IMPERIAL INSTITUTE
OF
AGRICULTURAL RESEARCH PUSA

PROCEEDINGS

OF THE

ROYAL SOCIETY OF LONDON

SERIES A

CONTAINING PAPERS OF A MATHEMATICAL AND
PHYSICAL CHARACTER.

VOL. CXLII.

314748
IARI

LONDON:
PRINTED FOR THE ROYAL SOCIETY AND SOLD BY
HARRISON AND SONS, LTD., ST. MARTIN'S LANE
PRINTERS IN ORDINARY TO HIS MAJESTY.
NOVEMBER, 1933.

LONDON
HARRISON AND SONS, LTD., PRINTERS IN ORDINARY TO HIS MAJESTY,
ST. MARTIN'S LANE

CONTENTS.

SERIES A. VOL. CXLII.

No A 846—October 1, 1933.

PAGE

Bakerian Lecture—The Neutron. By J. Chadwick, F R S . .. 1

Absorption Spectra of Burning Hydrocarbons By A Egerton, F R S, and L. M Pidgeon (Plate 1) . . . 26

The Spectrum of H_2 The Bands ending on $2p\ ^3\Pi$ Levels.—Part III. By O W Richardson, F R S, and P M Davidson Appendix by J Marsden and W M Evans 40

The Spectrum of H_2 The $3d^1\Delta$ and $4d^1$ Levels By O W Richardson, F R S, and P M Davidson 63

The Homogeneous Catalysis of Gaseous Reactions by Iodine The Decomposition of Propionic Aldehyde, and a General Discussion By S. Bairstow and C N Hinshelwood, F R S . . 77

On a New Type of Expansion Apparatus By C T R Wilson, F.R S 88

The Motion of a Rotor carried by a Flexible Shaft in Flexible Bearings By D M Smith Communicated by G Stoney, F R S . 92

The First Spark Spectrum of Gold Au II By B V. R. Rao Communicated by Lord Rayleigh, For Sec R S 118

Investigations in the Infra red Region of the Spectrum. Part IX—The Absorption Spectrum of Chlorine Monoxide (Cl_2O) By C R Bailey and A B D Cassie. Communicated by F. G. Donnan, F R S. 129

The Passage of Positive Ions through Gases By H S. W. Massey and R A Smith Communicated by P. A. M Dirac, F R.S 142

The Estimation of Electric Moment in Solution by the Temperature Coefficient Method Part I—Experimental Method and the Electric Moments of some Benzyl Compounds By F Fairbrother. Communicated by A. Lapworth, F.R S 173

The Thermal Expansions of Certain Crystals with Layer Lattices. By H D Megaw Communicated by A. Hutchinson, F R S. (Plate 2) . . . 198

The Internal Conversion of γ-Rays.—II By H M. Taylor and N F Mott Communicated by P. A. M. Dirac, F.R.S 215

The Thermal Expansion of Quartz by X-ray Measurements. By A H Jay Communicated by W. L. Bragg, F R S (Plate 3)... 237

On the Electric Charge Collected by Water Drops Falling through Ionised Air in a Vertical Electric Field. By J. P Gott. Communicated by C T R. Wilson, F.R.S. 248

PAGE

Quantization of the Kramers and Pauli Model By P M Davidson Communicated by O W. Richardson, F R S 269

The Behaviour of Metals, Particularly Lead and Bismuth, in Atomic Hydrogen, and Attempts to Prepare Atomic Hydrogen from Hydrides By T G Pearson, P L. Robinson and E M Stoddart Communicated by J Kendall, F.R S . 275

Perturbations in the Barium I Spectrum By G O Langstroth Communicated by O W. Richardson, F R S. 286

Interference Due to Walls of a Wind Tunnel By L. Rosenhead. Communicated by H G Glauert, F R S 308

The Inelastic Scattering of Slow Electrons in Gases —III By F H Nicoll and C B O Mohr Communicated by Lord Rutherford, O M , F R S 320

An X-ray Study of p Diphenylbenzene By L W Pickett Communicated by Sir William Bragg, O M , F R S 333

Analysis of the Long Range α-Particles from Radium C' by the Magnetic Focussing Method By Lord Rutherford, O M , F R S , W B. Lewis and B V Bowden 347

No A 847 —November 1, 1933

Spectrum of the Afterglow of Carbon Dioxide By A Fowler, F R S , and A G Gaydon (Plate 4) 362

Beryllium and Helium I —The Helium Contained in Beryls of Varied Geological Age. By Lord Rayleigh, For Sec R S 370

The Influence of the Underlying Surface on the Cataphoretic Mobility of Adsorbed Proteins By A Dummett and P Bowden Communicated by T M Lowry, F R S 382

The Structure of Surface Films Part XVIII —The Effect of Alkalinity in the Underlying Solution on Films of Fatty Acids By N K Adam and J G. F. Miller Communicated by F G Donnan, F R S 401

The Structure of Surface Films Part XIX — Influence of Alkaline Solutions on Films with Various End Groups By N K Adam and J G F Miller Communicated by F G Donnan, F R S . 416

The Reflection of X-rays from Anthracene Crystals By B W. Robinson Communicated by Sir William Bragg, O M , F.R S (Plate 5) 422

Exchange of Energy between Inert Gas Atoms and a Solid Surface By J. M. Jackson and A Howarth. Communicated by D R Hartree, F R S 447

A Comparison of the Catalytic Activity of Liquid and Solid Surfaces The Decomposition of Methanol on Solid and Liquid Zinc By E W R Steacie and E M. Elkin Communicated by H T Barnes, F R S. 457

The Emission Constants of Metals in the Near Infra-red. By C. Hurst Communicated by F A. Lindemann, F R S 466

The Flow of Viscous Liquid Past Spinning Bodies. By T E. Garstang Communicated by L. N G Filon, F R S 491

PAGE

The Scattering of Electrons by Metal Vapours II - Zinc By E C Childs and H S W. Massey Communicated by Lord Rutherford, O M., F R S .. 509

The Exchange of Energy between Gas Atoms and Solid Surfaces III.—The Accommodation Coefficient of Neon By J K Roberts Communicated by Lord Rutherford, O M, F R S . . 518

The Kinetics of the Reaction between Hydrogen and Nitrous Oxide —I By H. W. Melville Communicated by J Kendall, F R S 524

On the Two-Dimensional Steady Flow of a Viscous Fluid Behind a Solid Body —I By S Goldstein Communicated by L N G Filon, F R S Appendix by A Fage . 545

On the Two Dimensional Steady Flow of a Viscous Fluid Behind a Solid Body II By S Goldstein Communicated by L N G Filon, F R S 563

Some Intensity Measurements on the Band Spectrum of Helium (He_2) By R C Johnson and R C Turner Communicated by O W Richardson, F R S 574

The Change in the Absorption Spectrum of Cobalt Chloride in Aqueous Solution with increasing Concentration of Hydrochloric Acid By O R Howell and A. Jackson Communicated by E K Rideal F R S 587

The Transmission of Infra-red Radiation by a Thin Layer of Horn. By H J Taylor Communicated by Sir Leonard Hill, F R S 598

Power Loss Phenomena in Liquid Dielectrics By W Jackson Communicated by M. Walker, F.R S 606

On the Stability for Three-Dimensional Disturbances of Viscous Fluid Flow between Parallel Walls By H B Squire Communicated by R V Southwell, F R S 621

The Mechanism of the Oxygen Electrode By T P Hoar Communicated by E K Rideal, F R S . 628

The Inelastic Scattering of Slow Electrons in Gases —IV By F H Nicoll and C B O Mohr Communicated by Lord Rutherford, O M, F R S 647

Fourier Analysis of the Durene Structure By J M Robertson Communicated by Sir William Bragg, O M, F R S 659

The Crystalline Structure of Naphthalene A Quantitative X-ray Investigation. By J M. Robertson Communicated by Sir William Bragg, O M., F R S . 674

Collisions of Neutrons with Light Nuclei.—Part II By N Feather Communicated by Lord Rutherford, O M, F R S (Plates 6 and 7) 689

Index . . . 711

Title, Contents, etc

PROCEEDINGS OF

THE ROYAL SOCIETY.

Section A.—Mathematical and Physical Sciences.

Bakerian Lecture *The Neutron.*

By J Chadwick, F.R.S.

(Read May 25, 1933 Received June 27, 1933)

§ 1 In an earlier paper[*] I showed that the radiations excited in certain light elements by the bombardment of α-particles consist, at least in part, of particles which have a mass about the same as that of the proton but which have no electric charge These particles, called neutrons, have some very interesting properties Some of the more striking were described in the paper I have mentioned and in those of Dr Feather[†] and Mr. Dee[‡] which accompanied it. The most obvious properties of the neutron are its ability to set in motion the atoms of matter through which it passes and its great penetrating power From measurements of the momenta transferred to different atoms the mass of the neutron was estimated and shown to be nearly the same as the mass of the proton, while the penetrating power shows that the neutron can have no nett electric charge. The loss of energy of a neutron in passing through matter is due to the collisions with the atomic nuclei and not with the electrons. The experiments of Dee showed that the primary ionization along the track of a neutron in air was less than 1 ion pair in 3 metres path, while Massey has calculated that it may be as low as 1 ion pair per 10^5 km This behaviour is, of course, very different from that of a charged particle such as a proton, which dissipates its energy almost entirely in electron collisions. The contrast between the rate of loss of energy of a proton and a neutron of the same initial velocity is most striking A proton of velocity 3×10^9 cm./sec. travels about 1 foot in air, while a neutron of the same initial velocity will on the average make a close collision with a nitrogen nucleus only once in 300 to 400 yards' path and it may go a distance of a few miles before losing all its energy. The collision of a neutron with an atomic nucleus, although much more frequent than with an electron, is also a rare event, for the electric field between a neutron and a nucleus is small except at distances of the order of 10^{-12} cm. In such a close collision the neutron will be deflected from its path and the struck nucleus may acquire sufficient energy to produce ions. Thus the nuclei recoiling from encounters with neutrons can be detected by ionization measurements, using an ionization chamber with a sensitive electrometer or with an electrical counting apparatus, or by their ionized tracks when produced in an expansion chamber

---

[*] Chadwick, 'Proc Roy. Soc,' A, vol. 136, p. 692 (1932).

[†] Feather, *loc. cit.*, p. 709

[‡] Dee, *loc. cit.*, p 727

Neutrons can thus be detected only in an indirect way, by the observation of the recoil atoms For this reason, and also because they are produced as a result of a similar collision process only partly under our control, the study of their properties in detail has proved both difficult and tedious.

The nature and properties of the neutron are of interest not only because of their novelty but because the neutron is probably a very important unit in the structure of matter It is now generally assumed that atomic nuclei consist of protons and neutrons , then, because the mass of a nucleus is always equal to or greater than twice its charge, there must be more neutrons in matter than there are protons

In this lecture I shall give a brief survey of our knowledge of the neutron and indicate some directions in which progress has been made recently

§ 2 *Production of Neutrons.*—Neutrons have been produced so far only by bombarding certain elements by α-particles The process is assumed to be the capture of the α-particle into the atomic nucleus with the formation of a new nucleus and the release of a neutron The new nucleus will thus have a nuclear charge two units higher than that of the original nucleus and a mass number three units greater. The yield of neutrons is, of course, very low, and comparable to the yield of protons in the artificial transmutations by the same process. The greatest effect is given by beryllium, where the yield is probably about 30 neutrons for every million α-particles of polonium which fall on a thick layer of beryllium. For the elements of much higher atomic number the yield is very small, probably of the order of 1 or 2 neutrons per million α-particles. The yield can be increased by using bombarding α-particles of greater energy, *e.g* , using radon and its products as the source of α-particles, but here the γ-radiations from the source may interfere with the detection of neutrons unless suitable precautions are taken. The elements from which neutrons have been obtained are lithium, beryllium, boron, fluorine, neon, sodium, magnesium and aluminium. It is probable that most of the elements of higher atomic number up to argon will give neutrons when α-particles of sufficient energy are used.

It is noteworthy that, with the exceptions of helium, nitrogen, carbon and oxygen, all the light elements up to aluminium give neutrons, while some, *e.g.*, fluorine, give both neutrons and protons. Both results can be related to general rules of nuclear structure.* If a nucleus of mass number A and atomic number Z transforms by capturing an α-particle and emitting a neutron, the new nucleus will have a mass $A + 3$ and an atomic number $Z + 2$. Now all known types of atomic nuclei obey the rule that $A \geqslant 2Z$. If the new nucleus is to be subject to this condition then $A+3 \geqslant 2(Z + 2)$ or $A \geqslant 2Z+1$. This condition is not satisfied by He_2^4, C_6^{12}, N_7^{14}, or O_8^{16}, and we should therefore not expect to observe a disintegration of these nuclei with a neutron emission. The application of this condition also forbids the emission of neutrons from B_5^{10}, Ne_{10}^{20} and Mg_{12}^{24}. The neutrons must, therefore, be ascribed to the other isotopes of these elements.

The cases of fluorine and aluminium are interesting because these elements are both pure and yet they emit both protons and neutrons under the bombardment of α-particles. It seems then that the nuclei F^{19} and Al^{27} can disintegrate in either of two ways. For example, the capture of the α-particle may result in the reaction $F_9^{19} + He_2^4 \rightarrow Ne_{10}^{22} + H_1^1$, or in the reaction $F_9^{19} + He_2^4 \rightarrow Na_{11}^{22} + n_0^1$, *here forming a sodium isotope of mass 22 which* is certainly very rare in nature. If Na^{22} is stable its mass must be less than that of Ne^{22}, for otherwise the capture of a K electron would provoke the change $Na^{22} \rightarrow Ne^{22}$ with a release of energy. It follows that the maximum energy of the neutrons liberated from fluorine should be greater than the maximum energy of the protons. I have not yet been able to test this conclusion, for the yield of neutrons from fluorine is small. If it should prove that the neutrons have a smaller energy than the protons then we must conclude that the Na^{22} nucleus is unstable and transforms into Ne^{22} by capturing an electron, emitting some energy in the form of radiation. A similar argument may be applied to the dual transformation of aluminium which results in the formation of Si^{30} and an otherwise unknown P^{30}.

§ 3. *Boron and Beryllium.*—The production of neutrons from boron and beryllium has been investigated in some detail. These cases are of importance because in most experiments with neutrons boron and beryllium have been used as sources

---

* The following argument has also been pointed out independently by Dr. Feather in discussions in this laboratory.

The element boron consists of two isotopes B^{10} and B^{11}. When boron is bombarded by α-particles both neutrons and protons are emitted. The application* of the arguments used above leads to the conclusion that the protons are emitted in the disintegration of B^{10} and the neutrons from B^{11}. The velocity distribution of the neutrons from boron has not been examined in any detail, but the experimental results are consistent with the supposition that the neutrons liberated from a thin layer of boron by a homogeneous beam of α-particles would consist of a single group of definite velocity The velocity of the neutron liberated by an α-particle of velocity $1 \cdot 60 \times 10^9$ cm /sec. is about $2 \cdot 53 \times 10^9$ cm /sec There is no indication of a γ-ray emission connected with the neutrons †

The dependence of the neutron emission on the velocity of the bombarding α-particles has been examined The source of α-particles, a silver disk coated with polonium, was placed in an air-tight vessel at a distance of 2 05 cm from the boron target. The neutrons emitted from the target were detected in an ionization chamber connected to an amplifier and oscillograph To increase the effect, a sheet of paraffin wax was placed over the front of the ionization chamber Thus the deflexions of the oscillograph were due partly to nitrogen recoil atoms produced in the air of the chamber itself, and partly to protons ejected from the paraffin wax Carbon dioxide was then admitted to the source vessel at a pressure of 5 cm , thus reducing the velocity of the α-particles striking the boron target The number of oscillograph deflexions obtained under these conditions was again counted In this way, by successive additions of carbon dioxide, the variation of the emission of neutrons was found as the velocity of the impinging α-particles gradually decreased The results‡ are shown in fig 1, where the ordinates are the number of oscillograph deflexions observed in 30 minutes and the abscissæ are the maximum ranges of the α-particles incident on the boron, calculated on the assumption that the stopping power of carbon dioxide is 1·53 relative to air. It must be noted that this curve does not necessarily represent the true variation in the number of neutrons emitted as the range of the α-particles is varied. The number of deflexions observed in the chamber will depend not only on the number of neutrons but also upon their velocity, the probability of a collision between a neutron and a nitrogen atom in the chamber or a proton in the paraffin wax depends on the velocity of the neutron, and further, the slower the neutron the less is the energy of the recoil atoms and therefore the greater the chance that some of them will not give a measurable deflexion of the oscillograph. It is not possible at present to estimate the influence of these effects and to deduce from the observations of fig. 1 the true curve showing the variation in the emission of neutrons with the range of the bombarding α-particles

---

* *Cf.* Chadwick, Constable and Pollard, 'Proc Roy. Soc ,' A, vol 130, p 480 (1931).

† The γ-rays of energy about 3×10^6 electron volts emitted from boron bombarded by α-particles are connected with the proton emission from B^{10}.

‡ Similar results have been obtained by Curie and Joliot, 'C. R. Acad. Sci. Paris,' vol 196, p. 397 (1933)

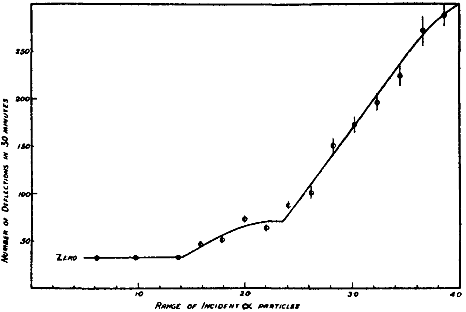

Fig. 1

It appears from fig 1 that no neutrons are liberated until the range of the α-particles is about 1 4 cm of air As the range of the α-particles is increased the emission of neutrons rises to a stationary value and then increases rapidly as the range of the α-particles is increased from about 2·4 cm up to the maximum of 3·86 cm. This suggests that the α-particles of 1·4 cm. range enter the boron nucleus through a resonance level, and those of 2·4 cm and greater range enter through and over the top of the potential barrier. The corresponding energies are 2·4 × 10^6 electron volts for the resonance level, and about 3·7 × 10^6 electron volts for the top of the potential barrier (or rather the point at which the α-particles begin to penetrate appreciably).

Since the velocity of the neutron liberated from boron by an α-particle of given velocity is known, the velocity distribution of the neutrons emitted from a thick layer of boron bombarded by polonium α-particles can now be deduced. The resonance level will give a group of neutrons of velocity about $1 \cdot 07 \times 10^9$ cm./sec, and penetration over the barrier will give neutrons with a continuous distribution of velocity between $1 \cdot 9$ and $2 \cdot 53 \times 10^9$ cm/sec The corresponding energies are $0 \cdot 6 \times 10^6$ volts for the resonance group and $1 \cdot 9$ and $3 \cdot 35 \times 10^6$ volts for the continuous distribution

The excitation of neutrons from a thick layer of beryllium by α-particles of different ranges was examined in a similar way, with the result shown in the full curve of fig 2 This curve suggests the existence of two resonance levels, the first, through which α-particles of 0·80 cm. range can enter the beryllium nucleus, and the second through which α-particles of 1·46 cm range enter A rapid increase in the emission of neutrons takes place when the range of the α-particles is increased beyond 2·25 cm This is taken to correspond to the penetration through and over the top of the potential barrier. The energies of the resonance levels are about $1 \cdot 4 \times 10^6$ and $2 \cdot 5 \times 10^6$ electron volts, and penetration through the top of the barrier begins at about $3 \cdot 5 \times 10^6$

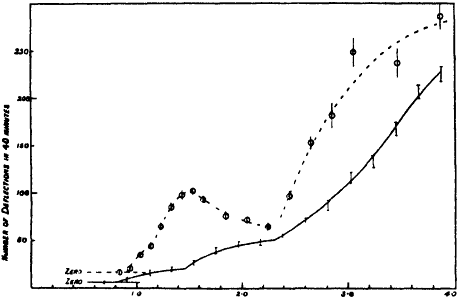

Fig 2

electron volts. As we should expect, the height of the potential barrier of beryllium is slightly less than that of boron.

The existence of the resonance levels in beryllium was confirmed by observing the neutron emission from a thin foil of beryllium. This was prepared by evaporating *in vacuo* a small piece of pure beryllium and allowing some of the vaporized metal to condense on a cooled copper disk. The thin layer of beryllium thus obtained was not quite uniform in thickness, but it was suitable for the present purpose The thick piece of beryllium used in the previous experiment was replaced by this thin foil, and the observations were repeated. The results are given in the dotted curve of fig. 2 The first resonance level is only vaguely indicated in this curve, but the second level is shown clearly There is a very definite decrease in the emission of neutrons from the thin foil when the range of the α-particles is increased from 1·6 cm. to 2·2 cm. followed by a rapid rise when the α-particles begin to penetrate the top of the barrier The correspondence between this curve and that for the thick layer of beryllium is not complete. The discrepancies are probably to be attributed to changes in the geometry of the experimental arrangement produced when replacing the thick piece of beryllium by the foil, and also to the fact that the foil is not uniform in thickness

The excitation curve for a thick layer of beryllium is not very different from that obtained by Rasetti[*] and by Curie and Joliot (*loc. cit*) in similar experiments, or from that found by Becker and Bothe[†] for the excitation of γ-rays from from beryllium bombarded by α-particles. It is to be expected that the two processes—the emission of neutrons and the emission of γ-rays—should have similar excitation functions, for both are due to the entry of an α-particle into the beryllium nucleus, and the excitation curve gives in effect the probability of the entry of α-particles of different ranges. These two processes are, however, more intimately connected Becker and Bothe found that the energy of the γ-ray is independent of the energy of the incident α-particle and may be greater than it and they pointed out that this means that the emission of the γ-ray is not an independent process; it is probably related to the neutron emission in a manner similar to that in which the γ-rays from B^{10} are related to the emission of two groups of protons. On this view, we should expect to find two groups of neutrons emitted from a thin foil of beryllium bombarded by a homogeneous beam of α-particles. Some observations suggest that this is so. Curie, Joliot, and Savel[*] found that the protons ejected from paraffin wax by the neutrons from a thick piece of beryllium bombarded by polonium α-particles consist mainly of a group with maximum range about 28 cm. in air and a weaker group of maximum range about 70 cm. This indicates that the main group of neutrons has a maximum velocity of about $2 \cdot 9 \times 10^9$ cm./sec and that there is also a small number of neutrons with velocities up to about $3 \cdot 8 \times 10^9$ cm /sec. Without further evidence it is not possible to decide how these groups are excited

---

[*] 'Z. Physik,' vol. 78, p 165 (1932)

[†] 'Z. Physik,' vol. 76, p. 421 (1932).

In my experiments I have examined the neutrons emitted from a thick layer of beryllium and from the thin foil The neutrons passed through a sheet of paraffin wax placed just in front of the face of the ionization chamber The ranges of the protons ejected by the neutrons from the wax were measured by observing the diminution in the number of protons as absorbing foils of aluminium were interposed between the wax and the ionization chamber The protons due to the neutrons from the thin foil of beryllium consisted mainly of a group with a fairly well defined range of 23 cm. to 24 cm in air, fig. 3 There were protons present with ranges much greater than this but their number was very small. Some indication was obtained that the maximum range was at least 100 cm. in air, but the difference between the number of oscillograph deflexions with and without the wax was so small that the range of these fast protons could not be fixed.

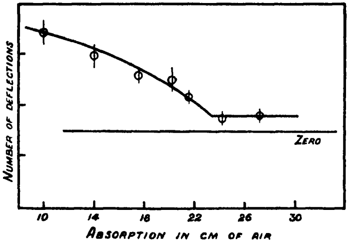

FIG 3

---

[*] ‘C A. Acad. Sci. Paris,’ vol. 194, p. 2208 (1932).

The results using a thick layer of beryllium showed again the presence of a group of protons of 24 cm range, and also a group of about 65 cm to 75 cm range, with a very doubtful indication of the presence of protons of still greater range.

The conclusions to be drawn from these experiments are not very definite. It is, however, certain that the neutrons liberated from beryllium by polonium α-particles of velocity $1 \cdot 6 \times 10^9$ cm /sec consist of at least two groups; the slower and more intense group has a velocity of $2 \cdot 8 \times 10^9$ cm /sec. (energy $4 \cdot 1 \times 10^6$ electron volts) and the faster group a velocity perhaps greater than 4×10^9 cm./sec. (energy greater than 8×10^6 electron volts). It remains to be seen how these results can be fitted into the disintegration process I assume that the reaction is

$$\mathrm{Be}_4{}^9 + \mathrm{He}_2{}^4 \rightarrow \mathrm{C}_6{}^{12} + n_0{}^1.$$

The masses of all the nuclei concerned are now known with reasonable accuracy, Bainbridge's measurement gives $\mathrm{Be}^9 = 9 \cdot 0132$, from Aston's measurements, $\mathrm{He}^4 = 4$ 00106 and $\mathrm{C}^{12} = 12 \cdot 0003$, and the mass of the neutron is $1 \cdot 0067$ (see § 4) Assuming that energy and momentum are conserved, the velocity and energy of the neutron liberated by an α-particle of polonium (velocity $= 1$ 60×10^9 cm /sec, energy $= 5 \cdot 3 \times 10^6$ electron volts) can be calculated Its velocity is 4 77×10^9 cm /sec and energy 11 9×10^6 electron volts These values are much greater than any found in the experiments described above Neutrons of this velocity would eject protons with ranges up to about 150 cm in air, while the greatest ranges found for the protons experimentally is 70 cm, with, however, indications of ranges greater than 100 cm. Some evidence of the presence of neutrons of high energy has been obtained from the examination of oscillograph records of the deflexions due to recoil atoms produced in an ionization chamber. The size of a deflexion is proportional, at least approximately, to the energy of the recoil atom, and therefore, for a given atom, proportional to the energy of the colliding neutron. Neutrons from the thin beryllium foil bombarded by polonium α-particles of full range were passed into an airtight ionization chamber, which was filled in turn with nitrogen, oxygen, and argon For each gas a large number of oscillograph deflexions was photographed, using the oscillograph at a convenient sensitivity The examination of the records for all three gases showed very clearly a strong and well defined group of recoil atoms which was attributed to the effect of the group of neutrons of energy about 4×10^6 electron volts, and in addition a much weaker group containing recoil atoms of high energy.

The maximum energy associated with this group was roughly three times the maximum energy of the short group, that is, about 12×10^6 electron volts The separation of the recoil atoms into these two groups is to some extent confirmed by an estimate of the number of ions corresponding to the oscillograph deflexions, from which the energies of the recoil atoms can be deduced. This estimation is, however, indirect and somewhat uncertain. With these reservations, the experiments provide fair evidence for the emission of neutrons of energies up to about 12×10^6 electron volts Some evidence has also been obtained by Feather, who has measured the ranges of recoil atoms of nitrogen, oxygen, and carbon produced in an expansion chamber He has observed several tracks which lead to values of the neutron energy of about 10×10^6 electron volts Feather's evidence is more direct and more trustworthy than that just given, but further data are needed before the maximum energy of the neutrons can be definitely ascertained

I shall suppose for the present that the energy of the faster group of neutrons emitted from beryllium does in fact agree with that calculated on the hypothesis that the disintegration process is $Be^9 + He^4 \rightarrow C^{12} + n^1$ and that energy and momentum are conserved On this view a thin foil of beryllium bombarded by α-particles of velocity $1 \cdot 60 \times 10^9$ cm /sec. should emit a strong group of neutrons with velocity $2 \cdot 8 \times 10^9$ cm./sec and a weak group of velocity $4 \cdot 7 \times 10^9$ cm /sec., and a γ-radiation of high energy, which is intimately connected with the emission of the neutrons.

These facts can be given a descriptive explanation in terms of the following picture of the disintegration process. Assume that the beryllium nucleus consists of an α-particle with 2 protons and 3 neutrons For some reason the formation of another α-particle by the further condensation of 2 protons and 2 neutrons cannot take place (or rather the chance of condensation is very small When it occurs the beryllium nucleus may break up into two α-particles and a neutron). The capture of an α-particle by the beryllium nucleus provokes the condensation, and usually the nuclear change takes place with the emission of a γ-ray and a neutron This neutron will belong to the group of lower velocity found experimentally. Sometimes, however, all the energy may be taken by the neutron, and this reaction will correspond to the emission of the group of neutrons of high velocity On this view we get a residual nucleus, C^{12}, consisting of three α-particles, and two groups of neutrons which should differ in energy by about the energy of the γ-ray (allowance must be made for the energy of the recoiling C^{12} nucleus) Taking the velocities given above for the two groups of neutrons, the energy of the γ-ray should be 7×10^6 electron volts. This is much higher than the value 5×10^6 electron volts deduced by Becker and Bothe from their measurements of the ranges in aluminium of the secondary electrons produced by this γ-radiation On the other hand, the measurements of the absorption coefficient of the radiation suggest an energy rather higher than 5 million volts, and there is no doubt, from expansion chamber observations, that the radiation does produce some secondary electrons of greater energy than 5 million volts Thus Auger observed one β-ray track due to this radiation which had an energy of $6 \cdot 5 \times 10^6$ electron volts, while out of 150 electron tracks measured by Blackett Occhialini and myself, 10 had energies between 5 and 7×10^6 volts Unless these were due to the penetrating radiation there must be some γ-radiation emitted from beryllium with an energy of about the required amount On the other hand, the analysis of the tracks suggests that a large fraction of the γ-radiation has an energy of about 5×10^6 volts The evidence about the energy of the γ-rays emitted from beryllium is unsatisfactory, but it is not definitely against the proposed scheme of disintegration

It is now possible to describe the velocity spectrum of the neutrons emitted from a thick layer of beryllium bombarded by polonium α-particles. Each resonance level will give rise to two homogeneous groups of neutrons, the slower group being much stronger than the faster. The groups from the first level will have velocities of about 1×10^9 cm /sec and $3 \cdot 92 \times 10^9$ cm./sec or energies of about $0 \cdot 5 \times 10^6$ electron volts and about $8 \cdot 0 \times 10^6$ electron volts.* The groups from the second level will have velocities of about $1 \cdot 68 \times 10^9$ cm /sec and $4 \cdot 18 \times 10^9$ cm./sec, corresponding to energies about $1 \cdot 47 \times 10^6$ electron volts and $9 \cdot 1 \times 10^6$ electron volts respectively Since general penetration through the top of the potential barrier begins when the α-particle has a range of 2·25 cm., there will be a group of neutrons with velocities between $2 \cdot 16 \times 10^9$ and $2 \cdot 8 \times 10^9$ cm./sec., or energies between 2·5 and $4 \cdot 1 \times 10^6$ electron volts, and a weaker group with velocities between $4 \cdot 4 \times 10^9$ and $4 \cdot 77 \times 10^9$ cm./sec, and energies between 10 1 and $11 \cdot 9 \times 10^6$ electron volts. The neutron emission from a thick layer of beryllium is thus relatively complicated The majority of the neutrons are contained in the slow groups and the velocities given for these should be fairly accurate. It must be remembered that there is little direct evidence for the velocities given for the faster groups The values are obtained on the assumptions that the disintegration proceeds in a certain way and that energy is conserved. The picture of the disintegration process adopted here can be tested in two ways—by a search for the group of very fast neutrons and by measurement of the energy of the γ-radiation The evidence now available on these points is inconclusive

---

* The group of neutrons of velocity about $3 \cdot 8 \times 10^9$ cm /sec observed from a thick layer of beryllium may correspond to this weak resonance group

It is possible that either or both the assumptions made above are untrue. It may be that the capture of an α-particle by the beryllium nucleus results in a complete breakdown of the nucleus, with the emission of three α-particles, a neutron, and a γ-radiation There seems, however, no reason to expect in such a process that the neutrons would be emitted in two definite groups as appears to be the case It is perhaps possible that both processes take place, sometimes a C^{12} nucleus being formed and sometimes three α-particles; one might then be able to account not only for the presence of the γ-ray of energy about 7×10^6 volts, but also for that of about 5×10^6 volts which is suggested by Becker and Bothe's measurements

In none of the examples of artificial transmutation so far examined, has there been any reason to suspect that energy is not conserved, in some cases it is certain that energy is conserved within narrow limits If it should fail in this particular case, one might be tempted to suppose that the missing energy is taken away by some yet undetected particle A suggestion has, indeed, been made at various times that neutral particles of very small mass may exist, and it has been revived recently to overcome the difficulty of explaining the continuous distribution of energy among the β-rays expelled from a radioactive body The emission of such a particle would be very difficult to detect in any cases of artificial transmutations owing to their infrequent occurrence, and the most favourable opportunity of finding it appears to be offered by a radioactive β-ray disintegration About two years ago Mr Tarrant kindly made some measurements for me to search for this neutral radiation in the emission from radium E, but we were unable to find any evidence of it Mr. Lea and I have recently made a stricter examination with the same result We conclude from our experiments that if a neutral radiation is emitted from radium E to compensate for the energy distribution of the β-rays, it must consist of particles of small mass and of such small magnetic moment that a particle cannot produce more than 1 pair of ions in 100 miles of path in air.

§ 4. *The Mass of the Neutron.*—While observations of the momenta transferred in collisions of a neutron with atomic nuclei are enough to show that the mass of the neutron is about the same as that of the proton, the measurements cannot be made with precision. For an accurate estimate of the mass of the neutron we must use the energy relations in a disintegration in which a neutron is liberated from an atomic nucleus. Assuming that energy and momentum are conserved in the disintegration, the measurement of the kinetic energy of the neutrons liberated by α-particles of known energy is sufficient to give the mass of the neutron if the masses of the nuclei concerned are known. In a previous paper I considered the disintegration

$$B^{11} + He^{4} \rightarrow N^{14} + n^{1}.$$

The kinetic energy of the neutrons liberated from boron by α-particles of polonium was found by measuring the maximum range of the particles ejected from paraffin wax. Using Aston's measurements of the masses of the nuclei, I obtained a value for the mass of the neutron of 1·0067.

Another value can be deduced from the process

$$Li^{7} + He^{4} \rightarrow B^{10} + n^{1}.$$

The mass of Li^7 is best obtained from the experiments of Cockcroft and Walton on the disintegration of lithium by fast protons. The lithium nucleus captures a proton and breaks up into two α-particles

$$Li^{7} + H^{1} \rightarrow 2He^{4}.$$

Cockcroft and Walton found that the range of the α-particles is 8·4 cm in air, corresponding to an energy of $8·7 \times 10^6$ electron volts, when protons of energy 300,000 volts were used. This leads to a mass of 7·0133 for the Li^7 nucleus. Aston's measurements give 4·00106 for the mass of He^4 and 10·01075 for B^{10}. The kinetic energy of the neutrons liberated from Li^7 by the α-particles of polonium (energy 0·00565 in mass units) has not been determined. It is small, perhaps less than $0·5 \times 10^6$ volts, for the neutrons are easily absorbed in a few millimetres of lead. If we assume that the neutrons are emitted with zero energy we shall get a maximum value for the mass of the neutron. We find in this way that the mass of the neutron cannot be greater than $1·0070 \pm 0·0005$. The uncertainty in this estimate arises mainly from the probable error in Aston's measurement of B^{10}.

If we assume that the hydrogen isotope of mass 2 consists of a proton combined with a neutron, we can obtain a minimum estimate for the mass of the neutron, for the sum of the masses of the two particles must be greater than the mass of the combination by an amount corresponding to the binding energy. The mass* of the nucleus of the H^2 isotope is 2·0130. Thus the mass of the neutron must be greater than 2·0130 − 1·0072, or

---

* Bainbridge, 'Phys. Rev.,' vol. 43, p. 103 (1933).

1 0058. The mass of the neutron therefore lies between 1·0058 and 1·0070. Provisionally we may retain the value 1·0067 which I deduced from the boron disintegration

There can be no doubt that the mass of the neutron is distinctly less than that of the hydrogen atom This is consistent with the view that the neutron consists of a proton and an electron The difference in mass, 0·0011, then represents the binding energy of the two particles and corresponds to 1 million electron volts. It may be significant that the change of mass corresponds to a change in the energy of the electron from $+mc^2$ to $-mc^2$. This argument from the mass is certainly in favour of the complex nature of the neutron but it is by no means conclusive The most direct proof would be the observation of the splitting of the neutron into a proton and an electron in a nuclear collision, but both calculation and experiment show that this must be a very rare event As I shall show later, some suggestion that either the neutron or the proton may be complex can be deduced from the collisions of neutrons with protons

On the other hand, certain arguments can be advanced to support the idea that the neutron is an elementary particle According to the present scheme of quantum mechanics the hydrogen atom represents the only possible combination of a proton and an electron However, the binding energy of the particles is greater than the proper mass of the electron and a relativistic mechanics would be required to describe their interaction

A further argument is based on the spin of the neutron This is deduced from the spins of the light elements on the assumption (1) that a nucleus is built up as far as possible of α-particles, then of protons and neutrons (no free electrons), (2) that the nuclear spin is given by the vector sum of its components' spins. It then appears that the neutron must have a spin $\frac{1}{2}h/2\pi$ and obey the Fermi statistics The proton has a spin $\frac{1}{2}h/2\pi$ and obeys Fermi statistics If the neutron is to be regarded as a proton combined with an electron a spin of 0 and Bose statistics must be ascribed to the electron. This is contrary to the behaviour of a free electron The statistics and spins of the lighter elements can only be given a consistent description if we assume that the neutron is an elementary particle.

A more general argument may be used. If the neutron is a proton and an electron why does not the hydrogen atom transform into a neutron with a release of energy? There is ample evidence to show that such a transformation must be exceedingly rare. This consideration seems to me to argue strongly for the elementary nature of the neutron.

It seems necessary for the present to recognize these difficulties and, while retaining the hypothesis that the neutron is complex for some purposes, to regard it as an elementary unit in the structure of atomic nuclei.

One might perhaps attempt to offer an alternative view, that the proton is the complex particle and regard it as a neutron plus a positive electron. The mass of the proton might perhaps be less than the sum of the masses of the neutron and positive electron, if the mass of the neutron is near the higher limit given above. But the difficulty with the spin remains We should be forced to assume that the spin of the positive electron is 0, and then the annihilation of the positive electron with the negative becomes difficult to understand.

§ 5. *Collisions of Neutrons with Atomic Nuclei.*—The elastic collisions of a neutron with an atomic nucleus can be briefly described in a general way Whatever view one takes of the nature of the neutron, its interaction with an atomic nucleus will be very small except at distances of the order of 10^{-12} cm In its passage through matter the neutron will not be deflected unless it suffers a very intimate collision. One may say that the scattering of the neutrons will be due mainly to the internal field of the nucleus; the cross-section for the collisions will be about the same as the cross-section of the potential barrier of the nucleus, and the distribution of the scattered neutrons will not be markedly anisotropic. As I have shown in a previous paper, this view gives a reasonable account of the scattering of neutrons by heavy nuclei.

This is, of course, only a rough picture of the collision process, but the calculations of Massey* lead to much the same conclusion. Massey assumed that the neutron was a hydrogen atom in a nearly zero quantum state. The field of such a neutron will be similar to that just outside the Bohr orbit of the hydrogen atom but on a much reduced scale It can be represented by

$$\mathrm{V}\,(r) = e^2\left(\frac{1}{r} + \frac{\mathrm{Z}}{a_0}\right)e^{-2\mathrm{Z}r/a_0},$$

where Z, the effective nuclear charge, will be very large, and a_0 is the radius of the first Bohr orbit of hydrogen The " radius " of the neutron will be a_0/Z.

The field of interaction between this neutron and a nucleus of charge Z′ at distances greater than the nuclear radius will be $\mathrm{Z}'\mathrm{V}(r)$ Now the experiments on the scattering of neutrons by lead show that the collision radius is about the same as the nuclear radius, and from this Massey was able to obtain a lower limit to the value of Z of 25,000. (This gives a maximum value of 2×10^{-13} cm. for the radius of the neutron.)

---

* 'Proc Roy. Soc,' A, vol. 138, p 460 (1932)

Applying this result for Z to the collisions of a neutron with the lighter nuclei, he was able to show that the collision radii should be proportional to the nuclear charge. This result does not correspond with experiment, which show that the radius varies slowly from carbon (*ca.* $3{\cdot}5 \times 10^{-13}$ cm.) to argon (*ca.* $5{\cdot}5 \times 10^{-13}$ cm.). He therefore concluded that the collision areas are determined by the internal field of the nucleus, that the external interaction is of such short range that the colliding systems penetrate.

The most interesting collisions of a neutron are those with a proton. The proton should behave as an elementary charge even at very small distances. If there were no other interaction between a proton and a neutron but that given by $V(r)$, the collision radius for these collisions must be less than $1{\cdot}4 \times 10^{-14}$ cm. The disagreement with experiment is startling, for the observed collision radius is about 4 to 5×10^{-13} cm. for neutrons of velocity $2{\cdot}7 \times 10^{9}$ cm./sec. and greater still for slower neutrons. Before proceeding to discuss the reasons for this discrepancy I will state briefly what is known about the neutron-proton collisions.

These collisions have not been studied in much detail owing to experimental difficulties. The most direct method would be to pass a known number of neutrons of definite speed into an expansion chamber filled with hydrogen and to photograph the hydrogen recoil tracks. This would give both the frequency of the collisions and the angular distribution of the struck protons. Unfortunately we have only very indirect methods of estimating the number of neutrons in a beam and the collisions are so infrequent as to make the experiment exceedingly tedious.

Some results on the angular distribution of the protons have been obtained by this method by Auger and Monod-Herzen,* and also by Kurie,† who used a slightly different arrangement. In both experiments the neutrons were obtained by bombarding a thick layer of beryllium by polonium α-particles. The neutrons were therefore heterogeneous, the greater part having speeds below $2{\cdot}8 \times 10^{9}$ cm./sec. In Auger's experiments a large majority of the recoil protons were due to collisions of slow neutrons. The angular distribution of the struck protons was roughly uniform. Kurie confined his attention to the protons produced by the faster neutrons but their distribution with angle was also fairly uniform relative to the centre of mass of the moving system.

---

* 'C. R. Acad. Sci. Paris,' vol. 196, p. 1102 (1933).

† 'Phys. Rev.,' vol. 43, p. 672 (1933).

Meitner and Philipp* have used the expansion chamber method to make an estimation of the collision radius. They assumed that 30 neutrons are emitted from a thick foil of beryllium for every 10^6 α-particles of polonium incident upon it, and they measured the time interval in which tracks were recorded in the chamber by an independent experiment with a source emitting a known number of α-particles. Then from the observed frequency of the proton tracks they estimated that the collision radius was not less than 8×10^{-13} cm. From the data given in their account, it would appear that most of the collisions were due to slow neutrons, of velocities around 10^9 cm./sec.

My own experiments, in which electrical counting methods were used, are in general agreement with these The angular distribution of the protons was measured by counting the number of protons ejected from annular rings of paraffin wax of different apertures The results, though rough, showed that the distribution with angle of the protons was approximately uniform Attempts to observe the angular distribution for a reasonably homogeneous beam of neutrons failed, owing to the smallness of the effects

The collision radius was determined by the method used previously. The neutron source was a thin foil of beryllium of about 5 mm air equivalent bombarded by polonium α-particles The neutron beam was therefore fairly homogeneous, the main part consisting of particles of velocity about $2 \cdot 7 \times 10^9$ cm /sec., with a weak group of much higher velocity. The source was fixed in position relative to an ionization chamber connected to an amplifier and oscillograph in the usual way The chamber could be evacuated and filled with different gases The number of deflexions was observed when the chamber was filled in turn with hydrogen or a heavier gas, *e.g.*, nitrogen, oxygen, or argon. Each deflexion corresponds to the production of a recoil atom by the collision of a neutron with a nucleus. Since the number of neutrons passing through the chamber was the same in each case, the number of deflexions should be proportional to the collision area of the nucleus concerned. It was found that the number of deflexions in hydrogen was slightly less than the number in nitrogen or oxygen. The collision radius for hydrogen should therefore be rather less than for these nuclei. The collision radius for carbon was estimated by measuring the reduction in number of the deflexions observed in a counter when a thick block of graphite was placed in the path of the neutrons. The value found was about $3 \cdot 5 \times 10^{-13}$ cm. The collision radii of nitrogen and oxygen may be somewhat greater and will be taken as 4×10^{-13} cm.

---

* 'Naturwiss.,' vol. 20, p 929 (1932).

The above comparison between hydrogen and nitrogen is subject to a small but uncertain error due to the fact that recoil atoms which make only a few ions will not be counted by the oscillograph This affects the number of deflexions both in hydrogen and nitrogen. The deflexions in hydrogen are on the whole smaller than those in nitrogen owing to the low ionizing power of the proton and the low density of the gas On the other hand the energy transfer is smaller in the nitrogen collisions and the more distant collisions may not be recorded An estimate of the fraction of the hydrogen collisions which were not recorded in pure hydrogen was made from experiments in which mixtures of hydrogen and nitrogen were used in the ionization chamber, but it has not been possible to make a correction for the unrecorded nitrogen collisions. Having regard to this source of error, we may take the collision radius for hydrogen to be about 4 to 5×10^{-13} cm for neutrons of velocity $2{\cdot}7 \times 10^{9}$ cm /sec

The same experiment was made with a neutron source consisting of a thick layer of boron bombarded by polonium α-particles These neutrons would have velocities up to about $2{\cdot}5 \times 10^{9}$ cm /sec the average being probably rather less than 2×10^{9} cm /sec The number of deflexions in hydrogen was now about twice the number in nitrogen, suggesting that the collision radius either of hydrogen or nitrogen varies rapidly with the velocity of the neutron Measurements of the scattering of these slower neutrons in graphite and paraffin wax showed that the variation was to be ascribed mainly to hydrogen From the comparison with nitrogen a value of 6×10^{-13} cm was deduced for the hydrogen collision radius, while the comparison between graphite and paraffin wax gave a value of about 7×10^{-13} cm. Some experiments with slower neutrons suggest that the radius for the proton collisions continues to increase as the velocity of the neutron decreases.

In the consideration* of the neutron-proton collisions we thus have to explain the observations that the angular distribution of the struck protons is roughly uniform, and that the collision radius is very large and increases as the velocity of the neutron decreases. If we assume that the hydrogen isotope of mass 2 consists of a proton and a neutron we have a further experimental fact, that the binding energy of this isotope is about 10^{6} volts.

The wave theory of the collisions of two independent particles gives for the collision cross-section

$$Q = \frac{h^2}{\pi M^2 v^2} \Sigma_n (2n + 1) \sin^2 \delta_n,$$

---

* I am much indebted to Mr H. S. W. Massey in this discussion of the collisions

where M is the reduced mass of the system, v the initial relative velocity of the particles, and the δ_n's are phase constants depending on M, v and $V(r)$, the interaction energy of the particles The angular distribution per unit angle of the particles in a system of co-ordinates in which the centre of mass is at rest is given by

$$I(\theta)\sin\theta = \frac{h^2}{8\pi^2 M^2 v^2}\left|\Sigma_n \left(e^{2i\delta_n} - 1\right)(2n+1)\,P_n(\cos\theta)\right|^2 \sin\theta,$$

where

$$P_0(\cos\theta) = 1, \qquad P_1(\cos\theta) = \cos\theta, \qquad P_2(\cos\theta) = \tfrac{1}{2}(3\cos^2 - 1), \text{ etc.}$$

The fact that the angular distribution is uniform shows that only the spherical harmonic of zero order is important, *i e*, the scattering depends mainly on the head-on collisions of the particles This means that the range of the neutron-proton interaction is small compared with

$$\frac{\text{wave-length}}{2\pi}\left(=\frac{h}{2\pi M v}\right),$$

i e., the interaction range $\lesssim 10^{-12}$ cm (This result agrees with the previous calculation of the collisions of neutrons in which the neutron was likened to an atom with an effective nuclear charge of at least 25,000.)

We must now examine the significance of the H^2 isotope, assuming it to consist of a proton and a neutron The potential field between a neutron and a proton is taken as in fig. 4 $V(r)$ is negligible for $r > r_0$. From the fact that an energy level of energy $-E_0$ ($=$ binding energy) exists we can deduce that $V(r)$ must be very great in the region $r < r_0$, for the field has to be so great as to compress a half wave-length into this region We have found that the wave-length of the incident protons is much greater than r_0 and their energy is of the same order as the binding energy E_0 Thus $V(r)$ must be $\gg E_0$ or E the energy of the incident protons

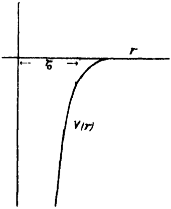

FIG 4

The potential field of a proton and a neutron may be roughly likened to a very deep hole of small radius. It can be shown that the effect of this deep hole is to make the wave function describing the collisions of a neutron and a proton nearly a maximum at $r = r_0$ instead of nearly zero, corresponding to a phase shift of nearly $\frac{1}{2}\pi$.

Thus $\delta_0 = \frac{1}{2}\pi$ approximately, and $Q \simeq \frac{h^2}{\pi M^2 v^2}$ about $2 \times 10^{-23} \times v^{-2}$ sq. cm. when v is measured in 10^9 cm./sec.

The collision radius $\simeq 2{\cdot}5 \times 10^{-13}/v$ cm. Since we have taken the maximum value of δ_0 this collision radius is a maximum also. It is most unlikely that δ_0 can be less than $\frac{1}{4}\pi$. A minimum value for the collision radius can therefore be obtained by putting $\delta_0 = \frac{1}{4}\pi$. The minimum collision radius is then $1{\cdot}8 \times 10^{-13}/v$ cm.

This result is in better accord with experiment than the previous one. The cross-section for proton collisions is large and varies with velocity in the way required. On the other hand, the cross-section is now too large. Putting $v = 2{\cdot}7 \times 10^9$ cm./sec. we obtain a collision radius of nearly 10×10^{-13} cm., certainly not less than 7×10^{-13} cm., whereas the observations give rather less than 5×10^{-13} cm. I do not think that the errors in the experiments can cover such a discrepancy, and an explanation must be sought elsewhere.

The explanation is perhaps to be found by introducing some type of exchange interaction between the neutron and proton. For example, if the neutron consists of a proton and an electron another kind of interaction between the proton and the neutron is possible—the change of the electron from the neutron to the proton and the exchange of protons. This interaction is analogous to that between a hydrogen atom and a proton. In effect it introduces a strong repulsive field and a strong attractive field, both of very small radius of action. The final result is to reduce the collision cross-section by a factor depending upon the spin of the proton. If the spin is $\frac{1}{2}h/2\pi$ the cross-sections may now be not smaller than one-quarter of those given above, *i.e.*,

Q is now

$$\simeq \frac{1}{4}\frac{h^2}{\pi M^2 v^2}$$
$$\simeq 5 \times 10^{-24} \times v^{-2}\ \text{cm.}^2,$$

where v is in units of 10^9 cm./sec. For neutrons of velocity $2{\cdot}7 \times 10^9$ cm./sec. this gives a collision radius of about 5×10^{-13} cm. in good accord with the experimental value.*

---

* The variation in the cross-section with the velocity of the neutron appears to be more rapid than is given by the above expression. This can be explained in a more detailed development of the theory. It is worthy of note that this rapid variation of the cross-section for hydrogen collisions accounts in part for the difficulty found in observing fast neutrons by their ejection of protons (§ 3). While the cross-section for collisions with other nuclei also depends on the velocity of the neutron the decrease with increasing speed is not so rapid as for hydrogen. The rapid variation in the cross-section for collision also explains the marked preponderance of short proton tracks in expansion chamber photographs, as observed in the experiments of Auger and of Meitner and Philipp.

It would be premature to conclude definitely that the neutron is a complex particle, for the theory of the collisions is not yet complete and the experimental observations are somewhat uncertain. It seems probable, however, that the experiments can only be explained if there is some kind of exchange interaction between a neutron and a proton. The nature of this interaction may be different from what has been assumed above and it may perhaps not be necessary to conclude that either of the particles is complex. In this discussion the spins of the particles and the effects of any possible magnetic forces have not been considered These may ultimately prove to be significant in these interactions

The interaction between a neutron and a proton is of great importance in the theory of nuclear structure If we assume that the atomic nuclei are built up from protons and neutrons then the binding forces in a nucleus are the interactions proton-proton, neutron-neutron, and proton-neutron The interaction between two protons should be due to Coulomb forces (neglecting any magnetic forces) and it is clear, from the nature of the nuclear fields, that these forces play only a small part inside a nucleus, certainly in the case of the lighter nuclei The interaction between two neutrons is probably small in comparison with the others. Thus the interaction between a neutron and a proton is the most significant for the structure of a nucleus and governs its stability.

§ 6. *Disintegration by Neutrons* –The majority of the collisions of neutrons with atomic nuclei are elastic, but occasionally inelastic collisions occur. These were first observed by Feather when studying the collisions of neutrons with nitrogen with the aid of the expansion chamber. Collisions of any kind are, of course, rare, but in 2000 photographs Feather obtained about 100 examples of recoil tracks of nitrogen obviously due to elastic collisions, and about 30 examples of paired tracks of quite a different type These were ascribed to a disintegration of the nitrogen nucleus which has been struck by a neutron In about half the cases observed it appears that the neutron was captured and an α-particle emitted, the final nucleus being therefore the boron isotope of mass 11.

$$N^{14} + n^1 \rightarrow B^{11} + He^4.$$

This is, of course, the reverse of the process in which a neutron is emitted from boron under the bombardment of α-particles. The mechanism of the disintegration in the other cases is not yet clear. It seems probable that the neutron was not captured and that the ejected particle was a proton. If this view should prove correct, we have here the first example of a transmutation in which the bombarding particle is not captured

Examples of disintegrations of nitrogen by neutrons have also been obtained by Meitner and Philipp (*loc. cit.*), by Harkins, Gans and Newson,* and by Kurie †

Feather‡ has also observed paired tracks in oxygen, in about the same proportion to the normal tracks of recoiling oxygen atoms as in nitrogen. In all the collisions observed the neutron was captured and an α-particle emitted, forming a nucleus C^{13}

$$O^{16} + n^1 \rightarrow C^{13} + He^4.$$

This transmutation is of special interest, for the oxygen nucleus appears to withstand bombardment both by α-particles and by protons

He has also found a few examples of disintegration when neutrons were passed through an expansion chamber filled mainly with acetylene Some of these appear to be due to a small impurity of air and only two can be definitely ascribed to the disintegration of carbon. It is obvious from the results so far obtained that inelastic collisions are much less frequent in carbon than in nitrogen or oxygen This is, indeed, to be expected, for the transition

$$C^{12} + n^1 \rightarrow Be^9 + He^4$$

requires a large amount of energy, about $7\frac{1}{2} \times 10^6$ electron volts, and few of the neutrons from the source used by Feather (beryllium bombarded by α-particles of polonium) possess such an energy Further, if the views expressed above about the constitution of the Be^9 and C^{12} nuclei are correct the change from C^{12} to Be^9 would be extremely unlikely, for an α-particle in the C^{12} nucleus would have to expand from a condensed system to a looser one

These are at present the only known examples of disintegration by neutrons but it is possible that many other elements will be transmuted in this way

The energy relations in the disintegrations produced by neutrons present some interesting features The disintegration $B^{11} + He^4 \rightarrow N^{14} + n^1$ takes place with an absorption of kinetic energy of $1 \cdot 4 \times 10^6$ electron volts. We should therefore expect the reverse process to take place with a liberation of energy of this amount. Feather showed that the measurements of 12 examples of this process corresponded in 10 to an absorption of energy, and that the energy change was not always the same This suggests that the disintegration takes place usually with the formation of an excited nucleus of B^{11}, the residual energy being emitted in the form of γ radiation To account for the different energy changes one must suppose that more than one excited state of B^{11} is possible Similarly, the analysis of the oxygen disintegrations leads to the conclusion that nuclei of C^{13} in different states of excitation may be formed

---

* 'Phys Rev,' vol 43, p. 208 (1933).

† 'Phys Rev,' vol. 43, p. 771 (1933).

‡ 'Nature,' vol 130, p 237 (1932)

In many disintegrations with the emission of protons the reaction takes place usually with the formation of an excited nucleus, but there is no evidence for more than one excited state * It must be pointed out that the calculated energy changes in the neutron disintegrations are subject to errors arising partly in the actual measurements of the tracks and partly in their interpretation ; while it seems certain that the residual nucleus is generally formed in an excited state the evidence for several excited states requires confirmation

§ 7 *Production of Positive Electrons* —As I have mentioned in § 3, the radiation excited in beryllium by the bombardment of α-particles consists not only of neutrons but also of a very penetrating γ-radiation, and it is sometimes difficult to decide whether the phenomena observed in experiments in which the beryllium radiation is used are to be ascribed to the neutrons or the γ-rays The most interesting example of this kind is the production of positive electrons, particles of the same mass as an electron but carrying a positive charge. The first evidence for the existence of positive electrons was given by the experiments of Anderson† and of Blackett and Occhialini‡ on the effects produced in an expansion chamber by the penetrating radiation of the atmosphere It seemed highly desirable to find some way of producing positive electrons by more ordinary means so that the evidence could be clinched and the properties of the particles studied Certain observations led Blackett, Occhialini and myself§ to consider the possibility that positive electrons might be produced in the interaction of the beryllium radiations and matter.

A capsule containing a polonium source and a piece of beryllium was placed outside an expansion chamber close to the wall. On the inside of the wall a target of lead, 2·5 cm square and 2 mm. thick, was placed. This target was thus exposed to the γ-rays and neutrons liberated from the beryllium Expansion photographs were taken by a stereoscopic pair of cameras. A magnetic field, usually of about 800 gauss, was applied during the expansion , any electrons liberated from the target would be bent in the field, the sense of the curvature indicating the sign of their charge and the amount of the curvature the Hρ value Of the electron tracks observed from the target about 200 were clearly due to negative electrons, but about 70 tracks showed a curvature in the opposite sense. There was a remote possibility that these tracks were due to negative electrons ejected in distant parts of the chamber and bent by the magnetic field so as to end on the lead target A statistical examination of all the tracks observed in the chamber was strongly in favour of the view that the tracks were due to positive electrons Definite proof was obtained in the following way A metal plate was placed across the expansion chamber so as to intercept the path of the particles, and some photographs were obtained in which a positively curved track passed through the plate, remaining in good focus throughout its path. The curvature of the track was less on the target side of the plate than on the further side, showing definitely that the particle travelled from the target and therefore carried a positive charge. In one case, the track had a curvature on the target side of the plate, a sheet of copper 0 25 mm thick, corresponding to a value of Hρ = 12,700, on the other side the curvature gave a value Hρ = 10,000, in another case, in which the plate was a sheet of aluminium 0 33 mm thick, the corresponding values of Hρ were 5000 and 4000.

---

* *Note added in proof* —Recent experiments on the disintegration of aluminium by α-particles give evidence of two excited states of the residual nucleus

† 'Science,' vol 76, p 238 (1932)

‡ 'Proc. Roy. Soc ,' A, vol. 139, p 699 (1933).

§ Chadwick, Blackett and Occhialini, 'Nature,' vol. 131, p. 473 (1933)

The observations of the ionizing power in the gas and loss of energy in the metal plates are consistent with the assumption that the mass and magnitude of the charge of the positive particle are the same as for the negative electron

Similar observations have been made by Meitner and Philipp* and by Curie and Joliot.† Some results of the latter workers suggest that the production of the positive electrons is, at least mainly, to be ascribed to the γ-radiation from beryllium and not the neutrons

That a γ-radiation can produce positive electrons has been shown in further experiments‡ we have made, in which the beryllium source was replaced by a very weak source of thorium active deposit, enclosed in a lead block, 1 cm. thick. In these experiments the lead target was bombarded by γ-radiation alone, the strongest component in the radiation being a ray of $h\nu = 2 \cdot 62 \times 10^6$ electron volts. Expansion photographs were taken as before, with a metal plate across the chamber to indicate the direction of the particles. Among about 1200 tracks of negative electrons, about 50 tracks due to positive electrons have been observed. These must certainly be ascribed to the action of a γ-radiation, very probably to the strong γ-ray of $h\nu = 2\cdot62\times10^6$ electron volts The ratio of positive to negative electrons is much lower than that observed with the beryllium radiations On the hypothesis, first suggested by Blackett and Occhialini, that a negative and a positive electron may be created simultaneously in some interaction of a γ-ray and the electric field of an atomic nucleus, it is not unlikely that the effect will increase very rapidly with the energy of the γ-ray, as the above observations suggest The creation of the two electrons will require an energy of $1\cdot02\times10^6$ electron volts, so that the energy of a positive electron produced by the γ-ray of $h\nu = 2\cdot62\times10^6$ electron volts should never be greater than $1\cdot60\times10^6$ electron volts.

---

* 'Naturwiss.,' vol 21, p. 286 (1933).

† 'C R Acad Sci. Paris,' vol. 196, p. 1105 (1933).

‡ Also in experiments by Anderson, 'Science,' vol. 77, p. 432 (1933)

The measurements of the energy distribution of the positive electrons are in agreement with this hypothesis of their origin, and in a few cases, both with the thorium active deposit and with the beryllium source, a negative track appeared to be associated with the positive The evidence, however, is not yet sufficient to decide how the positive electrons are produced.

Some observations have been made using a source of boron exposed to polonium α-particles. The target was thus bombarded by the neutrons liberated in the disintegration of B^{11} and by the γ-radiation accompanying the proton emission from B^{10}. The energy of this γ-radiation is rather less than 3×10^6 electron volts, so that the ratio of the number of positive to the number of negative electrons should have been of the same order as found in the experiments with thorium active deposit, *i.e.*, 1 to 25 Actually the fraction of positive electrons was much higher than this, but the total number of electrons observed in the experiments was small It seems likely that positive electrons can be produced not only by the action of γ-rays but also by neutrons, but more information is required before a definite decision can be made.

Absorption Spectra of Burning Hydrocarbons

By A. Egerton, F R S. and L. M Pidgeon, Clarendon Laboratory, Oxford.

(Received March 24, 1933—Revised June 7, 1933)

[Plate 1]

There is much yet to learn about the manner in which various hydrocarbons burn

The methods employed to gain information on the subject up to the present have been chiefly chemical, for instance, the estimation of the amount of products formed at different temperatures.

It was hoped that a different method might divulge new facts The idea was to pass a beam of ultra-violet light along a tube through which a mixture of combustible gas was passed at such temperatures that combustion was just commencing, and to observe by a spectrograph the changes in the absorption of the light Although for the combustion of hydrocarbons there is an essential difficulty, because the products of initial stages of the reaction are likely to be masked by the accumulation of the end products, yet certain interesting facts have been discovered, which it is the purpose of this communication to record The experiments are of a preliminary character designed to test in what directions the method can yield useful information about combustion

Experimental Details

Ultra-violet light from a large and powerful water-cooled hydrogen source, giving a continuous spectrum, was directed through quartz windows along a pyrex tube (1 m. long by 7 mm), and photographed with a quartz prism spectrograph (Hilger E 31) A mixture of hydrocarbon vapour and air (or nitrogen, etc) was passed through the tube. The rate and proportion of air and vapour were controlled by flow meters. In the case of liquid hydrocarbons, the vapour was obtained from the liquid in a glass vaporizer immersed in a bath at a definite temperature, the tube between the vaporizer and the long tube was kept warm by an electrically heated coil of wire to prevent condensation.

The long tube was maintained at an approximately uniform temperature throughout its length by surrounding it with a well lagged, electrically heated, copper tube furnace, provided with thermocouples in three positions along the length of the tube The lines in the spectrum of the light from a quartz mercury lamp served to establish the position of the absorption bands on the plate Little attempt was made to employ high dispersion, or photometric methods, as the method was used rather as a qualitative test than as a means of studying the nature of the band spectra obtained An exposure of 2 minutes was found to be sufficient, and was adhered to throughout most of the work Various tests showed that the thermal reactions were not appreciably altered by the photochemical effects of the light absorbed

Arrangement of Results

The hydrocarbon vapours of the paraffin series themselves do not absorb in the ultra-violet regions of greater wave-length than about λ 2000, and their absorption does not therefore interfere with that found for the products of combustion which mainly consists in general absorption beyond about λ 2300, and absorption bands in the region λ 2800–3580 The general absorption beyond 2300 will be alluded to as "extinction" in what follows

There is no object in giving in detail the results of 500 or more different exposures taken under a variety of conditions, therefore only a summary will be attempted.

It is first necessary to describe the nature of the absorption for those individual substances which may be formed during the combustion of a hydrocarbon, or which are of interest in studying that process —this is done in § A § B will indicate the character of the absorption due to the combustion of different hydrocarbons under various conditions § C will give further details of the investigation of the origin of the "extinction," and § D results of other special tests

§ A *Absorption by Various Vapours*

During the combustion of a hydrocarbon, alcohols, aldehydes, acids, unsaturated hydrocarbons, peroxides, etc, may be formed, the absorption of the vapour of some of these types of compound were therefore noted first in nitrogen, and then in presence of air in the heated tube.*

---

* *Cf* Purvis, 'J Chem Soc,' 1909–1915

Absorption by Aldehyde Vapours (The aldehydes from Kahlbaum or B D H, redistilled, and purity tested by boiling point.) The aldehydes—valeraldehyde, butyraldehyde, propionaldehyde or acetaldehyde—showed hardly any extinction at the far end of the spectrum when introduced along with air, the furnace being cold, or even with nitrogen when heated. Strong absorption occurs in the region λ 2600–3300 (maximum about 2900), consisting of a number of very hazy bands, about five heads of bands are usually distinctly visible

Acetaldehyde vapour exhibited a somewhat different absorption spectrum with numerous bands The concentration of the aldehyde must not be more than about 2%, otherwise only a continuous absorption is visible in the region 2850–3500, which extends in either direction as the concentration increases.

In pure nitrogen the temperature could be taken far above the temperature at which combustion would commence in air, without the "extinction," or change in the hazy bands, becoming noticeable—for instance, when propionaldehyde was heated in nitrogen to 425° C, the only appreciable difference was that the bands became more diffuse

On the other hand, when a trace of oxygen was present, or when the aldehyde was introduced along with air, combustion occurred, and the heads of the bands became sharpened. The series of bands obtained was identifiable with those of formaldehyde vapour,* but extinction also occurred at the far end of the spectrum. For instance, in the case of valeraldehyde there was slight extinction, and no formaldehyde bands were visible at 230° C, but considerable extinction and formaldehyde bands at 290° C, when combustion was more rapid, fig. 6, Plate 1.†

On passing the vapour of 40% formaldehyde solution along with air through the tube at 200° C, no extinction occurred, but faint bands characteristic of formaldehyde made their appearance † Even with high concentration of formaldehyde in nitrogen, though the bands in the region λ 2800-3200 were very strong, extinction (λ 2050) even at 310° C was hardly detectable, and there was no difference between the spectra in air or in nitrogen at this temperature, fig. 4, Plate 1.

Since the character of the absorption is similar in the case of all the higher aldehydes, presumably the hazy banded absorption is due to the electronic behaviour in reference to the —CHO group.

---

* Henri and Schou, 'Z. Physik,' vol 49, p. 774 (1928)

† The reproduction of this photograph does not show up the effect, which is quite distinct on the original plates.

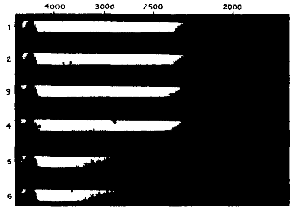

Fig 1 Combustion of butane and air showing induction period of 18′ (1-4) formaldehyde bands and absorption at 2600 (5) and disappearance of the latter (6)

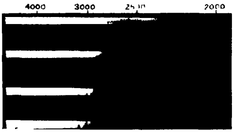

Fig 2 – Combustion of pentane and air

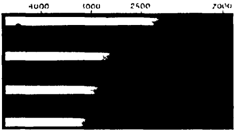

Fig 3 —Absorption of diethylperoxide

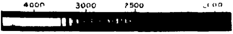

Fig 4 – Absorption of formaldehyde vapour

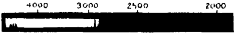

Fig 5 —Combustion of butane in oxygen

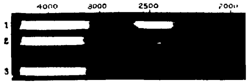

Fig 6 Absorption by valeraldehyde in N_2 (1 and 2) and its combustion in air (3)

The main point about the behaviour of these aldehydes, however, is that the "extinction" mentioned on p 28 is not dependent on the unchanged aldehyde molecule, but is connected with the process of combustion which is responsible for the formaldehyde bands

Alcohols.—Neither ethyl alcohol nor isobutyl alcohol vapour alone or with nitrogen, showed any appreciable absorption in the region investigated; even at 360° C., a 2% isobutyl alcohol-air mixture did not exhibit any extinction or bands Higher concentrations of alcohol, and higher temperatures, were needed before absorption was observed, under which conditions both extinction and the formaldehyde bands were obtained owing to the alcohol undergoing oxidation.

Acids —The vapours of the fatty acids absorb strongly, and cause "extinction" in the ultra-violet A 3% formic acid-air mixture at 310° C caused "extinction" to λ 2200, but the edge has a fine banded structure extending to λ 2500

Acetic acid-air mixtures gave no such bands, but only "extinction" Even at 1·5% concentration, no difference in the extent of extinction (to λ 2200) was noticed up to 400° C At 17% concentration extinction extended to λ 2500 The edge of the band was diffuse. The extinction for propionic acid at 11% concentration in air similarly extended up to about λ 2400.

The extinction due to 0·06% of butyric acid was barely perceptible, but at 0·6% quite definite (to λ 2100) No other bands became visible even in air at 363° C.

This "extinction" must be due to the —COOH group, it was not appreciably affected by temperature The acids mainly provide CO, CO_2 and water when further oxidation occurs (Ethyl acetate and other similar esters were found to absorb in accordance with the concentration of the acidic portion of the molecules.)

Peroxides. Diethyl peroxide $(C_2H_5)_2O_2$ *and ethyl hydrogen peroxide* $(C_2H_5O_2H)$ were prepared by methods described by Baeyer and Villiger,* and by Rieche† from hydrogen peroxide and diethyl sulphate. Lederle and Rieche have investigated the absorption of these peroxides in solution in hexane. The diethyl peroxide boiled at 62°–63° C at 740 mm. It has a very low flash point, but is comparatively stable The monoethyl peroxide boiled at 93°–97°, and inflamed quietly with a non-luminous flame When the vapour was passed along with nitrogen into the tube (at 19° C), extinction to the region λ 2900 occurred for high concentration (50%) and down to λ 2400 for lower concentration (about 10%), the extinction was not sharp, and was like that given by the fatty acids, fig. 3, Plate 1 When ethyl hydrogen peroxide was introduced into the tube at 83° C, extinction occurred up to λ 2800 depending on the concentration There were no other bands, in fact for both peroxides the results were much the same

---

* 'Ber deuts chem. Ges,' vol. 34, p 739 (1901)

† 'Ber. deuts chem Ges,' vol. 62, p. 218 (1929)

It is also probable that peracetic acid, and other similar peroxides obtained by the action of oxygen on aldehydes, absorb in the same region as the acids, and therefore there is no direct evidence of their formation obtainable from the extinction shown in the absorption spectra of the aldehyde-air mixtures

Ether readily gives a peroxide, and during slow combustion, evidence of its formation might be obtained At 426° C in nitrogen, ether vapour in fairly high concentration gave very little evidence of any absorption (extinction only to λ 2000) In the presence of air, extinction commenced at 187° C, but no aldehyde bands appeared till 200° C (air flow 45 c c. min) At 230° C aldehydes and peroxides were produced in profusion, extinction occurred from λ 2250 Formaldehyde bands became strong with fairly intense general absorption in the region of these bands at λ 2900 (probably due to acetaldehyde) It was noted that the extinction did not extend to more than λ 2250, even though the absorption due to the formaldehyde bands increased, so that the proportion of acid formed was unexpectedly small

Amongst the few classes of substances investigated which are likely to occur during hydrocarbon combustion, it is possible to distinguish by the nature of the absorption spectra, acids, aldehydes, and some higher unsaturated compounds, but the other substances cannot be directly identified, and it is necessary to deduce what is happening from a variety of different observations.

§ B. *Combustion of Hydrocarbons*

When hydrocarbon vapours are passed through the heated tube along with air, the first noticeable effect on the spectrum of the light from the hydrogen source is slight "extinction" of the far ultra-violet, then as combustion proceeds, the formaldehyde bands make their appearance, and the extinction increases In the case of the higher hydrocarbons (beyond and including butane), another band with a maximum about λ 2600 is distinctly visible during the early stages of combustion

The following notes, referring to the combustion of certain hydrocarbons, illustrate some of the observations made —

(*a*) *Propane,** 36% mixture in air at a rate of flow 70 c c. per minute gave practically no extinction up to 426° C. in spite of aldehyde being detectable (by Schiff's reagent). From 444° C. upwards, the extinction became marked, and then the formaldehyde bands made their appearance, and became pronounced at 484° C No continuous absorption occurred in the λ 2600 region·

(*b*) *Butane,** 43% in air, at a rate of flow 115 c c per minute (which implies 20 seconds exposure at 360° C. in the heated zone of the tube) just visibly gave rise to the formaldehyde bands The extinction (< λ 2300) was detected before the bands in the region λ 3000 became visible Halving the rate of flow caused the bands to stand out strong, and the extinction became marked At double the rate of flow neither the extinction nor the bands were visible On lowering the temperature to 340° C at 50 c c per minute the bands almost disappeared Continuous absorption occurred at λ 2600 when the formaldehyde bands became visible This absorption was particularly noticeable in the experiments with butane in an atmosphere enriched with oxygen (30%), the resulting absorption at 360° C was the same for a rate corresponding to the exposure of the gas mixture for 15 seconds in the heated tube as for 45 seconds when air instead of oxygen was used, fig. 5, Plate 1

(*c*). *N pentane,* 50% in air, at a rate of flow 45 c.c per minute at 275° C. seemed to show some extinction, and at 300° C. gave detectable aldehyde formation, but no formaldehyde bands were visible, there was slight continuous absorption in the region 2550–2750 At 317° C. this continuous absorption was very marked, and although only a comparatively small amount of aldehyde was noticed, the extinction extended from λ 2250 into the far ultra-violet. The extinction was complete to λ 2900 at 330° C, and the photograph showed strong formaldehyde bands, fig. 2, Plate 1.

(*d*) *Hexane* (boiling point 68°–69° C.), 14% in air, was passed through the tube at 352° C., very strong formaldehyde absorption bands and extinction were observed. At 324° C., and double the rate of flow, the absorption was only slight There was slight extinction observed, but no aldehyde bands visible, to as low a temperature as 259° C.

(*e*) A sample of *heptane* (kindly supplied by the Air Ministry Laboratory, S. Kensington) under similar circumstances at 283° C. burnt to give formaldehyde bands, but the extinction was very great, no light being transmitted beyond λ 3000 This extinction was found to be due to a small quantity of unsaturated impurity which was removed by treatment with fuming sulphuric acid. At 300° the purified heptane gave slight extinction, and a pronounced general absorption in the region λ 2600, like other higher hydrocarbons (A condensation product was formed during the heptane combustion which deposited on the windows of the tube, and gave rise to a series of sharp narrow bands at about λ 2600, 2530, 2470, 2420, 2350.) In all these cases the hydrocarbon itself showed no absorption at the temperatures mentioned when passed through the tube along with nitrogen at the same concentrations, so that none of the absorption effects recorded can be directly ascribed to dissociation products of the hydrocarbon

---

* Boiling point determinations showed that the gases kindly supplied by The Asiatic Petroleum Company were of satisfactory purity.

(*f*) The effect of *temperature* on a mixture of butane and air is illustrated by the following experiment A 45% mixture was let into the long tube at 351° C., and retained there, 2-second exposures being taken at ½-minute intervals. The products showed the extinction after 1 minute, together with faint formaldehyde bands At the end of 4 minutes, the absorption was fully developed, and was apparently unchanged after a further 10 minutes heating. For another charge let in at 334° C. both the extinction and the band became visible after 2½ minutes, and increased till 7 minutes, when no further change was noticeable up to 20 minutes. Similarly at 324° C. no absorption was visible for 13 minutes, then the extinction became just appreciable, followed by the bands, which became clearly marked after 20 minutes. The period of the induction increased as the temperature decreased The actual temperatures are of no great significance, as the surface of the tube would also influence the temperature at which combustion would commence to accelerate

Comparing all these observations with those in the previous § A, it is clear that the extinction could be connected with the production of acids or peroxides, or of both, and the bands with the formation of aldehydes (particularly formaldehyde),* but the absorption at λ 2600 for the higher hydrocarbons cannot be associated with any of the compounds in § A.

The experiments illustrating the effect of temperature, and influence of the rate of flow show that it takes an appreciable time to accumulate sufficient products of combustion to cause appreciable absorption of the light in the 1 metre length of column of gas It is improbable, therefore, that the initial unstable molecules taking part in the reaction chain process, would be present in sufficient quantity to show up, as once a chain is started, the final products are formed almost immediately For this reason, it was probable that the extinction, although the first effect to be observed, was due to the final acid residues of the combustion Nevertheless, it was thought that it might be possible to detect whether the extinction for the hydrocarbon combustion was greater than could be ascribed to the amount of acids produced, for if so, then the presence of other substances, such as peroxides stabilized from the reaction chain mechanism, might be established

---

* Whether these aldehyde bands are entirely due to the formaldehyde formed or whether the same vibrations can be set up in molecules of higher aldehydes undergoing combustion is a point which has not yet been settled experimentally, but it is perhaps worth noting that although other aldehydes are formed during the combustion of the higher hydrocarbons that there is no evidence of any absorption in this region until the formaldehyde bands make their appearance. Formaldehyde being a final product is no doubt in preponderance.

The next section deals with experiments attempting to elucidate such points

§ C *Origin of the " Extinction "*

A series of comparisons, taken on the same plate, of the absorption given by butane mixtures, and that afforded by butyraldehyde mixtures was made to test whether for the same intensity of formaldehyde bands, the same extinction occurred in both cases, for if the extinction were greater for butane, then it might be surmised that some product giving rise to extinction (such as peroxide) was formed during the hydrocarbon combustion before the production of aldehyde

A mixture of butane (45%) and air at 360° C gave the same absorption as a 2% butyraldehyde-air mixture passed through the tube at the same temperature and rate of flow When the intensity of the formaldehyde bands were similar, the quantity of aldehyde as measured by the bisulphite method was found to be approximately the same In several comparisons, when the intensity of the formaldehyde bands was the same for the hydrocarbon as for the aldehyde, the extinction was slightly greater for the hydrocarbon combustion, but the difference was not sufficiently marked to draw any definite conclusions The extinction was therefore certainly *mainly* due to the acid formed in proportion to the formaldehyde produced Similar comparisons were also made for pentane and valeraldehyde

In order to investigate the point further, the next series of experiments was made to determine the amount of absorption provided by the products of combustion of the hydrocarbon, compared with that of about 0 1% of acid under similar circumstances The tube was provided with heaters at the inlet and outlet to prevent condensation of acid Between each exposure titrations were made, the gases being bubbled through weak alkali solution, which was afterwards titrated back with N/100 acid, using various indicators :—

No.	Air, c.c. per min.	Butane, c.c. per min.	Butyric acid (estimate of concentration from vapour pressure).	Butyric acid from titration
			%	%
1	110	—	—	—
2	135		(0·26)	0·16
3	135	—	(0·13)	0·09
4	135		—	—
5	85	49		0·12
6	165	49	—	0·04
7	170	—	—	—

The amount of extinction given by 0·16% butyric acid (No. 2) was similar to that of 0·08% acid from the butane (between Nos. 5 and 6).

No.	Air, c.c. per min.	Butane, c.c. per min.	Butyric acid (estimate of concentration from vapour pressure)	Butyric acid from titration
			%	%
1	110	—		—
2	85	49	—	0·08
3	85	49	—	0·07
4	85		—	—
5	110	—	(0·15)	0·12

In this case 0·12% butyric acid (No. 5) seemed to give about the same extinction as 0·08% acid from the butane (No. 2).

It was necessary, however, to take into consideration the amount of CO_2 formed during the butane combustion, as this might be assumed to be derived from the breakdown of acid. Tests were carried out both by using phenolphthalein and methyl red as indicators, and also by direct determination of the CO_2 percentage in a Haldane apparatus. The outcome was to show that the percentage of CO_2 was about 0·1%. If this was all derived from acids—which could take part in the absorption—the combustion of the butane should give greater "extinction" than the butyric acid, for the same amount of organic acid found by titration. If the extinction for the hydrocarbon combustion was *more* than would be given by about double the concentration of the corresponding acid (as estimated by titration using methyl red) in the products obtained during the combustion of the hydrocarbon, then there would be evidence of some product being present, which was responsible for the absorption, over and above that due to the acid

The following is an example of some experiments made to test if this was so or not —

No	Air, c c per min	Butane, c c per min	Acid, etc	Organic acid %	Total % of organic acid + CO_2	Time of contact secs	Remarks
1	85	—			—	27	—
2	85	50		0 03	0 06	17	Slight extinction
3	120	50	—	—	0 008	11	-
4	110		Butyric (0 18%) at 28° C	0 06	0 08	21	Same extinction as for 2
5	110		Acetic (0 52%) at 0° C	—	0 6	21	Considerable extinction.
6	110		Acetic (0 16%) at −13° C	0 06 0 07	0 07 0 09	21	Extinction observed between that for Nos 3 and 4
7	110	—	Butyraldehyde (0 40%) at − 20° C	0 05	0 08	21	
8	110					21	-

The result of these tests was that butane appeared to give slightly greater extinction than the acid for the same total acid concentration, *i e*, including that which might have given rise to the carbon dioxide, but any difference obtained was too small to be convincing The combustion of the butyraldehyde also gave slightly more extinction, in comparison with that given by acetic acid vapour, than corresponded to the acid produced.

Thus aldehyde, and the hydrocarbon too, apparently gave an extinction slightly more than the quantity of acid formed from them would indicate This was the conclusion obtained from these tests, but it is not satisfactory to attempt to gauge accurately the extent of the extinction without using spectrophotometric methods

Similar experiments were also made using hexane and caproic acid, but the results did not provide any further positive support for the supposition that something besides acid was necessary to account for the extinction

The result of these tests has been to show that the extinction can be almost entirely ascribed to the acid produced during combustion, and that if there may be an intermediate product (*e g*, peroxide, etc.) formed on the way to the final stage, that its additional effect on the absorption is too small to be verified. As already explained, the accumulation of the final products would tend to mask any effect of earlier formed products. Furthermore, this spectroscopic test, though convenient, is not sensitive and the more transient products may not be present in sufficient quantity at any given moment to cause appreciable absorption.

Although the alcohols do not exhibit absorption, it is of interest to compare the absorption of the products of their combustion with that of the corresponding hydrocarbons The products which give rise to absorption were not generated to the same extent from alcohols as from the corresponding hydrocarbons exposed to the same temperature

N butyl alcohol does not itself absorb appreciably above λ 2000 At 426° C a 30% n butyl alcohol and air mixture, only gave slight extinction, and faint aldehyde bands, at 130° C the extinction extended to λ 2300, and the aldehyde bands were rather less marked than for butane-air mixtures at 360° C On cooling from 450° C. the formaldehyde bands were still visible at as low a temperature as 380° C, it is probable, therefore, that the products of reaction tend to assist the initiation of the combustion of the mixtures But even with a mixture over 50% butyl alcohol and air (when the extinction extended to λ 2700 and strong formaldehyde bands were visible at 380° C.) the bands at 370° C were very faint compared with those of a butane-air mixture at 360° C and the extinction, though detectable at 360° C, was not nearly so strong as with butane at a similar temperature, neither was the amount of aldehyde formed so great

These experiments indicate that the alcohol corresponding to a given higher hydrocarbon, such as butane, under the same conditions of combustion is not so readily oxidized, and if its formation is an initial step in the combustion of the hydrocarbon, it must owe its more rapid oxidation to activation by chemical reaction rather than to thermal exchange

It is interesting, however, that butyl alcohol gives rise during oxidation to strong absorption in the region λ 2550–2750 as in the case of butane. The aldehydes do not exhibit this absorption.

This other absorption band which only shows up during the combustion of hydrocarbons and alcohols, inclusive of and superior to butane in the series, will be referred to at the end of the next section, which describes certain other special experiments.

§ D. *Various other Experiments*

Another possibility was worth exploring, viz, to test whether an inhibitor could be found which would stop down the later reactions, and allow the initial reactions to proceed. Of all the antiknocks tried (see below), lead tetraethyl was the only one found which did not absorb in the ultra-violet. However, even lead tetraethyl in the presence of a trace of air absorbed strongly, giving an absorption somewhat similar to the peroxide absorption. 0·1% lead tetraethyl added to a butane air mixture stopped down the formation of acid, and prevented the production of aldehyde even when the temperature was taken 60° above that which gave strong aldehyde bands without the lead tetraethyl. But the lead tetraethyl itself absorbed as far as the region λ 2400 under these conditions, in fact, the extinction was much the same with lead tetraethyl at all temperatures, even in nitrogen.* For lead tetraethyl in butane alone there was no extinction, showing that the extinction was due to the oxidation of the lead tetraethyl. Owing to this absorption, lead tetraethyl cannot be used to trace out the initial stages of the reaction. It is interesting that the effect of the lead tetraethyl persisted in the tube for some time (10 minutes) after its introduction (for no aldehydes could be detected in the products by Schiff's reagent). This indicates that part of the effect of the lead is at the surface of the tube.

[Iron carbonyl cut off the whole of the ultra-violet region to λ 4000, butyl iodide to λ 3000, aniline to λ 3100, the latter at quite low concentration entirely prevented the oxidation of butane up to 420° C.]

A final series of experiments was made on the slow combustion of butane air mixtures by linking up the apparatus used by Pidgeon and Egerton† with the long tube used for these experiments, instead of the reaction bulb described in that paper. The connection was effected by a ground glass joint, a contact point to tell the height of the mercury was fitted, as in the previous work. Mixtures of butane and air could be made, and run into the long tube in its furnace, and by listening to the make of the contact from time to time, and measuring the height of the mercury in the manometer column, the pressure change during the oxidation could be determined. Spectrographs taken at regular intervals recorded the change in absorption of the mixture during its slow combustion.

The first plate showed that reaction occurred almost at once on letting in the butane air 50% mixture (the tube being at too high a temperature). The aldehyde bands are at first hardly visible, but the general absorption at λ 2600 was marked, this disappeared after some minutes, the formaldehyde bands then got stronger, towards the end of the observations, however, they got weaker again, and gave rise to more general absorption Several photographs had to be taken to get the right conditions Another plate was exposed with the furnace set at 357° C, during an induction period of 18 minutes nothing was visible on the plate, but after 22 minutes, aldehyde bands and absorption at λ 2600 were visible, the latter then disappeared, and at 37 minutes only the bands remained, fig 1, Plate 1.

---

* The nitrogen was passed over heated copper, but was evidently not completely free of oxygen.

† 'J. Chem. Soc.,' p. 661 (1932).

Similar experiments were attempted at 337° C, using flat polished silica discs placed across the section of the tube at 5 cm intervals, and kept in position by short lengths of closely fitting glass tube, 11 in all, so that the light had to pass 22 surfaces on which products might accumulate during the induction period

The gas (a 1 1 mixture) reacting at the surface gave rise to extinction and formaldehyde bands almost at once, no induction period was obtained

With a 2 air 1 butane mixture at 338° C the bands became visible after half an hour, before then very little extinction occurred At 347° C gradual development of extinction and bands occurred, but no real induction period was obtained, and no absorption in the λ 2600 region. The final experiment with 10 discs gave much the same result, at 330° C, after 30 minutes, the aldehyde bands began to show, but there was no absorption in the λ 2600 region

The attempt here described to measure the absorption of any product that might be stored on the surface during the induction period could hardly be expected to reveal anything, because the layer would almost certainly be too thin to absorb appreciably.

It was interesting to note in the experiment without discs the sudden appearance of the absorption band at λ 2600 at the end of the induction period, and its subsequent disappearance. This band which appeared to be formed prior to the appearance of the formaldehyde bands is not obtained during the combustion of the aldehydes, and is connected, therefore, with the process of combustion of the hydrocarbons and the alcohols prior to the formation of the aldehydes. Since it only appears with the higher hydrocarbons, it is possibly connected with a process of ring formation.

The significance of this change in the character of combustion for the higher hydrocarbons will be dealt with in another communication, and now that the possibilities of the method have been explored, it is proposed to use it for studies of a more quantitative nature.

Our thanks are due to Mr S. Barratt, M A, for information regarding the construction of the hydrogen source, and to Mr A R Ubbelohde, B A, for useful criticism and help

Summary

(1) The character of the absorption spectra of various substances likely to be formed during the combustion of a hydrocarbon was investigated, and compared with the absorption spectra of various hydrocarbons undergoing slow combustion

(2) The absorption spectra of the hydrocarbons during combustion exhibit three characteristics, an absorption in the far ultra-violet, bands identified with those of formaldehyde, and in the case of the higher hydrocarbons, a band with a maximum at about λ 2600

The absorption in the far ultra-violet was proved to be due mainly to the formation of acids

(3) The absorption of peroxide compounds is in the region in which the acids absorb and it would not be possible to determine the extent to which peroxides or other substances which may be formed, take part in the absorption obtained during the hydrocarbon combustion without more elaborate methods of measurement than have been attempted in these preliminary experiments

(4) During the induction period, no absorption is visible For butane and the higher hydrocarbons the band at λ 2600 is the first to make appearance, and is followed by the aldehyde bands The corresponding aldehydes on combustion do not give this band

The Spectrum of H_2. *The Bands ending on* $2p\,^3\Pi$ *Levels.* *Part* III.

By O. W. Richardson, F.R.S., Yarrow Research Professor of the Royal Society, King's College, London, and P. M. Davidson, Ph.D., with an Appendix by Miss J. Marsden and W. M. Evans, University College, Swansea

(Received May 5, 1933.)

§ 1. *The Band Lines which go down to* $2p\,^3\Pi$ *from the* $4d^3$ *Complex*

This paper is an immediate continuation of Part II† which described the band systems whose lower levels were $2p\,^3\Pi_{ab}$ and whose upper levels were $3d\,^3\Sigma_g$, $3d\,^3\Pi_b$, $3d\,^3\Pi_a$, and $3s\,^3\Sigma_g$. In the present paper (Part III) we start by describing the band systems which end on $2p\,^3\Pi_{ab}$ and come from $4d\,^3\Sigma_g$, $4d\,^3\Pi_b$, $4d\,^3\Pi_a$ and $4d\,^3\Delta_b$. After that we consider the properties and constants of all the various levels $2p\,^3\Pi_{ab}$, $3d\,^3\Sigma_g$, $3d\,^3\Pi_b$, $3d\,^3\Pi_a$, $3d\,^3\Delta_b$, $3d\,^3\Delta_a$, $4d\,^3\Sigma_g$, $4d\,^3\Pi_b$, $4d\,^3\Pi_a$, and $4d\,^3\Delta_b$. Most of these constants are worked out from the Appendix, in which the energy levels and the intensities in the bands are shown to be in good agreement with the wave mechanics.

The lines going down to $2p\,^3\Pi$ from $4d\,^3\Sigma$, Π_b, Π_a, Δ_b, are set out in Tables I to IV. The 0—0 bands are to be understood as replacing the tentative lines which were included in Part I. In these tables the first column gives the designation P, Q, R of the line followed by the K value of the final level. Transitions between weak (*s*) levels are distinguished by dashes from those between strong (*a*) levels. The remaining columns give in turn Gale, Monk, and Lee's‡ wave numbers, Kapuscinski and Eymers's§ intensity measures, Gale, Monk and Lee's‡ and Finkelnburg's‖ eye estimates of intensity, response to high (H) or low (L) pressure as recorded by Merton and Barratt,¶ Zeeman effect according to Dufour** or Croze,†† comparison of intensity at room temperature and with the discharge tube immersed in liquid air by McLennan, Grayson-Smith and Collins,‡‡ the excitation potential of the final level of the line as determined by Finkelnburg, Lau, and Reichenheim[†] and the effect of admixture of helium (He) as observed by Merton and Barratt.[‡] An asterisk after the wave number denotes an interferometer measure of Gale, Monk, and Lee. A comparison of the intensities given by Gale, Monk, and Lee with those of Finkelnburg often gives a valuable confirmation of the correctness of the line, because in a given band the lines with higher K numbers tend to become relatively more intense in Finkelnburg as compared with Gale, Monk, and Lee, and those with lower K numbers tend in the opposite direction. This is due to the higher temperature of the sources used by Finkelnburg.

---

† 'Proc. Roy. Soc.,' A, vol. 140, p. 25 (1933).

‡ 'Astrophys. J.,' vol. 67, p. 89 (1928).

§ 'Proc. Roy. Soc.,' A, vol. 122, p. 58 (1928).

‖ 'Z. Physik,' vol. 52, p. 27 (1928).

¶ 'Phil. Trans.,' A, vol. 222, p. 369 (1922).

** 'Ann. Chim. Phys.,' vol. 9, p. 361 (1906); 'J. Phys. Rad.,' vol. 8, p. 259 (1909).

†† 'Ann. Physique,' vol. 1, p. 58 (1914).

‡‡ 'Proc. Roy. Soc.,' A, vol. 116, p. 277 (1927).

These bands are very like the corresponding ones which go down to $2p\,^3\Pi$ from the levels $3d\,^3\Sigma$, $3d\,^3\Pi_b$, $3d\,^3\Pi_a$, and $3d\,^3\Delta_b$. Apart from the fact that they lie about 5500 wave numbers higher, corresponding to the change in the quantum number of the initial states from 3 to 4, the most noticeable difference is the absence of the high pressure and condensed discharge enhancements. There are no lines enhanced in the condensed discharge in Tables I–IV and there are about as many H as L lines. However, a considerable proportion both of the H and the L lines are coincident with lines of other systems, so it seems fairly sure that the lines of the $4d\,^3\Sigma\Pi\Delta \rightarrow 2p\,^3\Pi$ systems are unresponsive to pressure changes.

In every case the strength is practically confined to the diagonal bands. The strongest are $0' \rightarrow 0''$ and $1' \rightarrow 1''$ with about equal strength, then $2' \rightarrow 2''$, and $3' \rightarrow 3''$ weakest. In each system the strong lines of the $0' \rightarrow 0''$ bands are recorded by Merton and Barratt (*loc. cit.*) as strongly enhanced by admixture of helium, just as in the bands which come from the $n = 3$ levels, and, as is the case with those bands also, the lines of the $1' \rightarrow 1''$, $2' \rightarrow 2''$, and $3' \rightarrow 3''$ bands do not possess this property. The incidence of the Zeeman effect is also almost the same as that in the bands coming from corresponding levels with $n = 3$. Thus in $4d\,^3\Sigma \rightarrow 2p\,^3\Pi$ all the strong lines respond to the Zeeman effect, in $4d\,^3\Pi_b \rightarrow 2p\,^3\Pi$ most of them do, although in one or two cases this may come from the lines being blended with lines belonging to $4d\,^3\Sigma \rightarrow 2p\,^3\Pi$. In $4d\,^3\Pi_a \rightarrow 2p\,^3\Pi$ there is a fair number of lines definitely known not to respond to the Zeeman effect whilst for those for which it has been recorded, in every instance, the data are affected by blends. The properties of $4d\,^3\Delta_b \rightarrow 2p\,^3\Pi$ are probably very similar to those of $4d\,^3\Pi_a \rightarrow 2p\,^3\Pi$ as regards the Zeeman effect but, since the lines of this system are weaker, the data are less numerous.

[†] 'Z. Physik,' vol. 61, p. 782 (1930).

[‡] 'Phil. Trans.,' A, vol. 222, p. 369 (1922).

Table I —$4d\,^3\Sigma \to 2p\,^3\Pi_{ab}$

The 0 → 0 *band*

		K	G				R T	L.A	V.	
R′ 1	22477 97†	66 7	9	(4)F		Z	38	39	11 75	He++
R2	22410 40*	90 0	10	(8)F		Z	39	38	11 75	He++
R′ 3	22343 81	24 4	6	(4)F	H+	Z	15½	10½	11 37	He+−
R4	22285 97		*ab*	(3)F						
R′ 5	22237 62		0	(2)F						
? R6	22198 42		00	(0)F						
Q1	22476 06†	28 3	6	(4)F		Z	38	39	11 75	He++
Q′ 2	22357 05		1	UF	L+					
Q3	22230 34	9 2	3	(3)F						
Q′ 4	22105 74	3 1	1	*ab* F or U						
Q5	21991 63		00	(1)F						
Q′ 6	21889 22		*ab*	(0)F						
Q7	[21797 78]		*ab*	*ab*F						
P′ 1	22525 32	4 5	3	(2)F			6½	5		He++
P2	22355 31	12 6	3	(3)F	H−		10½	10½		
P′ 3	[22177 14]		*ab*	*ab*F						
P4	[21992·65]		*ab*	*ab*F						
P′ 5	[21812 07]		*ab*	*ab*F						
P6	21644 05		*ab*	(0)F						
P′ 7	21508·40		*ab*	(00)F						

R′ 1 is also R′ 2 of 1 → 1 $4d\,^3\Pi_a \to 2p\,^3\Pi$
Q′ 2 is also P3 of 0 → 0 $4d\,^3\Pi_b \to 2p\,^3\Pi$

R′ 3 is also R3 of 2 → 3 $3d\,^1\Pi_a \to 2p\,^1\Sigma$ and P′ 5 of 0 → 0 $4d\,^3\Pi_a \to 2p\,^3\Pi$
Q′ 4 is also R2 of 1 → 1 $4p\,^3\Pi \to 2s\,^3\Sigma$

P2 is also R3 of $3\,^1K \to 2p\,^1\Sigma$, 1′ → 1″

The 1 → 1 *band*

		K	G				R T	L.A	V.	
R′ 1	22286 17		2	(3)F						
R2	22225·34*	61 4	10	(5)F		Z	51	47	11 86	
R′ 3	22162 31	14 7	5	(3)F	H++					
R4	22097 47	27 1	7	(5)F	H++	Z	21	16	11 84	He0
Q1	22284·92	41 0	8	(3)F		Z	26	29	11 98	
Q′ 2	22171·16	3 6	2	(1)F			4½	6		
Q3	22054·01‡	*ca* 18	5U	*ab* or UF			24*a*	19*a*		
Q′ 4	21936·14	32	5	(3)F	L++		18½	14		
Q5	21817·66	..	00*a*	(0/1)F						

P′1	22335 79	0	*ab*F
P2	[22169 78]	*ab*	*ab*F
P′3 ?	21999 45	*ab*	(0)F
P4	[21827·10]	*ab*	*ab*F
P′5	[21655 75]	*ab*	*ab*F
P6	[21485 87]	*ab*	*ab*F

R2 is also R1 of 2 → 2 $4d\,^3\Pi_b \to 2p\,^3\Pi$ R4 is also P4 of 2 → 3 $3d\,^1\Pi_a \to 2p\,^1\Sigma$ Q′2 is also Q′5 of 1 → 1 $4d\,^3\Pi_b \to 2p\,^3\Pi$

Q′4 is also Q2 of 1 → 1 $4p\,^3\Pi \to 2s\,^3\Sigma$ Q5 is also R′2 of 3 → 3 $4d\,^3\Pi_b \to 2p\,^3\Pi$

	The 2 → 2 band								*The 3 → 3 band*	K.	G		*Non-diagonal lines*
R′1	22079 72		2	(1)F			6	8	21853 10		0	(00)F	1→ 0 Q3 = 24378 70 (0)F
R2	22024 35	8 2	5	(2)F	H++	Z	15	14½	21803 61	2 0	1	(1)F	1→ 0 Q5 = ’24116 66 (00)F
R′3	21963 56	17 6	3	(3)F	L+								2 → 1 P4 = 23837 59 (0*a*) *ab*F
R4	21896 92	21 1	3	2(F)			4	5					3→ 2 R2 = 23896 38 (0)F, (*r*)T
													3→ 2 P4 = ? 23516 94 (0)F
Q1	22073 37	7 6	5	(2)F			12	12½	21843 55	6 6	1*h*	(0)F	
Q′2	21970 34		1	(0)F					21749 20		0	UF	
Q3	21861 44		0	*ab*F or U					21648 95		0	(0)F	
Q′4	21748 69		0*a*	UF									
Q5	21631 16		*ab*	(0)F									
P′1	22114 63		1	(0)F					absent or ’21876 81		0	*ab*F	
P2	21963 56	17 6	3	(3)F	L+				[21739 06]		*ab*	*ab*F	
P′3	[21806 67]		interference						[21593 39]		*ab*	*ab* or UF	
P4	[21645 12]		*ab*	*ab* or < 0 F					[27442 91]		*ab*	*ab*F	
P′5	[21481 15]		*ab*	*ab*F									
P6	[21314 65]		*ab*	*ab*F									

R′1 is also P′4 of 1 → 1, $4d\,^3\Pi_b \to 2p\,^3\Pi$ R4 is also R1 of 0 → 1, $^1M \to 2p\ \Sigma$ Q1 is also R1 of 1 → 4, $^1X \to 2p\,^1\Sigma$

R′3, P2 is also R2 of 2 → 3, $3d\,^1\Sigma \to 2p\,^1\Sigma$ Q′4 is also P3 of 1 → 1, $4p\,^3\Pi \to 2s\,^3\Sigma$ Q1 is also Q1 of 3 → 3, $4d\,^3\Pi_a \to 2p\,^3\Pi$

---

† Properties are for both lines ‡ Properties are for a blend.

Table II —$4d\,{}^3\Pi_b \rightarrow 2p\,{}^3\Pi_{ab}$

The 0 → 0 *band*

		K.	G				R.T.	L.A.	V	
R1	22657·81*	86 0	8	(7)F		Z	35	30	11 74	He++
R′2	22643 75	21 5	3	*ab*F		Z				He− +
R3	22631 71	47 0	5	(6)F		Z	22	14	11 71	He−+
R′4	22619·03	6 4	1	(2)F						
R5	22604 65†		1	(3)F		? Z				? He++
Q′1	22622 48		0	(0)F						
Q2	22537 10	4 6	1	(1)F						He++
Q′3	22463 85	3 2	0	(1)F						
Q4	22394 07†	8 6	2	(2)F			8	5½		He++
Q′5	22325·17		*ab*	(1)F						
Q6	22256 87		0*a*	(2)F						
P′2	22501 71	9 4	2	(2)F	L+					
P3	22357·05		1	(U)F	L+					
P′4	[22225 84]		*ab*		*ab*F					
P5	22099 97		*ab*	(0)F						
P′6	21976 78		*ab*	(00)F						

R3 is also Q4 of 3 → 4, $3d\,{}^1\Pi_b \rightarrow 2p\,{}^1\Sigma$
P3 is also Q′2 of 0 → 0, $4d\,{}^3\Sigma \rightarrow 2p\,{}^3\Pi$
R5 is also R′1 of 1 → 1, $4d\,{}^3\Pi_a \rightarrow 2p\,{}^3\Pi$.

The 1 → 1 *band.*

R1	22489 64	72 1	7	(4)F		Z	23	22	11 71
R′2	22477·97	66·7	9	(6)F		Z	38	39	11 75
R3	22466 06	28 9	6	(4)F	H+		14½	10	
R′4	22451 67	13 9	3	(2)F					
R5	22436 59	8 8	2	(1)F					
R′6	? 22420 99	20·0	3	UF					

The 2 → 2 *band.*

	K.	G			R.T	L.A.	V.
22225 34*	61 4	10	(5)F	Z	51	47	11 86
22219·94		00	(0)F				
22218 21	8 6	2	(3)F				
22213 99		*ab*	(00)F				
22208 13	3 7	1	(3)F				

Q′1	[22448·26]		*ab*	*ab*F						[22179 91]		*ab*	*ab*F
Q2	[22374 50]		*ab*	*ab*F						22115 51		0	(1)F
Q′3	[22306·34]		*ab*	*ab*F						22056 15		*ab*	(0)F
Q4	22239 17		1	(2)F						[22001 89]		*ab*	*ab*F
Q′5	22171·16	3 6	2	(1)F			4½	6		[21946 45]		*ab*	*ab*F
Q6	22103·87		1	(0)F						21891 54		*ab*	(0)F
Q′7	?22040·16	11 4	2*h*	(2)F									
P′2	22333 24	6·7	1	(0/1)F						22070 50		0	(2)F
P3	22203 18		2	(2)F						21952 80		1*h*	(0)F
P′4	22079 80		2	(1)F	*d*(0)	MB	6	8		21841 25	3 2	1	(1)F
P5	21959 22		*ab*	(2)F						21736 08		*ab*	(0)F
P′6	[21840—]		*ab*	*ab*F						21632 10		*ab*	(00)F
P7	[21723 3–]		*ab*	*ab*F						[21530 0]		*ab*	*ab*F

R′2 is also R′1 of 0 → 0, $4d\,^3\Sigma \rightarrow 2p\,^3\Pi$
Q′5 is also Q′2 of 1 → 1, $4d\,^3\Sigma \rightarrow 2p\,^3\Pi$
R1 is also R2 of 2 → 2, $4d\,^3\Pi_a \rightarrow 2p\,^3\Pi$
? R′6 is also R′1 of 2 → 2, $4d\,^3\Pi_a \rightarrow 2p\,^3\Pi$
? Q′7 is also R2 of 0 → 0, $3d\,^1\Pi_a \rightarrow 2p\,^1\Sigma$

P′2 is also R1 of 0 → 2 $^1\mathrm{N} \rightarrow 2p\,^1\Sigma$
P′4 is also R′1 of 2 → 2, $4d\,^3\Sigma \rightarrow 2p\,^3\Pi$

R1 is coincident with R2 of 1 → 1, $4d\,^3\Sigma \rightarrow 2p\,^3\Pi$ which requires most of the strength
P′4 is also R2 of 6 → 0, $3p\,^3\Sigma \rightarrow 2s\,^3\Sigma$
R3 is also P5 of 1 → 1, $4d\,^3\Pi_b \rightarrow 2p\,^3\Pi$
R5 is also R′1 of 3 → 3, $4d\,^3\Pi_a \rightarrow 2p\,^3\Pi$

The 3 → 3 *band.*

R1	21820·60	13 4	4	(8)F	H++	Z	He++
R′2	21817 58		0*a*	(0/1)F			
R3	21813 48		0	(0)F			
Q′1	21771·28		0	*ab*F			
Q2	21716·11		*ab*	(0)F			
Q′3	21661·76		*ab*	(0)F			
Q4	21607 34	4·1	0*h*	(1)F			
P′2	21667 31		*ab*	(00)F			
P3	21561 33		*ab*	(0)F			
P′4	? 21457·81		*ab*	(0)F			
P5	21355·39	10·6	2	(3)F			

R′2 is also Q5 of 1 → 1, $4d\,^3\Sigma \rightarrow 2p\,^3\Pi$
P5 is also P6 of 1 → 2, $3d\,^1\Pi_a \rightarrow 2p\,^1\Sigma$

---

† Properties affected by blends

Table III —$4d\,^3\Pi_a \rightarrow 2p\,^3\Pi_{ab}$

	The 0 → 0 band	K G		RT	LA	V		*The 1 → 1 band*	K G		RT	LA	V	
R′1	22777 41	13 6 3 (2)F		9	7		He−−	22604 65†	1 (3)F	Z				He++
R2	22827 77	20 3 4 (4)F	Z=0	11	7½	11 78	He++	22666 05†	11 6 3h (3)F		10	4½		
R′3	22875 37†	2 0 0 (1)F		4	2½		He+−	[22725 05]	ab abF					
R4	22919 17	2 8 0a (2)F					He−	22778 47	4 3 1 (0/1)F					
R′5	22956 97	ab (0)F												
R6	’22984 62	ab (00)F												
Q1	22666 21†	11 6 3h (3)F		10	4½			22481 73	3 0 0 (1)F					
Q′2	22656 61†	10 6 2 (3)F	Z	35	30		He−+	22489 66	72 1 7 (4)F	Z	23	22	11 71	
Q3	22647 73	33 3 4 (5)F	Z=0	26	16		He++	22494 88	< 18 9 3 (3)F					
Q′4	22637 46	ca 5 2 (3)F					He+	22498 68	1 8 0h (0)F					
Q5	22624 96	7 5 1 (3)F					He−+	22498 80	1 8 0h (0)F					
Q′6	22608 47	ab (00)F												
P2	22545·28	5 3 1 (1)F		8½	5			[22366 57]	ab abF					
P′3	[22476 70]	ab abF						[22318 03]	ab abF					
P4	22410 04	U or U or ab ab F						22267 82	0 abF					
P′5	22343 79†	«24 4 6 (4)F H+	Z	15½	10½		He+−	22218 21	8 6 2 (3)F					
P6	[22277 29]	ab abF						22167 05	ab (0)F (r)D					
P′7	[22227 61]	ab abF												

Q′4 is also Q4 of 1 → 1, $3d\,^1\Pi_b \rightarrow 2p\,^1\Sigma$
Q1 is also R2 of te 1 → 1 band
P′5 is also R′2 of 0 → 0, $4d\,^3\Sigma \rightarrow 2p\,^3\Pi$ and R3 of 2 → 2, $3d\,^1\Pi_a \rightarrow 2p\,^1\Sigma$
The line has enough intensity for all three
R′1 is also R5 of 0 → 0, $4d\,^3\Pi_b \rightarrow 2p\,^3\Pi$

Q′2 is also R2 of the 2 → 2 band and R1 of 1 → 1, $4d\,^3\Pi_b \rightarrow 2p\,^3\Pi$
It seems strong enough for all three
R2 is also Q1 of the 0 → 0 band.
Q3 is also R5 of 0 → 2, $^1\mathrm{N} \rightarrow 2p\,^1\Sigma$ where it is probably too strong
R4 is also P7 of $^1\mathrm{N} \rightarrow 2p\,^1\Sigma$ where it is too strong
P′5 is also R3 of 2 → 2, $4d\,^3\Pi_b \rightarrow 2p\,^3\Pi$

The 2→ 2 band

		K	G				R.T	L.A.	V	
R′1	22420 99‡	13 0	3	(4U)F		Z	15½	10		He+
R2	22489 66‡	72 1	7	(4)F		Z	23	22	11 71	
R′3	22555 03	6 7	1h	(1)F						
R4	22616 53‡	*ca.*10	4	(3)F	L++					
Q1	22293 62		00	*ab*F						
Q′2	22311 59		00	(1)F						
Q3	22326 85		*ab*	(00)F						
Q′4	[22340 01]		*ab*	*ab*F						
Q5	[22350 78]		*ab*	*ab*F						
P2	22183 74		00	*ab*F						
P′3	22147 91	«9 3	3	(1)F						
P4	22110 43‡	‹20	3	(00)F	L+		10½	8		
P′5	22072 56‡	«12 4	2	(2)F			12	12½		
P6	?22034 53		*ab*	(0)F						

R′1 is also ? R′6 of 1 → 1, $4d\,^3\Pi_b \rightarrow 2p\,^3\Pi$

R2 is also Q′2 of the 1 → 1 band and R1 of 1 → 1, $4d\,^3\Pi_b \rightarrow 2p\,^3\Pi$ which requires most of the strength

R4 is also P5 of 1 → 1, $3d\,^1\Pi_a \rightarrow 2p\,^1\Sigma$, for which it is too strong

P′3 is also R1 of 4 → 4, $3d\,^1\Sigma \rightarrow 2p\,^1\Sigma$ and Q5 of $3d\,^1\Delta_b \rightarrow 2p\,^1\Sigma$

P4 is also Q5 of 2 → 3, $3d\,^1\Pi_b \rightarrow 2p\,^1\Sigma$, which requires most of it

The 3→ 3 band

		K.	G			R.T	L.A.
R′1	22208 13	3 7	1	(3)F			
R2	22287 71		0	(1)F			
R′3	22367 39	2 2	0	(0)F			
R4	22440 29		0	(0)F			
Q1	22073 35	7 4	5	(2)F		12	12½
Q′2	22104 18		?*ab*	*yab*F			
Q3	[22133 02]		*ab*	?*ab*F			
Q′4	[22163 07]		*ab*	*ab*F			
Q5	22188 23	34 2	6	(6)F	Z=0	15	8½
P2	?21969 00		*ab*	(00)F			
P′3	21948 45		*ab*	(0)F			
P4	21927 12		*ab*	(0,1)F			
P′5	21909 00		*ab*	(0)F			
P6	Interval unknown						

P′5 is also Q4 of 2 → 3, $3d\,^1\Pi_b \rightarrow 2p\,^1\Sigma$

R′3 is also P5 of 3 → 4, $3d\,^1\Pi_a \rightarrow 2p\,^1\Sigma$

Q1 is also ? Q1 of 0 → 4, $4d\,^1\Pi_b \rightarrow 2p\,^1\Sigma$

Q1 is also Q1 of 2 → 2, $4d\,^3\Sigma \rightarrow 2p\,^3\Pi$

R′1 is also ? R5 of 2 → 2, $4d\,^3\Pi_b \rightarrow 2p\,^3\Pi$

---

† Properties influenced by blends

‡ Properties affected by blends.

Table IV —$4d\,^3\Delta_b \rightarrow 2p\,^3\Pi_{ab}$

	The 0 → 0 band										The 1 → 1 band									
							R.T	L.A	V								R.T	L.A.	V	
R1	22888 79	6 8	1	(2)F			4	3		He⊤	22716 63†	3 3	3	*ab* or UF	L+⊤		13½	9½		He+
R′2	23004 64		*ab*	(0)F	(*r*)T						[22828 28]		*ab*	*ab*F						
R3	[23110 54]		*ab*	*ab*F							[22926 33]		*ab*	*ab*F						
Q2	22768 00	22 5	4	(4)F		Z=0	14½	9	11 93	He+⊤	22601 50†	21 1	3	(3)F			15	14		
Q′3	22824 69	3 5	1	(1)F							22656 63†	10 6	2	(3)F		Z	35	30		He++
Q4	22872 87	5 5	2	(3)F			4	2½		He+⊤	22699 42	6 7	1	(0)F						
P3	22587 98	15 2	2	(3)F			12	8½		He∔+	22430 19·	9 0	3	(2)F						
P′4	22586 89		0	(1)F			12	8½		He⊤+	22430 19·	9 0	3	(2)F						
P5	22578 51	6 3	0*h*	(3)F							22419 69		2	*ab*F						

Q′3 is also Q′2 of 0′ → 0″, $3d\,^3\Pi_a \rightarrow 2p\,^3\Pi$

Q4 is also P4 of 0′ → 0″, $3\,^1O \rightarrow 2p\,^1\Sigma$.

P5 is also R2 of 0′ → 0′, $3p\,^3\Pi \rightarrow 2s\,^3\Sigma$

	The 2 → 2 band										The 3 → 3 band									
R1	22541 71†	8 7	2	(2)F						He⊤	22361 47	3 7	1	(0)F						
R′2	22651 41	12 8	2	(3)F						He+⊥	[22460 65]		*ab*	*ab*						
R3	[22735 41]		*ab*	*ab*							[22526 29]		*ab*	*ab*						
Q2	22432 12†	26 4	3	(4)F		Z=0	24	21		He0	22256 87		0*a*	(2)F						
Q′3	22487 68		1	(0)F							22304 85†		1	(0)F	H⊤−		10	6½		He+⊤
Q4	22519 11	2 9	1	(1)F							22320 24	11 0	3	(2)F	L+−		6½	7		
P3	22269 39	5 9	1	(2)F							22102·12†	14 3	2	(2)F	L−	Z				
P′4	22272 69	3 9	1	(3)F							22100 76		0	*ab*F						
P5	22253 41		0	(00)F							22068 24		*ab*	(0)F						

Q′3 is also R2 of 1 → 1, $3d\,^1\Sigma \rightarrow 2p\,^1\Sigma$

R1 is also R2 of 1 → 1, $3\,^1K \rightarrow 2p\,^1\Sigma$

Q2 is also Q6 of 0 → 0, $3d\,^3\Pi \rightarrow 2p\,^3\Pi$

---

† Properties affected by blends

The excitation potentials of a good many of the lines have been determined by Finkelnburg, Lau, and Reichenheim.† The values for the final levels, given under V in the tables, do not agree so well with the theoretical values as do those got from the band systems which go down to $2p\,^3\Pi$ from levels with $n = 3$. However, according to our interpretation of them, an unusually high proportion of the stronger lines of those systems are blends Perhaps this is not surprising as the bands are all very close together and much interwoven. They are also embedded in the bands of $3p\,^3\Pi \rightarrow 2s\,^3\Sigma$ and $4p\,^3\Sigma \rightarrow 2s\,^3\Sigma$ as well as in the bands of a large number of strong systems which go down to $2p\,^1\Sigma$. In any event it is satisfactory to note that in $4d\,^3\Sigma \rightarrow 2p\,^3\Pi$ the only two really strong lines which are not believed to be blends, or for which the excitation potential data are free from suspicion of ambiguity, namely, R2 of the $0' \rightarrow 0''$ band and Q1 of the $1' \rightarrow 1''$ band have measured excitation potentials of the final levels of 11·75 and 11·98 volts respectively and these values are in agreement with the theoretical values to within the accuracy of the excitation potential measurements. When allowance is made for the probable influence of the blended constituents in the case of the remaining band lines for which excitation potential measurements are available it is doubtful if any of them differ from the theoretical values by more than the possible experimental error, which is rather considerable in these measurements

The effect of an admixture of helium on the lines of these systems is almost identical with the corresponding effect in the $3d\,^3\Sigma\Pi\Delta \rightarrow 2p\,^3\Pi$ systems All the strong lines in the $0' \rightarrow 0''$ bands of $4d\,^3\Sigma \rightarrow 2p\,^3\Pi$, $4d\,^3\Pi_b \rightarrow 2p\,^3\Pi$, $4d\,^3\Pi_a \rightarrow 2p\,^3\Pi$ and $4d\,^3\Delta_b \rightarrow 2p\,^3\Pi$, as well as some rather weak ones, are recorded by Merton and Barratt as enhanced by helium On the other hand in the $1' \rightarrow 1''$, $2' \rightarrow 2''$ and $3' \rightarrow 3''$ bands of all these systems, as well as in the non-diagonal bands, for which up to the present only a few lines have been found, there is only a single line which is recorded without ambiguity as enhanced by helium. There is also one line, R4 of the $1' \rightarrow 1''$ band of $4d\,^3\Sigma \rightarrow 2p\,^3\Pi$, which is definitely recorded as unaffected by admixture of helium. It seems clear, therefore, that the strong helium enhancement is confined to the $0' \rightarrow 0''$ band of each system

Considering the systems as a whole, the strongest are $4d\,^3\Sigma \rightarrow 2p\,^3\Pi$ and $4d\,^3\Pi_b \rightarrow 2p\,^3\Pi$, with not much to choose between them. $4d\,^3\Pi_a \rightarrow 2p\,^3\Pi$ is much weaker than these and is a little stronger than $4d\,^3\Delta_b \rightarrow 2p\,^3\Pi$. We have not been able to find $4d\,^3\Delta_a \rightarrow 2p\,^3\Pi$ which is presumably very weak in some respect. It is probable on theoretical grounds that this band has no detectable

† 'Z. Physik,' vol. 61, p. 782 (1930).

strength except in the P branches. This would account for the difficulty of detecting it, which does not necessarily imply that there are no lines of any strength in the system. This distribution of intensity among the bands as a whole is quite different from that in $3d\,{}^3\Sigma\Pi\Delta \rightarrow 2p\,{}^3\Pi$ where $3d\,{}^3\Delta_b \rightarrow 2p\,{}^3\Pi$ is the strongest system. It is similar to that in $4d\,{}^1\Sigma\Pi\Delta \rightarrow 2p\,{}^1\Pi$ and has considerable resemblance to that in $3d\,{}^1\Sigma\Pi\Delta \rightarrow 2p\,{}^1\Sigma$. The resemblance to the intensity distribution in $4d\,{}^1\Sigma\Pi\Delta \rightarrow 2p\,{}^1\Pi$ is not unreasonable since, as we saw in Part II, that of $3d\,{}^3\Sigma\Pi\Delta \rightarrow 2p\,{}^3\Pi$ was quite like that of $3d\,{}^1\Sigma\Pi\Delta \rightarrow 2p\,{}^1\Pi$.

In $4d\,{}^3\Sigma \rightarrow 2p\,{}^3\Pi$ the R branch is strong, the Q branch moderately strong and the P branch weak. In $4d\,{}^3\Pi_b \rightarrow 2p\,{}^3\Pi$ the R branch is strong and the Q and P branches both weak. In $4d\,{}^3\Pi_a \rightarrow 2p\,{}^3\Pi$ the R and Q branches are each of moderate intensity and the P branches weak. In $4d\,{}^3\Delta_b \rightarrow 2p\,{}^3\Pi$ the Q branch is moderately strong, the P branch is similar in intensity to the Q branch but a little weaker, and the R branch is much weaker than either and is, in fact, quite weak These are rough statements intended to give a general idea of the intensity distribution in the bands. In reality the intensity of the lines of a given branch varies considerably with K These peculiarities of intensity distribution are accounted for quantitatively so far as the $0 \rightarrow 0$ bands are concerned, as well as the $0 \rightarrow 0$ and $1 \rightarrow 1$ bands of the $3d\,{}^3\Sigma\Pi\Delta \rightarrow 2p\,{}^3\Pi$ systems, by the theoretical calculations in the Appendix.

We are inclined to consider the $2 \rightarrow 2$ and $3 \rightarrow 3$ bands of $4d\,{}^3\Pi_{ab} \rightarrow 2p\,{}^3\Pi_{ab}$ as less secure than the others and in all the bands with v' (or v'') > 1 there are lines involving transitions between weak (s) levels which it is difficult to be certain of.

§ 2. *The Vibrational Intervals.*

The additional data furnished by the $4d\,{}^3\Sigma\Pi\Delta \rightarrow 2p\,{}^3\Pi$ systems enable the final vibrational intervals given in Table VII of Part II to be extended somewhat. The values we now find for these intervals are given in Table V. Where

Table V.—Final Vibrational Intervals of $2p\,{}^3\Pi_{ab}$.

State.	Vibrational interval.	K = 1.	K = 2.	K = 3.	K = 4	K = 5.	K = 6.	K = 7.
$2p\,{}^3\Pi_b$	1—0		2333·26		2313·71		2283·31	
	2—1		2311·40		2192·35		2163·04	
	3—2		2092·75		2074·32			
$2p\,{}^3\Pi_a$ ...	1—0	2338·84		2324·54		2299·21		
	2—1	2216·77		2202·90		2178·36		2144·2
	3—2	2098·04		2084·61		2060·63		

these differ from the corresponding values in Part II the present ones are believed to be the more accurate.

The mean values of the initial vibrational intervals $\Delta v'$ (K) calculated from the final intervals in the preceding table and equations of the type

$$\Delta v'(\mathrm{K}) = \Delta v''(\mathrm{K}+1) + \mathrm{P}(\mathrm{K}+1)(v+1 \rightarrow \overline{v+1}) - \mathrm{P}(\mathrm{K}+1)(v \rightarrow v)$$

are set out in Table VI. As only the values for the strong a levels are known the successive values of K jump by 2 in each band, just as they did for the final intervals and for the same reason. If we compare these intervals with the corresponding intervals of the $3d\,^3\Sigma\Pi\Delta$ complex (Part II, Table VIII) the greatest similarity is at the Δ level, as is to be expected. The value of the lowest interval at $1' \rightarrow 0'$ for both $4d\,^3\Sigma$, $4d\,^3\Pi_b$ and $4d\,^3\Pi_a$ is much closer to that for H_2+, the end of the series $nd\,^3\Sigma$, Π, Δ, than is that for the corresponding interval of $3d\,^3\Sigma$, $3d\,^3\Pi_b$ and $3d\,^3\Pi_a$. This also is very reasonable.

Table VI.—Vibrational Intervals of $4d\,^3\Sigma$, $4d\,^3\Pi_b$, $4d\,^3\Pi_a$ *and* $4d\,^3\Delta_b$.

Level ↓	Δv ↓	K = 1	K = 2	K = 3	K = 4	K = 5	K = 6
$4d\,^3\Sigma$	From→	P2, Q1		P4, Q3, R2		P6, Q5, R4	
	1′—0	2147·71$_8$		2148·19		2125·14	
	2′—1′	2005 20		2010 37		1991 83	
	3′—2′	1868 23$_5$		1872 10			
$4d\,^3\Pi_b$	From→		P3, Q2, R1		Q4, R3		Q6, R5
	1′—0′		2170·663		2158·85		2130·1$_4$
	From→		P3, Q2, R1		P5, Q4, R3		P7, Q6, R5
	2′—1′		1952 47		1955 07		1950·90$_8$
	3′—2′		1693·3$_6$		1679·8$_8$		
$4d\,^3\Pi_a$	From→	P2, Q1		P4, Q3, R2		P6, Q5, R4	
	1′—0′	2154 4$_5$		2171 54		2173 03$_6$	
	2′—1′	2028·61		2034·95		2030·37$_3$	
	From→	P2, Q1		P4, Q3, R2		Q5, R4	
	3′—2′	1877·8$_9$		1890 9$_6$		1898 1$_6$	
$4d\,^3\Delta_b$	From→		P3, Q2		P5, Q4		
	1′—0′		2166·75$_5$		2140 32		
	2′—1′		2042·06		2012 06		
	3′—2′		1917·4		1875 47		

Note—When the last digit is depressed it means that the correct value is thought to lie within ± 5 units in the last decimal place

There is a very close resemblance between the distribution of intensity in the present band systems and those of the corresponding singlet systems $4d\,^1\Sigma\Pi\Delta \rightarrow 2p\,^1\Pi$. We should, moreover, expect a close resemblance between the vibrational intervals of $4d\,^3\Sigma\Pi\Delta$ and of $4d\,^1\Sigma\Pi\Delta$. The data for testing this question are very meagre. The $4d\,^1\Sigma\Pi\Delta$ levels are only known at the lowest vibrational interval $v = 0$, except in the case of $4d\,^1\Pi_b$, where $v = 1$ is known in addition. The 1 — 0 intervals of $4d\,^1\Pi_b$ are 2164·18 at K = 2 and 2155·40 at K = 4. The corresponding intervals of $4d\,^3\Pi_b$ are 2170·66 and

2158 85 respectively. Thus in the only instances where it is possible to test the question the resemblance is very close, as was anticipated.

§ 3. *The Initial Rotational Levels.*

The intervals between these have been measured by the same method as was adopted in dealing with the $3d\,{}^3\Sigma\Pi\Delta$ levels. As was explained in Part II, owing to the rotational doubling of the final levels, it is only possible to determine these intervals to within $\pm x_m$, where x_m is the height of the lowest s level above the lowest a level at the final vibrational level $v'' = v' = m$ of the bands from which the data are extracted. If we imagine for a moment that the x_m's are zero, then in the lower state the intervals between all the a and b levels at a given v are known completely and hence the rotational intervals in any upper state can be immediately calculated from the bands, in the usual way This gives Table VII It is to be remembered that x_m is not usually zero, and hence that in each $4d\,{}^3$ diagram in Table VII the whole of the dotted (s) levels are to be raised relatively to the solid (a) levels by the x_v of the corresponding lower vibrational state. Thus using F (K) for the true level, and considering, for instance, $4d\,{}^3\Pi_b$, $v = 0$, the number 35·19 is really $\mathrm{F}(2) - \mathrm{F}(1) + x_0$, while 106·85 is really $\mathrm{F}(3) - \mathrm{F}(2) - x_0$, and so on.

The corresponding singlet bands are included in the table for comparison. The singlet level differences do not involve any uncertainty corresponding to the small quantity $\pm x_m$ which enters into the triplet data; because these intervals have been measured, in our papers on the singlet systems, with reference to the $2p\,{}^1\Sigma$ state where this duplicity does not occur and in which, owing to its great regularity, all the intervals can be computed with an accuracy which is probably great

Although there is much similarity between the structure of the rotational levels of $4d\,{}^3\Sigma\Pi\Delta$ and that of the corresponding levels of $4d\,{}^1\Sigma\Pi\Delta$ it is not so close as that between the rotational levels of $3d\,{}^3\Sigma\Pi\Delta$ and the corresponding levels of $3d\,{}^1\Sigma\Pi\Delta$. This was discussed in Part II where it was shown that the triplet $3d\,\Pi_b$ and $3d\,\Delta_b$ levels were almost indistinguishable from the corresponding singlet levels. It is true that there is a similar resemblance between $4d\,{}^3\Delta_b$ and $4d\,{}^1\Delta_b$ but the lowest K interval of $4d\,{}^3\Pi_b$, if genuine, differs appreciably from $4d\,{}^1\Pi_b$.

In $4d\,{}^3\Sigma$, as in $3d\,{}^3\Sigma$, $\rightarrow 2p\,{}^3\Pi$ the status of the P′ 1 lines is less secure than that of the others, since there are no combinations. The main justification for the lines chosen is that (1) they continue down to $\mathrm{K} = 0$ the rotational structure of the levels at higher K which are made secure by the combinations

Table VII —Rotational Structure of $4d\,{}^3\Sigma\Pi\Delta$ and $4d\,{}^1\Sigma\Pi\Delta$ Levels.

K ↓	$4d\,{}^3\Sigma$ $v = 0$		$4d\,{}^1\Sigma$ $v = 0$		$4d\,{}^3\Sigma$ $v = 1$		$4d\,{}^3\Sigma$ $v = 2$		$4d\,{}^3\Sigma$ $v = 3$		
7											a
	308 64		278·79								
6		→62 91		→53 91							s
	245·73		224 88								
5		→65·90		→54 74							a
	179 83		170 14		161 90		149 31				
4		→66·34		→56·21		→53 43		→46 82			s
	113 49		113·93		108 47		102 49				
3		→60 31		→51 63		→54 16		→48 09			a
	53 18		+62 30		54 31		54 40		55·00		
2		→51 27		→81 75		→53 06		→48 05		→45 45	s
	+1 91		−19 45		+1 25		+6 35		+9 55		
1		→51 17		→ 6 50		→52 12		→47 61		→42·81	a
	−49 26		−25 95		−50 87		−41 26		−33 28?		
0											s

	$4d\,{}^3\Pi_b$ $v = 0$		$4d\,{}^1\Pi_b$ $v = 0$		$4d\,{}^3\Pi_b$ $v = 1$		$4d\,{}^1\Pi_b$ $v = 1$		$4d\,{}^3\Pi_b$ $v = 2$		$4d\,{}^3\Pi_b$ $v = 3$		
7													s
					317?								
6						→53?							a
	279 40				264 03				260·71				
5		→54 12				→51 69				→49 37			s
	225 28		225 81		212 34				211 34				
4		→57 47		→55 22		→52 81				→49 94			a
	167·81		170 59		159 53		157 26		161 40		151 20		
3		→60 96		→63 78		→56 18		→54 58		→57·39		→50·25	s
	106·85		106 81		103 35		102 68		104 01		100 95		
2		→71 66 ?		→92 66		→62 97		→67 54		→58 58		→51 63	a
	? 35 19		14 15		41 38		35 14		45 43		49 32		
1													s

	$4d\,{}^3\Pi_a$ $v = 0$		$4d\,{}^1\Pi_a$† $v = 0$		$4d\,{}^3\Pi_a$ $v = 1$		$4d\,{}^3\Pi_a$ $v = 2$		$4d\,{}^3\Pi_a$ $v = 3$		
7											a
	375 5?										
6		→43 9?									s
	331·59										
5		→50 00									a
	281·59				280 19		277 53		278·12		
4		→54 05				→49 73		→48 94		→43 18	s
	227 54		225·12		230 46		228 59		234 94		
3		→56 41		→77 71		→53 90		→50·06		→50·94	a
	171·13		147 41		176 56		178 53		184 00		
2		→59·77 ?		→88 88		→53 64		→51·16		→49·23	s
	? 111 36		58 53		122 92		127·37		134 77		
1											a

	$4d\,{}^3\Delta_b$ $v = 0$		$4d\,{}^1\Delta_b$ $v = 0$		$4d\,{}^3\Delta_b$ $v = 1$		$4d\,{}^3\Delta_b$ $v = 2$		$4d\,{}^3\Delta_b$ $v = 3$		
4											a
	285·92		285 68		269·36		247 30		220 39		
3		→49 28		→49 18		→42 58		→28·22		→17 17	s
	236 64		236 50		226 78		219·08		203·22		
2											a

---

† The validity of this level will be discussed in a different paper.

and (2) their intensities look reasonable and change in the right way in Finkelnburg's tables as compared with Gale, Monk and Lee's. The P′ 1 line of the $0 \rightarrow 0$ band has the further security that it is an He ++ line, of which very few now are unclassified.

Admitting the correctness of these $4d\,{}^3\Sigma$ P′ 1 lines (all the facts known about them are favourable to this identification) we see that the $K = 0$ level is inverted at each vibrational level In this respect $4d\,{}^3\Sigma$ resembles $3d\,{}^1\Sigma$ more closely than it resembles either $4d\,{}^1\Sigma$ or $3d\,{}^3\Sigma$, assuming that the irregularly placed $K = 0$ level of $3d\,{}^1\Sigma$ at $v = 2$ is to be relied on As v increases from 0 to 3 the extent of the inversion of the $K = 0$ level of $4d\,{}^3\Sigma$ diminishes. This trend is the opposite of that in $3d\,{}^1\Sigma$ where the inversion increases in going from $v = 0$ to $v = 2$ (the $K = 0$ level at $v = 3$ is unknown) and is more like that in $3d\,{}^3\Sigma$ where the $K = 0$ level is inverted at $v = 0$ and $v = 1$ but not at $v = 2$ and $v = 3$ Among the four levels $4d\,{}^3\Sigma$, $4d\,{}^1\Sigma$, $3d\,{}^3\Sigma$ and $3d\,{}^1\Sigma$, $4d\,{}^1\Sigma$ is unique in having both the $K = 0$ and the $K = 1$ level inverted. However, in $4d\,{}^3\Sigma$ the interval between $K = 1$ and $K = 2$ is very small; so that the $K = 1$ level is almost inverted. $4d\,{}^1\Sigma$ is known only at the vibrational level $v = 0$. The uncoupling effects are very pronounced in $4d\,{}^3\Sigma$ as in $4d\,{}^1\Sigma$, $3d\,{}^3\Sigma$ and $3d\,{}^1\Sigma$. This seems quite certain as it holds good even if we disregard the $K = 0$ levels, which depend on the P′ 1 lines which are less secure than the others in the case of $4d\,{}^3\Sigma$ and $3d\,{}^3\Sigma$.

$4d\,{}^3\Pi_b$ resembles $4d\,{}^1\Pi_b$ more closely than it resembles either of the two levels $3d\,{}^3\Pi_b$ and $3d\,{}^1\Pi_b$ which are very much alike.

In $4d\,{}^3\Pi_a$ there are several doubtful elements in the bands with $v > 0$ The difference in structure between $4d\,{}^3\Pi_a$ and $4d\,{}^1\Pi_a$ at $v = 0$ is chiefly due (see Appendix) to the $K = 1$ level of $4d\,{}^3\Pi_a$ being a long way from its theoretical position. This experimental level is rather uncertain. In view of the possibility of alternatives for some of the more doubtful levels in $4d\,{}^3\Pi_a$ as we have arranged it the apparent difference of its rotational structure when compared with $4d\,{}^1\Pi_a$, may not be very significant. It is, however, not very unlike that of the $3d\,{}^{3,1}\Pi_a$ levels.

As has been mentioned $4d\,{}^3\Delta_b$ has a rotational structure practically identical with that of $4d\,{}^1\Delta_b$ at $v = 0$, the only vibrational level at which $4d\,{}^1\Delta_b$ is known. $4d\,{}^3\Delta_b$ is also a good deal like the almost interchangeable levels $3d\,{}^3\Delta_b$ and $3d\,{}^1\Delta_b$. The most striking difference here is the rapid closing up of the interval between $K = 4$ and $K = 3$ of $4d\,{}^3\Delta_b$ as v increases from 0 to 3. However, as the $K = 4$ level of $4d\,{}^3\Delta_b$ is not too secure at $v = 1$, 2 and 3, perhaps too much emphasis should not be laid on this feature.

§ 4. *Various Constants.*

Table VIII gives a number of constants The five energy levels Σ, Π_b, Π_a, Δ_b, Δ_a are associated with three unperturbed levels (or more strictly one should say that the Π's coincide in that approximation, and so do the Δ's). It is to these unperturbed states that the constants refer. Many of the numbers are calculated from data in the Appendix, in which, also, the notation is referred to. For Table VIII, it need only be added that W_m means the minimum of W'_b, the curve of energy for fixed nuclei (defined, for example, by equation (21), page 16 in Kronig's book†). At each Λ a Rydberg formula is

Table VIII

	$\Lambda = 0$	$\Lambda = 1$	$\Lambda = 2.$
$3d^3$, W_m, above $2p\,^3\Pi$, $K = 1$, $v = 0$ (wave numbers)	15500	15760	16185
$4d^3$, W_m, above $2p\,^3\Pi$, $K = 1$, $v = 0$ (wave numbers)	21175	21265	21460
$3d^3$, W_m, below W_m of H_2+ (wave numbers)	12775	12485	12090
$4d^3$, W_m, below W_m of H_2+ (wave numbers)	7106	6980	6815
$3d^3$, energy of dissociation (volts)	2·83	2·79	2·74
$4d^3$, energy of dissociation (volts)	2·79	2·77	2·75
$3d^3$, W_m, denominator of the Rydberg formula	2·930	2·964	3·012
$3d^3$, ω_0 (wave numbers)	2240	2260	2350
$4d^3$, ω_0 (wave numbers)	2270	2296	2305
Three values of $2p\,^3\Pi$, $K = 1$, $v = 0$ below W_m of H_2+ (wave numbers)	28275	28245	28275
Average value of $2p\,^3\Pi$, $K = 1$, $v = 0$ below W_m of H_2+ (wave numbers)		28265	
W_m of $2p\,^3\Pi$ (wave numbers) below W_m of H_2+ (wave numbers)		29625	
$2p\,^3\Pi$, energy of dissociation (volts)		3·03	
$3p\,^3\Pi$, W_m above $2s\,^3\Sigma$, $K = 1$, $v = 0$ (wave numbers)		15306	
$4p\,^3\Pi$, W_m above $2s\,^3\Sigma$, $K = 1$, $v = 0$ (wave numbers)		20970	
$3p\,^3\Pi$, W_m below W_m of H_2+ (wave numbers)		12765	
$4p\,^3\Pi$, W_m below W_m of H_2+ (wave numbers)		7095	
$3p\,^3\Pi$, denominator of the Rydberg formula		2·932	
$2s\,^3\Sigma$, $K = 1$, $v = 0$, below W_m of H_2+ (wave numbers)	28065		
$2s\,^3\Sigma$, W_m below W_m of H_2+ (wave numbers)	29530		
$2s\,^3\Sigma$, W_m energy of dissociation (volts)	3·018		

applied to the W_m's of the 3 and 4 electronic levels, in order to estimate their position relative to the W_m of the hydrogen molecular ion. The corresponding constants for the α, β bands are also calculated, in order to compare the positions of the $2p\,^3\Pi$ and $2s\,^3\Sigma$ levels. The $K = 1$, $v = 0$ level of $2p\,^3\Pi$ is found to lie about 200 wave numbers below $K = 1$, $v = 0$ of $2s\,^3\Sigma$ (and hence about 11·74 volts above the ground level of the molecule; this agrees with the excitation potentials measured by Finkelnburg, Lau and Reichenheim and with the old extrapolation‡ from the Rydberg-Ritz formula).

In all three unperturbed states, both of $3d^3$ and $4d^3$, B_0 lies close to 29 and α is about 2. The value of $x\omega_0$ is about 75. In the lower state, $2p\,^3\Pi$, the rotational levels are of simpler type. As in the upper states, the Π_b and Π_a levels are associated with unperturbed states in which they coincide. Here, however, the perturbations are small. In an "average" state, obtained by taking the average of the two levels at each K, it is found that B_0 is $31 \cdot 075$; α is $1 \cdot 47$, and D is $-0 \cdot 019$, ω_0 is $2467\frac{1}{2}$, and $x\omega_0$ is $63\frac{1}{2}$. These are in terms of the new mechanics, if they are to be compared with constants of other systems, worked out on the old mechanics, B_0 must be changed to $30 \cdot 335$, α to $1 \cdot 45$, ω_0 to 2404 and $x\omega_0$ to $62\frac{3}{4}$.

---

† "Band Spectra and Molecular Structure," Camb. Univ. Press (1930).

‡ O W. Richardson, 'Proc Roy Soc.,' A, vol 113, p 399 (1926).

In Table VIII, the energy of dissociation means the amount by which the minimum of the energy curve (for fixed nuclei) lies below its asymptotic value at infinite nuclear separation

It will be seen from the table that the application of the Rydberg formula to the W_m's of $3p\,{}^3\Pi$ and $4p\,{}^3\Pi$ gives $2 \cdot 932$ for the denominator in $2p\,{}^3\Pi$ (and, of course, $3 \cdot 932$ in $4p\,{}^3\Pi$). If the W_m of $2p\,{}^3\Pi$ had denominator $1 \cdot 932$ it would lie 29390 below the W_m of $H_2{}^+$. According to the table this number is 235 greater, being 29625, this value being got by applying Rydberg formulæ to the $3d^3$ and $4d^3$ levels The value 29625 corresponds to a denominator 1 924 The small disagreement is not surprising; a Rydberg formula can hardly be expected to hold accurately as far as the 2-electronic states.

As remarked above, the B_0 of $2p\,{}^3\Pi$ (on the old mechanics) is about $30 \cdot 335$, at $3p\,{}^3\Pi$, the upper level of the α-bands, it is about $29 \cdot 69$, at $4p\,{}^3\Pi$ about $29 \cdot 35$ and at $5p\,{}^3\Pi$ about $29 \cdot 28$ The limit of the series should be the rotational constant of the lowest vibrational level of the molecular ion H_{2+} This quantity computed from Burrau's data is about $29 \cdot 1$.

At $v = 0$ the coefficient of $(K + \frac{1}{2})^4$ proves to be in the immediate neighbourhood of $-0 \cdot 02$ in all the $np\,{}^3\Pi$ states This is in close agreement with the value computed from $\beta_0 = -4B_0{}^3/\omega_0{}^2$ in each case.

The values of the rotational constants, as well as all the other properties, of the final levels of these bands are in excellent accordance with what we should anticipate for the member $n = 2$ of the series $np\,{}^3\Pi_{ab}$ from the known properties of the members $n = 3$, 4, 5 and ∞.

Summary.

This paper is a continuation of Part II which described the band systems of H_2 coming from $3d\,{}^3\Sigma_g$, $3d\,{}^3\Pi_b$, $3d\,{}^3\Pi_a$ and $3s\,{}^3\Sigma_g$ and ending on $2p\,{}^3\Pi_{ab}$. It describes the band systems which end on $2p\,{}^3\Pi_{ab}$ and come from $4d\,{}^3\Sigma_g$, $4d\,{}^3\Pi_b$, $4d\,{}^3\Pi_a$ and $4d\,{}^3\Delta_b$. The properties and constants of all the various

levels $2p\,^3\Pi_{ab}$, $3d\,^3\Sigma_g$, $3d\,^3\Pi_b$, $3d\,^3\Pi_a$, $3d\,^3\Delta_b$, $3d\,^3\Delta_a$, $4d\,^3\Sigma_g$, $4d\,^3\Pi_b$, $4d\,^3\Pi_a$ and $4d\,^3\Delta_b$ are then considered. Most of the constants are worked out from the Appendix, in which the energy levels and the intensities in the bands are shown to be in good agreement with the wave mechanics.

APPENDIX.

The rotational levels, of the $3d^3$ and $4d^3$ states, are very similar to the corresponding singlet levels, and may be subjected to an exactly similar theoretical treatment So may the intensity distribution, except that in the present bands the application of the theory is more limited, owing to the absence of the $2p\,^3\Sigma$ state, which is unstable In what follows, the notation used for the singlets[†] is retained throughout the text, tables and diagrams.

At $v = 0$ of $3d^3$ and $4d^3$ (figs. 1 and 2) the levels marked simply $W_\Lambda{}^\circ$ are got by assuming a formula $W_\Lambda{}^\circ = C_\Lambda + 29\,(K + \frac{1}{2})^2 - 0{\cdot}02\,(K + \frac{1}{2})^4$ The Σ, Π, Δ levels marked "calc" are obtained from these $W_\Lambda{}^\circ$'s by the perturbation theory. It will be seen that they agree fairly well with the levels (marked "obs") derived from the bands[‡] This is especially true in the 4-electronic states. In the others the method called "calc. 2"[†] was also used, giving somewhat different values for the W°'s In the above expression for the W°'s the values of $C_{0,\,1,\,2}$, all measured above the $K = 1$, $v = 0$ level of $2p\,^3\Pi$ are 16860, 17058, 17352 at $v = 0$ of the $3d^3$ states, 16593, 16835, 17228 at $v = 1$ of the $3d^3$ states; and 22547, 22587, 22607 at $v = 0$ of the $4d^3$ states. The calculated and observed intensities are set out in Tables IX–XI.

In these tables K is the (rotational) quantum number of the initial state From each K there are in general three transitions ($K \rightarrow K$, $K \pm 1$) down to $2p\,^3\Pi$, giving rise to a Q, P and R line respectively As the relative populations of the initial states are unknown the theory is only to be applied to each separate group of three lines, P, Q and R, coming from a given initial state such as, for example, $3d\,^3\Delta_b$, $v = 0$, $K = 2$. In the three theoretical intensities kx^2 for each group a common factor has been employed which makes the strongest line of the group agree with Kapuscinski and Eymer's measure of the intensity.[§]

[†] Davidson, 'Proc. Roy. Soc.,' A, vol. 138, p. 580 (1932).

[‡] *In $v = 1$ of $3d^3$, for which a diagram is not given, the number 29 in the above* expression for $W_\Lambda{}^\circ$ must be replaced by about 27 to give the best agreement with the observed levels

[§] In the bands considered by Davidson the relative intensities in transitions to two lower electronic states were considered Since we have here only one, the quantity k reduces simply to v^4 multiplied by the factor mentioned

Their measurements are given under E whilst the numbers under G are Gale, Monk and Lee's eye estimates. Lines absent from the tables are indicated by *ab* or .., lines claimed as blends on theoretical grounds by †, observational blends by U. Lines marked *a*, *b*, *c* or *h* are also likely, on observational grounds, to be blends (*cf.* Gale, Monk and Lee, *loc. cit.*). ? means that some of the strength may be wanted elsewhere, but that is not certain The agreement with theory is quite good In particular, nearly all the lines which should be very weak are found to be so.

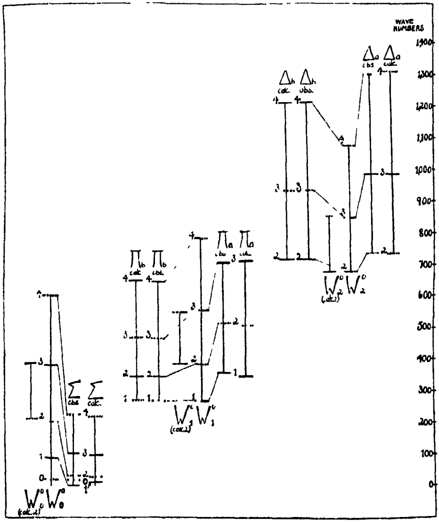

Fig. 1.—$3d\ {}^3\Sigma\Pi\Delta$ at $v = 0$.

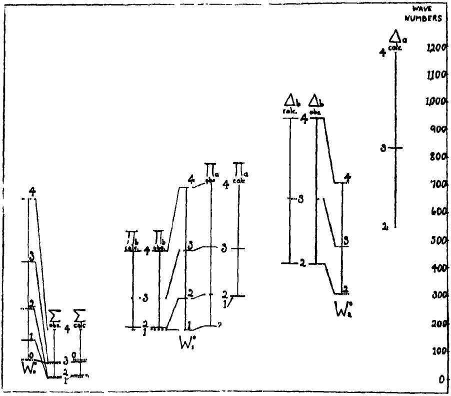

FIG. 2 —$4d\ ^3\Sigma\Pi\Delta$ at $v = 0$

In Fig. 2, the Π_b, K = 1, obs. level corresponds to lines which are alternatives to those in the text.

Table IX.—Intensities. 3-electronic states, $v = 0$.

		K = 1.				K = 2.				K = 3				K = 4			
		x^2.	kx^2.	E.	G	x^2	kx^2.	E.	G	x^2.	kx^2.	E.	G	x^2.	kx^2	E	G
$3d\,^3\Sigma$	P	0 125	2	11 0†	(4)†	0	0	*ab*	*ab*	0	0	*ab*	*ab*	0	0	*ab*	*ab*
$\rightarrow$	Q	2 07	*37·5*	37 5	(10)	1 14	*12*	12 0	(4)	0 7	13	18 1	(9)	0 51	8	8 7	(1)
$2p\,^3\Pi$	R					1 26	13	22 3†	(4)	1 95	*37 7*	37 7	(10)	2	36	U	(4)†
$3d\,^3\Pi_a$	P	2 4	17	17 0	(8)	1·19			(1)	0 41			(1)	0 154	1		*ab*
$\rightarrow$	Q	0 43	3		(1)	0 59			(1)	1 71			(0)	2 4	*17 1*	17 1	(4)
$2p\,^3\Pi$	R					1 61			(5)	2 46		19 6†	(8)†	1 62	12	12	(2U)
$3d\,^3\Delta_a$	P					1 65	9	9 3	(2)	2 55	*14·6*	14 6	(4)	2 94			(1)
$\rightarrow$	Q	Do not exist				1 8	*10*	10 0	(6)	1 34	8	9 6	(4)	0 93			(1)
$2p\,^3\Pi$	R					1·82	10 4	5 7	(5)	1 3	8	5 9	(3)	0 33		†	
$3d\,^3\Pi_b$	P	1 5		14 9	(3a)	0 98		16 3†	(5)†	0·67	2½		(1)	0 43			(1)
$\rightarrow$	Q	1 5			(2)	0 04			*ab*	0 04	0		*ab*	0·23			(0)†
$2p\,^3\Pi$	R					2 3		44 0†	(10)†	3 4	*14 3*	14 3	(4)	3 07		44 0†	(10)†
$3d\,^3\Delta_b$	P					1 01	12	13 9	(4)	1 85	5		(0a)	1 95	8	10 3	(2A)
$\rightarrow$	Q	Do not exist.				2 45	*30 7*	30·7	(10)	3 16	*9 6*	9 6	(3)	2 6	*11 1*	11 1	(4)
$2p\,^3\Pi$	R					2 21	29	34 6	(10)	2 4	7	3 3	(2)	0 7	3	5 0	(3)

Table X.—Intensities. 3-electronic states, $v = 1$.

		K = 1.				K = 2				K = 3.				K = 4.			
		x^2.	kx^2.	E.	G.	x^2.	kx^2.	E.	G	x^2	kx^2.	E.	G	x^2	kx^2.	E	G.
$3d\,^3\Sigma \rightarrow 2p\,^3\Pi$	P	0·23	3	30·6†?	(8)†?	0 01	0		*ab*	0	0		*ab*	0			*ab*
	Q	1·9	*27*	27 0	(9)	1 24	*15*	15 0	(5)	0 86	17	26 1	(7)	0 62			(1)
	R					1 10	13½	8 4	(3)	1 65	*34 7*	34 7	(10)	1 83		14 2	(5)
$3d\,^3\Pi_a \rightarrow 2p\,^3\Pi$	P	2 27	*39 4*	39·4	(9)	1 64		10 2	(3)	1 06	13½	10 4	(2)	0 45			*ab*
	Q	0 59	10*d*	22 7†?	(8)†?	0 20			(1)	0 85	11	15 0	(5)	1 70		9 3	(1)
	R					1 14			(4*h*)	1 66	*23*	23 0	(8)	1 55			(1)
$3d\,^3\Delta_a \rightarrow 2p\,^3\Pi$	P	Do not exist.				1 16	7½	10 2	(4)	1 98	14½		(3*a*)	2 65			(1)
	Q					2 07	14	15 6	(5)	2	*15 6*	15 6	(6)	1 5			(1)
	R					2 47	*17 1*	17 1	(6)	2 2	18	12 0	(5)	0 22			(1)
$3d\,^3\Pi_b \rightarrow 2p\,^3\Pi$	P	1 5			(1)	1 16	16	14 0	(5)	0 94	7	8 0	(1)	0·42			(1)
	Q	1 5		.. ..	(0)	0 12	1½	..	(1)†	0	0		*ab*	0 13			*ab*
	R			..		1 9	*28*	28 0	(10)	2 70	*22·7*	22 7	(8)	2 37		21 3	(6)
$3d\,^3\Delta_b \rightarrow 2p\,^3\Pi$	P	Do not exist.				0 84	13	17 6	(5)	1·32	5½		(2)	1·77	6½	9 8	(2)
	Q					2 38	*36*	37 0	(9)	2·76	11½	11 5	(3)	2 75	*11 7*	11.7	(5)
	R					2 60	40·3	40 3	(10)	2 73	*12 1*	12·1	(5)	0·98	4½	5 7	(4)

Table XI.—Intensities, 4-electronic states, $v = 0$.

		K = 1				K = 2				K = 3.				K = 4.			
		x^2	kx^2.	E	G	x^2	kx^2	E.	G	x^2.	kx^2	E	G	x^2.	kx^2.	E.	G.
$4d\,^3\Sigma$	P	0·014	~0	12 6	(3)	0 009	0		*ab*	0 007	0		*ab*	0 005	0		*ab*
→	Q	2·46	*28 3*	28 3	(6)	0 63	19		(1)	0 28	9	9 2	(3)	0 158	1½	3 1	(1)
$2p\,^3\Pi$	R					2 1	*66·7*	66 7	(9)	2 9	*90*	90 0	(10)	2 68	*24 4*	24 4	(6)
$4d\,^3\Pi_a$	P	2·5				0 007	0		*ab*	0·07	½		*ab*	0 11	0	†	†
→	Q	0·1				2 7	14	10 6†	(2)†	3·33	*33 3*	33·3	(4)	3 6	5	~5	(2)
$2p\,^3\Pi$	R	0				2 5	*13·6*	13 6	(3)	2·82	29	20 3	(4)	1 36	*2*	2 0†	(0)†
$4d\,^3\Delta_a$	P	Do not exist.				2 8				2 8				2 9			
→	Q					0 16				0 115				0 08			
$2p\,^3\Pi$	R					0 059				0 09				0 015			
$4d\,^3\Pi_b$	P	1 5		? 9 4	? (2)	0 25	5		(1)	0 143	½		*ab*	0 08	1		*ab*
→	Q	1·5		?..	? (0)	0·19	4	4 6	(1)	0 52	2½	3·2	(0)	0 737	9	8 6†	(2)†
$2p\,^3\Pi$	R					3 9	*86*	86 0	(8)	4 8	*21½*	21·5	(3)	3 6	*47*	47·0	(5)
$4d\,^3\Delta_b$	P	Do not exist.				1 74	15½	15 2	(2)	2 1	3½		(0)	2 3	*6 3*	6 3	(0½)
→	Q					2 46	22½	22 5	(4)	2 2	*3½*	3 4	(1)	2 11	6	5·5	(2)
$2p\,^3\Pi$	R					0 57	*5*	6·8	(1)	0 59	1		*ab*	0 134	½	..	*ab*

The Spectrum of H_2. *The* $3d\,^1\Delta$ *and* $4d^1$ *Levels*

By O. W. Richardson, F.R.S, Yarrow Research Professor of the Royal Society, King's College, London, and P. M Davidson, Ph D, Lecturer in the University College, Swansea.

(Received June 13, 1933)

We will begin with the lines which go down from $3d\,^1\Delta_{ab}$. We succeeded in identifying them some time ago, but apart from a single progression (called the progression starting from λ 4097·433) which we found some while before the others,* no account of them has been published, though they have been used by one of us† in a paper on the theoretical rotational and intensity structure in the singlet bands

These even singlet Δ levels go down to each of the odd singlet levels of H_2 at $n = 2$, namely, to $2p\,^1\Sigma_u$ and $2p\,^1\Pi_{a,b}$. Fig. 1, which is not drawn to scale, shows the transitions. The potential energy curves of the upper states are very similar to that of $2p\,^1\Pi$, whereas $2p\,^1\Sigma$ has a much flatter curve. Its minimum is at a much larger nuclear separation, and is some 9000 wave numbers below that of $2p\,^1\Pi$. Thus whereas, for example, the $3d\,^1\Delta \rightarrow 2p\,^1\Pi$

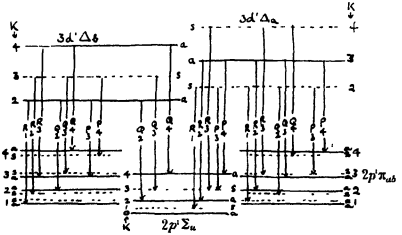

Fig 1.—Transitions from $3d\,^1\Delta_b$ and $3d\,^1\Delta_a$ down to $2p\,^1\Sigma_u$ and $2p\,^1\Pi$ at levels.

---

* It is one of the unassociated progressions included in Part 4 of our previous papers on the singlet systems ('Proc. Roy. Soc.,' A, vol. 124, p. 79 (1929)).

† Davidson, 'Proc. Roy. Soc.,' A, vol. 138, p 580 (1932), hereafter referred to as *loc. cit.*

bands (which are in the infra-red) are of the "diagonal" type, the corresponding bands to $2p\,{}^1\Sigma$ form long vibrational progressions in the visible, in fact, the intensity distribution in these progressions is, as it should be, very similar to that in the corresponding $3d\,{}^1\Sigma$ and $3d\,{}^1\Pi$ progressions, and shows a good general agreement with that predicted by the wave mechanics.* These $3d\,{}^1\Delta \rightarrow 2p\,{}^1\Sigma$ progressions are set out in Table I. The wave numbers are taken from Gale, Monk, and Lee's table,† and are followed by their eye estimates of intensity and preceded by Kapuscinski and Eymers' measured intensities ‡ These progressions are weaker than the corresponding ones from $3d\,{}^1\Sigma$ and $3d\,{}^1\Pi$, in fact, as may be seen, their strongest lines have intensity about 35 on Kapuscinski and Eymers' scale The strongest line in the whole H_2 spectrum occurs in the $3d\,{}^1\Sigma \rightarrow 2p\,{}^1\Sigma$ progressions, and has intensity 485, but there are only 13 lines in the spectrum with intensity greater than 160 We shall see later that the two strongest lines of the $3d\,{}^1\Delta \rightarrow 2p\,{}^1\Pi$ bands, though their intensities have not been measured, are probably about twice as intense as the strongest lines of the $3d\,{}^1\Delta - 2p\,{}^1\Sigma$ bands

In Table I a bar over a line means that the data refer to a blend with another line of at least comparable intensity. The letter F means that the data are taken from Finkelnburg's§ table instead of from Gale, Monk, and Lee's. Lines whose inclusion is doubtful are queried. We have examined the properties of the lines as set out in Merton and Barratt's table,‖ the Zeeman effect data of Dufour¶ and Croze,** and the effect of low temperature on the lines as recorded by McLennan, Grayson-Smith, and Collins †† Owing to insufficient resolution these observational data refer, in a large number of cases, not to a single line but to a group of two or more lines of which one of the lines in Table I forms a part However, it seems safe to say that the strongest line of $3d\,{}^1\Delta_b \rightarrow 2p\,{}^1\Sigma$, Q2 of the $0' \rightarrow 0''$ band, and the strongest line of $3d\,{}^1\Delta_a - 2p\,{}^1\Sigma$, P4 of the $0' \rightarrow 0''$ band, are both lines for which the Zeeman effect is definitely known to be absent. There seems no doubt of the conclusion in these two cases as the observations are either for uncontaminated lines or for blends with lines

---

* Davidson, 'Proc Roy. Soc,' A, vol 135, p 459 (1932), and actual calculations by Price, 'Proc. Roy Soc.,' A, vol. 136, p 264 (1932).

† 'Astrophys, J.,' vol. 67, p 89 (1928).

‡ 'Proc. Roy. Soc.,' A, vol. 122, p. 58 (1929).

§ 'Z. Physik,' vol. 52, p. 27 (1928).

‖ 'Phil. Trans.' A, vol. 222, p. 369 (1928).

¶ 'Ann. Chim. Physique,' vol. 9, p. 361 (1906), 'J. Physique,' vol. 8, p. 259 (1909).

** 'Ann. Physique,' vol. 1, p. 58 (1914).

†† 'Proc. Roy. Soc.,' A, vol. 116, p. 277 (1927).

Table I

The System $3d\,^1\Delta_g \rightarrow 2p\,^1\Sigma_u$

v' ↓	K ↓ v'' →	0		1		2		3		4	
	0										
	1										
0	2 Q	33·7	22206 34 (6)	$\overline{10\ 4}$	20893 78 $(\overline{2})$	4 6	19616 95 (1bh)		18374 88 (0)		
	3 Q	8·6	22308 89 (2)	7 6	21002 00 (1)						
	4 Q	26 4	22432 02 (3)	5 9	21132 38 (2)	$\overline{4\ 7}$	19866 70 $\overline{(1)}$				
	0										
	1										
	2 Q	32 7	24398 66 (3)	5 9	23088 09 (1)	9 3	21809 48 (2)		20566 99 (0)		19357 95 (0a)
1	3 Q	10·9	24479 87 (1)		23172 98 (0a)		21901 17 (1)				
	4 Q	33 7	24580 27 (1)	3 3	23280 55 (1)	9 0	22014 85 (2)		20782 31 (0a)		
	5 Q	8	24696 90 (1)		23406 11 (0a)	$\overline{9\ 3}$	22147 95 $(\overline{3})$		20922 09 (0)F	$\overline{23\ 1}$	19728·21 $(\overline{5})$
	6 Q	6·6	24830 20 (2) ?				22299 80 (00) ’	$\overline{18\ 8}$	21081 77 $(\overline{3})$?	$\overline{3\ 8}$	19895 10 (1) ?
	0										
	1										
2	2 Q		26467 83 (1a)	14 4	25155 14 (3)		23878 39 (0)F ?	7 1	22636 12 (1)†		
	3										
	4		26605 28 (0)	10 8	25305 63 (2)		[24040 04]		22807 41 (0)	4·1	21607 34 (0h)
	0										
	1										
3	2 Q		[28415 48]		27102 93 (0a)	$\overline{44\ 3}$	25826 42 (2)		[24583·95]		23374 88 (0)

$3' \rightarrow 5''$ Q2 = 22198 54 (00).

† Coincident with R2 of $1 \rightarrow 2$, $3\,^1O \rightarrow 2p\,^1\Sigma$

Table I—*continued*.

The System $3d\,{}^1\Delta_g \rightarrow 2p\,{}^1\Sigma_u$.

v' ↓	K ↓ v''→	0	1	2	3	4
0	0					
	1 R	3 2 22294·48 (1)	.. 20978 00 $\underline{(0)}$	[19698·29]		
	2 R	5 7 22455·06 (0)	$\overline{3{\cdot}4}$ 21142·46 $\overline{(1)}$			
	3 P	14·3 22102 13 (2)	4 4 20795 08 (0*a*)	.... 19523·42 (00)		
	4 P	34 2 22188 25 (6)	10 9 20888·53 (2)	3·6 19622·77 (1)	.. 18390·35 (00)	
	5 P	$\underline{3\ 2}$ 22294·48 $\underline{(1)}$	.. 21003·40 (0)F			
	6 P	$\overline{20{\cdot}0}$ 22421 63 (3)	2 9 21140·73 (1)	19891 49 (0*a*)		
1	0					
	1					
	2 R	10 2 24603 86 (1)	[23291 31]	$\overline{9\ 0}$ 22014 85 $\overline{(2)}$	.. 20772 11 (1)	
	3					
	4 P	16·8 24337 16 (2)	23037 49 (1)	11 6 21771 84 (2)		
2	0					
	1					
	2 R	.. .. 26640 44 (0*a*)	25327·97 (1)	24051 24 (4)†	22808 88 (0)	.... 21599·78 (0)

so weak that they would not be detected under the conditions of the Zeeman effect observations. Q4 of the $0' \rightarrow 0''$ band of $3d\,{}^1\Delta_b - 2p\,{}^1\Sigma$ is also a $Z = 0$ line, but here the evidence is not so clear as the observation may be for a group which includes a rather stronger line of the $4p\,{}^3\Sigma \rightarrow 2s\,{}^3\Sigma$ system, and this system does not give the Zeeman effect Nothing definite can be said about the other lines. It looks, then, as if these bands do not respond, or respond very weakly to the Zeeman effect (this places them in sharp contrast with, for example, the $3d\,{}^1\Sigma \rightarrow 2p\,{}^1\Sigma$ and $3d\,{}^3\Sigma - 2p\,{}^3\Pi$ bands). There seems a slight tendency for the bands to be enhanced at high pressures, to be exact, two lines in each system are recorded as so enhanced, and none are recorded as enhanced at low pressures.

The final vibrational and rotational intervals of the bands in Table I are identical with those which we have securely established for $2p\,{}^1\Sigma$ in our former papers dealing with the singlet systems. In particular, very accurate mean values were given.* The excitation potential of the line 22206·34 (Q2 of $0' \rightarrow 0''$, $3d\,{}^1\Delta_b \rightarrow 2p\,{}^1\Sigma$) has been measured by Finkelnburg, Lau, and Reichenheim,† and this determination further confirms the identification of the final level as $2p\,{}^1\Sigma$

As to the identification of the upper levels as $3d\,{}^1\Delta_{ab}$, it is to be noted that their denominators (m in $\nu_s = R/m^2$) are very nearly equal to 3, making a strong presumption that their electronic quantum number is 3 Granted this, and that they have only one excited electron, that the $K = 0$ and 1 levels are absent, and that the lines in the Δ_b band are indeed Q lines (and not R with very weak P, or *vice versa*), the identification is inevitable. More conclusively, it is shown by Davidson, *loc cit.*, that these levels together with the $3d\,{}^1\Sigma$, Π_{ab} levels given in our previous papers form a complete system whose detailed rotational intervals and transition intensities are in good accord with the wave-mechanics theory of uncoupling

It was shown by one of us‡ that most of the levels described in our previous papers, which give transitions to $2p\,{}^1\Sigma$ give rise also to lines of much longer wave-length, due to transitions to $2p\,{}^1\Pi$. The intervals between the $2p\,{}^1\Sigma$ and $2p\,{}^1\Pi$ levels were thus determined in detail and with accuracy. Hence when we had found the bands in Table I we were able to test at once whether there were corresponding transitions to $2p\,{}^1\Pi$. Table II is the result. The bands prove, indeed, to be about the strongest of those from 3-electronic levels

---

* 'Proc. Roy. Soc.,' A, vol 123, p. 54 (1929).

† 'Z. Physik,' vol. 61, p. 782 (1930).

‡ Richardson, 'Proc. Roy Soc.,' A vol. 126, p. 487 (1930).

Table II.

The Systems $3d\,^1\Delta_{ab} \rightarrow 2p\,^1\Pi_{ab}$

Initial state→	$3d\,^1\Delta_b$	$3d\,^1\Delta_b$	$3d\,^1\Delta$	$3d\,^1\Delta_b$	$3d\,^1\Delta_a$	$3d\,^1\Delta_a$	
Vibrational transition →	0′→0″	1′→1″	2′→2″	3′→3″	0′→0″	1′→1″	
K ↓							
1 Q							Q1
2 Q	13250 2 (3)	13143 3 (4)	13048 8 (2)	12951 3 (1*a*)	13264 4 (0)		Q2
3 Q	13283 7 (1) ?				13321 2 (1)	13180 3 (1)	Q3
4 Q	13315 7 (1*a*)	13195 2 (1)	*ab*				Q4
1 P							P1
2 P							P2
3 P	13072 5 (1)	12975 0 (1*a*)	12887 8 (00)	12809·9 (1*a*) ?	13076 8 (0)		P3
4 P					13072 0 (0)	*ab*	P4
1 R	13375 1 (2)	13261·9 (3)	13159 4 (3)	13067 0 (3)	13384 7 (1)		R1
2 R					13496 8 (1*a*)	13348 4 (1)	R2
3 R	13564 9 (00)	13423 3 (00)	13292 2 (00)				R3
4 R							R4

to the $2p\,^1\Pi$ state. Like the other $3d^1$ bands, they have an intensity distribution in agreement with Davidson's theoretical calculations As before, we give wave numbers from Gale, Monk, and Lee's table, followed by their eye estimates in brackets In one case, marked by the letter P, the wave number is taken from Poetker's* table, being absent from Gale, Monk, and Lee's. No "properties" of these infra-red lines are known, and the intensity measurements of Kapuscinski and Eymers do not extend to this part of the spectrum. Davidson (*loc cit.*) deduces a correlation between the infra-red eye estimates in this region and the intensity scale of Kapuscinski and Eymers It is, roughly $(00) < 10 < (0) < 18 < (1) < 45 < (2) < 65 < (3)$. This is based on calculations for the whole $3d^1$ system, and its justification rests on the success of the theory in the $4d^1$ system, where the bands both to $2p\,^1\Sigma$ and to $2p\,^1\Pi$ are in regions measured by Kapuscinski and Eymers.

Since we have previously found the rotational and vibrational intervals of $2p\,^1\Sigma$, those of the upper levels can be immediately found from the bands to $2p\,^1\Sigma$. (To be strictly accurate it is only intervals between *s* levels and between *a* levels which are actually observed, the whole singlet spectrum being thus divided into two non-combining groups, but the extreme regularity of the $2p\,^1\Sigma$ state enabled us to compute the relative position of the two groups with, we believe, considerable accuracy) The rotational intervals of $3d\,^1\Delta_b$ and $3d\,^1\Delta_a$ are shown in Table III Reference should also be made to Table VI, which shows the relationship between the five levels, and illustrates the uncoupling process.

The constants of the levels will be considered at the end of the paper.

Table III.

Rotational Structure of $3d\,^1\Delta_b$ and $3d\,^1\Delta_a$.

K	$3d\,^1\Delta_b$		$v = 0$	$3d\,^1\Delta_b$		$v = 1$	$3d\,^1\Delta_a$		$v = 0$
6	*a*			*a*					
					354 04 ?				
5	*s*			*s*		50 45 ?	*a*	—	
					303 59			347·90	
4	*a*	—		*a*	—	50 51	*s*		54·72
		274 81			252 08			293 18	
3	*s*		57 20	*s*		55·81	*a*	—	55·38
		217·61			196 27			237 80	
2	*a*	—		*a*	—		*s*		

The $0' \rightarrow 0''$ bands from $4d\,^1\Delta_b$ and $4d\,^1\Delta_a$ to $2p\,^1\Sigma$ and $2p\,^1\Pi$ will be found in Tables IV and V. The bands to $2p\,^1\Sigma$ are obtained by extending a provisional arrangement which we published early in 1929, and called $4\,{}^1\chi$.[*] At the same time the necessity for the whole set of $4d^1$ levels to form a group whose detailed structure and transition intensities shall be in fairly good quantitative accord with theory enables us to decide definitely the interpretation of the other 4-electronic singlet bands, which we called provisionally 4^1 A, B, C, E. Of these, $4\,{}^1$E is $4d\,{}^1\Sigma$, except that its R0 and, of course, P2, lines should be replaced by those of $4\,{}^1$C. (In the original paper such lines were called R1 and P3 To obtain the K values the old integers have always to be diminished by 1.) $4\,{}^1$B as slightly modified later by one of us[†] is $4d\,{}^1\Pi_b$, the lines originally called P are to be regarded as Q (They were at first called P in case some weak and dubious R lines associated with them were genuine) In the $4d\,{}^1\Pi_a$ band there is unfortunately a choice of lines between which it is difficult to decide with certainty. The possibilities are set forth in Table IV and the corresponding lines to $2p\,{}^1\Pi$ are arranged similarly in Table V. The lower alternatives for the P4 lines to $2p\,{}^1\Sigma$ are the same as the Q4 lines of $4d\,{}^1\Pi_b$ (and there is corresponding interference in the bands to $2p\,{}^1\Pi$) They assume, in other words, that the $K = 4$ level of $4d\,{}^1\Pi_b$ is practically coincident with the $K = 3$ level of $4d\,{}^1\Pi_a$. This, of course, is not very probable If it is so, most of the strength of the lines presumably belongs to $4d\,{}^1\Pi_b$, since the lines, as used in that band, are not perceptibly too strong It is true that if the lines are regarded as P4, two of the R2 lines calculated from them are found to exist, but practically all the strength of one of them (26246 05) seems to be required in the $3d\,{}^1\Sigma \rightarrow 2p\,{}^1\Sigma$ bands; on the other hand, it is also true that the R lines should theoretically be much weaker than the P lines. The lines used by Davidson in the theoretical paper, *loc cit.*, are in each case the upper of the two alternatives, they show on the whole a more satisfactory agreement with the theoretical intensities; in fact, the only real objection to them is the great strength of the Q1 line in the band to $2p\,{}^1\Pi$, which theoretically should be very weak Its apparent strength may, of course, be due to interference. An objection to the lower of the alternative P2 (and R0) lines is that they are present in Finkelnburg's table, but not in Gale, Monk, and Lee's. As a rule Finkelnburg's table does not enhance lines coming from such a low rotational level, though the rule is not universal On the other hand, the lines seem too numerous to be fortuitous. If they belong to this band, they should probably be associated with the lower of the alternative P4 (and R2) lines, since the upper alternative lines are not much stronger in Finkelnburg's table than in Gale's. The lower alternative

---

* 'Phys. Rev.,' vol. 30, p. 418 (1927)

---

[*] 'Proc. Roy Soc.,' A, vol. 123, p. 466 (1929).

[†] Richardson, 'Proc. Roy. Soc.,' A, vol. 126, p. 496 (1930).

Table IV

$4d\,^1\Pi_a \rightarrow 2p\,^1\Sigma_u$.

v' ↓	K ↓ v'' →	0	1	2	3	4	5	
0	0R	– 27487 25 (1) 27468·37 (1)F	.. 26149 84 (0)F	24887 49 (0)F 24868 64 (00)F	24 23640 67 (1)	22408 70 (0)F		
	1R							
	2R	– 27561 03?(0/1)F [27558·61]	19·0 26246 05 (1)	24969 36 (0)				
	2P	19 5 27371 04 (2) [27352 23]	22 3 26058 46 (2) 26039 69 (0)F	24781 84 (0) 24763 21 (00)F	2 8 23539 49 (0) 2·8 23520 62 (00)F	22311 57 (00)		
	3P							
	4P	– 27294 50 (0) 16·5 27291 87 (1*a*)	10 5 25994 82 (0) 19 4 25992 16 (1)	– 24729 13 (0)F 8 4 24726 47 (0*a*)	2 4 23493 95 (0)			

$4d\,^1\Delta_b \rightarrow 2p\,^1\Sigma_u$

v' ↓	K ↓ v'' →							
0	2Q	.. .. *27515 16 (1)	13 3 26202 65 (1)	6 3 24926 04 (0)	?23683 94 (0)F		?21298 60 (1)F	2Q
	3Q	.... *27636 60 (2)F	26330 00 (0)F	25057 67 (0)F	.. 23819 72 (0)F	22614·51 (00)F		3Q
	4Q	27770 59 (2)F	26470 85 (0/1)F	25205 20 (0)F	.. 23972·71 (0)F			4Q

$4d\,^1\Delta_a \rightarrow 2p\,^1\Sigma_u$.

								1P
								2P
0	3P	.... ..*27501·79 (1*a*)	.. 26194 74 (00*a*)	24922 93 (0)				3P
	4P	.... ..*27616 06 (1)	.. 26316 55 (1*a*)		.. 23818·24 (00)F			4P
	5P	[27758 83]	.. 26467 83 (1*a*)	25209 72 (0)F	.. ?23984 06 (0)F	22789 90 (00)F	?21627·96 (00)F	5P

Table V.

$0' \to 0''$ bands, $4d\,^1 \to 2p\,^1\Pi$.

	$4d\,^1\Sigma \to 2p\,^1\Pi$.	$4d\,^1\Pi_b \to 2p\,^1\Pi$	$4d\,^1\Pi_a \to 2p\,^1\Pi$	$4d\,^1\Delta_b \to 2p\,^1\Pi$	$4d\,^1\Delta_a \to 2p\,^1\Pi$
Q1	30 0 18260·26 (5)		52 1 18539 87 (6)		
Q2	2 8 18119·22 (1)	3 5 18327 61 (00)	—	13 4 18558 93 (2)	
Q3	4 9 18000 61 (1)	2 0 18250 40 (0)	22 18427 39 (4) ca 24 18425 06 (8)		3 4 18748 95 (0)†
Q4	17882·44 (0) ?	18175 67 (0)			
P2		2 7 18316 97	11 9 18414 66 (2)		
P3	17931 48 (0)	3 0 18150 08 (0)	—	10 6 18381 39 (3)	18476 47 (1)
P4	17751 35 (0)	2 9 18024 36 (1)	45 6 †18178·16 (9) 18175 67 (0)		3 4 18499·91 (0)
R1	ca. 12 18239 51 (10)	45 6 18452·56 (6)		4 7 18683 93 (1)	
R2	45 8 18178 16 (9)	14 6 18437 81 (2)	16 3 18604·96 (2)	16 0 18799 23 (5)	
R3	11·5 18108 03 (3)	24 18425·06 (8)			
R4	20 0 18035 41 (4)				

lines are certainly much enhanced in Finkelnburg's table, but it must be remembered that in any case very little of their strength can be in this band. It is possible that the lines 27294·50, etc, are really the Q4 lines of $4d\,^1\Pi_b$. This gives the lower alternative interval in $4d\,^1\Pi_b$, Table VI.

There are some fragments of the original 4^1 bands still to be interpreted. All the definitely genuine lines of $4\,^1\chi$ are used in $4d\,^1\Delta_{ab}$, with the exception of the R4 and associated P6 lines (in the present notation) We think they may safely be set down in the $v' = 3$ bands of $3d\,^1\Sigma \rightarrow 2p\,^1\Sigma$, where just such lines are missing. In the same way the R1 (present notation) and R3 lines of 4C, together with the P3 and P5 lines, may be placed in the $v' = 2$ bands of $3\,^1O$, though this is open to some objection Their intensity distribution is hardly what would be expected, and they predict a few uncertain lines to the $v'' = 0$ level of $2p\,^1\Pi$; if these are genuine the lines almost certainly belong to the $v' = 0$ bands of some 4-electronic level No doubt the 4-electronic levels of 3^1K and $3\,^1O$ should be represented by weak bands in this region of the spectrum, in fact, we have been able to fit up possible versions of them, but they are not very certain and will not be given here

The rotational intervals of the nd^1 states at $v' = 0$ are set out in Table VI. If we consider the $3d^1$ and $4d^1$ systems as a whole, we find that their rotational intervals and transition intensities, though decidedly similar, are by no means identical From the theoretical standpoint this is associated with the closer proximity of the three W'_s's (see § 2) in the $4d^1$ states At a given nuclear distance in the neighbourhood of the equilibrium value they should have, in rough approximation, about $(\frac{3}{4})^3$ of the corresponding separation in the $3d^1$ states, and this proves to be so The result is that at the $v = 0$ level the unperturbed states ($\Lambda = 0, 1, 2$) are much closer together, and their action on each other is greater. The theory predicts, for example, that in $3d\,^1\Sigma$ the $K = 1$ level should be depressed considerably below the $K = 0$ level (which is unperturbed), while the $K = 2$ level should not be depressed so far below that level. On the other hand, in $4d\,^1\Sigma$ the $K = 2$ level should lie even lower than the $K = 1$ level. This is found to be so. At the same time the intensity distributions will be modified. Taking again the $d\,^1\Sigma$ levels as an illustration, the theoretical intensity ratio of the P to the R line from a given upper K in the $3d\,^1\Sigma - 2p\,^1\Sigma$ band is about 0 4 at $K = 1$, falling off very rapidly as K increases (being only about 0·08 at $K = 3$). In the corresponding $4d\,^1\Sigma$ band the ratio is only about 0·2 at $K = 1$, again falling off very rapidly As stated previously, the quantitative measurements in all bands confirm the predictions quite well, with a few exceptions It is to be noted that from a

Table VI.

Rotational Structure of $nd\,^1\Sigma\Pi\Delta$ Complexes

K ↓		$4d\,^1\Sigma$ $v = 0$			$4d\,^1\Pi_b$ $v = 0$			$4d\,^1\Pi_b$ $v = 1$			$4d\,^1\Pi_a$ $v = 0$			$4d\,^1\Delta_b$ $v = 0$			$4d\,^1\Delta_a$ $v = 0$	
7	a																	
		278·79																
6	s		→53·91															
		224·88																
5	a		→54 74															
		170·14																
4	s		→56 21	a														
		113 93			167 93													
					or	61 12	a						a			s		
					170 59	or		157·26						285·68			329 72	
3	a		→51 63	s		→63 78	s		→54 58	a			s		→49 18	a		→63 76
		+62 30			106 81			102 68			190 20			236 50			265 96	
2	s		→81·75	a		→92 66	a		→67 54	s	or		a			s		
		−19 45			14·5			35 14			206 38 ’							
1	a		→6 50	s			s			a								
		−25 95																
0	s																	

		$3d\,^1\Sigma$ $v = 0$		K ↓	$3d\,^1\Pi_b$ $v = 0$			$3d\,^1\Pi_b$ $v = 1$			$3d\,^1\Pi_a$ $v = 0$			$3d\,^1\Delta_b$ $v = 0$			$3d\,^1\Delta_a$ $v = 0$	
7	a																	
		?270 97																
7	a		?53 52															
		?253 53																
6	s		→ ?36 08	6a			a											
		217 45			282 09			270 25										
5	a		→53 07	5s		→52 10	s		→48 11							a		
		164 38			229 98$_5$			222 13$_5$									347 90	
4	s		→51 90	4a		→52 97	a		→48 31	s			a			s		→54·72
		112 48			177 01$_5$			173 82$_5$			232 59			274 81			293 18	
3	a		→47 24	3s		→52 52	s		→47 54	a		→43 77	s		→57 20	a		→55·38
		65 24			124 50			126·29			188 82			217 61			237 80	
2	s		→42 54	2a		→49 77	a		→45 58	s		→41 75	a			s	– –	
		+22 70			74 73			80 71			147 07							
1	a		→30·23	1s			s			a								
		−7·53																
0	s																	

given upper K level there are in general five (or four) transitions whose relative intensities can be calculated—three transitions to $2p\,^1\Pi$ and two (or one) to $2p\,^1\Sigma$.

It would appear at first sight that the 3, $4d\,^1\Delta_{ab} \rightarrow 2p\,^1\Sigma$ bands should not exist since they break the selection rule $\Delta\Lambda = 0$ or ± 1. This is accounted for by the perturbation theory of uncoupling which shows that the actual perturbed wave functions for Δ_b are linear combinations of the unperturbed functions for $\Lambda = 2$ and $\Lambda = 1$; the wave function for Δ_a involves also the unperturbed function for $\Lambda = 0$. Thus the Δ levels can go down to the Σ level.

§ 2 *Energy of the Electronic Levels and various Constants*.—In deducing the constants of the $nd\,^1\Delta$ levels we must consider them not alone but in conjunction with the $nd\,^1\Sigma$ and $nd\,^1\Pi_{ab}$ levels. The five levels Σ, Π_b, Π_a, Δ_b, Δ_a may be regarded as formed by the mutual perturbations of three regular unperturbed levels. (There are really, of course, five unperturbed levels, but at each K the unperturbed Π_b and Π_a coincide, and so do the Δ_b and Δ_a.) Davidson, *loc. cit.*, gives diagrams showing quantitatively the relationship between the perturbed and unperturbed levels of the 3- and 4-electronic states. The constants calculated for the unperturbed levels are given in Table VII.

Table VII

Upper State	$3d\,^1\Sigma$	$3d\,^1\Pi_{ab}$	$3d\,^1\Delta_{ab}$	$4d\,^1\Sigma$	$4d\,^1\Pi_{ab}$	$4d\,^1\Delta_{ab}$
$W''^{e}_{b} - E''_{e}$	20860	21120	21605	26490	26610	26870
A	33565	33580	33670	33565	33580	33670
x	−·0614	−·0349	+·0154	−·0614	−·0349	+·0154
$\frac{109678}{(n+x)^2}$	12705	12460	12065	7075	6970	6800
D	2·84	2·81	2·76	2·80	2·78	2·76

W'^{e}_{b} is the minimum of W'_b (in wave numbers).

D is in volts, and is the energy at W'^{e}_{b}, measured downwards from its value at infinite nuclear separation. In other words, it is the energy of adiabatic dissociation of the molecule, with held nuclei.

A is the constant term in the Rydberg formula. If such formulae held accurately A should have the same value in all cases. As the values do not differ much we can take the mean value 33605 wave numbers.

E''_e is the value for $2p\,^1\Sigma$ of the $W_{e\Lambda}{}^e$ in equation (5) p. 32 in Kronig's book*, and A is the value of E''_e measured downwards from the minimum of W'_b for $H_2{}^+$.

B_e is close to 28·8 in all the upper states, and ω_e averages 2300.

* "Band Spectra and Molecular Structure," Cambridge (1930).

In calculating the electronic constants we have assumed that for each of the three unperturbed states a Rydberg formula connects the energies W'_b (in the notation of Kronig's book) in the various electronic levels $n = 3, 4, \ldots$, the nuclei being held fixed at the same separation (approximately the minimum of each W'_e curve) This is probably an improvement on previous methods of treating such data. It will be seen that a single value is given for all the B_0's. Actually there is evidence that in the $3d^1$ states B_0 is slightly different in the three unperturbed states, though in the $4d^1$ states the variation is hardly perceptible The three ω_0's also vary somewhat, and a mean value is given

Combining the results in Table VII with Burrau's value for the total negative energy of the hydrogen ion, we find 31 488 ± 0 035 volts for the total negative energy of H_2 in its ground state, and hence 4 428 ± 0·04 for the energy of dissociation in the ground state This differs only very slightly from the result 4 46_5 ± 0·04 we obtained when the analysis was less detailed than it is now *

Summary

The first part of this paper describes the bands which go down from $3d\,^1\Delta_{ab}$ to $2p\,^1\Sigma_u$ and $2p\,^1\Pi_{ab}$ These bands determine the $3d\,^1\Delta_{ab}$ levels, and complete the $3d\,^1\Sigma\Pi\Delta$ complex Analogy with these 3-electronic states now enables the previously known bands from 4-electronic states to $2p\,^1\Sigma$ and $2p\,^1\Pi$ to be extended and interpreted fairly satisfactorily The detailed spacing of the $4d\,^1\Sigma$, Π, Δ levels as well as the distribution of line intensities in the transitions from these levels down to $2p\,^1\Sigma$, Π levels is in substantial agreement with the results of the wave-mechanics theory of uncoupling. The same is true of the bands coming from $3d\,^1\Sigma$, Π, Δ down to $2p\,^1\Sigma$, Π. The existence of the bands coming from 3, $4d\,^1\Delta_{ab}$ levels down to $2p\,^1\Sigma$ has a peculiar interest since they are the only bands known in the H_2 spectrum which break the selection rule $\Delta\Lambda = 0$ or ± 1 This infraction is accounted for by the wave-mechanics theory. Various constants of the initial levels of the bands are calculated.

---

* 'Proc Roy Soc,' A, vol 123, p. 467 (1929).

The Homogeneous Catalysis of Gaseous Reactions by Iodine. The Decomposition of Propionic Aldehyde, and a General Discussion.

By S Bairstow and C. N. Hinshelwood, F R S

(Received June 13, 1933)

Introduction.

Previous papers* have dealt with the homogeneous catalysis of the decomposition of ethers and of acetaldehyde by iodine. The problem of the mechanism of these catalysed reactions can be approached in two ways: on the one hand, by seeking to obtain as complete a picture as possible of the types of chemical change which are susceptible to the action of a given catalyst, and, the catalysts which will promote a given chemical change; and, on the other hand, by investigating in detail the kinetics and molecular statistics of individual reactions

Experiments on the different kinds of reaction which iodine will catalyse are being published elsewhere Most of the chemical changes have involved too many side reactions, or secondary reactions with the catalyst, to be suitable for complete kinetic analysis Nevertheless, they show the chemical specificity of the action of iodine in the clearest manner, and this aspect of the problem is discussed from a general point of view in the last section of the present paper.

In one of the new examples, that of propionic aldehyde, the chemical changes have been found to be simple enough to justify a complete quantitative treatment. The results are of interest in that they reveal the operation of a factor not clearly in evidence in the examples of acetaldehyde and of the ethers previously studied, namely, a deactivating influence of the molecules of the reacting substance itself. Recognition of this factor leads to a more general and comprehensive view of the processes of molecular activation and deactivation.

Catalysed Decomposition of Propionic Aldehyde.

The method of measuring the rate of reaction has already been described. The iodine used as catalyst was prepared *in situ* by decomposing isopropyl iodide. The course of the reaction corresponds fairly closely to the equation $C_2H_5CHO = C_2H_6 + CO$. The products were found to have the composition :—

---

* Glass and Hinshelwood, 'J. Chem. Soc.,' p. 1815 (1929), Clusius and Hinshelwood, 'Proc. Roy. Soc.,' A, vol. 128, p. 82 (1930), Clusius, 'J. Chem. Soc.,' p. 2607 (1930).

Carbon dioxide	—
Unsaturated hydrocarbons	2·0%
Saturated hydrocarbons	45·7%
Carbon monoxide	52·3%

The saturated hydrocarbons gave on combustion Gas · Contraction · Oxygen used = 1·00 . 1·93 : 2·43 : 3·37, and thus consist almost entirely of ethane The pressure increase on decomposition is 80% of the initial pressure, instead of the theoretical 100%. This can be accounted for if 10% of the aldehyde condenses to products of high molecular weight. Since the extent of the condensation reaction is not very large, it can be corrected for accurately enough by substituting the observed "end-point" for the measured initial pressure in the kinetic equations. (There is evidence that the condensation is a heterogeneous reaction, and is probably approximately of the first order.)

The catalysed decomposition is homogeneous, as shown by experiments in a "packed" vessel.

For a given initial pressure of the aldehyde the rate of reaction is directly proportional to the concentration of catalyst, at least over a certain range. No experiments were made in which the concentration of catalyst was commensurate with that of the aldehyde.

Table I.—Temperature 398·5° C.

Catalyst, c.	$t_{\frac{1}{2}}$	$t_{\frac{1}{2}}\ c$
mm.	"	
2·3	190	437
5·0	97	485
10·0	47·5	475
11·5	39	448
16·5	26	429
20·0	22	440
27·5	17	468

For a given concentration of the catalyst the course of the reaction is not represented by a first order equation Unimolecular velocity constants show a regular and quite marked increase as the change proceeds; the ratio $t_{\frac{3}{4}}/t_{\frac{1}{2}}$, instead of being 2·0 is between 1·50 and 2·0. Moreover, the value of $t_{\frac{1}{2}}$, the half life, increases as the initial pressure of the propionic aldehyde increases;

that is, the aldehyde itself has a certain retarding influence on its own decomposition.

These observations can be correlated by the aid of a simple hypothesis. Activation is assumed to take place by the collision of an aldehyde molecule with an iodine molecule. But instead of immediate reaction there is a short time interval during which the iodine and the aldehyde remain associated as an activated complex. If the latter suffers a further collision with an aldehyde molecule it may be deactivated. Let n be the concentration of normal molecules of aldehyde, c that of catalyst molecules and X the concentration of activated complex established in the stationary state, then, since the rate of the uncatalysed reaction is negligible, we may write

$$k_1 . n . c - k_2 \; n . \mathrm{X} - k_3 . \mathrm{X} = 0$$

The first two terms are the rate of activation and deactivation respectively and the last term is the rate of transformation of the complex into the products of reaction From the equation we find for the rate of reaction

$$k_3 . \mathrm{X} = \frac{k_1 . n . c}{1 + \frac{k_2}{k_3} . n} .$$

Thus if a is the original amount of aldehyde, x the amount transformed at time t, and $k_2/k_3 = b$,

$$\frac{dx}{dt} = \frac{k . c . (a - x)}{1 + b\,(a - x)}$$

Thus

$$k . c \;\; t = \log\left(\frac{a}{a - x}\right) + bx.$$

The value of b may be found from the ratio of the three-quarter life to the half life, since

$$\frac{t_{\frac{3}{4}}}{t_{\frac{1}{2}}} = \frac{\log 4 + 0{\cdot}75\, ba}{\log 2 + 0{\cdot}50\, ba} .$$

Also in terms of $t_{\frac{1}{2}}$ we have

$$k = \frac{1}{c . t_{\frac{1}{2}}} . \left[\frac{b . a}{2} + \log 2\right].$$

That the formula represents the course of the reaction is shown by the figures in Table II.

According to the above formula, $t_{\frac{1}{2}}$, for a given catalyst concentration, should give a straight line when plotted against a. From the slope and intercept of this line an independent value of b can be found. The linear relation

Table II.—Temperature 365·5° C. $a = 168$, $b = 0·00756$.

t	x	$k.c.$
23	30	0·0184
39	50	0·0187
58	70	0·0185
80	90	0·0181
106	110	0·0179
135	130	0·0183
154	140	0·0185

is satisfied in practice as long as the ratio of aldehyde to catalyst remains large. For quite small pressures of aldehyde the value of $t_{\frac{1}{2}}$ decreases too rapidly, but at the same time the course of the reaction changes as shown by a fall in the "end point." For this reason results for the lowest pressures of aldehyde in Table III are ignored.

Table III.—Temperature 365°. 20 mm. decomposed iodide.

a.	a/p_0	$t_{\frac{1}{2}}$	$(t_{\frac{1}{2}} - 41)/a$.
272	0·80	104	0·232
249	0·79	99	0·233
227·5	0·80	94	0·233
136	0·79	72	0·228
73·5	0·79	58	0·231
(40·5	0·74	43	—)
(12·8	0·64	23	—)

a/p_0 is the ratio of the observed pressure increase to the initial pressure.

The slope is $b/2kc$ and the intercept, 41, is $\log 2/kc$. The mean value of the slope being 0·231, $b = 0·231 \times 2 \times \log 2/41 = 0·0078$.

Using this value of b, the course of a curve for a given initial pressure should be correctly represented. The calculation of the ratio $t_{\frac{3}{4}}/t_{\frac{1}{2}}$ is enough to test the agreement since the general applicability of the formula has already been shown.

a	$t_{\frac{3}{4}}/t_{\frac{1}{2}}$ (calculated)	$t_{\frac{3}{4}}/t_{\frac{1}{2}}$ (observed)
73·5	1·85	1·85
153	1·77	1·78
272	1·71	1·79

If there were no deactivation by aldehyde molecules, the rate of reaction would be $k . n . c$. This is therefore the quantity which should be compared with the number of collisions between aldehyde and iodine in considering the molecular statistics of the reaction. The quantity directly measured in any experiment is kc. Thus the absolute value of k depends on the units in which c is measured. The unit used is that concentration of iodine which produces a pressure of 1 mm. at 400° C. In determining the temperature coefficient of k 6·67 mm. iodine were used at each temperature but were expressed in terms of the above unit for the calculation.

k was worked out for five temperatures. Since the value of b is sensitive to small errors in the ratio $t_{\frac{1}{2}}/t_{\frac{1}{4}}$, the mean value of this ratio at each temperature was determined in several experiments.

Table IV

Temperature (absolute)	$k \times 10^3$.	k (average) $\times 10^3$.	k (calculated) $\times 10^3$
609°	0·765 0·756	0·760	0·767
623·5	1·55 1·56	1·55	1·46
638·5	2·58 2·59	2·58	2·77
653·5	5·29 5·24 5·37	5·30	5·08
668·5	8·84 9·15 9·45	9·15	9·09

The calculated values correspond to the equation

$$\log_e k = 20 \cdot 608 - \frac{33{,}500}{\mathrm{RT}}$$

The reaction, being homogeneous, must depend upon the collision of iodine molecules with aldehyde molecules. At 673° abs. with 760 mm. aldehyde and 6·67 mm. of iodine the number, Z, of these collisions is found from the usual formula* to be $4 \cdot 55 \times 10^{26}$. For the calculation the value of σ_{12}, the mean diameter, is taken as 5×10^{-8} cm. The number of collisions which can produce activated molecules is $Ze^{-E/RT}$ if the energy which counts as activation energy resides in two square terms. E, corrected for the variation of collision number with temperature is 32,800, whence the above expression is found to be $0{\cdot}94 \times 10^{16}$.

---

* Clusius and Hinshelwood, *loc. cit.*, p. 86.

The actual rate of reaction at 760 mm. pressure is much less than the rate of activation, on account of the deactivation of the active complexes by the aldehyde, but $k\,.\,n\,.\,c$ gives the rate when $b = 0$, that is, the rate if there were no deactivation. This is the quantity which should be compared with $Z\,.\,e^{-E/RT}$. At 673° abs. k for 1 mm. iodine is $0{\cdot}0107$, and thus $k\,.\,n\,.\,c = 0{\cdot}0107 \times 1{\cdot}1 \times 10^{19} \times 6{\cdot}67 = 7{\cdot}9 \times 10^{17}$ molecules per cubic centimetre per second. This is 84 times greater than the number calculated above for two square terms. For the uncatalysed decomposition the corresponding discrepancy is about 400. The differences, as is known, can be accounted for by the introduction of extra square terms in the activation energy. It is clear that fewer are required for the catalysed reaction. In some examples of iodine catalysis, such as the decomposition of isopropyl ether, the number of square terms reduces to two for the catalysed reaction. With propionic aldehyde the simplification of the activation mechanism, although considerable, has apparently not gone to the full extent where the energy is communicated in a collision to a single vital degree of freedom, as would be indicated if only two square terms were required. When activation energy is distributed in more than one degree of freedom, internal rearrangement of energy probably has to occur before decomposition. Thus the activated molecule, or complex of molecule and catalyst, may have a finite life, and therefore be subject to deactivation. It is significant, therefore, that, precisely in that catalysed reaction requiring the greatest number of square terms to account for its rate, a marked deactivation factor makes its appearance, as shown by the b term in the equations.

General Considerations about Activation and Deactivation in Catalysed Reactions.

Evidence from many different types of reaction now shows that almost any molecules present are capable of activating or deactivating to a greater or smaller exent. When this is taken into account, the most diverse relations between rates and concentrations are all seen to be derivable from one general formula by variation in the relative values of specific numerical constants.

Suppose there is a catalytic reaction in which molecules of a reactant, concentration n, can be activated by collision with one another or by collision with molecules of a catalyst, concentration c. For generality, we will assume that the molecules activated by the catalyst remain associated with it in the form of a complex which may be deactivated by collisions either with catalyst molecules or reactant molecules. Active molecules produced by collision between two reactant molecules can be deactivated in the same type of collision In the absence of catalyst the decomposition of this kind of active molecule gives rise to the well-known quasi-unimolecular reaction. In presence of catalyst, the energy of activation of the catalytic complexes is so much smaller that these latter are responsible for practically the whole decomposition. Equating rates of production, deactivation and chemical transformation of the activated complexes, of which a stationary concentration X is established, we have

$$k_1 . n \quad c - k_2 \quad n \quad \mathrm{X} - k_2 \quad c \quad \mathrm{X} - k_3 \quad \mathrm{X} = 0.$$

Whence, rate of reaction

$$k_3 . \mathrm{X} = \frac{k_1 \quad n \quad c}{\dfrac{k_2}{k_3} \; n + \dfrac{k_2'}{k_3} . c + 1}$$

When k_2 and k_2' are very small or k_3 is very large the rate of reaction is directly proportional to the catalyst concentration and the whole change is of the first order. With acetaldehyde and some of the ethers catalysed by iodine this state of affairs is nearly realized If k_2' is small, the formula reduces to the one used in the last section, and accounts for an increase in the half life of the reactant with its own initial pressure. This effect is marked with propionic aldehyde, but it is also observed that such departures from a strictly first order reaction as are found with the ethers (compare diisopropyl ether and methyl ethyl ether) are in this same direction

If, on the other hand k_2 is small but k_2 is comparable with k_3, then the reaction rate will not be linearly proportional to the catalyst concentration but will approach a limiting value as this is increased. Some particularly marked examples of this effect in various stages of development are to be found in the catalytic decompositions of the simple aliphatic amines by iodine

General Discussion of Iodine Catalysis.

In this and previous papers most of the possible kinetic relations have been exemplified and discussed. It now remains to survey the results as a whole, to see whether any generalization can be made about the relation between the properties of the catalyst and the structure of the compounds which it influences.

Since the results have not been collected together in any of the previous papers, it will be convenient to tabulate below the various types of reaction, involving different molecular structures, which have been investigated.

(*a*) *Decomposition of Ethers* —

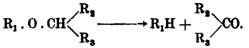

$$R_1 . O . CH\begin{matrix} \diagup R_2 \\ \diagdown R_3 \end{matrix} \longrightarrow R_1H + \begin{matrix} R_2 \diagdown \\ R_3 \diagup \end{matrix} CO.$$

This reaction has been found to be catalysed in the examples of diisopropyl, diethyl, isopropyl methyl and ethyl methyl ethers. The rate of reaction is multiplied by a factor varying from 10^2 to 10^5 by the presence of 10 mm. iodine.

Dimethyl ether is not catalysed, and in the mixed ethers containing a methyl group the movement of hydrogen is predominantly from the other group to the methyl.

(*b*) *Decomposition of Aldehydes* —

$$R . CHO \longrightarrow RH + CO.$$

Acetaldehyde and propionic aldehyde are both catalysed, the acceleration produced by 10 mm iodine being of the order 10^4

(*c*) *Decomposition of Ketones* —The decomposition of acetone and of methyl ethyl ketone is not catalysed

(*d*) *Decomposition of Alcohols* —Methyl alcohol is not catalysed by a factor of more than three.

(*e*) *Decomposition of Alkyl Halides.*—Ethyl chloride and ethyl iodide are not catalysed With ethyl bromide the rate is approximately doubled by 10 mm. iodine.

(*f*) *Decomposition of Esters* —Under the influence of iodine the following reactions have been shown to occur, with methyl formate and with methyl acetate respectively

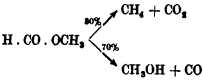

$$H . CO . OCH_3 \begin{matrix} \xrightarrow{30\%} CH_4 + CO_2 \\ \xrightarrow{70\%} CH_3OH + CO \end{matrix}$$

$$CH_3\ CO\ OCH_3 \longrightarrow CH_3CHO + HCHO.$$

The rate is multiplied about 50 times for 10 mm. iodine.

(*g*) *Decomposition of Acids.*—The reactions

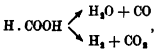

$$H . COOH \begin{matrix} \nearrow H_2O + CO \\ \searrow H_2 + CO_2 \end{matrix},$$

and the decomposition of acetic acid are uncatalysed.

(*h*) *Decomposition of Simple Aliphatic Amines* —

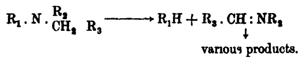

$$R_1 . N . \overset{R_2}{CH_2}\ R_3 \longrightarrow R_1H + R_3 . \underset{\substack{\downarrow \\ \text{various products.}}}{CH} : NR_2$$

With diethylamine and triethylamine the rate is multiplied by factors of the order 10^2 by 10 mm. iodine, while with the corresponding methyl compounds the factor is only of the order 10. Ethylamine is catalysed to a quite small extent

(*i*) *Decomposition of Hydrocarbons* —Iodine exerts a small effect on the decomposition of hexane, but how much of it can be called catalytic is not certain

The numerical factors which have been given are only approximate, since the conditions of comparison are not exactly the same in the different examples, but the differences are so striking that there is no difficulty whatever about classifying them It appears that, whenever there is any marked degree of catalytic influence, the reaction can be formulated as the movement of a hydrogen atom accompanied by the rupture of a bond * Ethers, amines, esters and aldehydes are all strongly catalysed The reactions of the amines are analogous to those of the ethers, and the reactions of the esters to those of aldehydes or ethers

The catalysis depends both on the nature of the bond to be broken and on the mode of attachment of the hydrogen atom, as may be seen by contrasting methyl ethyl ether with methyl ethyl ketone, on the one hand, and with dimethyl ether, on the other Methyl ethyl ether is catalysed. the ketone, which contains a similar set of hydrogen atoms, and which might quite well decompose into methane and methyl ketene, is not catalysed Dimethyl ether, which contains the C—O—C bond but no methylene hydrogen, is also not catalysed The insensitiveness of dimethyl ether is reflected in the relatively small catalysis of the methylamines compared with the ethylamines.

All the kinetic results prove that the energy of activation of the catalysed reaction is very much smaller than that of the uncatalysed reaction, *e.g.*, with diethyl ether 34,800 compared with 53,000 calories Furthermore, the activation mechanism is much simpler, the energy transferred in the encounter with the catalyst being located in fewer degrees of freedom. To take an extreme example, diisopropyl ether can be activated by collision with molecules of its own kind. The energy of activation is 60,500 calories and is distributed throughout the molecule in at least 13 degrees of freedom In the catalysed reaction only two square terms are necessary to account for the rate, and thus the much smaller amount of energy, 28,500 calories, appears to be made effective by being brought by the iodine to one vital degree of freedom.

---

* The decomposition of nitrous oxide is strongly catalysed by iodine. The effective catalyst is the iodine atom, so that the process is different from those discussed here. The rate of the reactions dealt with in this paper is usually directly proportional to the iodine concentration at least over a wide enough range to show that the molecule and not the atom is the catalyst.

The first question arising is whether there is any obvious mechanism whereby the iodine can place energy selectively in one bond of a molecule.* A property common to all the molecules which are subject to any very marked influence of iodine is the possession of a dipole moment, and with the ethers, esters and amines there is a moment located precisely in that bond which is broken in the catalytic reaction. The iodine molecule is known to be a very easily polarizable structure,† and therefore, as it approaches a molecule with a dipole moment it will have a moment induced in itself, and will be attracted to the position of the original dipole. The dipole aggregate may sometimes have a life considerably longer than the normal duration of a collision,‡ but, even without this, the orientation of the iodine with respect to the bond is unusually favourable for the transfer of vibrational energy. Ordinarily, as shown by evidence of several different kinds, such transfers are highly specific, and may be difficult unless helped in a way such as that suggested here Since this intimate association at the vital point can occur, a whole series of degrees of simplification of the activation mechanism are possible, up to the ideal limit where the iodine places the requisite energy straight into the weak bond and immediately breaks it. This point of view implies that the energy of activation is mostly stored as vibrational energy of the iodine molecule. As far as the mathematical evidence goes, it might equally well be the kinetic energy of approach, but if the relative velocity of the molecules is too great, there is unlikely to be time for orientation and, therefore, there will be no selective placing of the energy. (If dipole forces are in action, there may also be a somewhat augmented "collision diameter.")

---

* An extreme view of the process would be to assume a definite series of chemical reactions, *e.g.*, $CH_3CHO + I_2 = CH_3I + HI + CO$, and $CH_3I + HI = CH_4 + I_2$. Apart from the fact that such a formulation would be difficult with the esters, it is not helpful, because, while leaving unanswered the question as to how the iodine influences the bonds in the other molecule, it raises yet another question, namely, why the process should be resolved into two definite stages.

† The molecular refraction of iodine is 32 compared with values of 2·08 for hydrogen and 4·15 for the $C = O$ system.

‡ If a definite dipole aggregate is formed with a finite life then it is easy to see how the deactivation possibility appears, as with propionic aldehyde.

So far we have only been concerned with the directing of the energy to the vital point in the molecule, and with the ease of transfer. The energy of activation of the uncatalysed reaction, being wastefully distributed, is probably far greater than the actual work required to break the bond. In presence of iodine it may be more nearly a measure of the bond strength,* so that there will be a lowering of E to the extent of the originally wasted energy. But, in addition, the iodine probably weakens the bond itself and loosens the hydrogen atom. The extent to which this occurs is impossible to estimate, but relevant factors are the known affinity of iodine for hydrogen, and the loose attachment of the outer electrons in the iodine molecule. The whole complex of processes occurring seems to possess certain suggestive analogies to the proton donating and accepting mechanisms of acid and basic catalysis in solution.

We are indebted to the Royal Society and to Imperial Chemical Industries, Ltd., for grants for the purchase of apparatus.

Summary

(1) The homogeneous decomposition of propionic aldehyde, $C_2H_5CHO = C_2H_6 + CO$, is catalysed by iodine, the rate being proportional to the catalyst concentration, and increased about 10^4 times by 7 mm The aldehyde itself exerts a deactivating influence on the active complex involved in the reaction. Allowing for this the kinetics of the process can be accounted for quantitatively. The molecular statistics of the reaction are discussed, and compared with analogous examples

(2) A general theory of activation and deactivation by all the types of molecule present in a system is shown to explain the apparently diverse relations between rates and concentrations in various classes of catalytic reaction.

(3) From a general survey of the types of reaction which have been found to be markedly catalysed by iodine the following general conclusions are drawn.

---

* From the rather regular trend of activation energies in the series of homologous ethers, that of the "catalysed decomposition" of dimethyl ether can be estimated at about 42,000 calories. This is the only one of the E values which exceeds the heat of dissociation of iodine to any extent. Whether this is connected with the non-occurrence of the catalytic reaction might be determined by experiments with the other halogens.

All the reactions which are catalysed involve the movement of a hydrogen atom, and the breaking of a bond (although the decomposition of dimethyl ether, which can be formulated in this way, is not catalysed). In general the energy of activation of the catalysed reaction is very much lower than that of the uncatalysed reaction, and this energy, instead of being distributed through the whole molecule, appears to be placed in a part of the molecule where it can be efficiently used in breaking the bond The existence of a dipole moment in or near the bond broken suggests that the selective energy transfers are favoured by polarization and attraction of the iodine molecule Actual weakening of the bond and loosening of the hydrogen atom in the presence of the iodine must, however, be assumed also to play a part.

On a New Type of Expansion Apparatus

By C. T. R Wilson, F.R.S

(Received July 8, 1933)

The cloud-chambers hitherto used for the photography of tracks have all, so far as I am aware (with the exception of the Shimizu apparatus), been essentially of the same type. A definite volume change has been produced by the rapid motion of a piston or plunger (forming the " floor " of the chamber) which has been suddenly brought to rest by striking against a base plate While the volume thereafter remains constant the pressure increases as the temperature within the chamber rises

Whether a water, oil, or rubber " seal " is used to prevent leakage past the piston, rather exact workmanship is required in the construction of the apparatus; and the original form with the water-seal can hardly be used except with the axis vertical and with the plunger forming the bottom of the chamber.

In the apparatus now to be described the expansion is made by suddenly reducing the pressure from one definite value to another; the pressure thereafter remains constant while the gas expands as a result of the rising temperature.

The usual method of making the expansion by the sudden displacement of one end of a shallow cylinder avoids the stirring up of the air at the moment of expansion. This form of the apparatus lends itself also to the maintenance of an approximately uniform electric field within the chamber.

In the new type of apparatus these advantages are retained by giving the cloud chamber a fixed "floor" of wire gauze through which a portion of the air escapes at the moment of expansion The mechanism for allowing the pressure fall is attached to a second chamber separated from the cloud-chamber by this gauze partition. Any turbulent motion is prevented from reaching the cloud-chamber proper by the wire gauze partition, which also forms a convenient electrode for maintaining the necessary electric field. The necessary fall of pressure is effected by suddenly opening communication between the second chamber and the atmosphere or a large vessel at the desired final pressure.

If it is desired always to use the same gas in successive expansions, this gas is kept separate from the atmospheric air by a sheet of thin elastic membrane across the second chamber.

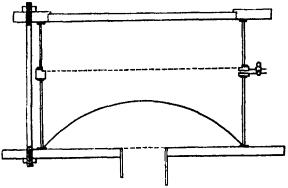

FIG 1

For the purpose of testing the working of this type of cloud-chamber the apparatus shown in fig. 1 was designed. It was constructed in the workshop of the Cavendish Laboratory by Mr. P C Ho It is shown as used for working with a final pressure equal to that of the atmosphere. The cloud-chamber is about 16 centimetres in diameter

Two glass cylinders, separated by a brass ring, to the top of which is soldered the wire gauze partition, are bolted together between the roof (a brass ring with a glass disc cemented into it) and the brass base plate. The base-plate has a central aperture to which is connected the mechanism for making sudden communication with the atmosphere. Rubber rings are inserted between the glass cylinders and the brass plates or rings to make an air-tight seal. The wire gauze partition is of copper wire about 0·2 mm. in diameter, spaced 1 mm. apart. A piece of similar gauze was inserted over the mouth of the aperture in the base-plate with the object of damping the oscillations of the air column

A sheet of thin balloon rubber is inserted below the lower glass cylinder; it is shown in the position it occupies when the air is in its compressed condition before an expansion.

The central brass ring which carries the gauze partition is insulated by the glass rings, so that the potential difference required for the removal of ions may be maintained between it and the rest of the apparatus.

The central ring is bored below the level of the gauze to receive two side-tubes, provided with stopcocks, for admitting gas and for connecting to a gauge for the measurement of the initial pressure

The initial pressure is adjusted to the value required to give the desired expansion by pumping air into the space below the rubber sheet, while the communication with the atmosphere or low pressure chamber through the wide exhaust tube is closed.

The sudden expansion is effected by suddenly opening this communication by the same kind of mechanism as is used in the ordinary type of expansion apparatus

After some preliminary tests made by Mr Ho in the Cavendish Laboratory, the apparatus was further tested by Mr Ho and Dr. E. C. Halliday at the Solar Physics Observatory by taking a number of track photographs. Arrangements for illumination and for timing the operations were in readiness for use with my old expansion apparatus, which was being applied by Dr. Halliday in an attempt to detect penetrating radiation from thunderclouds The new experimental apparatus could easily be substituted for the old, and a number of photographs of tracks due to electrons ejected by X-rays and to α- and β-rays were obtained

These photographs do not appear to be inferior to those obtained with the old apparatus Further tests are being made on such points as the extent to which the expansion is oscillatory, and the best amount of damping to be introduced into the exhaust tube. But even without further improvements on the form described above, which is that of the original design planned to test the possibilities of the method, the apparatus is suitable for giving good track photographs.

The apparatus is extremely simple to construct, and admits of much greater variations in shape or size than the older form, and it may be placed in any position.

It should be noticed that the thin rubber sheet is not really an essential part of the apparatus. If it is omitted, fresh dust-free air or gas has to be admitted after each expansion to replace that which has escaped. This may be a convenient method in certain circumstances, as for example, in experiments at low pressures

One might ask whether there is any advantage, apart from practical convenience, in making the expansion consist in a definite volume change followed by an increase in pressure as the temperature rises, or in a definite pressure change followed by an increase in volume So far as there is any difference, the advantage would seem, for certain purposes, to lie with the second method. For here the rise of temperature in one part of the cloud-chamber, due to heat conduction from the walls or condensation to form cloud, does not, as in the first method, cause simultaneous compression and consequent rise of temperature in the rest of the chamber; after an expansion a longer interval of time may therefore be available in which the super-saturation necessary for the production of sharp tracks persists.

It may finally be pointed out that the apparatus which has been described may be converted into one of the definite volume-change type with exceedingly light moving part by inserting the thin rubber sheet above instead of below the lower glass cylinder (*i.e*, immediately below the wire gauze) and placing below it a perforated platform against which it is tightly pressed by a large excess pressure at the completion of the expansion, the rubber sheet, the initial position of which is varied according to the expansion required, takes the place of the moving plunger or piston of the older type of apparatus

Summary

A new type of expansion apparatus is described which is more easily constructed than the usual form, and is less restricted as to the size and shape and position of the cloud-chamber.

The Motion of a Rotor carried by a Flexible Shaft in Flexible Bearings.

By D. M. Smith, D.Sc

(Communicated by G. Stoney, F R S.—Received February 7, 1933.)

(1) *Introduction.*

1 1 —*Scope of Investigation.*—This paper discusses the transverse motion of a rotor carried by a flexible shaft rotating in flexibly-supported bearings. The rotor is assumed to consist of one or more rigid bodies mounted on a shaft which is weightless and torsionally rigid. The rotor and shaft are in rotation; in the first place, it is taken that the speed of rotation is maintained constant, driving torques being applied if necessary about the shaft axis. Unsymmetrical flexibility of the bearing supports and unsymmetrical transverse flexibility of the shaft are taken into account, and the effect of damping which resists change of strain of the flexible members of the system is also considered. The work is mainly analytical, but reference is also made to experiments which have been carried out.

1 2. *Definitions* —The flexible members (shaft and bearing supports) are described collectively as the mounting An unstable speed is a speed of rotation at which a rotor, after receiving a small initial displacement from its equilibrium state of motion, tends to increase its amplitude of vibration beyond all bounds; while a critical speed is a speed at which out-of-balance alone tends to set up vibrations of very great amplitude.

(2) *Rotor consisting of a Single Concentrated Mass*

2 1. *Equations of Motion* —Axes OX, OY, OZ are chosen fixed in space such that OX, the bearing axis, coincides with the centre line of the undeflected bearings and OY, OZ lie in that transverse plane in which the concentrated mass M moves when shaft and bearings deflect. For reference, rotating axes OU, OV are also employed; these axes revolve in plane YOZ with the same constant angular velocity ω as the rotor, so that at time t the angle made by OU with OY is ωt. (Fig. 1.)

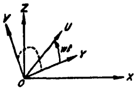

Fig. 1.

Let y, z in fixed axes, or u, v in rotating axes, be the co-ordinates of the rotor centre, that is, the point in the rotor which coincides with O when the mounting is undeflected; then y, z or u, v denote the total deflection of the mounting at the point of attachment of the rotor. Let y_m, z_m or u_m, v_m be the co-ordinates of the centroid of the mass M When the rotor is in perfect balance $y_m = y$, $z_m = z$, $u_m = u$, $v_m = v$; but when the balance is imperfect (due to lack of initial straightness in the shaft or to eccentric mounting of the rotor) the relationship in rotating co-ordinates is $u_m = u + g$, $v_m = v + h$ where g, h are the out-of-balance displacements which are constant in rotating axes The equations of motion of the rotor are

$$\mathrm{M}y_m - \mathrm{F}_y = 0, \qquad \mathrm{M}z_m - \mathrm{F}_z = 0,$$

where F_y, F_z are the forces acting on the rotor in directions OY, OZ respectively Transferring to the co-ordinates which express deflection of the mounting, these equations of motion become in fixed axes

$$\mathrm{M}y - \mathrm{F}_y - \mathrm{M}\omega^2 (g \cos \omega t - h \sin \omega t) = 0 \tag{1}$$

$$\mathrm{M}z - \mathrm{F}_z - \mathrm{M}\omega^2 (g \sin \omega t + h \cos \omega t) = 0, \tag{2}$$

or in rotating axes,

$$\mathrm{M}(u - 2\omega v - \omega^2 u) - \mathrm{F}_u - \mathrm{M}\omega^2 g = 0 \tag{3}$$

$$\mathrm{M}(v + 2\omega u - \omega^2 v) - \mathrm{F}_v - \mathrm{M}\omega^2 h = 0 \tag{4}$$

The applied forces F_y, etc., include (*a*) mounting forces, both elastic and damping, applied through the mounting and due to strain of the mounting, and (*b*) external disturbing forces applied otherwise than through the mounting So far as (*a*) is concerned it is assumed that the reaction transmitted in any principal direction across any member of the mounting is the sum of two terms, one (the elastic force) being proportional to the strain of the member, and the other (the damping force) being relatively small and proportional to the rate of strain of the member It is also assumed that the shaft does not cross clearances in the bearings, so that deflection of the rotor may be completely expressed in terms of strain of the members of the mounting Hence, for any given orientation of the shaft in the bearings (*i.e.*, for any given angle UOY) the terms representing elastic and damping forces are linear functions of the co-ordinates and their first derivatives As the shaft rotates in the bearings the coefficients of those co-ordinates may vary so that the complete expressions in the equations of motion may include periodic functions of the time The only external disturbing forces (*b*) considered are constant or are periodic functions of the time It follows that the equations of motion, expressed either in fixed or in rotating co-ordinates, are always linear differential equations (not necessarily with constant coefficients) Further, the out-of-balance terms and the external disturbing forces do not affect the complementary function and therefore do not influence the stability of the motion, but merely determine the particular integral and hence fix the amplitude of the steady station of motion. The form of the out-of-balance terms in the equations of motion shows that out-of-balance has the same effect as an externally applied force of constant magnitude rotating in plane YOZ with the rotor speed, and therefore that a critical speed is a speed at which the system is in resonance with such a disturbing force. In subsequent analysis external disturbances and out-of-balance terms are to be taken as zero unless the contrary is expressly stated. The generality of the investigation as to stability of motion is not thereby diminished

2 2 *Symmetrical Shaft, Symmetrical Bearings* —The shaft and the bearings have elastic and damping characteristics uniform in all transverse directions Where the constraint exercised on the shaft by the bearings is such that the reactions at the bearings are statically determinate, the relation of the reaction across any member of the mounting to the resultant mounting forces is determined solely by the geometry of the system, and the total deflection (y, z) or (u, v) of the rotor centre is the sum of two independent parts, of which one (y', z') or (u', v') arises in deflection of the bearing supports and the other (y'', z'') or (u'', v'') arises in deflection of the shaft The bearing characteristics are such that

$$F_y = -b'y' - c'y'$$
$$F_z = -b'z' - c'z',$$

where c' is the stiffness coefficient and b' the damping coefficient of the bearings The shaft characteristics must be expressed in the first place in rotating co-ordinates, since damping in the shaft is brought about by change in configuration of the rotating shaft, the characteristics are

$$F_u = -b''u'' - c''u''$$
$$F_v = -b''v'' - c''v'',$$

where c'' is the stiffness coefficient and b'' the damping coefficient of the shaft. b' and b'' are assumed so small compared with c' and c'' that the damping forces are small compared with the elastic forces The shaft characteristics when transferred to fixed co-ordinates become

$$F_y = -b''(y'' + \omega z'') - c''y''$$
$$F_z = -b''(z'' - \omega y'') - c''z''.$$

The terms in ω represent the circumferential drag experienced if a rotating shaft with inherent damping is held deflected at a fixed position in space. From the relations $y = y' + y''$, $z = z' + z''$ the forces may be expressed as follows correct to small quantities of the first order —

$$F_y = -b'\left(\frac{c''}{c'+c''}\right)^2 y - b''\left(\frac{c'}{c'+c''}\right)^2 (y + \omega z) - \frac{c'c''}{c'+c''}\, y$$

$$F_z = -b'\left(\frac{c'}{c'+c''}\right)^2 z - b''\left(\frac{c'}{c'+c''}\right)^2 (z - \omega y) - \frac{c'c''}{c'+c''}\, z,$$

and hence the equations of motion of the mass M may be written—

$$y + (m+n)\, y + \omega n z + \mu y = 0 \qquad (5)$$

$$z + (m+n)\, z - \omega n y + \mu z = 0, \qquad (6)$$

where $m = \frac{b'}{M}\left(\frac{c''}{c'+c''}\right)^2$ = stationary damping coefficient representing effect of damping in the bearing supports;

$n = \frac{b''}{M}\left(\frac{c'}{c'+c''}\right)^2$ = rotating damping coefficient representing effect of damping in the shaft,

$\mu = \frac{c'c''}{M(c'+c'')}$ = $\frac{\text{overall stiffness of mounting}}{\text{mass}}$

When there is no damping the equations of motion take the simple form $\dot{y} + \mu y = 0$, $z + \mu z = 0$, the free motion is simple harmonic, and therefore always stable, the angular frequency of this motion is $\sqrt{\mu}$ in either transverse direction, so that the critical speed is given by $\omega = \sqrt{\mu}$ Frequencies and speeds are stated throughout this paper in radian measure.

When there is stationary damping but no rotary damping the equations separate out to $y + my + \mu y = 0$, $z + mz + \mu z = 0$; the free motion is damped oscillatory and is therefore always stable; critical speed is still given by $\omega = \sqrt{\mu}$ correct to small quantities of the first order, but the amplitude of steady motion due to a given out-of-balance remains finite at the critical speed.

When rotary damping is present, either with or without stationary damping, the equations of motion are coupled by the terms $\omega n z$, $\omega n y$, and the determinantal equation formed from them is of the fourth degree. The stability of the motion is conveniently examined by Routh's criterion* and it is found that the motion is stable up to the speed

$$\omega = \left(\frac{M}{n} + 1\right)\sqrt{\mu}$$

and is unstable at all higher speeds. Hence a system which includes rotary damping but no stationary damping is unstable at all speeds above the critical speed; while a system which contains both stationary and rotary damping is unstable at all speeds above a certain transition speed which is higher than the critical speed.

A detailed investigation of the character of the free motion can be made by transformation to polar co-ordinates It is found that at any speed the free motion is compounded of two whirls, each in an Archimedean spiral, one with the direction of rotation and the other against it, the angular velocity in either spiral is approximately $\sqrt{\mu}$. At speeds below the transition speed both spirals are of decreasing amplitude, but at speeds above the transition speed the whirl in the direction of rotation is of increasing amplitude. The physical explanation of the tendency of damping in the shaft to produce instability at super-critical speeds may be realized by noting that if there is a possible free vibration, without damping, which consists of circular motion about the bearing axis in the direction of rotation, then rotation of a damped shaft at any speed higher than the free vibration will urge on that motion and therefore tend to increase its amplitude.

Investigation of the out-of-balance motion shows (as might have been expected from physical theory) that stationary damping restricts the amplitude of out-of-balance motion but rotary damping does not.

It was first suggested by Kimball† that rotary friction is a possible cause of shaft whirling at high speeds, and Newkirk outlined the physical explanation of increase of amplitude by rotary friction at high speeds, and showed experimentally the building up of the whirl in shafts where rotary friction due to cramping fit was present. Similar phenomena have been observed as occurring erratically in model rotor tests where there was no deliberate provision of rotary damping, but where occasional slight working loose of the rotor on its shaft may have permitted a rotary frictional effect.

2 3. *Symmetrical Shaft, Unsymmetrical Bearings.*—In this system the shaft characteristics remain symmetrical, but the stiffness and damping of the

---

* 'Advanced Dynamics,' par 287.

† Newkirk, 'Gen. Elec Rev.,' vol 27, p. 169 (1924).

bearing supports vary in different transverse directions. (These conditions are often realized in practice since the bearings of machines with horizontal shafts are usually more flexible in the lateral than in the vertical direction). Choose OY, OZ in the direction of the principal axes of bearing stiffness and in the first place take the principal axes of bearing damping effect as in the same direction. Then bearing characteristics are

$$\mathrm{F}_y = -b'_1 y' - c'_1 y'$$
$$\mathrm{F}_z = -b'_2 z' - c'_2 z'$$

where b'_1 differs from b'_2 and c'_1 and c'_2. The equations of motion formed in the same way as in the previous paragraph are

$$y + (m_1 + n_1)\, y + \sqrt{n_1 n_2}\, \omega z + \mu_1 y = 0 \qquad (7)$$

$$z + (m_2 + n_2)\, z - \sqrt{n_1 n_2}\, \omega y + \mu_2 z = 0 \qquad (8)$$

where m_1, m_2 are stationary damping coefficients, n_1, n_2 are rotary damping coefficients, and μ_1, μ_2 are stiffness/mass coefficients.

When there is no damping the equations are uncoupled, the free motion is simple harmonic with frequency $\sqrt{\mu_1}$ in direction OY and simple harmonic with frequency $\sqrt{\mu_2}$ in direction OZ, the motion is always stable and critical speeds are given by $\omega = \sqrt{\mu_1}$ and by $\omega = \sqrt{\mu_2}$.

When there is stationary damping but no rotary damping, the equations still separate out, the free motion consists of a damped oscillation in each principal direction, the motion is always stable and the critical speeds are practically unchanged.

When rotary damping is present, with or without stationary damping, the equations are coupled. By inspection of the determinantal equation it can be seen (as also in the conditions stated in the previous paragraph) that if the damping coefficients are of the first order of smallness, and if ω is of the same order as $\sqrt{\mu_1}$ and $\sqrt{\mu_2}$, then the presence of the damping coefficients affects the imaginary parts of the roots only to the extent of quantities of the second order of smallness, hence, just as with light stationary damping,* the presence of light rotary damping leaves the natural frequencies of the system unaffected correct to small quantities of the first order. The effect on frequencies of rotary damping becomes sensible, however, when ω is very large in comparison with $\sqrt{\mu_1}$ and $\sqrt{\mu_2}$

---

* Lord Rayleigh, "Theory of Sound," vol. 1, pars. 45 and 102. Macmillan, London (1877).

Examination of the transition speed given by Routh's criterion shows that when μ_1 differs appreciably from μ_2 (that is, when there is considerable lack of symmetry in the bearing stiffness) the transition speed is very high compared with the critical speeds even if there is no stationary damping; that increase in dissymmetry of the bearing stiffness and in intensity of stationary damping relatively to rotary damping raises the transition speed; and that the transition speed is always higher than either critical speed. The physical explanation of the effect of unsymmetrical bearing stiffness in restraining instability due to rotary damping is that since the natural frequencies of the system are different in the two principal transverse directions, there is no tendency to set up a whirl of the type which can be dragged forward by rotary damping until the rotary damping forces have been so far increased by rising speed that they are commensurate with the difference between elastic restoring forces in the two principal directions.

When the principal axes of bearing stiffness do not coincide with the principal axes of damping reaction, additional frictional terms appear in the equations of motion, but the general character of the motion is not thereby altered, except that the equations of motion do not separate out even when there is no rotary damping.

With unsymmetrical bearing stiffness the amplitude of steady motion due to out-of-balance is restricted by rotary damping as well as by stationary damping, but rotary damping has smaller influence in this respect especially if there is only slight dissymmetry of bearing stiffness

The effect of flexibility of the bearings in producing stability at speeds well above the critical speeds in a rotor with rotary damping was discovered experimentally by Newkirk (*loc. cit.*), but it appears doubtful whether he realized that the *unsymmetrical* flexibility of the bearings is the essential feature inducing stability even in the absence of damping in the bearings.

2.4. *Unsymmetrical Shaft, Symmetrical Bearings.*—When the bearings are symmetrically supported, but the shaft has elastic and damping properties varying in transverse directions (such as may be realized in practice by cutting a keyway along a round shaft) the mounting forces when expressed in terms of fixed co-ordinates include coefficients which are periodic functions of the time; but when reference is made to rotating axes, the equations of motion may be brought to the form

$$u + (m_3 + n_3)\, u - 2\omega v + (\mu_3 - \omega^2)\, u - \sqrt{m_3 m_4}\, \omega v = 0 \qquad (9)$$

$$v + (m_4 + n_4)\, v + 2\omega u + (\mu_4 - \omega^2)\, v + \sqrt{m_3 m_4}\, \omega u = 0, \qquad (10)$$

where m_3, m_4 are stationary damping coefficients; n_3, n_4 are rotary damping coefficients, and μ_3, μ_4 are stiffness/mass coefficients. In this form, the equations of motion are linear differential equations with constant coefficients.

When there is no damping the equations of motion become

$$u - 2\omega v + (\mu_3 - \omega^2)\, u = 0$$

$$v + 2\omega u + (\mu_4 - \omega^2)\, v = 0$$

so that even in this case the equations are coupled. The free motions represented by these equations are harmonic referred to rotating axes, and therefore stable, so long as ω lies outside the range $\sqrt{\mu_3}$ to $\sqrt{\mu_4}$; when ω lies within this range the free motion is exponentially increasing, and is therefore unstable. The frequency is zero in rotating co-ordinates at $\omega = \sqrt{\mu_3}$ and at $\omega = \sqrt{\mu_4}$; hence these speeds are critical speeds $\sqrt{\mu_3}$ and $\sqrt{\mu_4}$ are also the irrotational frequencies of the system, *i.e.*, the natural frequencies when the shaft is not rotating. Hence for this system, in the absence of friction, there are two critical speeds which are numerically equal to the irrotational frequencies; motion is unstable at all speeds between these two critical speeds, and stable at all speeds outside that range. When the rotor is acted upon by a transverse disturbing force steady in space (such as gravitational force on a rotor with horizontal shaft), the system vibrates with a whirling motion at a frequency (in fixed axes) which is twice the speed of rotation, and this motion exhibits a sharply resonant increase of amplitude at a speed which is approximately half the mean of the critical speeds.

When there is stationary damping but no rotary damping, the two critical speeds remain equal to the irrotational frequencies and the range of speeds between them is still unstable; speeds outside that range are stable and are characterized by a damped oscillatory free motion.

The determinantal equation for the general case shows that small damping coefficients, representing either stationary or rotary damping, affect the frequencies (referred to rotating axes) by small quantities of the second order when the speed is very low or when the frequency is very low but by small quantities of the first order in other circumstances. Critical speed occurs when one frequency becomes zero in rotating axes; hence the critical speeds are unaltered by damping, correct to small quantities of the first order. When there is rotary damping only, or when the stationary damping is small in comparison with the rotary damping, the motion is stable at all speeds up to the lower critical speed and is unstable at all speeds above. When both practical importance. When ρ is small a sufficiently accurate expression for the four principal critical speeds is

$$\frac{\mu}{\omega^2} = 1 \pm \frac{\rho}{2} \pm \sqrt{\sigma^2 + \left(\frac{\rho}{2}\right)^2}.$$

The system when not rotating has two frequencies in each orientation of the shaft, but these frequencies vary with the orientation over the ranges defined by upper pair and lower pair of angular frequencies f where $\mu/f^2 = 1 \pm \sigma \pm \rho$. The extreme principal critical speeds always lie between the extreme irrotational frequencies. When ρ is large compared with σ, the principal unstable speed ranges cover nearly the whole range between the extreme irrotational frequencies with only a narrow gap of stable speeds about $\omega = \sqrt{\mu}$. When σ is large compared with ρ, each principal unstable speed range covers approximately the middle half of each range of irrotational frequencies. The two frequencies given by $\mu/f^2 = 1 \pm \sigma$ always lie one within each principal unstable speed range; while the odd submultiples of these two frequencies always lie one very close to each minor unstable speed range. High divergence in stationary flexibility favours widely separated unstable speed ranges, high divergence in rotating flexibility favours wide ranges of unstable speed.

Close to each principal critical speed, and at all other speeds excepting close to minor speeds, the steady motion due to out-of-balance is mainly of frequency equal to the rotor speed; but very close to each nth minor critical speed, the largest term in the infinite series for the particular integral represents motion with frequency $n\omega$.

The "even" periodic solutions represent speeds at which resonant vibration occurs under a steady disturbing force of the gravitational type. The highest pair of "even" solutions is given approximately by $\mu/4\omega^2 = 1 \pm \sigma - \frac{3}{8}\rho^2$. The gravitational resonance is fairly sharp at these speeds if ρ is small, and is always very sharp (and easily suppressed by friction) at the submultiple "even" solutions.

With regard to steady motion of the system under a periodic disturbing force in one principal direction of the bearings, rotating unsymmetry introduces coupling between the two principal directions of bearing flexibility and also induces a linkage between motions differing from one another in frequency by 2ω and its multiples; the result of this coupling is that besides the principal resonance of the ordinary type, a sub-principal resonance is introduced for motion in the perpendicular direction, and pairs of minor resonances (very sharply resonant and easily damped out) are set up through motions linked in frequency to that of the disturbance.

When damping is taken into account, additional terms in y, z, ωy and ωz appear in the equations of motion; these terms have as coefficients periodic functions of the time. It is evident by comparison of the characteristics with those already established for the limiting conditions of symmetry in stationary parts alone, or in rotating parts alone, that damping can never render a stable motion unstable below the lowest principal critical speed; but that, at speeds well above the lowest principal critical speed, rotary damping may impart instability to a motion otherwise stable, the transition speed is raised by increase of stationary damping relatively to rotary damping, and by divergence in the principal bearing flexibilities For quasiharmonic motion of another system (see paragraph 6 2) the writer has made detailed calculations of the effect of damping on the principal and minor unstable speed ranges, and has shown that light damping does not appreciably affect the principal unstable speed ranges, but that very light damping is sufficient to render stable the minor unstable speed ranges That a rule of this type holds for all quasiharmonic motion, would be expected from physical theory.

2 6. *Statically Indeterminate Bearings*—When the constraint exercised on the shaft by the bearings is such that the bearing reactions are statically indeterminate (for instance when there are two bearings each constraining the shaft in direction as well as in transverse position) the deflection of the rotor under given mounting forces is no longer the simple sum of two parts, one determined solely by shaft characteristics and the other solely by bearing characteristics. When the elastic and damping characteristics of each portion of the system are known, the overall characteristics are determined by elimination between a number of simultaneous equations; this process yields a result of which the most general form is

$$\mathrm{F}_y = -b_{11}y - b_{12}z - b_{33}\omega y - b_{34}\omega z - c_{11}y - c_{12}z \tag{13}$$

$$\mathrm{F}_z = -b_{22}z - b_{21}y - b_{44}\omega z + b_{43}\omega y - c_{22}z - c_{21}y \tag{14}$$

where c_{11}, c_{12} . . are stiffness coefficients and b_{11}, b_{12} ... damping coefficients; these coefficients are independent of the orientation of the shaft if the shaft is symmetrical, but are periodic in $2\omega t$ if the shaft is unsymmetrical. If the coefficients are constant, transformation to principal elastic axes eliminates the coupling coefficients $c_{12} = c_{21}$, and if the principal axes of damping are in the same direction as the principal elastic axes, the same transformation eliminates $b_{12} = b_{21}$, b_{33}, and b_{34}. Hence the equations of motion for statically indeterminate cases take the same general forms as already discussed in paragraphs 2.2 to 2.5, and the character of the motion is the same.

(3) *Rotor consisting of a Series of Concentrated Masses.*

3 1. *Series of Concentrated Masses.*—The next system discussed is that consisting of a series of concentrated masses mounted at intervals along a weightless flexible shaft which runs in flexibly supported bearings, fig. 2. Symbols referring to the successive masses M_1, M_2, M_3 . M_r are distinguished by the corresponding subscripts. General treatment of this system involves only slight extension of the work of the previous section. The equations of motion (1), (2), (3), (4) remain correct for each individual mass but the forces F_{y_1}, &c., must now be expressed as functions of other co-ordinates as well as of y_1.

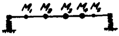

FIG. 2

When connected characteristics influencing the system are arranged with their principal axes oblique to one another, the system is said to be skew For example, if in a two-bearing system with horizontal shaft the principal elastic axes at one bearing support are horizontal and vertical, and at the other bearing support are inclined to the vertical, the bearings in that system are skew. Although a skew case is mathematically more general than an unskewed one, systems which arise in engineering practice are commonly almost completely devoid of skew characteristics. The treatment of unskewed systems is relatively simple since there is no coupling between the two principal transverse directions.

3.2. *Symmetrical Shaft, Symmetrical Bearings.*—Let the system be referred to those co-ordinates θ_1, θ_2 which would have been normal co-ordinates if there had been no damping present. Since the system has $2r$ degrees of freedom there are $2r$ such co-ordinates; they fall into two groups, one group $\theta_1, \theta_2 \,..\, \theta_r$ being formed by certain relations from the y— co-ordinates, and the other group θ_{r+1} . θ_{2r} by identical relations from the z· co-ordinates. The equations of motion then fall into pairs of the type

$$\theta_1 + m_{11}\dot{\theta}_1 + m_{12}\dot{\theta}_2 + \quad + n_{11}(\theta_1 + \omega\theta_{r+1})$$
$$+ n_{12}(\theta_2 + \omega\theta_{r+2}) + \ldots + \mu_{11}\theta_1 = 0 \quad (15)$$
$$\theta_{r+1} + m_{11}\theta_{r+1} + m_{12}\theta_{r+2} + \ldots + n_{11}(\theta_{r+1} - \omega\theta_1)$$
$$+ n_{12}(\theta_{r+2} - \omega\theta_2) + \,..\, + \mu_{11}\theta_{r+1} = 0 \quad (16)$$

where θ_1 and θ_{r+1} are complementary normal co-ordinates.

By the same process which was applied by Lord Rayleigh (*loc. cit.* par. 102) for non-rotating systems, it may be seen that the vibrations mainly in one normal co-ordinate θ_1 are approximately the same as they would have been if the coupling damping coefficients n_{12} . had been absent, unless the frequency in θ_1 is very close to the frequency in another normal mode represented in the same equation. Now θ_1, θ_2 . θ_r all give different frequencies; but θ_{r+1} gives the same frequency as θ_1, θ_{r+2} as θ_2, and so on. Hence the state of affairs for one normal co-ordinate θ_1 is to a first approximation the same as if all the damping terms except m_{11} and n_{11} were suppressed; and consequently the properties established in paragraph 2.2 for a system containing a single mass also characterize the motion of this system in each normal mode, the only important effect of the coupling damping terms being to entail along with forced or free motion in one normal co-ordinate, smaller out-of-phase movements in the other normal co-ordinates to which it is coupled. The r different critical speeds are equal to the respective irrotational frequencies. If there is no rotary damping, the system is stable at all speeds, if there is rotary damping but no stationary damping, the system is stable up to its lowest critical speed and is unstable at all speeds beyond, if there are both stationary damping and rotary damping, the system is stable up to a certain transition speed which is higher than the lowest critical speed, and is unstable at all speeds beyond. The instability due to rotary damping is characterized by the very gradual building up of a whirl in the direction of rotation, of frequency equal to the fundamental critical speed.

3.3 *Symmetrical Shaft, Unsymmetrical Bearings.*—In this case the $2r$ normal frequencies of vibration are independent of the speed, and are in general all different; or if two of them happen to lie close (for any other cause than small divergence in the bearing flexibilities) this can only occur at some frequency high in comparison with the lowest frequency of the system, hence the normal modes of vibration of the system are to a first approximation independent of one another, and as in paragraph 2.3 stability is ensured, even in the presence of rotary damping, up to a speed which is high in comparison with the lowest pair of critical speeds.

3.4. *Unsymmetrical Shaft, Symmetrical Bearings.*—Consider in the first phase an unskewed shaft in a system free from damping. When the equations of motion (referred to axes rotating with the shaft) are rearranged in terms of those co-ordinates which would have been normal co-ordinates if the shaft had not been in rotation, they fall into complementary pairs of the type

$$\theta_1 - 2k\omega\theta_{r+1} + (\mu_1 - \omega^2)\,\theta_1 = 0 \tag{17}$$

$$\theta_{r+1} + \frac{2}{k}\,\omega\theta_1 + (\mu_{r+1} - \omega^2)\,\theta_{r+1} = 0. \tag{18}$$

The solution of these equations indicates that the critical speeds are numerically equal to the irrotational frequencies, and that the system is violently unstable between these two critical speeds but is stable (so far as movements in θ_1 and θ_{r+1} are concerned) at all higher and lower speeds When the shaft is skew, the disentanglement of the normal rotating co-ordinates is less obvious; but examination of the equations of motion of the individual masses shows that the determinant defining the frequencies for zero speed is identical with the determinant defining the speeds for zero frequency. Now zero frequency (referred to rotating co-ordinates) corresponds to a critical speed and to a transition between stability and instability in one pair of degrees of freedom; and by considering the transformation from an unskewed condition to a skewed one by gradual twisting of the shaft, it is evident that the critical speeds occur in pairs complementary to one another and that each pair includes a range of unstable speeds. Hence for any unsymmetrical shaft, whether skew or not, running in symmetrical bearings, the $2r$ critical speeds are respectively equal to the irrotational frequencies, and occur in complementary pairs each of which includes a range of unstable speeds; it is possible for such ranges to overlap one another. The presence of rotary damping, with no stationary damping, renders unstable all speeds above the lowest critical speed; when stationary damping and rotary damping are both present, all speeds above a certain speed higher than the lowest critical speed are rendered unstable by the rotary damping. The system also exhibits resonant vibration (whether or not damping is present) under steady (gravitational) disturbing force at about half the mean speed of each unstable range.

3.5 *Unsymmetrical Shaft, Unsymmetrical Bearings.*—Purely analytical investigation of this case would be cumbersome, but it is clear from physical considerations that the motion of this system is similar to that discussed in paragraph 2.5 but with the phenomena repeated for every additional pair of degrees of freedom, there are $2r$ principal unstable speed ranges, bounded by $4r$ principal critical speeds, all of which lie between the highest and the lowest irrotational frequencies of the system; if the system has no appreciable damping, minor critical speeds may show themselves near the odd submultiples of the frequencies which would be obtained if the shaft were rendered symmetrical (each portion retaining its mean transverse flexibility) while the bearing flexibilities remained unchanged. Gravitational resonances occur near the half and possibly near the other even submultiples of those frequencies.

3.6. *Dynamic Balancing.*—The dynamic balancing of a system consisting of a number of masses, slightly out of balance, carried by a symmetrical shaft in symmetrical bearings, has been studied by Blaess.* He shows that such a system can usually be brought into dynamic balance at a given speed by placing the correct balance weights in any two assigned transverse balancing planes; but that owing to the change in configuration of the unbalanced shaft with speed, the necessary balance weights change with the speed, and that at certain speeds complete balancing in the two assigned balancing planes may be impossible. The same holds good for an unsymmetrical shaft running in symmetrical bearings at any stable speed; but when the bearings are unsymmetrical (whether with symmetrical or with unsymmetrical shaft) the unbalanced shaft changes its configuration during rotation at one given speed as well as changing from one speed to another, in consequence, complete balancing is no longer possible if there are out-of-balance masses not in the assigned balancing planes. The only method of obtaining a perfect balance of a series of masses carried by a flexible shaft in unsymmetrical flexible bearings is to balance each mass separately on the shaft

(4) *Rotor consisting of a Single Uniaxial Rigid Body*

4 1. ***Equations of Motion.***—Consider next the system illustrated in fig 3, where the rotor is a single rigid body, uniaxial about the rotor axis O′A; this axis, fixed in the body, coincides with the bearing axis when the mounting is undeflected. O′ lies in the same transverse plane as the centroid and O′B, O′C are transverse axes fixed in the body and therefore rotating with it, fig. 4. The mass of the body is M and the moments of inertia are A, B and C (which equals B) about the axes O′A, O′B, O′C respectively. If the balance about the rotor axis is imperfect, the static out-of-balance is represented by small centroid displacements u, v, as in Section 2, and the dynamic out-of-balance by small products of inertia E, F about the axes O′B, O′C respectively. The equations of motion of the centroid, referred either to fixed axes OX, OY, OZ or to rotating axes OX, OU, OV, are the same as were established for a concentrated mass in paragraph 2.1. The angular motion of the rotor axis O′A relatively to the bearing axis OX is designated in fixed axes by the angles

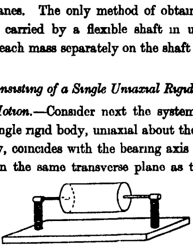

FIG 3

---

* ‘Z angew. Math Mech.,’ vol. 6, p 429 (1926).

ϕ, ψ representing turning about OY, OZ respectively, and in rotating axes by the angles β, γ representing turning about OU, OV respectively. Provided the angles of displacement remain small, the angular equations of motion are in fixed axes

$$B\phi + \omega A\psi - M_\phi + \omega^2 E \cos \omega t + \omega^2 F \sin \omega t = 0 \tag{19}$$

$$B\psi - \omega A\phi - M_\psi + \omega^2 E \sin \omega t - \omega^2 F \cos \omega t = 0, \tag{20}$$

and in rotating axes

$$B\beta - \omega\,(2B - A)\,\gamma - \omega^2\,(B - A)\,\beta - M_\beta + \omega^2 E = 0 \tag{21}$$

$$B\gamma + \omega\,(2B - A)\,\beta - \omega^2\,(B - A)\,\gamma - M_\gamma - \omega^2 F = 0, \tag{22}$$

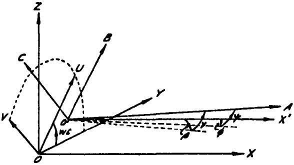

FIG 4

where M_ϕ, M_ψ, etc., are the transverse moments applied to the rotor, either through the elastic and damping reactions of the mounting or by external disturbances. The angular equations of motion are more complicated than those for motion of the centroid on account of the presence of the gyroscopic terms in A, but they are still linear differential equations which when the bearings are symmetrical have constant coefficients if referred to fixed axes, and when the shaft is symmetrical have constant coefficients if referred to rotating axes.

4.2. *Angular Motion uncoupled from Motion of Centroid.*—In many important practical cases (including all those in which the mounting is symmetrical axially about the centre of the rotor) there is no coupling between linear and angular elastic reactions and deflections at the rotor centre; then the moments M_ϕ, M_ψ so far as they arise from elastic and damping reactions can be completely expressed in terms of ϕ, ψ, ϕ and ψ in a manner analogous to the expressions for F_u, F_v in Section 2; the angular movements of the rotor axis are then independent of the movements of the centroid. The characteristics of motion of the centroid are exactly as have been established for a single concentrated mass in Section 2. The characteristics of the angular motion alone are briefly stated in the following paragraphs 4.21 to 4 24.

4.21. *Angular Motion . Symmetrical Shaft, Symmetrical Bearings.*—When shaft and bearings are symmetrical there is only one angular irrotational frequency which is the same in every direction , this frequency is $\sqrt{S/B}$ where S is the angular stiffness of the mounting At any given running speed there are two angular frequencies, one of which is higher than the irrotational frequency and is characterized by forward precession of the rotor axis (*i e.*, revolution of the axis in a cone in the same sense as that of rotation of the rotor) while the other is lower than the irrotational frequency and is marked by backward precession of the axis As the speed increases the higher frequency rises, asymtotically approaching $A/B\ \omega$ which is independent of the elastic properties of the mounting, while the lower frequency falls towards zero For all rotors there is a " backward critical speed " $\omega = \sqrt{S/(B+A)}$ at which the running speed is numerically equal to the frequency of backward precession , mathematically this is not a true critical speed, since analysis shows that out-of-balance alone does not give rise to increase of amplitude at this speed if the conditions of symmetry in the mounting are fulfilled ; but in tests, considerable increase in amplitude when passing this speed has been observed * A critical speed of forward precession occurs at $\omega = \sqrt{S/(B-A)}$ with a long rotor ($B > A$), but with a short rotor ($A > B$) there is no such critical speed In experiments made by the writer, it was observed that a long rotor exhibited very violent vibration at its forward critical speed, and also exhibited some vibration, but less violent and very sharply resonant, at its backward critical speed ; while a short rotor exhibited a small amount of vibration at its backward critical speed.

When there is no damping, or when the damping present is in the stationary parts only, the motion is stable at all speeds. For a short rotor the motion is also stable at all speeds so far as angular movements are concerned even if rotating damping is present When a long rotor is running in a mounting where rotary damping but no stationary damping is present, the motion is stable up to the forward critical speed and unstable at all higher speeds. When both stationary damping and rotary damping act on a long rotor, the angular motion is either stable at all speeds or is unstable at speeds above a certain transition speed which is higher than the forward critical speed ;

---

* First noted by Stodola, " Steam and Gas Turbines " (English Trans.), p. 434 (1927).

stability is favoured by decrease in "length" of the rotor (*i.e.*, by decrease in the ratio B/A) and by increase in intensity of stationary damping relatively to rotary damping.

4.22. *Angular Motion · Symmetrical Shaft, Unsymmetrical Bearings*.—When the bearings are unsymmetrical there are two angular irrotational frequencies. As the speed rises the higher frequency is raised (again ultimately approaching A/B ω) and the lower frequency is lowered. Each normal type of vibration involves precession of the rotor axis in a cone of elliptical section, the higher frequency exhibiting forward precession and the lower frequency backward precession. For long rotors there are two angular critical speeds—the lower one backward and the higher forward—but for short rotors there is only one angular critical speed, that of backward precession Calculation predicts that for long rotors the increase of amplitude due to small out-of-balance should be smaller and more sharply resonant at the lower angular critical speed than at the higher one, and experiments carried out by the writer on rotors running in unsymmetrical bearings have verified this prediction. The amplitude of the motion at the lower critical speed is greater the greater the lack of symmetry of the bearing flexibility.

When no damping is present, or when there is stationary damping only, or when the rotor is short, the angular motion is stable at all speeds. When the rotor is long and rotary damping is present, the motion is sometimes unstable above a transition speed which is always higher than the higher critical speed

4.23. *Angular Motion Unsymmetrical Shaft, Symmetrical Bearings*.—In this system also there are two angular standing frequencies With a short rotor there is no true critical speed, and the angular motion is stable at all speeds, whatever the damping characteristics may be. For a long rotor there are two angular critical speeds which are higher than the respective standing frequencies and the whole range of speeds between is violently unstable. When rotary damping alone is present with a long rotor all speeds above the higher critical speed are rendered unstable by damping; when both stationary and rotary damping are present there may be damping instability above a certain speed not lower than the higher critical speed. With all rotors there is a speed at which a disturbing moment steady in space (analogous to "gravitational" disturbance) sets up resonant vibrations.

4.24. *Angular Motion Unsymmetrical Shaft, Unsymmetrical Bearings*.—The angular motion with shaft and bearings both unsymmetrical is somewhat similar to that for motion of the centroid (paragraph 2.5) but complicated by the gyroscopic action. For the long rotor there are two principal unstable speed ranges, bounded by principal critical speeds, which do not necessarily lie within the range of possible irrotational frequencies; and there are minor unstable speed ranges which are no longer close to exact submultiple speeds For the short rotor, there is only one principal unstable speed range but the minor unstable speed ranges still occur in pairs Principal and minor resonances with steady disturbing moment also occur in pairs. The minor critical and unstable speed phenomena are easily suppressed by damping.

4 3. *General Case. Angular and Linear Motions Coupled.*—When the angular and linear elastic reactions and deflections are coupled at the rotor centre, the angular and linear motions are not independent, but nevertheless over a limited range of speeds the normal modes of vibration of such a system can usually be divided into mainly-linear movements approximating to those described in Section 2 and mainly-angular movements approximating to those described in paragraphs 4 2 to 4 24

A rotor with symmetrical shaft (and therefore with motion harmonic in fixed co-ordinates) has at any speed four definite frequencies in fixed axes, at low speeds the two mainly-linear frequencies are very close to the mainly linear irrotational frequencies, while the mainly-angular frequencies vary quite rapidly with speed owing to the gyroscopic action At high speeds one angular frequency is very low, while the other is very high and asymptotically approaches $A/B\omega$ which is independent of the elastic constraints, the two remaining frequencies approach steady values equal to the frequencies which would be obtained if transverse couples were applied to the rotor constraining its axis to remain parallel to the bearing axis. Such a rotor has three critical speeds if short, and four critical speeds if long. Frequencies and critical speeds are found by solution of determinantal equations of standard type. In the absence of rotary damping, the motion is stable at all speeds, with rotary damping the motion may be unstable above a certain transition speed, which is never lower than the lowest critical speed of forward precession, stability up to high speeds is favoured by increase in relative stationary damping and by increase in lack of symmetry of the bearing flexibilities

The particular integral representing the steady motion of this rotor under out-of-balance conditions in a frictionless mounting has been studied by Blaess (*loc. cit.*), who shows that in steady motion the axis of the unbalanced rotor traces out a surface of which every transverse cross-section save two is an ellipse; but at each of two sections, the ellipse degenerates to a finite straight line. These two straight lines are in general oblique to one another even when the principal axes of the bearings are not skew and the surface changes in form as well as in scale with change in rotor speed. Blaess describes the motion as an "Astigmatic" vibration. It is this astigmatism which obstructs attempts to determine the location of out-of-balance by scribing methods.

A rotor mounted on an unsymmetrical shaft in symmetrical bearings exhibits two ranges of violently unstable speed if long, or one range if short; these ranges are bounded by the critical speeds. This rotor also exhibits two resonant speeds under gravitational disturbances. If the bearings are unsymmetrical as well as the shaft, the principal unstable speed ranges number four (for a long rotor) or three (for a short rotor) and are bounded by the principal critical speeds while minor unstable ranges and minor critical speeds show themselves if the system is sufficiently devoid of damping.

(5) *Rotor consisting of a Series of Uniaxial Rigid Bodies.*

5.1. *Equations of Motion.*—When the rotor consists of r uniaxial rigid bodies (distinguished by subscripts 1, 2, … r) mounted at intervals along a weightless flexible shaft which runs in flexibly supported bearings, the system has $4r$ degrees of freedom. The four equations of motion for the pth disc may be written

$$M_p y_p + \frac{\partial F}{\partial y_p} + \frac{\partial R}{\partial [y_p + \omega z_p]} + \frac{\partial V}{\partial y_p} = 0 \tag{23}$$

$$M_p z_p + \frac{\partial F}{\partial z_p} + \frac{\partial R}{\partial [z_p - \omega y_p]} + \frac{\partial V}{\partial z_p} = 0 \tag{24}$$

$$B_p \phi_p + \omega A_p \psi_p + \frac{\partial F}{\partial \phi_p} + \frac{\partial R}{\partial [\phi_p + \omega \psi_p]} + \frac{\partial V}{\partial \phi_p} = 0 \tag{25}$$

$$B_p \psi_p - \omega A_p \phi_p + \frac{\partial F}{\partial \phi_p} + \frac{\partial R}{\partial [\psi_p - \omega \phi_p]} + \frac{\partial V}{\partial \psi_p} = 0 \tag{26}$$

where the non-rotating dissipation function F is a homogeneous quadratic function of the velocities $y_1, y_2 \ldots; z_1, z_2 \ldots, \phi_1, \phi_2 \ldots; \psi_1, \psi_2 \ldots;$ the rotary dissipation function R is a homogeneous quadratic function of terms of the type $[y_1 + \omega z_1], \ldots; [z_1 - \omega y_1], \ldots; [\phi_1 + \omega \psi_1], \ldots; [\psi_1 - \omega \phi_1], \ldots$, and the potential V is a homogeneous quadratic function of the co-ordinates of the system. The coefficients in the functions F, R, V, are independent of time only when the shaft is symmetrical; otherwise, the coefficients are periodic in 2ω with time. When the shaft is symmetrical the functions F and V possess the properties established by Rayleigh (*loc. cit.*, Chapter IV), and the rotary dissipation function R is similar in character to F.

The equations of motion are always linear differential equations, but if referred to fixed axes have constant coefficients only when the shaft is symmetrical, and if referred to rotating axes have constant coefficients only when the bearings are symmetrical When the equations of motion have constant coefficients a considerable amount of information as to the stability of the motion is gained by inspection of the character of the coefficients in accordance with rules established by Routh* and this inspection is supplemented by analysis similar to that employed in Section 3

5.2. *Symmetrical Shaft.*—When the shaft is symmetrical, the motion is stable at all speeds in the absence of rotary damping. When rotary damping but no stationary damping is present, the motion is unstable above the lowest critical speed of positive precession if the bearings are symmetrical, but is stable up to a much higher speed if the bearings are unsymmetrical. The addition of stationary damping raises the speed of transition to instability. At any speed, there are $4r$ different natural frequencies, these frequencies vary with speed, some slowly and some rapidly When the speed is very great, the motion of the system bears certain resemblances to that of the "gyrostatically dominated" systems investigated by Thomson and Tait,† but (as may be seen by inspection of the fundamental determinant) differs from the latter in that the system here under examination is under gyrostatic domination in only half of its degrees of freedom; the result is that at high speed, of the $4r$ normal frequencies, r are very small, $2r$ are of the same order as the irrotational frequencies, and r are very great, the latter frequencies being commensurate with the speed and nearly proportional to it, and almost independent of the elastic characteristics of the mounting.

If among the r discs constituting the rotor, p are short and $(r - p)$ are long, the number of real critical speeds of the system is $(4r - p)$ This may be proved by counting the number of real critical speeds when the elastic coupling coefficients between the different discs are made zero and then observing that the real roots of the determinant for critical speeds do not alter in number, although they alter in value, when the coupling coefficients are varied in any manner physically possible. When the bearings are unsymmetrical all these $(4r - p)$ speeds which give one frequency numerically equal to the speed are true critical speeds at which out-of-balance alone excites resonant amplitudes; when the bearings are symmetrical, $2r$ of these speeds are "backward critical speeds," at which calculation does not indicate resonance due to out-of-balance alone, although pronounced vibration may be observed in practice at these speeds.

---

* 'Advanced Dynamics,' par. 310, *et seq*

† 'Natural Philosophy,' par. 345.

5.3. *Unsymmetrical Shaft.*—A series of r discs, of which p are short, mounted on an unsymmetrical shaft in symmetrical bearings, exhibits $(2r - p)$ ranges of violently unstable speed, each bounded by two critical speeds This system provides $2r$ gravitational resonances. When the bearings also are unsymmetrical, the system exhibits quasiharmonic motion in which (by analogy with systems previously investigated) there appear $(4r - p)$ principal ranges of unstable speed, bounded by principal critical speeds, and $4r$ principal gravitational resonances, as well as minor resonance phenomena if the system is sufficiently devoid of damping. At speeds above the highest range of unstable speeds, the motion of any system with unsymmetrical shaft is very similar to that of the similar system having a symmetrical shaft of the same mean stiffness.

(6) *Rotor consisting of a Series of Balanced Rigid Bodies of any Shape*

6.1. *Equations of Motion for Unsymmetrical Rotor.*—Consider the case where the rotor is a single rigid body, mounted on the shaft with one principal axis nearly or exactly coincident with the shaft axis, but with the moments of inertia about the other principal axes unequal. Refer to the same axes as in paragraph 4.1, fig. 4, but choose the transverse axes O′B, O′C, in orientation such that there is no product of inertia between them. The notation is unchanged except that B is no longer equal to C. The equations of motion of the rotor for small angular movements are then in fixed axes

$$\frac{\mathrm{B}+\mathrm{C}}{2}\,\phi + \frac{\mathrm{B}-\mathrm{C}}{2}\cdot\frac{d}{dt}\{\phi\cos 2\omega t + \dot{\psi}\sin 2\omega t\}$$
$$+ \omega\mathrm{A}\psi - \mathrm{M}_{\phi} + \omega^2\mathrm{E}\cos\omega t + \omega^2\mathrm{F}\sin\omega t = 0 \quad (27)$$

$$\frac{\mathrm{B}+\mathrm{C}}{2}\,\psi + \frac{\mathrm{B}-\mathrm{C}}{2}\cdot\frac{d}{dt}\{-\psi\cos 2\omega t + \phi\sin 2\omega t\}$$
$$- \omega\mathrm{A}\phi - \mathrm{M}_{\psi} + \omega^2\mathrm{E}\sin\omega t - \omega^2\mathrm{F}\cos\omega t = 0 \quad (28)$$

and in rotating axes

$$\mathrm{B}\beta - \omega y\,(\mathrm{B}+\mathrm{C}-\mathrm{A}) - \omega^2\beta\,(\mathrm{C}-\mathrm{A}) - \mathrm{M}_{\beta} + \omega^2\mathrm{E} = 0 \quad (29)$$

$$\mathrm{C}y + \omega\beta\,(\mathrm{B}+\mathrm{C}-\mathrm{A}) - \omega^2\gamma\,(\mathrm{B}-\mathrm{A}) - \mathrm{M}_{\gamma} - \omega^2\mathrm{F} = 0. \quad (30)$$

The equations of motion of a system including such bodies are therefore always linear differential equations, but the inertia terms expressed in fixed axes include coefficients which are periodic functions of the time; so that the motion of such a system with unsymmetrical bearings is quasiharmonic even if the shaft is perfectly symmetrical. When the bearings are symmetrical, the motion of the system is harmonic in rotating axes whatever the shaft characteristics may be.

6 2. *Quasiharmonic Motion with One Degree of Freedom.*—With an unsymmetrical rotor it is possible to realize a motion of one degree of freedom which is quasiharmonic, and thereby to undertake detailed calculations which would be extremely cumbersome for a system of more than one degree of freedom. The system in question is provided by an unsymmetrical rotor, mounted on rigid shaft, running in bearings which are flexible in one transverse plane only and which provide linear and angular movements uncoupled at the rotor centre; the equation of motion for the angular movement is

$$\frac{\mathrm{B}+\mathrm{C}}{2}\psi-\frac{\mathrm{B}-\mathrm{C}}{2}\cdot\frac{d}{dt}\{\psi\cos 2\omega t\}+\mathrm{R}\dot{\psi}+\mathrm{S}\psi=0, \tag{31}$$

where R is the damping coefficient and S the stiffness coefficient of angular flexibility of the bearings. For this system, in the absence of damping, and with $\rho=\frac{\mathrm{B}-\mathrm{C}}{\mathrm{B}+\mathrm{C}}$, the principal critical speeds which enclose the principal range of unstable speed are given by

$$\frac{2\mathrm{S}}{\mathrm{B}+\mathrm{C}}\cdot\frac{1}{\omega^2}=1-\tfrac{1}{2}\rho-\frac{9}{32}\rho^2+\frac{9}{512}\rho^3 \quad .$$

$$\frac{2\mathrm{S}}{\mathrm{B}+\mathrm{C}}\,\frac{1}{\omega^2}=1+\tfrac{1}{2}\rho-\frac{9}{32}\rho^2-\frac{9}{512}\rho^3$$

and the minor critical speeds and unstable speed range of third order by

$$\frac{2\mathrm{S}}{\mathrm{B}+\mathrm{C}}\cdot\frac{1}{\omega^2}=9-\frac{207}{64}\rho^2-\frac{9}{512}\rho^3 .$$

$$\frac{2\mathrm{S}}{\mathrm{B}+\mathrm{C}}\cdot\frac{1}{\omega^2}=9-\frac{207}{64}\rho^2+\frac{9}{512}\rho^3 \ldots$$

If damping moments of the first order of smallness are present the boundaries of the principal range of unstable speeds are narrowed by amounts of the second order of smallness, and the minor unstable speed range of third order is completely suppressed by damping if the damping coefficient R is greater than a very small value approximately equal to $\frac{27}{512}\rho^3\sqrt{\frac{\mathrm{S}\,(\mathrm{B}+\mathrm{C})}{2}}$.

6.3. *Motion of Unsymmetrical Rotor.*—The only case of motion of an unsymmetrical rotor which the writer has investigated in detail is that of the angular motion of a single unsymmetrical rigid body so mounted that the angular motion is uncoupled from the motion of the centroid. When such a rotor is mounted, on a shaft either symmetrical or unsymmetrical, in symmetrical bearings, there are two true critical speeds enclosing a range of unstable speed if the rotor is long (B and C both greater than A); there is no true critical speed or range of unstable speeds if the rotor is short (B and C both less than A); while if the axis of rotation is the intermediate principal axis ($B > A > C$ or $C > A > B$) there is one critical speed, and all speeds above this are unstable. Unsymmetry of the rotor, when the shaft is symmetrical, does not give rise to "gravitational" resonance When the bearings are unsymmetrical the motion exhibits quasiharmonic characteristics somewhat similar to those produced with an unsymmetrical shaft in symmetrical bearings (paragraph 4 24).

6.4. *Motion of Rotor including a Series of Unsymmetrical Bodies.*—When the bearings are symmetrical, inspection of the equations of motion expressed in rotating co-ordinates shows that critical speeds and unstable ranges of speed occur in a manner very similar to that obtained with uniaxial bodies mounted on an unsymmetrical shaft. When the bearings are unsymmetrical the motion is quasiharmonic and its character is too complicated to be inferred by mere inspection of the equations of motion, but is evidently analogous to those cases of quasiharmonic motion already investigated, the critical speed and unstable speed phenomena being repeated for each additional pair of degrees of freedom of the system

6 5. *Acknowledgments.*—The writer desires to thank Messrs. Metropolitan Vickers Electrical Co., Ltd , for making provision for the experimental work and for other facilities afforded him in the course of preparation of the paper

(7) *Summary and Application of Results.*

7.1. *Outline of Analytical Work.*—It has been shown in the previous sections that the equations of motion of a rotor conforming to the assumptions made are always linear differential equations and are of the following types :—

(*a*) When the rotating parts (rotating masses and shaft) are symmetrical all coefficients are constant in the equations when referred to fixed axes. The motion then exhibits critical speeds, but in the absence of damping in the rotating shaft there are no ranges of unstable speed. When there is damping in the rotating shaft, motion may be unstable above a certain speed which is never lower than the lowest critical speed of positive precession. The speed of transition to instability is raised by increasing the relative intensity of damping on the bearing supports and by rendering the bearing supports unsymmetrical.

(*b*) When the bearing supports are symmetrical, the equations of motion have constant coefficients when referred to rotating axes. If the rotating parts are unsymmetrical, the critical speeds occur in pairs which enclose ranges of violently unstable speed, and, in addition, instability may be produced by shaft damping at speeds above the lowest range of unstable speeds

(*c*) When both stationary and rotating parts are unsymmetrical, the equations of motion when referred to either fixed or to rotating axes include coefficients which are periodic functions of the time The type of motion, called quasiharmonic, is characterized by principal unstable speed ranges bounded by principal critical speeds and also, if the damping in the system is extremely light, by sharply resonant minor critical speeds and minor unstable speed ranges at speeds lower than the principal critical speeds

7 2 *Driven and Free Rotor* —The analysis has assumed a rotor driven from outside the system at constant speed of rotation Examination of the motion of a rotor in free rotation shows that the fluctuation in speed of rotation is a quantity of the second order of smallness, provided that the rotor is in good balance relatively to its inertia about the axis of rotation, that the transverse movements are small, and that the external disturbing forces (if any) produce about the rotor axis a moment which is small compared with the elastic transverse moments involved in the motion , and hence that the analysis of this paper remains valid for a free rotor when those conditions are fulfilled.

7 3. *Validity of Assumptions* —In those practical high-speed rotors where serious vibration trouble may be apprehended, the assumptions as to good balance and as to small amplitude of vibrations are sufficiently well fulfilled. The assumption as to linear relation between deflection and elastic reactions is closely fulfilled unless the vibration is so violent as to cause the journals to cross the clearances in the bearings The assumption as to viscous law of damping, however, is not even approximately fulfilled, and analytical predictions as to the effect of damping are, in consequence, only qualitative. In practice frictional forces arise in various ways and follow various laws ; a severe type of rotary friction sometimes experienced is due to working of the shaft in a cramping fit of the rotor and the effect of this in bringing about instability at super-critical speeds shows itself erratically.

7.4. *Influence of Results on Machine Design.*—This paper indicates certain principles which should be followed in the design and running of high speed machinery in order to secure maximum immunity from vibration trouble.

Unsymmetrical flexibility of the shaft should always be avoided, especially if the machine has to run through a critical speed, and unsymmetrical rotors are likewise undesirable. Damping in the flexible bearing supports always favours stability, but damping in the rotating parts should be avoided when the machine has to run above a critical speed. If instability due to rotary damping has shown itself, the running may be improved by provision of unsymmetrical flexibility in the bearing supports. Unsymmetrical bearing supports may increase the difficulty of balancing a flexible rotor running at a high speed. A rotor should not be run for any length of time close to a critical speed and preferably not at a speed which is close to half one of the normal frequencies of the system.

The First Spark Spectrum of Gold. Au II.

By B. V. Raghavendra Rao, M.Sc., Physics Laboratory, Central College, Bangalore.

(Communicated by Lord Rayleigh, For Sec R S —Received March 16, 1933.)

The spark lines of gold have been measured and wave-length data recorded by a number of observers; chief among these are Exner and Haschek,* Eder and Valenta,* Handke,* L. and E. Bloch,† R J. Lang,† and Takamine and Nitta.† On the basis of their own photograph of the spark spectrum of gold, McLennan and McLay‡ gave the first analysis of Au II. Of the configurations $5d^9\,6s$, $5d^9\,7s$, $5d^9\,6p$, $5d^9\,6d$, and $5d^8\,6s^2$, they have found all the terms resulting from the first three, while for the $5d^8\,6s^2$ and $5d^9\,6d$ configurations only some of the terms have been fixed.

The application of Hund's theory has led to the recognition of the essential regularities in a large number of spectra rich in lines which previously defied analysis. Every new investigation in this field only serves to confirm the view that Hund's theory correctly predicts the important features of a spectrum. This is particularly so if, as is usual, research is confined to the strongest lines and the lowest configurations But when the analysis is sufficiently exhaustive as in the beautiful work of Russell* on Ni I, it is seen that there are some levels which, with our present knowledge cannot be assigned to any electronic configuration, and again there are a number of weak lines remaining unclassified, particularly in the extreme ultra-violet and the infra-red. When as many lines as possible have been analysed on the present ideas in a number of spectra, the residuum of unassignable terms and weak lines will have to form the material for fresh developments Such considerations have prompted the extension of the analysis of the Au II spectrum forming the subject matter of the present paper.

---

* Kayser's "Handbuch der Spectroscopie."

† See R. J. Lang, 'Phil. Trans.,' A, vol. 224, p. 371 (1924).

‡ 'Trans. Roy. Soc. Canada,' vol. 22, p. 103 (1928).

As a result of the present investigation all the terms of the configuration $5d^8\ 6s^2$ have been identified, and nearly all the terms arising from the configuration $5d^9\ 6d$ have been fixed, while a number of terms arising from the configuration $5d^8\ 6s7s$ have been located. More than a hundred lines come under the present classification.

The electronic configurations and the terms expected from each configuration according to Hund's theory are given in Table I.

Table I

Configuration.	Expected terms
$5d^9\ 6s$	^{3}(D), ^{1}(D).
$5d^9\ 6p$	^{3}(F D P), ^{1}(F D P)
$5d^9\ 6d$	^{3}(G F D P S), ^{1}(G F D P S).
$5d^9\ 7s$	^{3}(D), ^{1}(D)
$5d^8\ 6s^2$	^{3}(F P), ^{1}(G D S)
$5d^8\ 6s7s$	^{5}(F P), ^{3}(F F D P P S), ^{1}(G F D P S).

Table II gives the positions of all the levels calculated from $5d^9\ 6s\ ^3D_3$ as zero. This list does not include a large number of terms that were found to give only three combinations and were therefore not considered certain Some thirteen terms whose designations could not be definitely fixed have been marked by the letters *a*, *b*, *c*, *d*, etc. The low group marked *a*, *b*, *c*, *d* is interesting because it is difficult to find a place for these terms in Hund's scheme. They cannot be considered spurious because of the large number of accurate combinations they give rise to. As has already been pointed out similar unaccountable terms are met with in about the same region also in Ni I (Russell, *loc. cit.*).

---

* 'Phys. Rev.,' vol. 34, p. 821 (1929).

Table II.

Configuration.	Term designation.		Term value.
	McLennan and McLay	Author.	
$5d^9\ 6d$	$^3G_5$	$^3G_5$	101952 2
	$^3G_4$	$^3G_4$	101904 2
	—	$^3G_3$	105982 9
	$^3F_4$	$^3F_4$	103126 6
	$^3F_3$	$^3F_3$	102941 6
	—	$^3F_2$	
	$^3D_3$	$^3D_3$	102470 0
	$^3D_2$	$^3D_2$	102988 0
	—	$^3D_1$	106171 0
	—	$^3P_2$	102147 3
	$^3P_1$	$^3P_1$	102256 1
	—	$^3P_0$	104105 1
	$^3S_1$	$^3S_1$	101008 8
	—	$^1D_2$	106425 0
	—	$^1P_1$	102686 8
	$^1S_0$	$^1S_0$	103212 6
	—	$^1G_4$	
	—	$^1F_3$	
$5d^8\ 6s^2$	$^3F_4$	$^3F_4$	25439 3
	—	$^3F_3$	27217 2
	—	$^3F_2$	28808 0
	—	$^3P_2$	32234 0
	—	$^3P_1$	32530 2
	—	$^3P_0$	33242 0
	—	$^1G_4$	32838 0
	$^3P_2$	$^1D_2$	33471 6
$5d^8\ 6s7s$	—	$^5F_4$	94644 2
	—	$^5F_3$	93828 6
	—	$^5F_2$	93184 6
	—	$^5P_3$	100099 5
	—	$^5P_2$	100630 5
	—	$^5P_1$	100875 8
	—	$^3G_4$	101787 6
	—	$^3G_3$	101615 0
	—	$^3F_4$	101034 9
	—	$^3F_3$	101769 3
	—	$^3F_2$	102442 4
	—	$^3D_3$	114271 0
	—	$^3D_2$	119518 0
	—	$^3D_1$	124996 4
	—	$^3P_2$	110771 4
	—	$^3P_1$	112390 3
	—	$^1D_2$	125283 7

Unidentified Terms

a	37137·2	*g*	101637 0
b	42905 8	*h*	102345 1
c	43152·4	*i*	113651 2
d	44164 4	*j*	114356 0
e	93336 4	*k*	126021 2
f	98112 3	*l*	126890·4
		m	130699·1

Table III.

	$5d^9\,6p$	$^3F_4$ 57455 7	$^3F_3$ 49964 2	$^3F_2$ 61620 5	$^1F_3$ 70660 8	$^3D_3$ 59752 1	$^3D_2$ 58138 8	$^3D_1$ 70668 0	$^1D_2$ 71526 0	$^3P_2$ 48014 0	$^3P_1$ 58364 5	$^3P_0$ 67574 5	$^1P_1$ 66820·2
$5d^8\,6s^2$													
$^3F_4$	25439 3	(6) 32016 4	(1) 24524·9	—	(2) 45221·4	(7) 34312 7	—	—	—	—	—	—	—
$^3F_3$	27217 2	—	(1*u*) 22744 1	(3) 34402 3	(1) 43444 6	—	—	—	(1) 44313 7	—	—	—	—
$^3F_2$	28808 0	—	—	—	(3) 40856 4	(3) 30944 5	—	(1) 41859 5	(3) 42718 1	—	(1*u*) 29559 8	—	—
$^3P_2$	32234 0	—	—	—	—	(4) 27515 8	(1*u*) 25904 1	—	(2*r*) 39292 5	—	(2*u*) 26131 6	—	(4) 34383 7
$^3P_1$	32530 2	—	—	—	—	—	—	—	—	(1) 15484 0	(1) 25835 2	(1) 35046 2	(4) 34094 3
$^3P_0$	33242 0	—	—	—	—	—	—	—	—	—	(1) 25121 4	—	(5*r*) 33379 3
$^1G_4$	32838 0	(1*u*) 24617 5	(8) 17126 1	—	—	—	—	—	—	—	—	—	—
$^1D_2$	33471 6	—	—	(1) 28148 8	(3) 37189 3	(6) 26280 8	(6) 24667 2	—	(2) 38054 3	—	(5) 24893 1	—	(2) 33148·8

Table IV

	$5d^9\,6p$	$^3F_4$ 57455 7	$^3F_3$ 49964 2	$^3F_2$ 61620 5	$^1F_3$ 70660 8	$^3D_3$ 59752 1	$^3D_2$ 58138 8	$^3D_1$ 70668 0	$^1D_2$ 71526 0	$^3P_2$ 48014 0	$^3P_1$ 58364 0	$^3P_0$ 67574 5	$^1P_1$ 66620 2
$5d^9\,6d$													
$^3G_5$	101962 2	(6) 44496 5	—	—	—	—	—	—	—	—	—	—	—
$^3G_4$	101904·2	(2) 44449 2	(5) 51941 0	—	—	(2) 42152·7	—	—	—	—	—	—	—
$^3G_3$	105982 9	—	—	(1) 44362 4	(1) 35322 0	—	—	—	—	—	—	—	—
$^3F_4$	103126 6	(5) 45671 0	(2) 53163 0	—	—	(7) 43374 5	—	—	—	—	—	—	—
$^3F_3$	102941 6	—	(2) 52978 0	(2) 41321 4	—	—	(6) 44803 4	—	—	—	—	—	—
$^3D_3$	102470 0	(1) 45014 8	(3) 52506 0	—	—	(3) 42718 1	(1) 44332 1	—	(3) 30944 5	(3) 54434 0	—	—	—
$^3D_2$	102988 0	—	—	(1u) 41367 5	—	(1) 43235·7	(3) 44849 2	(1) 32318 6	—	(8) 54972 2	(2) 44624 0	—	(2) 36368 8
$^3D_1$	106171 0	—	—	—	—	—	—	—	(2) 34644 9	(4) 58156 9	—	(2) 38597·0	—
$^3P_2$	102147·3	—	—	—	—	—	—	—	—	(1) 54133 1	(3) 43782 9	—	—
$^3P_1$	102256 1	—	—	—	—	—	(1) 44118·1	(1) 31587 5	—	—	(4) 43891 6	—	(3) 35636 2
$^3P_0$	104105 1	—	—	—	—	—	—	—	—	—	(1) 45740 5	—	(1) 37484·9
$^3S_1$	101006 8	—	—	—	—	—	( ) 42869 8	—	—	—	(1) 42644 1	—	—
$^1D_2$	106425 0	—	—	(2) 44803 4	(1) 35760 6	—	—	(1) 35757 3	(1) 34899 3	—	—	—	—
$^1P_1$	102686·8	—	—	—	—	—	—	—	—	(2) 54671·7	—	(2) 35113 3	—
$^1S_0$	103212·6	—	—	—	—	—	—	—	—	—	(3) 44849 2	—	(2u) 36592·4

	$5d^9\,6p$	$^3F_4$ 57455 7	$^3F_3$ 49964 2	$^3F_2$ 61620 8	$^1F_3$ 70660 8	$^3D_3$ 59752 1	$^3D_2$ 58138 8	$^3D_1$ 70668 0	$^1D_2$ 71526 0	$^3P_2$ 48014 0	$^3P_1$ 58364·5	$^3P_0$ 67574 5	$^1P_1$ 66620·2
$5d^8\,6s7s$													
$^5F_4$	94644 2	(3) 37189 3	(2) 44679 2	—	—	—	—	—	—	—	—	—	—
$^5F_3$	93828 6	(8) 36375 9	—	(1*u*) 32208 2	(5*u*) 23167 7	—	—	(5) 23167·7	—	—	—	—	—
$^5F_2$	93184 6	—	—	—	(3*r*) 22529 9	(5) 33432 0	(1) 35046 2	—	—	(2) 45169 7	—	—	—
$^5P_3$	100099 5	(1) 42644 1	—	—	—	(2) 41346 8	(1) 41961 3	—	—	(6) 52083 3	—	—	—
$^5P_2$	100630 5	—	—	(1) 39011 0	—	(1) 40878 2	(3) 42491 9	—	—	—	(2) 42271 8	—	—
$^5P_1$	100875 8	—	—	—	—	—	—	(1) 30203 7	—	—	(1) 42511·6	—	(2) 34255·6
$^3G_4$	101787 6	(1) 44332 1	(½) 51823 1	—	—	—	—	—	—	—	—	—	—
$^3G_3$	101615 0	(2) 44161 6	(3) 51652 9	—	(3) 30944 5	(1) 41859 9	—	—	—	—	—	—	—
$^3F_4$	101034 9	(1) 43579 9	(2) 51069 9	—	—	—	—	—	—	—	—	—	—
$^3F_3$	101769 3	(1) 44313 7	(½) 51805 1	—	—	(1) 42018 6	(3) 43625 5	—	—	(4) 53757 7	—	—	—
$^3F_2$	102442 4	—	(1) 52476 9	—	(1) 31782 1	(1) 42691 1	—	(1) 31773 5	—	(3) 54433 6	—	—	—
$^3D_3$	114271 6	—	—	—	—	(2) 54519 7	(2) 56132 5	—	—	(2) 66260 3	—	—	—
$^3D_2$	119518 0	—	—	—	—	(5) 59765 7	(3) 61379 8	—	—	—	—	—	(2) 52891 5
$^3D_1$	124996 4	—	—	—	—	—	—	(3) 54330 1	—	—	(3) 66631 1	—	(1) 58377 1
$^3P_2$	110771·4	—	(1) 60819·1	—	—	—	(2) 52629 9	(1) 40106 3	—	(2) 62758 9	(1) 52405·4	—	—
$^3P_1$	112390 3	—	—	—	—	—	—	—	(1) 40868 2	—	(4) 54024·9	—	(1) 45770·9
$^1D_2$	125283·7	—	—	—	(2) 54618·0	(1) 65530·8	—	(2) 54618·0	(4) 53757·7	—	—	—	—

Tables III, IV, V give respectively the multiplet schemes for the configurations $5d^8\,6s^2$, $5d^9\,6d$ and $5d^8\,6s7s$ Considering that these multiplets result from the combination of high terms with middle terms the absence of certain combinations is to be expected

The terms $^1S_0$ of $5d^8\,6s^2$, $^3F_2$, $^1G_4$ and $^1F_3$ of $5d^9\,6d$, and $^3G_5$, $^1G_4$, $^5F_5$, $^3F_{4,3,2}$, $^1F_3$, $^3P_{2,1,0}$, $^1P_1$, $^3S_1$, $^1S_0$ of $5d^8\,6s7s$ could not be identified with certainty, since some of them do not give many combinations and there are no other reliable criteria available for their location.

The designations here proposed for the terms are based on combining properties, line intensities and the several interval separations. The following comparison with similar spectra, viz, Pd I, Ag II and Ni I, supports the present allocation and justifies the few changes that have been made in the previous analysis of McLennan and McLay.

Configuration.	Terms.	Au II	Ag II.	Pd I.
$nd^9\,(n+1)d$	$^3G_5$			
		−48 0	−12·6	5·0
	$^3G_4$			
		4078 7	4573 2	3538 0
	$^3G_3$			
	$^3F_4$			
		−184 8	−117·3	−13 0
	$^3F_3$			
		?	4664 4	3544·0
	$^3F_2$			
	$^3D_3$			
		518 0	308 0	51·0
	$^3D_2$			
		3183 0	3983 0	3410 0
	$^3D_1$			
	$^3P_2$			
		108 8	3 5	2 0
	$^3P_1$			
		1849 0	1767 7	550 0
	$^3P_0$			

Configuration.	Terms	Au II	Ni I	Configuration.	Terms.	Au II.	Ni I.
$nd^8\,(n+1)\,s^2$	$^3P_2$			$nd^8\,(n+1)s\,(n+2)\,s$	$^5F_4$		
		296	124			−815 6	692 0
	$^3P_1$				$^5F_3$		
		712	283			−644 0	569 0
	$^3P_0$				$^5F_2$		
	$^3F_4$				$^3F_4$		
		1778	1332			735·0	840·0
	$^3F_3$				$^3F_3$		
		1591	884			673·1	734·0
	$^3F_2$				$^3F_2$		

The present assignment of terms in the configuration $5d^8\,6s^2$ also shows an approximate conformity with theoretical predictions of Goudsmit and Pauling* regarding the multiplet separations as will be seen from the following table According to the theory the interval factors of the ^{3}F and ^{3}P terms should be equal. The instance of the similar configuration for Ni I is also given to show that exact conformity with theoretical predictions is not to be expected

Term	Interval factor A	
	Au II	Ni I
$5d^8\,6s^2\ {}^3F$	481 2	317 0
$5d^8\,6s^2\ {}^3P$	336 0	102 0

A list of all the lines involving the terms given in Table II is given in order of decreasing wave-length. The wave-lengths have been taken from the lists in Kayser's "Handbuch" and from the paper of Lang (*loc. cit.*). The wave-lengths are in I.A. The intensities are given as noted by the different observers so that they are not comparable

Observer.	Intensity	I A.	Observed ν vac	Calculated ν vac	Designation.
E. & V	1	6456 52	15483 9	15483 8	$6s^2\,{}^3P_1-6p\,{}^3P_2$
,,	1	6022 74	16599 2	16599 7	$c\ -6p\,{}^3D_2$
,,	8	5837 44	17126 1	17126·2	$6s^2\,{}^1G_4-6p\,{}^3F_3$
,,	1	5726 82	17456 9	17456 1	$d\ -6p\,{}^3F_2$
E & H	2	4760 22	21001 6	21001 6	$a\ -6p\,{}^3D_2$
,,	1u	4583·7	21810 4	21810 4	$6p\,{}^1D_2-\ e$
,,	3r	4437 30	22529 9	22523 8	(?) $6p\,{}^1F_3-6s7s\,{}^5F_3$
,,	2	4420 64	22614 8	22614 9	$a\ -6p\,{}^3D_3$
,,	1u	4410 2	22668 4	22668 4	$6p\,{}^3D_1-\ e$
,,	1u	4395 4	27744 7	22747 0	$6s^2\,{}^3F_3-6p\,{}^3F_3$
,,	5u	4315 14	23167 7	23167 8	$6p\,{}^1F_3-6s7s\,{}^5F_3$
,,	1	4259 97	23467·8	23467 8	$c\ -6p\,{}^1P_1$
,,	2	4083 27	24483·1	24483 3	$a\ -6p\,{}^3F_3$
,,	2	4076 34	24524 9	24524·9	$6s^2\,{}^3F_4-6p\,{}^3F_3$
,,	1u	4061 0	24617 5	24617·7	$6s^2\,{}^1G_4-6p\,{}^3F_4$
,,	6	4052·83	24667 2	24667 2	$6s^2\,{}^1D_2-6p\,{}^3D_2$
				24668 7	$b\ -6p\,{}^3P_0$
,,	5	4016 05	24893 1	24892 9	$6s^2\,{}^1D_2-6p\,{}^3P_1$
,,	1	3979 55	25121 4	25122 5	$6s^2\,{}^3P_0-6p\,{}^3P_1$
,,	1	3880 22	25764 8	25761·9	$6p\,{}^3P_0\ -\ e$
,,	1	3869 60	25835 2	25834·3	$6s^2\,{}^3P_1-6p\,{}^3P_1$
,,	1u	3859 3	25904 1	25904 8	$6s^2\,{}^3P_2-6p\,{}^3D_2$
,,	2u	3825 7	26131 6	26130 5	$6s^2\,{}^3P_2-6p\,{}^3P_1$
,,	6	3803 99	26280 5	26280 5	$6s^2\,{}^1D_2-6p\,{}^3D_3$
,,	1	3773 15	26495 6	26496·4	$d\ -6p\,{}^1F_3$

---

* "Structure of Line Spectra," p. 162.

Observer.	Intensity.	I A	Observed ν vac	Calculated. ν vac.	Designation.
E & H	1u	3653·5	27363 2	27361·6	$d - 6p\,{}^1D_2$
,,	1u	3642 8	27443 6	27444 3	$6p\,{}^3D_1 - f$
,,	2	3635·13	27501 5	27508 4	(?) $c - 6p\,{}^1F_3$
,,	4	3633 25	27515 8	27515 6 27518 1	$c - 6p\,{}^3D_1$ $6s^2\,{}^3P_2 - 6p\,{}^3D_2$
,,	1	3601 08	27761 8	27762 2	$b - 6p\,{}^3D_1$
,,	1	3551 54	28148 8	28148 9	$6s^2\,{}^1D_2 - 6p\,{}^3F_2$
,,	1	3523·35	28374 0	28373 6	$c - 6p\,{}^1D_2$
,,	1	3492 95	28620 9	28620·2	$b - 6p\,{}^1D_2$
,,	1u	3382 0	29559 8	29556 5	$6s^2\,{}^3F_2 - 6p\,{}^3P_1$
,,	1	3320·21	30109 9	30111 0	$6p\,{}^1D_2 - g$
,,	1	3309 90	30203 7	30207 8	$6p\,{}^3D_1 - 6s7s\,{}^3P_1$
,,	1	3273 69	30537 8	30537·8	$6p\,{}^3P_0 - f$
,,	1	3243 37	30823 4	30819·1	$6p\,{}^1D_2 - h$
,,	3	3230 66	30944 5	30944 0 30947 0 30944·1	$6p\,{}^1D_2 - 6d\,{}^3D_3$ $6p\,{}^1F_3 - 6s7s\,{}^3G_3$ $6s^2\,{}^3F_3 - 6p\,{}^3D_3$
,,	1	3228 00	30970 0	30971 0	$6p\,{}^3D_1 - g$
,,	1u	3164 9	31587 5	31588 1	$6p\,{}^3D_1 - 6d\,{}^3P_1$
,,	2	3156 57	31670 8	31677 1	(?) $6p\,{}^3D_1 - h$
,,	1	3146 37	31773 5	31774 4	$6p\,{}^3D_1 - 6s7s\,{}^3F_2$
,,	1	3145 52	31782·1	31781 6	$6p\,{}^1F_3 - 6s7s\,{}^3F_2$
,,	5	3122 50	32016·4	32016 4	$6s^2\,{}^3F_4 - 6p\,{}^3F_4$
,,	1u	3103 9	32208 2	32208 1	$6p\,{}^3F_2 - 6s7s\,{}^3F_3$
,,	1u	3093 3	32318 6	32320 2	$6p\,{}^3D_1 - 6p\,{}^3D_2$
,,	2	3015 82	33148 8	33148 6	$6s^2\,{}^1D_2 - 6p\,{}^1P_1$
,,	5r	2995 00	33379·3	33378 2	$6s^2\,{}^3P_0 - 6p\,{}^1P_1$
,,	5r	2990 28	33432 0	33432·5	$6p\,{}^3D_2 - 6s7s\,{}^3F_2$
,,	2	2982 11	33523 6	33523 6	$a - 6p\,{}^1F_3$
,,	4	2932 19	34094 3	34090 0	$6s^2\,{}^3P_1 - 6p{}^1P_1$
,,	2	2918 40	34255 3	34255 6	$6p\,{}^1P_1 - 6s7s\,{}^3P_1$
,,	10	2913 52	34312·7	34312 8	$6s^2\,{}^3F_4 - 6p\,{}^3D_3$
,,	4	2907 07	34388·7	34386·2 34383 3	$6s^2\,{}^3P_2 - 6p\,{}^1P_1$ $a - 6p\,{}^1D_2$
,,	3	2905 93	34402 3	34403 3	$6s^2\,{}^3F_3 - 6p\,{}^3F_2$
,,	2	2885 58	34644 9	34645 0	$6p\,{}^1D_2 - 6s\,{}^3D_1$
,,	1	2864 54	34899 3	34899 0	$6p\,{}^1D_2 - 6d\,{}^1D_2$
,,	1	2852 54	35046 2	35044 3 35045 8	$6s^2\,{}^3P_1 - 6p\,{}^3P_0$ $6p\,{}^3D_2 - 6s7s\,{}^3F_2$
,,	2	2847 09	35113 3	35112 3	$6p\,{}^3P_0 - 6d\,{}^1P_1$
,,	1	2830·26	35322 1	35322 1	$6p\,{}^1F_3 - 6d\,{}^3G_3$
,,	2	2805 31	35636 2	35635 9	$6p\,{}^1P_1 - 6d\,{}^3P_1$
,,	1	2795·55	35760 6	35764 0	$6p\,{}^1F_3 - 6d\,{}^1D_2$
,,	1u	2748 8	36368 8	36367 8	$6p\,{}^1P_1 - 6d\,{}^3D_2$
,,	8	2748 26	36375·9	36372 9	$6p\,{}^3F_4 - 6s7s\,{}^3F_3$
,,	2U	2732 00	36592 4	36592 4	$6p\,{}^1P_1 - 6d\,{}^1S_0$
,,	3	2688 15	37189 3	37186·5 37189 2	$6p\,{}^3F_4 - 6s7s\,{}^3F_4$ $6s^2\,{}^1D_2 - 6p\,{}^1F_3$
,,	1	2666·95	37484 9	37484 9	$6p\,{}^1P_1 - 6d\,{}^3P_0$
,,	2	2627 04	38054·3	38054 4	$6s^2\,{}^1D_2 - 6p\,{}^1D_2$
,,	2u	2590 10	38597 0	38596 5	$6p\,{}^3P_0 - 6d\,{}^3D_1$
,,	1	2562 61	39011 0	39010 0	$6p\,{}^3F_2 - 6s7s\,{}^3P_2$
,,	2r	2544 25	39292 5	39292 0	$6s^2\,{}^3P_2 - 6p\,{}^1D_2$
,,	1	2515·10	39747 9	39747 8	$6p\,{}^3P_1 - f$
,,	1	2492 62	40106·4	40106 3	$6p\,{}^3D_1 - 6s7s\,{}^3P_2$
,,	2	2477 76	40346 8	40347·4	$6p\,{}^3D_2 - 6s7s\,{}^3P_2$
,,	1	2446 15	40868 2	40868 2	$6p\,{}^1D_2 - 6s7s\,{}^3P_1$
,,	1	2445 55	40878·2	40878 4	$6p\,{}^3D_3 - 6s7s\,{}^3P_2$
,,	1u	2419 32	41321 4	41321·1	$6p\,{}^3F_3 - 6d\,{}^3F_3$
,,	1u	2416 62	41367 5	41368 5	$6p\,{}^3F_2 - 6d\,{}^3D_1$
,,	1	2388 39	41856 4	41852 8	$6s^2\,{}^3F_2 - 6p\,{}^1F_3$

Observer	Intensity	I.A.	Observed ν vac.	Calculated. ν vac.	Designation
E & H	1	2388 10	41859 9	41862·9	$6p\ ^3D_3-6s7s\ ^3G_3$
				41860 0	$6s^2\ ^3F_2-6p\ ^1D_2$
,,	1	2382·42	41961 3	41960·7	$6p\ ^3D_2-6s7s\ ^5P_2$
E	1	2379 17	42018 6	42017 2	$6p\ ^3D_2-6s7s\ ^3F_2$
E & H.	1	2373·18	42124·7	42125 2	$6p\ ^1D_2-\ i$
,,	2	2371 60	42152 7	42152 1	$6p\ ^3D_3-6d\ ^3G_4$
,,	2	2364 58	42277 9	42266 0	(?) $6p\ ^3P_1-6s7s\ ^5P_2$
,,	3	2352·67	42491·9	42491 7	$6p\ ^3D_2-6s7s\ ^5P_2$
,,	1	2351·58	42511 6	42511 3	$6p\ ^3P_1-6s7s\ ^5P_1$
,,	1	2347 13	42592 2	42593 0	$6p\ ^3D_2-\ h$
,,	1	2344 27	42644 1	42643 8	$6p\ ^3F_4-6s7s\ ^5P_3$
				42644 3	$6p\ ^3P_1-6d\ ^3S_1$
E.	1	2341 69	42691 1	42690·3	$6p\ ^3D_3-6s7s\ ^3F_2$
E & H.	3	2340 21	42718 0	42718 1	$6s^2\ ^3F_4-6p\ ^1D_2$
,,	1*n*	2334·1	42829 9	12830 0	$6p\ ^1D_2-\ j$
,,	?	2331 93	42869 8	42870 0	$6p\ ^3D_2-6d\ ^3S_1$
,,	1	2325·74	42983 8	42983 2	$6p\ ^3D_1-\ i$
,,	1	2312·27	43235 7	43235 9	$6p\ ^3D_2-6d\ ^3D_2$
,,	4	2304·82	43375 8	43372 2	$6p\ ^3F_3-\ e$
				43374 5	$6p\ ^3D_3-6d\ ^3F_4$
,,	1	2301 07	43444 6	43442 6	$6s^2\ ^3F_3-6p\ ^1F_3$
E.	1	2298·18	43499 2	43498 2	$6p\ ^3D_2-\ g$
E & H	1	2293 93	43579 9	43579 2	$6p\ ^3F_4-6s7s\ ^3F_4$
,,	3	2291 53	43625 5	43630 5	$6p\ ^3D_3-6s7s\ ^3F_3$
,,	1	2288·25	43688 0	43688 0	$6p\ ^3D_1-\ j$
,,	1	2287 68	43698 9	43695·2	$6p\ ^1F_3-\ j$
,,	3	2283 35	43782 9	43782 8	$6p\ ^3P_1-6d\ ^3P_2$
,,	2	2277 68	43891 9	43891 6	$6p\ ^3P_1-6d\ ^3P_1$
,,	1	2266 03	44118 1	44117 3	$6p\ ^3D_2-6d\ ^3P_1$
,,	2	2263·81	44161·6	44159 3	$6p\ ^3F_4-6s7s\ ^3G_3$
,,	1	2261·38	44207 1	44206 3	$6p\ ^3D_1-\ h$
,,	1	2255 94	44313 7	44313 6	$6p\ ^3F_4-6s7s\ ^3F_3$
				44308 8	$6s^2\ ^3F_3-6p\ ^1D_2$
,,	1	2255 0	44332·1	44331 9	$6p\ ^3F_4-6s7s\ ^3G_4$
				44331 2	$6p\ ^3D_3-6d\ ^3D_3$
,,	1	2253 46	44362 4	44362 4	$6p\ ^3F_2-6d\ ^3G_3$
,,	1	2249 06	44449 2	44448·5	$6p\ ^3F_4-6d\ ^3G_4$
,,	2	2246 66	44496 5	44496 5	$6p\ ^3F_4-6d\ ^3G_5$
,,	1	2240 33	44624 0	44623 5	$6p\ ^3P_1-6d\ ^3D_2$
,,	1	2237 48	44679 2	44680·0	$6p\ ^3F_3-6s7s\ ^3F_4$
,,	2	2231 33	44803 4	44802 8	$6p\ ^3D_3-6d\ ^3F_3$
				44804 5	$6p\ ^3F_3-6d\ ^1D_2$
,,	3	2228 98	44849 2	44849 2	$6p\ ^3D_3-6d\ ^3D_3$
				44848 1	$6p\ ^3P_1-6d\ ^1S_0$
McLennan	1	2220 82	45014 8	45014 3	$6p\ ^3F_4-6d\ ^3D_3$
E & H	2	2213 19	45169 7	45170 6	$6p\ ^3P_2-6s7s\ ^5F_3$
,,	2	2210 68	45221 4	45221 5	$6s^2\ ^3F_4-6p\ ^1F_3$
,,	1	2205·90	45318 8	45322 4	$6p\ ^3P_2-\ e$
E.	1	2188·89	45671·0	45670 9	$6p\ ^3F_4-6d\ ^3F_4$
,,	1	2185 56	45740 5	45740 6	$6p\ ^3P_1-6d\ ^3P_0$
,,	1	2184·11	45770·9	45770 1	$6p\ ^1P_1-6s7s\ ^3P_1$
		λ vac.			
,,	1	1996 08	50098 2	50098·3	$6p\ ^3F_2-\ f$
H.	2	1958·1	51069·9	51070·7	$6p\ ^3F_3-6s7s\ ^3F_4$
,,	3	1936·0	51652 9	51650 8	$6p\ ^3F_3-6s7s\ ^3G_3$
,,	2	1935·1	51676 9	51672·8	$6p\ ^3F_2-\ g$
E	½	1930·31	51805·1	51805·1	$6p\ ^3F_3-6s7s\ ^3F_3$
,,	½	1929·64	51823·1	51823 4	$6p\ ^3F_3-6s7s\ ^3G_4$
,,	5	1925·28	51941·0	51940 0	$6p\ ^3F_3-6d\ ^3G_4$

Observer.	Intensity	λ vac	Observed ν vac	Calculated ν vac	Designation.
E.	6	1920 0	52083 3	52085 5	$6p\,{}^3P_2-6s7s\,{}^3P_2$
,,	1	1908 2	52405 4	52406 0	$6p\,{}^3P_1-6s7s\,{}^3P_2$
,,	1	1905 6	52476 9	52478 2	$6p\,{}^3F_3-6s7s\,{}^3F_3$
McLennan	1*u*	1904 57	52506 0	52505 8	$6p\,{}^3F_2-6d\,{}^3D_2$
H	2	1900·6	52629 9	52633 4	$6p\,{}^3D_2-6s7s\,{}^3P_2$
,,	6	1891 1	52891 5	52897 8	$6p\,{}^1P_1-6s7s\,{}^3D_2$
,,	6	1887 6	52977 4	52977 4	$6p\,{}^3F_3-6d\,{}^3F_3$
McLennan	2	1881 01	53163 0	52172 4	$6p\,{}^3F_3-6d\,{}^3F_4$
H	4	1860 2	53757 7	53757 7 53755 3	$6p\,{}^1D_2-6s7s\,{}^1D_2$ $6p\,{}^3P_2-6s7s\,{}^3F_2$
,,	4	1851 0	54024 9	54025·8	$6p\,{}^3P_1-6s7s\,{}^3P_1$
,,	1	1847 3	54133 1	54133·3	$6p\,{}^3P_2-6d\,{}^3P_2$
,,	3	1840 6	54330 1	54328 4	$6p\,{}^3D_1-6s7s\,{}^3D_1$
,,	3	1837·1	54433 6	54428·4	$6p\,{}^3P_2-6s7s\,{}^3F_2$
McLennan	4*d*	1836·2	54458 0	54456 0	$6p\,{}^3P_2-6d\,{}^3D_3$
H.	3	1835 0	54495 9	54495 2	$6p\,{}^1D_2-\ k$
,,	2	1834 2	54519 7	54519 5	$6p\,{}^3D_2-6s7s\,{}^3D_3$
,,	2	1830 9	54618 0	54615 7	$6p\,{}^3D_1-6s7s\,{}^1D_2$
,,	1	1829·1	54671 7	54672 8	$6p\,{}^3P_1-6d\,{}^1P_1$
,,	3	1819 1	54972 2	54974 0	$6p\,{}^3P_2-6d\,{}^3D_2$
,,	4	1806 6	55352 6	55353 2	$6p\,{}^3D_1-\ k$
,,	2	1781 5	56132 5	56132 8	$6p\,{}^3D_2-6s7s\,{}^3D_3$
,,	4	1719 5	58156 4	58157 0	$6p\,{}^3P_2-6d\,{}^3D_2$
,,	1	1713 0	58377 1	58376 2	$6p\,{}^1P_1-6s7s\,{}^3D_1$
,,	5	1673 2	59765 7	59765 9	$6p\,{}^3D_3-6s7s\,{}^3D_3$
,,	1	1665 6	60038 4	60038 3	$6p\,{}^1F_3-\ m$
,,	2	1659 2	60270 0	60270 2	$6p\,{}^1P_1-\ l$
,,	1	1644 2	60819 9	60807 2	$6p\,{}^3F_2-6s7s\,{}^3P_2$
B	3	1629 2	61379 8	61379 2	$6p\,{}^3D_2-6s7s\,{}^3D_2$
,,	2	1593·4	62758 9	62767 4	$6p\,{}^3P_2-6s7s\,{}^3P_2$
,,	1	1552·8	64399 8	64391 8	$6p\,{}^3F_2-\ j$
,,	1	1526 0	65530 8	65531 6	$6p\,{}^3D_2-6s7s\,{}^1D_2$
,,	2	1509 2	66260 3	66257 6	$6p\,{}^3P_2-6s7s\,{}^3D_2$
,,	3	1500 8	66631 1	66631 9	$6p\,{}^3P_1-6s7s\,{}^3D_1$
,,	1	1459 3	68526 0	68525 9	$6p\,{}^3P_1-\ l$
,,	1	1454·5	68753 2	68751·6	$6p\,{}^3D_2-\ l$
,,	1	1447 1	69075 4	69078 6	$6p\,{}^3F_2-\ m$
Lang	1	1378 5	72542 0	72560 3	$6p\,{}^3D_2-\ m$

NOTE.—E & V, Eder and Valenta, E & H, Exner and Haschek, E, Eder, H., Handke B, L. and E. Bloch.

In conclusion I desire to express my best thanks to Professor B Venkatesachar and T. S. Subbaraya for their kind interest and helpful criticism.

Summary

The paper embodies an extension of the analysis of the Au II spectrum. The configurations considered are $5d^8\,6s^2$, $5d^9\,6d$ and $5d^9\,6s7s$. Of the terms arising from the first two configurations, some definitely and some tentatively have been fixed by McLennan and McLay, the first to classify the lines of this spectrum. In the present paper thirty terms have been newly located and more than one hundred lines classified. To make the list self-contained other relevant lines have been included.

Investigations in the Infra-Red Region of the Spectrum. Part IX — *The Absorption Spectrum of Chlorine Monoxide* (Cl_2O).

By C R Bailey and A. B. D Cassie, The Sir William Ramsay Laboratories of Inorganic and Physical Chemistry, University College, London

(Communicated by F G Donnan, F R S —Received April 13, 1933)

Recent applications of quantum mechanics to polyatomic molecules have given new theoretical rules governing molecular structure, and seem likely to provide much information regarding the nature of the forces acting between the constituent atoms In many cases we find that the bonds between neighbouring atoms may be classified according to the resultant component of angular momentum of the bonding electrons in the direction of the line joining the atoms Thus bonds may be of the σ-, π-, δ- and similar types, together with the non-localized bond obtained when the electrons available for bond formation are present in excess of the number usually required Theory has almost outrun experiment in that data, especially of a spectroscopic nature, are at present confined to the simpler triatomic molecules in which no great constitutional difficulties are to be expected, and apart from the somewhat indefinite and doubtful hypotheses of semipolar and one-electron bonds, there is no experimental result which contradicts classical theory yet finds a natural explanation in quantum mechanics

The structure of Cl_2O provides such a crucial test. The molecule consists of two atoms of chlorine each of large polarizability compared with the central oxygen atom to which they are joined, if the stability of a molecule be determined by the polarizability of the constituent atoms, the substance should have a linear structure, apart from any *ad hoc* evidence adduced from other sources as to the angle between two oxygen bonds. According to the quantum mechanics, however, the stable structure of a molecule is determined not by the polarizability alone, but rather by a combination of the polarizability of the atoms, and by the interactions of the valency electrons, the second factor playing by far the larger part in determining the structure. We shall see that the triangular molecule with a vertical angle not far removed from 90° is demanded by the quantum theory and supported by the experimental evidence. The gas absorbs continuously in the ultra-violet, and evidence as to the fundamental frequencies and force constants must consequently be sought in the infra-red.

Experimental.

The apparatus was similar to that used in the investigation of chlorine dioxide * The gas required careful drying since the presence of traces of water vapour leads to rapid attack of the rocksalt end-plates, and the samples used were obtained by repeated distillation over phosphoric oxide We are indebted to Mr and Mrs Goodeve of this Department for their kind advice in the preparation of this substance

Observations

The region investigated lay between 1 and 18 μ, and four bands were observed Their characteristics are recorded in Table I

Table I —The Infra-red Absorption Spectrum of Cl_2O

Band	Band centre		Maxima		$\Delta\nu$ for P − R (cm^{-1})	Intensity	Prism
	λ (μ)	ν_e (cm^{-1})	λ	ν			
A	15 63	640	15 91	628	23	30 (5)	Sylvine
			15 35	651			
B	10 28	973	10 33	967	13	50 (5)	Rocksalt
			10 28	973			
			10 20	980			
C	8 033	1245	8 111	1233	27	20 (10)	Rocksalt
			7 937	1260			
D	7 625	1311	7 625	1311	-	10 (10)	Rocksalt

The estimates of intensity at the slit-width used (the figure in brackets gives the extent of spectrum included in wave numbers) are rough approximations, the maximum pressure used for the preliminary exploration being that of Cl_2O at 0° C., some 70 cm of mercury.

Individual Bands

***Band A at* 15·63 μ**—This is shown in fig. 1, in company with the 14 87 μ band of CO_2. The two bands always appeared together and with much the same relative intensities, curve (*a*) was obtained with a smaller slit-width and lower pressure, and the doublet separation is the same as that given by

---

* Part VI, 'Proc. Roy. Soc.,' A, vol. 137, p. 622 (1932).

Schaefer and Philipps* for the long-wave CO_2 fundamental, the band centres also coinciding. When the origin of the more intense component was suspected, fresh samples of the monoxide were prepared, but it was found impossible to remove the impurity. It is probable that CO_2 dissolves in liquid Cl_2O, and the maintenance of the relative intensities indicates that we may be dealing with a constant boiling point mixture, we have since learnt that solid sodium hypochlorite or normal calcium hypochlorite may be obtained, and distillation of a sample over either of these substances might offer a means of purification, but this has not been tried. No appreciable absorption was observed in the neighbourhood of the 4·25 μ CO_2 band but Burmeister's original examination† shows that this band has only approximately one-tenth of the intensity of the band at 14·87 μ. On freezing the mixture, CO_2 seemed to be given off, since a white frost appeared on the central stem of the trap, but even by warming the upper part while keeping the monoxide frozen effected no appreciable separation on pumping off. The frequent attempts to remove the impurity were made not so much because of doubt as to the origin of the band, but because consideration of the isotope effect shows that it is possible that there may be a second Cl_2O band obscured by the CO_2.

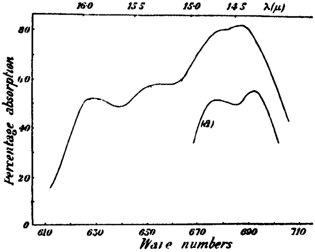

FIG 1

Band B at 10·28 μ (973 *cm.*$^{-1}$); fig 2.—Trouble was experienced in the examination of this band since it appeared to gain in intensity with time;

---

* 'Z. Physik,' vol. 36, p. 641 (1926).

† 'Verh. deuts. phys Ges,' vol 15, p. 589 (1913).

the peculiarity was due to the presence of traces of water vapour which caused the monoxide to attack the rocksalt plates. Repeated distillation over phosphoric oxide at length produced a sample without effect on these, and with the band intensity completely under control. The solid obtained in the reaction may be sodium hypochlorite, the attacked plates absorbing at exactly the same wave-length as the gas. The band appears to have a Q branch, and is considerably narrower than the others.

Band C at 8·033 μ (1245 *cm.*$^{-1}$); fig. 3.—No difficulty was experienced in reproducing the observations for this band, and the peculiar contour with the flat portion between the two somewhat indistinct maxima is characteristic and definite. It will be seen that consideration of the isotope effect is required for the interpretation of the envelope.

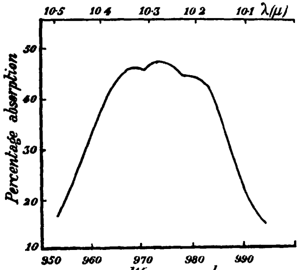

Fig. 2.

Band D at 7·625 μ (1311 *cm.*$^{-1}$).—No resolution was achieved, and the single maximum obtained is indicated at the short wave end of fig. 3.

The Band Assignments

From the intensity of the bands, and from the isotope effect, it seems reasonable to assume that in Dennison's classification,* ν_1 and ν_3 are to be allotted to the two strong bands at 8·03 and 10·28 μ. One of these must be the asymmetrical vibration ν_3, and since band B at 10·28 μ is much the more intense in the infra-red, it is probable that it represents this fundamental mode, and that ν_1 is band C at 8·03 μ. The long-wave fundamental, ν_2, is more difficult to place, on account of the rigidity of the molecule as defined below, it is very likely that this symmetrical mode is responsible for band A at 15·63 μ, and consistent solutions for the force constants are obtained on this supposition. In spite of the comparative heaviness of the atoms, the type of structure for this molecule (as in H_2O and H_2S) demands a rather high frequency for this mode. The possibility that the observed band is the first harmonic of another at some 340 cm $^{-1}$ has not been neglected, but does not lead to concordant solutions. Band D at 1311 cm $^{-1}$ is probably $2\nu_2$, the calculated value is 1280 cm $^{-1}$, and although it is uncommon to find the observed value of a band

---

* 'Rev. Mod. Phys.,' vol. 3, p. 289 (1931).

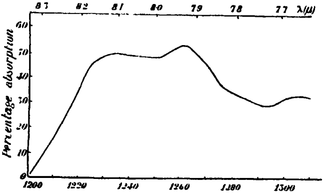

FIG. 3.

greater than the calculated value, the effect may be due to interaction between the electron shells of the chlorine atoms. It is to be noticed that unlike SO_2 and ClO_2, the monoxide has the asymmetric vibration, ν_3, at a lower frequency than the symmetric ν_1. The effect depends upon the masses of the atoms and upon the ratio of the force constants in the molecule, and a full discussion is given by Kohlrausch* when various vertical angles are considered.

The Chlorine Monoxide Molecule

When the fundamental frequencies have been selected, and inserted in formulæ (1) and (3) of Part VI (*loc. cit.*) various possible semi-vertical angles emerge, and for each possible value one of the fundamental frequencies corresponds to a mode whose effective electric doublet lies perpendicular to the bisector of the vertical angle, the other two having effective doublets parallel to this line. Again, the least axis of inertia must be parallel or perpendicular to this bisector, and the choice between the two directions is determined by the known vertical angle Hence the orientation of the various effective electric doublets relative to the least axis of inertia is known for all possible angles, and the selection rules tell us that for fundamental bands Q branches should appear only when the effective electric doublet is parallel to the least axis of inertia. The presence or absence of Q branches is thus final in deciding which of the possible vertical angles is correct.

---

* "Der Smekal-Raman Effekt," p. 173 (1931)

Table II --Possible Semi-vertical Angles, Transverse Frequencies, and Force Constants for Cl_2O

Transverse frequency, ν_3 (cm $^{-1}$)	Central force system			Valence force system		
	Possible semi-vertical angle, α	K(Cl—O) dynes/cm × 10^5	K(Cl—Cl) dynes/cm × 10^5	Possible semi-vertical angle, α	K(Cl—O) dynes/cm × 10^5	K dynes/cm. × 10^5
	°			°		
640	25	4·7	15	35	3·5	68
	17	5·8	11			
973	54	5·1	12	No solution		
	36	7·8	4·5			
1245	No solution			No solution		

The solutions obtained when the three fundamental frequencies are in turn considered as the asymmetric frequency, ν_3, are given in Table II. The force constants K (Cl—O) and K (Cl—Cl) are the ordinary linear coefficients, K_ϕ is the tangential restoring force per unit arc displacement of the vertical angle and appears only in the valence force system. The only possible solution with the latter system is provided by the unlikely assumption that the long-wave fundamental, A, represents the asymmetric vibration, and the value of K_ϕ obtained on this supposition is so large as to exclude this possibility, apart from other considerations. The solution in the same system with band B at 973 cm $^{-1}$ as ν_3 gives $\sin \alpha$ as 1·06; with the approximations of the theory, this value might represent a rectilinear molecule, but in this case the asymmetric frequency becomes the asymmetric linear vibration, and the Cl—O force constant drops to 3·5 × 10^5 dynes/cm., and by analogy with other triatomic molecules is excluded. Furthermore, simple calculation supplies the approximate positions of the other bands, and no agreement with observed results is found It is unfortunate that no Raman spectrum is available for either Cl_2O or the hypochlorites, since the most powerful line in this spectrum has a displacement corresponding to the most symmetrical vibration, ν_1. The highest fundamental frequency in a rectilinear molecule is invariably the asymmetric mode, and if the binding corresponds to a single valence stroke as is probable in this case, the force constant is some 6×10^5 dynes/cm Band B is too intense to be any but a fundamental tone, and it cannot be the symmetrical vibration in a symmetrical triatomic molecule as it must then be inactive in the infra-red The possibility of the rectilinear structure is thus excluded on several counts

In the possible triangular forms we have to determine the orientation of the least axis of inertia with respect to the bisector of the vertical angle This axis is parallel or perpendicular to the bisector as $\tan^2 \alpha <$ or $> 1/(1 + 2m/M)$, and for Cl_2O this gives a critical value for the vertical angle, 2α, of 46° The transverse fundamental mode has an effective electric doublet normal to the bisector, and the symmetric modes have doublets parallel to this line, the effective doublets for the harmonics of the transverse mode are alternatively parallel and normal to the bisector, while the doublets for the harmonics of the symmetric modes are always parallel to this line Knowing the possible solutions of the frequency equations, we can orientate the effective electric doublets with regard to the least axis of inertia; the results are summarized in Table III.

Table III —Orientation of the effective electric doublets with respect to the least axis of inertia for possible solutions of the frequency equation.

Band, cm⁻¹	Central force system			Valence force system
	Vertical angle 2α			Vertical angle 2α
	50°	34°	72° or 108°	70°
640	Parallel	Perpendicular	Perpendicular	Parallel
973	Perpendicular	Parallel	Parallel	Perpendicular
1245	”	”	Perpendicular	”
1311	”	”	”	”

The band at 973 cm.$^{-1}$ is the only fundamental whose contour definitely suggests the presence of a Q branch due to asymmetry of the moments of inertia, and Table III indicates that the only solutions consistent with the observed contours are those with 973 cm $^{-1}$ as the asymmetric frequency, giving on the central force system vertical angles of either 72 or 108°. The oxygen angle in the ethers has been determined by collision area methods, and from considerations of the dipole moments, and the bonds are found to be almost invariably at an angle of 110° to each other.* The approximations introduced enable us to say that in the case of chlorine monoxide, the vertical angle is slightly greater than 90°.

The Isotope Effect

Further supporting evidence is provided by the isotope effect. The principal isotopes of chlorine have atomic weights of 35 and 37, in the frequency ratio of three to one. The probability of the chlorine atom in the dioxide having mass 35 is $\frac{3}{4}$ and for mass 37 is $\frac{1}{4}$, and the ratio of the intensity of the bands $Cl^{35}O_2$ to those of $Cl^{37}O_2$ is 3 : 1. Since the bands overlap to a large extent, the latter are almost unobservable with the resolution attained, but conditions are much more favourable with the monoxide. The relative intensity of the bands due to $(Cl^{35})_2\,O$ and $(Cl^{35}Cl^{37})\,O$ gives a ratio of less than 3 : 1, the probability of the first molecule is 9/16, of the second 6/16, and of $(Cl^{37})_2O$ is 1/16 bands due to the last molecule may be neglected as too weak to detect under the experimental conditions, but the $(Cl^{35}Cl^{37})_2O$ band has an intensity 2/3 of that of the $(Cl^{35})_2O$ band, and should therefore be observable.

The isotope separation can be estimated from the frequency formula, and the central force system is adopted as giving the possible solution. The frequency of the asymmetric mode is given by

$$n_3^2 = K_1\,[1/m + (2\sin^2\alpha)/M], \tag{1}$$

where n is $2\pi c\nu$, M and m the masses of the oxygen and chlorine atoms, α the semi-vertical angle, and K_1 the Cl—O force constant. Differentiating with respect to m gives

$$\Delta n_3 = -\,\Delta m K_1/2m^2 n_3. \tag{2}$$

Formula (2) gives the isotope separation of bands due to $(Cl^{35})_2O$ and $(Cl^{37})_2O$, and we shall assume that the separation of bands due to $(Cl^{35})_2O$ and $(Cl^{35}Cl^{37})_2O$ is one-half this value.

---

* Freudenberg, "Stereochemie," p. 262 (1932)

The symmetrical frequencies are given by

$$n_{1,2}^2 = \frac{1}{2m}\left[2K_2 + \left(1 + \frac{2m}{M}\cos^2\alpha\right)K_1 \pm \sqrt{4K_2 + \left[4 - 8\left(1 + \frac{m}{M}\right)\cos^2\alpha\right]K_1K_2 + \left(1 + \frac{2m}{M}\cos^2\alpha\right)^2 K_1^2}\right], \tag{3}$$

where K_2 is the Cl—Cl force constant Differentiating with respect to m we have

$$\Delta n_i = -\frac{\Delta m}{2m}n_i + \frac{\Delta m K_1\cos^2\alpha}{mMn_i}\cdot\frac{mn_i^2 - 2K_2}{2mn_i^2 - \left[2K_2 + \left(1 + \frac{2m}{M}\cos^2\alpha\right)K_1\right]} \tag{4}$$

The required separation is again assumed to be one-half that given by (4)

On insertion of the experimental value $\nu_3 = 973$ cm.$^{-1}$ in (2), we obtain an isotope separation of 4 cm.$^{-1}$ for the transverse mode This separation depends only on the O—Cl force constant, K_1, which we have taken as 7×10^5 dynes/cm , the actual value as seen from Table II may be slightly less, but it can never be sufficiently small to influence appreciably the calculated separation, which is likely to lead only to a blurring of the contour of the band, as shown in fig 2

The isotope separations of the symmetrical modes, ν_1 and ν_2, depend not only on K_1, but also on K_2 and the semi-vertical angle, α The solutions of the frequency equations give a rather large range of possible values of K_2 and α, and we have accordingly calculated isotope separations for these modes from formula (4) for representative values of the variables, they are reproduced in Table IV The separation for the ν_1 mode is seen to be comparatively insensitive to changes in K_2 and α, but the variation for the long wave ν_2 is considerable

Table IV —Calculated Isotope Separations

Semi vertical angle, α	38°			45°			55°		
K_2 (dynes/cm × 10^{-5})	2	7	14	2	7	14	2	7	14
$\Delta\nu_2$ cm^{-1} (ν_2 = 640 cm^{-1})	13	6	3	14	6	3	22	6	2
$\Delta\nu_1$ cm^{-1} (ν_1 = 1245 cm^{-1})	13	13	15	13	13	16	14	14	16

It will be gathered from the above that the band at 1245 cm.$^{-1}$ must consist of two superposed bands which have their centres some 13 cm.$^{-1}$ apart, and of relative intensities 3 . 2. Fig. 3 indicates that the observed band is in fact composite, as is shown by the rapid change in slope near 1220 cm.$^{-1}$, and by the flat portion between the extreme maxima. The latter accordingly represent the R branch of the shorter wave component and the P branch of the longer wave band, and an envelope resembling that observed can be constructed from two bands of the given relative intensities, with P and R branches separated as in band B by some 13 cm.$^{-1}$, and with band centres differing by 13 cm.$^{-1}$.

The general shape of the contour of the fundamental at 640 cm $^{-1}$ may be reasonably due to an isotope separation of some 6 cm $^{-1}$, but the interference of the CO_2 band prevents definite measurement

The Force Constants

Table II indicates the rapid increase of the force constant for the external atoms in a symmetrical triatomic molecule governed by central forces as the vertical angle is opened out. Owing to the uncertainty in the value of the vertical angle, we can only say that since it is not far removed from 90°, the force constant K_2 will lie in the neighbourhood of 7×10^5 dynes/cm This is of the order corresponding to a single chemical bond, and at first sight seems large when we realize that the two atoms in question are probably not in chemical combination. It is twice that observed for SO_2 and ClO_2 (3 5 $\times 10^5$ dynes/cm), in which the valence force system provides the only possible solutions , the rigidities are not in the same ratio, since the valence system constant, K_θ, refers to the tangential restoring force per unit arc displacement, while the central force constant, K_2, refers to the restoring force per unit central displacement of the length of the triangle base

We have to consider what is meant by the success of the valence force system in the one case, and its failure in the other. A possible solution with the valence force frequency equation implies a potential field such that the direction of least rate of increase of potential for motion of either atom at the base of the triangle is normal to the side of the triangle , and this in turn implies that the force constant acting along the side of the triangle is considerably greater than the force constant effective for displacements normal to this line On the other hand, failure of the valence force system signifies that the force constant effective for displacements normal to the side of the triangle is comparable with, or even greater than that for displacements in the direction of the side. In fact a system that gives a solution with a large vertical angle with central forces clearly increases the length of either side rather than displaces the vertical angle from its equilibrium position. Thus we say that the vertical angle rigidity of Cl_2O is of a greater order than that of either SO_2 or ClO_2.

Similar Molecules.

The electronic structures of water vapour and hydrogen sulphide would suggest that these molecules are spectroscopically like chlorine monoxide. Considerable uncertainty still exists as to the fundamental frequencies of the first two compounds, but Plyler concludes that in the case of water vapour, they are given by $\nu_2 = 1597$, $\nu_3 = 3745$, and $\nu_1 = 5307$ cm $^{-1}$. On insertion of these values in the frequency equations, we find in confirmation of our conclusions that a possible solution is provided only by the central force system, the vertical angle is some 110°, the O—H force constant is $7 \cdot 5 \times 10^5$ dynes/cm., and the H- -H force constant, K_2, is 5×10^5 dynes/cm. The value for the vertical angle is only approximate, as the fundamental frequencies are not greatly sensitive to changes in its value The rules developed in Part VI (*loc cit*) indicate from the presence of a Q branch in the 3745 cm $^{-1}$ band that the vertical angle is greater than 85°, and since this is the asymmetrical frequency for the possible solution, the least axis of inertia must be perpendicular to the bisector of the vertical angle, and the larger value for this angle is confirmed. The deductions are in agreement with the absence of a Q branch in both the other fundamentals For hydrogen sulphide the vertical angle must be greater than 88°, and the force constants are of the same order

Electronic Structure

Both H_2O and Cl_2O have a central oxygen atom which requires two $(2p)$ electrons to complete its shell, while both hydrogen and chlorine require one electron. If we regard the electrons required to complete a shell as equivalent to electrons outside a closed one, we can say that oxygen has two $(2p)$ electrons, hydrogen one $(1s)$ electron, and chlorine one $(3p)$ electron. The difference between the quantum orbits in the last two cases is not of vital importance in determining the configuration of the molecule ; for Slater, Pauling, and Hund have all shown that a central atom with two $(2p)$ electrons available for binding always tends to form bonds which lie at right angles to each other. Departure from this configuration will be due chiefly to other chemical bonds within the molecule, and these are lacking in the two cases considered, which form a close approximation to the ideal case of two p-electron bonds originating in one atom, and resulting in the attachment of external atoms by σ-bonds.

This discussion ignores the difference between the $(3p)$ chlorine electron and the $(1s)$ hydrogen electron. If the chlorine electron be placed in a $(3p_0)$ proper function with respect to the O—Cl direction, the binding power of this electron will be little different from that of a $(3s)$ electron ; the resulting effect will be to give a larger separation for O—Cl than for O—H, and the chlorine atom will have a larger polarizability, the last factor might be expected to constitute the greatest difference between the two molecules, and one would have anticipated its effect on the configuration of the molecule to be greater than the analyses of the infra-red bands suggests The reasonable conclusion is that the polarizabilities of the constituent atoms are of much less importance than are the values of the exchange integrals The main distinction between the two molecules lies in the values of the Cl—Cl and H—H force constants, both are large, but that for Cl—Cl is greater than that for H—H, and the difference may be due to exchange of electrons between the two chlorine atoms. If the angle ClOCl is approximately 90°, as is required by the infra-red data, and also theoretically by the orthogonality of the linear combinations of the *p* proper functions of oxygen, then there must be overlapping of the electron clouds of the two chlorine atoms We might thus expect exchange integrals to be finite for two electrons one on each chlorine atom, with a resulting attraction. The chlorine shells are only virtually closed, certainly not in the same way as those of the inert gases. Cl_2O should thus be a rigid molecule on two counts, and the large force constant K_2 is consistent with the structure proposed. With the smaller hydrogen nucleus the rigidity is presumably due entirely to the fixed orientation of the oxygen bonds

Other Molecular Data

The rotational fine structure within the vibrational bands of an asymmetric rotator is extremely complex The maximal separation within a Bjerrum doublet for such a molecule will accordingly give only approximate values for the moment concerned, and only an approximate estimate of the molecular dimensions can be made The asymmetric vibration gives a rough indication of the greatest moment of inertia, and for Cl_2O the P and R branches in this band are separated by some 13 cm^{-1}. The moment of inertia corresponding to this is 274×10^{-40} g cm^2, and the calculated value for the O—Cl distance is then 1·8 A There is a general tendency for the interatomic distance to increase as one proceeds along a period towards Group VII (r_e for N_2, O_2, and F_2 is 1·1, 1·2 and 1·5 A.; and for CO, NO, and O_2 is 1·15, 1·15, and 1·20 A.; for SO it is 1·49 and for Cl_2, 1·98 A.), and taking into account the large force constants of the molecule, we shall perhaps be not far out in suggesting some 1·6 A for the Cl—O distance, and accordingly some 2·5 A for the Cl—Cl separation

The breaking of each O—Cl link in Cl_2O requires the same energy, approximately 45 k cals.,* and the phenomenon appears to be characteristic of the $p\sigma$ molecular bonds from a $(2p)^2$ atom, since we have the value of 111 k.cals for each link in the H_2O molecule, and may be taken as another tribute to the fixed direction in space of these bonds. With ClO_2, where the available electrons are one in excess of those required for normal bond formation, we have an electronic rearrangement consequent upon dissociation of the first oxygen atom which involves some 66 k cals., the second requiring again 46 k cals. Similarly for SO_2 (where the rearrangement is greater with two excess electrons) the first oxygen needs some 149 k cals and the second, 103 k cals. The two latter molecules are governed by valence forces, the vertical angle is slightly greater than 120°, and the comparative looseness of the structure is a result of the electronic arrangement indicated. It seems to be doubtful whether the first type of molecule can dissociate completely to give $O + Cl_2$, or $O + H_2$† as a first stage reaction, but it was shown in Part VIII‡ that SO_2 may reasonably give $S + O_2$ when the molecule collapses.

The force constant between the external atoms exists mainly by virtue of the rigidity of the structure, and although it is large, it does not contribute in any marked degree to the heat of dissociation of the molecule. Hence we are not dealing with a true chemical bond, and if the resonance effect referred to earlier exists between the chlorine shells, the bond is more of the type of the polarization bonds of metals.

The authors are glad to acknowledge their indebtedness to Professor Donnan, C.B.E., F.R.S., for his constant interest and help, and to the Department of Scientific and Industrial Research for a Senior Award to A. B. D. C.

Summary

(1) The infra-red absorption spectrum of chlorine monoxide, Cl_2O has been examined between 1 and 18 μ and four bands have been isolated.

(2) Fundamental frequencies have been assigned, and the molecular dimensions approximately evaluated.

(3) The isotope effect has been considered, and is shown to account for the envelopes of certain of the bands.

(4) Cl_2O and H_2O belong to the group of molecules whose vibrations are governed by central forces, and are characterized by a vertical angle of slightly greater than 90°, and a strong resistance to angular deformation.

(5) The electronic structure of the substance is discussed.

---

* Finkelnburg, Schumacher and Stieger, 'Z. phys. Chem.,' B, vol. 15, p. 127 (1932).

† Finkelnburg, Schumacher and Stieger, *loc. cit.*

‡ 'Proc. Roy. Soc.,' A, vol. 140, p. 605 (1933).

The Passage of Positive Ions through Gases.

By H. S W Massey, Ph D, Senior 1851 Exhibitioner, Trinity College, Cambridge, and R A Smith, M A, Emmanuel College, Cambridge, Charles Maclaren Scholar, Edinburgh University

(Communicated by P. A. M Dirac, F R S —Received April 25, 1933)

A large number of investigations have been carried out on the motion of charged particles through gases, and the subject has received added impetus from the introduction of quantum mechanics, as this theory is capable of dealing with collision phenomena in a manner that was beyond the reach of Bohr's quantum theory. In the early days of the wave theory, many experiments were devised with a view to testing the validity of the theory , but now the foundations of quantum mechanics have been so firmly laid that we may use the theory to clarify the more complicated phenomena observed in the passage of charged particles through gases

Both from the experimental and theoretical point of view the most convenient particles to study are electrons ; and, as a consequence, the phenomena observed in the collisions of electrons with gas molecules are well known and to a large extent understood Well-marked diffraction phenomena have been observed and the relative probabilities of elastic and inelastic collisions measured for a number of gases. Although detailed theoretical explanations have not always been given, it is possible in nearly all cases to give a general description of the main processes contributing to the observed effects. For example, the Ramsauer effect is now completely explained †

As well as the large amount of attention devoted to electrons, a large number of experimental investigations have been concerned with the passage of positive ion beams through gases Recent developments of technique have also made experiments possible with fast beams of neutral atoms. In nearly every case the investigator has been concerned with detecting analogies with the behaviour of electrons, and phenomena supposedly analogous to the Ramsauer effect have been described

From a theoretical point of view, however, we would expect the behaviour of positive ions and neutral atoms to be markedly different to that of electrons, both on account of their much greater mass and of the opposite sign of their interaction with gas molecules. It is therefore very necessary to consider the hitherto neglected theoretical side of this subject, and this paper represents a first step in this direction.

---

† Faxèn and Holtsmark, 'Z Physik,' vol 45, p. 307 (1927), Holtsmark, 'Z. Physik, vol. 55, p 437 (1929), Allis and Morse, 'Z Physik,' vol 70, p 567 (1931).

When a homogeneous positive ion beam passes through a gas, it may be weakened by elastic collisions with the gas atoms, resulting in deviations from the original path, by loss of energy owing to inelastic collisions with the gas atoms, or by neutralization through electron capture. The last process is a special type of inelastic collision, except in the special case of exact resonance which occurs when the ion beam is passing through a gas of similar atoms (i.e., He$^+$ ions in helium). In this case no kinetic energy is lost, but the ion which results from the transfer is not in general moving in the same direction as the beam, and the process may be considered as an elastic collision which results in a large deviation. We require to determine the relative importance of these processes under different experimental conditions, but as we are concerned only with ions and atoms with velocities considerably less than those of the orbital electrons of the atoms with which they collide, it is necessary to develop a theory of the collisions which is applicable under these conditions. Such a theory is developed and applied to a number of illustrative cases. The bearing of the results on the interpretation of the experimental material is also considered in detail.

§ 1. *Theory of Collisions*

Let us consider the impact of two atoms A and B. We denote the co-ordinates of the atomic electrons with respect to the centres of mass of the respective atoms by $\mathbf{r}_a$, $\mathbf{r}_b$ and the relative co-ordinates of the centres of mass by $\mathbf{r}$. The centre of mass of the combined system may be separated out to give the wave equation

$$\left[\frac{h^2}{8\pi^2 M}\nabla^2 - H_a(\mathbf{r}_a) - H_b(\mathbf{r}_b) - V(\mathbf{r}, \mathbf{r}_a, \mathbf{r}_b) + E\right]\Psi = 0 \qquad (1)$$

In terms of the co-ordinates $\mathbf{r}_a$, $\mathbf{r}_b$, $\mathbf{r}$, M is the reduced mass $M_aM_b/(M_a + M_b)$ of the atoms, $H_a(\mathbf{r}_a)$, $H_b(\mathbf{r}_b)$ are the Hamiltonians of the atomic electrons referred to the centres of mass of the respective atoms, ∇^2 is the Laplacian operator in the relative co-ordinates $\mathbf{r}$ of the centres of mass and $V(\mathbf{r}, \mathbf{r}_a, \mathbf{r}_b)$ is the interaction energy of the two atomic systems.

Before proceeding further it is convenient to introduce a notation for the wave functions and energies of the atomic electrons when unperturbed. We denote these wave functions by $u_n(\mathbf{r}_a)$, $v_m(\mathbf{r}_b)$ and the corresponding energies by E_n^a, E_m^b. We have, then,

$$\left.\begin{aligned}[H_a - E_n^a]\, u_n &= 0\\ [H_b - E_m^b]\, v_m &= 0\end{aligned}\right\} \tag{2}$$

For convenience of notation we will not distinguish the separate states of the two atomic systems, but will denote a pair of states n, m by a single suffix n. A wave function $\psi_n(\mathbf{r}_a, \mathbf{r}_b)$ is then to be understood to be a product $u_n(\mathbf{r}_a)$ $v_m(\mathbf{r}_b)$, while E_n represents the sum $E_n^a + E_m^b$.

In order to calculate the probabilities of excitation, ionization, or charge transfer on impact of two atoms, we must obtain a solution of equation (1) which has the asymptotic form for large r

$$\Psi \sim e^{ikr\cos\theta}\, \psi_0(\mathbf{r}_a, \mathbf{r}_b) + \sum_{n=0}^{\infty} f_n(\theta, \phi) \frac{e^{ik_n r}}{r}\, \psi_n(\mathbf{r}_a, \mathbf{r}_b) \tag{3}$$

Here

$$k^2 = 8\pi^2 M\, [E - E_0]/h^2$$

$$k_n^2 = 8\pi^2 M\, [E - E_n]/h^2$$

Thus $k_n/2\pi$ is the wave number for the relative motion after excitation of the nth state. By computing the scattered current we find that the cross-section for excitation of the nth state of the system by the impact, is given by

$$Q_n = \int_0^{\pi}\int_0^{2\pi} \frac{k_n}{k}\, |f_n(\theta, \phi)|^2 \sin\theta\, d\theta\, d\phi \tag{4}$$

The usual method of calculating f_n approximately is to expand Ψ in a series of the form

$$\Psi = \Sigma_n\, F_n(\mathbf{r})\, \psi_n(\mathbf{r}_a, \mathbf{r}_b) \tag{5}$$

Substituting in (1) and using (2) gives

$$\Sigma_n \left[\frac{h^2}{8\pi^2 M}\nabla^2 - V(\mathbf{r}, \mathbf{r}_a, \mathbf{r}_b) + E - E_n\right] F_n(\mathbf{r})\, \psi_n(\mathbf{r}_a, \mathbf{r}_b) = 0 \tag{6}$$

Multiplying by $\psi^*_n(\mathbf{r}_a, \mathbf{r}_b)$ and integrating over the co-ordinate space of the electrons, we obtain by virtue of the orthogonal properties of the atomic wave functions,

$$[\nabla^2 + k_n^2]\, F_n = \Sigma_m\, U_{mn} F_m, \tag{7}$$

where

$$U_{mn} = \frac{8\pi^2 M}{h^2} \iint V(\mathbf{r}, \mathbf{r}_a, \mathbf{r}_b)\, \psi^*_n(\mathbf{r}_a, \mathbf{r}_b)\, \psi_m(\mathbf{r}_a, \mathbf{r}_b)\, d\tau_a\, d\tau_b$$

Under certain conditions these simultaneous equations may be simplified sufficiently to give formulæ for $f_n(\theta, \phi)$. This is so when the velocity of relative motion is high compared with that of the internal motion considered. For then we may neglect all the scattered waves on the right side of (7) and take

$$[\nabla^2 + k_n^2]\, F_n = U_{0n} F_0 = U_{0n}\, e^{ik\mathbf{n}_0 \cdot \mathbf{r}}, \tag{8}$$

where $\mathbf{n}_0$ is a unit vector in the direction of incidence. Solving the equation asymptotically by the method of Green's Functions one obtains the formula ("Born's approximation")

$$f_n(\theta, \phi) = -\frac{1}{4\pi}\int U_{0n}\, e^{i(k\mathbf{n}_0 - k_n\mathbf{n})\cdot \mathbf{r}}\, d\tau, \tag{9}$$

where $\mathbf{n}$ is a unit vector in the direction (θ, ϕ), $\mathbf{n}_0$ being in the direction $\theta = 0$.

A less drastic simplification may be made when the non-diagonal matrix elements U_{nm} are small compared with the diagonal elements U_{mn}. In this case† we may consider the interaction of two states only in (7), and solve the resulting simultaneous equations by successive approximations, commencing with the solution of the equation for the elastic scattering

$$[\nabla^2 + k^2 - U_{00}]\, F_0 = 0$$

In one other case we need only consider the interaction of two states o and n. This arises when the states n and o are in close resonance, but all other pairs of states in poor resonance. As the matrix element U_{0n} is not necessarily small in the case of close resonance, the problem is reduced to that of solving the coupled equations

$$\left.\begin{aligned} [\nabla^2 + k^2 - U_{00}]\, F_0 &= U_{n0} F_n \\ [\nabla^2 + k_n^2 - U_{nn}]\, F_n &= U_{0n}\, F_0 \end{aligned}\right\} \tag{10}$$

These equations have been discussed by Stueckelberg,‡ who applies the solution to the problem of the ionization of rare gas atoms by alkali ions.

When we examine the problem with which we are concerned, it is clear that not only is Born's approximation invalid owing to the small relative velocity of the ions and atoms concerned, but that the non-diagonal matrix elements U_{nm} are not small compared with the diagonal elements. In most cases the excited state is not in closer resonance with the ground state than with all the neighbouring states. In fact, the energy difference between any two excited states is usually much less than that between the initial state and the excited state concerned. These considerations indicate the necessity of developing a method in which the interaction between all the states is taken into account to some degree of approximation Such a method may be obtained by considering the physical aspects of the problem The relative velocity of the atoms is small compared with the velocity of the atomic electrons, so it is natural to treat the two atomic systems as if at rest and then introduce the relative motion as a perturbation

---

† *Cf.* Jackson and Mott, 'Proc. Roy. Soc.,' A, vol. 137, p. 703 (1932).

‡ 'Helv. Phys. Acta,' vol. 5, p. 370 (1933).

We therefore first consider the equation

$$[\mathrm{H}_a(\mathbf{r}_a) + \mathrm{H}_b(\mathbf{r}_b) + \mathrm{V}(\mathbf{r}, \mathbf{r}_a, \mathbf{r}_b) - \mathrm{E}]\chi = 0, \tag{11}$$

in which the relative motion of the two systems does not appear Let us suppose this equation to be solved for any value of $\mathbf{r}$, leading to a set of proper functions $\chi_n(\mathbf{r}, \mathbf{r}_a, \mathbf{r}_b)$ and proper values of the energy $\varepsilon_n(r)$ † These functions are classified by their behaviour for large r We distinguish by the suffix n that energy value which tends to E_n as $r \to \infty$ We may therefore write

$$\varepsilon_n(r) = \mathrm{E}_n - \eta_n(r), \tag{12}$$

where $\eta_n(r) \to 0$ as $r \to \infty$ The corresponding wave functions χ form, for all $\mathbf{r}$, a set normal and orthogonal with respect to $\mathbf{r}_a$, $\mathbf{r}_b$. It is therefore possible to expand Ψ in the form

$$\Psi = \Sigma_n \chi_n(\mathbf{r}, \mathbf{r}_a, \mathbf{r}_b)\,\mathrm{F}_n(\mathbf{r}), \tag{13}$$

and as before we require solutions for the functions $\mathrm{F}_n(\mathbf{r})$ such that Ψ has the asymptotic forms (3), *i e*, we must have

$$\left.\begin{aligned} \mathrm{F}_n(\mathbf{r}) &\sim e^{ik_n r} r^{-1} f_n(\theta, \phi) \\ \mathrm{F}_0(\mathbf{r}) &\sim e^{ikz} + e^{ikr} r^{-1} f_0(\theta, \phi) \end{aligned}\right\} \tag{14}$$

On substituting (13) in (1), remembering that

$$[-\mathrm{H}_a(\mathbf{r}_a) - \mathrm{H}_b(\mathbf{r}_b) - \mathrm{V}(\mathbf{r}, \mathbf{r}_a, \mathbf{r}_b)]\chi_n = [\eta_n(r) - \mathrm{E}_n]\chi_n,$$

we obtain

$$\Sigma_n \frac{h^2}{8\pi^2 \mathrm{M}}[\mathrm{F}_n\nabla^2\chi_n + 2\,\mathrm{grad}\,\mathrm{F}_n \cdot \mathrm{grad}\,\chi_n + \chi_n\nabla^2\mathrm{F}_n] = \Sigma_n[\mathrm{E}_n - \eta_n(r) - \mathrm{E}]\chi_n\mathrm{F}_n. \tag{15}$$

---

† Throughout this calculation it is assumed that the interaction energy between the two atomic systems, in both initial and final states, is a function of r only When this is not so the effect of the angular momentum associated with the electron orbital motion in the pseudo-molecule must be taken into account This effect will be small, except for high excited states

We now multiply both sides of this equation by χ^*_n and integrate over the co-ordinate space of $\mathbf{r}_a$ and $\mathbf{r}_b$.

This gives

$$\frac{h^2}{8\pi^2 M}\nabla^2 F_n + [E - E_n + \eta_n(r)] F_n = -\Sigma_m F_m(\mathbf{r})\frac{h^2}{8\pi^2 M}\iint \chi^*_n \nabla^2 \chi_m \, d\tau_a \, d\tau_b$$

$$- 2 \sum_{m \neq n} \frac{h^2}{8\pi^2 m} \operatorname{grad} F_m \iint \chi^*_n \operatorname{grad} \chi_m \, d\tau_a \, d\tau_b. \quad (16)$$

In deriving this formula we have used the result

$$\iint \chi^*_n \operatorname{grad}_r \chi_n \, d\tau_a \, d\tau_b = 0,$$

which follows from the normalizing condition

$$\iint \chi^*_n \chi_n \, d\tau_a \, d\tau_b = 1,$$

on the assumption that χ_n is a real function of the co-ordinates $\mathbf{r}$ The generalization for cases when this is not so presents no difficulty, but it will not be considered further as it involves considerable increase in the length of the resulting formulæ without any appreciable modification of the final expressions for the cross-sections

These equations replace equations in the usual method where expansions are made in terms of the unperturbed stationary state wave functions. To obtain approximate solutions we neglect all non-diagonal matrix elements except those which refer to the initial state This leads to the equations

$$\left.\begin{aligned} &\nabla^2 F_0 + \left[k^2 + \frac{8\pi^2 M}{h^2}\eta_0(r) + \iint \chi^*_0 \nabla^2 \chi_0 \, d\tau_a \, d\tau_b\right] F_0 = 0 \\ &\nabla^2 F_n + \left[k_n{}^2 + \frac{8\pi^2 M}{h^2}\eta_n(r) + \iint \chi^*_n \nabla^2 \chi_n \, d\tau_a \, d\tau_b\right] F_n \\ &\quad = - F_0 \iint \chi^*_n \nabla^2 \chi_0 \, d\tau_a \, d\tau_b - 2 \operatorname{grad} F_0 \, . \iint \chi_n{}^* \operatorname{grad} \chi_0 \, d\tau_a \, d\tau_b \end{aligned}\right\} . \quad (17)$$

The asymptotic forms of the solutions of these equations satisfying the boundary conditions (14) may be obtained in terms of the solutions of the homogeneous equation

$$\nabla^2 F_n + \left[k_n{}^2 + \frac{8\pi^2 M}{h^2}\eta_n(r) + \iint \chi^*_n \nabla^2 \chi_n \, d\tau_a \, d\tau_b\right] F_n = 0 \quad (18)$$

If we denote by $\mathfrak{F}_n(r, \theta)$ that solution of (18) which is finite at the origin and has the asymptotic form

$$\mathfrak{F}_n(r, \theta) \sim e^{ik_n r \cos\theta} + r^{-1} e^{ik_n r} \times \text{function of } \theta, \phi, \tag{19}$$

the solution of (17) satisfying the required conditions has the asymptotic form

$$\mathrm{F}_n \sim r^{-1} e^{ik_n r} \iiint \mathfrak{F}_n(r', \pi - \Theta) \chi^*_n [\nabla^2 \chi_0 + 2 \operatorname{grad} \chi_0 \ \operatorname{grad}] \mathrm{F}_0(r', \theta') \, d\tau_a \, d\tau_b \, d\tau', \tag{20}$$

where

$$\cos\Theta = \cos\theta' \cos\theta + \sin\theta' \sin\theta \cos(\phi' - \phi).$$

Hence we have

$$f_n(\theta, \phi) = \iiint \mathfrak{F}_n(r', \pi - \Theta) \chi^*_n [\nabla^2 \chi_0 + 2 \operatorname{grad} \chi_0 \ \operatorname{grad}] \mathrm{F}_0(r', \theta') \, d\tau_a \, d\tau_b \, d\tau'. \tag{21}$$

To compare this formula with that obtained by the method of expansion in unperturbed stationary state wave functions, we shall use functions obtained from a first order perturbation method (treating $\mathrm{V}(\mathbf{r}, \mathbf{r}_a, \mathbf{r}_b)$ as small). We thus take for χ_n, ε_n,

$$\chi_n = \psi_n + \sum_{m \neq n} \mathrm{V}_{nm} \psi_m / (\mathrm{E}_n - \mathrm{E}_m)$$

$$\varepsilon_n = \mathrm{E}_n + \mathrm{V}_{nn} + \Sigma \frac{\mathrm{V}_{nm} \mathrm{V}_{mn}}{\mathrm{E}_n - \mathrm{E}_m},$$

where

$$\mathrm{V}_{nm} = \frac{h^2}{8\pi^2 \mathrm{M}} \mathrm{U}_{nm}. \tag{22}$$

Substitution in (17) then gives

$$\begin{aligned}
\nabla^2 \mathrm{F}_n + \left[k_n{}^2 - \mathrm{U}_{nn} - \sum_{m \neq n} \frac{\mathrm{V}_{nm}}{(\mathrm{E}_m - \mathrm{E}_n)^2} \left\{\nabla^2 + \frac{8\pi^2 \mathrm{M}}{h^2} (\mathrm{E}_m - \mathrm{E}_n)\right\} \mathrm{V}_{mn}\right] \mathrm{F}_n \\
= - \mathrm{F}_0 \left[\frac{\nabla^2 \mathrm{V}_{0n}}{\mathrm{E}_n - \mathrm{E}_0} - \sum_{m \neq n} \frac{\mathrm{V}_{nm} \nabla^2 \mathrm{V}_{m0}}{(\mathrm{E}_n - \mathrm{E}_m)(\mathrm{E}_m - \mathrm{E}_0)}\right] \\
- 2 \operatorname{grad} \mathrm{F}_0 \left[\frac{\operatorname{grad} \mathrm{V}_{0n}}{\mathrm{E}_n - \mathrm{E}_0} - \sum_{m \neq n} \frac{\mathrm{V}_{nm} \operatorname{grad} \mathrm{V}_{m0}}{(\mathrm{E}_n - \mathrm{E}_m)(\mathrm{E}_m - \mathrm{E}_0)}\right].
\end{aligned} \tag{23}$$

Neglecting the effect of the summation terms and of the potentials U_{nn}, U_{00} we obtain

$$f_n(\theta, \phi) = \int e^{-i\mathbf{k}_n \ \mathbf{r}} (\nabla^2 \mathrm{V}_{0n} + 2 \operatorname{grad} \mathrm{V}_{0n}{}^{\circ}) \operatorname{grad} e^{i\mathbf{k}_0 \cdot \mathbf{r}} \, d\tau. \tag{24}$$

Making use of the fact that

$$[\nabla^2 + k^2]\, e^{ik\mathbf{n}_0 \cdot \mathbf{r}} = 0,$$

this formula may be reduced to Born's approximation (9) When the interaction V ($\mathbf{r}$, $\mathbf{r}_a$, $\mathbf{r}_b$) can no longer be treated as small, the formula (21) will not in general reduce to Born's, even for the highest velocities of impact In such cases it must be remembered that (21) is derived on the assumption of low velocity impacts and cannot be expected to give correct results when the velocity of relative motion is greater than the orbital velocity of the atomic electrons concerned Born's formula must then be used.

We see also from this perturbation treatment how the formula (21) takes into account the interaction of the various stationary states to some degree of approximation

We shall now consider the various phenomena associated with the passage of beams of heavy particles through matter in terms of this theory.

§ 2. *Elastic Collisions.*

For the elastic scattering we have the equation

$$\left[\nabla^2 + k^2 + \frac{8\pi^2 M}{h^2}\eta_0(r) + \iint \chi^*_0 \nabla^2 \chi_0\, d\tau_a\, d\tau_b\right] F_0 = 0, \tag{25}$$

which represents the motion in a field of force of potential

$$V = -\eta_0(r) + \frac{h^2}{8\pi^2 M}\iint \chi^*_0 \nabla^2 \chi_0\, d\tau_a\, d\tau_b. \tag{26}$$

This is the interaction energy of the ion and atom in their normal states, and so includes,† besides the Coulomb repulsion of the charge distributions, the exchange energy and the polarization. As we are not concerned in this section with the exact calculation of cross-sections we will assume that only the Coulomb repulsions are important This assumption is probably valid in any case for collisions involving heavy ions or atoms, as it has been found that exchange is relatively less important in the theory of chemical combination of such atoms than it is for light atoms. We shall therefore consider the elastic scattering of protons by various atoms assuming that the potential acting on the protons is just that of the Hartree field of the atom.

---

† *Vide* Lennard-Jones, 'Proc Phys. Soc Lond.', vol 43, p. 461 (1930).

The cross-section for elastic scattering is given by†

$$Q_0 = \frac{4\pi}{k^2} \Sigma_s (2s+1) \sin^2 \delta_s, \tag{27}$$

where δ_s is defined by the asymptotic form of that solution of the equation

$$\frac{d^2}{dr^2}(r\mathrm{F}_0{}^s) + \left\{k^2 - \frac{8\pi^2 \mathrm{M}}{h^2} \mathrm{V} - \frac{s(s+1)}{r^2}\right\}(r\mathrm{F}_0{}^s) = 0, \tag{28}$$

which is finite at the origin, this asymptotic form being written

$$r\mathrm{F}_0{}^s \sim \sin(kr - \tfrac{1}{2}s\pi + \delta_s).$$

The convergence of the series (27) is determined by the fact that δ_s is small for such s that

$$\frac{8\pi^2 \mathrm{M}}{h^2} \mathrm{V}(r) \ll \frac{s(s+1)}{r^2},$$

for

$$kr \simeq s + \tfrac{1}{2} \tag{29}$$

When this condition is satisfied δ_s is given with close approximation by the formula‡

$$\delta_s = \frac{4\pi^3 \mathrm{M}}{h^2} \int_0^\infty J r \mathrm{V} \{_{s+\frac{1}{2}}(kr)\}^2 \, dr \tag{30}$$

On application of these formulæ to the scattering of protons by helium atoms it is found that, for energies of impact between 50 and 1000 volts, s must be equal to about 100 in order that δ_s be sufficiently small to make (30) applicable. For values of s less than this, δ_s is greater than $\frac{1}{2}\pi$, and $\sin^2 \delta_s$ therefore oscillates between values of 0 and 1 in this range of s For greater values of s, δ_s converges uniformly to zero as $s \to \infty$. This behaviour of the phases is illustrated diagrammatically in fig 1

Because of this behaviour of the terms of the series (27), we may sum the series approximately in the following way We break up the sum into two parts $Q_0{}^S$, $Q_S{}^\infty$, the first being the sum of the first S terms, the second the sum from S to ∞ We take S as being the order of that phase δ_S which first attains the value of $\frac{1}{2}\pi$ As S is a large number we have

$$Q_0{}^S \simeq \frac{4\pi}{k^2} \int_0^S 2x \sin^2 \{f(x)\} \, dx \tag{31}$$

---

† Faxén and Holtsmark, 'Z Physik,' vol. 45, p 307 (1927).

‡ Mott, 'Proc. Camb Phil. Soc.,' vol 25, p 304 (1928)

$f(x)$ is such that $\sin^2\{f(x)\}$ oscillates rapidly in the range considered and may be replaced by its mean value of $\frac{1}{2}$. This gives

$$Q_0^S = 2\pi S^2/k^2.$$

To calculate Q_S^∞ the sum is again transformed to an integral and evaluated by graphical integration. To do this it is only necessary to calculate the phases δ_s from formula (30) at a small number of suitable values of s. As tables of Bessel functions of order greater than 37/2 do not exist, a special method must be devised to make the evaluation of (30) possible The method used is discussed in Appendix I As high accuracy is not required S was chosen using the formula (30) which is not strictly applicable when δ_s is as great as $\frac{1}{2}\pi$.

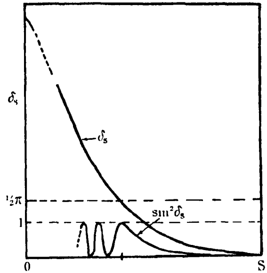

FIG 1.—Illustrating behaviour of phase constants δ as functions of the order s for collisions of positive ions with gas atoms

The elastic cross-sections calculated for collisions of protons with helium and argon atoms are given in Table I.

Table I

Gas.	Proton energy (in e volts)	Cross-section (in units of πa_0^2)	Gas-kinetic cross section (in units of πa_0^2).
He	90	3·75	2·6
	800	2·0	—
A ..	73	16·4	7·3
	650	10·7	—

It will be seen that the cross-sections in the voltage range given do not differ greatly from the gas kinetic cross-sections This result appears at first sight to be definitely contradictory to a number of experimental results Thus Dempster† and Ramsauer, Kollath, and Lilienthal‡ found that the total cross-section (including inelastic as well as elastic collisions) for protons with energies between 50 and 2000 volts in helium is very much less than gas-kinetic The explanation of this apparent discrepancy lies in the form of the angular distribution of the scattered protons, nearly all the collisions result in such slight deviations that the angular resolution of the apparatus used in the experiments cited above was not great enough to permit of their detection

The number of protons scattered through an angle θ into the solid angle $d\omega$ is given by

$$\mathrm{I}(\theta)\,d\omega = \frac{1}{4k^2}\left|\Sigma\,(2s+1)\,(e^{2i\delta_s}-1)\,\mathrm{P}_s(\cos\theta)\right|^2 d\omega \tag{32}$$

As the convergence of the series in (32) is very slow, the direct numerical evaluation of the angular distribution would be virtually impossible, if it were not for the fact that the scattering may be calculated by classical theory except at very small angles of scattering The condition for classical scattering§ at an angle θ is that the value s_0 of s such that

$$\frac{\partial\delta_s}{\partial s} = \tfrac{1}{2}\theta,$$

must be large and δ_s must also be large for this value of s This condition is satisfied for proton collisions for all angles θ appreciably greater than the first zero, π/s, of the harmonic $\mathrm{P}_s(\cos\theta)$ which is associated with a phase $\delta_s = \frac{1}{2}\pi$. Thus for 90-volt protons in helium the classical formula holds for angles greater than 3° and for 72-volt protons in argon for angles greater than 30′. We are therefore able to use the classical formula over a wide angular range, and it is only necessary to calculate $\mathrm{I}(\theta)$ for $\theta = 0$ in order to determine the complete form of the angular distribution with sufficient accuracy.

For $\theta = 0$ we have $\mathrm{P}_s(\cos 0) = 1$, so

$$\begin{aligned}\mathrm{I}(0) &= \frac{1}{4k^2}\left[\{\Sigma_s\, 2\,(2s+1)\sin^2\delta_s\}^2 + \{\Sigma_s\,(2s+1)\sin 2\delta_s\}^2\right] \\ &= \frac{k^2\mathrm{Q}_0^{\,2}}{16\pi^2} + \frac{1}{4k^2}\{\Sigma_s\,(2s+1)\sin 2\delta_s\}^2.\end{aligned} \tag{33}$$

---

† 'Phil. Mag.,' vol. 3, p. 115 (1927).

‡ 'Ann. Physik,' vol 8, p 709 (1931).

§ Unpublished work by N. F. Mott to appear shortly in "The Theory of Atomic Collisions," by Mott and Massey, The Clarendon Press, Oxford.

The second term, which is usually small, may be summed by numerical integration, just as in the calculation of Q_0. Use is also made of the fact that the mean value of $\sin 2\delta_s$ is zero over the range of s where the phases are greater than $\frac{1}{2}\pi$.

In the range of validity of the classical theory of scattering the angular distribution is given by

$$I(\theta) = \frac{s}{k^2}\frac{ds}{d\theta}\frac{1}{\sin\theta},$$

where s is given by

$$\theta = \pi - 2s\int_{r_0}^{\infty} r^{-2}\left\{k^2 - \frac{8\pi^2 MV}{h^2} - \frac{s^2}{r^2}\right\}^{-\frac{1}{2}} dr,$$

and r_0 is the greatest zero of

$$k^2 - \frac{8\pi^2 MV}{h^2} - \frac{s^2}{r^2} \tag{34}$$

Using (33) and (34) we obtain the following values for the variation of intensity of scattering with angle of scattering for 110-volt protons in helium and 72-volt protons in argon.†

Table II.

Angle of scattering (relative co-ordinates)	$I(\theta)$ in units of a_0^2.			
	Argon		Helium	
	Hartree field	Coulomb	Hartree field	Coulomb.
°				
0	16×10^4	∞	9×10^3	∞
12	22 0	$1\ 58 \times 10^4$	7·85	124 0
28	7 20	770	2 00	6 10
34	2 76	365	0 72	2 85
57	0 93	51	0 21	0 40
80	0 48	15	0 08	0·12
114	0 14	5 3	0 04	0 04
137	0 08	3 5	—	0 03
167	0 05	2 6	—	0 02

The great concentration of the scattering at small angles even for the low energy protons considered is clear. This concentration becomes more marked as the energy increases, and for 1000-volt protons in argon the intensity per unit solid angle at 0° is at least 10^5 times that at 10°. The calculations for the Hartree fields are also compared with the Coulomb scattering by the unshielded nuclei in order to illustrate the effect of the screening of the nuclei by the electron distributions.

---

† These energies are reckoned on the assumption that the protons are fired into a gas of atoms at rest.

Ramsauer and Kollath† have recently measured the angular distributions of 64-volt protons scattered by helium and argon, and the curves obtained agree satisfactorily with those calculated over the angular range of the observations (15°–167·5°). Actually the observed curves are somewhat steeper at small angles than the calculated, but this is to be expected as electron exchange and polarization have been neglected throughout. These will have the effect of increasing the interaction at large distances and hence the intensity of small angle scattering. Ramsauer and Kollath found that the angular distribution for helium is steeper than for argon in the observed angular range, just as is indicated by the calculations. They also found that the Coulomb scattering law does not fit the observations satisfactorily as it gives much too steep an angular distribution. This is also in agreement with the calculations. This is therefore one of the few cases where *classical* theory has been applied successfully to the scattering by a field of force other than Coulomb.

§ 3. *Excitation and Charge Transfer for Protons in Helium.*

Referring to (21), it will be seen that we require the wave functions χ which represent the motion of electrons in the combined fields of the helium and hydrogen nuclei supposed held at rest. As there is no method known for obtaining these functions exactly, we are forced in this preliminary discussion to assume forms which are not exact, but which contain the essential properties. We therefore make the following assumptions in evaluating the probability amplitude $f_n(\theta, \phi)$ (equation (21)).

Firstly, we take F_0, $\mathfrak{F}_n$ to be the plane waves $e^{ik\mathbf{n}_0 \cdot \mathbf{r}'}$, $e^{-ik\mathbf{n} \cdot \mathbf{r}'}$ respectively. This is legitimate when the energy of the incident protons is so high that the plane waves are only distorted by the interaction at distances much smaller than those at which the remaining terms in the integrand of (21) are appreciable. We choose our axis along $\mathbf{n}_0$, so that

$$\mathbf{n}_0 \cdot \mathbf{r}' = r' \cos\theta', \qquad \mathbf{n} \cdot \mathbf{r}' = r' (\cos\theta \cos\theta' + \sin\theta \sin\theta' \cos(\phi - \phi')).$$

Secondly, we take for the final electronic wave function χ_n just that of the undisturbed systems, *i.e.*, a combination of two atomic wave functions having the correct symmetry. This is admittedly very rough, but as we are not in a position to obtain the initial wave function with accuracy it is not worth while to complicate further a necessarily complicated calculation by allowing χ_n to depart from its unperturbed form as well as χ_0.

---

† 'Ann. Physik,' vol. 16, p. 570 (1933).

In any accurate treatment the wave functions χ_0 can only be determined by the use of a variation method in which a suitable form involving one or more arbitrary constants is assumed and the constants fixed by a minimal condition. In the problem in hand a suitable form for χ_0 is

$$\chi_0 = \mathrm{N}_0 \exp \{- \mathrm{Z}(r_1 + r_2) - \mathrm{Z}'(p_1 + p_2)\}, \tag{35}$$

where Z and Z′ are functions of the nuclear separation r, distances from the helium nucleus being denoted by r_1, r_2, and from the proton by p_1, p_2, for the two electrons respectively. Z and Z′ must satisfy the conditions†

$$\left.\begin{aligned} Z &\rightarrow 1{\cdot}69 \\ Z' &\rightarrow 0 \end{aligned}\right\} \text{ as } r \rightarrow \infty$$

$$\mathrm{Z} + \mathrm{Z}' \rightarrow 2{\cdot}69 \qquad \text{as } r \rightarrow 0.$$

At intermediate distances Z, Z′ can only be fixed by minimizing the energy given by the assumed form of the wave function, but as this is somewhat laborious the approximation was made of assuming Z and Z′ to be given by

$$\left.\begin{aligned} \mathrm{Z} &= 1{\cdot}69 \\ \mathrm{Z}' &= 0 \end{aligned}\right\} r > r_0$$

$$\left.\begin{aligned} \mathrm{Z} &= 2{\cdot}19 \\ \mathrm{Z}' &= 0{\cdot}50 \end{aligned}\right\} r = 0,$$

$$\frac{\partial \mathrm{Z}}{\partial r}, \frac{\partial \mathrm{Z}'}{\partial r} \text{ constant for } r < r_0, \text{ and zero for } r > r_0. \tag{36}$$

By comparison with the known variation with distance of the effective nuclear charge for the only analogous case which has been worked out, that of the hydrogen molecular ion‡ $\mathrm{H_2}^+$ and hydrogen molecule§ $\mathrm{H_2}$, this approximation is seen to be reasonably accurate, and r_0 may be taken as a little greater than the sum of the radii of the hydrogen and helium atoms. A value of $1{\cdot}75\ a_0$ was therefore adopted for r_0. Actually, in carrying out the calculation, the discontinuity in $\partial Z/\partial r$ was allowed for to some extent in the manner indicated below (see fig 2).

---

† This behaviour of Z for helium is that obtained by Hylleraas. (Z Physik, vol. 54, p. 347 (1929))

‡ Condon and Morse, "Quantum Mechanics," p. 178 (1929).

§ N. Rosen, 'Phys Rev.,' vol. 38, p. 2099 (1931).

Finally, we note that the term in (21) involving $\nabla^2\chi_0$ may be neglected in comparison with that involving grad χ_0, since the method is applied only to slowly moving atoms and ions

For the two cases considered here, that of the excitation of the $2\,^1$P states of He, and that of electron capture by a proton, we use respectively the final wave functions† —

$$\chi_n = \mathrm{N}_n \left\{ r_1 \begin{matrix}\cos\,\theta_1 \\ \sin\,\theta_1\end{matrix} e^{\pm i\phi_1} e^{-0{\cdot}5r_1-2r_2} + r_2 \begin{matrix}\cos\,\theta_2 \\ \sin\,\theta_2\end{matrix} e^{\pm i\phi_2} e^{-0{\cdot}5r_2-2r_1} \right\} \text{for excitation}$$

$$\chi_n = \mathrm{N}_n \{e^{-2r_1-\rho_2} + e^{-2r_2-\rho_1}\} \text{ for capture}$$

Inserting these functions in (21) we obtain —

For excitation

$$f_n(\theta, \phi) = \frac{ik}{2\pi} \int \left\{ \begin{matrix} \cos^2\theta' \mathrm{W}_1(r') - \sin^2\theta' \mathrm{W}_2(r') \\ \cos\theta' \sin\theta' (\mathrm{W}_1(r') + \mathrm{W}_2(r')) \end{matrix} \right\} \mathrm{E}(r', \theta')\, d\tau'$$

For capture

$$f_n(\theta, \phi) = \frac{ik}{2\pi} \int \cos\theta'\, \mathrm{W}_3(r')\, \mathrm{E}(r', \theta')\, d\tau_1.$$

In these formulæ

$$\mathrm{E}(r', \theta') = \exp\,[ir' \{(k - k_n \cos\theta) \cos\theta' + k_n \sin\theta \sin\theta' \cos\phi'\}]$$

and W_1, W_2, and W_3 are defined in terms of certain integrals over the electronic co-ordinates. They are given by —

$$\left.\begin{aligned} \mathrm{W}_1 = 2\mathrm{N}_n \frac{\partial \mathrm{N}_0}{\partial r} \mathrm{I}_1\mathrm{J}_1 - 2\mathrm{N}_0\mathrm{N}_n \Big[\frac{\partial Z}{\partial r} (\mathrm{I}_1\mathrm{J}_2 + \mathrm{J}_2\mathrm{I}_1) &+ \frac{\partial Z'}{\partial r} (\mathrm{I}_1\mathrm{J}_3 + \mathrm{J}_3\mathrm{I}_1) \\ &+ rZ' (\mathrm{I}_1\mathrm{J}_4 + \mathrm{J}_4\mathrm{I}_1) - Z' (\mathrm{I}_1\mathrm{J}_5 + \mathrm{J}_5\mathrm{I}_1)\Big] \\ \mathrm{W}_2 = 2\mathrm{N}_0\mathrm{N}_n Z' \{\mathrm{I}_6\mathrm{J}_1 + \mathrm{I}_7\mathrm{I}_1\} \\ \mathrm{W}_3 \text{ is of the same form as } \mathrm{W}_1 \text{ with K in place of I.} \end{aligned}\right\}. \quad (38)$$

The integrals I, J, K are defined below. As this type of integral occurs in all problems involving two centres of force, we give a detailed treatment of their evaluation in Appendix 2

---

† The wave function, χ_n, for excitation is that of the $2\,^1$P state of helium in the approximate form given by Eckart ('Phys. Rev.,' vol. 36, p. 878 (1930)).

$$
\begin{aligned}
\mathrm{I}_1 \cos\theta' &= \int r_1 \cos\theta_1\, e^{-ar_1-bp_1}\, d\tau_1 & \mathrm{J}_1 &= \int e^{-cr_1-dp_1}\, d\tau_1 \\
\mathrm{I}_2 \cos\theta' &= \int r_1^2 \cos\theta_1\, e^{-ar_1-bp_1}\, d\tau_1 & \mathrm{J}_2 &= \int r_1\, e^{-cr_1-dp_1}\, d\tau_1 \\
\mathrm{I}_3 \cos\theta' &= \int r_1 p_1 \cos\theta_1\, e^{-ar_1-bp_1}\, d\tau_1 & \mathrm{J}_3 &= \int p_1\, e^{-cr_1-dp_1}\, d\tau_1 \\
\mathrm{I}_4 \cos\theta' &= \int r_1 p_1^{-1} \cos\theta_1\, e^{-ar_1-bp_1}\, d\tau_1 & \mathrm{J}_4 &= \int p_1^{-1}\, e^{-cr_1-dp_1}\, d\tau_1 \\
\mathrm{I}_5 \cos\theta' &= \int r_1 p^1 \cos\theta_1 \cos\gamma\, e^{-ar_1-bp_1}\, d\tau_1 & \mathrm{J}_5 &= \int r_1 p_1^{-1}\, e^{-cr_1-dp_1} \cos\gamma\, d\tau_1 \\
\mathrm{I}_6 &= \int r_1^2 p^{-1}\, e^{-ar_1-bp_1}\, d\tau_1 & \mathrm{J}_6 &= \int r_1 p_1^{-1}\, e^{-cr_1-dp_1}\, d\tau_1 \\
\mathrm{I}_7 &= \int r p^{-1}\, e^{-ar_1-bp_1} \sin\gamma \frac{\partial\gamma}{\partial\theta'}\, d\tau_1, & \cos\gamma &= \cos\theta_1 \cos\theta' \\
& & &\quad + \sin\theta_1 \sin\theta' \cos(\phi_1 - \phi').
\end{aligned}
$$

The K's are of the same form as the corresponding J's, but have e, f in place of c, d. The values of the constants a, b, c, d are as follows —

For excitation, $a = \mathrm{Z} + 0{\cdot}5$, $b = \mathrm{Z}'$, $c = \mathrm{Z} + 2$, $d = \mathrm{Z}'$

For capture, $c = \mathrm{Z} + 2$, $d = \mathrm{Z}'$, $e = \mathrm{Z}$, $f = \mathrm{Z}' + 1$.

As will be seen, these integrals are complicated functions of the nuclear separation r' To avoid an extremely lengthy numerical integration over the r' co-ordinate the functions W were computed numerically and the values obtained fitted in the best possible way by functions of the form $r^l e^{-\lambda r^2}$. The actual functions used were

$$
\left.
\begin{aligned}
\mathrm{W}_1(r) &= \mathrm{C}_1 [16{\cdot}2 r^6 e^{-2{\cdot}56 r^2} + 15{\cdot}5 r^2 e^{-3{\cdot}535 r^2}] \\
\mathrm{W}_2(r) &= \mathrm{C}_2 [2{\cdot}035 r^6 e^{-2{\cdot}56 r^2} + 6{\cdot}25 r^2 e^{-3{\cdot}535 r^2}] \\
\mathrm{W}_3(r) &= \mathrm{C}_3 [24{\cdot}1 r^5 e^{-1{\cdot}55 r^2} + 31{\cdot}0 r\, e^{-4{\cdot}16 r^2}]
\end{aligned}
\right\}. \tag{39}
$$

The exact form of the W's are compared with the forms (39) in fig. 2. It will be seen that the latter correct the assumed discontinuous behaviour of $\partial\mathrm{Z}/\partial r$, $\partial\mathrm{Z}'/\partial r$, Z, Z′ to some extent.

Returning now to (37), the θ' and ϕ' integrations may be performed using the integral†

$$\int_0^{2\pi} \exp\{irk' \sin\theta' \cos\phi' \sin\theta\}\, e^{-im\phi'}\, d\phi' = 2\pi i^m J_m(k'r \sin\theta' \sin\theta),$$

and the Gegenbauer integral‡

$$\int_0^{\pi} \exp\{ir(k\cos\theta' - k_n \cos\theta' \cos\theta)\} \times J_m(k'r\sin\theta'\sin\theta)\, P_l^m(\cos\theta')\sin\theta'\, d\theta' = \sqrt{\frac{2\pi}{K}}\, J_{l+\frac{1}{2}}(Kr)\, i^{l-m}\, P_l^m(\cos\psi).$$

$$K^2 = k^2 + k_n^2 - 2kk_n\cos\theta$$

and

$$\cos\psi = (k - k_n\cos\theta)/K$$

Using the forms (40), the integration over the r co-ordinate may be carried out by use of Weber's integral§

$$\int_0^{\infty} J_\nu(Kr)\, e^{-\lambda r^2} r^{\nu+1}\, dr = K^\nu (2\lambda)^{-\nu-1} \exp(-K^2/4\lambda)$$

This completes the evaluation of the probability amplitude $f_n(\theta, \phi)$. To complete the calculation of the total cross-section, it is necessary to integrate over all values of θ and ϕ. This is most easily done by changing to the momentum variable K. We can then express $f_n(\theta, \phi)$ as a function of ϕ, K, and $k - k_n$, and the final integration may be carried out numerically. The results of the calculation are illustrated in fig. 3. For comparison the cross-section for excitation calculated by use of Born's approximation (9) is also given. It will be seen that the latter formula predicts much too big a cross-section for the lower energy encounters. This is to be expected, as the velocity of impact is so slow that multiple transitions take place between the colliding atoms. As a result a number of transitions which take place at the beginning of the encounter are reversed before the atoms are separated.

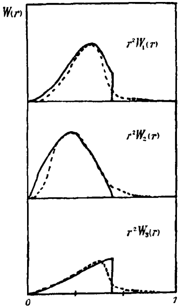

FIG. 2.

- - - - Actual form of curve
— Form assumed to simplify the calculation

---

† Watson, "Theory of Bessel Functions," (1922), p. 19.

‡ *Ibid.*, p. 379.

§ *Ibid.*, p. 393.

Born's approximation gives only the probability of the first of these transitions

§ 4 *Discussion of Results.*

An important feature of the results is that the probability of an inelastic collision is negligibly small unless the kinetic energy of the relative motion is greater than a certain value, which may be many times the least energy required for the process to be possible As this energy is not an ionization or excitation energy in the true sense, it is advisable to have a more satisfactory nomenclature; we propose the term activation energy or potential, as the case may be. It may be shown, by consideration of the form of the final integral expression for the excitation cross-section

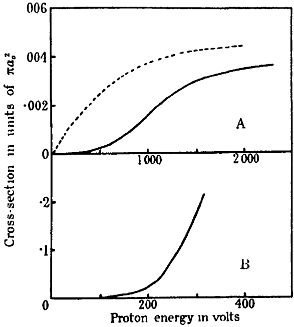

FIG. 3 —Calculated cross-sections for excitation and capture by protons in helium. A, excitation of 2 ¹P of He B, capture - - - calculated by Born's approximation

$$Q_n = \frac{k_n}{k}\int_0^{\pi}\int_0^{2\pi} |f_n(\theta, \phi)|^2 \sin\theta \, d\theta \, d\phi,$$

where $f_n(\theta, \phi)$ is given by (38) and (39), that the activation energy† is roughly proportional to

$$M(\Delta E)^2 r_0^2, \tag{40}$$

---

† This is the energy of relative motion and must not be confused with the energy measured with respect to a system in which one of the atoms is initially at rest.

where ΔE is the energy difference between the initial and final stationary states of the system and r_0 is a quantity approximately equal to the sum of the gas-kinetic radii of the ion and atom concerned.

For we may change the variable in the expression for Q_n to the momentum variable

$$K = (k^2 + k_n^2 - 2kk_n \cos\theta)^{\frac{1}{2}},$$

giving

$$Q_n = \int_{k-k_n}^{k+k_n} F_n(K, k, k_n)\, dK,$$

where $F_n(K, k, k_n)$ is only appreciable for such values of K that

$$Kr_0 < 1,$$

where r_0 is as defined in equation (36) Q_n is therefore negligible unless

$$(k - k_n)\, r_0 < 1,$$

i e.,

$$(k^2 - k_n^2)\, r_0 < k + k_n$$

Since

$$k^2 - k_n^2 = \frac{8\pi^2 M}{h^2}\,\Delta E$$

$$k + k_n \simeq 2k,$$

we have then

$$k > \frac{4\pi^2 M}{h^2}\,\Delta E\, r_0.$$

On substitution for k we obtain the result (40)

The existence of an activation energy is in accord with the observations of excitation and ionization by heavy particles. Direct experiments on excitation of helium by hydrogen canal rays (a mixture of protons and neutral hydrogen atoms) have recently been carried out by Dopel † The excitation curve he obtains for the excitation of the 4 ^{1}P level of helium is illustrated in fig 4 and compared with the corresponding curve for electrons. Absolute values of the cross-sections have been obtained from the known values for electrons ‡ It will be noticed immediately that the form of the excitation curve is very similar to that calculated for protons , but the activation energy is somewhat higher than that calculated. In view of the rough nature of the wave functions used in the calculations, this is not surprising.

Döpel states that protons are at most only one-tenth as effective as hydrogen atoms in exciting helium atoms, but he obtains this result from measurements of the intensity of excitation of the 3 ^{3}P—2 ^{3}S line. This line could not, in fact, be excited by protons at all, as a transition from the ground state of helium to the 3 ^{3}P state requires a reversal of electron spin , hence the presence of a third electron is necessary to change places with one of the helium electrons Such an electron may be supplied by impact with an electron or hydrogen atom, but not with a proton It is therefore difficult to say how much of the observed excitation of the 4 ^{1}P level is due to protons and how much to hydrogen atoms All one can say by reference to fig. 3 is that the observed cross-section is of the same order of magnitude as that calculated for protons

---

† 'Ann Physik,' vol. 5, p. 1 (1933).

‡ Massey and Mohr, 'Proc. Roy. Soc.,' A, vol. 140, p. 613 (1933).

The experiments show also that, for the lower voltages of impact, a greater proportion of the collisions between hydrogen atoms and helium atoms result

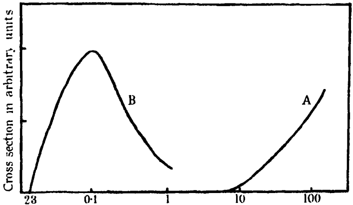

FIG 4.—Observed cross-sections for excitation of the 4 ^{1}P level of helium by hydrogen canal rays (H + H+) and by electrons. A, canal rays , B, electrons. The scale is such that the maximum value of the cross section for electron excitation is 0 01 πa^2

in the excitation of hydrogen lines than of helium lines, a result which is reversed at the higher energies This is to be expected, since ΔE is only 10 volts for hydrogen excitation, but 20 volts for helium excitation. The respective activation energies are then in the ratio of 1 4 At higher energies the helium excitation is fully activated, but that of hydrogen has passed through its maximum.

Döpel has also carried out experiments on the excitation of sodium, potassium, and mercury by the hydrogen canal rays, and obtains the striking result that, although the heavy atoms are strongly excited by the impact of the canal rays there is no evidence of any excitation of the hydrogen atoms themselves. This is explicable in terms of (40), for the ratio of the activation potentials is equal to the square of the ratios of the excitation potentials. For potassium this ratio is as high as 70, and even for mercury it is as great as 4. The reason why the activation energy for excitation of hydrogen atoms by collision with these heavy atoms is so much greater than that for excitation of helium by canal rays is that r_0 is much larger for the large heavy atoms (see (40)).

Similar results have been obtained by investigation of the probabilities of ionization by positive ions and neutral atoms.[†] The existence of an activation potential is well established, and it appears that neutral atoms are more effective ionizers than the corresponding slow ions. This is probably due to the decrease of r_0 for neutral atom collisions owing to the screening effect of the external atomic electrons Such a decrease not only reduces the activation potential, but also increases the gradient of the initial wave function χ_0 with respect to nuclear separation, thereby increasing the corresponding matrix element

We see then that the theory introduced above is capable of providing a qualitative explanation of a number of the experimental results, but in order to obtain quantitative results it will be necessary to use wave functions which have been determined by a variation method This will be carried out in a later paper.

The only evidence available as to the cross-section for capture comes from observations of the total absorbing cross-sections of various gases for protons Ramsauer, Kollath, and Lilienthal[‡] have carried out such measurements in argon, hydrogen, nitrogen, neon, and helium, their results for protons with energies between 50 and 1000 volts are illustrated in fig. 5 It will be seen that, although the observed cross-section is comparable with the gas kinetic in argon, hydrogen, and nitrogen, it is very much smaller than the gas kinetic for neon and helium Further, although the cross-section for helium decreases continually as the protons energy increases, the cross-section for the other gases at first decreases and then, for protons with energies greater than about 300 volts, begins to increase again Since the velocities of the protons used in these experiments is such that the minima occur at nearly the same velocities as in the Ramsauer effect for electrons, it has been suggested that the explanation of the latter effect may also apply to the proton results This is, however, inconceivable, because the Ramsauer effect is determined by the wave-length and not the velocity of the particles, and in any case cannot occur for a repulsive field of force. Also we have shown in § 2 that the angular distribution of the elastically scattered protons falls off so rapidly with increase of angle that experiments such as those of Ramsauer, Kollath, and Lilienthal could only measure a small percentage of the elastic cross-section except at very low energies The most probable explanation of the observed minima can be given in terms of the theory of this paper For low proton voltages excitation and capture processes are of negligible importance, as in no case is an activation energy exceeded The observed cross-section must then be mainly that due to elastic scattering This cross-section as measured will decrease rapidly with increase of proton energy, because the elastic angular distribution increases in steepness as the energy increases, and fewer elastic collisions result in sufficient deviation to make possible their detection in the experiments. As the voltage increases, capture and excitation processes set in with increasing probability. When the rate of increase of the inelastic cross-section equals the rate of decrease of the measured elastic cross-section, the minimum appears in the observed curves. Consideration of the energy loss ΔE involved in electron capture by the protons from the gas atoms indicates that the activation energies for this process in helium should be higher than in neon, and that for neon should be higher than for the remaining gases. The minimum should therefore occur at a higher voltage for helium than for neon, and higher for neon than for the other three gases. This is in agreement with the observations Further, the high activation energies for helium and neon explain the low values observed for their cross-sections.

[†] *Vide* Thomson and Thomson, "Conduction of Electricity in Gases," Pt II chap. IV

[‡] 'Ann Physik,' vol. 8, p. 709 (1931).

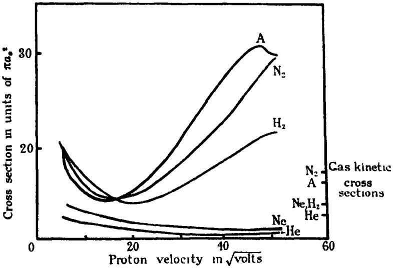

Fig. 5 —Observed total absorption cross sections for protons.

Evidence in favour of the correctness of this explanation is afforded by certain results obtained by Ramsauer, Kollath, and Lilienthal with the same apparatus. They find that for low proton energies (up to a few hundred volts) there is no evidence of the occurrence of any excitation or capture process, as no very slow ions or electrons were detected in the experimental chamber during the passage of the protons, for higher energies slow ions were observed, which were undoubtedly formed by electron transfer to the proton beam Even at the highest energies investigated no slow electrons were observed, showing that ionization by the protons was still very small As the activation energy for excitation and ionization is much larger than that for electron capture (ΔE being much larger) this last result is also to be expected

If one refers to fig 3, it appears that the calculated activation potential for neutralization of protons by helium atoms is too low to explain the observed results. A similar discrepancy was noted above for excitation, and is undoubtedly due to the crudeness of the wave functions χ_0 and χ_n used in the calculations As the activation potential is roughly proportional to $r_0{}^2$ a slightly larger value of r_0 would remove the discrepancy

Somewhat similar experiments have been carried out by Dempster,[†] who found that protons with energies between 14 and 930 volts have very long free paths in helium, just as observed by Ramsauer, Kollath, and Lilienthal The explanation is the same as that given above. The experiments detect few elastic collisions, owing to the small deviations involved, and in the voltage range used the lowest activation potential, that for capture, has been barely exceeded

§ 5 *Electron Transfer in the Case of Exact Resonance*

When we consider the collisions of ions with similar atoms (such as He^+ with He), it is necessary to modify the method of calculation If He^+ ions are scattered by helium gas, it is impossible to determine whether an observed ion has been directly scattered, or whether it is a knocked-on atom which has lost an electron This must be taken account of in the theory, just as in the theory of the scattering of α-particles by helium nuclei.[‡]

The wave equation for the complete system is as before

$$\left[\frac{h^2}{8\pi^2 M}\nabla^2 - H_a(\mathbf{r}_a) - H_b(\mathbf{r}_b) - V(\mathbf{r}, \mathbf{r}_a, \mathbf{r}_b) + E\right]\Psi = 0, \qquad (41)$$

[†] 'Phil. Mag.,' vol. 3, p. 115 (1927).

[‡] Mott, 'Proc. Roy Soc.,' A, vol. 126, p. 259 (1930).

and again we have the equation

$$[-H_a(\mathbf{r}_a) - H_b(\mathbf{r}_b) + E - V(\mathbf{r}, \mathbf{r}_a, \mathbf{r}_b)]\chi = 0, \tag{42}$$

for the functions χ. Owing, however, to the indistinguishability of the nuclei, we now have two sets of electronic states to deal with, one set symmetric in the nuclei, the other, antisymmetric For the purpose in hand we consider only those two states which result from the ground states of the ion and atom when the two are brought together adiabatically These differ in nuclear symmetry, we denote them by χ_S, χ_A, the suffices indicating the type of nuclear symmetry.

Writing

$$\Psi' = \chi_S F_S(\mathbf{r}) + \chi_A F_A(\mathbf{r}), \tag{43}$$

we obtain, by following the same procedure as in § 1,

$$\left.\begin{aligned} &\nabla^2 F_A + \left\{k^2 + \eta_A(r) + \iint \chi^*{}_A \nabla^2 \chi_A \, d\tau_a \, d\tau_b\right\} F_A \\ &\qquad = - F_S \iint \chi^*{}_A \nabla^2 \chi_S \, d\tau_a \, d\tau_b - 2 \operatorname{grad} F_S \iint \chi^*{}_A \operatorname{grad} \chi_S \, d\tau_a \, d\tau_b \\ &\nabla^2 F_S + \left\{k^2 + \eta_S(r) + \iint \chi^*{}_S \nabla^2 \chi_S \, d\tau_a \, d\tau_b\right\} F_S \\ &\qquad = - F_A \iint \chi^*{}_S \nabla^2 \chi_A \, d\tau_a \, d\tau_b - 2 \operatorname{grad} F_A \,.\iint \chi^*{}_S \operatorname{grad} \chi_A \, d\tau_a \, d\tau_b \end{aligned}\right\} \tag{44}$$

The interaction terms on the right-hand sides of these equations are small, on account of the opposing symmetry, and may be neglected, we are left with two uncoupled equations which represent elastic scattering by the fields of force resulting respectively from the two types of interaction We may therefore obtain solutions which have the asymptotic form

$$\left.\begin{aligned} F_S &\sim \alpha\{e^{ikz} + r^{-1} e^{ikr} f_S(\theta, \phi)\} \\ F_A &\sim \beta\{e^{ikz} + r^{-1} e^{ikr} f_A(\theta, \phi)\} \end{aligned}\right\}, \tag{45}$$

for large r.

Substituting in (45) we obtain for Ψ' the asymptotic form

$$\Psi' \sim (\alpha\chi_S + \beta\chi_A) e^{ikz} + r^{-1} e^{ikr} \{\alpha\chi_S f_S(\theta, \phi) + \beta\chi_A f_A(\theta, \phi)\}. \tag{46}$$

This form for Ψ' is unsymmetric in the nuclei, and we must form the symmetric and antisymmetric solutions Ψ_S, Ψ_A, from Ψ' by linear combination. We find

then

$$\Psi'_S \sim 2\alpha\chi_S \cos kz + 2i\beta\chi_A \sin kz + r^{-1} e^{ikr} [\alpha\chi_S \{f_S(\theta, \phi) + f_S(\pi - \theta, \phi)\} + \beta\chi_A \{f_A(\theta, \phi) - f_A(\pi - \theta, \phi)\}], \quad (47)$$

and a similar expression for Ψ'_A. In what follows we assume that the nuclei obey the Bose-Einstein statistics, so that Ψ'_S is the function which must be used to describe the scattering

To complete the solution we must fix α and β. To do this we make use of the initial condition that the incident ion is moving in the direction of the positive z axis. For simplicity we consider only one electron whose co-ordinates we denote by $\boldsymbol{\rho}$ We also distinguish the co-ordinates of the nuclei by suffixes 1 and 2 so

$$|\mathbf{r}_1 - \mathbf{r}_2| = r$$

$$z_1 - z_2 = z.$$

Now we have for large r,

$$\chi_S \sim \psi(|\mathbf{r}_1 - \boldsymbol{\rho}|) + \psi(|\mathbf{r}_2 - \boldsymbol{\rho}|)$$

$$\chi_A \sim \psi(|\mathbf{r}_1 - \boldsymbol{\rho}|) - \psi(|\mathbf{r}_2 - \boldsymbol{\rho}|),$$

so, using (45), we see that the incident wave in Ψ'_s is given by

$$e^{ik(z_1-z_2)} \{(\alpha + \beta)\psi(|\mathbf{r}_1 - \boldsymbol{\rho}|) + (\alpha - \beta)\psi(|\mathbf{r}_2 - \boldsymbol{\rho}|)\} + e^{-ik(z_1-z_2)} \{(\alpha - \beta)\psi(|\mathbf{r}_1 - \boldsymbol{\rho}|) + (\alpha + \beta)\psi(|\mathbf{r}_2 - \boldsymbol{\rho}|)\}.$$

To satisfy the condition that the ion (i e, the nucleus without an electron) is moving in the positive z direction (wave function e^{+ikz}) we must have $\alpha = -\beta$. This gives for the incident wave

$$2\alpha \{e^{ik(z_1-z_2)}\psi(|\mathbf{r}_2 - \boldsymbol{\rho}|) + e^{ik(z_2-z_1)}\psi(|\mathbf{r}_1 - \boldsymbol{\rho}|)\} \quad (48)$$

Using (45) and (47) we now have for the asymptotic form of the scattered wave

$$\alpha r^{-1} e^{ikr} [\psi(|\mathbf{r}_1 - \boldsymbol{\rho}|) \{f_S(\theta) + f_S(\pi - \theta) - f_A(\theta) + f_A(\pi - \theta)\} + \psi(|\mathbf{r}_2 - \boldsymbol{\rho}|) \{f_S(\theta) + f_S(\pi - \theta) + f_A(\theta) - f_A(\pi - \theta)\}]. \quad (49)$$

The scattered amplitude associated with an incident wave of unit amplitude moving in the direction of positive z is then

$$f(\theta) = \tfrac{1}{2}\{f_S(\theta) + f_S(\pi - \theta) + f_A(\theta) - f_A(\pi - \theta)\} \quad (50)$$

The scattered intensity of ions per unit solid angle is then given in terms of relative co-ordinates by $|f(\theta)|^2$.

If we have a beam of ions passing through a gas we may change directly to a co-ordinate system (Θ, Φ), in which the gas atoms are initially at rest, by writing $\theta = 2\Theta$. This gives the intensity of scattering of the ions per unit angle in the form

$$2\pi I(\Theta) \sin \Theta = \pi \left| f_S(2\Theta) + f_S(\pi - 2\Theta) + f_A(2\Theta) - f_A(\pi - 2\Theta) \right|^2 \sin 2\Theta \tag{51}$$

Now the functions $f_S(\theta)$, $f_A(\theta)$ are known to have negligible values, except when θ is small. Hence $f(\theta)$ and $f(\pi - \theta)$ overlap very little, and we may write

$$2\pi I(\Theta) \sin \Theta = \pi \{ |f_S(2\Theta) + f_A(2\Theta)|^2 + |f_S(\pi - 2\Theta) - f_A(\pi - 2\Theta)|^2 \} \sin 2\Theta \tag{52}$$

The first term may be regarded as due to direct elastic scattering of the ions, the second to electron transfer. The cross-section for the latter process will then be

$$Q_0{}^t = \tfrac{1}{2}\pi \int_0^\pi |f_S(\theta) - f_A(\theta)|^2 \sin \theta \, d\theta$$

Following the method of Faxèn and Holtsmark (*loc. cit.*) we may write

$$\left. \begin{aligned} f_S(\theta) &= \frac{1}{2ik} \Sigma_s (e^{2i\beta_s} - 1)(2s + 1) P_s(\cos \theta) \\ f_A(\theta) &= \frac{1}{2ik} \Sigma_s (e^{2i\gamma_s} - 1)(2s + 1) P_s(\cos \theta) \end{aligned} \right\}, \tag{53}$$

where the phases β_s, γ_s are determined from the solutions of the equation (44). The cross-section for transfer then becomes

$$Q_0{}^t = \frac{\pi}{k^2} \Sigma_s (2s + 1) \sin^2 (\beta_s - \gamma_s) \tag{54}$$

This result was also obtained by London,[†] who, however, did not consider the symmetry properties of the system. It must be remembered that the cross-section $Q_0{}^t$ is arbitrarily chosen on the assumption that all ions scattered at large angles are atoms which have lost an electron in the collision, an assumption which has no meaning experimentally. Since we know, however, that, when resonance is not exact, there is no appreciable large angle scattering of the incident ions, the transfer process may be separated out as above; thus the treatment represents the limiting case of approximate resonance. If accurate formulæ for the angular distribution of the scattered ions at intermediate angles are required, this arbitrary separation of direct scattering and transfer is no longer valid, and the more accurate formula (52) must be used.

[†] 'Z. Physik,' vol. 74, p. 143 (1932).

5 1. *Calculation for Helium Ions in Helium.* --The evaluation of Q_0^t for this case may be carried out in exactly the same way as the calculation of elastic cross-sections in § 2 The phases β_n, γ_n are just those which occur in the elastic scattering by the two possible fields of interaction These interaction energies have been worked out for a considerable range of nuclear separation by Pauling,† and his values were extrapolated when necessary The series for Q_0^t was summed in the same way as that for Q_0 in § 2.

The value 6 7 πa_0^2 was obtained in this way for Q_0^t for 1000-volt ions This may be compared with the value, 11 3 πa_0^2, of the absorbing cross-section for 600-volt He^+ ions in helium measured by Dempster ‡ As the absorption in these experiments must result mainly from large angle scattering (which we interpret as due to charge transfer), it will be seen that the agreement is quite satisfactory. Kallmann and B Rosen§ have found much bigger cross-sections (of the order 60 πa_0^2) for A^+ in argon, N_2^+ in nitrogen and H_2^+ in hydrogen, but they find much smaller values for He^+ in helium in agreement with the above

As the theoretical values for these cross-sections depend on the exchange energy, the agreement with experiment provides a further verification of the theory of interaction of atoms, which has already been so successful in the interpretation of chemical phenomena.

Summary.

The collisions with gas atoms of slow positive ions (velocity less than the orbital velocity of atomic electrons) are discussed in terms of a quantum mechanical theory of collisions. This theory treats the relative motion of the centres of mass of the ions and atoms as a perturbation, and is applied to both elastic and inelastic collisions. It is found possible to correlate most of the experimental results in terms of the theoretical formulæ, and good agreement is found between observed and calculated collision cross-sections

The case of collisions of ions with similar atoms is also considered in detail, taking account of nuclear symmetry.

---

† 'J. Chem. Phys.,' vol. 1, p 56 (1933).

‡ 'Phil. Mag ,' vol. 3, p. 115 (1927).

§ 'Z Physik,' vol. 61, p. 61 (1930).

APPENDIX 1.

Calculation of the phases δ_n *for large* n —We have to evaluate

$$\int_0^\infty r\mathrm{V}(r)\,\{\mathrm{J}_{n+\frac{1}{2}}(kr)\}^2\,dr,$$

when n is large. To do this[†] we break up the range of integration and write

$$\int_0^\infty r\mathrm{V}(r)\,\{\mathrm{J}_{n+\frac{1}{2}}(kr)\}^2\,dr = \left\{\int_{r_0}^\infty + \int_0^{r_0}\right\} r\mathrm{V}(r)\,\{\mathrm{J}_{n+\frac{1}{2}}(kr)\}^2\,dr,$$

where r_0 is the first zero of $\mathrm{J}_{n+\frac{1}{2}}(kr)$

To evaluate the first of these integrals we use the formula[‡]

$$\mathrm{J}_n(n\sec\beta) \sim \cos\left[n(\tan\beta - \beta) - \tfrac{1}{4}\pi\right]\left[\tfrac{1}{2}n\pi\tan\beta\right]^{-\frac{1}{2}},$$

for large n, this shows that $\mathrm{J}_{n+\frac{1}{2}}(kr)$ oscillates rapidly for $r > r_0$ with an amplitude which is given to a close approximation by

$$(\tfrac{1}{2}\pi)^{-\frac{1}{2}}(k^2r^2 - n^2)^{-\frac{1}{4}}$$

Replacing the oscillatory function by its mean value we obtain

$$\int_{r_0}^\infty r\mathrm{V}\,[\mathrm{J}_{n+\frac{1}{2}}(kr)]^2\,dr \simeq \frac{1}{\pi}\int_{r_0}^\infty r\mathrm{V}\,(r^2k^2 - n^2)^{-\frac{1}{2}}\,dr$$

The integral on the right-hand side can be evaluated numerically without difficulty, making use of the result that the position of the zero is given accurately by[§]

$$kr_0 = n + 1\cdot 86\, n^{1/3}$$

The contribution from the range $r < r_0$ is quite small, and it is sufficient to estimate it from the known position r_0 of the zero and the position, r_m, of the first maximum of $\mathrm{J}_{n+\frac{1}{2}}(kr)$, which is given by[||]

$$kr_m = n + 0\cdot 81\, n^{1/3}.$$

APPENDIX 2

(*a*) ***Evaluation of the integrals*** I_1, I_2, I_3, I_4 —The integrals required may all be obtained from the integral

$$\mathrm{I}_4 = \sec\theta\int\cos\theta_1\, r_1\, p_1^{-1}\, e^{-ar_1 - bp_1}\, d\tau_1,$$

by differentiation with respect to a and b.

[†] We are indebted to Dr. C B. O Mohr for suggesting this procedure

[‡] Watson, "Theory of Bessel Functions" (1922), p. 234.

[§] *Ibid.*, p. 516.

[||] *Ibid.*, p. 521.

To evaluate I_4 we expand $p^{-1} e^{-bp}$ in a series of spherical harmonics† —

$$p_1^{-1} e^{-bp_1} = (rr_1)^{-\frac{1}{2}} \sum_{n=0}^{\infty} (2n+1) \gamma_n(r, r_1) P_n(\cos\gamma),$$

where

$$\cos\gamma = \cos\theta\cos\theta_1 + \sin\theta\sin\theta_1\cos\phi$$

$$\begin{aligned} \gamma_n &= K_{n+\frac{1}{2}}(br_1)\, I_{n+\frac{1}{2}}(br) \qquad r_1 > r \\ &= I_{n+\frac{1}{2}}(br_1)\, K_{n+\frac{1}{2}}(br) \qquad r_1 < r. \end{aligned}$$

Now

$$\begin{aligned} P_n(\cos\gamma) = {} & P_n(\cos\theta) P_n(\cos\theta_1) \\ & + 2 \sum_{m=1}^{n} \frac{(n-m)!}{(n+m)!} (-1)^m P_n^m(\cos\theta) P_n^m(\cos\theta_1) \cos m\phi. \end{aligned}$$

On integrating with respect to ϕ all the terms vanish for which $m \neq 0$, while the only harmonic which gives a contribution on integrating with respect to θ_1 is that of order 1 The integral therefore reduces to

$$\begin{aligned} I_4 = \frac{2\pi}{br} \Bigg\{ & e^{-br}\left(1 + \frac{1}{br}\right) \int_0^r \left[e^{-(a-b)r_1}\left(1 - \frac{1}{br_1}\right) + e^{-(a+b)r_1}\left(1 + \frac{1}{br_1}\right)\right] r_1^2 dr_1 \\ & + \left[e^{br}\left(1 - \frac{1}{br}\right) + e^{-br}\left(1 + \frac{1}{br}\right)\right] \int_r^{\infty} e^{-(a+b)r_1}\left(1 + \frac{1}{br_1}\right) r_1^2 dr_1 \Bigg\}. \end{aligned}$$

The integration with respect to r_1 is straightforward, and leads to

$$\begin{aligned} I_4/2\pi = r^{-2}(a^2 - b^2)^{-3} [& e^{-br}\, 16a(1 + br) - e^{-ar}\{16a(1 + ar) \\ & + 8ar^2(a^2 - b^2) + 2r^3(a^2 - b^2)^2\}]. \end{aligned}$$

From this integral we deduce

$$\begin{aligned} I_1/2\pi = -\frac{I}{2\pi}\frac{\partial I_4}{\partial b} = r^{-2}(a^2 - b^2)^{-4} [& 16\, e^{-br}\{abr^2(a^2 - b^2) - 6ab(1 + br)\} \\ & + 4e^{-ar}\{24ab(1 + ar) + 8abr^2(a^2 - b^2) + br^3(a^2 - b^2)^2\}], \end{aligned}$$

$$\begin{aligned} I_2/2\pi = -\frac{1}{2\pi}\frac{\partial I_1}{\partial a} = r^{-2}(a^2 - b^2)^{-5} [& 16\, e^{-br}\{(b^3 + 5a^2b)(a^2 - b^2) r^2 \\ & - 6(b^3 + 7a^2b)(1 + br)\} + 4\, e^{-ar}\{24(b^3 + 7a^2b)(1 + ar) \\ & + 8(8a^2b + b^3)(a^2 - b^2) r^2 + 12abr^3(a^2 - b^2)^2 + br^4(a^2 - b^2)^3\}], \end{aligned}$$

$$\begin{aligned} I_3/2\pi = -\frac{1}{2\pi}\frac{\partial I_1}{\partial b} = r^{-2}(a^2 - b^2)^{-5} [& 16\, e^{-br}\{abr^3(a^2 - b^2)^2 \\ & - (a^3 + 11ab^2)(a^2 - b^2) r^2 + 6(a^3 + 7ab^2)(+ 1\, br)\} \\ & - 4\, e^{-ar}\{24(a^3 + 7ab^2)(1 + ar) \\ & + 8(a^3 + 11ab^2)(a^2 - b^2) r^2 + (a^2 + 3b^2)(a^2 - b^2)^2 r^3\}]. \end{aligned}$$

---

† Watson, "Theory of Bessel Functions," p. 366 (1922)

(*b*) *Evaluation of the integrals* J *and* I_6.—These integrals are evaluated by exactly the same method. When we perform the θ_1 integration this time, however, only the zero order harmonic will contribute Thus we have

$$J_4 = \int p_1^{-1} e^{-cr_1 - dp_1} \, d\tau_1$$

$$= 4\pi r^{-\frac{1}{2}} \left[\int_0^r r_1^{-\frac{1}{2}} e^{-cr_1} I_{\frac{1}{2}}(dr_1) \, K_{\frac{1}{2}}(dr) \, r_1^2 \, dr_1 + \int_r^\infty r_1^{-\frac{1}{2}} e^{-cr_1} I_{\frac{1}{2}}(dr) \, K_{\frac{1}{2}}(dr_1) \, r_1^2 \, dr_1 \right],$$

which, on inserting the expressions for the Bessel functions becomes

$$(4\pi/dr) \left[\sinh dr \int_r^\infty r_1 \, e^{-(c+d)\, r_1} \, dr_1 + e^{-dr} \int_0^r r_1 \, e^{-cr_1} \sinh dr_1 \, dr_1 \right].$$

Performing the r-integration we obtain

$$J_4/4\pi = r^{-1} (c^2 - d^2)^{-2} \left[2c \, e^{-dr} - e^{-cr} \{ 2c + r(c^2 - d^2) \} \right]$$

From this integral we deduce that

$$J_1/8\pi = -\frac{1}{8\pi} \frac{\partial J_4}{\partial d} = (c^2 - d^2)^{-3} r^{-1} \left[r e^{-dr} \{ r(c^2 - d^2) - 4d \} \right.$$
$$\left. + \, d e^{-cr} \{ r(c^2 - d^2) + 4c \} \right],$$

$$J_2/8\pi = -\frac{1}{8\pi} \frac{\partial J_1}{\partial c} = r^{-1} (c^2 - d^2)^{-4} \left[e^{-dr} \{ -r(c^2 - d^2)^2 + 4(d + c^2 r)(c^2 - d^2) \right.$$
$$\left. - 24c^2 d \} + e^{-cr} \{ r^2 d + 4d(2cr - 1)(c^2 - d^2) + 24c^2 d \} \right],$$

$$J_3/8\pi = -\frac{1}{8\pi} \frac{\partial J_1}{\partial d} = r^{-1} (c^2 - d^2)^{-4} \left[e^{-dr} \{ r^2 c (c^2 - d^2)^2 \right.$$
$$- 4c(2dr - 1)(c^2 - d^2) + 24cd^2 \} - e^{-cr} \{ (c^2 - d^2)^2 r$$
$$\left. + \, 4(c + d^2 r)(c^2 - d^2) + 24cd^2 \} \right].$$

It can be shown by integrating with respect to θ_1 and ϕ_1 that $J_5 = \frac{1}{3} J_6$ (*cf* I_5), for which we obtain the expression

$$J_6/4\pi = -\frac{1}{4\pi} \frac{\partial J_4}{\partial c} = r^{-1} (c^2 - d^2)^{-3} \left[2e^{-dr} (3c^2 + d^2) + e^{-cr} \{ -r^2 (c^2 - d^2)^2 \right.$$
$$\left. + \, 2(1 - 2cr)(c^2 - d^2) - 8c^2 \} \right].$$

Finally, we have

$$I_6/4\pi = \frac{1}{4\pi} \frac{\partial^2 I_4}{\partial a^2} = r^{-1} (a^2 - b^2)^{-4} \left[24 e^{-br} a (a^2 + b^2) - e^{-ar} \{ r^3 (a^2 - b^2)^3 \right.$$
$$\left. + \, 6ar^2 (a^2 - b^2)^2 + 6r(3a^2 + b^2)(a^2 - b^2) + 24a(a^2 + b^2) \} \right].$$

(*c*) *Evaluation of* $I_5 = \sec\theta \int r_1 p_1^{-1} e^{-ar_1-bp_1} \cos\gamma \cos\theta_1 \, d\tau_1$.—In order to apply the former method to this integral we use the recurrence formula

$$(2n+1)\cos\gamma \, P_n(\cos\gamma) = (n+1) P_{n+1}(\cos\gamma) + n P_{n-1}(\cos\gamma).$$

Hence

$$I_5 \cos\theta = \int \sum_1^{\infty} \{(n+1) P_{n+1}(\cos\gamma) + n P_{n-1}(\cos\gamma)\} F_n(r_1) \cos\theta_1 \, d\tau_1,$$

where

$$F_n(r_1) = (r_1 r)^{-\frac{1}{2}} e^{-ar_1} I_{n+\frac{1}{2}}(br_1) K_{n+\frac{1}{2}}(br) \; r_1 < r.$$

Now

$$\int_0^{\pi}\int_0^{2\pi} P_n(\cos\gamma) \cos\theta_1 \sin\theta_1 \, d\theta_1 \, dp_1 = \frac{4\pi}{3}\cos\theta, \; n = 1$$

$$= 0, \qquad n \neq 1,$$

so

$$I_5 = \frac{4\pi}{3}\int_0^{\infty} (F_0 + 2F_2) \, dr_1$$

The first term of the integral gives $\frac{1}{3} I_6$ On substituting for the Bessel functions the second term may be evaluated to give

$$I_5 = \frac{4\pi}{3r^3}(a^2-b^2)^{-5}[e^{-ar}\{-2r^5(a^2-b^2)^4 - 12ar^4(a^2-b^2)^3 - 48a^2r^3(a^2-b^2)^2$$
$$+ 48ar^2(b^2-3a^2)(a^2-b^2) - 288a(1+ar)\}$$
$$+ e^{-br}\{288a(1+br) + 96ab^2r^2(a^2-b^2)\}] + \tfrac{1}{3} I_6$$

(*d*) *Proof that* $I_7 = \int r_1 p_1^{-1} e^{-ar_1-bp_1} \sin\gamma \frac{d\gamma}{d\theta} d\tau_1 = 0$ —The angular integration gives

$$\int_0^{\pi}\int_0^{2\pi} \Sigma_n F_n(r_1) P_n(\cos\gamma) [\sin\theta\cos\theta_1 - \cos\theta\sin\theta_1\cos\phi_1] \sin\theta_1 \, d\theta_1 \, d\phi_1$$

$$= F_1 \int_0^{\pi}\int_0^{2\pi} \cos\gamma [\sin\theta\cos\theta_1 - \cos\theta\sin\theta_1\cos\phi_1] \sin\theta \, d\theta \, d\phi$$

$$= 2\pi F_1 \int_0^{\pi} \sin\theta\cos\theta [2\cos^2\theta_1 - 1] \, d\theta_1$$

$$= 0.$$

The Estimation of Electric Moment in Solution by the Temperature Coefficient Method. Part I.—Experimental Method and the Electric Moments of some Benzyl Compounds

By FRED FAIRBROTHER, D Sc, The Chemical Department, The University, Manchester

(Communicated by A. Lapworth, F R S —Received April 29, 1933)

1 *Introduction.*

The theory of the estimation of the electric moment of molecules dissolved in a non-polar solvent is now well known* The fundamental equation† is

$$P_{2\infty} = \frac{4\pi}{3} N \left(\alpha_0 + \frac{\mu^2}{3kT}\right) \tag{1}$$

in which the symbols have the following significance · $P_{2\infty}$ the total polarizability of the solute per gram molecule at infinite dilution, N Avogadro's number, α_0 the moment induced in a single molecule by unit electric field, k the Boltzmann gas constant, T the absolute temperature, and μ the permanent electric moment of the molecule This equation is of the form

$$P_{2\infty} = A + B/T, \tag{2}$$

where

$$A = \frac{4\pi}{3} N\alpha_0 \quad \text{and} \quad B = \frac{4\pi}{9} \frac{N\mu^2}{k},$$

from which it follows that if A and B are constant, *i e.*, independent of temperature, then each may be evaluated from a series of measurements of $P_{2\infty}$ at different temperatures or alternatively B (and hence μ) may be obtained from one value of $P_{2\infty}$ at one temperature, provided that A can be obtained by some independent method

Of such measurements, by far the majority have been made at one temperature only, A being estimated either from the polarization of the substance in the solid state, or more usually from measurements of the refractive indices of the solutions. The latter method may, however, lead to inaccuracy in the value of μ on account of the uncertainty regarding the magnitude of the atomic polarization P_A.

---

* *Cf.* Debye, "Polar Molecules," New York (1929); Smyth, "Dielectric Constant and Molecular Structure," New York (1931).

† Debye, 'Phys Z.,' vol. 13, p. 97 (1912), "Handb. Radiologie" (Marx), Leipzig, vol. 6, p. 597 (1925).

On the other hand, the evaluation of A and B in equation (2) by measurements made at several temperatures, is theoretically more free from objection, but introduces certain practical difficulties In particular, the usual available accuracy of measurement of dielectric constant requires for anything more than an approximate estimation of the electric moment by this method, a temperature range greater than is possible in the solvent most widely used, namely, benzene, since in order to eliminate the effect of molecular association it is necessary to work in dilute solution in which the temperature coefficient of the polarization is correspondingly small Several investigators have measured the polarization of substances dissolved in benzene at various temperatures, but the limited range of temperature within which benzene is liquid renders the exact location of the $P_{2\infty} - 1/T$ curves very difficult [*] Measurements in solution over wider ranges of temperature have been carried out chiefly by Smyth and his collaborators,[†] who have measured the polarization of a number of substances dissolved in normal hexane and normal heptane over temperature ranges from − 90° or − 100° to 60° or 70° (the actual range differed in the various cases) Morgan and Lowry[‡] have also measured the polarization of the methyl halides in hexane and carbon tetrachloride between − 100° and + 40°, and Bretscher[§] has measured the polarization of several benzene derivatives in solution in dekalin, tetrachloroethylene and *p*-cymene from 25° to 90° The only measurements of polarization in solution that appear to have been made at temperatures higher than 90° are those of the polarization of diethyl succinate in kerosene from 0° to 200° carried out by Smyth, Dornte, and Wilson [||]

In the present work an attempt has been made to estimate the electric moment of several compounds from measurements in solution over temperature ranges of 100° and 140° and from measurements of the refractive index, and polarizability of the substance in the solid state, to obtain some information as to the approximate magnitude of the atomic polarization and of the change of moment with temperature in certain cases.

---

[*] *Cf.* Wolf and Fuchs in Freudenberg "Stereochemie," p 209, and Smyth, 'J Amer Chem Soc,' vol 53, p 545 (1931).

[†] 'J. Amer Chem. Soc.,' vol. 50, p 1547 (1928); vol 51, p 3312 (1929); vol. 52, p. 2227 (1930); vol 53, pp 545, 4242 (1931)

[‡] 'J. Phys. Chem.,' vol. 34, p 2385 (1930)

[§] 'Phys. Z,' vol 32, p 767 (1931)

[||] 'J Amer. Chem. Soc,' vol. 53, p. 4242 (1931)

In the first place a search was made for a non-polar solvent with a high boiling point and low melting point, which would therefore have a long range of temperature over which measurements could be made Hexane, heptane, or carbon tetrachloride could have been used if low temperatures were to be included, but from the outset it was decided to make the measurements at higher temperatures which, if the volatility of the solute is sufficiently low, have a number of advantages over low temperatures for this purpose (1) a greater solubility of the polar compound in the non-polar solvent, (2) greater ease of experimental working, particularly as regards ease of maintenance of constant temperatures and avoidance of condensation of atmospheric moisture, and (3) decreased molecular association The decrease in molecular association at higher temperatures is of considerable importance since it permits of the use of more concentrated solutions, for, as the results in the later part of the paper show, the effect of molecular association on the polarization and hence change of the polarization with concentration, are much less at higher temperatures. As a consequence, the extrapolation to infinite dilution can be carried out with a correspondingly greater accuracy.

Two solvents have so far been used: decahydronaphthalene, in which measurements were made from 20° to 160°, and *p*-xylene, in which measurements were made from 20° to 120° Measurements at temperatures nearer to the boiling points of the solvents were avoided on account of the possible loss of the solvent by evaporation.

Compounds which are too volatile for the polarization to be measured in solution except at low temperatures are probably best examined in the vapour state

2 *Experimental*

Since many methods for the measurement of the dielectric constant of a liquid have already been published, an additional description of experimental method may appear unnecessary On the other hand, the development of methods using thermionic valves and high frequencies has made comparatively easy of attainment results which are reproducible to a high degree of precision, and it is only from a consideration of the details of a method that it is possible to judge whether or not large systematic errors may be present

Dielectric Constant.—This was measured at approximately 1000 kc. (300 metres) by a resonance method using a piezo-electrically controlled oscillator The electrical circuits and arrangement of the standard condenser were essentially as described elsewhere.* The measuring circuit is shown in fig. 1, the original arrangement being modified to include provision for applying a small direct e.m.f. to the carborundum-steel rectifier, to permit of the rectification and measurement of smaller resonance voltages.

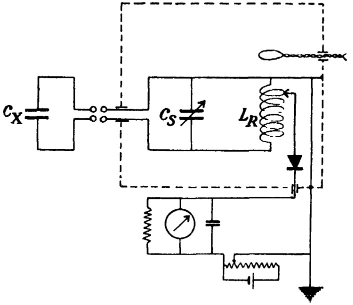

FIG 1

The test condenser C_X used for the solutions, which is shown in section in fig. 2, was made from three seamless platinum cylinders, 0·1 mm. thick, 9 cm. in length and of outside diameters respectively 18 mm , 19 mm , and 20 mm , the first and third being connected together electrically and to earth The cylinders were held relative to one another by four small glass beads at each end, fused to the platinum, very little glass being actually between the plates of the condenser On measurement, the electrical capacity in air was found to be about 215 μμF of which more than9 9% was located in the dielectric between the plates. The rigidity of the arrangement was shown by the constancy of the capacity in dry air, this being measured before every measurement of a solution. The platinum leads were 0·4 mm. diameter, 10 cm. long and fixed 1·3 cm apart in parallel glass tubes, the upper portions of which formed mercury contact cups. The condenser is somewhat similar in design to the one described by Smyth† but differs from it as regards the glass spacers, the inner "dead space" and the smaller distance between the leads As will be shown, wide spacing of the leads is inadvisable when the condenser is to be used in a resonance circuit at high frequencies

---

* Fairbrother, 'J. Chem. Soc.,' p. 43 (1932).

† "Dielectric Constant and Molecular Structure," New York, p 60 (1931).

The condenser, which required only 21 c c. of liquid, was immersed in a large bath of a second quality medicinal paraffin, heated electrically, so that the top of the plates was about 6 cm below the surface The temperature was controlled by means of a mercury contact thermometer with fixed points at about 20° intervals between 20° and 160°. At each temperature halt the bath was maintained constant to ± 0·1° for at least half an hour before a reading, trial estimations having shown that this time was sufficient to attain a constant value of the dielectric constant Since some of the points on the contact thermometer were not quite evenly spaced and since, moreover, the equilibrium temperatures varied over a few tenths of a degree on different occasions, the dielectric constant measurements are given in the following tables at equal intervals of 20° or 40° The interpolation was carried out arithmetically by using the mean temperature coefficient of ε at each experimental point, obtained graphically. In many cases no correction was necessary, in the remainder, the smallness of the temperature coefficient and of the temperature range over which the correction was made, give the values of ε the significance in all cases of actual experimental values

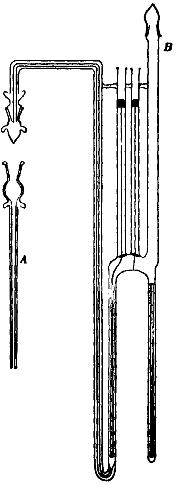

FIG 2.

Calibration of the apparatus · the measuring circuit, fig. 1, can be arranged diagrammatically as in fig. 3, the complete circuit consisting of three parts, comprising respectively C_X, C_S, and L_R each with their respective leads, the common points to these being A and B. The inductance of the leads to L_R may be included in the value of L_R itself and in the present work the capacity of these leads was negligible, this being the only portion of the whole circuit in which the leads were well spaced. Let l_X and l_S be respectively the self-inductance of the leads between AB and the plates of the two condensers. The calibration consists in the first place of the evaluation of the effect of the inductance of the leads on the apparent capacity of C_X and C_S, and of the fixed, lead, and stray capacities associated with C_X The circuit, including C_X, is brought into resonance by adjustment of C_S to a value, say, C'_S C_X is then

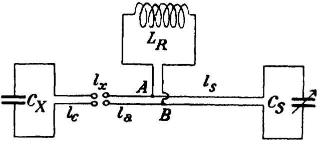

FIG. 3

removed and C_S adjusted to a value C''_S to give resonance again C_X, however, may be taken as equal to $C''_S - C'_S$ only at low frequencies at which the effect of the inductance of the leads is negligible. It may easily be shown that a condenser of capacity C at the end of leads of inductance l is equivalent to a condenser without leads of capacity $C/(1 - l\omega^2C)$ where $\omega = 2\pi f$, f being the frequency of the measuring current. At high frequencies the term $l\omega^2C$ may become quite large. For example, Lattey and Gatty* calculate that a condenser of 1000 cm. capacity at the end of leads 1 mm. diameter, 3 cm apart and 10 cm long, has an effective capacity of 1016 cm. when measured at a frequency corresponding to a wave-length in air of 200 metres Hence, if the condenser C_S is a semi-circular plate condenser with a linear relation between the capacity and the angular displacement of the plates when measured at low frequencies, unless the points AB are situated at the plates of the condenser (and therefore l_S zero), the scale will no longer be a linear one when measured at high frequencies Since the dielectric constant is measured as a ratio, the value of C_S in absolute units is not required, but only its capacity relative to some scale on the instrument. The most convenient procedure therefore is to calibrate C_S and l_S together by a step-by-step method. In the present work this was done with the aid of another variable air condenser in parallel with C_S and a small air condenser of fixed capacity equivalent with its leads to about 10° on the scale of C_S, which could be switched in and out of circuit in the position of C_X. A linear scale in arbitrary units was then calculated and a curve drawn so that angular readings of C_S could be interpreted in terms of capacity on this scale, much as a slightly conical graduated tube is calibrated in units of volume. The leads were of fairly thick copper wire enclosed in a double cover of insulating sleeving and twisted together; this procedure resulted in an increase of lead capacity but a decrease of inductance and is considered preferable to an increase of the latter by the use of thin wire and spaced leads. To prevent any change in the characteristics of the leads, they were firmly attached by sealing wax to insulated supports. The inductance l_X consists of two parts, l_A the inductance of the leads from AB up to and including the links of the mercury cup switch and l_C the inductance of the two platinum wires between the mercury cups on the condenser and the plates of the condenser. l_A could be evaluated by measurements at different frequencies as carried out by Lattey and Gatty (*loc. cit.*) and by Watson,* but in the present case this was inapplicable as the frequency was fixed. The following procedure was therefore adopted, which is similar to a second method used by Watson. Two small fixed capacity mica condensers (Dubilier type 620) of nominal capacities 0.0003 μμF and 0.0005 μμF respectively, were taken and small mercury cups, 2 mm. diameter, made in the tops of the ebonite casings. The mercury cups were about 1·3 cm. apart, the same as the distance of the mercury cups of the test condenser, and were connected to the terminals on the fixed condenser. Two vertical nickel wires, 1 mm. diameter, 1 cm. long and 1.3 cm. apart were soldered to the leads at AB. The two mica condensers could then be arranged successively at AB, in place of the test condenser, and removed altogether; from the corresponding resonance settings of C_S the change in apparent capacity of each mica condenser on being removed from AB to C_X could then be calculated, and hence the inductance l_A of the fixed leads. Measurements with each condenser gave results which were in good agreement. Since the links of the mercury cup switch in the second case were in the position they were later to occupy relative to the test condenser, their inductance was included in the calculation. The inductance of the platinum leads of the test condenser was then calculated from their dimensions and distance apart.†

---

* 'Phil. Mag.,' [7] vol 7, p. 985 (1929).

---

* 'Proc. Roy. Soc.,' A, vol. 117, p. 43 (1927).

† 'Circ. Bur. Stand., No. 74,' p. 245 (1924).

From the known value of l_X in units corresponding to the arbitrary units in which C_S was measured, the true value of C_X could then be calculated by means of the equation

$$C_{X_{meas}} = \frac{C_{X\,true}}{1 - l_X\ \omega^2\ C_{X\,true}}$$

Since the solution of this equation for every measurement would be laborious, values of

$$\frac{C}{1 - l_X\omega^2 C} - C$$

were calculated for a large number of values of C and plotted on a large scale against $C/(1 - l_X\omega^2 C)$. From these curves the value of the difference between the observed and the true capacity could be readily obtained and the correction made. The neglect of the effect of the inductance of the leads in a resonance or heterodyne method at high frequencies, where a substitution of capacities is made, may easily lead to errors of several cubic centimetres in the estimated polarization of the solute. In the present work, an error in ε of 0·001 causes an error of about 0·1% in P_{12}. The corresponding uncertainty in P_2 is dependent upon the concentration of the solution, in the very dilute solutions in which P_2 is calculated from a small difference between the two relatively large magnitudes P_1f_1 and P_{12}, the uncertainty may rise to as much as ± 2 c.c.

The true capacity of C_X obtained as above, consists partly of the capacity of the leads and stray capacities to earth, and partly of the fixed capacity located in the solid dielectric (glass) through which a small fraction of the total lines of force pass, and partly of the capacity between the plates, located in air or the liquid under consideration as the case may be. It is only this last "replaceable capacity" which is changed when the air in the condenser is replaced by a liquid. The correction for the "non-replaceable" capacity has been discussed in several papers* and consists briefly in evaluating the replaceable capacity C_0 by means of measurements of the capacity of the condenser filled with air (C_{air}) and with a liquid, for example benzene, whose dielectric constant is accurately known (C_{benz}). Then if ε is the dielectric constant of the liquid used for calibration

$$\varepsilon\,(C_{air} - x) = C_{benz} - x, \qquad x = C_{air} - C_0,$$

and

$$C_0 = C_{air} - \frac{\varepsilon C_{air} - C_{benz}}{\varepsilon - 1}.$$

---

* Oliver and Hartshorn, 'Proc. Roy. Soc.,' A, vol. 123, p. 664 (1929).

In the present case, Kahlbaum's benzene "for analysis and molecular weight determination," after a preliminary drying and distillation, was dried for several days over purified phosphoric oxide and distilled directly into the test condenser from an all-glass apparatus. The dielectric constant of this benzene was taken as 2·283 at 20°. The calculated dielectric constants of the solutions and liquids were finally corrected to vac = 1, this correction is small but affects the last decimal place in many cases by one unit.

The capacity of the test condenser when filled with air increased by about 0·2% over the range from 20° to 160° which is about that which would be expected from the dimensions of the plates and the thermal expansion of the platinum and of the glass spacers The actual capacity was separately estimated at each temperature halt and the capacity at 20° redetermined before the introduction of a fresh liquid The solutions, which were prepared in stoppered flasks of about 100 c c capacity, were introduced into the test condenser through A, gentle suction (via a drying tube) being applied at B, taking care to avoid the inclusion of air bubbles The tube A was then replaced by the small ground cap. After use the condenser was emptied and washed at least seven times with pure benzene and a current of dry nitrogen passed through for several hours, during which the condenser was warmed to about 110° in an electrically heated pyrex tube

An attempt was also made to gain an approximate idea of the magnitude $P_A + P_E$ by the measurement of the polarization of the substances in the solid state at 20°, which is sufficiently below the melting point in each case. For this purpose the substances were introduced into the test condenser in a molten state and allowed to solidify slowly As it was felt that the considerable contraction on solidification might have distorted the plates of the condenser, which was not designed for such experiments (although subsequent estimation of the capacity when filled with air showed that no detectable permanent change of capacity had occurred), another condenser was made for the purpose This, which is shown in fig 4, consisted of three brass plates, respectively 6 mm, 1 mm, and 6 mm thick, held together by brass screws at the corners The thinnest plate (of which the length and width were each 1 cm. less than those of the thicker ones, for screening purposes), was separated from the outer ones by four small blocks of glass on each side, the whole being held together by the clamping action of the screws This condenser, which had a capacity when filled with air of about 92 μμF, fitted closely into a rectangular glass trough and only required 10 c c. of substance. The brass plates were chromium plated and the leads arranged to have approximately the same length and configuration as the leads on the other condenser, thus avoiding a re-calibration for the effect of inductance The calibration for replaceable capacity was carried out in the usual manner The substance was introduced into the condenser by pouring it in whilst molten, to a height of a few millimetres above the tops of the plates, trapped air bubbles being removed by moving the plates up and down Solidification from the bottom upwards was secured by standing the condenser in a shallow layer of cold water The polarization results with both condensers agreed to ± 1 5 c c , the mean values are therefore given The values of the dielectric constants of the solids are probably not better than the second significant figure This difficulty of measurement of the dielectric constant of a solid which has been introduced into the condenser in the liquid state, has been commented upon by several authors[*] The source of the difficulty appears to lie in the considerable contraction of the substance which occurs on change of state from liquid to solid.

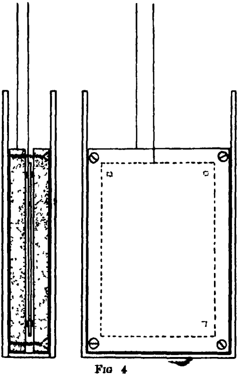

Fig 4

---

[*] *Cf.* Morgan and Lowry, 'J. Phys. Chem.,' vol. 34, p. 2385 (1930), Kamerling and Smyth, 'J. *Amer.* Chem Soc,' vol. 55, p. 462 (1933).

This contraction results in the formation of cracks in the solid and gas pockets either in the solid or between the solid and the plates of the condenser. In addition, with the above method of filling the condenser, it is very unlikely that we are dealing with a completely random orientation of the small crystals of which the solid mass is composed. Consequently, the crystals all being doubly refracting, the dielectric constant of the solid will depend upon the manner of crystalline growth.

Refractive Indices.—These were measured with a Pulfrich refractometer at 20·0° for the wave-lengths 6708 A. (Li), 5893 A. (Na), 5461 A. (Hg), 4358 A. (Hg). The optical polarizations were calculated by means of the modified Lorentz-Lorenz formula for dilute solutions and the molar polarizations of the solutes calculated in a manner similar to that used for the dielectric polarizations. The extrapolations of refractive index to zero frequency were carried out graphically with the aid of the simplified Cauchy extrapolation formula $n_\lambda = n_\infty + a/\lambda^2$. In the case of the pure liquids the refractive indices are given in full in the following tables, but for the solutions, for the sake of brevity, only the molar refractivities of the solutes at $\lambda = 5893$ A. (Na) and $\lambda = \infty$ are given.

3 (*a*) *Purification of Materials.* *

Decahydronaphthalene.—This liquid was selected as a solvent on account of its high boiling point (185°–193°) and also because it is obtainable cheaply as a commercial solvent. It has the disadvantage, however, of being a mixture of two isomers. W. Hückel† showed that the isomers are cis and trans forms, the isomerism being of the type required by the theory of strainless ring systems. Traces of unsaturated compounds were removed from the commercial "Dekalin" by repeated treatment with 100% sulphuric acid. The liquid was dried by refluxing over sodium for at least 8 hours followed by standing in contact with purified phosphoric oxide before the final distillation. By repeated fractionation of the purified dekalin two samples were obtained, boiling at 187·5°–189·8° (757·8 mm.) and at 195·7°–196·5° (757·3 mm.), and which consisted mainly of the trans and cis isomers respectively (Hückel gives boiling point, trans 185°, cis 193°). The separation was not complete, particularly the trans fraction, which, however, contained probably not more than 5%

---

* Purification of materials, preparation and densities of solutions with Mr. J. Rigg, M.Sc.

† 'Ann. Chem.,' vol. 441, p. 1 (1925).

of the other isomer Both fractions solidified to crystalline masses when cooled in carbon dioxide and acetone, whereas the unfractionated mixture had to be cooled in liquid air in order to solidify and then gave a transparent glass. The polarizations of these two fractions, termed "Trans" and "Cis" respectively in the following tables, when measured over the whole temperature range as described, showed that both isomers were non-polar The remaining fractions were then mixed together and distilled and used as a "solvent mixture" The polarization of this mixture, which was sufficient in amount for all the measurements recorded, was also measured and its non-polar nature confirmed The polarizations of this mixture are used as P_1 in calculating P_2 for the solutions of benzyl alcohol and benzyl chloride

p-*xylene* —This solvent was used on account of its good solvent properties, the nitrobenzylchlorides, for example, dissolving readily in it, whereas the solubility of these compounds in decahydronaphthalene was found to be insufficient for the present purpose A very good product "*p*-xylol-rein" was dried over purified phosphoric oxide for 5 weeks and fractionated The final product had boiling point 138·2°–138 5° (764 5 mm.) and freezing point 12·9° ("International Critical Tables," boiling point 137 7°, melting point 13 2°)

Benzyl Alcohol —A good commercial product was dried over anhydrous sodium sulphate and fractionated twice The final product distilled between 205 8° and 206·1° (760 mm.) ("International Critical Tables," boiling point 205·8°)

Benzyl Chloride —A good commercial "redistilled benzyl chloride" was dried over phosphoric oxide and fractionated three times. The fraction used distilled between 178·6° and 179·0° at 766 mm ("International Critical Tables," boiling point 179·4°)

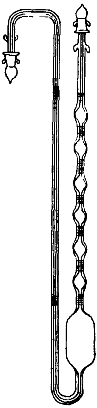

FIG 5.

o-, m- *and* p-*nitrobenzylchlorides* —Commercial products were used after purification by recrystallization, *p*- from 95% ethyl alcohol, and *o*- and *m*- from a mixture of "80°–100°" light petroleum and benzene The crystals were well dried *in vacuo* before use. Melting points, ortho 48·4°, meta 45 0°, para 72·2° ("International Critical Tables," melting points, ortho 49°, meta 44·5°, para 71°).

Densities.—These were measured by means of a dilatometer of the form shown in fig. 5, immersed in medicinal paraffin in a bath with a glass window. Several observations were made as the liquid rose through each capillary portion of the right-hand limb, and the corresponding densities plotted against the temperature on a large scale. The densities at the required temperatures were then interpolated by means of these curves which were generally almost linear.

(*b*) *Dielectric Constants, Densities and Refractive Indices*

ϵ, dielectric constant, d, density. P_{12}, polarization of solution, P_2, polarization of solute. f_2, mol fraction of solute.

"Trans" Decahydronaphthalene

t	ϵ	d	P	t	ϵ	d.	P.
°			c.c.	°			c.c.
20	2·165	0·8723	44·31	100	2·061	0·8125	44·43
40	2·139	0·8572	44·36	120	2·034	0·7968	44·45
60	2·113	0·8420	44·40	140	2·007	0·7808	44·47
80	2·087	0·8271	44·43	160	1·980	0·7648	44·48

"Cis" Decahydronaphthalene

t	ϵ	d	P	t	ϵ	d	P.
°			c.c.	°			c.c.
20	2·182	0·8941	43·68	100	2·081	0·8343	43·87
40	2·157	0·8793	43·74	120	2·055	0·8189	43·92
60	2·131	0·8644	43·77	140	2·029	0·8028	43·95
80	2·106	0·8494	43·82	160	2·003	0·7870	43·99

Decahydronaphthalene "Solvent Mixture"

t	ϵ	d	P	t	ϵ	d	P
°			c.c.	°			c.c.
20	2·165	0·8830	43·77	100	2·063	0·8230	43·93
40	2·140	0·8681	43·83	120	2·037	0·8073	43·97
60	2·114	0·8533	43·85	140	2·011	0·7916	44·00
80	$2{\cdot}088_5$	0·8382	43·89	160	1·986	0·7759	44·05

p-xylene

t	ϵ	*d.*	P	t	ϵ	*d.*	P.
°			c.c.	°			c.c.
20	2·267	0·8609	36·60	80	2·165	0·8075	36·74
40	2·233	0·8432	36·66	100	2·130	0·7897	36·76
60	2·199	0·8254	36·71	120	2·095	0·7718	36·77

Refractive Indices.

	6708 A	5893 A	5461 A	4359 A	MR_{∞}	$P_A = P - MR_{\infty}$.
					c.c	c.c
$C_{10}H_{18}$ "trans"	1·4680	1·4709	1·4729	1·4817	43·3	1·0
$C_{10}H_{18}$ "cis"	1·4780	1·4809	1·4831	1·4920	43·0	0·7
$C_{10}H_{18}$ "solvent mixture"	1·4730	1·4760	1·4782	1·4869	43·1	0·7
p-xylene	1·4909	1·4962	1·4999	1·5268	34·6	2·0

Benzyl Alcohol in Decahydronaphthalene

	$f_2 = 0·007812$				$f_2 = 0·01493$			
t	ϵ	d	P_{12}	P_2.	ϵ	d	P_{12}	P_2
°			c.c.	c.c.			c.c.	c.c.
20	2·184	0·8837	44·17	93·4	2·197	0·8840	44·44	88·4
60	2·131	0·8539	44·23	92·4	2·144	0·8545	44·50	87·2
100	2·076	0·8235	44·23	81·0	2·089	0·8243	44·50	82·1
140	2·023	0·7922	44·28	78·5	2·033	0·7925	44·51	77·8
160	1·997	0·7765	44·31	77·6	2·006	0·7766	44·54	76·5

	$f_2 = 0·03035.$				$f_2 = 0·05048$			
$t.$	ϵ	d	P_{12}	P_2	ϵ	d	P_{12}	P_2
°			c.c.	c.c.			c.c.	c.c.
20	2·227	0·8856	44·99	84·0	2·265	0·8875	45·67	81·4
60	2·176	0·8558	45·17	87·3	2·216	0·8573	45·98	86·0
100	2·116	0·8253	45·10	82·4	2·152	0·8267	45·87	82·3
140	2·055	0·7932	45·02	77·4	2·085	0·7950	45·66	76·6
160	2·027	0·7778	45·01	75·6	2·053	0·7791	45·57	74·2

Benzyl Alcohol in Decahydronaphthalene—(continued)

	$f_2 = 0\ 06474$				$f_2 = 0\ 1025$			
t	ϵ	d	P_{12}	P_2	ϵ	d.	P_{12}	P_2
°			c c	c c			c c	c c
20	2 294	0 8890	46 18	81 0	2 394	0 8952	47 88	83 8
60	2 245	0 8587	46 53	85 3	2 344	0 8639	48 38	88 1
100	2 177	0 8279	46 37	81 6	2 263	0 8325	48 08	84 4
140	2 105	0 7963	46 05	75 6	2 177	0 8004	47 56	78 7
160	2 072	0 7803	45 96	73 6	2 135	0 7846	47 26	75 4

t.	$P_{2\infty}$
°	c.c
20	(103 0)
60	(94 0)
100	83 4
140	79 4
160	77 6

$MR_D = 33\ 3$ c c
$MR_\alpha = 31\ 0$ c c

Benzyl Chloride in Decahydronaphthalene

	$f_2 = 0{\cdot}008853$				$f_2 = 0\ 01794$			
t	ϵ	d	P_{12}.	P_2	ϵ	d	P_{12}	P_2
°			c c	c c			c c	c c
20	2 189	0 8842	44 32	106 3	2 214	0 8856	44 88	105 7
60	2 134	0 8545	44 33	97 5	2 155	0 8558	44 82	97 7
100	2 060	0 8242	44 35	90 9	2 099	0 8257	44 80	92 5
140	2 026	0 7929	44 38	86 9	2 042	0 7939	44 80	88·7
160	2·001	0 7772	44 45	89 1	2 015	0 7780	44 83	87 6

	$f_2 = 0{\cdot}02833$.				$f_2 = 0{\cdot}04695$.			
t.	ϵ	d	P_{12}.	P_2	ϵ	d.	P_{12}	P_2.
°			c c	c c			c c	c c
20	2 243	0 8871	45 52	106 6	2 294	0 8906	46 57	103 1
60	2 179	0 8572	45 37	97 5	2 224	0 8599	46 38	97 5
100	2 118	0 8266	45 28	91 5	2 156	0·8293	46 16	91 2
140	2 060	0 7950	45 28	89 1	2 091	0 7976	46 02	86 8
160	2·030	0 7792	45 22	85 2	2 060	0 7815	45 98	85 0

Benzyl Chloride in Decahydronaphthalene—(continued).

$f_2 = 0\cdot06500$

t.	ϵ	d	P_{12}	P_2	t	$P_{2\infty}$	
°			c c.	c c	°	c c	
20	2 347	0 8927	47 59	102 6	20	108 0	
60	2 268	0 8627	47·22	95 6	60	100 0	
100	2 194	0·8317	46·93	90 1	100	93 8	MR_D = 37 0 c c
140	2 124	0·8009	46·66	84 9	140	90 0	MR_∞ = 36 6 c c
160	2 092	0 7855	46 58	83 0	160	87 8	

p-nitrobenzyl chloride in *p*-xylene

	$f_2 = 0$ 005650				$f_2 = 0$ 01052			
t	ϵ	d	P_{12}	P_2	ϵ	$d.$	P_{12}	P_2
°			c c	c c			c c	c c
20	2 343	0 8644	38 09	301 2	2 407	0 8665	39 35	298 3
40	2 302	0 8464	38 07	287 6	2 361	0·8487	39 27	285 4
60	2 263	0 8285	38 08	278 9	2 316	0 8308	39 20	273 3
80	2 222	0 8106	38 02	262 5	2 271	0 8129	39 10	260 5
100	2 183	0 7926	37 99	254 5	2 228	0 7950	39·02	251 0
120	2 143	0 7746	37 92	240 7	2 184	0 7770	38 90	238 9

	$f_2 = 0\cdot02105$				$f_2 = 0\cdot03066.$			
t	ϵ	d	P_{12}	$P_2.$	ϵ	d	P_{12}	P_2
°			c c	c c			c c	c c
20	2 550	0 8722	41 98	292 2	2 682	0 8768	44 30	288 7
40	2 491	0 8543	41 77	279 6	2 609	0 8589	43 94	276 2
60	2·434	0 8363	41 57	267 4	2 543	0 8410	43 66	263 5
80	2 380	0 8184	41 38	256 9	2 479	0 8230	43 38	253 1
100	2 328	0 8005	41 20	247 5	2 419	0 8050	43 13	244 3
120	2·277	0 7823	41·02	238 8	2 362	0 7870	42 90	236 5

$f_2 = 0\cdot03417.$

t	ϵ	d	$P_{12}.$	P_2	t	$P_{2\infty}.$	
°			c.c	c c	°	c c	
20	2 733	0 8777	45 20	288·3	20	308 0	
40	2 657	0 8600	44·83	275·8	40	293 2	
60	2 585	0 8422	44 47	263·9	60	280 4	MR_D = 41 5 c.c.
80	2 517	0 8243	44 14	250 4	80	268 0	MR_∞ = 39 5 c c
100	2 454	0 8064	43 86	244 4	100	255 2	
120	2 393	0 7885	43 57	235 8	120	243 8	

m-nitrobenzyl chloride in *p*-xylene.

	$f_2 = 0·005003$				$f_2 = 0·007682.$			
t	ϵ.	d	P_{12}	P_2.	ϵ	d.	P_{12}.	P_2
°			c.c.	c.c.			c.c.	c.c.
20	2·343	0·8637	38·11	338·0	2·382	0·8651	38·87	331·9
40	2·302	0·8459	38·08	321·4	2·338	0·8474	38·81	316·3
60	2·262	0·8281	38·06	306·4	2·296	0·8296	38·77	305·0
80	2·223	0·8102	38·05	296·6	2·254	0·8118	38·71	293·0
100	2·184	0·7924	38·01	285·8	2·213	0·7939	38·66	284·2
120	2·145	0·7745	37·96	275·0	2·171	0·7760	38·57	271·3

	$f_2 = 0·01041.$				$f_2 = 0·02012$			
t	ϵ	d	P_{12}	P_2	ϵ.	d	P_{12}	P_2.
°			c.c.	c.c.			c.c.	c.c.
20	2·425	0·8664	39·69	333·9	2·575	0·8713	42·45	327·2
40	2·378	0·8487	39·61	319·9	2·513	0·8537	42·19	311·5
60	2·332	0·8310	39·51	306·2	2·456	0·8361	41·98	298·8
80	2·287	0·8132	39·42	294·1	2·401	0·8181	41·80	288·1
100	2·243	0·7954	39·33	283·5	2·349	0·8002	41·64	279·2
120	2·199	0·7776	39·23	274·1	2·297	0·7823	41·45	269·3

	$f_2 = 0·03029.$						
t	ϵ	d	P_{12}	P_2	t	$P_{2\infty}$	
°			c.c.	c.c.	°	c.c.	
20	2·734	0·8770	45·15	318·8	20	341·2	
40	2·659	0·8592	44·80	305·4	40	324·8	
60	2·588	0·8413	44·47	293·0	60	311·0	$MR_D = 41·5$ c.c.
80	2·523	0·8234	44·20	283·0	80	298·6	$MR_\infty = 39·2$ c.c.
100	2·460	0·8055	43·93	273·3	100	287·8	
120	2·400	0·7876	43·67	264·5	120	278·2	

o-nitrobenzyl chloride in *p*-xylene

	$f_2 = 0·005011.$				$f_2 = 0·007633$			
t	ϵ.	d	P_{12}	P_2	ϵ.	d	P_{12}.	P_2
°			c.c.	c.c.			c.c.	c.c.
20	2·350	0·8636	38·25	366·2	2·394	0·8651	39·10	363·8
40	2·300	0·8459	38·22	349·4	2·348	0·8474	39·00	344·2
60	2·268	0·8281	38·19	331·7	2·305	0·8296	38·96	331·1
80	2·228	0·8104	38·15	316·7	2·261	0·8118	38·86	314·4
100	2·188	0·7926	38·09	302·1	2·219	0·7940	38·80	302·9
120	2·149	0·7748	38·04	291·0	2·177	0·7762	38·70	289·9

o-nitrobenzyl chloride in *p*-xylene—(continued)

	$f_2 = 0·01024$				$f_2 = 0·02020$			
t	ϵ	d	P_{12}	P_2	ϵ	d	P_{12}	P_2
°			c.c.	c.c.			c.c.	c.c.
20	2·436	0·8664	39·90	358·7	2·600	0·8713	43·04	355·7
40	2·387	0·8487	39·78	341·5	2·544	0·8536	42·77	339·0
60	2·340	0·8309	39·68	326·9	2·483	0·8358	42·52	324·4
80	2·294	0·8131	39·58	313·2	2·424	0·8180	42·27	310·5
100	2·249	0·7952	39·47	301·2	2·369	0·8001	42·07	298·9
120	2·204	0·7773	39·33	288·0	2·314	0·7822	41·83	287·5

	$f_2 = 0·03052$					
t	ϵ	d	P_{12}	P_2	t	$P_{2\infty}$
°			c.c.	c.c.	°	c.c.
20	2·794	0·8758	46·19	350·9	20	371·0
40	2·711	0·8580	45·76	334·9	40	350·8
60	2·634	0·8402	45·37	320·5	60	334·8
80	2·563	0·8223	45·03	308·0	80	319·2
100	2·495	0·8043	44·70	296·2	100	304·8
120	2·430	0·7863	44·38	286·1	120	293·0

$MR_D = 41·5$ c.c.
$MR_\infty = 39·5$ c.c.

Polarization of Solids

	ϵ	d	P.
			c.c.
p-nitrobenzyl chloride	3·33	1·45	52
m-nitrobenzyl chloride	3·29	1·44	52
o-nitrobenzyl chloride	2·98	1·48	46

4 *Discussion.*

The polarizations of the decahydronaphthalenes agree with the observations of Hückel (*loc. cit.*) who found that the cis form had a higher boiling point, density, and refractive index, but a lower molecular refraction, than the trans form; the above figures show that the dielectric constant of the cis isomer is higher, but its polarization less, than that of the trans isomer. In all three the nearness of the dielectric polarization to the extrapolated refractivity indicates that the liquids are non-polar with, moreover, a very small atomic polarization.

The same holds for *p*-xylene. All four liquids show a small but definite increase of polarization with rise of temperature instead of the usual decrease observed with substances which possess a moment. This small increase of polarization with temperature with presumably non-polar substances has been observed by other workers. Sanger* came to the conclusion that the divergence from the Clausius-Mosotti expression shown by the values for the polarization of benzene was the result of an incorrect assumption as to the value of the constant of the internal field ($4\pi/3$), or to the limits of accuracy of measurement then attainable. Since that time, however, experimental methods of measurement of the dielectric constant have been much improved and other instances of such an increase of polarization observed, for example, by Smyth and Stoops† for heptane and its isomers, and by Dornte and Smyth‡ for a number of other saturated paraffins. The increase cannot be due to a direct intramolecular effect of temperature since the polarization of the vapour does not increase with temperature as is shown by the recent work of McAlpine and Smyth§ on the polarization of benzene vapour. It must therefore be a consequence of a partial restriction of the displacement of the electrons responsible for the cohesive forces between the molecules.

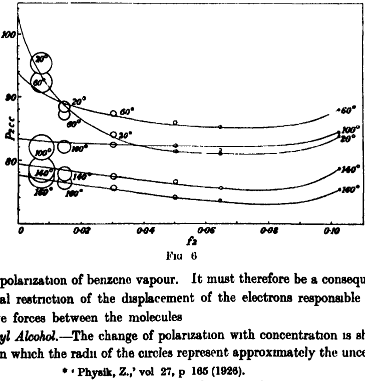

FIG. 6

Benzyl Alcohol.—The change of polarization with concentration is shown in fig. 6, in which the radii of the circles represent approximately the uncertainty in the polarization corresponding to an error of $\pm$ 0 0005 in ϵ, the experimental point being at the centre of the circle.

---

* 'Physik, Z.,' vol 27, p 165 (1926).

† 'J. Amer. Chem. Soc.,' vol 50, p. 1883 (1928).

‡ *Ibid.*, vol. 52, p. 3545 (1930)

§ *Ibid.*, vol. 55, p. 453 (1933)

From this can be seen the great difficulty of accurate extrapolation to infinite dilution at the lower temperatures in a strongly associated solute · for one less strongly associated, or at higher temperatures, the change of polarization with concentration in dilute solution is much less, and the uncertainty in P_2 therefore of less significance in the extrapolation. The results also show that the polarization of benzyl alcohol, except in very dilute solution, at first increases with rise of temperature It is evident that we are here concerned with some effect, which is probably due to molecular association, which decreases the polarization of the solute at the lower temperatures. Such an effect of molecular association was discussed by Debye* in his theoretical treatment of dielectric polarization and has been found for some aliphatic alcohols by Smyth and his co-workers Also, as with the aliphatic alcohols, there is evidence here of a second type of association which increases the moment, in the slight upward trend of the curves at the higher concentrations ; Sidgwick† has suggested that the latter may be due to the formation of co-ordinate links between the oxygen of one molecule and the hydroxyl hydrogen of another. We are, however, here mainly concerned with the first kind of association, which is probably electrostatic in nature, the dipoles opposing one another, the moments cancelling When P_2 is plotted against $1/T$ the curves of the more dilute solutions straighten out above about 100°, beyond which we may assume therefore that the molecular association is small The extrapolation of P_2 to $f_2 = 0$, at 100°, 140°, and 160°, may be carried out to $\pm$ 0·5 c c and gives three points which lie almost on a straight line, the slope of which indicates a moment of $\mu = 1\ 6 \times 10^{-18}$ e.s.u. This value is necessarily approximate owing to the limited number of experimental points on the linear portion of the curve and to the small temperature range (60°), it is, however, probably correct to the two significant figures given and is theoretically more free from objection than that calculated from measurements at a single lower temperature. It is slightly lower than the moments of methyl and ethyl alcohols (1·7) which may be attributed to the slightly greater repulsion between the hydroxyl hydrogen and the large group of the benzene nucleus, leading to a widening of the oxygen valence angle. Benzyl chloride, in contrast to benzyl alcohol, is associated in solution to a much less degree and the $P_{2\infty} - 1/T$ relation appears to be linear over the whole temperature range examined. The equation to this line (which as in the other cases is calculated by the method of least squares), is

---

* Marx, "Handb Radiologie," vol. 6 (1925).

† "The Electronic Theory of Valency," Oxford, p. 134 (1927).

$$P_{2\infty} = 45 \cdot 8 + \frac{18,200}{T},$$

from which $\mu = 1 \cdot 72 \times 10^{-18}$ e.s u. with a probable error of ± 0·02 unit

p-nitrobenzyl chloride.—Plotting $P_{2\infty}$ against 1/T we obtain

$$P_{2\infty} = 58 \cdot 2 + \frac{73,600}{T},$$

from which $\mu = 3 \cdot 45 \times 10^{-18}$ e s u ± 0·02 unit

The moment of *p*-nitrobenzyl chloride has been measured in benzene solution at 25° and 50° by Smyth and Walls * Taking $P_E + P_A$ equal to the molar refractivity for the sodium D line, they calculate a moment of $3 \cdot 58 \times 10^{-18}$ e s u at 25° and $3 \cdot 60 \times 10^{-18}$ e s u at 50°, the same assumption applied to the present results leads to apparent moments of $3 \cdot 56 \times 10^{-18}$ e s.u at 20° and $3 \cdot 59 \times 10^{-18}$ e s u at 60°, which are in excellent agreement with these values. It is clear, however, from a consideration of the polarization of the solid and of the temperature variation of the solute polarizations that $P_E + P_A$ has a much higher value than the refractivity for the sodium D line Also, it is difficult to understand how the moment of *p*-nitrobenzyl can increase with rise of temperature since rotation of the —CH_2Cl group around the C—C bond as axis would not change the angle between the —NO_2 moment and that of the benzyl group, we should therefore expect that all the rotational isomers would have the same moment, unless the C—Cl moment were affected by its position relative to the plane of the benzene ring, or the —NO_2 moment were not, as is generally assumed, directed through the centre of the ring If we make the assumption that the moment is constant, we obtain the value given above, $\mu = 3 \cdot 45 \times 10^{-18}$ e s u and also $A = P_E + P_A = 58$ c c This latter value is slightly higher than the value obtained from the polarization of the solid, which is, however, almost certainly a minimum value on account of the difficulties already mentioned, in the way of an accurate measurement of the polarization of the solid

m- *and* o-*nitrobenzyl chlorides.*—The polarizations of ortho- and meta-nitrobenzyl chlorides, when plotted against 1/T, also give, within the error of measurement, straight lines over the whole temperature range,

$$P_{2\infty} = 91 \cdot 9 + \frac{73,000}{T},$$

---

* 'J. Amer. Chem. Soc.,' vol 54, p. 1854 (1932).

for *m*-nitrobenzyl chloride, and

$$P_{2\infty} = 69\cdot5 + \frac{89{,}700}{T},$$

for *o*-nitrobenzyl chloride.

The large differences, however, between the intercepts at $1/T = 0$ and the polarizations of the solids, suggests that for these two the intercept cannot be taken as indicating a large value of $P_A + P_E$, but is partly due to an increase of moment with rise of temperature. Also, as for the *p*-isomer, the polarizations of the solids are much higher than the optical polarizations, and although the former may possibly be on the low side, the values of the electric moment obtained as a result of taking $P_A + P_E = P_{solid}$, will probably be approximately correct.

Calculating then $\mu = 0\cdot01273\sqrt{(P_{2\infty} - P_{solid})\,.\,T}$ for *m*-nitrobenzyl chloride, we obtain,

t	20°	40°	60°	80°	100°	120°
$\mu \times 10^{18}$ (e s u) ..	3·71	3·72	3·74	3·76	3·78	3·80

showing a marked increase in the moment with rise of temperature which is too great to be attributed to any small residual error in the value of $P_A + P_E$.

A change of moment with rise of temperature also appears to occur with *o*-nitrobenzyl chloride With this substance the polarization of the solid was found to be less than for the other isomers, when measured by the same method and with presumably the same accuracy, this was observed with both test condensers and may be a consequence of the restriction of the vibrations associated with the two groups, brought about by their close proximity. Calculating the electric moment as before

$$\mu = 0\cdot01273\sqrt{(P_{2\infty} - P_{solid})\,T},$$

we obtain for ortho-nitrobenzyl chloride·

t	20°	40°	60°	80°	100°	120°
$\mu \times 10^{18}$ (e s.u) ...	3·93	3·93	3·95	3·95	3·96	3·97

or about half the rate of increase compared with the *m*-isomer.

The change of moment with temperature in both isomers is most probably a consequence of the rotation of the $-CH_2Cl$ group, as may be seen from a comparison between the observed moments and those calculated vectorially from the moments associated with the nitro- and $-CH_2Cl$ groups respectively. Such calculations can only be approximate in view of the assumptions which are involved, in particular, that the moment of one group attached to the benzene nucleus is uninfluenced by the introduction of a second substituent.

The agreement between the polarization of benzyl chloride in decahydronaphthalene at 20° with the values obtained by other workers in benzene solution, suggests that similar results would be obtained in *p*-xylene, we are therefore justified in using the value of $\mu = 1{\cdot}72 \times 10^{-18}$ e.s.u. for the moment of benzyl chloride in the following calculations. For the moment of the nitro group in the absence of any value obtained by the temperature coefficient method over a wide range of temperature, we may take $\mu = 3{\cdot}9 \times 10^{-18}$ e.s.u.* If, then, we assume that the moment of the nitro group is directed through the centre of the ring, the angle θ which it makes with the $-CH_2Cl$ group in *p*-nitrobenzyl chloride, may be calculated by means of the usual equation for the resultant of two vectors

$$\mu = \sqrt{m_1^2 + m_2^2 + 2m_1m_2 \cos \theta},$$

in which m_1 = the moment of the $-NO_2$ group, m_2 = the moment of the $-CH_2Cl$ group and μ = the moment of *p*-nitrobenzyl chloride, from which we obtain $\theta = 118°$. The difference between this and the theoretical tetrahedral angle of 109° 28′ may easily arise from the approximate nature of the assumptions involved, as well as from small errors in the values of m_1, m_2 and μ. The angle, however, may actually be different from the tetrahedral angle, since it is the angle of the group moment as a whole. The value obtained is within the limits of the angles obtained by Smyth and Walls† from the moments of a number of para substituted benzyl halides. We shall therefore take $\theta = 118°$ in the following calculations; the values are such that the conclusions arrived at would not be affected qualitatively if θ lies between 118° and 109·5°.

For *m*-nitrobenzyl chloride the angle between the moments is not independent of the rotational position taken up by the $-CH_2Cl$ group, values between $120° - \alpha$ and $120° + \alpha$, $(\alpha = 180° - \theta)$, being possible, corresponding to a kind of "cis" and "trans" positions respectively. Taking θ, which is the angle between the moment and the adjacent C—C bond, as 118°, the corresponding possible moments for these extreme positions are $2{\cdot}28 \times 10^{-18}$ e.s.u. and $5{\cdot}03 \times 10^{-18}$ e.s.u., neither of which is close to the values actually found (3·71 to 3·80). If we assume complete freedom of rotation about the C—C bond joining the $-CH_2Cl$ group to the benzene ring, that is assuming an equal probability for all positions around the solid angle described by the $-CH_2Cl$ group, the moment should be

---

* Smyth, "Dielectric Constant and Molecular Structure," New York (1931).

† 'J. Amer. Chem. Soc.,' vol. 54, p. 1854 (1932).

$$\mu = \sqrt{m_1^2 + m_2^2 - m_1 m_2 \cos \alpha}.^*$$

Making the substitutions we find $\mu = 3 \cdot 88 \times 10^{-18}$ e.s u. We must therefore conclude that the $-CH_2Cl$ group in the meta position has a fairly large freedom of rotation, but that the positions near that of maximum potential energy, when the dipoles are most closely orientated, are rather less frequently occupied. As the temperature rises the increased rotational energy acquired by the group results in the more frequent close approach of the dipoles.

o-nitrobenzyl chloride is similar, but is complicated by the possibility of the mutual interaction of the groups as a whole, as well as of the dipole repulsion. The calculated moment, if the rotation were unhindered and the moment of each group uninfluenced by the other (assumptions which are certainly not strictly correct), would be $4 \cdot 62 \times 10^{-18}$ e s u The mutual repulsion of the groups as a whole would make this figure lower The values actually found (3·93 to 3·97) again indicate a certain degree of freedom of rotation

For the sake of comparison, in the following table are given the moments of benzyl alcohol, benzyl chloride, and *p*-nitrobenzyl chloride, calculated from the present results (*a*) from the temperature variation of the polarization, and (*b*) by taking A in equation (2) equal to MR_D. Values obtained by other observers are also given, together with the method of calculation

	Present results		Previous results (in benzene)		
	$\mu \times 10^{18}$ (e s u)				
	B = $\delta P/\delta(1/T)$.	B = $(P-MR_D)T$	$\mu \times 10^{18}$. (e s u)	B.	Authors
Benzyl alcohol	1·6	1·7	1·68	$[P-(MR_\infty+15\%)]T$	Bodenheimer and Wehage.[†]
Benzyl chloride	1·72	1·83	1·82 1·84 1·87	$(P-MR_{5461})T$ $(P-MR)T$ $(P-MR_D)T$	Sutton.[‡] Bergmann, Engel, and Sandor.[§] Weissberger and Sangewald.[‖]
p-nitrobenzyl chloride	3·45	3·56	3·58	$(P-MR_D)T$	Smyth and Walls.[¶]

[†] 'Z. phys. Chem.,' B, vol. 18, p. 343 (1932).
[‡] 'Proc. Roy Soc,' A, vol 133, p. 668 (1931).
[§] 'Z. phys. Chem.,' B, vol. 10, p 397 (1930)
[‖] 'Z phys. Chem,' B, vol. 9, p. 133 (1930).
[¶] 'J Amer. Chem. Soc,' vol. 54, p 1854 (1932).

---

[*] *Cf.* Fuchs, 'Z phys Chem.,' vol. 14, p. 339 (1931).

The values of μ calculated with the use of the molecular refraction are in excellent agreement with the results of other workers; but the variation of the polarization with temperature shows that the atomic polarization of these substances cannot be neglected.

Thanks are due to Messrs Imperial Chemical Industries, Ltd., for a grant for the purchase of apparatus, and to the Department of Scientific and Industrial Research for a maintenance grant to J R.

Summary.

(1) The estimation of electric moment in solution by means of measurements of dielectric constant and density in solution over a wide range of temperature is discussed.

(2) Technical "Dekalin" has been fractionated into two samples consisting mainly of the cis and trans isomers respectively, and the dielectric polarizations separately estimated. Both isomers as well as a mixture used in the rest of the work as a solvent are shown to be non-polar *p*-xylene is also shown to be non-polar. In all these substances the polarization increases slightly with rise of temperature

(3) The polarizations of benzyl alcohol and benzyl chloride have been measured in decahydronaphthalene solution from 20° to 160°. The estimated electric moments are, benzyl alcohol $\mu = 1 \cdot 6 \times 10^{-18}$ e s.u., benzyl chloride $\mu = 1\ 72 \times 10^{-18}$ e.s.u The polarization of benzyl alcohol except in very dilute solution is shown to rise at first with temperature, which is attributed to a decrease of molecular association It is shown that for an associated solute, the extrapolation of the polarization to infinite dilution can be carried out with much greater accuracy at higher temperatures.

(4) The polarizations of *o*-, *m*-, and *p*-nitrobenzyl chlorides have been measured in *p*-xylene from 20° to 120°.

(5) With the aid of measurements of the polarizations of the solids it is shown that the moments of *o*- and *m*-nitrobenzyl chlorides increase with temperature whilst that of *p*- is probably constant. Results, *o*-, 3·93 to 3·97; *m*-, 3 71 to 3·80, *p*-, 3·45. ($\times 10^{-18}$ e s u. in each case)

(6) It is shown that these results are consistent with a rotation of the—CH_2Cl group about its axis, which is unhindered in the *p*- compound, suffers a slight hindrance in the *m*- which decreases with rise of temperature and experiences a greater hindrance in the *o*-.

The Thermal Expansions of Certain Crystals with Layer Lattices.

By HELEN D. MEGAW, M A., Yarrow Research Student of Girton College, Cambridge

(Communicated by A Hutchinson, F R S —Received May 5, 1933)

[PLATE 2]

The methods for the determination of linear expansion coefficients which are applicable to anisotropic substances fall into two main groups, the optical and the X-ray methods. Of these the former have hitherto been much more extensively used. They consist essentially in measuring the change in distance between two plane surfaces of the crystal Thus, Fizeau* investigated a large number of crystals by an interferometer method, and much of the subsequent work on single crystals has been done by modifications of this method. An optical lever method was applied by Roberts† to the measurement of the expansion of single crystals of bismuth The X-ray method determines directly the change in lattice spacing of the crystal. It was first employed by Backhurst,‡ who used an ionization spectrometer to find the expansion of diamond, and that of graphite perpendicular to its cleavage plane The same method has been used by Goetz and Hergenrother§ for the expansion of bismuth crystals Becker|| employed a photographic method, calculating the expansion from the shift of the lines on a powder photograph He investigated several cubic and uniaxial substances up to temperatures of about 850° C A similar method was used by McLennan and Monkman¶ to examine zinc and cadmium at liquid air and room temperatures, and by Müller** to find the expansion of long-chain paraffins up to their melting point

The X-ray methods of determining thermal expansion possess two advantages over any optical method. The first concerns the material used Since it is the change in spacing and not the actual external change in size of the specimen which is directly measured, neither the size nor shape of the crystal affects the

---

* 'C. R. Acad Sci Paris,' vol. 62, pp. 1101, 1133 (1866); vol. 66, pp. 1005, 1072 (1868)

† 'Proc. Roy. Soc.,' A, vol. 106, p. 385 (1924).

‡ 'Proc Roy. Soc.,' A, vol 102, p 340 (1923).

§ 'Phys. Rev ,' vol. 40, p. 643 (1932).

|| 'Z. Physik,' vol 40, p. 37 (1926).

¶ 'Proc Roy. Soc. Canada,' vol 23, Sect 3, p 255 (1929).

** 'Proc Roy. Soc.,' A, vol. 127, p 417 (1930).

accuracy appreciably (provided that it is so small that geometrical errors are not introduced; this depends on the particular experimental arrangement). Thus very small crystals can be used, and it is immaterial what external faces they show; it is not necessary to grind and polish surfaces perpendicular to the direction in which the expansions are to be measured. The only conditions fixing a lower limit to the size of the crystals are the practical ones of convenience in setting the crystals and the lengths of exposure necessary Given sufficiently long exposure times, the substance may even be examined in the form of a powder, as in the work referred to above, but in general the photographs so obtained are liable to be too complicated to interpret satisfactorily for any substances but those with cubic and uniaxial symmetry.

The second advantage of X-ray methods is that they determine the expansion of the lattice as distinct from the macroscopic expansion It has been shown by Goetz and Hergenrother (*loc cit*) that these two are not necessarily the same They measured the thermal expansion of bismuth along its trigonal axis up to the melting point, and showed that while the expansion coefficient as measured by X-rays increased with the temperature, the expansion coefficient measured optically remained constant till near the melting point, when it decreased rapidly The results for the macroscopic expansion are in general agreement with those of Roberts Goetz suggests as a possible explanation that the crystals possess a mosaic structure, the layers between the microcrystals being occupied by amorphous or "decrystallized" atoms with a small expansion coefficient Whatever the explanation, it is clear that it is the lattice expansion which should be calculable from the lattice theory of crystal structure; if the macroscopic expansion is different, it must involve factors which are not dealt with by the lattice theory This is in accordance with the experimental result of Goetz and Hergenrother that the expansion coefficients determined by X-rays obey Gruneisen's law, $\alpha/c_p =$ const whereas those determined macroscopically do not On the other hand, there is no evidence that an appreciable difference between the lattice and macroscopic expansions is of universal or even common occurrence, indeed it is much more likely that for ordinary crystals far from their melting points the difference is small But until there is more information available on this subject, it is desirable that the actual lattice expansions, as determined by X-rays, should be used when strict comparison is to be made with theoretical results.

The theory of homogeneous deformation* shows that a sphere of unit radius at a given temperature in any crystal changes at a neighbouring temperature into an ellipsoid, whose axes serve, in length and direction, to determine the expansion of the crystal over this temperature range. Let the expansion coefficients in the direction of the axes be ϵ_1, ϵ_2, ϵ_3. Then the semi-axes of the ellipsoid corresponding to a temperature change of 1° C. are $1 + \epsilon_1$, $1 + \epsilon_2$, $1 + \epsilon_3$, and the expansion coefficient ϵ in any other direction making angles θ_1, θ_2, θ_3, with the axes of the ellipsoid is given by the equation

---

* Fizeau, 'C. R. Acad. Sci. Paris,' vol 66, p. 1005 (1868); Fletcher, 'Z Kristallog.,' vol. 4, p. 337 (1880); Voigt, "Lehrbuch der Kristallphysik," p. 171 (1910).

$$\frac{1}{(1+\epsilon)^2} = \frac{\cos^2\theta_1}{(1+\epsilon_1)^2} + \frac{\cos^2\theta_2}{(1+\epsilon_2)^2} + \frac{\cos^2\theta_3}{(1+\epsilon_3)^2}.$$

The symmetry of the ellipsoid must be consistent with the symmetry of the crystal The crystals dealt with in this paper belong to the rhombohedral and monoclinic systems In all uniaxial crystals the ellipsoid becomes an ellipsoid of revolution with its axis coincident with the crystallographic axis, its orientation is thus fixed, and $\epsilon_1 = \epsilon_2$. Hence two measurements of the expansion coefficients parallel and perpendicular to the trigonal axis serve to determine the ellipsoid completely. In the monoclinic system, one axis of the ellipsoid coincides with the symmetry axis of the crystal, but the others may lie anywhere in the plane perpendicular to it. The problem then is to find the length and direction of the axes of an ellipse lying in the (010) plane; there are three unknowns, so measurements of the expansion in three known directions in this plane are required to solve it. Measurement of the expansion along the symmetry axis fixes the remaining axis of the ellipsoid

For purposes of calculation, it is more convenient to use Voigt's " deformation tensor " This is a conic with its axes in the same direction as those of the ellipsoid previously described, but involving the expansion coefficients directly. It is given by the equation

$$\epsilon = \epsilon_1 \cos^2\theta_1 + \epsilon_2 \cos^2\theta_2 + \epsilon_3 \cos^2\theta_3.$$

It can be derived from the previous ellipsoid by neglecting the squares of the expansion coefficients. Since the expansion coefficients may be negative, the conic may be a hyperboloid. Its semi-axes are inversely proportional to the square root of the expansion coefficient where this has a maximum or minimum value.

Experimental Details.

The method adopted in this research uses small single crystals. By a suitable choice of X-ray wave-length, a reflection from some order of the plane to be investigated is obtained at a glancing angle of nearly a right-angle, and recorded on a film in a back-camera (see fig. 1) in the way proposed by van Arkel [*] Then in accordance with Bragg's law, $n\lambda = 2d \sin\theta$, a change Δd in the spacing corresponds to a change $\Delta\theta$ in the glancing angle given by

$$\frac{\Delta d}{d} = \cot\theta\,\Delta\theta$$

Since θ is nearly $\pi/2$, a small change of spacing thus gives a large change of angle, making possible accurate determinations of the spacing From measurements of the position of the spot produced by the ray reflected from the crystal at the different temperatures, the thermal expansion normal to the reflecting plane is calculated.

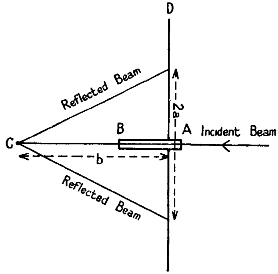

FIG 1 —Experimental arrangement.

The substances investigated were brucite $Mg(OH)_2$, calcium hydroxide $Ca(OH)_2$, and hydrargillite (gibbsite) $Al(OH)_3$. The two former are isomorphous. They belong to the rhombohedral system, and possess a simple layer structure consisting of a plane of cations between two planes of hydroxyl ions. The only parameter in the structure defines the distance between the cation and hydroxyl layers. Hydrargillite is monoclinic, with certain pseudo-hexagonal features. Its structure is closely related to the others, consisting of a similar layer lattice, but is much less simple.[†] They all have a very well-marked basal cleavage. This series of substances was chosen for examination because their layer structure was expected to give rise to a large anisotropy, and because the simplicity of the structure of the first two is a convenience in practical work, and gives some hope that the theoretical calculation of the expansion coefficient may be possible. The substances are also of interest because of the relationship which exists between them and silicates with a layer structure, such as the micas, the chlorites, and kaolinite.*

---

[*] 'Z. Kristallog.,' vol. 67, p. 235 (1928)

[†] [*Note added in proof.*—The structure has now been determined by the author, and will be published shortly in 'Z. Kristallog ']

The apparatus consisted of a Bernal photogoniometer, fitted with a back-camera which could be used instead of the ordinary cylindrical camera. The back-camera consisted essentially of a film-holder moving on a slide, by which it could be set at any desired distance from the crystal, and carrying a vernier by which its position could be read A brass tube of 3 mm diameter penetrated the holder, holes being punched in the films to accommodate it; it carried the aperture, which was about 0·3 mm. in diameter. The aperture was adjustable and could be set so that the distance from aperture to crystal was equal to that from crystal to spot, as calculated from preliminary measurements, thus fulfilling the focussing condition

Small natural crystals from 1 mm to 3 mm. in size were used Besides a well-developed basal plane, all possessed a few other faces, small but good enough to allow the crystal to be set optically to within a degree or so The final adjustments were made from trial photographs The crystals were given an oscillation of 2° about the calculated reflecting position; reflections from the plane examined were obtained in turn on each side of the direction of incidence of the beam

The temperatures at which the spacings have been measured are room temperature and 100° C. It is hoped later to go down to liquid air temperatures. For the higher temperature the heating arrangement consisted of a double-walled water-jacket of brass fitted with a short condenser of copper tubing, fig 2, it was wound with a heating coil lagged with asbestos and taking 50 watts. The crystal was mounted with a drop of "Durofix" on a glass fibre held in position on the arcs with a small pellet of fireclay; the arcs were heat-insulated from the rest of the goniometer by a layer of asbestos. The jacket slipped over the arcs carrying the crystal, and rested on a stand attached to the base of the goniometer, from which it was heat-insulated with asbestos. A window of about 25° aperture allowed the passage of the incident and reflected X-rays It was covered with a thin piece of paper to prevent disturbance of the temperature by draughts. The crystal and its arcs were thus almost enclosed in an oven at a uniform temperature. The temperature was measured by a mercury thermometer reading to $\frac{1}{5}$° which passed through a hole in the top of the oven; it was found to remain constant to within $\frac{1}{2}$° C.

---

* Pauling, 'Proc Nat. Acad Sci. Wash.,' vol. 16, pp. 123, 578 (1930).

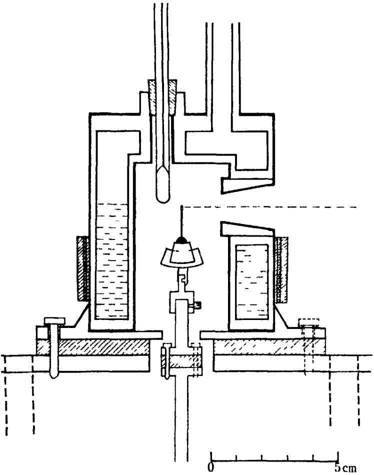

FIG. 2.—Diagram of the heating apparatus.

The X-ray source consisted of a Shearer gas tube, taking 2 mA. to 15 mA. at about 20 KV. to 35 KV. The anticathode was removable, and the copper one ordinarily used could be replaced by whatever else was needed for any particular purpose. During the latter part of the work, a tube specially designed for it was used, in which all the demountable parts were sealed with rubber washers held tight by brass nuts. This made it very easy to change the anticathode as often as it was needed

A certain amount of preliminary work was necessary with each crystal. The order of the plane chosen for measurement of the thermal expansion must satisfy two conditions: it must be of reasonable intensity, so that the exposures need not be unduly long; and it must give a reflection with some convenient wave-length at nearly 90°. The second condition necessitates an accurate knowledge of the spacing, as, owing to the high dispersion, small changes of d are accompanied by large changes of θ. The values quoted in the Strukturbericht are not sufficiently accurate. The spacing was found from the highest order reflection obtainable with copper radiation, this in general gave sufficient accuracy for the purpose. Using the value thus obtained, a wave-length was chosen which would give a reflection with a reasonably strong order of the plane at an angle θ greater than 78°. (This is the practical limit set by the construction of the heater, as rays reflected at any smaller angle are cut off by its walls; but in any case the dispersion would not be great enough much below this angle.) For each order there is only a very small range of wave-length which gives reflections at such angles; and it was sometimes difficult to find a convenient emission line with which to work. Experiments had to be made with anticathodes of different elements so as to find one which worked smoothly and gave an appropriate line of good intensity

The lines used for the different expansion measurements were Cu $K\alpha$ and β, Zn $K\alpha$, Fe $K\alpha$, Ni $K\alpha$, Mn $K\beta_1$, and Ce $L\beta_1$. For the first three, the whole anticathode was made of the element or its alloy, copper, brass, and steel respectively For the Ni line, a copper anticathode was plated with a thick layer of nickel, about 0·3 mm. thick, this still gave the Ni line strongly after about 30 hours use. For the Mn line, a disc of a manganese-copper alloy containing about 30% manganese was spun into a copper anticathode. The author wishes to express her thanks to Dr. Stockdale for preparing the alloy from which the anticathode was made. With the tube running at a fairly low potential, the disc of alloy lasted about a week before it needed renewal. For the Ce line, powdered cerium was fused on to a copper anticathode with borax in a blowpipe flame at a dull red heat; the cathode was set at 5 cm. from the anticathode instead of the 4 cm. at which it was in focus, and the tube was run at a low potential. After about 8 to 10 hours running the cerium needed renewal. With this long wave-length, the usual window of aluminium foil was replaced by a piece of celluloid covering a small hole in lead. A reasonably strong beam was obtained. The lines given by these anticathodes of manganese and cerium were examined by photographing the spectrum obtained from the (111) plane of diamond, all the expected lines occurred in both cases, including the lines required for use.

Preliminary photographs recording separately the spots due to the hot and the cold crystals were first obtained, to determine whether the change of spacing on heating was an expansion or a contraction When possible, for the actual measurement of the expansion, the two sets of spots were recorded on the same film, but when the spot was too large or irregular this would have led to confusion, and separate films were then used. In every case at least two independent measurements of the expansion were made Two examples of the photographs obtained are given in fig 4, Plate 2 The exposure time needed for each spot was from 2 to 6 hours.

Measurements of the distance between the spots on the film were made on an accurate glass scale against an illuminated background, the scale was graduated in millimetres, and 0·1 mm could be estimated. The focussing condition secures that the width of the spot shall be equal to the width of the slit, provided that the crystal is perfect. In this case its position can be read to 0·1 mm. But with some of the crystals used, the spot was drawn out or irregularly shaped, owing to imperfections in the crystal When this happened, it was generally possible to make measurements to corresponding parts of the spots; the error might then be as much as 0·3 mm.

The films were found to shrink during development, the shrinkage was measured on films of two separate batches and found to be about 0·3% in both. This introduces an error into the measurement of the position of the spot, and hence into the spacing, but if it is uniform it gives only a negligible error in the expansion coefficient The results show that it is justifiable to consider it uniform · for the expansions agree with each other within the estimated error, whether the measurements of the spacings at the two temperatures were made on the same or different films. A correction for shrinkage was made in calculating the spacings given in Table I.

The distance from specimen to film was obtained from the scale reading of the camera's position. To find the absolute value corresponding to a given scale reading, the distance from the axis of the goniometer to the film was found with a distance rod, and a constant correction thus obtained to be applied to all scale readings. The scale could be read to less than 0·05 mm., the error in the determination of the absolute distance is about 0·05 mm. The setting on the axis of rotation of the crystal face used had a possible error of 0·1 mm. Where the crystal had not a large face parallel to the plane to be investigated, its geometrical shape introduced another small error into the distance; as the crystals used were small, this was probably never greater than 0·3 mm It was also possible that the crystal might change its position on heating, owing to the uneven expansion of the arcs on which it was mounted. To determine whether this occurred, when the crystal and its arcs were at the high temperature, the oven was removed and the setting of the crystal quickly examined. No change could be observed. The error from any source in the distance from crystal to film was therefore probably not greater than 0·3 mm.

If the measured distance between the spots on opposite sides of the aperture is $2a$, the distance from crystal to film b, the glancing angle θ is given by

$$\tan(\pi - 2\theta) = \frac{a}{b}$$

The error in the spacing is given by

$$\frac{\Delta d}{d} = \tfrac{1}{4}\sin 4\theta \cot\theta \left\{\frac{\Delta a}{a} + \frac{\Delta b}{b}\right\},$$

where Δa, Δb are the errors in a, b respectively For $b = 7$ cm, $\theta = 80°$, the error is about 0·03%. The change in spacing due to the expansion is of the order of 0·3%; hence the error in determining the coefficient of expansion is very roughly 10%. This can be considered in another way: if e is the shift of the spot due to expansion, Δe the error in its measurement, the error in the expansion coefficient is given by $\Delta e/e$. Now Δe, for a good crystal, depends only on the width of the aperture; therefore the greater the shift of the spot, the greater the accuracy with which the expansion can be measured. For an imperfect crystal, Δe increases with e, and the same advantage cannot be obtained by increasing the displacement

The temperature is measured accurately to about 1° C., that is, to 1% An error of this amount is negligible compared with the above.

The values used for the wave-lengths are those given by Siegbahn.*

Results.

The values obtained for the thermal expansions are given in Table I, along with the exact spacings of the planes used and the estimated error of the determinations. A more detailed account of the work on each substance is given below.

Calcite, $CaCO_3$.—Before beginning work on the hydroxides, it was considered desirable to determine the expansion of a substance which was already

---

* "Spektroskopie der Rontgenstrahlen," 2nd ed. (1931).

Table I

Substance	Plane perpendicular to which expansion is measured	Line used	Plane used to measure expansion	Angle $\frac{\pi}{2} - \theta$	Spacing * A	Expansion coefficient × 10^5
				° ′		
Calcite, $CaCO_3$	0001	Cu K β_1	000 24	11 46	[17 020]	2 53 ± 0 15
	$10\bar{1}0$	Zn K α_1	$60\bar{6}0$	4 30	[4 312]	−0 52 ± 0 07
Brucite, Mg $(OH)_2$	0001	Ce L β_1	0004	8 40	4 758 ± 0 003	4 47 ± 0 20
	$10\bar{1}0$	Cu K α_1 α_2	$22\bar{4}0$	11 46 11 3	3 142 ± 0 003	1 10 ± 0 15
Calcium hydroxide, $Ca(OH)_2$	0001	Fe K α_1 α_2	0005	9 26 8 12	4 805 ± 0 003	3 34 ± 0 20
	$10\bar{1}0$	Cu K α_1 α_2	$40\bar{4}0$	7 56 6 52	3 5853 ± 0 0007	0 98 ± 0 08
Hydrargillite, Al $(OH)_3$	010	Ni K α_1 α_2	060	11 20 10 38	5 0602 ± 0 0006	1 09 ± 0 08
	001	Mn K β_1	00 10	9 48	9 669 ± 0 003	1 54 ± 0 10
	100	Zn K α_1	12 00	4 49	8 6236 ± 0 0007	1 31 ± 0 07
	$10\bar{1}$	Ni K α_1 α_2	$80\bar{8}$	9 43 8 30	6 707 ± 0 001	3 90 ± 0 20
	101	Cu K α_1 α_2	808	7 10 5 53	6 1972 ± 0 0005	−0 56 ± 0 07
Phlogopite (mica)	001	Cu K α_1 α_2	00 13	7 38 6 27	10 0844 ± 0 001	1 49 ± 0 15

* The spacings enclosed in square brackets are quoted from the Strukturbericht.

known, in order to test the method and check its accuracy. The expansion of calcite has not previously been determined by X-ray methods, but it is unlikely that its lattice expansion differs from its macroscopic expansion by as much as the experimental error of the present method. The planes (000 24) and ($60\bar{6}0$) gave reflections in suitable positions with Cu Kβ_1 and Zn Kα_1 respectively. The crystal used showed a hexagonal prism terminated by a rather imperfect basal plane; it was about 4 mm long and 3 mm. in diameter. The accuracy could probably have been increased by the use of a better crystal. The values obtained for the coefficients of expansion agree within the limits of error with those found from interferometer methods, which are given for comparison in Table II. The coefficient of expansion perpendicular to the axis is negative, showing that a contraction occurs in that direction.

Brucite, Mg $(OH)_2$.—The crystals used were from a specimen in the Mineralogical Collection of Cambridge University, and came from Wood's Mine, Texas, Pennsylvania. They occurred in thin flat plates with a hexagonal outline, the side faces were found to belong to the prism $\{10\bar{1}0\}$. The measured cell dimensions were $c = 4{\cdot}758$, $a = 3{\cdot}142$, as compared with the values 4·73, 3·12 respectively quoted in the Strukturbericht. For the expansion parallel to the axis, a piece about 1·5 × 1 mm. in area, of thickness 0·1 mm, was used. The spot was considerably drawn out horizontally, indicating a variation of spacing throughout the crystal For the expansion perpendicular to the axis, a larger crystal was taken, about 0·3 mm. thick, 5 mm. long and 3 mm wide. The plane $(22\bar{4}0)$ was used with the Cu Kα doublet The spots were drawn out horizontally, and also reduplicated in a vertical direction, indicating differences in orientation between different parts of the crystal

Table II —Expansion coefficients of calcite × 10^5.

	Present experiment.	Fizeau.*	Benoit.†
Parallel to axis	2·53 ± 0·15	2·621	2·5135
Perpendicular to axis	−0·52 ± 0·07	−0·540	−0·5578

* 'C R. Acad Sci Paris,' vol 66, p 1005 (1868).
† 'Trav Mem. Bur. Int Poids et Mes.,' vol 6 (1888).

Calcium Hydroxide, $Ca(OH)_2$.—The crystals of this substance came from the Imperial Chemical Industries, Northwich, where they had been found in a disused lime kiln. The specimen used for the expansion measurements was a small thin plate about 2 × 1 × 0·2 mm. The measured spacings were $c = 4{\cdot}895$, $a = 3{\cdot}585$, as compared with those found by Harrington,‡ $c = 5{\cdot}030$, $a = 3{\cdot}580$, who, however, obtained his results from powder photographs. There was no sign of chemical decomposition of the crystals after some weeks' exposure to air, and no change could be detected either in the spacings or in the intensities of the basal plane as measured on an ionization spectrometer.

For the expansion parallel to the axis the strong plane (005) gave a reflection at a suitable angle with the Fe Kα doublet, and a steel anticathode was accordingly used. The spots were drawn out horizontally as in brucite and were even more irregular in a vertical direction.

For the expansion perpendicular to the axis, a suitable reflection was obtained with Cu Kα from the plane $(30\bar{3}0)$. With this reflection the spots were small, single, and only very slightly drawn out horizontally; consequently the accuracy could be increased by using a camera distance of 10 cm.

---

‡ 'Amer. J. Sci,' vol 13, p. 467 (1927).

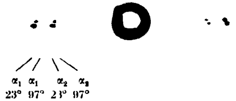

(*a*) Expansion of hydrargillite perpendicular to (101) Distance, 10 cm, copper Kα

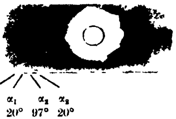

(*b*) Expansion of phlogopite perpendicular to (101) Distance 7 cm, copper Kα

Fig. 4

Hydrargillite, Al$(OH)_3$.—The crystals used came from Langesundsfjord, Brevig, Norway. The thanks of the author are due to Dr. L J Spencer for the gift of one of these crystals, and to Professor Schetelig and Dr I Oftedal for the gift of the others. The crystals were about 1 × 0·5 × 0·3 mm. in size, they showed the faces (001), (100), (10$\bar{1}$), (110), the measurements of the angles agreeing with those quoted by Dana. Optically they were positive and practically uniaxial, the optic axis being inclined at an angle of about −20° to the *c*-axis One crystal appeared to be twinned on the *c* plane (this was shown by a Weissenberg photograph of the *h*0*l* zone); but the other, on which all the measurements of expansions in the *h*0*l* zone were made, was a good single crystal. The spacings found were $a = 8·624$, $b = 5·060$, $c = 9·669$, as compared with the values given by Pauling,* $a = 8·70$, $b = 5·09$, $c = 9·76$. The *c* plane (001) corresponds to the (0001) plane in brucite.

Expansions have been measured perpendicular to the planes (010), (001), (100), (10$\bar{1}$), (101) All these gave good spots, permitting accurate measurement. For the wave-lengths and orders of plane used, see Table I A camera distance of 10 cm. was used in each case except that of (100), where the inconvenience of making long exposures with the Mn anticathode prevented it A photograph showing the expansion (negative in sign) perpendicular to (101) is given in fig. 4, *a*, Plate 2.

It is required from any three of the measurements in the (010) plane to calculate the direction and magnitude of the axes of the conic representing the expansion in that plane. The expansion in the fourth direction can then be calculated and compared with that observed Let one axis of the conic make an angle α with a fixed direction in the crystal, say the normal to the (001) plane, and let the expansion coefficients be ε_a, ε_b, ε_c in three different directions making angles ϕ_a, ϕ_b, ϕ_c respectively with the fixed direction. Then the equation to the conic gives

$$\varepsilon_a = \varepsilon_1 \cos^2(\phi_a - \alpha) + \varepsilon_3 \sin^2(\phi_a - \alpha),$$

and similarly for ε_b and ε_c. These three equations can be solved for ε_1, ε_3, α. The solutions are

$$\varepsilon_1 = \tfrac{1}{2}\{A + B + \sqrt{(A - B)^2 + C^2}\}$$

$$\varepsilon_3 = \tfrac{1}{2}\{A + B - \sqrt{(A - B)^2 + C^2}\}$$

$$\alpha = \tfrac{1}{2}\tan^{-1}\frac{C}{B - A},$$

---

* 'Proc. Nat. Acad. Sci. Wash.,' vol. 16, p. 123 (1930).

where

$$A = -\left\{\frac{\epsilon_a \cos\phi_b \cos\phi_c}{\sin(\phi_c - \phi_a)\sin(\phi_a - \phi_b)} + \frac{\epsilon_b \cos\phi_c \cos\phi_a}{\sin(\phi_a - \phi_b)\sin(\phi_b - \phi_c)} + \frac{\epsilon_c \cos\phi_a \cos\phi_b}{\sin(\phi_b - \phi_c)\sin(\phi_c - \phi_a)}\right\},$$

$$B = -\left\{\frac{\epsilon_a \sin\phi_b \sin\phi_c}{\sin(\phi_c - \phi_a)\sin(\phi_a - \phi_b)} + \frac{\epsilon_b \sin\phi_c \sin\phi_a}{\sin(\phi_a - \phi_b)\sin(\phi_b - \phi_c)} + \frac{\epsilon_c \sin\phi_a \sin\phi_b}{\sin(\phi_b - \phi_c)\sin(\phi_c - \phi_a)}\right\},$$

$$C = +\left\{\frac{\epsilon_a \sin(\phi_b + \phi_c)}{\sin(\phi_c - \phi_a)\sin(\phi_a - \phi_b)} + \frac{\epsilon_b \sin(\phi_c + \phi_a)}{\sin(\phi_a - \phi_b)\sin(\phi_b - \phi_c)} + \frac{\epsilon_c \sin(\phi_a + \phi_b)}{\sin(\phi_b - \phi_c)\sin(\phi_c - \phi_a)}\right\}.$$

An alternative method of calculating ϵ_1, ϵ_3, and α is that of successive approximations. It is seen from Table I that the expansion coefficients normal to (001) and (100) are roughly equal, hence one axis of the conic must nearly bisect the angle between them, *i.e.*, it lies nearly normal to (10$\bar{1}$). Assuming this to be exactly true, ϵ_1 is given by $\epsilon_{10\bar{1}}$, then from ϵ_{100} and ϵ_{001} separately ϵ_3 is calculated, and a mean taken of the two values thus obtained, which is then substituted in the equation and used to calculate α. This is used for a further approximation, and the process is continued until values are obtained for ϵ_1, ϵ_3, and α which are consistent with the observed results within the experimental error.

Table III —Thermal expansion of hydrargillite in the (010) plane

	Calculated from (100), (001), (101)	Calculated from (100), (001), (10$\bar{1}$)	Weighted mean.
$\epsilon_1 \times 10^5$	3·75 ± 0·20	3·92 ± 0·20	3·84 ± 0·20
$\epsilon_3 \times 10^5$	−0·56 ± 0·07	−0·67 ± 0·30	−0·56 ± 0·07
α	−45° 44′ ± 15′	−46° 0′ ± 10′	−45° 54′ ± 10′

The constants for the conic have been calculated by the above formula in two ways, in the first using the measured expansions perpendicular to (100), (001), and (101), the second those perpendicular to (100), (001), and (10$\bar{1}$). The results are shown in Table III, the two sets agree within experimental error. (They were also checked by the method of successive approximations) Here α is the angle between the normal to (001) and the axis of the conic along which greatest expansion occurs, the negative sign of α implying that this axis lies in the quadrant between the normals to (001) and ($\bar{1}00$). The negative sign of ϵ_3 shows that the conic is a hyperbola; this was obvious from the fact that contraction occurs in a direction normal to (101).

The orientation of the axes of the hyperbola in the (010) plane is represented in fig. 3, which also shows the direction of the optic axis. This figure may be compared with those of Fizeau* for the only other monoclinic crystals which have been investigated.

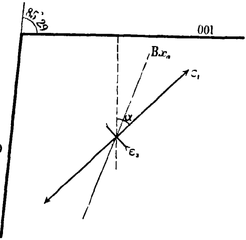

FIG. 3.—Thermal expansion of hydrargillite in the (010) plane.

Phlogopite (Magnesia Mica).—A cleavage flake of phlogopite was used, taken from a specimen from Ceylon in the Mineralogical Collection of Cambridge University. Only the expansion perpendicular to the cleavage plane was measured; for this, the Cu $K\alpha$ doublet was used with the plane (00 13).

The results are shown in Table I. A photograph from which the expansion was measured is reproduced in fig. 4, *b*, Plate 2.

Discussion of Results.

The thermal expansion of a crystal must depend on the third power terms in the expression connecting the energy of the atoms with their displacement. If Hooke's law were strictly obeyed, an increase of energy would not affect their mean positions but only the amplitude of their vibrations; but if the expression

---

[*] 'C. R. Acad. Sci. Paris,' vol. 66, p. 1072 (1868).

for the energy contains a term involving the cube of the displacement, the mean position changes as the energy increases, and thermal expansion occurs. A formal expression for the thermal expansion has been derived by Born[*] from the lattice theory; the expansion along any axis i is given by

$$u_i^0 = \sum_{j=1}^{n} s_{ij}\widetilde{K}_j^0,$$

where s_{ij} are the elastic moduli of the crystal, and $\widetilde{K}_j^0$ involves its Debye and optical frequencies. It is apparent that large elastic moduli (and therefore large compressibilities) are associated with large thermal expansion. The elastic moduli and the characteristic frequencies can themselves be derived by Born's theory from a knowledge of the laws of force in the crystal. Actually the calculation has only been carried out for isotropic substances, in particular for the rock-salt type. It is clear from the above that close relations exist between the thermal expansion and the specific heat and the melting point, which also depend on the characteristic frequencies of the crystal. But here again the theory has only been worked out in detail for isotropic substances. In particular, Gruneisen's law has been derived theoretically by Born for crystals of the rock-salt type, but not for anisotropic crystals. Neither the elastic moduli nor the characteristic frequencies of the crystals dealt with in this paper are known.

Though no exact calculation of the thermal expansion of anisotropic crystals has been made, it is possible to form some qualitative idea of the expansion to be expected in a given structure. It is probably legitimate to assume that weak cohesive forces in the lattice will be associated with large thermal expansion. Thus in calcium hydroxide a single $Ca(OH)_2$ layer is held together by *strong* electrostatic forces, whereas two layers are only held by *weak van der Waals* forces; corresponding to this, a marked anisotropy is to be expected, the expansion coefficient perpendicular to the layers being greater than that in the layers. The same considerations apply to brucite. Since hydrargillite probably has a very similar layer structure, it is not surprising that the two expansions in the layer, those normal to (010) and (100) respectively, are not greatly different from those of the other hydroxides. But in this mineral the greatest expansion coefficient occurs in a direction inclined at about 45° to the normal to the layer, which seems to suggest that here expansion occurs by the slipping of one layer relative to the next. A more detailed explanation cannot be given till the structure of the hydrargillite has been determined. It is interesting to compare the expansion of these layer hydroxides with that of the oxides of the same elements, corundum Al_2O_3, periclase MgO, and spinel Al_2MgO_4. (The expansion of CaO has not been measured.) The structure of each of these substances is a three-dimensional network in which all the bonds are ionic; the two latter substances are cubic, while corundum is rhombohedral. From Table IV it is apparent that their expansion coefficients are all of the same order as those in a layer of the hydroxides; and for the uniaxial corundum the anisotropy is very much less than that which exists in the hydroxides.

---

[*] "Atomtheorie des Festen Zustandes" (1923).

Table IV.—Expansion coefficients of substances related to those investigated.

Corundum—	
Parallel to axis	0.62×10^{-5}
Perpendicular to axis	0.54
Periclase	1.043
Spinel	0.593
Cristobalite	0.97

The coefficient of expansion of phlogopite perpendicular to its cleavage plane is considerably smaller than those of brucite and calcium hydroxide. No measurements have been made of its expansion in other directions; as it is monoclinic, the same effect may occur as in hydrargillite, the expansion being greater in some direction inclined to the normal to the cleavage plane. But considering only the direction normal to the plane, it is possible to see that the expansion is consistent with Pauling's (*loc. cit.*) suggested structure. He supposes that a "uniaxial" mica like phlogopite is built up of a brucite layer between two layers of silica tetrahedra such as occur in cristobalite, the composite layer being held together by sheets of potassium ions. The linear expansion coefficient of cristobalite is quoted in Table IV. (Since cristobalite is cubic, it is one-third of the volume expansion coefficient, given in the International Critical Tables.) It is apparent that the coefficient of expansion of phlogopite is intermediate between those of brucite and cristobalite, which is in accordance with the proposed structure.

I wish to express my thanks to Mr. J. D. Bernal for suggesting this investigation, and for his advice and criticism throughout the work; and to Dr. W. A. Wooster for his helpful interest. I am also indebted to Girton College for the

Yarrow Studentship which made the work possible, and to the Department of Scientific and Industrial Research for a grant I wish also to acknowledge a grant from the Royal Society for apparatus.

Summary

The thermal expansions of certain crystals have been measured from the change in their lattice spacings as determined by X-rays To measure the spacings with sufficient accuracy, reflections at a glancing angle of nearly a right angle have been used, where the dispersion is high The crystals investigated all possess layer structures Complete determinations have been made of the thermal expansions of brucite $Mg(OH)_2$, calcium hydroxide $Ca(OH)_2$, and hydrargillite $Al(OH)_3$, the last-mentioned being monoclinic, and the expansion of a mica (phlogopite) perpendicular to its cleavage plane has also been measured. The hydroxides are found to show marked anisotropy, the expansion coefficient perpendicular to the layer being greater than those in the layer. The determinations so far have been made over the range from 0° to 100° C., it is hoped later to work down to liquid air temperatures The values obtained for the coefficients of expansion are discussed, and compared with those of related substances.

The Internal Conversion of γ-Rays.—II.

By H M TAYLOR, B A , Clare College, Cambridge, and N. F. MOTT, M A , Gonville and Caius College, Cambridge

(Communicated by P A M Dirac, F R S —Received May 6, 1933)

§ 1 *Introduction* —The Internal Conversion Coefficient of γ-rays has recently been calculated by Hulme[†] and by Taylor and Mott [‡] The assumptions on which both of these calculations rest may be analysed as follows

I —A nucleus, originally in an excited state of energy W_n, radiates, corresponding to the transition to each lower state of energy W_m, an electromagnetic field which may be either that of a dipole or that of a quadripole For a dipole such a field has scalar and vector potentials given by

$$A_0 = \mathscr{A}_0 + \mathscr{A}^*_0 \quad \text{and} \quad \mathbf{A} = \mathscr{A} + \mathscr{A}^*,$$

where

$$\left.\begin{aligned} \mathscr{A}_0 &= Br^{-1}\, e^{iqr} \cos\theta\,(1 + i/qr)\, e^{-2\pi i\nu t}, \\ \mathscr{A}_x &= \mathscr{A}_y = 0, \\ \mathscr{A}_z &= Br^{-1}\, e^{iqr}\, e^{-2\pi i\nu t}. \end{aligned}\right\} \qquad (1.1)$$

B is here an (unknown) constant , the asterisks indicate that complex conjugate values are to be taken , and

$$q = 2\pi\nu/c \quad \text{and} \quad \nu = (W_n - W_m)/h.$$

II.—The probability per time dt ($= b\,dt$) that an electron is ejected from the K shell may be calculated by the ordinary methods used in the photoelectric effect. It follows that[§]

$$b = \frac{4\pi^2}{h}\left|\int \psi^*_f\,\{-\epsilon\mathscr{A}_0 - \epsilon\rho_1\,(\mathscr{A}\sigma)\}\,\psi_0\,d\tau\right|^2, \qquad (1.2)$$

where ψ_0 is the initial wave function of the K electron, and ψ_f is the wave function of its final free state [||]

[†] 'Proc Roy. Soc.,' A, vol 138, p. 643 (1932), referred to as H II.

[‡] 'Proc. Roy. Soc.,' A, vol. 138, p 665 (1932), referred to as T M.

[§] *Cf.* Hulme, 'Proc. Roy. Soc.,' A. vol. 133, p 381, *et seq* (1931), referred to as H I.

[||] See a note in § 2 as to the normalization of the wave function ψ_f. Throughout this paper $-\epsilon$ is used for the charge on the electron. If there are several possible final states for the electron, (1.2) is, of course, summed for all such states.

III.—The probability per time dt ($= pdt$) that the nucleus shall make the transition $W_n \rightarrow W_m$, either a γ-quantum or an extra-nuclear electron being ejected from the atom, is the *same as it would be if the K electron were not present.* Thus p may be calculated by evaluating the rate at which energy is radiated by the field (1.1) and dividing by $h\nu$. This gives

$$p = 16\pi^2 B^2 \nu / 3hc \tag{1.3}$$

The internal conversion coefficient was then defined as the ratio

$$\alpha = b/p,$$

from which the unknown constant B disappears. The probability gdt per time dt that a γ-quantum is emitted is clearly

$$(p - b)\, dt$$

The number

$$b/(p - b) = \alpha/(1 - \alpha)$$

is the quantity which is measured experimentally,[†] namely, the ratio of the β-particles to γ-quanta for a given γ-ray frequency.

We have been led to re-examine these assumptions, owing to the disturbing fact that it is possible to construct a model nucleus, of smaller atomic number Z and larger nuclear radius r_0 than that of the actual radioactive nuclei, for which the value of α calculated in this way is greater than unity.

We find that the assumptions I and II are correct, but that III is valid only if $\alpha \ll 1$. Thus our previous calculations are correct for hard γ-rays but require modification for soft γ-rays. The assumption III is not correct, because the K electron perturbs the nucleus, and so the total probability, pdt, that in the time dt the nucleus will fall to the ground state, is *greater* than it would be if the K electron were not there. Thus the ejection of a β-particle is to be thought of partly as due to absorption of a γ-ray and partly to direct interaction between the nucleus and the electron. It is, however, impossible to separate the two effects, and the total probability of electron emission due to both causes is correctly given by (1.2). This point has already been discussed (T M, § 3), and is further considered below.

The quantity (1.3) is, therefore, not the correct expression for p. In this paper we calculate g by considering the rate of γ-radiation from the complete system consisting of the nucleus coupled to the two K electrons, by methods which are discussed below.

[†] *Cf.* Rutherford, Chadwick and Ellis, "Radiations from Radioactive Substances," p. 512.

We find that the *probability of γ-radiation* (g, not, as in III above, p) is always very nearly the same as it would be if the K electron were not there, and thus nearly equal to (1.3), being less only by a term of order of magnitude $g\epsilon^2/hc$. Thus in cases where $b/g \gg \epsilon^2/hc$ the electron ejection may be considered to be nearly all due to direct interaction. Thus the quantity calculated in T M, fig 1, is really b/g, the experimental points $\alpha = b/(g-b)$ should be changed to $b/g = \alpha/(1-\alpha)$, and thus raised somewhat The agreement with experiment is slightly less good than before

The term "internal conversion coefficient" thus loses its meaning The theory gives directly the quantity which is measured, namely b/g.

§ 2. *General Theory* —We first show that (1 2) does give the correct value for the probability of β-ray emission by the complete system [†] For the sake of argument we consider the γ-rays to be emitted by an excited particle of charge η in the nucleus We assign to this particle wave functions $\Psi_n(\mathbf{R})$ and $\Psi_0(\mathbf{R})$ in its excited and normal states We suppose the K electron to be in its normal state with wave function $\psi_0(\mathbf{r})$. Then a transition analogous to the Auger effect is possible, whereby the electron is ejected and the nucleus returns to its normal state [‡] According to *non-relativistic* quantum mechanics we can calculate the probability $b\,dt$ per time dt of the transition between these two states of equal energy, it is given by the familiar formula

$$b\,dt = \frac{4\pi^2}{h}\left|\int \Psi^*_0(\mathbf{R})\,\psi^*_f(\mathbf{r})\,\frac{\epsilon\eta}{|\mathbf{R}-\mathbf{r}|}\,\Psi_n(\mathbf{R})\,\psi_0(\mathbf{r})\,d\mathbf{R}\,d\mathbf{r}\right|^2 dt \qquad (2\ 1)$$

This formula is the result of a first order perturbation calculation The general criterion for the validity of such a calculation is that $b\tau \ll 1$, τ being a time of the order of $1/\nu$, where ν is the frequency of the γ-ray which *would* be emitted if the nucleus alone made the transition $\Psi_n \rightarrow \Psi_0$. If this condition were not satisfied it would be impossible to define the initial state of the system, and therefore we conclude that in our case there is no question as to the sufficiency of the perturbation method

If in (2 1) we perform the integration over the co-ordinate **R**, we obtain

$$b = \frac{4\pi^2}{h}\left|\int \psi^*_f(\mathbf{r})\,V_{0n}(\mathbf{r})\,\psi_0(\mathbf{r})\,d\mathbf{r}\right|^2 \qquad (2\ 2)$$

[†] This point has been discussed in less detail in our earlier paper (T M), § 3.

[‡] This was first suggested by Smekal, 'Z. Physik,' vol. 10, p. 275 (1922).

where, if we assume the nuclear transition $n \rightarrow 0$ to be a dipole transition, it may easily be shown that

$$\mathrm{V}_{0n} = \mathrm{C}r^{-2}\cos\theta, \qquad \mathrm{C} = \epsilon\eta \int z\Psi^*_0(\mathbf{R})\,\Psi_n(\mathbf{R})\,d\mathrm{R}, \tag{2 3}$$

or for a quadripole transition

$$\mathrm{V}_{0n} = \mathrm{C}'r^{-3}\,\mathrm{P}_2(\cos\theta).$$

The result (2 3) is, of course, valid only when r is greater than the "radius of the nucleus," *i e*, $r > 10^{-12}$ cm, say Now Møller† has recently shown how to treat the interaction of two particles by a relativistic perturbation theory, according to which (1.2) is just the relativistic generalization of (2 2), to which it clearly tends as $c \rightarrow \infty$ According to Møller's theorem, we must replace $\mathrm{V}_{0n}(\mathbf{r})$ in (2 2) by the perturbation due to the electromagnetic field radiated by the charge density

$$\eta\Psi^*_n(\mathbf{R})\,\Psi_0(\mathbf{R})\,e^{-2\pi\nu t} + \text{complex conjugate}$$

If $n \rightarrow 0$ is a dipole transition, this field is simply (1 1) with $\mathrm{C} = -\epsilon\mathrm{B}/q$. The expression (1 2) thus gives correctly the probability per unit time that an electron is ejected, whether this is considered to be due to "direct interaction" (Auger effect) or to "absorption of a γ-ray." On the relativistic theory the distinction between these two processes loses its meaning, and one cannot separate the two effects In fig 1 we show the variation of the radial part of $r\mathrm{A}_0$ (*cf.* (1.1)), with r, and we see that, for $r > \frac{1}{2}\lambda$ the important part of A_0

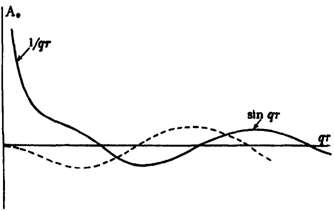

FIG. 1—Scalar potential of dipole, $r\mathrm{A}_0 = 2\mathrm{B}\,\{\cos(qr - \omega t) - (qr)^{-1}\sin(qr - \omega t)\}$. Full line, $\omega t = \frac{1}{2}\pi$, dotted line, $\omega t = 0$.

---

† 'Ann. Physik,' vol. 14, p. 531 (1932).

is the term in $r^{-1} e^{\pm iqr} \cos\theta$, while for $r < \frac{1}{2}\lambda$ the important part of A_0 has the form $r^{-2} \cos\theta$. Thus we may say roughly that in the integral in (1.2), the part for $r < \frac{1}{2}\lambda$ corresponds to direct interaction, and the part for $r > \frac{1}{2}\lambda$ to photoelectric absorption. It is, however, important to notice, as was emphasized in TM, § 3, that it is the probability *amplitudes* for these two terms which we add, *not* the probabilities themselves This is quite clear from the formula (1 2).

From these considerations it appears incorrect to obtain the number of γ-rays emitted in time dt by subtracting the number of electrons from the number of quanta which would have been emitted had the K electron not been present The correct procedure is to calculate the rate of radiation from the system

(nucleus + K electron)

as a whole. Now if a system of two particles, whose charges are η and $-\varepsilon$ and whose co-ordinates are $\mathbf{R}$ and $\mathbf{r}$, jumps from a state

$$\Phi_i(\mathbf{R}, \mathbf{r}) \exp(-2\pi i W_T^i t/h)$$

to a state $\Phi_f(\mathbf{R}, \mathbf{r}) \exp(-2\pi i W_T^f t/h)$, the radiating charge density corresponding to the transition† is given by

$$\left\{\eta \int \Phi^*_f \Phi_i \, d\mathbf{r} - \varepsilon \int \Phi^*_f \Phi_i \, d\mathbf{R}\right\} e^{-2\pi i\nu t} + \text{complex conjugate}, \qquad (2.4)$$

where $h\nu = W_T^i - W_T^f$, W_T denoting the energy of the total system

We have now to determine the form of the wave functions Φ_i and Φ_f. To the approximation of zero order in the interaction between nucleus and K electron, our initial system is an excited particle in the nucleus, described by the wave function $\Psi_n(\mathbf{R}) \exp(-2\pi i W_n t/h)$, together with an electron in the K state, described by the wave function $\psi_0(\mathbf{r}) \exp(-2\pi i E_0 t/h)$; the total system, therefore, is described by the wave function

$$\Psi_n(\mathbf{R}) \, \psi_0(\mathbf{r}) \exp\{-2\pi i (W_n + E_0) t/h\} \qquad (2\ 5)$$

In the first order approximation we take into account the interaction V between the nuclear particle and the electron. The system therefore no longer stays in the state (2 5). We suppose for simplicity that there is only one other nuclear state available, of energy W_0 ($< W_n$), and then, if we suppose the interaction V " switched on " at time $t = 0$, the state of the total system at time t can be expressed in the form

---

† *Cf.* Klein, 'Z. Physik,' vol. 41, p. 407 (1927).

$$a_0(t)\, \Psi_n(\mathbf{R})\, \psi_0(\mathbf{r}) \exp\{-2\pi i (\mathrm{W}_n + \mathrm{E}_0)\, t/h\} + \Psi_0(\mathbf{R})\, \chi(\mathbf{r}, t) \exp\{-2\pi i \mathrm{W}_0 t/h\}, \tag{2.6}$$

where $\chi(\mathbf{r}, t)$ represents a wave diverging from the atom, corresponding to the ejected K electrons. To find χ we expand it in the form

$$\chi = \sum_{ku} \sum_{\mathrm{E}_j < mc^2} a_{jku}(t)\, \psi_{jku}(\mathbf{r}) \exp\{-2\pi i \mathrm{E}_j t/h\} + \sum_{ku} \int_{mc^2}^{\infty} a(\mathrm{E}, k, u;\; t)\, \psi(\mathrm{E}, k, u,\; \mathbf{r}) \exp(-2\pi i \mathrm{E} t/h)\, d\mathrm{E}, \tag{2.7}$$

where ψ_{jku} denotes a normalized wave function of the discrete spectrum, $\psi(\mathrm{E}, k, u, \mathbf{r})$ a normalized† wave function of the continuous spectrum, and k and u are the angular quantum numbers as defined by Darwin.‡ At time $t = 0$ all the coefficients a are zero except a_0, which has the value unity. Bethe§ has shown that the wave function (2.7), calculated by the method of variation of parameters, represents an outgoing wave only, the terms of the type $\exp(-2\pi i mvr/h - 2\pi i \mathrm{E}t/h)$ vanishing, and further that if v is the velocity with which the photoelectrons are ejected, (2.7) becomes very small for $r > vt$. The coefficient $a_0(t)$ is such that $|a_0(t)|^2 = e^{-pt}$, we consider only t such that $pt \leqslant 1$, so that $a_0(t)$ may be replaced by unity.

We return later to the discussion of the values of the coefficients a

---

† The normalization of the continuous-energy wave functions calls for some comment. In H I, H II, and T M, the wave functions were normalized, following Gaunt (‘ Phil. Trans.,’ A, vol. 229, p 163 (1930)) *per unit frequency range* That is to say

$$\int \psi^*(\mathrm{E}')\, \psi(\mathrm{E})\, d\tau = \delta(\nu - \nu'), \qquad \mathrm{E} = h\nu,$$

whence it follows that (with certain restrictions on f)

$$\iint \psi^*(\mathrm{E}')\, f(\mathrm{E})\, \psi(\mathrm{E})\, d\tau\, d\mathrm{E}/h = f(\mathrm{E}').$$

In this paper we adopt the principle of normalization *per unit energy range* Thus in our case

$$\iint \psi^*(\mathrm{E}')\, \psi(\mathrm{E})\, f(\mathrm{E})\, d\tau\, d\mathrm{E} = \int \delta(\mathrm{E} - \mathrm{E}')\, f(\mathrm{E})\, d\mathrm{E} = f(\mathrm{E}')$$

Our normalising factor $\xi(\mathrm{E}, k, u)$ is therefore $h^{-\frac{1}{2}}$ times the normalizing factor of these other papers. This accounts for the coefficient $4\pi^2/h$ in our equation (1.2) as compared with the coefficient $4\pi^2/h^2$ in T M (2.4) or H II (3).

‡ ‘ Proc. Roy Soc.,’ A, vol. 118, p. 667 (1928), *cf.* our equations (3.4A) and (3.4B).

§ ‘ Ann. Physik,’ vol. 4, p. 445 (1930).

We note that the initial state of the system is not a *stationary* state, though it is a state of almost definite total energy. It is a state similar to the quasi-stationary nuclear states that, in the Gamow-Condon-Gurney theory, describe an α-particle's escape from a radioactive nucleus.

The final state to which the system can jump, with emission of a quantum of γ-radiation, is clearly the state in which both electron and nuclear particle are in their lowest energy levels, *i.e.*, the state

$$\Phi_f(\mathbf{R}, \mathbf{r})\, e^{-2\pi i(W_0+E_0)t/h} = \Psi_0(\mathbf{R})\, \psi_0(\mathbf{r})\, e^{-2\pi i(W_0+E_0)t/h} \qquad (2.8)$$

To obtain the radiating charge density for the transition of the whole system from the initial state, with energy $W_0 + E_0 + h\nu$, to the state with energy $W_0 + E_0$, we substitute in (2.4), putting Φ_i equal to (2.6), and Φ_f equal to (2.8). We thus obtain, for the radiating charge density

$$\eta\, \Psi^*_0\, \Psi_n\, e^{-2\pi i\nu t} - \varepsilon\, \psi^*_0(\mathbf{r})\, e^{2\pi i E_0 t/h}\, \chi(\mathbf{r}, t) \qquad (2.9)$$

The first term in (2.9) is just the radiating charge density corresponding to the nuclear transition, and the electromagnetic field radiated is simply the dipole field (1.1) with which we start, with $B = \eta q \int \Psi^*_0\, z\, \Psi_n\, d\tau$. We shall now calculate the field radiated by the second term in (2.9), and shall show that this field, interfering with (1.1), produces a small *diminution* in the intensity of the outgoing γ-ray wave, but that this diminution is *not* the same as that obtained by subtracting the number, *b*, of β-particles given by (1.2). However, when a similar calculation is carried out (§ 3), taking for the perturbing field that of a light wave coming from *outside* the atom, it is found that the diminution in intensity *is* equal to the number of β-particles. This is what we should expect, because there is here no possibility of "direct" interaction between the atom and the source of the light waves.

We must now evaluate the coefficients *a* in (2.7) by the method of the variation of parameters. In order to do this we need to know the interaction V, and according to Møller's theory that is to be obtained as follows. We write down the electromagnetic potentials A_0 and $\mathbf{A}$ which the nuclear particle would radiate in making the jump $\Psi_n \rightarrow \Psi_0$; V is then given by

$$V = -\varepsilon\{A_0 + \rho_1(\boldsymbol{\sigma}\mathbf{A})\}/c. \qquad (2.10)$$

If, for example, the nuclear particle has made a dipole jump, then the quantities which occur in (2.10) are just the potentials of (1.1), with $h\nu = W_n - W_0$. If then we write

$$V = ve^{-2\pi i\nu t} + v^* e^{2\pi i\nu t} \tag{2.11}$$

we at once obtain† from (2.7), by the usual method of variation of parameters

$$\begin{aligned} a_0(t) &\simeq 1 \\ a(\mathrm{E}, k, u, t) &= -v_-(\mathrm{E}, k, u)\,\frac{\exp\{2\pi i(\mathrm{E} - \mathrm{E}_0 - h\nu)t/h\} - 1}{\mathrm{E} - \mathrm{E}_0 - h\nu} \\ &\quad - v_+(\mathrm{E}, k, u)\,\frac{\exp\{2\pi i(\mathrm{E} - \mathrm{E}_0 + h\nu)t/h\} - 1}{\mathrm{E} - \mathrm{E}_0 + h\nu} \end{aligned} \tag{2.12}$$

with similar equations for $a_{jku}(t)$. The coefficients are given by

$$\left.\begin{aligned} v_-(\mathrm{E}, k, u) &= c\int \psi^*(\mathrm{E}, k, u, \mathbf{r})\, v\psi_0(\mathbf{r})\, d\tau \\ v_+(\mathrm{E}, k, u) &= c\int \psi^*(\mathrm{E}, k, u, \mathbf{r})\, v^*\, \psi_0(\mathbf{r})\, d\tau \end{aligned}\right\} \tag{2.13}$$

Thus the wave function $\chi(\mathbf{r}, t)$ in (2.7) becomes—omitting the summation over the quantized states‡—

$$-e^{-2\pi i(\mathrm{E}_0 + h\nu)t/h}\int v_-(\mathrm{E})\,\psi(\mathrm{E}, \mathbf{r})\,\frac{1 - e^{-2\pi i(\mathrm{E} - \mathrm{E}_0 - h\nu)t/h}}{\mathrm{E} - \mathrm{E}_0 - h\nu}\, d\mathrm{E} \tag{2.14}$$

Bethe (*loc. cit.*) has shown that at points outside the atom ($\mathbf{r}$, t large) nearly all this integral comes from the neighbourhood of $\mathrm{E} = \mathrm{E}_0 + h\nu$, corresponding to the fact that electrons are only ejected with this energy. For t large but r small (*i.e.*, within the atom) this however is not so; here χ may be split up into two terms; we may write

$$\chi(\mathbf{r}, t) = \chi_{\mathrm{A}}(\mathbf{r}, t) + \chi_{\mathrm{B}}(\mathbf{r}, t),$$

where

$$\left.\begin{aligned} \chi_{\mathrm{A}}(\mathbf{r}, t) &= -e^{-2\pi i(\mathrm{E}_0 + h\nu)t/h}\int v(\mathrm{E})\,\psi(\mathrm{E}, \mathbf{r})\,\frac{i\sin\{2\pi(\mathrm{E} - \mathrm{E}_0 - h\nu)t/h\}}{\mathrm{E} - \mathrm{E}_0 - h\nu}\, d\mathrm{E} \\ &\text{and} \\ \chi_{\mathrm{B}}'(\mathbf{r}, t) &= -e^{-2\pi i(\mathrm{E}_0 + h\nu)t/h}\int v(\mathrm{E})\,\psi(\mathrm{E}; \mathbf{r})\,\frac{1 - \cos\{2\pi(\mathrm{E} - \mathrm{E}_0 - h\nu)t/h\}}{\mathrm{E} - \mathrm{E}_0 - h\nu}\, d\mathrm{E} \end{aligned}\right\}. \tag{2.15}$$

---

† *Cf.* H I, p. 389. There is a misprint in his equation; the exponential in the second matrix element should be $\exp\{-2\pi i\nu_0 z/c\}$.

‡ The quantum numbers k, u are here omitted from v, ψ. A summation over all k, u is to be understood. The term involving v_+ is small for large r, and is omitted.

The integrand in χ_A has a strong maximum for $E = E_0 + h\nu$; as $\nu t \rightarrow \infty$ it tends to

$$\chi_A \rightarrow -e^{-2\pi i(E_0+h\nu)t/h}\, \pi i\, v(E_0 + h\nu)\, \psi(E_0 + h\nu,\ \mathbf{r}) \tag{2.16}$$

In χ_B, on the other hand, one may neglect the cosine as $\nu t \rightarrow \infty$ and write

$$\chi_B \rightarrow -e^{-2\pi i(E_0+h\nu)t/h} \int v(E)\, \psi(E,\ \mathbf{r})\, \frac{dE}{E - E_0 - h\nu}, \tag{2.17}$$

where the integration over the infinite point is to be carried out by means of the convention†

$$\int_A^B \frac{d\zeta}{\zeta} = \lim_{\epsilon \rightarrow 0} \left[\int_A^{-\epsilon} \frac{d\zeta}{\zeta} + \int_{\epsilon}^{B} \frac{d\zeta}{\zeta} \right]$$

We now consider the oscillating charge density (2.9). The second term is

$$-\epsilon\, \psi^*_0(\mathbf{r})\, e^{2\pi i E_0 t/h} \{\chi_A + \chi_B\}, \tag{2.18}$$

and using the asymptotic forms (2.16), (2.17) the two terms in (2.18) are

$$\left.\begin{array}{ll} \text{(A)} & \epsilon\, e^{-2\pi i\nu t}\, \psi^*_0(\mathbf{r})\, \psi(E_0 + h\nu,\ \mathbf{r})\, \pi i\, v(E_0 + h\nu) \\ \text{(B)} & \epsilon\, e^{-2\pi i\nu t}\, \psi^*_0(\mathbf{r}) \displaystyle\int \frac{v(E)\, \psi(E,\ \mathbf{r})}{E - E_0 - h\nu}\, dE \end{array}\right\}. \tag{2.19}$$

The electromagnetic wave radiated by (B) is the ordinary "scattered" wave given by the Kramers-Heisenberg dispersion theory.‡ We emphasize here that the phase of this wave must, if the formula is to be physically significant, be such that the *phase* of the original γ-ray wave at infinity is altered, but not its intensity. The term (B) will thus represent the "refracting effect" of the K ring on the outgoing γ-ray. This term, therefore, contributes nothing to the diminution of intensity of the original γ-ray (1.1).

It is the term A in (2.19) which radiates a wave which interferes with the original γ-ray, and produces a diminution of intensity. We believe that this is the correct interpretation of this term, because of the following facts in the classical theory. If a charged particle, bound so that it can vibrate with natural frequency ν_0, is acted on by a light wave of frequency ν, it will execute forced oscillations with amplitude proportional to

$$1/(\nu_0^2 - \nu^2)$$

---

† *Cf.* Kramers, 'Atti. Cong. Int. Fis.,' (1927).

‡ *Cf.* Waller, 'Z. Physik,' vol. 58, p. 75 (1929).

The wave radiated by the particle is the scattered light in the classical dispersion theory No energy is absorbed by the particle; it follows that the phase of the scattered wave must be such that the total energy (flux of Poynting's vector) crossing a sphere surrounding the atom is zero (*cf.* § 3). If, however, $\nu = \nu_0$ the amplitude increases indefinitely with the time, and then, on the classical theory, the light radiated by the oscillating particle, interfering with the original wave, *must* result in a wave of decreased intensity—since in classical electrodynamics the conservation of energy is valid, and the increasing energy of the oscillating particle must come from the light wave. Thus the energy flowing *into* a large sphere is more than that flowing *out* † We are thus led to suspect that the wave radiated by the term A, which comes from the neighbourhood of the resonance spot in the Kramers-Heisenberg dispersion formula, must be capable of interfering with the original wave and producing a diminution of intensity.

Writing out the term (A) in full, we obtain from (2 10), (2 11) and (2 13)

$$\rho_{0n}\, e^{-2\pi i\nu t} = -\pi i\epsilon^2 e^{-2\pi i\nu t}\, \psi^*{}_0(\mathbf{r}) \sum_{ku} \psi(\mathrm{E}_0 + h\nu, k, u,\ \mathbf{r})$$
$$\int \psi^*(\mathrm{E}_0 + h\nu, k, u,\ \mathbf{r})\, \{\mathcal{A}_0 + \rho_1(\boldsymbol{\sigma}\cdot\mathcal{A})\}\, \psi_0(\mathbf{r})\, d\tau \qquad (2.20)$$

We have to calculate the field radiated by this charge density, the scalar potential, for instance, is

$$\mathrm{A}_0{}^1 = e^{-2\pi i\nu t} \int \frac{e^{iq|\mathbf{r}-\mathbf{r}'|}}{|\mathbf{r}-\mathbf{r}'|}\, \rho_{0n}(\mathbf{r}')\, d\tau' + \text{complex conjugate} \qquad (2\ 21)$$

We note that $\mathrm{A}_0{}^1$ is proportional to B (1 1) The scalar potential for the wave radiated by the whole system is

$$\mathrm{A}_0 + \mathrm{A}_0{}^1,$$

where A_0 is given by (1 1). The vector potential may be calculated in a similar way, and g deduced We note that g is proportional to $|\mathrm{B}|^2$, as is

---

† This is not difficult to prove directly by the method of § 3. We note that if $\nu \neq \nu_0$, the oscillating particle is in phase with the light wave, *i.e.*, if the light wave is E sin $2\pi\nu t$, the displacement of the particle at time t is proportional to

$$(\nu_0{}^2 - \nu^2)^{-1}\, \mathrm{E}\epsilon \sin 2\pi\nu t, \qquad (a)$$

whereas, if $\nu = \nu_0$, it is proportional to

$$\mathrm{E}\epsilon\, t \cos 2\pi\nu t. \qquad (b)$$

As may easily be seen by the method of § 3, the difference of phase of $\frac{1}{2}\pi$ is responsible for the fact that the wave radiated by (*a*) does not change the total flux of energy, whereas that by (*b*) does.

also b. Thus this unknown constant B does not occur in the ratio $b \cdot g$. The detailed calculations are carried out in § 4

§ 3. *External Photoelectric Effect.*—The methods of the last section may be applied to the ordinary photoelectric effect. The electromagnetic field radiated by the electrons in jumping from bound to free states, *i.e.*, by the term (2 17), interferes with the original beam, and in this case one would expect the number of light quanta removed from the beam to be equal to the number of photoelectrons ejected The analysis given below shows that this is so, if we neglect terms of the order $(\varepsilon^2/hc)^2$. This is justifiable, firstly, because a relativistic quantum mechanics on the lines of Møller's theory is accurate only to this order, and secondly, because the Compton absorption will be of order $(\varepsilon^2/hc)^3$, and has not been allowed for

We consider a beam of light travelling in the positive z-direction and with the magnetic vector in the $x0z$ plane For the field perturbing the electrons we may therefore write

$$\left.\begin{aligned} \mathcal{A}_0 = \mathcal{A}_x = \mathcal{A}_z = 0 \\ \mathcal{A}_y = \mathrm{E}e^{i(qz-2\pi\nu t)} \end{aligned}\right\}. \tag{3 1}$$

We represent the ejected electrons as before by the wave function

$$\chi(\mathbf{r}, t),$$

and the radiating charge and current densities of the type (2 19 A) due to the transitions are therefore, from (2 20), given by

$$\left.\begin{aligned} \rho(\mathbf{r}) &= -\pi i\varepsilon^2 e^{-2\pi i\nu t}\, \psi^*{}_0(\mathbf{r})\, \psi_n(\mathbf{r})\, \mathrm{ME} \\ \mathbf{j}(\mathbf{r}) &= +\pi i\varepsilon^2 e^{-2\pi i\nu t}\, \psi^*{}_0(\mathbf{r})\, \rho_1\sigma\psi_n(\mathbf{r})\, \mathrm{ME} \end{aligned}\right\} + \begin{array}{c}\text{conjugate}\\ \text{complex,}\end{array} \tag{3 2}$$

where for simplicity we have assumed that there is only one possible final free state n, and have therefore dropped the summation of (2 20) and where

$$\left.\begin{aligned} \mathrm{M} &= \int e^{iqz}\, \mathrm{J}_y(\mathbf{r})\, d\tau \\ \text{with} \qquad \mathbf{J}(\mathbf{r}) &= \psi^*{}_n(\mathbf{r})\, \rho_1\sigma\psi_0(\mathbf{r}). \end{aligned}\right\} \tag{3.3}$$

The radiated vector potential is given by

$$\mathcal{A}_\mu(\mathbf{r}) = \int \frac{e^{iq|\mathbf{r}-\mathbf{r}_1|}}{|\mathbf{r}-\mathbf{r}_1|}\, j_\mu(\mathbf{r}_1)\, d\tau_1 \qquad \mu = x, y, z, \tag{3.4}$$

which, for large values of r may be written

$$\mathcal{A}_\mu(\mathbf{r}) \sim r^{-1} e^{i(qr-2\pi\nu t)} f_\mu(\mathbf{n})\, \mathrm{E},$$

where
$$\mathbf{n} = \mathbf{r}/r$$
and
$$f_\mu(\mathbf{n}) = \pi i e^2 \mathrm{M} \int e^{-iq(\mathbf{n}\mathbf{r}_1)} \mathrm{J}^*_\mu(\mathbf{r}_1)\, d\tau_1 \tag{3.5}$$

This wave has now to interfere with the incident wave (3.1), and in order to calculate the rate of radiation of energy by the combined wave we may proceed as follows. We calculate the magnetic vector H and write down the energy per unit volume $(\mathbf{E}^2 + \mathbf{H}^2)/8\pi = \mathbf{H}^2/4\pi$. We subtract from this the energy per unit volume in the incident wave and then calculate the amount of this energy difference enclosed between two large spheres of radii r and $r + \Delta$ (where $\Delta r \gg \lambda$). If $\mathrm{W}\Delta r$ be the energy so obtained, then the number of quanta absorbed per unit time is $\mathrm{W}c/h\nu$.

If now we reject terms of order M^2, the only term in $\mathrm{H}_x^2 + \mathrm{H}_y^2 + \mathrm{H}_z$ which differs from the original value is H_x^2. We have

$$\mathrm{H}_x = -iq\mathrm{E}\left[e^{iqz} + r^{-1} e^{iqr}\left\{\frac{z}{r} f_y(\mathbf{n}) - \frac{y}{r} f_z(\mathbf{n})\right\}\right] e^{-2\pi i\nu t}$$
$$+ \text{ conjugate complex.} \tag{3.6}$$

If now we write $\mathrm{H}_x = ae^{-2\pi i\nu t} + a^* e^{2\pi i\nu t}$, then the time-average value H_x^2 is $2aa^*$. Thus the average value of H_x^2, less the original average value if given by

$$\overline{\delta \mathrm{H}_x^2} = 2q^2\mathrm{E}^2\left[e^{-iqz}\frac{e^{iqr}}{r}\left\{\frac{z}{r} f_y(\mathbf{n}) - \frac{y}{r} f_z(\mathbf{n})\right\}\right] + \text{ conjugate complex} \tag{3.7}$$

This we now integrate over the space between the spheres of radii r and $r + \Delta r$. Now, we have for large r

$$e^{-iqz} = \sum_{n=0}^{\infty} (2n+1)(-i)^n \mathrm{P}_n(\cos\theta) \frac{\sin(qr - \frac{1}{2}n\pi)}{qr}, \tag{3.8}$$

and therefore, since $\Delta r \gg \lambda$, we obtain

$$\int_r^{r+\Delta r} r^{-1} e^{iqr} e^{-iqz} r^2\, dr = \sum_n \frac{(2n+1)\mathrm{P}_n(\cos\theta)}{-2iq} \Delta r$$

But if $\mathrm{F}(\theta, \phi)$ is any function of position on a sphere,

$$\sum_n \iint (2n+1)\mathrm{P}_n(\cos\theta)\mathrm{F}(\theta, \phi) \sin\theta\, d\theta\, d\phi = 4\pi \mathrm{F}_{\theta=0}, \tag{3.9}$$

and therefore, carrying out the θ and ϕ integrations, we obtain from (3.7) for the energy deficit between the two spheres

$$-\mathrm{W}\Delta r = 2q^2\mathrm{E}^2 \frac{f_y(\mathbf{n}_0)}{-2iq} \Delta r + \text{ conjugate complex,}$$

where $\mathbf{n}_0$ denotes unit vector along the z-axis.

Now $f_\nu(\mathrm{n}_0) = \pi i \varepsilon^2 \mathrm{MM}^*$ from (3 5). Thus the number of quanta *absorbed* per unit time is

$$q\pi \mathrm{E}^2 c \varepsilon^2 \mathrm{MM}^*/h\nu + \text{conjugate complex},$$

i e,

$$4\pi^2 \mathrm{E}^2 \varepsilon^2 |\mathrm{M}|^2/h,$$

which, by (1.2) is just the number of electrons ejected.

The term (B) in (2 20), as already stated, is the charge density to which is due the Kramers-Heisenberg scattered wave It is easy to see that the wave radiated by (B) differs in phase by $\pi/2$ from the wave radiated by (A), and hence that, to the first order in the quantity $\varepsilon^2|\mathrm{M}|^2/h \lesssim \varepsilon^2/hc$, the change in the energy between the spheres of radii r, $r + \Delta r$ is zero

We see that the proof of this section depends on the fact that for the external photoelectric effect the same matrix elements occur in the probability for the ejection of an electron as those that occur in the probability of spontaneous emission of radiation When the atom is perturbed by a field diverging from the centre, however, quite different matrix elements occur

§ 4 In this section we calculate the electromagnetic field given by equation (2 21), which interferes with the original γ-ray wave The integral in (2.20), giving the probability that an electron makes a transition to the free state $\psi(\mathrm{E}_0 + h\nu, \mathbf{r})$, has already been calculated in TM. We have thus only to calculate the electromagnetic field radiated in a transition from the free state to the bound state in the K ring

Of the two possible bound states for the electron, corresponding to its spin being directed along the positive or negative z-axis, we take for the present the first only, and discuss later the question of an arbitrary orientation of the spin. Thus we take the four components of the initial wave function ψ_i to be

$$\left.\begin{array}{ll} (\psi_i)_1 = -if\cos\theta & (\psi_i)_2 = -if\sin\theta e^{i\phi} \\ (\psi_i)_3 = g & (\psi_i)_4 = 0 \end{array}\right\}, \qquad (4\ 1)$$

where

$$f = \frac{\gamma}{1 + (1-\gamma^2)^{\frac{1}{2}}}\,\xi(\mathrm{E}_0)\, r^\beta e^{-r/a_0},$$

$$g = \xi(\mathrm{E}_0)\, r^\beta e^{-r/a_0},$$

$\xi(\mathrm{E}_0)$ being the normalizing factor, γ being $2\pi\varepsilon^2\mathrm{Z}/hc$, β being $(1-\gamma^2)^{\frac{1}{2}} - 1$, and a_0 being the radius of the first Bohr orbit for a hydrogen-like atom of nuclear charge $\mathrm{Z}\varepsilon$.

Let us now confine ourselves to the case of the quadripole nuclear field discussed in T M ; the results for a dipole are similar. The field of a quadripole with axis along Oz has scalar and vector potentials

$$\left.\begin{aligned} A_0 &= \mathscr{A}_0 + \mathscr{A}_0^*, \\ \mathbf{A} &= \mathscr{A} + \mathscr{A}^*, \end{aligned}\right\} \tag{4.2}$$

where

$$\left.\begin{aligned} \mathscr{A}_0 &= Cr^{-1} e^{i(qr-2\pi\nu t)} \left\{2P_2(\cos\theta)\left[1 + \frac{3i}{qr} - \frac{3}{q^2r^2}\right] + 1\right\} \\ \mathscr{A}_x &= \mathscr{A}_y = 0 \\ \mathscr{A}_z &= 3Cr^{-1} e^{i(qr-2\pi\nu t)} \left[1 + \frac{i}{qr}\right] \end{aligned}\right\} \tag{4.3}$$

with $q = 2\pi\nu/c$ It is shown (TM, § 2) that under the influence of this field an electron initially in the K state (4 1) may make transitions only to one or other of the final states, whose wave functions have components given by putting $k = 2$ and $u = 0$ in the equations

$$\left.\begin{aligned} (\psi_f)_1 &= -i\,F_k P^{k}_{u+1}, & (\psi_f)_2 &= -i\,F_k P^{u+1}_{k+1}, \\ (\psi_f)_3 &= (k+u+1)\,G_k P_k{}^u, & (\psi_f)_4 &= (-k+u)\,G_k P_k^{u+1}, \end{aligned}\right\} \tag{4 4A}$$

and

$$\left.\begin{aligned} (\psi_f)_1 &= -i(k+u)\,F_{-k-1} P^u_{k-1} & (\psi_f)_2 &= -i(-k+u+1)\,F_{-k-1} P^{u+1}_{k-1} \\ (\psi_f)_3 &= \qquad G_{-k-1} P^u_k & (\psi_f)_4 &= \qquad G_{-k-1} P^{u+1}_k \end{aligned}\right\} \tag{4.4B}$$

where F_k and G_k are solutions of

$$\left.\begin{aligned} \left(A^2 + \frac{\Upsilon}{r}\right) F_k + \frac{dG_k}{dr} - \frac{k}{r} G_k = 0 \\ \left(B^2 - \frac{\Upsilon}{r}\right) G_k + \frac{dF_k}{dr} + \frac{k+2}{r} F_k = 0 \end{aligned}\right\}, \tag{4 5}$$

$$A^2 = 2\pi(mc^2 + E)/hc, \qquad B^2 = 2\pi(mc^2 - E)/hc,$$

and $P_k{}^u$ is the associated Legendre function defined by

$$P_k{}^u = (k-u)!\,\sin^u\theta\left(\frac{d}{d\cos\theta}\right)^{k+u} \frac{(\cos^2\theta - 1)^k}{k!\,2^k}\,e^{iu\phi}.$$

The energy E of the electron is, of course, the same for both of these states, being given in terms of the energy E_0 of the ground state by $E = E_0 + h\nu$. Our problem is therefore to evaluate the electromagnetic potentials radiated by an electron making either of the two possible transitions from the states A, B above to the ground state.

The radiating charge and current densities corresponding to the transition of the electron with charge $-\varepsilon$ between two states ψ_i and ψ_f having an energy difference $h\nu = E_f - E_i$ are given by

$$\left.\begin{aligned} \rho(\mathbf{r}) &= -\varepsilon\,\psi_i^*(\mathbf{r})\,\psi_f(\mathbf{r})\,e^{-2\pi i\nu t} + \text{complex conjugate} \\ \mathbf{j}(\mathbf{r}) &= +\varepsilon\,\psi_i^*(\mathbf{r})\,\boldsymbol{\alpha}\,\psi_f(\mathbf{r})\,e^{-2\pi i\nu t} + \text{complex conjugate} \end{aligned}\right\}, \tag{4 6}$$

where the suffixes i, f refer to the initial and final states respectively, and where the components of the vector $\boldsymbol{\alpha}$ are the Dirac current matrices Thus the quantities $\mathcal{A}_0$ and $\mathcal{A}$ defining the scalar and vector potentials radiated by the transition are given by

$$\left.\begin{aligned} \mathcal{A}_0(\mathbf{r}) &= -\varepsilon\,e^{-i\omega t}\int \frac{e^{iq|\mathbf{r}-\mathbf{r}_1|}}{|\mathbf{r}-\mathbf{r}_1|}\,\psi_i^*(\mathbf{r}_1)\,\psi_f(\mathbf{r}_1)\,d\tau_1 \\ \mathcal{A}(\mathbf{r}) &= +\varepsilon\,e^{-i\omega t}\int \frac{e^{iq|\mathbf{r}-\mathbf{r}_1|}}{|\mathbf{r}-\mathbf{r}_1|}\,\psi_i^*(\mathbf{r}_1)\,\boldsymbol{\alpha}\,\psi_f(\mathbf{r}_1)\,d\tau_1 \end{aligned}\right\}, \tag{4.7}$$

where $\omega = 2\pi\nu$ and $q = \omega/c$.

Now in order to calculate the rate of radiation of energy by the system we need to determine the field only for large values of r Thus in (7) we may put

$$\frac{e^{iq|\mathbf{r}-\mathbf{r}_1|}}{|\mathbf{r}-\mathbf{r}_1|} = \frac{e^{iqr}}{r}\,.\,e^{-iq(\mathbf{n}\ \mathbf{r}_1)},$$

where $\mathbf{n}$ denotes unit vector in the direction $\mathbf{r}$, *i e.*, $\mathbf{n} = \mathbf{r}/r$. To evaluate the potentials (4.7) we make use of the following lemma (*cf* equation (3.8)). If $\mathbf{r}$ and $\mathbf{r}_1$ are the position vectors of two points whose polar co-ordinates are (r, θ, ϕ) and (r_1, θ_1, ϕ_1) and if $f(\mathbf{r}_1)$ is any function of position which may be expanded in a series of spherical harmonics

$$f(\mathbf{r}_1) = \sum_{n,m} S_{n,m}(\theta_1, \phi_1)\,f_{n,m}(r_1), \tag{4.8}$$

then

$$\int e^{-iq(\mathbf{n}\ \mathbf{r}_1)} f(\mathbf{r}_1)\,d\tau_1$$
$$= 4\pi\left(\frac{\pi}{2q}\right)^{1/2}\sum_{n,m}(-i)^n\,S_{n,m}(\theta,\phi)\int f_{n,m}(r_1)\,J_{n+1/2}(qr_1)\,r_1^{3/2}\,dr_1, \tag{4 9}$$

where the integration is taken throughout any sphere with centre at the origin.

We now divide the discussion into two cases, according as the electronic transition is from the state (4.1) to the state (4.4A) or (4.4B).

Case A.—Inserting the explicit forms for ψ_i, ψ_f and α in (4.7) and using (4.8) and (4.9) we obtain

$$\left.\begin{aligned}
\mathscr{A}_0(\mathbf{r}) &= r^{-1}e^{i(qr-\omega t)}\,.\,6\mathrm{A}_2\mathrm{P}_2{}^0(\cos\theta)\\
\mathscr{A}_x(\mathbf{r}) &= r^{-1}e^{i(qr-\omega t)}\\
&\quad\times\{2\mathrm{P}_3{}^1(\cos\theta)[(\mathrm{C}_2-\tfrac{1}{5}\mathrm{B}_2)\cos\phi+i(\mathrm{C}_2+\mathrm{B}_2)\sin\phi]\\
&\qquad\qquad-\tfrac{12}{5}\mathrm{D}_2\mathrm{P}_1{}^1(\cos\theta)\cos\phi\}\\
\mathscr{A}_y(\mathbf{r}) &= r^{-1}e^{i(qr-\omega t)}\\
&\quad\times\{2\mathrm{P}_3{}^1(\cos\theta)[(\mathrm{C}_2-\tfrac{1}{5}\mathrm{B}_2)\sin\phi-i(\mathrm{C}_2+\mathrm{B}_2)\cos\phi]\\
&\qquad\qquad-\tfrac{12}{5}\mathrm{D}_2\mathrm{P}_1{}^1(\cos\theta)\sin\phi\}\\
\mathscr{A}_z(\mathbf{r}) &= r^{-1}e^{i(qr-\omega t)}\{6(\mathrm{C}_2-\tfrac{1}{5}\mathrm{B}_2)\mathrm{P}_3{}^0(\cos\theta)+\tfrac{24}{5}\mathrm{D}_2\mathrm{P}_1{}^0(\cos\theta)\}
\end{aligned}\right\},\qquad(4.10)$$

where

$$\left.\begin{aligned}
\mathrm{A}_2 &= \left(\frac{8\pi^3}{q}\right)^{1/2}\varepsilon\int_0^\infty(f\mathrm{F}_2+g\mathrm{G}_2)\,\mathrm{J}_{5/2}(qr)\,r^{3/2}dr\\
\mathrm{B}_2 &= \left(\frac{8\pi^3}{q}\right)^{1/2}\varepsilon\int_0^\infty f\mathrm{G}_2\mathrm{J}_{7/2}(qr)\,r^{3/2}\,dr\\
\mathrm{C}_2 &= \left(\frac{8\pi^3}{q}\right)^{1/2}\varepsilon\int_0^\infty g\mathrm{F}_2\mathrm{J}_{7/2}(qr)\,r^{3/2}\,dr\\
\mathrm{D}_2 &= \left(\frac{8\pi^3}{q}\right)^{1/2}\varepsilon\int_0^\infty f\mathrm{G}_2\mathrm{J}_{3/2}(qr)\,r^{3/2}\,dr
\end{aligned}\right\}.\qquad(4.11)$$

Now there must obviously be a relationship between these four quantities A_2, B_2, C_2, D_2, since A_0 and $\mathbf{A}$ satisfy the identity $c\,\mathrm{div}\,\mathbf{A}+\partial\mathrm{A}_0/\partial t=0$. In order to obtain this relationship we return to the equations (4.5) which may be written in the more symmetrical form

$$\left.\begin{aligned}
\left(\mathrm{A}^2+\frac{\gamma}{r}\right)(r\mathrm{F}_k)+(r\mathrm{G}_k)'-\frac{k+1}{r}(r\mathrm{G}_k)&=0\\
\left(\mathrm{B}^2-\frac{\gamma}{r}\right)(r\mathrm{G}_k)+(r\mathrm{F}_k)'+\frac{k+1}{r}(r\mathrm{F}_k)&=0
\end{aligned}\right\}.\qquad(4.12)$$

But f and g also satisfy these equations, with $k=0$ and with

$$\mathrm{A}^2=2\pi(mc^2+\mathrm{E}_0)/hc$$

and

$$\mathrm{B}^2=2\pi(mc^2-\mathrm{E}_0)/hc.$$

Thus, eliminating γ between corresponding pairs of the equations (4.12) and the similar equations for f and g, and noting that $2\pi(\mathrm{E}-\mathrm{E}_0)/hc = q$, we obtain

$$\left.\begin{aligned} q(r\mathrm{F}_k)(rf) + (rf)(r\mathrm{G}_k)' - (rg)'(r\mathrm{F}_k) - \frac{k+1}{r}(rf)(r\mathrm{G}_k) & \\ + \frac{1}{r}(rg)(r\mathrm{F}_k) &= 0 \\ -q(r\mathrm{G}_k)(rg) + (rg)(r\mathrm{F}_k)' - (rf)'(r\mathrm{G}_k) + \frac{k+1}{r}(rg)(r\mathrm{F}_k) & \\ - \frac{1}{r}(rf)(r\mathrm{G}_k) &= 0 \end{aligned}\right\}. \tag{4.13}$$

If we now multiply each of these equations by $r^{-1/2}\mathrm{J}_{n+1/2}(qr)$ and integrate, the terms containing derivatives of F_k, G_k, f and g can be eliminated by one partial integration, and, using the recurrence formulæ for the Bessel functions, we obtain

$$\left.\begin{aligned} &(2n+1)\int_0^\infty (f\mathrm{F}_k + g\mathrm{G}_k)\,\mathrm{J}_{n+1/2}(qr)\,r^{3/2}\,dr \\ &= \int_0^\infty f\mathrm{G}_k\{(k-n-1)\,\mathrm{J}_{n+3/2}(qr) + (k+n)\,\mathrm{J}_{n-1/2}(qr)\}\,r^{3/2}\,dr \\ &+ \int_0^\infty g\mathrm{F}_k\{(k+n+1)\,\mathrm{J}_{n+3/2}(qr) + (k-n)\,\mathrm{J}_{n-1/2}(qr)\}\,r^{3/2}\,dr \end{aligned}\right\} \tag{4.14}$$

Putting $n = 2$, $k = 2$ in (2.14) we have the desired relationship, namely,

$$5\mathrm{A}_2 = -\mathrm{B}_2 + 5\mathrm{C}_2 + 4\mathrm{D}_2. \tag{4.15}$$

Using this result we may simplify the potentials (4.10), for if we write

$$\left.\begin{aligned} \mathscr{A}'_0(\mathbf{r}) &= \mathscr{A}_0(\mathbf{r}) + \frac{1}{c}\frac{\partial\lambda(\mathbf{r})}{\partial t} \\ \mathscr{A}'(\mathbf{r}) &= \mathscr{A}(\mathbf{r}) - \operatorname{grad}\lambda(\mathbf{r}) \end{aligned}\right\} \tag{4.16}$$

with

$$\lambda(r) = -\frac{e^{i(qr-\omega t)}}{iqr}\{10(\mathrm{C}_2 - \tfrac{1}{5}\mathrm{B}_2)\,\mathrm{P}_2{}^0(\cos\theta) + 2(\mathrm{C}_2 - \tfrac{1}{5}\mathrm{B}_2) - \tfrac{12}{5}\mathrm{D}_2\}, \tag{4.17}$$

then we obtain

$$\left.\begin{aligned} \mathscr{A}'_0(r) &= \mathrm{H}_2\{2\mathrm{P}_2{}^0(\cos\theta) + 1\}\,r^{-1}e^{i(qr-\omega t)} \\ \mathscr{A}'_x(r) &= i\mathrm{K}_2\mathrm{P}_3{}^1(\cos\theta)\sin\phi\,.\,r^{-1}e^{i(qr-\omega t)} \\ \mathscr{A}'_y(r) &= -i\mathrm{K}_2\mathrm{P}_3{}^1(\cos\theta)\cos\phi\,.\,r^{-1}e^{i(qr-\omega t)} \\ \mathscr{A}'_z(r) &= 3\mathrm{H}_2\mathrm{P}_1{}^0(\cos\theta)\,.\,r^{-1}e^{i(qr-\omega t)} \end{aligned}\right\}, \tag{4.18}$$

where

$$H_2 = -2(A_2 - 2D_2)$$

and

$$K_2 = +2(C_2 + B_2),$$

and of course these potentials give rise to the same values of E and H as do the potentials (4 10).

Case B —Starting from the wave functions (4.1) and (4.4B) we find that the potentials radiated by a transition to the state of type (B) are given by

$$\left.\begin{aligned}
\mathscr{A}_0(\mathbf{r}) &= +r^{-1}e^{i(qr-\omega t)}\ \ 2A_{-3}P_2^0(\cos\theta)\\
\mathscr{A}_x(\mathbf{r}) &= -r^{-1}e^{i(qr-\omega t)}\\
&\quad\times\{\tfrac{4}{5}B_{-3}P_3^1(\cos\theta)\cos\phi - P_1^1(\cos\theta)[(E_{-3}+\tfrac{1}{5}D_{-3})\cos\phi\\
&\qquad\qquad + i(E_{-3}+D_{-3})\sin\phi]\},\\
\mathscr{A}_y(\mathbf{r}) &= -r^{-1}e^{i(qr-\omega t)}\\
&\quad\times\{\tfrac{4}{5}B_{-3}P_3^1(\cos\theta)\sin\phi - P_1^1(\cos\theta)[(E_{-3}+\tfrac{1}{5}D_{-3})\sin\phi\\
&\qquad\qquad - i(E_{-3}+D_{-3})\cos\phi]\},\\
\mathscr{A}_z(\mathbf{r}) &= -r^{-1}e^{i(qr-\omega t)}\{\tfrac{12}{5}B_{-3}P_3^0(\cos\theta)\\
&\qquad\qquad + 2(E_{-3}+\tfrac{1}{5}D_{-3})P_1^0(\cos\theta)\},
\end{aligned}\right\}\qquad(4.20)$$

where

$$\left.\begin{aligned}
A_{-3} &= \left(\frac{8\pi^3}{q}\right)^{1/2}\varepsilon\int_0^\infty (fF_{-3}+gG_{-3})\,J_{5/2}(qr)\,r^{3/2}\,dr,\\
B_{-3} &= \left(\frac{8\pi^3}{q}\right)^{1/2}\varepsilon\int_0^\infty fG_{-3}J_{7/2}(qr)\,r^{3/2}\,dr,\\
D_{-3} &= \left(\frac{8\pi^3}{q}\right)^{1/2}\varepsilon\int_0^\infty fG_{-3}J_{3/2}(qr)\,r^{3/2}\,dr,\\
E_{-3} &= \left(\frac{8\pi^3}{q}\right)^{1/2}\varepsilon\int_0^\infty gF_{-3}J_{3/2}(qr)\,r^{3/2}\,dr.
\end{aligned}\right\}\qquad(4.21)$$

The relation between these four coefficients is obtained from (4.14) by putting $n = 2$ and $k = -3$; it is

$$5A_{-3} = -6B_{-3} - D_{-3} - 5E_{-3}. \qquad (4.22)$$

Thus we may transform (4.20) to the equivalent form

$$\left.\begin{aligned}
\mathscr{A}'_0(\mathbf{r}) &= H_{-3}\{2P_2^0(\cos\theta)+1\}\,r^{-1}e^{i(qr-\omega t)},\\
\mathscr{A}'_x(\mathbf{r}) &= iK_{-3}P_1^1(\cos\theta)\sin\phi\,.\,r^{-1}e^{i(qr-\omega t)},\\
\mathscr{A}'_y(\mathbf{r}) &= -iK_{-3}P_1^1(\cos\theta)\cos\phi\,.\,r^{-1}e^{i(qr-\omega t)},\\
\mathscr{A}'_z(\mathbf{r}) &= 3H_{-3}P_1^0(\cos\theta)\,.\,r^{-1}e^{i(qr-\omega t)},
\end{aligned}\right\}\qquad(4.23)$$

where

and

$$\left.\begin{aligned} H_{-3} &= -\tfrac{1}{3}(2A_{-3} + D_{-3} + 5E_{-3}) \\ K_{-3} &= -(D_{-3} + E_{-3}) \end{aligned}\right\}. \qquad (4.24)$$

Comparing the potentials (4 18) and (4 23) with the field of a quadripole (4 3), we see that, on the relativistic theory, an electron making a jump between two states for which $\Delta k = 2$† does not radiate a simple quadripole field This point will be discussed in more detail at the end of the section, but we may notice here that, in the non-relativistic limit where f and F_k both tend to zero, the extra terms in $\mathscr{A}_x$ and $\mathscr{A}_y$ tend to zero and we are left with the field (4.3) of a simple quadripole.

We have next to evaluate the coefficients H_k and K_k defined in equations (4 19) and (4.24). For this purpose we write the Bessel functions in the exponential form, *e g* ,

$$J_{5/2}(z) = \left(\frac{2}{\pi z}\right)^{1/2} \cdot \tfrac{1}{2}\left\{ie^{iz}\left(1 + \frac{3i}{z} - \frac{3}{z^2}\right) + \text{complex conjugate}\right\},$$

which at once gives

and

$$\left.\begin{aligned} H_2 &= -\frac{4\pi\epsilon i}{q}[\Omega_2 - \Omega^*_2] \\ H_{-3} &= -\frac{2\pi\epsilon i}{3q}[\Omega_{-3} - \Omega_{-3}^*] \end{aligned}\right\} \qquad (4.25)$$

where

and

$$\left.\begin{aligned} \Omega_2 &= \int_0^\infty \left\{(fF_2 + gG_2)\left(1 + \frac{3i}{qr} - \frac{3}{q^2r^2}\right) - 2ifG_2\left(1 + \frac{i}{qr}\right)\right\} e^{iqr}\, r\, dr \\ \Omega_{-3} &= \int_0^\infty \left\{2(fF_{-3} + gG_{-3})\left(1 + \frac{3i}{qr} - \frac{3}{q^2r^2}\right)\right. \\ &\qquad\qquad \left. + i(5gF_{-3} + fG_{-3})\left(1 + \frac{i}{qr}\right)\right\} e^{iqr}\, r\, dr. \end{aligned}\right\} \qquad (4.26)$$

These integrals occur in the discussion of the probability that the electron will make a transition from the K state to a state of positive energy, and it has been shown in TM how they may be evaluated in terms of two quantities

---

† k is the suffix of equations (4.4A) and (4.4B). It corresponds in the non-relativistic theory to the quantum number l giving the orbital angular momentum of the electron.

P_k and Q_k defined by hypergeometric series. It is there shown (*cf.* TM equations (2.12) to (2.25)) that

$$\left.\begin{aligned}\Omega_2 &= -\frac{\xi(E_0)\,\xi(E,2,0)}{2(\beta+2)}\left\{A|B|\sqrt{\left(\frac{2}{A^2+|B|^2}\right)}\right\}^{-1}\mathfrak{Z}_2\\ \text{and}\qquad \Omega_{-3} &= +\frac{\xi(E_0)\,\xi(E,-3,0)}{2(\beta+2)}\left\{A|B|\sqrt{\left(\frac{2}{A^2+|B|^2}\right)}\right\}^{-1}\mathfrak{Z}_{-3}\end{aligned}\right\}, \tag{4.27}$$

where[†] $\mathfrak{Z}_k = \mathscr{P}_k P_k + \mathscr{Q}_k Q_k + \quad + \mathscr{U}_k U_k$. We have here inserted the normalizing factor $\xi(E, k, u)$ for the state of positive energy

In a similar fashion we may express K_2 and K_{-3} in terms of the known quantities P_k and Q_2 We have

$$\left.\begin{aligned}K_2 &= \frac{4\pi\varepsilon}{q}[\Lambda_2 + \Lambda_2^*]\\ \text{and}\qquad K_{-3} &= -\frac{2\pi\varepsilon}{q}[\Lambda_{-3} + \Lambda_{-3}^*]\end{aligned}\right\}, \tag{4.28}$$

where

$$\left.\begin{aligned}\Lambda_2 &= \int_0^\infty (fG_2 + gF_2)\left(1 + \frac{6i}{qr} - \frac{15}{q^2r^2} - \frac{15i}{q^3r^3}\right)e^{iqr}\,r\,dr\\ \text{and}\qquad \Lambda_{-3} &= \int_0^\infty (fG_{-3} + gF_{-3})\left(1 + \frac{i}{qr}\right)e^{iqr}\,r\,dr\end{aligned}\right\}. \tag{4 29}$$

These two integrals may be expressed in terms of the quantities already calculated, P_k and Q_k. The relations are similar to those for Ω_2 and Ω_{-3}.

According to equations (2 20) and (2 21) we now obtain the radiation from the total system by multiplying[‡] (4.18) by $-2\pi i(-\varepsilon)M_2$ and (4.23) by $-2\pi i(-\varepsilon)M_{-3}$ and then adding these two fields and the original quadripole field, M_2 and M_{-3} here stand for the integral in (2.20). But it has been shown[§] (TM, equations (2 14) and (2 24)) that

$$\left.\begin{aligned}M_2 &= -\frac{24\pi C\,\xi(E_0)\,\xi(E,2,0)}{5(\beta+2)}\left\{A|B|\sqrt{\left(\frac{2}{A^2+|B|^2}\right)}\right\}^{-1}\mathfrak{Z}_2\\ \text{and}\qquad M_{-3} &= \frac{4\pi C\,\xi(E_0)\,\xi(E,-3,0)}{5(\beta+2)}\left\{A|B|\sqrt{\left(\frac{2}{A^2+|B|^2}\right)}\right\}^{-1}\mathfrak{Z}_{-3}\end{aligned}\right\}. \tag{4.30}$$

[†] The coefficients $\mathscr{P}_k$, .., $\mathscr{U}_k$ are defined in TM (2.15), (2 18) and (2.25). The quantities R_k, S_k, T_k, U_k are determined from the known quantities P_k and Q_k by the recurrence relations TM (2.20) and (2.21).

[‡] The extra 2 in these factors is for the two electrons.

[§] Our C is the − C of TM (*cf.* TM (2.1) and our (4.3)). We have again inserted the normalizing factor for the free state omitted in TM (2.14) and (2.24).)

We thus obtain the field radiated by the total system in the form

$$\left.\begin{aligned}\mathscr{A}_0(\mathbf{r}) &= \mathrm{C}\{1+\lambda_2+\lambda_{-3}\}\{2\mathrm{P}_2{}^0(\cos\theta)+1\}\,r^{-1}e^{i(qr-\omega t)}\\ \mathscr{A}_x(\mathbf{r}) &= -\mathrm{C}\{\eta_2\mathrm{P}_3{}^1(\cos\theta)+\eta_{-3}\,\mathrm{P}_1{}^1(\cos\theta)\}\sin\phi\,.\,r^{-1}e^{i(qr-\omega t)}\\ \mathscr{A}_y(\mathbf{r}) &= \mathrm{C}\{\eta_2\mathrm{P}_3{}^1(\cos\theta)+\eta_{-3}\,\mathrm{P}_1{}^1(\cos\theta\}\cos\phi\quad r^{-1}e^{i(qr-\omega t)}\\ \mathscr{A}_z(\mathbf{r}) &= 3\mathrm{C}\{1+\lambda_2+\lambda_{-3}\}\,\mathrm{P}_1{}^0(\cos\theta)\quad r^{-1}e^{i(qr-\omega t)}\end{aligned}\right\},\quad(4.31)$$

where

$$\lambda_2=\frac{24\pi}{5q}\left\{\frac{2\pi\epsilon\,\xi(\mathrm{E}_0)\,\xi(\mathrm{E},2,0)}{\beta+2}\right\}^2\frac{\mathrm{A}^2+|\mathrm{B}|^2}{2\mathrm{A}|\mathrm{B}|}\{\aleph_2{}^2-|\aleph_2|^2\}$$

and

$$\lambda_{-3}=\frac{2\pi}{15q}\left\{\frac{2\pi\epsilon\,\xi(\mathrm{E}_0)\,\xi(\mathrm{E},-3,0)}{\beta+2}\right\}^2\frac{\mathrm{A}^2+|\mathrm{B}|^2}{2\mathrm{A}|\mathrm{B}|}\{\aleph_{-3}{}^2-|\aleph_{-3}|^2\}\quad,(4.32)$$

with similar expressions for η_2 and η_{-3}.

The rate of radiation of energy by the field (4 31) is

$$\frac{48\pi^3\nu^2}{5c}\mathrm{C}^2\mathrm{J},$$

where

$$\mathrm{J}=|1+\lambda_2+\lambda_{-3}|^2+\tfrac{10}{7}|\eta_2|^2+\tfrac{5}{9}|\eta_{-3}|^2,\qquad(4.33)$$

and thus the number, g, of γ-quanta emitted per second by the total system is given by

$$g=\frac{24\pi}{5}\;\frac{q}{h}.\,\mathrm{C}^2\mathrm{J}.\qquad(4.34)$$

The numerical evaluation of J shows that it does not differ from unity by more than a few per cent. in the experimental range of ν, the quantities λ_2, η_2, etc., being of the order ϵ^2/hc

We have still to discuss the question of the other possible initial state for the electron, given by

$$\left.\begin{aligned}(\psi_i)_1&=if\sin\theta e^{-i\phi}\qquad&(\psi_i)_2&=-if\cos\theta,\\ (\psi_i)_3&=0&(\psi_i)_4&=-g.\end{aligned}\right\}\qquad(4\;35)$$

We may notice at once that, according to the exclusion principle, if one of the K electrons is in the state (4.1) then the other must be in the state (4 35) and so our multiplication of the radiated wave by the factor 2 in (4.30) is justifiable only if transitions to either of these states from the free state gives rise to the same radiation. That this is the case is readily verified. The only possible final free states for electrons initially in the state (3.35) are given by (4 4A) and (4.4B) with $k=2$ and $u=-1$, and the matrix elements M_2 and M_{-3} corresponding to these transitions are identical with those of (4.30) as are also the potentials corresponding to (4.18) and (4.23).

That an electron initially in a state formed by superposing states (4.1) and (4.35) with arbitrary phase factors also gives rise to the same radiation on jumping to its possible free states may be readily verified by a method analogous to that of equations (2.28) to (2.31) of TM, and therefore the total rate of emission of γ-quanta by the system consisting of the nucleus coupled to the two K electrons is correctly given by (4.34).

Interpretation of the terms in the potentials (4.18) *and* (4.23) *which do not arise as the radiation from a simple electric quadripole.* The potentials (4.18) and (4.23) differ from those of an oscillating quadripole (4.3) only by the extra terms in $\mathscr{A}_x$ and $\mathscr{A}_y$. Now a small magnet of moment M placed at the origin of co-ordinates pointing along the positive z-axis has a vector potential whose components at any point (x, y, z) are given by

$$\frac{\mathrm{M}}{r^3}(y, -x, 0),$$

and comparing this with (4.23) we readily see that the additional terms in (4.23) arise as the radiation from an oscillating magnetic dipole. Similarly the additional terms in (4.18) arise as the radiation from a magnetic octopole.

If we write down the potentials radiated by a relativistic electron making a jump between two states for which $\Delta k = 1$, *i.e.*, a dipole jump, we find in a similar way that the potentials are those of an oscillating electric dipole plus the potentials of an oscillating magnetic quadripole. This is to be expected from the picture of a relativistic electron as a point electric charge plus a small magnetic dipole.

In conclusion, we should like to express our thanks to Professor Dirac for his advice and encouragement during the preparation of this work.

Summary.

It is shown that, if a γ-ray escaping from a nucleus be represented by an electromagnetic wave, then the reduction of intensity suffered by this wave in passing through the K ring is *not* equal to the number of electrons ejected, and is in general small, even when the number of electrons ejected is comparable with the number of γ-ray quanta emitted. It is shown that the quantity calculated by Hulme, and by Taylor and Mott in recent papers should be interpreted as being nearly equal to the ratio, b/g, of electrons to γ-quanta which is observed, not to the "internal conversion coefficient" $b/(g+b)$, as there stated. The agreement with experiment in the radium B region is slightly less good than before; for radium C the alteration is negligible.

The Thermal Expansion of Quartz by X-Ray Measurements.

By A. H. Jay, M Sc, Beyer Fellow of the University of Manchester.

(Communicated by W. L Bragg, F.R S—Received May 6, 1933)

(Plate 3)

The study of the coefficients of thermal expansion of substances has in the past, for the most part, been confined to direct measurement by optical methods. At the present time X-rays are being used for determining the expansion of the atomic lattice as distinct from the specimen block A question has arisen as to the relation between the coefficient of expansion as measured visually and that measured by X-rays From theoretical considerations Zwicky* has predicted that the two are not identical. X-ray measurements on the thermal expansion of single crystals of bismuth by Goetz and Hergenrother† have shown that there is a difference between the values obtained by the two methods of measurement On the other hand Y Tu‡ finds no evidence in his experiments on rock salt of the secondary structure described by Zwicky. The question to be answered is thus one of great importance The present paper gives evidence to show that for silver and quartz there is no difference between the coefficients of expansion as measured by X-rays and those from optical measurements

Present Work

The work described in this paper was carried out to measure the thermal expansion of quartz by X-rays and by comparing the results with those from optical measurements to test the validity of the assumption, made in previous papers,§|| that the coefficient of thermal expansion of silver is the same whether measured by X-rays or optical methods

Experimental

The X-ray photographs were taken in a high temperature camera¶ of the Debye-Scherrer type in which the specimen is heated by surrounding furnaces.

---

* 'Proc. Nat. Acad. Sci. Wash.,' vol. 15, pp 253, 816 (1929); 'Hel. Phys. Acta.,' vol. 3, p. 629 (1930).

† 'Phys. Rev.,' vol. 40, pp. 137, 643 (1932).

‡ 'Phys. Rev.,' vol 40, p. 662 (1932).

§ Jay, communicated to the Physical Society.

|| Jay, 'Z. Kristallog.,' vol. 86, p. 150 (1933).

¶ Jay, *loc. cit.*.

Experimental conditions are such that the $K\alpha$ doublets at high angles of reflection are well resolved and accurate measurement of line position is possible.

The powder was obtained by finely grinding a clear colourless crystal of quartz.* This was mounted on a thin silica rod which was supported vertically along the axis of the camera. The powder was thus held in the path of the X-ray beam and rotated throughout the exposure. The specimen was heated by two small surrounding furnaces, arranged one above the other with a small gap between for the X-rays to pass through. This arrangement has been shown to give a uniform temperature throughout the scattering mass. The energy input was measured by the product of the current (0 to 6 amps.) and the voltage drop (0 to 40 volts) across the furnaces The measuring instruments showed steady conditions throughout an exposure, variations not exceeding 0·01 amps and 0·1 volts. The temperature of the specimen was deduced from the measured energy input and the watts-temperature calibration curve of the camera (see previous papers) and read off the curve with an error not exceeding 2° C. Photographs were taken for a number of temperatures ranging from room temperature to 730° C The experiments were not carried out with any temperature sequence but in an order chosen to detect the possibility of a systematic change in the quartz after heat treatment The specimen powder was heated for about 20 minutes to bring it to a steady temperature state before the exposure was made, fig 1, Plate 3

General Discussion.

From previous work on the powder photographs of quartz crystals the indices (*hkl*) of the reflections are known. The photographs taken at different temperatures show a progressive inward displacement of the high angle lines with increasing temperature. Because of the unequal expansion of quartz in directions parallel and perpendicular to the principal axis, the relative position of different lines also depends on the temperature. Lines which superimpose at one temperature become separated at another temperature. Moreover, the intensities of lines vary gradually with temperature owing to small structural changes which occur even below the α–β transformation. It must be emphasized that only where lines are resolved into a distinct $K_{\alpha_1\alpha_2}$ doublet can any high accuracy be claimed for the individual measurements,

---

* Bradley and Jay, 'Proc. Phys. Soc.,' vol. 45. p. 507 (1933). It was shown that clear colourless quartz crystals possessed unit cell dimensions identical to 1 part in 80,000 at 18° C.

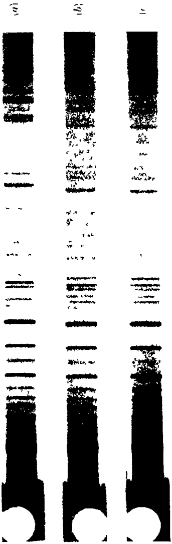

Fig. 1.—Powder photographs of quartz

(*a*) 203° C (*b*) 557° C (*c*) 615° C

and this resolution of doublets was always obtained at high angles of reflection. In some measurements, however, two doublets overlapped and then they were used only to identify the reflection and to serve as a check on the axial ratio

The specimen powder is in the form of a cylindrical shell around a thin fused silica rod. Considering a particular reflection at a high angle on the film, at any instant during the exposure only that portion of the specimen opposite the line can contribute to the reflection, the rays from the rest of the shell being absorbed by the rod. This effect is roughly equivalent to an eccentricity of the specimen To obtain accurate values of the lattice spacing the following procedure* was used. The evaluation of the lattice spacing was made by plotting the observed spacings for individual lines against the corresponding values of $\cos^2\theta$ and extrapolating by a straight line through them to $\cos^2\theta = 0$

The accuracy of lattice spacing determinations depends on two main factors —the photograph and the method of measurement. Powder photographs of crystalline substances obtained by using this type of camera have the $K_{\alpha_1\alpha_2}$ lines at high angles well resolved with a definite peak,† and with our methods of evaluating the lattice spacing it can be stated that the final accuracy is largely governed by the care taken in measuring the film. As previously stated experiments on clear colourless quartz crystals at room temperature 18° C showed a variation in lattice dimensions of not more than 1 part in 80,000, which can be regarded as the experimental error. In the present investigation this extreme accuracy is unlikely It might be claimed, however, from the consistency of the individual readings that the values of the c and d_{100} spacings given in Table I, are subject to an error not greater than 1 in 30,000 (0·2 X.U.) and 1 in 40,000 (0·1 X.U.) respectively The axial ratio is probably correct to 1 part in 20,000.

Determination of Lattice Spacings.

The determination of the lattice spacing for a cubic crystal, where there is only one unknown the a spacing, has been dealt with in a previous paper.‡ It was shown that for large angles of reflection the error da between the true and observed spacing is related to the true spacing a and the glancing angle θ by the expression

$$\frac{da}{a} = \mathrm{K}\cos^2\theta, \qquad (1\mathrm{A})$$

---

* Bradley and Jay, 'Proc. Phys Soc.,' vol. 44, p. 563 (1932).

† See photometer curves of quartz, Bradley and Jay, *loc. cit.*

‡ Bradley and Jay, *loc. cit.*

where K is a constant depending on the eccentricity and absorption of the specimen The above equation may be written

$$a - a_m = da = a\text{K} \cos^2 \theta,$$

where a_m is the spacing calculated from the measured angle θ; or

$$a = a_m + a\text{K} \cos^2 \theta. \qquad \text{(1B)}$$

Hence the measured lattice spacings when plotted against the corresponding values of $\cos^2 \theta$ lie along a straight line of slope given by aK. The true spacing a is then given by the intercept which this straight line makes with the spacing axis where $\cos^2 \theta = 0$.

In the present investigation with an hexagonal crystal, the problem is more complex because there are two unknowns, the c spacing parallel to the principal axis and the d_{100} spacing of the (100) planes of the basal plane. If we knew the axial ratio correctly then the problem would be the same as for a cubic crystal and spacing values of either c or d_{100} calculated for all values of hkl would lie on a straight line which on extrapolation to $\cos^2 \theta = 0$ would give the correct spacing value. Actually we do not know the axial ratio If this had been chosen in error it will be shown on plotting the spacing values against $\cos^2 \theta$ by a systematic departure of the points from a straight line. If, for example, the c spacings are plotted and the axial ratio c/a is too big the points corresponding to values of c deduced from reflections with small l indices will be above and those with large l indices will be below a mean straight line. A value of the axial ratio is found which brings all the points on the same line, apart from random errors of measurement. The true c spacing is then found by extrapolation and from this value and the axial ratio the d_{100} spacing is calculated The results are given in Table I for a number of temperatures The spacings are expressed as expansions per unit length in columns 4 and 5, taking as standard the spacing values for 18° C. previously determined.

Comparison of X-ray and Optical Measurements.

(*a*) *Expansion Parallel to the Principal Axis.*—By the use of optical methods the thermal expansion of quartz parallel to the principal axis has been measured accurately over an extended range of temperatures by Randall,* Müller,† and Lindman.‡ The results of Lindman deviate slightly at the higher temperatures from those of Randall and Müller, which are in good agreement with each other, the values of Randall and Müller being therefore chosen for making the comparison with the present X-ray measurements along the principal axis The continuous curve shown in fig 2 represents the results of Randall and Müller and has been drawn to express the measured expansions in terms of unit length at 18° C The results of the lattice expansion parallel to the principal c-axis as obtained by the present X-ray measurements and given in Table I, column 4, as expansions per unit length, are plotted for the corresponding temperatures as circles in the same figure. It is seen that the circles lie along the continuous curve within a small experimental error This agreement between the results obtained by X-rays and optical methods proves that in both cases the same changes are measured

---

* 'Phys Rev.,' vol 20, p. 10 (1905).

† 'Phys. Z.,' vol 17, p. 29 (1916).

‡ 'Acta Soc. Sci fenn.,' vol. 46, No. 5 (1916).

Table I —Expansion of Quartz in directions Parallel and Perpendicular to the Principal Axis

Temperature of specimen	Accurate value of lattice spacing, X units		Expansion expressed in terms of unit length, 18° C	
° C	c	d_{100}	c	d_{100}
18*	5393 3	4246 0	—	—
118	5398 1_5	4252 3	0 00090	0 00148
203	5402 7	4258 4_5	0 00174	0 00293
280	5406 8	4264 6_5	0 00250	0 00439
366	5412 8_5	4272 3	0 00362	0 00619
418	5416 3_5	4277 7	0 00427	0 00747
494	5424 1_5	4287 0_5	0 00572	0 00967
525	5427 0	4291 8_5	0 00634	0 01080
558	5433 8	4299 0	0 00752	0 01248
567	5435 5	4302 7	0 00782	0 01335
579	5446 4	4318 1	0 00984	0 01698
590	5447 3	4319 6	0 01001	0 01733
610	5447 0	4319 6	0 00996	0 01733
665	5446 4	4319 6	0 00984	0 01733
730	5445 9	4319 5	0 00975	0 01731

* Bradley and Jay, *loc cit*

The X-ray measurements were in addition carried out at temperatures up to 730° C, which is beyond the limit of the present optical measurements. However, it is known from the earlier work of Mallard and Le Chatelier† by the use of approximate methods of measurement that on approaching the α–β change point the coefficient of expansion becomes very large and that beyond the change point a slight contraction of the crystal takes place The dotted line, fig. 2, has been drawn through the X-ray points for temperatures higher than 500° C. and may be regarded as a continuation of the curve from Randall and Müller's data This line shows that the coefficient of expansion of the lattice increases rapidly as the temperature approaches 579° C. At this point there is an abrupt change followed by a contraction of the lattice Thus the present high-temperature X-ray measurements confirm the characteristics in the quartz expansion as found by Mallard and Le Chatelier.

---

† 'C. R. Acad. Sci. Paris,' vol. 108, p. 1046 (1889).

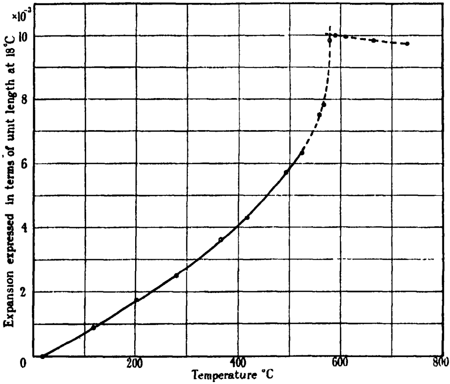

Fig. 2 —Expansion parallel to the principal axis. —— from Randall and Müller's data, ○ present X-ray measurements; - - - curve through X-ray points at higher temperatures

A comparison of the expansion curve along the principal axis as measured by X-rays and other methods shows that they are in good agreement from room temperature to 500° C, this being the range over which an accurate comparison is possible From the form of the expansion curve above and below the α–β change point the transformation is given as 579° C. which agrees within experimental error with the acknowledged temperature 575° C.

(*b*) *Expansion Perpendicular to the Principal Axis*.—The accurate measurements which have previously been made on the expansion perpendicular to the principal axis have for the most part been confined to a comparatively small range of temperatures. Lindman (*loc. cit.*), however, has carried out experiments at temperatures up to 330° C. and so a critical comparison of optical and X-ray measurements can be made over this temperature range. The curve, fig. 3, has been drawn from Lindman's values of the expansion coefficient. The circles in the same figure represent the expansion of the lattice expressed in terms of unit length at 18° C. It is seen that there is a very good agreement between the two series of measurements. This confirms the result found for the principal axis, that the expansion coefficient of the atomic lattice is the same as for the crystal block.

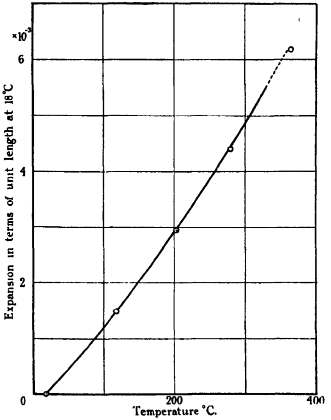

FIG. 3.—Expansion perpendicular to the principal axis. —— Optical expansion (Linderman); ⊙ present X-ray measurements.

The X-ray results for both directions of the crystal, expressed as expansions per unit length, see Table I, columns 4, 5 are shown in fig. 4. It will be seen that both expansion curves are of the same type, the coefficient of expansion increasing with temperature up to the α–β change point beyond which a contraction takes place. Le Chatelier found that while there was an appreciable contraction parallel to the principal axis the contraction in a perpendicular direction is much smaller. These characteristics are shown in the X-ray measurements

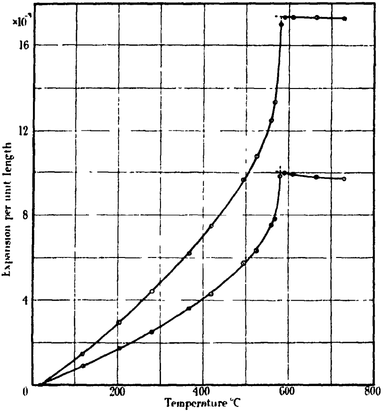

FIG 4 —X-ray measurements expressed in terms of unit length at 18° C.

The agreement of the observed α–β change point 579° C, as shown by the abrupt change in the expansion curves, with the acknowledged temperature 575° C. suggests that the temperature scale is correct and the validity of the assumption, previously made, that the coefficient of expansion of silver is the same whether measured optically or by X-rays is sound. This is further substantitated by the agreement shown in the comparison of optical and X-ray measurements for both axes of quartz at all temperatures investigated.

To sum up it can be stated that for silver and quartz the coefficient of thermal expansion of the lattice is identical with that of the crystal block.

Variation in the Axial Ratio c/a with Temperature.

The d_{100} spacing is related to the a-axis by the expression

$$a = \frac{2}{\sqrt{3}} \cdot d_{100}$$

The value of c/a for quartz at 18° C. was given in a previous paper as $1\cdot10002^* \pm 0\cdot00004$ Because the lattice has a greater coefficient of expansion in the basal plane than along the principal axis the value of c/a decreases with increasing temperature. The relation of c/a with temperature is shown in fig. 5 The curve shows (1) a steady decrease in the value of c/a from room temperature to about 560° C., (2) a rapid decrease up to the α–β change point

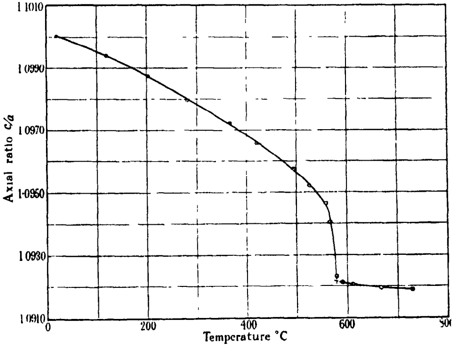

FIG 5 —Variation of axial ratio c/a with temperature.

---

* Value of c/a given by Tutton is $1\cdot1000$.

(579° C.), (3) an arrest at 579° C. followed by a slight and steady fall in the c/a value.

Discussion of the Changes in the Quartz Structure.

The structure of α- and β-quartz has been the subject of many investigations, namely, those of W H. Bragg and Gibbs, and Wyckoff,[*] to whose work for a detailed analysis reference should be made An examination of the X-ray powder photographs confirms the results of their intensity measurements. The photographs of both α- and β-quartz at different temperatures show that the intensity differences are surprisingly small and the slight variations which are seen appear to be gradual. A point which may be considered is the question whether after heating and cooling the quartz returns to its original state, *i e*, whether the modifications in the α- and β-forms and transformation are reversible As stated previously these X-ray observations were carried out in a random order at temperatures above and below the change point A certain time was allowed for the specimen to reach a steady state before the exposure was made From the spacing measurements it appears that the structure had been given the opportunity of returning to a state of equilibrium. Gibbs found that when the temperature was changed slowly between observations at various temperatures the X-ray measurements were reproducible.

In previous paragraphs the expansion of the lattice has been discussed. The results show a steady increase in the lattice up to the change point, the expansion becoming more and more rapid as the transformation point is approached. Lattice spacing measurements therefore confirm measurements on the crystal block. The modification of α-quartz probably can be seen better from a consideration of the variation in the axial ratio, see fig. 5 It would appear that while the α-structure changes continuously, yet there is a state just before the transition where the lattice dimensions suffer a rapid change, witnessed in the sudden fall of the axial ratio values. At the change point this fall is arrested and the changes in the β-form are small in comparison. This phenomena is not difficult to visualize and something very similar was found by Gibbs. The suggestion that the structure is passing through a state of thermally unstable equilibrium appears to be substantiated, and that the transition is abrupt seems certain.

---

[*] Bragg and Gibbs, 'Proc Roy. Soc, 'A, vol. 109, p. 405 (1925); Gibbs, 'Proc. Roy. Soc.,' A, vol 107, p 561 (1925), vol. 110, p. 443 (1926), Wyckoff, 'Amer. J. Sci.,' vol. 11, p. 62 (1926).

Acknowledgments.

I wish to express my best thanks to Professor W. L Bragg, F.R.S., and Dr A J. Bradley for their encouraging interest in the work, which was carried out in the Physical Laboratories of the University of Manchester I am also indebted to Mr. A. P. M Fleming, C.B E , Director-Manager, Research and Education Departments, Metropolitan-Vickers Electrical Co., Ltd., for his interest and permission to publish the work.

Summary.

X-ray powder photographs of clear colourless quartz have been taken for a number of temperatures from 18° C. to 730° C., and the lattice dimensions found corresponding to each temperature observation By using the lattice expansion of silver, described elsewhere, and assuming the ordinary expansion law, a temperature scale for the camera was obtained which, when used in conjunction with the quartz spacing measurements, gave (1) the α-β change point of quartz at 579° C as compared with the acknowledged temperature 575° C., thus proving the validity of the above assumption, (2) an expansion law for each of the directions parallel and perpendicular to the principal axis which was identical with those found by using optical methods of measurement.

The X-ray results indicate that for silver and quartz the coefficients of thermal expansion, over the range investigated, are the same whether measured by X-rays or optical methods

On the Electric Charge Collected by Water Drops falling through Ionized Air in a Vertical Electric Field.

By J P Gott, M.A , Trinity Hall, Cambridge.

(Communicated by C T. R. Wilson, F.R.S.—Received May 11, 1933)

1. *Introduction*

In connection with the theory of thunderclouds and of the electric charge brought down by rain, Wilson has suggested* the following mechanism Consider an uncharged water drop falling vertically through ionized air Let there be a vertical electric field, so that ions of one sign are moving down in the same direction as the drop falls, while ions of the other sign are moving up against the drop The electric field induces equal charges of opposite signs on the upper and lower halves of the drop Suppose now that the electric field has such an intensity that the velocity of the descending ions is less than the velocity of the falling drop. Under these conditions those descending ions which are above the drop, cannot overtake the drop and so do not reach it, although attracted by the charge on its upper half Those descending ions which are below and which the drop overtakes, are first repelled by the lower charge on the drop before being attracted by the upper charge and, since these charges are equal in the neutral drop, it is to be expected that these ions will not reach it Ions coming up to meet the drop are attracted to the lower charge and give the drop a net charge This destroys the equality of the induced charges and some of those ions which the drop overtakes are now attracted to it. A limiting condition will be approached in which the net charge is equal to some fraction of the induced charge.

This mechanism does not depend on whether the electric field is directed vertically upwards or vertically downwards and for this reason specific mention of the sign of an ion has been avoided In a particular case, suppose the potential gradient, measured upwards, to be negative, so that positive ions move up and negative ions move down. The charges on the upper and lower halves of the falling drop will then be positive and negative respectively. If the water drop falls more rapidly than the negative ions move down, it will collect a net positive charge, by selective absorption of positive ions at its lower negatively charged surface Since a drop of 1 mm radius has a terminal velocity of about 6 metres per second, the electric field must not exceed 400 volts/cm for ions of mobility 1·5 cm /sec /volt/cm

---

* 'J. Franklin Inst.,' vol. 208, p. 1 (1929).

Rain brings down an excess of positive electricity The potential gradient under a shower cloud or a thundercloud is usually negative and rain, possibly leaving the cloud with a negative charge, collects in accordance with this theory, more positive than negative ions and so arrives at the ground with a positive charge (Rain can also gain a positive charge if there is an excess of positive ions produced by point discharges from objects on the ground)

In the application of the theory to explain the development of the internal fields of thunderclouds, it is necessary to assume that the ions have their mobility reduced to that of large ions, by attachment to nuclei or small cloud particles Even in the large fields occurring in thunderclouds (up to 10,000 volts/cm) they will then move with a velocity of only a few centimetres per second Any rain drop, large enough to fall more quickly than these ions move down, will collect a net charge of such sign that its fall will tend to add to the already existing field of the thundercloud, as has been suggested by Wilson, *loc cit*

The work described in this paper was undertaken to obtain a direct experimental check on the working of the mechanism which has been outlined

2 *Experimental Method*

For an experimental check on this theory it is necessary to ionize the air in a region in which there is a vertical electric field and to measure the charge collected by a water drop when it falls through this region The ionization is conveniently produced by a beam of X-rays. Three series of experiments have been carried out of which the first was divided into two parts These were as follows

Series 1*a* —A thin beam of X-rays was directed along the upper surface of the lower of two horizontal plates used to produce the electric field. Under these conditions the drop fell through a stream of ions of one sign rising up to meet it and it collected a charge for all values of the electric field. This experiment gives the magnitude of the charge collected under the most favourable circumstances

Series 1*b*.—A similar thin beam of X-rays was directed along the under surface of the upper field plate. Ions of one sign then moved down in the same direction as the drop fell Starting with a large value of the electric field, the drop collected a charge, because ions overtaking the drop were attracted to its upper surface. When the field was diminished to a value somewhat less than that which gave to the ions a velocity equal to that of the drop, the charge collected diminished to zero in accordance with the theory

Series 2 – In these experiments the beam of X-rays was directed through the middle of the space between the field plates so that the drop in the first half of its fall, met ions which were moving up to meet it and in the second half of its fall, ions of opposite sign were moving down with it The interaction is thus divided into two stages. For large fields where the descending ions overtook the drop, it collected only a very small charge, as was to be expected since it would lose in the second stage the charge which it collected in the first stage For small fields where the descending ions could not overtake the drop, it collected a considerable charge It was then retaining most of the charge which it collected in the first stage Any loss of charge in the second stage was due to its net charge, collected in the first stage and of opposite sign compared with the ions which it was meeting in the second stage.

Series 3.—In these experiments the whole height between the plates was exposed to ionization by X-rays, so that the falling drop was meeting ions of both signs for the whole of the time that it was between the plates The results of these experiments, as was to be expected from the theory, were similar to those of the second series of experiments It should be noted that the conditions are more complicated when the whole space between the plates is ionized Instead of a uniform density of ions of one sign, there is a distribution of positive ions increasing from zero density at the surface of the positive plate to a greatest density at the negative plate, with a similar distribution in the opposite direction for the negative ions

The first two series of experiments were somewhat affected by a non-uniform electric field This does not destroy the general conclusion to be drawn from these experiments It was eliminated in the third series of experiments

3 *Experimental Details.*

The vertical electric field was maintained between two circular plates which, at first, had a diameter of 55 cm These were separated by a distance of 28 cm. by ebonite insulators. In the centre of each plate was a circular hole of 3 cm. diameter and on the upper plate there was erected a vertical brass tube about 10 cm. in diameter and a metre in length. This carried, at the top, a water dropping appliance, consisting of a reservoir, screw valve and a drawn out glass tube to form the drops. The height from the lower surface of the upper plate to the tip of the water dropper was almost exactly 100 cm. The apparatus had to be carefully adjusted into the vertical, for the drop to fall clear through the holes in both plates. It had, moreover, to be fairly rigidly supported against vibration.

This apparatus is illustrated in fig. 1, *a*. A and B are the plates and C the water dropper. The drop after passing through the field, was collected in a small Faraday cylinder D, insulated by sulphur and contained in an earthed metal case. E is a removable metal cover shielding the top of the Faraday cylinder. The Faraday cylinder was connected to the leaf system of a small gold leaf electrometer and to an earthing key. This electrometer, which has a linear scale for about 20 volts on each side of zero, has been described by Wilson.[*] Under these conditions the total capacity was 45 cm. This arrangement was not sufficiently sensitive to measure the charge on a single drop, which under the experimental conditions had a maximum value of about one-hundredth of an electrostatic unit, but by collecting one hundred drops reasonable deflections could be obtained. The results are in most experiments accurate to 5%, though the measurement of very small charges is more uncertain. This estimate includes all sources of irregularity.

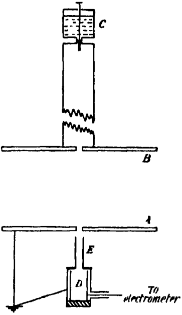

Fig. 1, *a*.

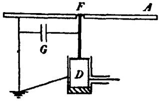

Fig. 1, *b*.

The ionization current per square centimetre flowing between the plates was measured by means of a small disc electrode inserted in the central hole in the lower plate. The water dropper was turned off. As shown in fig. 1, *b*, the cover E was removed and the disc F supported from the top of the Faraday cylinder, so making connection with the electrometer and, at the same time, connecting a large capacity (up to 900 cm.) to the system, as shown at G. This was necessary to obtain a suitable rate of deflection of the electrometer.

[*] 'Proc. Camb. Phil. Soc.,' vol. 13, p. 184 (1905).

In the use of the Faraday cylinder trouble was occasionally experienced owing to splashing. When this occurred it could always be detected at once and so does not produce any uncertainty in the observations, it was almost eliminated in the later experiments. Moist air, round the Faraday cylinder, at first sometimes caused electrical leaks This trouble was entirely eliminated by blowing a very slow stream of dry air through the apparatus

The X-rays were generated by a Coolidge tube worked by an induction coil and gas break Measurements of the ionization current were made both before and after the measurement of the charge brought down by one hundred drops During this time the ionization current usually remained constant to 2% or 3%. Ideally the beam of X-rays used in the first and second series of experiments should be very thin, but in practice a finite thickness is required to obtain sufficient output The beam used had a thickness, in the path of the drop, of about 4 cm, calculated from the relative positions of diaphragm and focal spot. In making observations the X-rays could be cut off by means of a shutter This shutter was held open while 100 drops were collected

Potentials up to 20,000 volts (in one case up to 30,000 volts) were maintained on the upper plate, the lower plate being earthed. In the more important region, up to 10,000 volts, the potential was measured by means of an electrostatic voltmeter. For higher potentials a sphere gap was used The potential was obtained from a Wimshurst machine.

Careful tests were made to ensure that the charge observed was never spurious. Thus the drops alone brought down no detectable charge and the electric field or the X-rays acting alone did not cause the drops to acquire any charge

It will be convenient, at this stage, to consider the velocity of the falling drop. The drops were formed, as already stated, at the end of a glass tube, supplied through a screw valve with distilled water from an approximately constant head. The volume of a drop was measured by counting the number required to fill a 10 c c measuring vessel The size of drop formed in this way remains remarkably constant The same glass tube was used to form the drops in all the observations and the average of several determinations of the radius of the drops, made at different times during the work, is 0 224 cm. and can be regarded as accurate to 1%. The terminal velocity of drops has recently been investigated by Flower.* For the drops used the terminal velocity is 774 cm /sec. but the drop must fall more than 3 metres to acquire this velocity. In the present experiments the drop fell 100 cm to the upper plate and 128 cm. to the lower plate. The velocity of a drop at points in its path before it has reached its terminal velocity does not seem to have been determined. From general considerations it is suggested that the velocity of the drop in the present experiments cannot be less than that due to gravity by more than a few per cent The velocity calculated in this way, increases from 443 cm./sec. at the upper plate to 500 cm /sec at the lower plate The fields which give the ions velocities equal to these are, for positive ions 317 and 357 volts/cm , taking the mobility to be 1 4 and for negative ions 296 and 333 volts/cm , taking the mobility to be 1·5 These are the values which are indicated in the diagrams.

---

* 'Proc. Phys. Soc.,' vol. 40, p. 167 (1928).

4 *Experimental Results*

The object of the experiments was to obtain curves connecting charge per drop with electric field, each curve corresponding to a constant ionization current flowing between the plates To obtain the points on such curves directly was not convenient, as it was difficult, with the X-ray apparatus used, to adjust the ionization current exactly to a predetermined value and then maintain it at that value The ionization current was measured by stop-watch readings On the other hand, the electric field, usually measured directly on an electrostatic voltmeter, was easily adjusted to a predetermined value Consequently the method adopted consisted in first obtaining curves connecting the charge on a drop with the ionization current, where each curve corresponds to a constant electric field Taking the charges given by a set of these curves for a constant ionization current and plotting against the corresponding fields gave the required curve The number of points on the final curves is thus small, being equal to the number of curves in the first set but, being taken from smooth curves drawn through the experimental points, they are equivalent to averages and are of high accuracy

Coming now to the first series of experiments, fig 2 is a specimen curve showing actual experimental points The accuracy indicated may be taken as average The points obtained when the electric field was very small, or the charge collected was very small, showed a greater uncertainty In the former case the ionization current was no longer saturated. The latter case will be discussed later. Under these conditions the curves were based on a greater number of observations. The curve of fig 2 is for negative ions moving down and a field of 268 volts/cm. Complete sets of curves are shown in figs. 3 and 4, where to avoid confusion the experimental points are not indicated. During these observations the upper field plate was negative with respect to the lower which was earthed Fig 3 refers to the case of positive ions moving up to meet the drop, the charge collected being positive, and fig. 4 gives the negative charge collected when negative ions move down. In each figure the ordinate is the charge on 100 drops in e.s.u. and the abscissa is the ionization current in e.s.u. per square centimetre. The electric field to which each curve

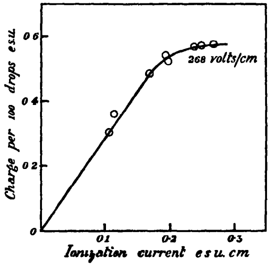

Fig. 2.—Specimen curve.

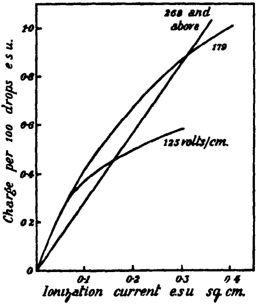

Fig. 3.—Positive ions moving up.

refers is indicated in the figure. The straight line occurring in each diagram represents some two or three curves in each case, since all curves obtained for values of the electric field greater than that indicated against the straight line in the diagram coincided to our order of accuracy. It should be noted that these straight lines have the same slope in each figure. In fig. 4 certain curves are shown coinciding near the origin. The observations are not sufficiently accurate to prove exact coincidence, but any difference must be small

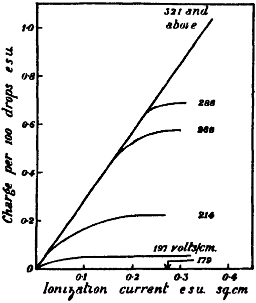

FIG 4 —Negative ions moving down

Fig 5 is of more direct interest This is constructed from figs. 3 and 4 and shows the charge (ordinate) against the electric field (abscissa), when the ionization current has the constant values 0 05, 0·1, 0 2 and 0·3 electrostatic units per square centimetre The full line curves were obtained from fig 4 and refer to ions moving down. The points taken from the curves are indicated. The broken line curves, which in the right-hand part of the diagram coincide with the full lines, were obtained from fig. 3 and refer to ions moving up. They are included chiefly for the sake of comparison. The critical values of the electric field, giving the ions and the falling drop equal velocities, are indicated by arrows. It will be seen that, for somewhat smaller values of the field, the charge collected from descending ions, which now cannot overtake the drop, falls to zero. This is in qualitative agreement with the theory.

The charge collected from ions moving up, shown by the broken lines, does not diminish in this region, and this is in agreement with the theory On the contrary, it shows an unexpected increase Referring back to fig 3, it will be seen that this rise is related to the curvature of the curves for 125 and 179 volts/cm and to the fact that their slopes near the origin are greater than the slope of the straight line for 268 volts/cm. and large fields. These two curves only provide two points on the rising part of the curves of fig. 5, but these points can be regarded as accurate although they cannot, of course, determine the precise shape of these curves This effect will be further discussed later.

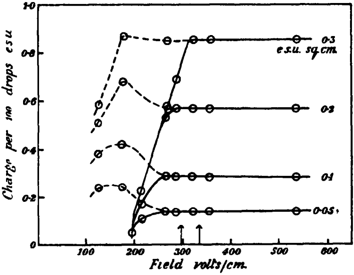

FIG 5 — —— Ions moving down , - - - ions moving up

The results of the second series of experiments are shown in the curves of fig 6, which were obtained by the same process as the curves of fig. 5 Here the beam of X-rays was directed through the middle of the space between the field plates and the upper plate was negative. In the first half of its fall between the plates the drop was meeting ascending positive ions and, in the second half, descending negative ions. The curves show the positive charge per 100 drops against the electric field for the constant ionization currents of 0·05, 0 1 and 0 2 e s.u. per square centimetre The critical fields, giving ions and drop equal velocities, are again indicated by arrows For greater fields (descending ions overtaking the drop) the charge collected is small, but this increases rapidly for fields less than the critical field. This is in agreement with the theory since the descending ions do not overtake the drop for small enough fields and therefore it retains most of the charge gained from the ascending ions Any loss of charge under these conditions is due to the attraction for the descending ions exerted by the net charge gained from ascending ions This effect must, however, be small in these experiments since curves very similar to those of fig. 6 can be constructed by taking half the difference of the curves of fig. 5.

In the third series of experiments the whole height between the plates was exposed to X-rays, so that the falling drop was meeting ions of both signs simultaneously It was when these experiments were undertaken, that the distortion of the electric field, already mentioned, was discovered. As already stated the field plates used had a diameter of 55 cm. and a separation of 28 cm. giving a ratio of 2 to 1 These dimensions were chosen from purely mechanical convenience when the possibility of observing the required effect was being investigated. A distortion of the field, corresponding to a bulging of the lines of force symmetrical about the plane mid-way between the field plates, would not have been of great consequence The magnitude of the effect was increased and it was made more serious by the fact that, the lower plate being earth connected, the lines of force from the upper plate spread out to the surroundings and so do not all terminate on the lower plate This gives an unsymmetrical field, strongest at the surface of the upper plate and weakest at the surface of the lower plate.

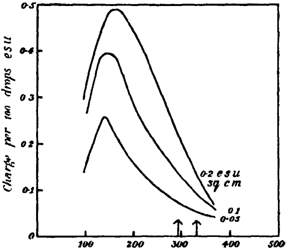

FIG 6 —Ionization in the middle of the field.

This effect first showed itself as a charging of the drops for fields well above the critical field and therefore under conditions where no charge was to be expected. Under these conditions the descending ions overtake the drop and no net charge is gained, providing the currents carried by the positive and negative ions are equal. Consider now the effect of the distorted field. The intensity of ionization (number of ions generated per cubic centimetre per second) may be taken to be uniform throughout the field. These ions follow the lines of force as they move in the field. Thus negative ions, say, spread out as they move down and the average current density, due to negative ions, is less than it would have been had the field been uniform. Positive ions moving up contract inwards and the average current density is increased There is thus an excess current of positive ions moving up and this gives a positive charge to the drop even when the field is above the critical value.

The distortion of the field was measured independently in the following manner A diaphragm with two openings was arranged to direct two identical beams of X-rays, one to the top of the field and the other to the bottom. A shutter was arranged to cover one or other of the openings in the diaphragm The measured ionization current, which has been used in the diagrams, is the current density at the surface of the lower plate. Using the lower beam of X-rays, the ionized region is just above the lower plate and the current density is not affected by spreading of the ions Using the upper beam of X-rays, the ions spread out before reaching the lower plate and the current density is diminished The ratio of these two current densities gives a measure of the spreading of the lines of force and therefore of the variation of the field. The observed ratio was 1 5

Various methods were tried to overcome this difficulty, but the only satisfactory solution lay in the use of larger field plates Field plates were constructed having a diameter of 4 feet (122 cm.) giving a ratio of diameter to separation of a little over 4 to 1. The remaining distortion of the field, using these plates, was about 5% This was measured in the same way, but the method was not very suitable for measuring such a small variation. With the larger plates the X-ray tube had to be moved further away from the centre of the field and to obtain X-ray beams of the same thickness as before, in the centre of the field, narrower slits had to be used. Small errors in their width or position then became serious. The change also had the disadvantage of diminishing the available intensity of ionization from the apparatus used. The effect of this distortion of the field, on the first two series of experiments, will be discussed later.

The third series of experiments was carried out with the large plates and the final curve of charge against field, for a constant ionization current, is shown in curve A of fig 7, for which the ionization current was 0·4 e s.u per square centimetre In these experiments the upper field plate was positive. As it will be required for the discussion of the experiments, the set of curves on which fig 7 is based is given in fig 8 Other curves similar to curve A could easily be constructed from it Returning to fig 7, the critical field corresponding to curve A is indicated by two vertical lines In fields smaller than the critical field the drop collects a charge, while in larger fields the charge is small

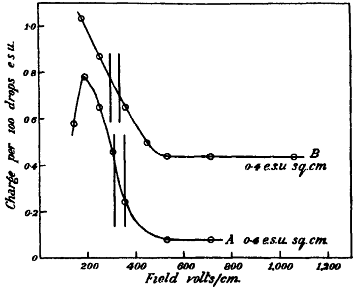

FIG. 7 —Whole field ionized

though not zero The charge collected diminishes very rapidly as the field increases through the critical value Curve B on the same diagram gives the corresponding curve obtained with the first field plates and the critical field is indicated in the same way. Actually curve B was obtained with the upper plate negative. It may be mentioned at this point that, although complete sets of observations have not been made with potentials of both signs on the upper plate, sufficient work has been done to show that the only difference between these two cases is that due to the difference in mobility for positive and negative ions. Curve B shows the proper variation of charge in the region of the critical field, but it is superimposed on the constant charge due to the distortion of the field. (The observations on which curve B is based were not extended to the smallest fields.) Curve B falls less steeply through the critical field than curve A and this, also, can be accounted for by the distortion of the field which affected curve B. Curve B is of interest in showing that the selective absorption of ions of one sign shows up quite clearly when superimposed on another effect

Curve A, obtained with the apparatus using the large field plates, still shows some charge above the critical field The 5% distortion remaining in the field would give an effect like this but, by comparison with curve B, where the distortion was 50%, it seems improbable that this can account for the whole effect. The measurement of these small charges was subject to greater error than in any other observations None the less, it appeared that observations on different occasions showed a greater variation than was warranted by experimental error It is probable that this residual charge together with its uncertainty is partly accounted for by the presence of large ions These would be formed by the attachment of the normal ion to nuclei, such as dust particles During the experiments a large Wimshurst machine was running continuously in the room and this, by producing ozone and oxides of nitrogen, might maintain a supply of nuclei It is to be expected that the number of such nuclei and therefore the number of large ions, would be different on different occasions and this would have its effect on the observations

A few experiments were carried out to detect the presence of large ions The method employed was to switch off the X-rays and raise the electrometer earthing key a fraction of a second later All the ions of one sign remaining in the space between the field plates, or more exactly in the volume above the collecting electrode, are then collected and measured If the interval between switching off the X-rays and raising the key is properly adjusted, all the ions of normal mobility will have been removed by the field and any charge observed will be due to slow ions. The switching was done by means of a falling weight. The charges observed were small, but by working with small electric fields, it was possible to make an estimate of them without difficulty since, for a given current, the charge density is inversely proportional to the field The removal of the ions of normal mobility could be followed and a residual effect remained This appeared to be due to ions having about one-fiftieth of the normal mobility and an estimate of the current they carried could be made This current showed considerable variations on different occasions. The drop would always fall more quickly than the large ions moving down and hence would collect a charge from large ions moving up. The order of magnitude of this charge can be estimated from the available data.

The actual result of the estimate is from one-third to one-fifth of the charge observed in fields greater than the critical field. This agreement is satisfactory. As a separate research is being made to determine the charge collected by a drop in the presence of large ions or charged cloud particles, it did not seem necessary to pursue the matter further.

It is reasonable to conclude that no charge is collected in fields greater than the critical field There is no evidence to the contrary in these experiments.

5 *Discussion.*

The experimental work which has been described clearly establishes the general accuracy of the theory outlined in the first section of this paper In particular, the third series of experiments indicates that the charge collected by the drop is cut off quite sharply at the critical field, for which ions and drop have equal velocities.

It is possible to proceed to somewhat greater detail A conducting sphere of radius, a, in a uniform electric field of strength, F, has positive and negative induced charges, each equal to $\frac{3}{4}Fa^2$, on the two hemispheres into which it is divided by a plane normal to the direction of the electric field. Consider all the lines of force which terminate on one of these induced charges At a distance from the sphere, such that the disturbance in the field caused by the induced charges is negligible, these lines of force form a cylindrical bundle, whose area of cross-section is easily shown to be equal to three times the area of cross-section of the sphere. In an electric field ions follow the lines of force. Suppose the sphere, at rest in the air, to be in a stream of ions of one sign only. It follows that all ions following lines of force which end on an induced charge will reach the sphere and hence, that the rate at which it gains charge is given by the ionization current per square centimetre multiplied by three times the area of cross-section of the sphere. This is the initial rate at which the sphere gains charge. When the sphere has a net charge, the distribution of charge on its surface is altered and, as has been shown by Pauthenier and Mme. Moreau-Hanot,* the limiting charge which the sphere can gain, in the presence of ions of one sign only, is equal to $3Fa^2$. When this limiting charge is reached the charge on the surface of the sphere has everywhere the same sign. If, for instance, the sphere has a net positive charge, this will increase the positive charge on its surface and diminish the negative charge. This will increase the area defined by the lines of force from the positive charge and diminish the corresponding area for the negative charge. Thus the sphere will gain positive charge at a decreased rate. Alternatively it can lose positive charge in a stream of negative ions at an increased rate.

---

* 'J. Phys. Rad.,' vol. 3, p. 590 (1932).

It has been assumed that the sphere is at rest in the air In the application of these considerations to a falling water drop it is necessary to consider the effect of the motion of the sphere through the air. In the first instance consider a stream of air blowing ions against the sphere This process alone cannot give the sphere a charge, for the air blows round the sphere and carries the ions with it For the falling drop the air stream, treating the drop as at rest with the air blowing up, and the electric field are in the same direction For ions moving up the air stream increases their velocity This is equivalent to increasing the ionization current flowing through any small area just below the drop, but the air blows outwards round the drop and carries some of the ions with it, so preventing them from reaching the drop. This introduces a compensating effect and it appears that the compensation is, at least approximately, exact. It can be shown that it would be exact for a true stream line motion, though it is conceivable that it might be modified by turbulence. Thus the rate of collection of charge is independent of the motion of the drop

Consider now the ions moving down. The air stream now decreases their velocity and decreases the effective ionization current, but above the drop the air blows inwards and causes more ions to reach the drop than would otherwise do so. This produces a similar compensating effect, so long as the velocity (relative to the drop) of the ions is not reduced to zero. No amount of " blowing in " can change zero into a finite quantity and so the drop then collects no charge. This is the cut off at the critical field. For smaller values of the electric field, we have the conditions already considered in the first section of this paper. Ions blowing round the neutral drop from below are first repelled and then attracted by equal and opposite induced charges which produces no net effect For a drop having a net charge, these induced charges are not equal and some of the ions reach the drop.

According to this theory, the charge collected by the drop is independent of the motion of the drop relative to the air, providing the field is greater than the critical field. This may be compared with the measurement of the conductivity of air with, for example, the Gerdien apparatus. In such measurements the charge reaching the collecting electrode is independent of the velocity of the air stream providing this velocity is great enough.

It is important to observe that the quantities which determine the charge are the current density, the area and the time. There is no question of ions being swept up by the falling drop

The experimental results may now be examined in the light of these considerations Turning to the results of the first series of experiments given in figs. 3 and 4 we see that, for large fields, the charge against ionization current curve is a straight line and, as already mentioned, it is the same straight line in each figure This means that, for large fields, the drop collects the same charge for a given ionization current whether that current is carried by ions overtaking the drop from above or by ions coming up to meet the drop In effect, the charge collected is independent of the motion of the drop, providing the field is greater than the critical field This implies that, in the presence of ions of both signs carrying equal currents, the drop collects no net charge in fields greater than the critical field The straightness of these lines indicates that the charge collected is far from the limiting value, as is also clear from the magnitude of the charge The rate of collection of charge may therefore be taken to be the initial rate and this may be compared with the value calculated in the way indicated above There are two sources of uncertainty in the experimental conditions One is the non-uniform field used in these experiments and the other is the thickness of the beam of X-rays. The measured ratio of the current densities at top and bottom of the field was 1 5. Since the charge depends on the current only and not on the field, in this case, we may allow for the distortion of the field by using the average ionization current, which is 25% greater than the observed value We must consider the collection of charge in two stages First, where the drop is exposed to ions of one sign only and second, where the drop is in the X-ray beam and is exposed to ions of both signs. The latter condition is the same as in the third series of experiments above the critical field, save that the drop has an initial charge and we will assume that no change of charge occurs. The thickness of the beam of X-rays has been given as 4 cm , but the beam was not very precisely defined and it was probably a little greater The drop takes about 0·06 second to fall the 28 cm between the plates. In round numbers we may say that it will collect charge during 0·05 second The radius of the drop, 0·224 cm , gives for three times the area of cross-section, the value 0·46 sq. cm. Since the drops had not approached their terminal velocity they were not distorted from the spherical shape. From the curve, when the observed ionization current is 0·1 e.s.u. per square centimetre, the charge collected is $2\cdot8\ 10^{-3}$ e.s.u. Taking the average ionization current to be 0·125, the calculated charge is $0\cdot46 \times 0\cdot125 \times 0\cdot05 = 2\cdot87\ 10^{-3}$ e.s.u. The difference is much smaller than the uncertainty of the calculation. Thus, at least approximately, the drop collects the ionization current from three times its area

In the experiments with the descending ions the quickness of the cut off at the critical field would be diminished by the distortion of the field The same consideration will apply to the second series of experiments, the results of which were given in fig 6 The values of the electric field given for these experiments are, of course, average values. In these experiments observations were not carried very far above the critical field, so it is not known how far the small charge remaining at about 370 volts/cm. would have diminished The beam of X-rays passed through the middle of the field and the current densities are again affected by the distortion of the field. In the upper half of the field we have a current due to ions going up and in the lower half a current due to ions going down. These currents are equal in the middle but, owing to the distortion of the field, the average current density in the upper half will be greater than that in the lower half This is similar to the excess current going up which was observed when the third series of experiments was attempted with the distorted field, save that the two currents now act successively instead of simultaneously, and it appears that a charge should be collected when the field is greater than the critical value. The small charge remaining at 370 volts/cm. is of about the magnitude which would be produced in this way The effect is not as prominent as it was in the other case

In many respects the most important experiments are those of the third series, in which the drop meets ions of both signs simultaneously. It is the charge collected in the presence of ions of both signs that is of importance in atmospheric phenomena In curve A of fig. 7 we have this charge and it has already been indicated that the curve shows the expected variation in the neighbourhood of the critical field. As the field diminishes below the critical value, the charge increases to a maximum and then diminishes A falling drop exposed for a great enough time, in a field smaller than the critical field, to ions of both signs will acquire a limiting value of net charge, which will be equal to some fraction of the induced charge. This limiting charge has no relation to the limiting charge in the presence of ions of one sign only, which has already been mentioned. When a drop has a net charge, so that the positive and negative charges on its surface are not equal, it collects a smaller number of the ions coming up to meet it and also some of the descending ions which it overtakes. When the limiting charge has been gained these two processes balance one another. The reason for the maximum in curve A is now apparent. When the field diminishes just below the critical value, the charge collected increases as the drop collects charge from ascending ions without losing much to descending ions This charge is greater than the limiting charge for small fields and so, for small fields the charge collected diminishes That this is so can be seen from the set of curves in fig. 8 from which curve A was constructed. The curves corresponding to the two smallest fields, 143 and 196 volts/cm. flatten out for large currents, showing that the limiting charge has been attained.

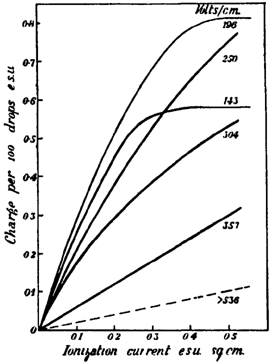

FIG 8

It is important to distinguish between the limiting charge collected in the presence of equal currents carried by positive and negative ions and the limiting charge under the conditions of these experiments. In the experiments the whole space between the field plates is ionized. We then have a density of negative ions increasing from zero at the negative plate to a greatest value at the positive plate and a density of positive ions increasing from zero at the positive plate to a greatest value at the negative plate. Thus when the drop falls between the plates it, at first, meets an excess of ascending ions from which it gains a charge and later it falls, with an initial charge, into a region in which there is an excess of descending ions. In this latter condition the drop may lose charge. Hence it is probable that the limiting charge under these conditions will be different from the limiting charge in the more simple case of equal currents carried by positive and negative ions.

The limiting charges observed are, for a field of 143 volts/cm. $0 \cdot 58 \; 10^{-2}$ e.s.u. and for a field of 196 volts/cm. $0 \cdot 81 \; 10^{-2}$ e.s.u. The corresponding induced charges ($\frac{3}{4}Fa^2$) are $1 \cdot 8 \; 10^{-2}$ and $2 \cdot 47 \; 10^{-2}$. Expressed as fractions of the induced charges, these limiting charges are $0 \cdot 322$ and $0 \cdot 328$ respectively. These fractions may be taken as one-third

The only matter which remains for consideration is the charge observed for small fields in the first part of the first series of experiments, where the current was carried by ions moving up For large fields it has been shown that the drop collects the ionization current from an area equal to three times its area of cross-section, this giving the straight line in fig 3 In the theory as it has been given, there is no reason why this should be changed when the field is diminished, unless the field becomes so small that the limiting charge becomes comparable with the observed charge. Then the charge collected would diminish. Actually, for small fields we have the two curves of fig 3, which rise above the straight line for small ionization currents and fall below it for larger currents. As has been pointed out, this produces the rise in the dotted curves of fig. 5. Clearly, if such curves had been plotted in fig 5 for larger ionization currents, the rise would have disappeared, for the curves of fig 3 fall below the straight line for large ionization currents.

The shape of these curves may be due to the departure of the experimental conditions from the intended simplicity. It was intended that the drop should collect its charge from a stream of ions of one sign moving up, but to produce these ions there was the X-ray beam at the bottom. The conditions when the drop is in the beam are the conditions of the third series of experiments For large fields it has already been assumed that the drop collects no charge while in the X-ray beam. In accordance with the theory and the experimental work, the drop will collect a charge while in the X-ray beam, as soon as the field is smaller than the critical field This can account for the increased charge in fields smaller than the critical field, observed for small ionization currents. In the third series of experiments a limiting value of charge was found, equal to one-third of the induced charge. For the larger ionization currents, assuming the drop to collect charge normally, it will fall into the X-ray beam with a charge greater than this limiting value and under these circumstances it will lose, instead of gaining, charge. This can account for a diminished charge for large ionization currents. The values of the limiting charges make such an explanation reasonable The conditions are complicated and an elaborate investigation would be necessary to be more definite. The most serious objection to this explanation is the magnitude of the effect to be accounted for. The drop is in the X-ray beam for not more than one-fifth of the time that it is in the field above the beam The ionization current does not change on entering the region of ionization and with due regard to the distribution of the ions, a maximum effect of 10% would be expected.

While the above explanation is qualitatively satisfactory, it is unsatisfactory when considered quantitatively, for the observed effect is much greater than 10%. With the smallest fields the ionization current was unsaturated and it is possible to think of ways in which this might account for the magnitude of the effect observed, but nothing definite can be said The more obvious supposition, that the curves show the normal charge collected by the drop in fields smaller than the critical field, must not be overlooked. In this connection it is worthy of note that a similar effect was present in the second series of experiments Then again, there was an X-ray beam giving an ionization current which was unsaturated for the smallest fields and the charge collected, fig 6, in fields smaller than the critical field was too great for a drop collecting normally from three times its area. The same considerations apply in this case

In the second part of the first series of experiments, where the X-ray beam was at the top and the current was carried by ions moving down, no corresponding effect was observed With fields smaller than the critical field the drop would collect a charge while in the X-ray beam, but this charge would probably be lost before the drop fell out of the field and so would not be observed.

The assumption that no change of charge occurs while the drop is in the X-ray beam when the field is greater than the critical field is not affected A drop with an initial charge would lose charge but this effect would be small, since the charges observed for large fields are small compared with the limiting charge. The question of unsaturation does not arise.

The largest charges observed in the course of this work were equal to about 10^{-2} e.s u. per drop. Since the volume of a drop was equal to $4 \cdot 7$ 10^{-2} c c, this is equal to $0 \cdot 2$ e.s.u. per cubic centimetre.

In conclusion, it may be said that the charge collected by water drops under the conditions of these experiments is in accordance with the considerations given in the first section of this paper.

These experiments were suggested by Professor C. T. R. Wilson The author is very gratefully indebted to him for his continued advice throughout their progress The work was carried out at the Cavendish Laboratory, Cambridge, and the author desires to express his thanks to Lord Rutherford for providing the necessary facilities

6. *Summary.*

Experiments have been made to determine the charge collected by a water drop falling through ionized air in a vertical electric field In the presence of ions of one sign only rising up to meet the falling drop, it collects a charge for all values of the electric field. When ions of one sign only are moving down in the same direction as the drop falls, the charge collected depends on the velocities of the drop and the ions If the descending ions have the greater velocity, so that they overtake the drop, then it collects a charge, but if the drop has the greater velocity, so that the descending ions cannot overtake it, then it collects no charge. The electric field which gives to the descending ions a velocity equal to that of the drop is the critical field for the phenomenon

In the presence of ions of both signs, carrying equal currents, the drop collects no net charge in fields greater than the critical field In fields less than the critical field it collects more ascending than descending ions and so gains a net charge This charge does not increase indefinitely but tends to a limiting value.

Experiments have been made with one size of drop only In fields greater than the critical field, the initial rate at which the drop collects charge in the presence of ions of one sign only is equivalent to collecting the ionization current from an area equal to three times the area of cross-section of the drop This applies both for ascending and for descending ions. In fields less than the critical field, the initial rate at which the drop collects charge from ascending ions appeared, in the experiments, to be different from this value, but this difference may not be a true effect. In the experiments the drop was not distorted from the spherical shape

These experimental results are in accordance with a theory proposed by Professor C T R. Wilson to account for the mechanism of thunderstorms and the electric charge brought down by rain.

Quantization of the Kramers and Pauli Model.

By P M. Davidson, Lecturer in the University College of Swansea

(Communicated by O W Richardson, F R S —Received May 12, 1933)

Ten years ago Kramers and Pauli quantized the diatomic molecular model* which bears their names, obtaining the formula which has played so large a part in band spectroscopy It is sometimes pointed out in modern text-books that these results, founded on the old mechanics, do not offer a very far-reaching analogy to those which the wave mechanics give for the real diatomic molecule I think the reason will be seen on closely examining the classical calculation, either in the original papers,† or in Born's "Atommechanik,"‡ Without adequate cause, all types of motion save one were rejected in the quantization; all that remained was the simple type of motion which, apart from the gyroscope's axial spin consists merely of a steady precession of the body as a whole about the invariable axis It will here be shown that in reality we can have Kramers and Pauli models performing a very different type of motion, while completely satisfying the old-quantum equations (which were determined in the original papers). In these motions the gyroscope precesses not only about the invariable axis but also about the nuclear axis Kemble§ proposed that in a modified model, having an elastically mounted gyroscope, motions of this more complex type should be possible as quantized states, though his actual treatment is confined to motions of the simpler type As stated above, we shall see that the original model can have the more complex type of motion, in strictly quantized states Kemble§ also proposed an energy formula for the corresponding motions of the real molecule; it is with this and with the well-established molecular formulæ of the wave mechanics that results obtained from the model are to be compared.

For specifying orders of magnitude it is convenient to think what happens when the mass of the nuclei is made very great, their angular momentum retaining the same order of magnitude as that of the gyroscope. Then the existence of quantized motions other than those prescribed by Kramers and Pauli is not surprising, for by analogy with the vectorial conception of the real molecule (described, notably, by Hund and Weizel),* we should expect, in these circumstances, to find models in whose quantized states the nuclei, if of great mass, will rotate about the invariable axis very slowly in comparison with the gyroscope's precession about the nuclear axis For the real molecule, wave mechanics equations such as Kronig's (22)† will hold with an accuracy increasing with the nuclear mass, in the sense that though the main rotational terms will become smaller, the neglected perturbations (if so they may be called) will diminish far more rapidly.

---

* The simple diatomic Kramers and Pauli model may be regarded (fig. 1) as consisting of two nuclei (point masses A and B) held at a fixed separation by a weightless frame within which a gyroscope, representing the electrons, is mounted rigidly, *i. e.*, at a fixed angle to the internuclear axis.

† 'Z Physik,' vol. 13, pp. 343, 351 (1923).

‡ English edition, pp 110–114 and 118–121.

§ "Report on Molecular Spectra in Gases," 'Bull. Nat. Res. Coun. Wash.,' chapter 7, §§ 2, 3 and 4.

In the model, it will be convenient to describe the motions first and then apply the quantum conditions It will be sufficient for our purposes to consider a model in which the centre of gravity of the gyroscope coincides with that of the nuclei, though the results are not limited to that case. For the dynamical argument we shall think of the model in terms of its two parts—the gyroscope and the nuclei (the latter being regarded as point masses); not until the quantization need we introduce the principal axes of the body as a whole It is essential to distinguish clearly between the gyroscope's axial component of angular momentum (which is of constant magnitude during the motion, and is quantized) and its total angular momentum (which need be neither) If this total angular momentum of the gyroscope is of strictly constant magnitude, we can only have the simpler type of motion, but in the motions to be considered the fluctuation of this magnitude, though slight, is compatible with a rapid precession of the gyroscope about the nuclear axis.

We consider first (fig 2) a simple motion in which the model precesses about a line OA, which lies in the plane of the gyroscope's axis and of the nuclear axis ON, and makes a small angle with the latter. Ω is the axial component of the gyroscope's angular momentum, differing from its total angular momentum L by the perpendicular component M_p proportional to the precessional velocity (and depending slightly on the small angle spoken of) The precession gives the nuclei an angular momentum m_1 (perpendicular to ON) proportional to the precessional velocity and the small angle. For this motion to be possible the resultant of L and m_1 must, of course, lie on OA. We will think of Ω and M_p retaining their magnitudes when the nuclear mass is made great, then the small angle is inversely proportional to the nuclear mass, or very nearly so. When this mass is great the energy of the nuclei (associated with the angular momentum m_1) is small compared with that part of the gyroscope's energy which is associated with the angular momentum M_p. This is the case we shall consider. The gyroscope's precessional velocity is great compared with the velocity which would have to be superposed about some new axis such as J (fig. 3) in order to generate in the nuclei an angular momentum m_2 of the same order as Ω. We cannot actually obtain the more

---

* *Cf.* Weizel's "Bandenspektren" ('Handbuch der Experimentalphysik,' 1931), chapter I, § 1 and § 5.

† "Band Spectra and Molecular Structure," p. 16. Camb. Univ. Press.

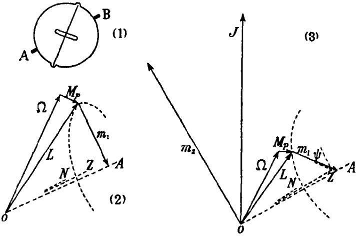

FIGS. 1, 2 and 3.

general motion merely by superposing on the simple motion a slow steady precession about OJ, for then Ω and the total angular momentum and the total energy would be fluctuating, by small fractions of their magnitudes, with the high frequency of the gyroscope's precession about OA. In the real motion, of course, they remain constant, while other quantities fluctuate. But the true motion of the nuclei only differs from the hypothetical one by quantities whose contribution to the nuclear angular momentum is of smaller order than m_1 and m_2. The axis OZ, which is needed in the quantization, is that principal inertial axis which is adjacent to ON, with which it makes a small angle inversely proportional to the nuclear mass. ON, OZ, and the gyroscope's axis are coplanar in our cases. ψ is the angle between the plane defined by OZ and the gyroscope's axis, and that defined by OZ and J. If all the angular momenta are measured in units of $h/2\pi$, we see from fig. 3 that the nuclear energy, apart from smaller orders, is

$$\frac{h^2}{8\pi^2 I_0}\{(m_2 - m_1 \cos\psi)^2 + (m_1 \sin\psi)^2\} = B_0\,(m_2^2 + m_1^2 - 2m_2 m_1 \cos\psi),$$

where I_0 is the nuclear moment of inertia, and B_0 is $h^2/8\pi^2 I$. Thus the energy of the gyroscope can be written, to this order, as

$$\bar{\bar{\mathrm{E}}} + \mathrm{B}_0\,(2m_2 m_1 \cos\psi), \tag{1}$$

where $\bar{\bar{\mathrm{E}}}$ is the mean energy of the gyroscope (the average with respect to ψ). The fluctuating term expresses, apart from the smaller orders, the energy transferred to and from the gyroscope by the nuclei (by a process easily traced), causing a fluctuation in its angular momentum component M_p The total energy may thus be written

$$\bar{\bar{\mathrm{E}}} + \mathrm{B}_0\,(m_2{}^2 + m_1{}^2) \tag{2}$$

The three quantum equations, which we have now to apply, were determined by Kramers and Pauli Both the constants J and Ω are quantum numbers. As a third we have the average, with respect to ψ, of the component of J along the axis OZ. We will call this third quantum number Λ, for purposes of a later comparison. For our purpose it is convenient to think of it as defined in this vectorial form, rather than in its geometrical form * The expression (2) may thus be written

$$\mathrm{E} + \mathrm{B}_0\,(\mathrm{J}^2 + \overline{\mathrm{L}_p{}^2} - \Lambda^2), \tag{3}$$

in which $m_1{}^2$ has been replaced by $\bar{\mathrm{L}}_p{}^2$, the mean square component of the gyroscope's angular momentum perpendicular to the nuclear axis. We could equally well replace it by any of the instantaneous values of $\mathrm{L}_p{}^2$, the changes only affect the higher orders.

It must be emphasized that the equation as it stands tells us nothing of the quantized energies, for we have not yet shown that $\bar{\bar{\mathrm{E}}}$ is independent of J to the accuracy considered That it is so might be guessed from fig 3, considering the quantum conditions, but it must be remembered that a very

---

* The surface of constant energy considered by Kramers and Pauli is, as they point out, a plate-like ellipsoid, though in the present cases their expression (1) does not adequately represent the total energy diminished by the constant energy $\Omega^2/2\mathrm{D}$ (in their units). In a case such as fig. 3, the plate has its centre inside, and its periphery far outside, the sphere of constant J It intersects the sphere in two separate curves, representing two entirely separate motions, which happen to have the same total energy and the same J. One motion can be obtained from the other by reversing the direction of the gyroscope's precession (this is possible in the model), and making adjustments in its magnitude and in other quantities, OA is moved to the other side of ON If either of the curves cuts off from the sphere an area satisfying the quantum condition, that curve represents a quantized state of the model (provided, of course, the other quantum conditions are satisfied).

small change in M_p alters the gyroscope's energy by an amount of the order of a rotational energy However, on making a rather more detailed treatment of the motion, and applying the quantum conditions, it will easily be found that $\overline{E}$ is indeed independent of J, to the desired accuracy, provided the nuclear mass is large enough to make the nuclear energy small compared with the energy associated with M_p. The calculation is quite simple if we note the orders of magnitude. In applying the third quantum condition we have evidently to write an algebraic expression for the component Λ, taking account of terms of the order ε (the ratio of the gyroscope's mass to that of the nuclei). Now the whole nuclear angular momentum, say m_n, is necessarily perpendicular to the nuclear axis, and OZ only makes with that axis an angle of order ε, hence to express to an order ε the part of Λ due to m_n we need only consider the principal terms in m_n. Also the component of the gyroscope's angular momentum perpendicular to the plane of OZ and its axis contributes nothing to Λ, and only represents an energy of smaller order than a rotational energy (it is limited by the rigid mounting of the gyroscope), so that to our accuracy the whole of the gyroscope's energy (1) consists of the constant part associated with Ω and the part associated with the main component of M_p (the component in the plane of OZ and the gyroscope's axis) Bearing these points in mind, the result is easily established

One point may be noted in passing, it is evident from the diagrams that for a given Ω and Λ the value which $\overline{M}_p$ must have in the quantized motions depends on the angle at which the gyroscope's axis is mounted relative to the nuclear axis To obtain a given precessional velocity in the quantized states, we must mount the gyroscope at the correct angle. Evidently if its precessional velocity is to be only a small fraction of its axial velocity, the angle at which it must be mounted will not differ very greatly from $\cos^{-1} \Lambda/\Omega$.

As remarked at the outset, we should expect the results to show an analogy with the wave mechanics equations, such as Kronig's (22) We insert there for W''_b its well-known value $B\{J(J+1) - \Lambda^2\}$,[*] and note that by definition $\overline{U}_b$ is B times $\overline{L_p{}^2}$ the mean square component of the electronic angular momentum perpendicular to the nuclear axis (apart from a term of an entirely different nature, which will have no counterpart in the model) Our J^2 has become $J(J+1)$, corresponding to the well-known difference between the old and the new quantum theories With this change the analogy is all that could be desired. In further analogy, we note from fig. 2 that the magnitude of the slightly fluctuating component of the gyroscope's angular momentum along the nuclear axis is very nearly the integer Λ, to which it tends as the nuclear mass increases, while the magnitude of $\overline{L}^2$ differs more perceptibly from Ω^2 All this is exactly as in the wave mechanics, except that again Ω^2 is to be replaced by $\Omega(\Omega+1)$.

---

[*] In this expression Kronig used the symbol K, not J.

To omit $\overline{U}_b$ from the wave equation would evidently correspond to omitting m_1^2 from our (2) or $\overline{L}_p^2$ from our (3). To obtain the higher approximations which represent rotational uncoupling (which corresponds to taking account of those "perturbations" neglected in the approximation (22)) we must, like Kemble, relax the rigidity of the gyroscope's mounting, but the motions will not be those which he treated. And if we wish to permit vibration we must set the nuclei themselves on springs, in that case to obtain the expression corresponding to Kronig's (5)[*] we must, of course, replace the vibrational action integral by the Wentzel-Brillouin-Kramers series, of which it is the first term.

Summary

It is shown that the quantized motions which the old quantum theory permits in simple Kramers and Pauli diatomic models are not limited to those specified by the original authors The present quantized motions and their energy formulæ offer a close analogy to those given by the wave mechanics for the corresponding molecule.

---

[*] *Loc. cit*, p. 32.

The Behaviour of Metals, particularly Lead and Bismuth, in Atomic Hydrogen, and attempts to prepare Atomic Hydrogen from Hydrides.

By Thomas Gibson Pearson, Percy Lucock Robinson and Eric Maurice Stoddart, Armstrong College, Newcastle-on-Tyne.

(Communicated by J Kendall, F R S —Received May 17, 1933.)

The preparation of free radicals from lead tetraethyl and tetramethyl has been described by Paneth and Hofeditz* and, having fully confirmed their work with the former compound† we sought, at the commencement of this investigation, to apply a similar technique to an analogous problem · the preparation of atomic hydrogen by the thermal dissociation of metallic hydrides Preliminary experiments on the dissociation of certain of the more accessible hydrides showed, however, that those of sulphur, selenium, tellurium, arsenic, antimony and tin, under the conditions employed, failed to yield hydrogen which was capable of removing even the most sensitive metallic mirror—such a mirror, we had been able to show, disappears quickly and completely when atomic hydrogen is present It is really not surprising that the hydrogen from these compounds is inactive since the accepted accommodation coefficients of the elements involved are relatively low In this respect, the hydrides of lead and bismuth promised greater success.

Hitherto, the hydrides of lead and bismuth have been obtained only in minute quantities, and have been characterized entirely by circumstantial evidence, hence it was necessary to discover means whereby they might be prepared on a larger scale Bismuth hydride, as it proved, did not present much difficulty , the yields from the dissolution of a magnesium-bismuth alloy in acid, although small, sufficed for our purposes On the other hand, the results accruing from the whole of our work on the lead compound are so meagre, and so dependent on inexplicable circumstances, as to leave a sense of uncertainty regarding the nature of the traces of lead-carrying body produced in the operations. Neither the dissolution of the magnesium alloy, nor the reduction of lead salts by magnesium gave the hydride, whilst a change of the alloying metal to lithium, the use of which in these preparations is new, resulted in the merest trace of a very impure, volatile lead compound from 20 gm of the alloy, and was without promise of yielding either a pure product or a sufficient quantity About fifty experiments with the oscillating arc, sometimes in its original form* and sometimes, modified so as to reduce the by-products contaminating the lead-containing condensate, agreed down to the minutest detail with the recorded observations of Paneth and Nórring, but, incidentally, gave uselessly small yields They found the presence of carbon to be a condition essential to the appearance of lead in the effluent gases, and of this there can be no question That our lithium contained carbon, whereas our magnesium was practically free from it is also significant in this connection

---

* 'Ber. deuts chem Ges ,' vol. 62, p. 1335 (1929)

† 'Nature,' vol 129, p 832 (1932).

From these abortive attempts to obtain lead hydride by classical chemical methods, attention was turned to atomic hydrogen as a means of its direct synthesis this Schultze and Muller† claim to have effected Early failure, on our part, to confirm the results of these workers, directed attention to the action of atomic hydrogen on solid elements in general, and the behaviour of a number of these in the gas was examined Several elements which do not react with molecular hydrogen yielded hydrides and new and interesting phenomena were observed, but despite improved technique, neither lead nor bismuth could be induced to form hydrides by this means

In the absence of lead hydride the bismuth compound was used in the thermal dissociations It did not, however, yield hydrogen atoms in detectable quantity presumably because their recombination, well known to be entirely a surface reaction, takes place instantly on the metal particles formed concurrently in the dissociation of the hydride Thus they fail to give evidence of independent existence

The Thermal Dissociation of Hydrides

The half life period of free methyl and ethyl is approximately one hundred times shorter than that of atomic hydrogen under similar conditions of pressure and wall-confinement The recombination of the free alkyls is, furthermore, a wall-reaction of the same character as that which accounts for the conversion of atomic to molecular hydrogen These considerations led to the attempted preparation, herein described, of hydrogen atoms by the thermal dissociation of hydrides Using a technique similar to that employed for the alkyls, a number of hydrides borne by a stream of hydrogen moving at a velocity of about ten metres per second and at a pressure ranging from 0·1 to 3 mm, were dissociated by heating the silica tube with a bunsen flame at various distances from "detector mirrors" of antimony, which was shown to be very sensitive to atomic hydrogen Hydrides having two, three or four atoms of hydrogen to the molecule, and varying considerably in decomposition temperature were used they included the hydrides of sulphur, selenium, arsenic, and antimony, and also those of tellurium, tin, and bismuth which were considered most promising The hydrides of sulphur, selenium, arsenic, and tellurium gave solid deposits which extended along the tube considerable distances beyond the source of heat, but those of bismuth and tin behaved more in the manner of lead tetraethyl. In no experiment, however, did dissociation result in detectable quantities of hydrogen atoms, and none of these mirrors showed the sharply defined back edge found when free alkyl radicals are being produced The diffuse posterior boundary was taken as additional evidence of the absence of free atoms in the gas stream (This criterion was inadmissible for bismuth hydride since, as is shown below, the metal does not unite with hydrogen atoms)

---

* Paneth and Nörring, 'Ber deuts chem Ges.' vol 53, p 1693 (1920).

† 'Z Phys. Chem' vol 6, p 267 (1929)

Atomic Hydrogen.

Since the preparation of atomic hydrogen by Wood* comparatively little has been added to our knowledge of its reactions with other substances Wood, himself, showed that sulphur is converted to hydrogen sulphide, and Bonhoeffer† described its action on the oxides, sulphides, chlorides, bromides and iodides of certain metals and pointed out that the compounds suffering reduction to the metal are those which would be similarly affected if heated in molecular hydrogen He also showed that phosphorus, arsenic and sulphur give hydrides, thereby confirming Wood's conclusions regarding the last element, and that palladium, tungsten, iron, chromium, silver, copper, lead, and mercury are unattacked by atomic hydrogen, but actively catalyse its recombination to the molecular condition. Duane and Wendt‡ stated that the gas is without effect on metallic bismuth, and Schultze and Müller§ described lead as being attacked by atomic hydrogen with the formation of the hydride, and sought, incidentally, to ascribe Paneth's free methyl phenomena to the formation of atomic hydrogen, rather than CH_3, on the dissociation of the alkyl.

---

* 'Phil. Mag.,' vol. 42, p. 729 (1921), 'Proc Roy. Soc,' A, vol 102, p 759 (1922)

† 'Z. Phys. Chem.,' vol. 113, p 203 (1924)

‡ 'Phys Rev,' vol. 10, p. 116 (1917)

§ 'Z. Phys. Chem,' vol 6, p 267 (1929)

The apparatus used by the authors in the preparation of atomic hydrogen consisted of a source of hydrogen, moist but otherwise uncontaminated, a discharge tube, a replaceable silica working-unit and a suitably protected and efficient pump system The electrolytic hydrogen employed was washed with alkaline pyrogallol, A, fig 1, before use and, in the course of the work, was repeatedly tested for volatile metallic impurities, using the Marsh test, after it had actually passed through the system It entered the discharge tube by

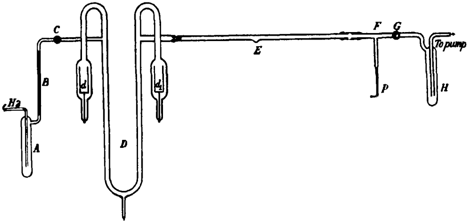

Fig 1

way of the capillary tube, B, the rate of flow being finally adjusted by the tap, C. The discharge tube, D, was constructed in Monax glass and had the form shown, the distance between the points of entry and exit of the gas stream being 60 cm and the diameter of the tube 1·8 cm. The cylindrical electrodes were sealed into compartments *d* and d_1 so disposed that material sputtered from the electrodes was prevented from falling into the middle portion of the tube, there to settle on the walls and serve as points catalysing the association of the atoms. The gas, for the activation of which an alternating current of 500 mA. at a potential of 5000 v was available, passed from the discharge tube directly into the clear silica working-tube, the precise form of which varied according to the requirements of the individual experiments, and thence *via* the T-tube, F, the tap, G, and the vessel, H, surrounded by liquid air, to the pumps. The evacuating system consisted of a Kaye annular jet mercury vapour pump, backed by a Hyvac. In order to facilitate changing, the silica working-tubes were incorporated in the apparatus by a spigot-joint with the discharge tube and by a sleeve-joint with the T-tube, F, the joints being sealed with picëin. The central portion of the discharge tube was cleaned, from time to time, by treating it with hot chromic-nitric solution and thoroughly washing with distilled water, and, after drying, it was uniformly coated with syrupy phosphoric acid. Immediately before attaching the silica tube, the inside and outside of the spigot were smeared with the same material and a layer of it was applied to the inside of that part of the silica tube forming the joint.

In carrying out the experiments with metals, a small piece of the pure element was placed in a slight depression which had been previously blown in the quartz tube at E, and, after the system had been evacuated, sufficient material was distilled from the reservoir to give a heavy mirror of metal, 2–3 cm long, situated about 2 cm. from the opening into the discharge tube This deposit was heated in a current of molecular hydrogen at 0·3 mm pressure, in order that a fraction, containing presumably the more volatile impurities, if any should be present, might be carried towards the reservoir by the gas stream After a second, thorough evacuation, a portion was moved backwards in the direction of the discharge tube, and the residue was driven with the assistance of a current of hydrogen, towards the reservoir by suitably heating the tube. By this means, a middle fraction of metal was obtained wherewith to fashion the testing mirror. This mirror lined the tube for about 1 mm of its length, being reduced to these dimensions by cutting away those portions farthest from the discharge tube by aid of a fine blowpipe flame, the metal thus volatilized being removed in a stream of hydrogen The operation involved repeated spreading and cutting and was greatly facilitated by pads of wet cotton wool encircling the tube at appropriate positions Practice enabled mirrors of identical size and density to be readily constructed After the formation of the mirror, the tube on either side of it was strongly heated to remove metal which had become dispersed in the process, the mirror, itself, being protected, meanwhile, by a pad of wet cotton wool, the position of which was adjusted so that the flame could be brought, in turn, closely up to each edge of the deposit The mirrors were used immediately after preparation as a decrease in their activity was occasionally observed on standing.

The experimental procedure then consisted in adjusting the rate of admission of hydrogen so as to maintain a suitable pressure in the system in spite of the withdrawal of gas by the pumps, activating the streaming hydrogen by means of the discharge, and, thereby, subjecting the mirrors to the action of atomic hydrogen Meanwhile, the quartz tube in the region of the deposit was kept cool by the usual cotton wool pad The phenomena observed differed greatly from metal to metal, but mirrors of all the elements tried, provided they were slight enough, could be made to disappear As, however, some of the metals employed were known to possess no volatile hydride, it was realized that the disappearance of a mirror is not, of itself, a sufficient criterion of hydride formation, since, as the sequel conclusively demonstrates, it may be due to the distillation of the metal by the heat evolved in the combination of hydrogen atoms on its surface. Such visual observations were, therefore, supplemented by an examination, with the aid of the sensitive Marsh test, of any product of the attack condensable at the temperature of liquid air. For this purpose, a quartz tube of the form shown in fig. 2 *a* was employed, the mirror occupying a position at I, and the reaction products being condensed by immersing the U-portion, J, in liquid air. After the passage of sufficient atomic hydrogen, the tap G was closed, and ordinary hydrogen was allowed to pass into the system until a pressure slightly above that of the atmosphere was reached. The tip of the silica Marsh tube, P, was then opened, the issuing hydrogen ignited, and the tube was heated at a point immediately before the capillary which was cooled by a pad of wet cotton wool to facilitate condensation of the metallic vapour. At this stage, the condensate in the U-tube was allowed to warm up by removing the bath of liquid air, any volatile material being carried forward to the Marsh tube, where the presence of hydrides was disclosed by the formation of deposits which were subsequently proved to be due to the particular element under test and not to adventitious impurity.

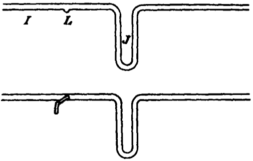

FIG. 2.—*a*, above ; *b*, below.

Mirrors of the elements arsenic, antimony, selenium, tellurium, germanium, and tin very readily suffered attack by atomic hydrogen, the first evidence of which was an increase in the definition of the boundary of the mirror adjacent to the discharge tube. This phenomenon was invariably accompanied by an evolution of heat. Opaque mirrors of these elements about 3 mm. in length completely disappeared within 5 min. of starting the discharge, even when the silica tube was cooled by pads of cotton wool kept at − 10° by means of a calcium chloride solution The speed of attack was at a minimum with tin, and increased from element to element through the series, tin, germanium, tellurium, selenium, antimony, arsenic In every case the presence of a hydride was established by condensing it in liquid air, and subsequently allowing the collected material to vaporize in a current of hydrogen, whereby it was carried to the silica Marsh tube for detection

With bismuth, interesting but completely different phenomena were witnessed. Instead of being eaten away *in situ* by atomic hydrogen, after the manner just described, bismuth mirrors, if sufficiently faint, moved along the tube at a rate of approximately 1 cm per minute, becoming, as they moved, progressively fainter and, finally, so attenuated as to be invisible Furthermore, all attempts to condense a hydride were abortive That failure was due to the hydride having a boiling point so excessively low as to prevent its retention in the liquid air trap seemed unlikely, in view of the behaviour, under identical conditions, of arsine and stibine, both of which are more volatile than any hydride of bismuth The progression of the mirrors along the tube must, therefore, be ascribed to the distillation of the metal brought about by the heat liberated in the recombination of hydrogen atoms on its surface. This view accords well with the observations made on heavier bismuth mirrors, the front edge of which, under the influence of atomic hydrogen, became at once sharply defined, and following this, a second mirror, very faint at its first appearance, began to be built up about two centimetres beyond the sharpened edge and continued to grow at the expense of material derived from the first mirror which eventually vanished In the course of these experiments the temperature of the quartz tube rose suddenly at the position occupied by the front edge of the first mirror and remained sensibly higher than the rest of the tube for about 2 cm beyond this point an observation which serves to explain the gap between the two mirrors where visible deposition was absent, and, also, the position taken up, just beyond the warm zone, by the second mirror The possibility of these phenomena being due to the formation of a hydride possessing so short an average life-period that it travelled only 2 cm., and hence existed only 2×10^{-3} sec , before dissociating was dismissed as a less probable explanation than simple distillation

It seemed, however, that the distillation hypothesis might best be tested by substituting for bismuth a metal of similar physical properties, but one which was known to form no volatile hydride under any conditions. For this purpose cadmium was selected, and, as had been anticipated, gave results which differed only in degree from the behaviour exemplified by bismuth ;

since, whilst cadmium has a similar catalytic activity in regard to the combination of hydrogen atoms, its hydrogen overvoltage (1·134 v.) being near to that of bismuth (1·050 v.), yet its boiling point in vacuo is 543° lower than that of this metal. In atomic hydrogen, a fairly heavy cadmium deposit caused the liberation of so much heat that the tube became appreciably warm in 30 sec. The front edge of the mirror turned from black to grey through the segregation of the metal from a uniform film into minute globules, and presented an appearance, reminiscent of the form frequently assumed by mercury mirrors, which was clearly due to the metal having reached temperatures in excess of its melting point. Following this change in appearance, the mirror progressed along the tube at an almost uniform speed, which, according to observations made on a number of similar deposits, was about 0·75 cm per minute. Bismuth mirrors of comparable intensity moved at a rate of about 0·35 cm per minute: the difference is significant, in that the ratio of the velocities Cd/Bi, 2·14, is very close to the reciprocal of the boiling points Cd/Bi, 2·21, and supports the ascription of the movement to distillation. The formation of a second mirror behind the first was also observed with cadmium; thus a cadmium mirror, 1·7 cm wide, gave, after 12 sec., a deposit 2·0 cm. behind its front edge, that is, again, just beyond the zone heated by the recombination of the hydrogen atoms. Once more the second mirror grew at the expense of the first and involved its complete disappearance in about 3 min. Measured by the displacement of the front edge, the total movement in 5 min. was 3 cm.

It has been recorded, above, that faint bismuth mirrors progressed along the tube with a gradual diminution in intensity until they finally vanished and it should be pointed out that this observation is compatible with the deductions just drawn, the vanishing being simply explained by dispersion of the metal. Faint mirrors are frequently lost from the same cause whilst being worked with the blowpipe in a stream of hydrogen, and, furthermore, the disappearance of both bismuth and cadmium deposits in atomic hydrogen is greatly facilitated by slightly warming the tube externally.

In another experiment, a bismuth mirror, 5 cm. long, in a working-tube of the type *a*, fig. 2, was subjected for 90 minutes, in 10-min. periods with 3-min. intervals, to the action of atomic hydrogen. The discharge tube, as judged by control experiments both before and after the run, was yielding a high concentration of atoms and thus the conditions must have been good for hydride formation. During the whole period the U-tube was submerged in liquid air, but when its contents were eventually tested in the usual manner, no trace of metal was found in the Marsh tube. Moreover, there was no evidence of a metallic hydride having decomposed in the U-tube since this appeared as clean at the end of the experiment as it had at the beginning. As, however, any hydride formed at I had to pass over a considerable area of metal collected about the reservoir L, whereon it might suffer dissociation, and thus avoid detection, for the final experiments we used a working-tube of type *b*, fig 2, provided with a side limb wherefrom the metal for the formation of the mirror might be distilled. Thus the main tube was occupied by a single narrow mirror which, in the course of a 30-min. run, moved 9 cm from its original position Evidently, as was anticipated, bismuth particles are captured more readily by a bismuth surface than a silica one, for a distinct ring was deposited on the surface of the U-tube immediately above the level of the surface of the liquid air The position occupied by this deposit rendered improbable the idea that its presence was due to a localized dissociation, and incidentally a similar line in the U-tube was obtained by vaporizing metal in the silica tube by heat from an external source, so that the phenomena described can only be interpreted as supporting the explanation advanced.

Schultze and Müller, *loc cit*, described the formation of lead hydride by the action of atomic hydrogen on mirrors of the metal In the light of our results with bismuth, this conclusion is difficult to believe since Paneth found, in all the methods tried by him, that positive indications of a hydride are much more difficult to obtain with lead than with bismuth. From the outset of our repetition of the work, it was realized that the yields of lead hydride, if produced at all, would be small and, therefore, every precaution was taken to ensure favourable conditions for formation and high sensitivity in detection

In the first experiment, very faint mirrors, situate 3 cm from the jet of the discharge tube, were repeatedly subjected to the action of atomic hydrogen over long periods broken only by short intervals to allow the discharge tube to cool somewhat There was evidence of these deposits heating up under the attack, but the only change observed after treatment for 90 min was in the front edge of the mirror which became slightly more clearly cut. This trifling improvement in definition was, however, unaccompanied by any recognizable movement of the edge or any decrease in the opacity of the mirror as a whole. Six repetitions of the experiment, employing a freshly reconditioned discharge tube the efficiency of which was demonstrated on mirrors of other metals, failed to disclose any evidence of hydride formation, despite a variation in the pressures of hydrogen from about 0·1 mm to 3·0 mm. and a concentration of atoms so great as to occasion a segregation phenomenon akin to that displayed by cadmium. The formation of two deposits ringing the tube, the one before and the other behind the original mirror, described by Schultze and Müller, may very well have been a special instance of a similar segregation. As, however, the mirrors of Schultze and Müller had been prepared by the decomposition of a lead alkyl, suitable modifications of the experimental arrangements were made to allow the behaviour of such mirrors to be studied Deposits from this source behaved in a manner identical with those prepared from metal, and, in particular, gave no evidence of yielding a hydride with atomic hydrogen

For the sake of substantiating the evidence, a lead mirror of considerable dimensions was subjected to the action of atomic hydrogen for 90 min, in periods of 5 min, and any volatile product was condensed by means of liquid air and subsequently tested by the Marsh method An exceedingly small, very faint stain was observed in the silica Marsh tube, but it was very much further from the heated zone than is normal for lead deposits which, in the experience of both Paneth and ourselves, are invariably found very near to the point of heating Actually, when tested chemically, this stain proved to be antimony, due, presumably, to a trace of that element in the lead and showing, incidentally, the selective nature of the atomic hydrogen attack and the sensitivity of the methods employed in detecting hydride formation Since treatment with atomic hydrogen had removed some of the antimony it appeared conceivable that in a second run the same mirror might give less stibine, or, possibly, none at all. The lead mirror was, therefore, reactivated by heating, without the addition of fresh material, and treated with atomic hydrogen, whereafter, the Marsh test was negative In these and other runs the U-tube was scrupulously examined for any trace of deposit which might have owed its origin to the decomposition of volatile lead compounds during their storage at the temperature of liquid air, but no evidence of this was forthcoming Schultze and Müller's U-tube deposit may possibly have been caused by electrode sputtering, *vide supra*, but can hardly have been due as they suggest to the decomposition of lead hydride

A critical examination of the evidence leads to the conclusion that lead hydride is not formed by the action of atomic hydrogen on lead at temperatures up to its melting point; furthermore, that the phenomena described by Schultze and Müller are not observed when aged electrodes, and pure lead mirrors are employed.

The authors wish to express their indebtedness to the Research Committee of this College for grants which provided the electrical and silica equipment

employed in this research, and to record their appreciation of the assistance rendered by the skilful glassblowing of Mr G Ellison of this Department. Grateful acknowledgment is made to Capt F P. Mills of the Northumberland and Durham Rescue Brigade who generously supplied the liquid air necessary in this work.

A Summary of Conclusions

1 The experiments of Paneth on the dissociation of lead tetraethyl have been repeated, and the results have confirmed his isolation of free ethyl and his value for its average life

2 Atomic hydrogen has not been found in the products of the thermal dissociation of hydrides in a stream of hydrogen, at low pressure, moving with a high velocity

3 The formation of bismuth hydride described in the literature has been confirmed

4 The necessity for the presence of carbon in all the methods whereby lead hydride has been alleged to be prepared has been confirmed The present authors hold the view, however, that further work is imperative, which, incidentally, should demonstrate, the composition of the volatile lead compound, before it can be safely assumed that the traces of material hitherto obtained are actually lead hydride They consider the diminution of the yield, following the reduction of the amount of carbon carrying material, needs more explanation than it has hitherto received, and that the possibility of the observed phenomena arising from compounds other than the hydride has by no means been excluded

5 Atomic hydrogen reacts with a number of elements of the B groups of the Periodic Table which do not combine directly with molecular hydrogen , these are indicated by heavy type in the Table

Table

Gp. 4	Gp 5	Gp 6	Gp 7
C	N	O	F
	P	S	Cl
Ge	**As**	**Se**	Br
Sn	**Sb**	**Te**	I

6. Contrary to all expectations, atomic hydrogen does not react with either of the metals lead or bismuth.

Perturbations in the Barium I Spectrum.

By G. O LANGSTROTH, Ph.D., 1851 Exhibition Scholar, Rijks Universiteit, Utrecht, Holland.

(Communicated by O W Richardson, F R S —Received May 23, 1933)

Quantum mechanics predicts that mutual interactions occur between adjacent spectral terms of the same j value arising from similar (odd or even) electron configurations. These interactions affect both the series term values and the intensities of transitions from the involved levels, and the normal multiplet intensity formulæ* no longer hold Theoretically, one expects that when such perturbations occur, the intensity† sum of each enlarged j group of the transition array for all the interacting configurations should be invariant,‡ *i e.*, equal to the theoretical sum which is obtained if the intensities in each multiplet be calculated separately for isolated LS coupling. These theoretical sums depend on uncalculated parameters (concerned with the radial functions) which connect the intensities in one multiplet with those of another arising from a different electron configuration, and which must be determined from the experimental data. The adjustment is easily made, however, if there exist transitions in each multiplet which are perturbed very slightly or not at all

It has been possible to identify the interacting terms which influence the intensities of the first three multiplets of the diffuse and of the fundamental series in the Ba I spectrum, and to show that for the most part, the experimental results confirm the theoretical prediction that each enlarged j group intensity sum should be invariant. Three striking exceptions occur, but they have an explanation other than a failure of the theory. This agreement is highly encouraging in view of the fact that the perturbations are in some instances several times the normal line intensity. For the present, no attempt has been made to calculate the perturbation to be expected in individual lines. The spin-orbit interaction matrices, for example, can be determined,§ but owing to the fact that the parent electron configurations are not known for all the perturbing terms, calculations which would give a more detailed test of theory, are at present impracticable [*]

---

* The Kronig-Russell-Sommerfeld-Honl formulæ since confirmed by wave mechanics. Dirac, 'Proc Roy. Soc ,' A, vol. 111, p. 281 (1926)

† The experimental intensities with the ν^4 and excitation corrections applied.

‡ Harrison and Johnson, 'Phys. Rev.,' vol. 38, p. 757 (1931).

§ Johnson, 'Phys. Rev.,' vol 38, p. 1628 (1931), also Brinkman, 'Z. Physik,' vol. 79, p. 753 (1932).

The group of mutually perturbed multiplets[†] in the diffuse series consists of transitions to the $2\,{}^3\mathrm{P}$ ($6s6p$) levels from $4\,{}^3\mathrm{D}$ ($6s6d$), $5\,{}^3\mathrm{D}$ ($6s7d$), $6\,{}^3\mathrm{D}$ ($6s8d$), $3\,{}^3\mathrm{P}$ ($6p^2$), ${}^3\mathrm{D}$ ($5d7s$), and an unclassified level q_λ at 6688·1 cm^{-1}[‡] The $4\,{}^3\mathrm{D}$ and $6\,{}^3\mathrm{D}$ transitions are only slightly perturbed In the fundamental series it consists of transitions to the $3\,{}^3\mathrm{D}$ ($6s5d$) levels from $5\,{}^3\mathrm{F}$ ($6s5f$), ${}^3\mathrm{F}$ ($5d7p$), a ${}^3\mathrm{F}$ term at 4561·6, 4750·5, and 4969 3 cm^{-1}, and $4\,{}^3\mathrm{F}$ ($6s4f$), and $6\,{}^3\mathrm{F}$ ($6s6f$) While the term value perturbations are felt in the latter two terms the intensities of transitions from them show no initial term perturbations large enough to be apparent

The perturbations in the fundamental series term values are relatively large and all members of the term series are affected This can only occur if the interactions are of electrostatic origin [§] For reasons to be discussed later, it is believed that the interactions in the diffuse perturbation group are of magnetic origin.

It is a general thing in both perturbation groups that the weakest multiplets show the largest percentage intensity perturbations as required by theory Configurations with two excited electrons appear to be more sensitive to perturbations than those with one electron in the ground state There is definite evidence that the $3\,{}^3\mathrm{D}_3$ level is perturbed, although no adjacent terms capable of interacting with it are known It may be connected with the circumstances determining the normal state of the atom ($-\,5s^2\,5p^6 6s^2$).

A very striking point in the intensity analysis is the manner in which it enables us to understand certain apparently anomolous lines in the spectrum. A weak multiplet may, by perturbation, have one (or more) of its lines intensified until it becomes strong compared to other lines in the spectrum, while its remaining lines are so weak as to escape notice. Several such " fragments " must be considered in the present instance Naturally their j values are not known uniquely from their combining properties, but only as one of two or three It has been possible from the intensity analysis to assign them j values without ambiguity, to show the source of their "borrowed" intensity, and to indicate what their intensities would be if unperturbed. Moreover, from similar considerations it has been possible to identify a line hitherto unclassified, whose intensity is for the most part the result of the same general process These examples serve to illustrate how such data can be used to further our knowledge and understanding of the more irregular spectral lines.

---

[*] The writer is aware of only one case in which the results of such calculations have been compared with experiment (Kast, 'Z. Physik,' vol. 79, p 731 (1932)) In this case (Sr spectrum) only two terms were involved and the perturbations were not so large as one might wish, in view of the magnitude of the experimental error. There was agreement within the experimental error.

[†] This will be referred to as a " perturbation group."

[‡] Russell and Saunders, 'Astrophys. J ,' vol 61, p 39 (1925). The usual (*e g.*, Fowler's) term values have been increased by 3 units in accordance with Shenstone and Russell's suggestion, 'Phys. Rev.,' vol. 39, p. 415 (1932).

[§] Shortley, 'Phys. Rev.,' vol. 40, p. 185 (1932).

A generalized Ritz equation, derived by perturbation theory,* has had remarkable success in describing perturbed term value series,† in the form

$$\nu_n = \frac{R}{(n + \mu + \alpha\nu_n + \sum_k \beta_k/\nu_n - \nu_k)^2},$$

where β_k is a "perturbation constant" which is a measure of the interaction of the term ν_n with some other at ν_k, R, μ, and α are constants, and n is the series order number. The very elegant graphical method of determining the constants, given by Shenstone and Russell, does not, however, permit one to find small β_k's, although if $\nu_n - \nu_k$ is small, the perturbation effect may be appreciable Neglect of a small β_k term in an analysis may produce a material discrepancy between the calculated and observed values for a particular level while those immediately before and after show good agreement This type of "isolated" discrepancy is well illustrated in the fundamental series, and is satisfactorily accounted for by the above explanation. The constants for the $n\text{F}_{4,\,3,\,2}$ series are given.

2. *Procedure.*

The following procedure was adopted in identifying the interacting terms and comparing experiment with theory Fortunately, the barium spectrum is well known and only very weak lines have not had their initial and final term values assigned Moreover, as pointed out later in this paper, it is sufficient to consider only the triplet systems.

A multiplet is chosen which exhibits departures from the normal relative intensity values, *e g.*, $2\,^3\text{P} - 5\,^3\text{D}$. From an examination of all known term values in the standard tables‡ it is possible to pick out all terms, of the same kind (odd or even) as the chosen initial term, which lie within a few hundred cm $^{-1}$ from it. The intensities of the transitions from these levels to the final levels ($2\,^3P$) are then determined. In the present instance, other important transitions from the initial levels do not occur.

---

* Langer, 'Phys Rev,' vol. 35, p 649 (1930).

† Shenstone and Russell, *loc cit*

‡ Especially "Atomic Energy States," Bacher and Goudsmit (McGraw-Hill), 1932.

In order to test if all the interacting configurations have been considered, the sum rule for the final levels is applied When the final levels are unperturbed it is sufficient that the intensity sums of transitions to them be in the ratio of their statistical weights It has been pointed out by Bartlett* that if some of the initial levels arise from configurations containing equivalent electrons, allowance must be made for those terms excluded by the operation of Pauli's equivalence principle. In the present work, the sums are still in the ratios of the statistical weights after such corrections have been made If the sum rule is found not to hold, the discrepancies may be attributed to failure to include all perturbing initial levels, or to perturbations in the final levels. If the latter is so, it can readily be seen from a comparison of the intensities of the chosen multiplet (with the known initial term perturbations removed), and the intensities in other multiplets of the same series which are not strongly perturbed in the initial levels If, however, it is the former, it is necessary to extend the measurements to include other transitions from initial levels lying at a greater distance from the chosen multiplet initial levels, or to look for unidentified lines which have sufficient intensity to affect the sums

When the measurements are complete, a transition array for all the perturbing configurations is drawn up, and the parameters which connect the theoretical intensities of one multiplet with those of another from a different electron configuration are adjusted. The guiding principle is to seek for certain unperturbed or slightly perturbed transitions, which are sufficient to fix the theoretical intensities for most multiplets The remaining "complete" multiplets can be given rough values from consideration of their intensities in general. One can then without ambiguity assign to definite enlarged j groups those "fragments" of multiplets (whose initial j values are not uniquely known), from consideration of the surplus or deficit of the experimental intensity in each group This is possible because the fragments in the present case are strong and consist mostly of "borrowed" intensity. The roughly adjusted parameters can then be finally determined, thus making possible the comparison of each enlarged j group sum with the theoretically predicted value, and the determination of the intensity perturbations in the individual lines.

---

* 'Phy. Rev.,' vol 35, p 229 (1930).

3 *Experimental*

For the most part an arc with carbon electrodes cored with a mixture of KCl and $BaCl_2$ was used as a source. This arc in air gives too much background for an accurate determination of relative intensities because of the presence of oxide bands. When operated in nitrogen, however, this difficulty disappears. In general arc currents of about 3·5 amperes were used. Owing to the interference of certain potassium lines this source could not be used for measurements of the $2\,^3P - 4\,^3D$ multiplet, but an arc cored with LiCl and $BaCl_2$ in air was found to be satisfactory. Special precautions had to be taken in photographing the $2\,^3P - 6\,^3D$ and the $3\,^3D - 6\,^3F$ multiplets, for when the arc was operated under the usual conditions, their lines were so broadened as to have almost the appearance of bands. This broadening increased with the arc current and was worse with low concentrations of $BaCl_2$. By increasing the concentration of the $BaCl_2$, and running the arc at the lowest current at which it would operate (about 0·8 amps.), it was possible to obtain sharp lines. The broadening is thought to be due to a Stark effect caused by the fields of charged particles in the arc. The fact that it depends on the arc current and apparently on the ionization potential of the coring material supports this view.

The coring material (KCl) usually contained only 1% $BaCl_2$ by weight, which corresponds to about 0·2% of barium atoms. Since no change in the relative intensities within strong multiplets occured when the concentration of $BaCl_2$ was increased to several times this amount, the effects of self-absorption were taken to be negligible. The final levels lie at approximately 13,000 and 9000 cm.$^{-1}$ above the ground level. Results of test measurements are contained in the data.

A standard Hilger E1 quartz spectrograph with a dispersion of about 10 A./mm. at $\lambda 3800$ was used. Intensity blackening marks were put on each plate by means of a step slit and a standard lamp whose intensity wave-length distribution was known as a function of the current. Exposure times for the barium spectrum and the intensity marks were made equal. For measurements below $\lambda 4000$ A. quartz optics and a quartz standard lamp were used.

The blackening measurements were made on a Moll microphotometer. The intensities were determined from these in the usual way.* Corrections for the background were made when it was present by subtracting the intensity of the background from the intensity of the line plus the background. In the few experiments in which overlapping lines occurred, their intensity curves were determined from their photometer curves on a special apparatus,* and these were analysed to give the separate intensities in the usual way *

---

* Ornstein, Moll and Burger, "Objektive Spektralphotometrie" (Vieweg), 1932.

The strongest lines of strontium and calcium were faintly present on most plates, owing to impurities in the arc carbons and coring. The sodium D lines were also present Special care was taken to prevent blends from passing unnoticed, not only by reference to standard wave-length tables, but by comparison with a special control plate This plate was obtained by photographing the spectrum of an arc cored with KCl and $SrCl_2$ in the ratio 3 · 1, which mixture is almost certain to contain all the impurities present in the KCl — $BaCl_2$ coring. One spectrum on the control plate was strongly overexposed, so that if there was a possibility of any blends occurring in the barium lines to be measured, it was immediately indicated, in "matching" the plate with the control plate, Such blends were very rare, and when present are noted in the data

In order to measure arc temperatures, which determine the populations in the initial levels (Boltzman distribution), photographs were taken of the spectrum of an arc cored with powdered carbon and the 1% $BaCl_2$— KCl mixture in equal parts The relative intensities of the bandheads of the $0 \rightarrow 0$, $1 \rightarrow 1$, $2 \rightarrow 2$, and $3 \rightarrow 3$, CN bands at λ3884 were measured and from these the arc temperatures were determined.† The transition probabilities of the lines of $2\,^3P - 3\,^3P'$‡ were then calculated by applying the ν^4 and excitation corrections to their intensities measured in the same exposures The arc temperature for any plate could then be determined from measurement of the intensities of two or more lines of $2\,^3P - 3\,^3P'$ and calculation from their known transition probabilities

It should be stressed that a specially prepared source is necessary to obtain a primary standard of temperature measurement. Temperatures found from the intensities of the CN bands on the usual plates cannot be used, since the CN bands and the Ba lines are radiated from different parts of the arc. For example, for one plate the temperature found from the CN bands on it was 5700° K, while that determined from $2\,^3P - 3\,^3P'$ was 3600° K. With the specially prepared source in which the coring contains a large percentage of powdered carbon, however, it is believed that no serious error is made in assuming that the temperatures at which the CN bands and the Ba lines are emitted, are identical.

---

* Wouda, 'Z. Physik,' vol 79, p. 511 (1932).

† Ornstein and Brinkman, 'Proc. Acad. Sci Amst.,' vol. 34, p. 33 (1931).

‡ For the nomenclature used in this paper, see Table I.

Two primary temperature determinations were made. The first gave three values which differed from the mean by less than 130° K, while in the second, the maximum variation from the mean was 250° K The largest temperature correction was about 30% ($2\,^3P - 3\,^3P'$)

The experimental error in individual intensity determinations is less than 8% Since it is more important to know accurately the intensities within the multiplets than it is to know the relative intensity of one multiplet to another, more determinations have been made for the former

4 *Results*

In this section are included the results of (*a*) the identification of the interacting terms by the procedure outlined in section 2, (*b*) the intensity measurements in the diffuse series group, (*c*) the intensity measurements in the fundamental series group, (*d*) measurements of the triplet singlet ratios in the fundamental series; and (*e*) a term value analysis of the fundamental series using two perturbing terms.

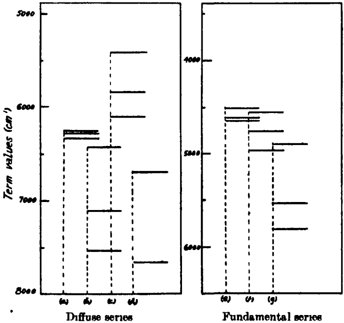

FIG. 1.

(*a*) Fig 1 Interacting terms lying near $5\,^3D$ and $5\,^3F$ The $4\,^3D$ and $6\,^3D$, and the $4\,^3F$ and $6\,^3F$ levels have been omitted in the diagram, although intensities of transitions from the former indicate slight perturbations in the initial levels. For (*a*), (*b*), (*c*), etc., see Table I.

Table I —Term Values for the Interacting Terms *

A	Symbol †	Shortened Symbol.	$j = 0$	$j = 1$	$j = 2.$	$j = 3$	$j = 4$
a	5 ^{3}D (6*s*7*d*)	5 ^{3}D	—	6323 1	6270·3	6247 2	—
b	3 ^{3}P (6*p*^{2})	3 ^{3}P′	7538 6	7208 9	6415 8	—	—
c	^{3}D (5*d*7*s*)	^{3}D″	—	6098 5	5832 0	5403 4	—
d	12‡	q_k	—	—	6688 1	—	—
	→§	q_e	7654 0	—	—	—	—
—	4 ^{3}D (6*s*6*d*)	4 ^{3}D	—	11336 9	11282 0	11214 6	—
—	6 ^{3}D (6*s*8*d*)	6 ^{3}D	—	4070 5	4058 4	4044 0	—
e	5 ^{3}F (6*s*5*f*)	5 ^{3}F	-	-	4637 0	4613 4	4508 3
g	^{3}F (5*d*7*p*)‖	^{3}F′	—	—	5797 3	5521 2	4900 5
f	^{3}F ( )¶	^{3}F″		—	4969 3	4750 5	4561 6
—	4 ^{3}F (6*s*4*f*)**	4 ^{3}F	—	—	7429 8	7415 8	7410 6
—	6 ^{3}F (6*s*6*f*)**	6 ^{3}F	-	-	3216 8	3213 1	3207 4

A —Denotes the symbols used in fig 1

* The usual values (*e g*, Fowler's) have been increased by three units in accordance with Shenstone and Russell's suggestion (*loc cit*)

† As given in Bacher and Goudsmit's " Atomic Energy States "

‡ *j* value assigned from the data of this paper

§ Found and classified from the data of this paper It is probably a level of the term to which q_k belongs If so, both are ^{3}P levels

‖ Found by Shenstone and Russell and assigned to *5d7p*

¶ This term has been assigned to *5d7p* in Bacher and Goudsmit's book, but Shenstone and Russell's more recent assignment has been adopted

** These terms are included for completeness, although transitions from them show no apparent intensity perturbation due to the group of levels about 5 ^{3}F

(*b*) In Tables II to VII are given the results of the intensity measurements within the multiplets Table VIII contains the averaged results from which the relative intensity of one multiplet to that of another was calculated. All values for the intensities have had the ν^4 and excitation corrections applied.

Table II.—2 ^{3}P — 5 ^{3}D.

Δj Conc / λ	3 → 2 4489 00	2 → 2 4493 66	2 → 1 4323 63	1 → 2 —	1 → 1 4332 96	1 → 0 4264 43
% 1	48 0	28 2	10 2	—	6 35	7 00
1	47·8	27 5	10 7	—	6 70	7 30
1	47·6	28 7	10 2	—	6 41	7 04
1	47 6	29 0	9 95	—	6 38	7 04
1	48 3	27 5	9 98	—	6 78	7 40
1	48 1	27 7	10 2	—	6 30	7 65
1	46 5	28 0	10 7	—	6 98	7 75
1	45 5	29·6	11 0	—	7 37	7 13
10	44 8	29 3	11 2	—	7 00	7 63
10	48·2	26 0	11 1	—	6 98	7 60
Average 10%	46 5	27 7	11 2	—	6 99	7 69
Average 1 %	47 4	28 3	10 4	-	6 66	7 34
Theory	46 7	8 36	25 0	0 56	8 36	11 1

Table III —2 ^{3}P — 3 ^{3}P′.

Temp.	Δ_j Conc / λ	2 → 2 4523 24	2 → 1 4350 37	1 → 2 4691 63	1 → 1 4505 94	1 → 0 4431 91	0 → 1 4573 38
°	%						
4700	1	18 5	12 0	26 1	12 6	17 4	13 6
4500	1	19 3	11 5	23 7	13 8	17 7	14 0
3600	1	19 0	11 4	25 5	13 1	17 7	13 3
6000	1	18 2	11 8	24 2	12 9	19 5	13 4
5600	1	18 0	12 8	24 8	12 7	19 7	12 4
5000	1	18 2	12 2	23 4	13 5	19 8	12 9
3700	10 (Average)	18 6	11 9	26 0	13 2	16 6	13 5
Average 1%		18 5	12 0	24 6	13 1	18 6	13 3
Theory*		65 9	22 0	22 0	13 2	17 6	17 6

* For the reasons for this adjustment, see the discussion

Table IV.—2 ^{3}P — ^{3}D″

Temp.	Δ_j Conc / λ	3 → 2 4325 11	2 → 2 4406 83	2 → 1 4242 61	1 → 2 —	1 → 1 4291 16	1 → 0 4223 96
°	%						
3700	10	19 4	25 3	15 8	—	20 1	19 2
3700	10	19 4	24 3	15 8	—	20 1	19 5
3500	10	19 1	25·1	14 9	—	20 7	19 9
3900	10	19 4	24 5	15 3	—	19 6	21·2
Average		19 3	24 8	15 5	—	20 1	20 0
Theory		19 3	3 5	10 4	—	3 5	4 6

Table V.—2 ^{3}P — q_k

Δ_j. Conc / λ.	k → 2 4579 67	k → 1 4402 55
%		
0 5	75 0	25 3
0 5	71·8	28 4
1 0	75 2	24 9
Average	73·9	26·2

Table VI.—$2\,^3P - 4\,^3D$.

Δj Conc /λ	3 → 2 5777 70	2 → 2 5800 30	2 → 1 5519 12	1 → 2 5818 91	1 → 1* 5535 93	1 → 0 5425 55
%						
0 9	48 6	7 32	24 0	- -	—	9 28
0 9	49 6	8 33	22 3	—	—	8 92
0 9	48 6	8 40	22 7	–	—	9 80
0 9	49 5	8 80	22 0	-	—	9 50
0 9	49 0	7 58	23 1		—	9 70
0 9	48 7	7 11	23 8	—	—	9 92
0 9	46 8	7 20	23 9	—	—	10 8
0 9	48 0	8 66	24 2		—	9 28
0 9	48 6	—	22 9	- -	- -	—
Average	48 6	7 92	23 2	—	-	9 65
Theory	46 7	8 36	25 0	0 56	8 36	11 1

* This line is blended with a very strong principal series lines at λ 5535 53

Table VII—$2\,^3P - 6\,^3D$

Δj Conc /λ	3 → 2 4084 87	2 → 2† 4087 31	2 → 1 3945 61	1 → 2 —	1 → 1 3947 51	1 → 0 3890 57
%						
50	-		22 1	—	11 0	12 0
50	48 4	—	22 0	-	10 2	11 4
50	48 1	-	22 5	—	10 1	10 9
50	48 1	—	22 3	-	10 4	11 6
50	48 1		21 6	- -	11 1	13 1
50	48 1	—	22 6	—	10 2	11 2
Average	48 2	—	22 2	- -	10 5	11 7
Theory	46 7	8 36	25 0	0 56	8 36	11 1

† A blend with the sharp series line λ 4087 31

As previously stated, this multiplet showed Stark broadening if precautions were not taken to prevent it As a check on the above maximum blackening measurements the areas under the intensity curves found with the Wouda apparatus were measured and compared The results, as follows, confirm the above measurements For λ3946 λ3948 the m b measurements gave

Table VIII—Relative Intensities of the Various Multiplets.

$\dfrac{2\,^3P_2-5\,^3D_3}{2\,^3P_1-q_k}$	$\dfrac{2\,^3P_1-3\,^3P'_2}{2\,^3P_1-q_k}$	$\dfrac{2\,^3P_2-{}^3D''_2}{2\,^3P_1-5\,^3D_2}$	$\dfrac{2\,^3P_1-3\,^3P'_1}{2\,^3P_1-4\,^3D_2}$	$\dfrac{2\,^3P_1-{}^3D''_1}{2\,^3P_1-6\,^3D_2}$
0 60	0 77	0 86	0 35	0 45

in two instances 22·3 10·3 and 22·4 10·1, while for the same two instances the area measurements gave the ratios 22·0 . 10·2, and 22·3 10·4

These results are the averages for several determinations From them, it is possible to calculate the intensities of all the measured lines in the same units, so that they can be compared The above values have had the ν^4 and excitation corrections applied. This table has been used in drawing up Table XVII of the discussion, section 5.

(c) In Tables IX to XIII are given the results of intensity measurements within the multiplets Table XIV contains the averaged results from which the relative intensity of one multiplet to that of another was calculated All values for intensities have had ν^4 and excitation corrections applied

Table IX —$3\,^3D - 5\,^3F$

Δj Conc /λ	4 → 3 3579·67	3 → 3 3593·20	3 → 2 3544·66	2 → 3 3596·33	2 → 2* 3547·70	2 → 1 3524·97
%						
1	35·0	5·4	32·0	–	4·8	23·0
1	34·2	6·1	32·3	—	4·8	23·0
1	33·7	5·9	32·6		4·8	23·3
1	34·0	6·4	31·2	—	5·5	22·8
1	34·8	7·3	29·8	--	5·9	22·4
Average	34·4	6·2	31·6	—	5·2	22·9
Theory	49·0	4·2	33·0	0·12	4·2	22·9

* This may be a blend with a very faint unknown line as shown by matching with the control plate

Table X.—$3\,^3D - 4\,^3F$.

Δj Conc /λ	4 → 3 3993·40	3 → 3 3995·66	3 → 2 3935·72	2 → 3 3997·92	2 → 2 3937·88	2 → 1 3909·92
%						
1	45·8	3·6	28·4	—	3·1	19·0
1	47·5	3·6	28·1	-	3·0	19·4
0·2	44·0	(4·4)	28·4	—	(4·0)	18·7
0·2	47·0	3·9	28·7	—	3·3	18·7
0·2	44·2	(5·6)	28·2	—	(4·5)	18·7
0·2	45·0	(2·7)	27·0	—	(2·4)	18·7
Average	45·6	3·9	28·1	—	3·4	18·9
Theory	40·5	3·5	28·0	0·10	3·5	18·9

The bracketed values are measurements on weak intensity plates where the plate grain effects are felt in the very weak lines This accounts for their variations

Table XI —$3\,^3D - 6\,^3F$.

Δj Conc /λ	4 → 3 3420 32	3 → 3 3421 01	3 → 2 3376 98	2 → 3 3421 48	2 → 2 3377 40	2 → 1 3356 80
Average 50%	46 0	3 6	27 8	1 8	4 3	17 5
Theory	40 5	3 5	28 0	0 10	3 5	18 9

This multiplet like $2\,^3P - 6\,^3D$ showed Stark broadening unless precautions were taken to prevent it Due to the small splitting of the initial levels, lines ending on each final level were not separated on the photometer curve. In order to obtain maximum blackening measurements of them the composite intensity curves had to be analysed, and separated into their component lines To provide a check on the work the area under each composite intensity curve corresponding to all transitions to a final level was measured. The intensity ratios for the sum of the transitions to each final level were then

Table XII —$3\,^3D - {}^3F'$.

Δj Conc./λ.	4 → 3 3631 7	3 → 3* —	3 → 2 3663 6	2 → 3* —	2 → 2* 3701 0	2 → 1* 3676 3
%						
1	88 2	—	12	—	—	—
1	86 5	—	13	—	—	—
1	90 0	—	10	—	—	—
1	89 5	—	11	—	—	—
1	89 8	—	10	—	—	—
Average	88 8	—	11	—	—	—

* Do not appear on plates suitably exposed for the measurement of the 4 → 3 and 3 → 2 lines 4 → 3 was generally compared with $3\,^3D_3 - 5\,^3F_4$ at the same time

Table XIII —$3\,^3D - {}^3F''$.

Δj Conc /λ	4 → 3 3586 50	3 → 3 3610 96	3 → 2 3561 94	2 → 3† 3639 72	2 → 2† 3589 95	2 → 1 3566 66
%						
1	33	36	15	—	—	15
1	33	35	18	—	—	14
Average	33	36	16	—	—	15

† These lines were too weak to measure The multiplet intensities are in general, weak, and the background corrections were large. Accordingly the intensities in this table are not as accurate as those in the previous tables

calculated from the m b. measurements, and the two sets of values were compared. The area measurements gave the following ratios for the intensities of transitions ending on the $j = 3$, 2 and 1 levels, 53·7 30 8 . 17·3. The ratios calculated from the analysed lines in Table XI are 51 3 32·1 17 5 which is in satisfactory agreement.

Table XIV —Relative Intensities of the Various Multiplets

$\frac{3\,{}^3D_3-5\,{}^3F_4}{3\,{}^3D_1-4\,{}^3F_2}$	$\frac{3\,{}^3D_2-{}^3F'_4}{3\,{}^3D_2-5\,{}^3F_4}$	$\frac{3\,{}^3D_3-{}^3F''_3}{3\,{}^3D_3-5\,{}^3F_4}$	$\frac{3\,{}^3D_3-6\,{}^3F_4}{3\,{}^3D_1-5\,{}^3F_2}$
0 41	0 63	0 12	0 85

This table has been used in drawing up Table XIX in the discussion, section 5

(*d*) The intensity of the singlet relative to the total intensity of the corresponding triplet in the fundamental series is given in three instances in Table XV, in the column headed "Ratio" The singlet series given by Shenstone and Russell (*loc. cit.*) has been used ν^4 and excitation corrections have been applied

Table XV —Singlet-Triplet Intensity Ratios (DF Series)

$3\,{}^1D-4\,{}^1F$	$3\,{}^3D_2-4\,{}^3F_3$	Ratio	$3\,{}^1D-5\,{}^1F$	$3\,{}^3D_2-5\,{}^3F_3$	Ratio.	$3\,{}^1D-6\,{}^1F$	$3\,{}^3D_3-6\,{}^3F_4$	Ratio
λ 4283 11* 118	3935 72 69 2	2 1	3861 91 15 9	3544 66 17 6	3 5	3636 83 9 2	3420 32 10 8	2 6

* Blended with the calcium line λ 4283 17 It was possible to estimate a correction for this from the intensities of the calcium lines at λ 4289 and λ 4299, which are of nearly the same intensity as the blended calcium line and which lie near enough to it to make such a procedure feasible The lower limit of the corrected value is given in Table XV It is important to know this, for the singlet intensity is too large

(*e*) The following term analyses using two perturbing terms have been made for the reasons given in the discussion. Shenstone and Russell's analyses with one perturbing term are also given

5 *Discussion*

From the results of (*b*) and (*c*), section 4, it is possible to draw up transition arrays for the perturbed configurations in the diffuse, and in the fundamental series perturbation groups This is done in Tables XVII and XIX, in which the intensities of all measured lines are comparable Estimated intensities of other lines (adjusted to the same scale to make them comparable with the measured results) have been included in the tables for the purpose of showing that those transitions which have not been measured and which should strictly be considered in a test of the theory, are so weak that they cannot appreciably affect the experimental sums

Table XVI —Constants for Langer's Formula for the $n\,^3F$ term values *

	nF_4		nF_3		nF_2	
	Author	S and R	Author	S and R	Author	S and R.
ν_{01}	4900 5	4900 5	5521 2	5521 2	5797 3	5797 3
ν_{02}	4561 6	—	4750 5		4969 3	—
β_{01}	−32 7	−33	30	−32 3	−26 5	−28
β_{02}	− 0 50	—	− 0 40	-	− 0 38	—
μ	− 0 1963	− 0 1980	− 0 1965	0 1956	− 0 1930	0 1934
a	$8\ 15 \times 10^{-6}$	$8\ 33 \times 10^{-6}$	$8\ 00 \times 10^{-6}$	$8\ 016 \times 10^{-6}$	$7\ 10 \times 10^{-6}$	$7\ 23 \times 10^{-6}$

nF_4 residuals −†1, (−1), ν_{01}, ν_{02}, −1, (−19), −1, (−2), 0, (−1), −3, (3), −4 (−5), −3, (−3)
1, (−1), 1, (−1), 0, (0), 0, (0), 2, (2)

nF_3 residuals −0, (−1), ν_{01}, ν_{02}, 0, (−1), −2, (0), 0, (2), −1, (0), 1 (1), −2, (−2), −2, (−2);
−1, (−1), 0, (0)

nF_2 residuals 0 (0), ν_{01}, ν_{02}, −1, (0), −1, (0), 2, (2), 1, (1), 8, (8), −1, (−1), −1, (−1)

S and R = Shenstone and Russell

* Usual term values increased by three units

†Residuals calculated using Shenstone and Russell's constants are given in brackets

In both transition arrays the triplet intensity sum in each enlarged j group, theoretically should be "invariant" to at least the degree to which the experimental values are known. For instance, in the diffuse series array (Table XVII), an examination shows that the three known intercombination lines are weak and cannot materially affect the intensity sums, and that strong singlets (singlets of "perturbing" configurations are not known and are therefore extremely weak) have their initial levels at large distances from the nearest "perturbing" terms of like j value (1300 cm $^{-1}$ for $5\,^1D$)

Following the procedure of section 2, we apply the sum rule for the final levels of the diffuse series perturbation group to test whether all interacting terms have been considered The intensity sums of the triplet transitions to $2\,^3P_2$, $2\,^3P_1$ and $2\,^3P_0$ (excluding $2\,^3P_1 - q_0$ which will be dealt with later) are 473, 268 and 90·5, in the ratio 5·1 2 9 0·98. This agrees within the experimental error (3%) with the ratios of the statistical weights of the final levels, and therefore all important perturbing configurations have been con-

Table XVII.—Diffuse

Initial levels.*

Final Levels.† j		0			1					
		$^1S'$	$^3P'$	^3q	$^3P'$	$4\,^3D$	$5\,^3D$	$6\,^3D$	$^3D''$	^3q
0	$2\,^3P$	—	—	—	42·4 (40·0)	35·6 (41·2)	3·31 (5·03)	4·95 (4·69)	4·19 (0·96)	*a*
1	$2\,^1P$	*a*	[3]	—	—	—	—	—	[1]	—
	$2\,^3P$	—	30·0 (40·0)	8·50 *t*	29·8 (30·0)	B (30·8)	3·00 (3·77)	4·45 (3·52)	4·22 (0·72)	*a*
2	$2\,^3P$	—	—	—	56·0 (50·0)	*w* (2·0)	*w* (0·25)	*w* (0·24)	*w* (0·05)	*a*

The measured intensities are given above the theoretical values for isolated terms in LS coupling which are contained in the round ( ) brackets

* *Initial Configurations*

$6s7d \rightarrow 5\,^1D,\ 5\,^3D$

$6p^2 \rightarrow {}^1S',\ {}^1D',\ {}^3P'$

$5d7s \rightarrow {}^1D'',\ {}^3D''$

A (?) $\rightarrow {}^3q$.

$6s6d \rightarrow 4\,^1D,\ 4\,^3D$

$6s8d \rightarrow 6\,^1D,\ 6\,^3D$

† *Final Configuration.*

$6s6p \rightarrow 2\,^1P,\ 2\,^3P$

sidered. Including $2\,^3P_1 - q_0$ gives a ratio somewhat nearer to the ratio 5 : 3 : 1. The sum rule still holds if $2\,^3P - 4\,^3D$ and $2\,^3P - 6\,^3D$ are omitted, but since they show slight perturbations in some of their lines for which no other explanation has been found, they have been included in this perturbation group. Two lines in these multiplets are blends and their intensities cannot be measured. However, since appreciable perturbations in these multiplets are rare, and since those which occur are small, the error in the sums introduced by assuming these lines to be of normal intensity is very small. It is also a fortunate fact that both blended lines are weak transitions in their respective multiplets.

The first step in adjusting the parameters which connect the theoretical intensities of one multiplet with those of the others, is to make the theoretical values for $2\,^3P_2 - 5\,^3D_3$ and $2\,^3P_2 - {}^3D''_3$ equal to their respective experimental intensities (Table XVII). This adjustment is possible because the separation of $5\,^3D_3$ and ${}^3D''_3$ is great, and there are no other perturbing $j = 3$ levels near. It fixes the theoretical intensities for $2\,^3P - 5\,^3D$ and $2\,^3P - {}^3D''$, and a consideration of the agreement with theory of the other lines in these multiplets confirms the adjustment. Naturally, the $2\,^3P_2 - 4\,^3D_3$ and $2\,^3P_2 - 6\,^3D_3$ transitions may also be taken as unperturbed so that the theoretical parameters are adjusted for all except $2\,^3P - 3\,^3P'$, and the "fragment" with the initial

Series Perturbation Group

2											3			
4^1D	5^1D	6^1D	$^1D'$	$^1D''$	$^3P'$	4^3D	5^3D	6^3D	$^3D''$	^3q	4^3D	5^3D	6^3D	$^3D''$
—	—	—	—	—	—	—	—	—	—	—	—	—	—	—
b	*c*	*d*	*a*	*a*	—	—	—	—	—	[2]	—	—	—	—
—	—	—	—	—	27 4 (50 0)	85 7 (92 9)	4 68 (11 3)	9 40 (10 5)	3 26 (2 16)	35 5 *r*	—	—	—	—
—	—	—	—	—	42 1 (150)	29 2 (30 8)	12 8 (3 77)	B (3 52)	5 20 (0 72)	100 *s*	179 (173)	21 3 (21 1)	20 0 (19 7)	4 04 (4 04)

a Denotes a line expected but not found and therefore extremely weak
— Denotes a line forbidden by the j selection rule, or an intercombination which is not found
[ ] Estimated intensity
w Denotes a line too weak to appear on the plate under the ordinary conditions of measurement.
B Blend as indicated in (*b*), section 4
r, *s*, *t* Small theoretical intensities which are estimated in the discussion
b, *c*, *d* Since the triplet sums are expected to be invariant, we are not directly concerned with these lines.

level q_k A rough adjustment can be made for the parameter of $2\,^3P - 3\,^3P'$ (actually $2\,^3P_1 - 3\,^3P'_0$ was made equal in theory and experiment) A comparison of the theoretical and experimental intensity sums in each enlarged j group can then be made, omitting the strong transitions from q_k, the level of unknown j value. It is found that in J_2^3 and J_1^3 the experimental deficits are about 96 and 37, while in J_2^1 and J_1^1 there are surpluses of 2 or 3 Since we expect that the transitions from q_k are lines of a weak multiplet greatly strengthened by "borrowed" intensity, it is at once obvious that the only place these transitions can fit is in J_2^3 and J_1^3. This fixes the j value of q_k without ambiguity. The parameter of $2\,^3P - 3\,^3P'$ is then finally adjusted by making the theoretical intensity sum in J_1^1 equal to the experimental sum, and calculating in this way the theoretical value for $2\,^3P_1 - 3\,^3P'_1$. This fixes the intensities for this multiplet and completes the adjustment of the parameters.

It now remains to compare the theoretical and experimental intensity sums in each enlarged j group. The experimental sum J_1^0 shows a deficit of 25% This group contains only $2\,^3P_1 - 3\,^3P'_0$ and there are no known transitions from adjacent levels capable of perturbing it. If its intensity has been "loaned," then the line which has "borrowed" it must be included in the array. A careful examination of my plates showed only one line in this region at λ4600, for which the initial and final levels were not known, and which had sufficient intensity to account for this behaviour. All other lines were either identified, and if so it was known that they could not perturb, or were so faint that they could not account for the discrepancy in the J_1^0 sum If λ4600 belongs in J_1^0, its initial level is at 7654 cm. $^{-1}$, which is just 118 cm $^{-1}$ from $3\,{}^3P'_0$ so that a large perturbation is practically certain Moreover, it is in a reasonable position for the $j = 0$ level of the term to which q_k belongs On this evidence, it is believed that λ4600 is $2\,{}^3P_1 - q_0$ and has been inserted as such in the tables It follows that q_k and q_0 are ${}^3P_2$ and ${}^3P_0$ levels

It is now possible to test the theory by comparing the theoretical and experimental sums in each enlarged j group The results are given in the following table. -

Table XVIII —Comparison of Theoretical and Experimental j Group Sums (Diffuse series)

Enlarged j Group.	Experiment	Theory	—
J_3^2	224	218	—
J_2^2	193	$189 + s$	$s \sim 4$
J_1^2	166	$167 + r$	$r \sim 0$
J_0^1	91	92	
J_1^1	72	69	
J_2^1	56	50	
J_1^0	38 5 (+ 3)	$40 + t$	$t \sim 1$

Examination of the table shows that the intensities of the transitions from q_k and q_0 if unperturbed (*i e* , s, r, t) are very small, being less than the error in the j group sums This was just what was expected in order to account for the absence (extreme weakness) of the other lines of the multiplet The sources of the borrowed intensity are apparent from Table XVII *Table XVIII shows the agreement with theory to be surprisingly good in view of the complicated nature and of the magnitude of the perturbations* In all except one case (J_2^1) there is agreement within the error of measurement (3%)

The general procedure of section 2 is also followed in the fundamental series group Here, however, the sum rule for the $3\,{}^3D_3$, $3\,{}^3D_2$ and $3\,{}^3D_1$ final levels gives the ratio 8·0 5 0 3·0, when all the measured triplet transitions are included The $3\,{}^3D - 4\,{}^3F$ and $3\,{}^3D - 6\,{}^3F$ multiplets do not show any appreciable perturbation which can be attributed to the levels which perturb $5\,{}^3F$. The sum rule for the final levels applied separately to the transitions from 4 ^{3}F, 6 ^{3}F, and 5 ^{3}F levels with the known initial term perturbations removed, gives respectively the ratios, 7·9 5 0 3·0, 8 5 5 0 3·0 and 8 5 5 3 2 9. The fact that these ratios are similar shows that none of the perturbing terms considered is responsible for the excess of intensity of transitions to 3 ^{3}D$_3$ If it were due to other unconsidered initial levels they would have to be situated similarly for each term in order to produce similar perturbations in each multiplet No levels capable of doing this are known Moreover, when the theoretical parameters are adjusted, as in Table XIX, the $J_3{}^4$, $J_3{}^3$ and $J_3{}^2$ intensity sums all show a surplus of experimental intensity These circumstances can only arise from a perturbation in the final levels, although no adjacent terms capable of causing such perturbations are known Because transitions to the 3 ^{3}D$_2$ and 3 ^{3}D$_1$ levels appear to be normal, it is thought that the perturbation is in the 3 ^{3}D$_3$ level That the 3 ^{3}D$_2$ and 3 ^{3}D$_1$ levels should be each perturbed in exactly the right manner to make them appear relatively normal, is a coincidence that appears highly improbable The adjustment of the parameters in Table IX has been made accordingly

There is no apparent reason why the 3 ^{3}D$_3$ level should be perturbed The interval ratio for the 3 ^{3}D term is greater than 3 . 2 instead of less as it should be if the perturbation were due to a repulsion from terms higher in the energy diagram. It may be connected with the fact that in building up the Ba atom two 6*s* electrons are added to the Xe configuration, while the first 5*d* electron is not added until the next element La

Examination of Table XX shows that there is agreement with the theory within the experimental error of measurement for all transitions not involving the* 3 ^{3}D$_3$ *level. The latter *j* groups show in all cases a surplus of experimental intensity. ***It is not, however, a true disagreement with theory but rather is due to the effect of unconsidered factors, as has been pointed out*** The source of the intensity "borrowed" by 3 ^{3}D$_3$ — ^{3}F$'_4$ is obviously 3 ^{3}D$_3$ — 5 ^{3}F$_4$ and when this is "restored" the former has an intensity comparable with the other lines of its multiplet (see Table XIX)

A very elegant graphical method for determining the constants in Langer's equation for the term values has been given by Shenstone and Russell The observed quantum defects multiplied by $(\nu_n - \nu_0)$, the separation of the "perturbed" and "perturbing" levels, are plotted against ν_n for all the levels of a series, and the perturbation constant β_0 is given by the intercept of $\nu_n = \nu_0$ with this curve. This enables one to find β_0 when it is large but not when it is very small, owing to the small scale necessary, and to the errors inherent in graphical methods. It is possible, however, for the perturbation

Table XIX.—Fundamental

Initial Levels *

Final Levels.†

j		0	1			2							
		$^3P'$	$^1P'$	$^3P'$	$^3D'$	$^1D'$	$^3P'$	$^3D'$	$4\,^3F$	$5\,^3F$	$6\,^3F$	$^3F'$	$^3F''$
1	$3\,^3D$	[1]	—	[1]	[1]	—	—	[1]	46.5 (46.5)	12.8 (12.8)	4.11 (4.20)	*a*	0.96 *x*
2	$3\,^1D$	—	[2]	[0.2]	[0.2]	[2]	[1.5]	—		—	—	—	—
	$3\,^3D$	—	[0.3]	[1.5]	[0.3]	[1]	[1]	[0.3]	8.4 (8.6)	2.9‖ (2.4)	1.0 (0.78)	*a*	*a*
3	$3\,^3D$	—	-	—	—	—	[1.5]	[0.2]	*w* (0.24)	*w* (0.06)	0.42 (0.02)	*a*	*a*

The measured intensities are given above the theoretical values for isolated LS coupling which are contained in round ( ) brackets.

* *Initial Configurations*

$6s5f \rightarrow 5\,^1F,\ 5\,^3F.$ $6s4f \rightarrow 4\,^1F,\ 4\,^3F$

$5d7p \rightarrow {}^1(P', D', F'),\ {}^3(P', D', F')$ $6s6f \rightarrow 6\,^1F,\ 6\,^3F$

$B\,(?) \rightarrow {}^3F''.$

† *Final Configuration*

$6s5d \rightarrow 3\,^1D,\ 3\,^3D$

term $\beta_0/\nu_n - \nu_0$ to be appreciable even if β_0 is very small, *i.e.*, if $(\nu_n - \nu_0)$ is also small Under these circumstances neglect of the small β_0 term leads to poor agreement with experiment for the level near ν_0, but does not appreciably affect the agreement for other levels of the series. Such a case occurs in the fundamental series which has been analysed by Shenstone and Russell using one perturbing term The analysis in Table XVI is given to point out how a large "isolated" discrepancy in the calculated values may be explained; $5\,^3F_4$ is an example, and the corrected value is given; $9\,^3F_2$ is possibly another example of the same thing The corrections involve the recalculation of the constants for all three series nF_4, nF_3 and nF_2. The

Table XX —Comparison of Theoretical and Experimental j Group Sums (Fundamental Series)

Enlarged j Group.	Experiment	Theory
J_2^3	96	94
J_2^2	12.3	11.8
J_1^3	64	64
J_3^4	156	136
J_2^3	16.5	11.8
J_3^1	(0.42)	(0.02)

Series Perturbation Group.

3										4				
4^1F	5^1F	6^1F	$^1F'$	$^3D'$	4^3F	5^3F	6^3F	$^3F'$	$^3F''$	4^3F	5^3F	6^3F	$^3F'$	$^3F''$
—	—	—	—	—	—	—	—	—	—	—	—	—	—	—
118‡ (78)§	15 9 (21 3)§	9 2 (7 0)§	[1 5]	—	—	—	—	[0 7]	—	—	—	—	—	—
—	—	—	—	[1 5]	69 2 (69 0)	17 6 (18 9)	6 52 (6 22)	1 5 *t*	1 0 *u*	—	—	—	—	—
—	—	—	—	[3]	9 8 (8 6)	3 5 (2 4)	0 85 (0 78)	*a*	2 3 *v*	112 (100)	19 2 (27 4)	10 8 (9 0)	12 1 *r*	2 1 *s*

a Denotes a line expected but not found and therefore very weak
— Denotes line forbidden by j selection rule, or an intercombination line which is not found
w Denotes a line too weak to appear on a plate under ordinary conditions of measurement
[ ] Estimated intensity
‡ Corrected lower limit as explained in (*d*), section 4
§ One third of the unperturbed triplet intensity
‖ Possibly a blend with a faint line as indicated in (*c*), section 4
r, *s*, *t*, *u*, *v*, *x* Theoretical intensities normally very weak

small β_0's were found by trial and error, but the trials can be made so that the approximations converge rapidly to give the best agreement with experiment Langer's formula may be expected to hold only so long as the perturbation is small compared to the distance between the perturbed and perturbing levels, the ratio of the latter to the former is about 3 1 for this. This is apparently within the region of validity, for the formula describes the term value series surprisingly well

I have found the perturbation constants in Langer's formula by the graphical method, for the terms which perturb the diffuse series intensities They are all very small if not zero, so that the interactions which affect the intensities, do not affect the series term values to any extent Since the main term value perturbations in the diffuse series near 2800 cm $^{-1}$ and 1400 cm.$^{-1}$ (probably *5d4f*) are due to terms whose precise values are not known, no analysis has been made

It is possible to draw some conclusions from the data concerning the nature of the interactions in the diffuse, and in the fundamental series groups. Shortley (*loc. cit*) has pointed out that magnetic interaction between two configurations can only occur if the *n* value of at least one electron in each is the same. The interactions in the fundamental series are then obviously of electrostatic origin, for terms arising from *5d7p* (and the other unknown configuration) interact with terms arising from the 6*snf* configurations, and perturb the whole series of term values.

On the other hand, in the diffuse group the term values series show little effect of interaction with the terms which perturb the intensities. Moreover, it appears to be a general thing that perturbations of electrostatic origin occur only between terms of the same L and S, as well as J value, for Russell and Saunders coupling. This rules out the possibility of the interaction being electrostatic. An examination of the electron configurations involved (Table I) shows that all terms, including $4\,^3D$ and $6\,^3D$, are capable of interacting magnetically with some other term in the perturbation group. It is therefore believed that the interactions are of magnetic origin.

The following observations have been made. While the term value perturbations due to the $^3F'$ (and $^3F''$) levels are strongly felt both in $4\,^3F$ and $6\,^3F$, the *intensity perturbations due to them in the corresponding multiplets* do not appear to be appreciable. As shown by the behaviour of the doubly excited configuration terms in the diffuse series group, intensities of transitions from terms of this type appear to be more sensitive to perturbations than those from terms of singly excited configurations. The weakest multiplets show the largest percentage intensity perturbations as required by theory, as reference to Tables XVII or XIX shows.

The measurements of the triplet singlet intensity ratio have been given (Table XV). When departures from extreme LS coupling are not great (when there are no intercombination lines), and when there are no perturbations due to neighbouring terms, the total triplet intensity is expected to be three times the corresponding singlet intensity. The results show that there are departures from this rule in the fundamental series. It is difficult to trace the causes for this, for the singlet series as well as the triplet series is perturbed by adjacent terms. One thing can, however, be said in general, and that is that the singlet intensity tends to be too large. (Both the triplet and singlet 5F transitions are too strongly perturbed to be of much value in discussing this point.) There are no intercombination lines to account for it. The following circumstances may, however, provide the correct explanation. Randall has found the combination $4\,^3D - 4\,^3F$ with some intensity in the infra-red, but I have not been able to find in his papers* any reference to a line at λ15,375 where $4\,^1D - 4\,^1F$ is expected. It may be that if the intensity sum of $3\,^3D - 4\,^3F$ and $4\,^3D - 4\,^3F$ (for example) were compared with the intensity of $3\,{}^1D - 4\,{}^1F$, which has no corresponding strong transition $4\,{}^1D - 4\,{}^1F$, the expected result would be obtained.

---

* 'Astrophys. J.,' vol 34, p 1 (1911), vol 42, p 195 (1915).

In conclusion, I wish to express my thanks to Professor L S Ornstein for discussion, and for many suggestions I am also indebted to Mr G G Zaalberg for assistance in carrying out some of the experimental work, and to the Royal Commission for the Exhibition of 1851 for the award of a scholarship.

Summary

(1) It has been possible to show that the large departures from the normal intensities which occur in certain barium multiplets are due to interactions of "overlapping" electron configurations, and to identify the mutually perturbed terms

(2) The method by which this is done is described The intensity measurements include transitions to the $2\,{}^3P$ levels from $4\,{}^3D$, $5\,{}^3D$, $6\,{}^3D$, $3\,{}^3P'$ and a level at 6688 1 cm $^{-1}$ and to the $3\,{}^3D$ levels from $4\,{}^3F$, $5\,{}^3F$, $6\,{}^3F$, ${}^3F'$ and ${}^3F''$, which form the two perturbation groups For the nomenclature, see Table I

(3) The ratio of the singlet to the total triplet intensity has been obtained for the first three members of the fundamental series

(4) An arc in nitrogen was used, for the most part, as a source Special precautions were taken to render the effects of self-absorption negligible, and tests were made to show that this was so

(5) The multiplets arising from $6\,{}^3D$ and $6\,{}^3F$ showed pronounced Stark broadening under ordinary conditions of arc current and $BaCl_2$ concentration The method used to obtain suitable conditions is described

(6) A method of measuring the arc temperature which corresponded to the temperature of the region from which the barium lines were emitted is given

(7) The intensity sum of each enlarged j group in the transition array for each perturbation group usually agrees with the theoretically predicted sum. Where this is not so, it is shown that other factors enter, so that the discrepancies are not " real " disagreements with the theory

(8) Examples of how such measurements can be used to assign definite j values, and to classify certain "irregular" lines, are given. The presence of certain "fragments" of multiplets is explained

(9) The perturbations in the diffuse series are probably of magnetic origin, while those in the fundamental series are certainly of electrostatic origin.

(10) There is definite evidence that the $3\,{}^3D_3$ level is perturbed, but no explanation has been found.

(11) An explanation is offered of the occurrence of certain "isolated" disagreements in term value analyses by Langer's formula An example is furnished in the fundamental series analysis which has been made for two "perturbing" terms

(12) The ratio of the singlet intensity to that of the corresponding triplet in the fundamental series is too large. An explanation is offered

(13) Some general observations on the perturbations are made

Interference Due to Walls of a Wind-Tunnel

By L Rosenhead, Ph D, Professor of Applied Mathematics, The University,
Liverpool; Fellow of St. John's College, Cambridge

(Communicated by H G Glauert, F R S—Received May 23, 1933)

1. *Introduction*

This paper arose out of a discussion with Mr. Glauert on the validity of certain results on wind-tunnel interference given in a recent paper by Theodorsen,* and I am greatly indebted to him for several very valuable suggestions. In his paper Theodorsen investigated, on the lines of the approximate theory laid down by Glauert,† the interference factors due to rectangular tunnels in the following five conditions (1) tunnel entirely enclosed, (2) free jet, (3) horizontal boundaries only, the vertical sides being free surfaces, (4) vertical boundaries only, the horizontal sides being free surfaces, (5) bottom boundary only, the remaining sides being free surfaces Apart from one or two minor errors, Theodorsen's paper has to face a more serious objection on the score that the approximate method employed is not always valid This objection to the approximate method was raised rather briefly in a previous paper,‡ but at that time all the cases discussed, using the approximate method, were those due to Glauert, and they were such that the approximate method did not come into conflict with the exact theory The more complicated method was, however, of some practical importance as it enabled additional refinements to be introduced into the numerical evaluation of the interference factors, and it enabled Glauert* to show that there is an appreciable drop in the interference factor in the Duplex Tunnel (height/breadth equal to one half) as the span of the aerofoil increases Some of the cases discussed by Theodorsen are such that they *must* be considered according to the exact theory. The crux of the matter is as follows —

---

* 'Nat Adv Ctee for Aeronautics,' No 410 (1931).

† "Aerofoil and Airscrew Theory," p 189 (1930), or 'Aero Res. Cttee Rep and Mem,' No 867 (1923)

‡ 'Proc. Roy Soc.,' A, vol. 129, p. 135 (1930).

The basis of the theory of wind-tunnel interference is due to Prandtl,† and he investigated several cases himself On the assumption that trailing vortices spring from the aerofoil and extend downstream without distortion, Prandtl showed that the whole problem can be converted into one dealing with the flow in a transverse section of the wake far behind the aerofoil, the necessary boundary conditions being that the velocity potential is constant over the surface of the free jet, and the stream function constant over the rigid boundary. The theory was extended by Glauert and others,‡ and applied particularly to the case of the small aerofoil in a rectangular tunnel When the aerofoil is very small the exact distribution of vorticity is not of extreme importance as, to a first approximation, they all give the same result The simplest case is that of "uniform vorticity," and far downstream an aerofoil of span $2s$ is represented by two line vortices of strengths $\pm\kappa$ at the points $\pm s$ In order to satisfy the boundary conditions appropriate "image vortices" are introduced, and the interference velocities inside the wind-tunnel are those due to this image system In order to calculate the interference velocities it is necessary to differentiate at some stage or other, an appropriate complex potential function, and in the approximate theory this fundamental complex potential function is of the form

$$w = \phi + \iota\psi = -\frac{\iota\kappa}{4\pi}\log \Pi\,(z - z_n), \tag{1}$$

where the infinite product Π contains a factor $(z - z_n)$ corresponding to every positive vortex, and a factor $1/(z - z_n)$ corresponding to every negative vortex. The function $\Pi\,(z - z_n)$ is, however, *not absolutely convergent*, and extreme care has to be taken in the differentiation, integration, approximation, etc. In determining the interference velocities by the approximate method the expression $dw/dz\ (= u - \iota v)$ is first formed, and the resulting doubly infinite series is summed by an approximate method. From the nature of the summation, it might be expected that in some cases this doubly infinite series will *not be absolutely convergent* and will have no "sum" in the usual sense of the word—in fact, different groupings of the terms may give different sums.

---

* 'Aero. Res Ctee. R. and M,' No. 1459 (1932)

† 'Gött Nacht.,' p 107 (1919)

‡ Glauert, *loc cit*, and also 'R. and M,' Nos 1453, 1470 (1932); Terazawa, 'Rep Res. Inst. Tokyo Imp. Univ,' vol. 4, p 69 (1928); Rosenhead, *loc cit*

If, however, each factor of the infinite product Π is multiplied by an appropriate exponential function so as to ensure the convergence of the infinite product without introducing additional zeros

$$w = -\frac{\iota\kappa}{4\pi}\log \Pi \left[\left(1-\frac{z}{z_n}\right)\exp\left(\frac{z}{z_n}+\frac{1}{2}\frac{z^2}{{z_n}^2}\right)\right],$$

we obtain an expression which is the logarithm of a quasi-doubly periodic function. If that part within the square bracket be treated as one unit, the w function is *absolutely convergent*, and it can be differentiated and have its terms rearranged in any way without altering the convergence or the sum. Further, the introduction of the exponential factors does not alter the nature of the flow. This is the basis of the exact theory, and when it was applied to the cases investigated by Glauert, his results emerged as first approximations of the general expressions and there is no question as to their validity. Some of the series given by Theodorsen are not absolutely convergent and have no "sum". All his cases have, therefore, been re-examined, and the results are given below.

2. *Tunnel Entirely Enclosed* (δ_1)

This case has been investigated previously by Glauert (*loc. cit.*) and Rosenhead (*loc. cit.*), but the results may be summarized briefly as follows. Let h and b be the height and breadth of the tunnel, λ the ratio h/b. The boundaries are lines $x = \pm b/2$, $y = \pm h/2$ and the semi-infinite trailing vortices $\pm \kappa$ are at the points $x = \pm s$, where $2s$ is the span of the aerofoil. The total lift L experienced by the aerofoil in free air can be expressed in either of the following forms

$$\mathrm{L} = 2s\rho\mathrm{V}\kappa = k_{\mathrm{L}}\rho\mathrm{S}\mathrm{V}^2, \tag{1}$$

where S is the area of the aerofoil, ρ the density of the medium, V the velocity of the aerofoil, and k_{L} the lift coefficient. The symbol $\mathrm{C}(= hb)$, the cross-sectional area of the tunnel, will also be used.

The complex potential function $w(= \phi + \iota\psi)$ must have logarithmic singularities at the vortices and must have ψ constant over the boundaries. The image system is therefore as shown in fig. 1, where + denotes a positive vortex pair, thus ↻ ↺, and — denotes a negative vortex pair, thus ↺ ↻.

There are positive vortices at $z = s + mb + \iota 2nh$, $z = -s + mb + \iota(2n+1)h$, and negative vortices at $z = -s + mb + \iota 2nh$, $z = s + mb + \iota(2n+1)h$, where m and n assume all positive and negative integral values from $-\infty$ to $+\infty$, and we arrive at the unique expression

$$\left.\begin{aligned} w &= -\frac{\iota\kappa}{4\pi}\log\frac{\vartheta_1(z-s/b)\,\vartheta_4(z+s/b)}{\vartheta_1(z+s/b)\,\vartheta_4(z-s/b)}, \\ &= -\frac{\iota\kappa}{4\pi}\log\frac{\vartheta_1(z-s/2\iota h)\,\vartheta_2(z+s/2\iota h)}{\vartheta_1(z+s/2\iota h)\,\vartheta_2(z-s/2\iota h)}, \end{aligned}\right\} \qquad (2)$$

where $q = \exp(-2\pi\lambda)$ in the first expression and $q_1 = \exp(-\pi/2\lambda)$ in the second one It might be noted that this pair of expressions, and similar pairs

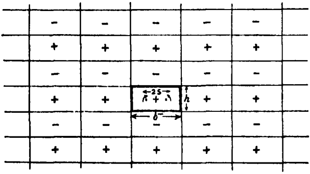

Fig 1 —Tunnel entirely enclosed Interference factor δ_1

occurring later in the paper, are connected by the "Jacobi imaginary transformation" (The notation used for the quasi-doubly periodic ϑ functions is that of Tannery and Molk "Fonctions Elliptiques")

Since the span is small the interference velocity over the aerofoil is assumed to be equal to that at the origin, and therefore,

$$\left.\begin{aligned} v &= \frac{\kappa}{2\pi b}\left[\frac{\vartheta'_4(s/b)}{\vartheta_4(s/b)} - \frac{\vartheta'_1(s/b)}{\vartheta_1(s/b)} + \frac{b}{s}\right]_q, \\ &= \frac{\kappa}{2\pi(2\iota h)}\left[\frac{\vartheta'_2(s/2\iota h)}{\vartheta_2(s/2\iota h)} - \frac{\vartheta'_1(s/2\iota h)}{\vartheta_1(s/2\iota h)} + \frac{(2\iota h)}{s}\right]_{q_1}. \end{aligned}\right\} \qquad (3)$$

If $\Delta\alpha$ and Δk_D are the corrections to be added to the wind-tunnel observations of angle of incidence and drag coefficient, we have, according to the usual formula,

$$\Delta\alpha = \frac{v}{V} = \delta\frac{S}{C}k_L, \qquad \Delta k_D = k_L\Delta\alpha = \delta\frac{S}{C}k_L^2.$$

In the present instance we derive a first approximation to δ_1 (the value of δ

in the closed tunnel) by neglecting second and higher powers of s in equation (3), and we get

$$\left.\begin{aligned}\delta_1 &= \pi\lambda\left[\frac{1}{12}+2\sum_1^\infty \frac{pq^p}{1+q^p}\right],\\ &= \frac{\pi}{\lambda}\left[\frac{1}{24}+\sum_1^\infty \frac{(2p-1)\,{q_1}^{4r-2}}{1-{q_1}^{4r-2}}\right],\end{aligned}\right\} \tag{4}$$

or

$$\delta_1 = \pi\lambda\left[\frac{1}{12}+2\sum_1^\infty \frac{p}{e^{2p\pi\lambda}+1}\right], \tag{4A}$$

$$= \frac{\pi}{\lambda}\left[\frac{1}{24}+\sum_1^\infty \frac{(2p-1)}{e^{(2p-1)\pi/\lambda}-1}\right]. \tag{4B}$$

Equation (4A) is useful for numerical evaluation when $\lambda > 1$, and (4B) when $\lambda < 1$

3. *Free Jet* (δ_2)

In this case the images are as shown in fig 2, and the distribution is positive vortices at $z = s + 2mb + \iota nh$, $z = -s + (2m+1)b + \iota nh$, and negative vortices at $z = -s + 2mb + \iota nh$; $z = s + (2m+1)b + \iota nh$.

The appropriate w function is

$$\left.\begin{aligned} w &= -\frac{\iota\kappa}{4\pi}\log\left[\frac{\vartheta_1(z-s/2b)\,\vartheta_2(z+s/2b)}{\vartheta_1(z+s/2b)\,\vartheta_2(z-s/2b)}\right]_q,\\ &= -\frac{\iota\kappa}{4\pi}\log\left[\frac{\vartheta_1(z-s/\iota h)\,\vartheta_4(z+s/\iota h)}{\vartheta_1(z+s/\iota h)\,\vartheta_4(z-s/\iota h)}\right]_{q_1},\end{aligned}\right\} \tag{1}$$

where $q = e^{-\pi\lambda/2}$ and $q_1 = e^{-2\pi/\lambda}$, so that the real part of w is constant over the surface of the jet, and by repeating the process of the previous section we get

$$\left.\begin{aligned}\delta_2 &= -\pi\lambda\left[\frac{1}{24}+\Sigma\frac{(2p-1)}{e^{(2p-1)\pi\lambda}-1}\right],\\ &= -\frac{\pi}{\lambda}\left[\frac{1}{12}+2\Sigma\frac{p}{e^{2p\pi/\lambda}+1}\right],\end{aligned}\right\} \tag{2}$$

4. *Horizontal Boundaries only, the Vertical Sides being Free Surfaces* (δ_3).

The images are as shown in fig. 3. There are positive vortices at

$z = s + 2mb + \iota 2nh$, $\quad z = -s + (2m+1)b + \iota 2nh$,

$z = s + (2m+1)\,b + \iota\,(2n+1)\,h$; $\quad z = -s + 2mb + \iota\,(2n+1)\,h$, and negative vortices at

$$z = -s + 2mb + \iota 2nh\,; \qquad z = s + (2m+1)\,b + \iota 2nh\,,$$
$$z = -s + (2m+1)\,b + \iota\,(2n+1)\,h\,, \quad z = s + 2mb + \iota\,(2n+1)h.$$

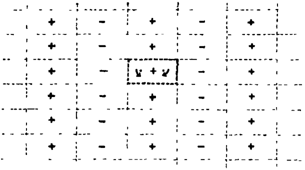

FIG. 2.—Free jet. Interference factor δ_2

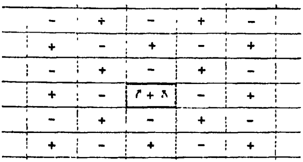

FIG. 3.—Horizontal boundaries only, the sides being free surfaces. Interference factor δ_3

A w function with the appropriate singularities is

$$\left.\begin{aligned} w &= -\frac{\iota\kappa}{4\pi}\log\left[\frac{\vartheta_1(z-s/2b)\,\vartheta_2(z+s/2b)\,\vartheta_3(z-s/2b)\,\vartheta_4(z+s/2b)}{\vartheta_1(z+s/2b)\,\vartheta_2(z-s/2b)\,\vartheta_3(z+s/2b)\,\vartheta_4(z-s/2b)}\right]_{q=e^{-\pi\lambda'}} \\ &= -\frac{\iota\kappa}{4\pi}\log\left[\frac{\vartheta_1(z-s/2\iota h)\,\vartheta_2(z+s/2\iota h)\,\vartheta_3(z-s/2\iota h)\,\vartheta_4(z+s/2\iota h)}{\vartheta_1(z+s/2\iota h)\,\vartheta_2(z-s/2\iota h)\,\vartheta_3(z+s/2\iota h)\,\vartheta_4(z-s/2\iota h)}\right]_{q_1=e^{-\pi/\lambda'}} \end{aligned}\right\} \quad (1)$$

but it is *not unique*. This can be seen as follows:—If $w_1\,(=\phi_1 + \iota\psi_1)$ is a complex potential function satisfying the following conditions: (1) positive vortex at $z = s$, (2) negative vortex at $z = -s$, (3) ψ_1 constant along $y = \pm h/2$; (4) ϕ_1 constant along $x = \pm b/2$, then $w = w_1 + Az$ will also satisfy the conditions if A is a purely real number. The number A is determined by the condition that as b and h become infinitely large the equation (1) should reduce to

$$w = -\frac{\iota\kappa}{4\pi}\log\left(\frac{z-s}{z+s}\right).$$

After some calculation it is found that A is equal to zero, and ultimately

$$\left.\begin{aligned} \delta_3 &= \pi\lambda\left[-\frac{1}{24}+\Sigma\frac{2p-1}{e^{(2p-1)\pi\lambda}+1}\right], \\ &= \frac{\pi}{\lambda}\left[\frac{1}{24}-\Sigma\frac{2p-1}{e^{(2p-1)\pi/\lambda}+1}\right], \end{aligned}\right\} \qquad (2)$$

and in particular $\delta_3 = 0$ when $\lambda = 1$

5 *Vertical Boundaries only, the Horizontal Sides being Free Surfaces* (δ_4)

The system is shown in fig. 4 There are positive vortices at $z = s + mb + \iota nh$, and negative vortices at $z = -s + mb + \iota nh$, so that a complex potential

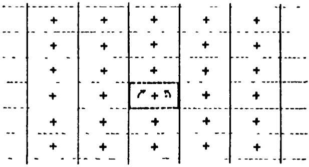

FIG 4 —Vertical boundaries only, the other sides being free surfaces Interference factor δ_4

satisfying the conditions of the problem, namely, logarithmic singularities at the vortices, ψ constant over the lines $x = \pm b/2$ and ϕ constant over the lines $y = \pm h/2$, is given by

$$w_1 = -\frac{\iota\kappa}{4\pi}\log\frac{\vartheta_1(z-s/b)}{\vartheta_1(z+s/b)}. \qquad (1)$$

As in the previous section this function is not unique, for

$$w = w_1 + \iota Bz \qquad (2)$$

will also satisfy the conditions if B is a perfectly real number. The quantity B is determined by the condition that the system reduces to

$$-\frac{\iota\kappa}{4\pi}\log\left(\frac{z-s}{z+s}\right)$$

when b and h become infinitely large. The effect of the term ιBz is to superpose a velocity $(-B)$ in the y-direction and to alter the momentum of the whole system. The momentum of the fluid within the region $x = \pm\frac{1}{2}b$, $y = \pm\frac{1}{2}h$ is

$$\left.\begin{aligned} M_y &= \iint v\,dx\,dy = \iint \frac{\partial\phi}{\partial y}\,dx\,dy \\ &= \int dx[\phi_{\frac{1}{2}h} - \phi_{-\frac{1}{2}h}] \end{aligned}\right\} \qquad (3)$$

From (2), however, the value of w on the line $y = \frac{1}{2}h$ is

$$\begin{aligned} w &= -\frac{\iota\kappa}{4\pi}\log\frac{\vartheta_1(\frac{1}{2}\iota h - x - s/b)}{\vartheta_1(\frac{1}{2}\iota h - x + s/b)} + \iota B\,(x + \iota\tfrac{1}{2}h) \\ &= -\frac{\iota\kappa}{4\pi}\log\frac{\exp\,[-\,\iota\pi\,(x - s/b)]\,\vartheta_4\,(x - s/b)}{\exp\,[-\,\iota\pi\,(x + s/b)]\,\vartheta_4\,(s + s/b)} + \iota Bx - \tfrac{1}{2}Bh \\ &= \left(\frac{\kappa s}{2b} - \frac{Bh}{2}\right) - \frac{\iota\kappa}{4\pi}\log\frac{\vartheta_4\,(x - s/b)}{\vartheta_4\,(x + s/b)}, \end{aligned}$$

where τ, the ratio of the periods of the ϑ functions, is equal to $\iota h/b$, so that

$$\phi_{\frac{1}{2}h} = \left(\frac{1}{2}\frac{\kappa s}{b} - \tfrac{1}{2}Bh\right) \qquad (4)$$

Similarly

$$\phi_{-\frac{1}{2}h} = -\left(\frac{1}{2}\frac{\kappa s}{b} - \tfrac{1}{2}Bh\right), \qquad (4\text{A})$$

and finally

$$M_y = b\left[\frac{\kappa s}{b} - Bh\right] = [\kappa s - Bhb] \qquad (5)$$

As h and b become very big the quantity $[\kappa s - Bhb]$ must tend to the momentum associated with

$$-\frac{\iota\kappa}{4\pi}\log\left(\frac{z-s}{z+s}\right), \qquad (6)$$

and it must be independent of the way in which b and h tend to infinity. This momentum is obtained as follows :—

Let us put

$$z - s = re^{i\theta}, \qquad z + s = r_1 e^{i\theta_1},$$

where

$$r^2 = (x - s)^2 + y^2, \qquad r_1{}^2 = (x + s)^2 + y^2,$$

$$\theta = \tan^{-1} y/(x - s), \qquad \theta_1 = \tan^{-1} y/(x + s),$$

and then ϕ, the velocity potential at the point z, is

$$\phi = \frac{\kappa}{4\pi}(\theta - \theta_1) = \frac{\kappa}{4\pi}\left[\tan^{-1}\frac{y}{x - s} - \tan^{-1}\frac{y}{x + s}\right]$$

$$= \frac{\kappa}{4\pi}\tan^{-1}\frac{2ys}{x^2 + y^2 - s^2}.$$

If the polar co-ordinates of the point z are R and ε, we get

$$\phi = \frac{\kappa}{4\pi}\tan^{-1}\frac{2s\mathrm{R}\sin\varepsilon}{\mathrm{R}^2 - s^2}$$

$$\rightarrow \frac{\kappa s}{2\pi\mathrm{R}}\sin\varepsilon,$$

when R is very big in relation to s. Hence the momentum of the system is

$$\mathrm{M}'_y = \int\limits_{x=-\infty}^{x=\infty}\int\limits_{y=-\infty}^{y=\infty}\frac{\partial\phi}{\partial y}\,dx\,dy = \int\limits_{x=-\infty}^{x=\infty} dx\,[\phi]_{y\to-\infty}^{y\to\infty}$$

$$= \mathop{\mathrm{Lt}}_{\mathrm{R}\to\infty}\int dx\left(\frac{\kappa s}{\pi\mathrm{R}}\sin\varepsilon\right),$$

where we have integrated along a line parallel to the y-axis, from $-\infty$ to $+\infty$. If now we put $x = \mathrm{R}\cos\varepsilon$, we get

$$\mathrm{M}'_y = \mathop{\mathrm{Lt}}_{\mathrm{R}\to\infty}\int_{\pi}^{0}(-\mathrm{R}\sin\varepsilon\,d\varepsilon)\;\frac{\kappa s}{\pi\mathrm{R}}\sin\varepsilon$$

$$= \frac{2\kappa s}{\pi}\int_0^{\frac{1}{2}\pi}\sin^2\varepsilon\,d\varepsilon = \tfrac{1}{2}\kappa s \tag{7}$$

Hence from (5)

$$[\kappa s - \mathrm{B}hb] \rightarrow \tfrac{1}{2}\kappa s$$

and must be independent of the way in which (hb) tends to infinity. Therefore

$$\mathrm{B} = \frac{\kappa s}{2hb}(\Gamma), \tag{8}$$

where Γ is a non-dimensional function of h and b, that is a function of (h/b), which tends to the limit 1 as h and b become infinite, and yet is independent of the manner in which h and b tend to infinity. There is only one possibility and that is $\Gamma = 1$ The final result is therefore

$$\left.\begin{aligned} w &= -\frac{\iota\kappa}{4\pi}\log\frac{\vartheta_1(z - s/b)}{\vartheta_1(z + s/b)} + \frac{\iota\kappa s}{2hb}\,z, \\ &= -\frac{\iota\kappa}{4\pi}\log\frac{\vartheta_1(z - s/\iota h)}{\vartheta_1(z + s/\iota h)} - \frac{\iota\kappa s}{2hb}\,z, \end{aligned}\right\} \qquad (9)$$

where $q = e^{-\pi\lambda}$ in the first expression and $q_1 = e^{-\pi/\lambda}$ in the second This leads to the result

$$\left.\begin{aligned} \delta_4 &= -\tfrac{1}{4} + \frac{\pi\lambda}{12} - 2\pi\lambda\,\Sigma\frac{p}{e^{2p\pi\lambda} - 1}, \\ &= \tfrac{1}{4} - \frac{\pi}{12\lambda} + \frac{2\pi}{\lambda}\Sigma\frac{p}{e^{2p\pi/\lambda} - 1}, \end{aligned}\right\} \qquad (10)$$

and in particular $\delta_4 = 0$ when $\lambda = 1$

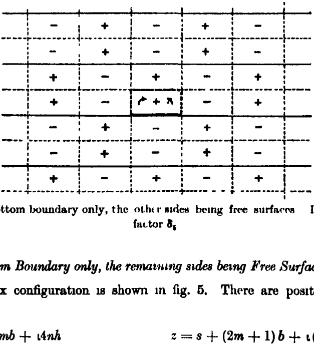

FIG 5.—Bottom boundary only, the other sides being free surfaces Interference factor δ_5

6 *Bottom Boundary only, the remaining sides being Free Surfaces* (δ_5).

The vortex configuration is shown in fig. 5. There are positive vortices at:—

$$\begin{array}{ll} z = s + 2mb + \iota 4nh & z = s + (2m+1)b + \iota(4n+2)h \\ z = -s + (2m+1)b + \iota 4nh & z = -s + 2mb + \iota(4n+2)h \\ z = s + 2mb + \iota(4n+1)h & z = s + (2m+1)b + \iota(4n+3)h \\ z = -s + (2m+1)b + \iota(4n+1)h & z = -s + 2mb + \iota(4n+3)h, \end{array}$$

and negative vortices at points obtained by putting $-s$ for s in the above expressions The complex potential function is

$$-\frac{\iota\kappa}{4\pi}\log\,[\mathrm{FF}_1]_{q\to e^{2\pi\lambda}},$$

where

$$\mathrm{F}=\frac{\vartheta_1(z-s/2b)\,\vartheta_2(z+s/2b)\,\vartheta_3(z-s/2b)\,\vartheta_4(z+s/2b)}{\vartheta_1(z+s/2b)\,\vartheta_2(z-s/2b)\,\vartheta_3(z+s/2b)\,\vartheta_4(z-s/2b)},$$

$$\mathrm{F}_1=\frac{\vartheta_1\left(\frac{1}{2}\frac{z-s}{b}-\frac{1}{4}\tau\right)\vartheta_2\left(\frac{1}{2}\frac{z+s}{b}-\frac{1}{4}\tau\right)\vartheta_3\left(\frac{1}{2}\frac{z-s}{b}-\frac{1}{4}\tau\right)\vartheta_4\left(\frac{1}{2}\frac{z+s}{b}-\frac{1}{4}\tau\right)}{\vartheta_1\left(\frac{1}{2}\frac{z+s}{b}-\frac{1}{4}\tau\right)\vartheta_2\left(\frac{1}{2}\frac{z-s}{b}-\frac{1}{4}\tau\right)\vartheta_3\left(\frac{1}{2}\frac{z+s}{b}-\frac{1}{4}\tau\right)\vartheta_4\left(\frac{1}{2}\frac{z-s}{b}-\frac{1}{4}\tau\right)}$$

The velocity at the origin $z=0$ is

$$-\frac{\iota\kappa}{4\pi}\left[\frac{\mathrm{F}'}{\mathrm{F}}+\frac{\mathrm{F}'_1}{\mathrm{F}_1}\right]_{z=0}$$

but the value of $\mathrm{F}'_1/\mathrm{F}_1$ at $z=0$ is of the second order in s, and can therefore be neglected Finally we get that

$$\left.\begin{aligned}\delta_5&=\pi\lambda\left[-\frac{1}{24}+\Sigma\frac{2p-1}{e^{2(2p-1)\pi\lambda}+1}\right],\\&=\frac{\pi}{4\lambda}\left[\frac{1}{24}-\Sigma\frac{(2p-1)}{e^{(2p-1)\pi/2\lambda}+1}\right],\\&=\tfrac{1}{2}\delta_3(2\lambda),\end{aligned}\right\}\qquad(1)$$

and in particular $\delta_5=0$ when $\lambda=0\cdot5$

The results are embodied in the following table -

$\lambda=h/b$	δ_1	δ_2	δ_3	δ_4	δ_5
0·1	1·309	−2·618	1·309	−2·368	0·327
0·125	1·047	2·094	1·047	1·844	0·262
0·250	0·524	−1·047	0·524	−0·797	0·125
0·333	0·393	−0·786	0·393	0·535	0·077
0·500	0·274	0·524	0·250	−0·274	0·000
1·000	0·274	−0·274	0·000	0·000	0·125
2·000	0·524	−0·274	−0·250	0·274	−0·262
3·000	0·785	0·393	−0·393	0·535	−0·393
4·000	1·047	−0·524	−0·524	0·797	−0·524

Fig. 6 shows these results in diagrammatic form.

7 *Glauert's General Theorem on Wind-Tunnel Interference*

The results obtained in the previous pages concerning the values of δ_2, δ_3 and δ_4 for small aerofoils are covered by Glauert's general theorem on wind-tunnel interference, and are in complete agreement with it The theorem* as originally stated is "The interference on a very small aerofoil in an open tunnel of any shape is of the same magnitude, but opposite in sign, as that on the same aerofoil, rotated through a right angle, in a closed tunnel of the same shape," and it was proved for wind-tunnels which were either entirely closed or entirely open The result of this paper is to show that the theorem is true also, in the particular cases considered, even when the tunnel is partially "closed" and partially "open," and Mr Glauert has stated in a recent letter that an extension of his method proves the following more general theorem :—

"The interference on a very small aerofoil in a tunnel, whose boundaries are partly rigid walls and partly free surfaces, is of the same magnitude but opposite in sign, as that on the same aerofoil rotated through a right angle in a tunnel

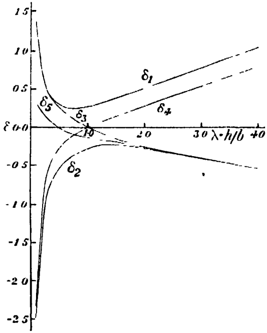

FIG 6 —Diagram showing the variation of δ with λ ([height/breadth] of tunnel)

of the same shape as the previous one but where rigid walls replace free surfaces, and free surfaces replace rigid walls "

---

* 'R and M,' No. 1470 (1932).

From this it becomes immediately clear that

$$\delta_2(\lambda) = -\delta_1(1/\lambda), \qquad \delta_3(\lambda) = -\delta_3(1/\lambda), \qquad \delta_4(\lambda) = -\delta_4(1/\lambda),$$

and proves incidentally that $\delta_3(1) = \delta_4(1) = 0$. In Theodorsen's paper $\delta_4(1)$ was not equal to zero, and it was this fact which led Mr. Glauert to suspect the validity of his results

8 *Summary*

This paper discusses the validity of the approximate method of determining the interference on aerofoils due to wind-tunnels The correct solutions of various cases recently investigated by Theodorsen are given and are illustrated by diagrams and tables

---

The Inelastic Scattering of Slow Electrons in Gases —III

By F H Nicoll, M Sc, Trinity College, Cambridge, 1851 Exhibitioner, University of Saskatchewan, and C B O Mohr, B A, M Sc, 1851 Exhibitioner, University of Melbourne

(Communicated by Lord Rutherford, O M, F R S —Received May 23, 1933)

Introduction

The subject of electron scattering in gases has received considerable attention within the last four years, and the very interesting results obtained have greatly assisted the wave mechanical study of collision processes The investigation of the angular distribution of the scattered electrons has proved particularly valuable The elastic scattering* has been studied systematically in a number of gases over a wide range of velocities and angles of scattering The inelastic scattering, however, has not been so exhaustively studied, the measurements in general being limited to small angles of scattering (less than 60°) and to high velocities of impact (above 50 volts) Recently Hughes and McMillen† have investigated the inelastic scattering of 25-, 35-, and 50-volt electrons in hydrogen for angles of scattering between 10° and 165°; the curves were found to rise slightly at large angles. Tate and Palmer,[*] and Hughes and McMillen[†] have measured the angular distribution of electrons which have been ejected from the atom with only a few volts energy; the curves obtained were on the whole fairly flat, although the latter observers find in some experiments sharp peaks at large angles.

---

* For a list of all the papers on this subject, *vide* Childs and Massey, 'Proc Roy Soc,' A, vol 141, p 473 (1933).

† 'Phys Rev,' vol 41, p. 39 (1932)

In two previous papers,[‡] the angular distribution of inelastically scattered electrons which have lost a discrete amount of energy were investigated in several gases for large angles of scattering, and for electrons with energies greater than about 40 volts At large angles, diffraction maxima and minima were found similar to those which occur for the elastic scattering, although the similarity between the two sets of curves was less marked at the lower velocities The present work was therefore undertaken to investigate this more interesting region While the previous apparatus proved entirely satisfactory for the purposes for which it was used, it was found that at low velocities, troubles due to intensity and "background" indicated that it was desirable to construct an apparatus in which every possible precaution was taken to avoid these difficulties.

In the present paper, experiments on the inelastic scattering are described in which the measurements were extended down to about 3 volts above the excitation potential of the gas atom, and over the angular range 10° to 155°

Description of the Apparatus

The apparatus used in these experiments is shown in fig 1 The end view of the apparatus is similar to that of the previous apparatus as shown in

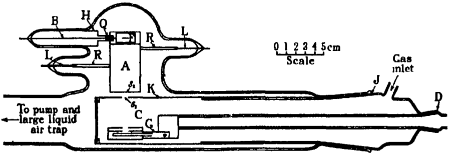

FIG. 1.—Diagram of apparatus.

---

[*] 'Phys. Rev.,' vol. 40, p. 731 (1932).

[†] 'Phys. Rev.,' vol. 39, p. 585 (1932), vol 41, p. 39 (1932).

[‡] I, 'Proc. Roy. Soc.,' A, vol. 138, p. 229 (1932); II, *ibid*, p. 469.

fig. 1A of I. The essential parts of the apparatus are the cylindrical chamber C in which the electron collisions occurred, and the analyser A in which the scattered electrons of various energies were separated

The electron gun G consisted of a filament and case containing two slits 6 mm. apart, the outer slit being 1·1 × 6 mm and the inner slit 0·47 × 6 mm ; the gun was supported by the ground-glass joint D and so could be rotated about the axis of the scattering chamber.

The electrons scattered at the centre of the collision chamber C passed through two slits, S_1 (0 27 × 8 mm) in the side of the cylinder K, and S_2 (0·4 × 5 mm.) on the front of the analyser about 7 mm distant from S_1 The electrons then passed between the curved plates of the electrostatic analyser A, and finally entered the Faraday cylinder F through a slit (0 6 × 5 mm).

The apparatus was designed so that the chamber containing the analyser could be evacuated to the lowest possible pressure, while a considerably higher pressure of gas was maintained in the scattering space To accomplish this, the inner part of the large ground-glass joint J was extended inwards, and a tightly-fitting copper can K slipped over this extension The pumping speed was sufficiently great to maintain a large pressure difference between the two sides of the slit S_1 This arrangement has great advantages over the usual method in which a sealed-in " pumping slit " separates the scattering and analysing chambers The final alignment of the slit S_1, when the apparatus is evacuated, may easily be effected by optical means, using the light from the filament of the gun, and when this was done it was found that maximum intensity of scattered electrons was secured The copper can K could easily be removed in order to replace the filament

The analyser A was constructed from two cylindrically-curved plates, 0·4 mm thick and 3 cm wide, accurately turned from a piece of duralumin , these plates were held a uniform distance of 1·3 cm. apart by two thin side plates of copper screwed to the duralumin by small screws, and insulated by means of small pieces of thin mica. The inner surfaces of the curved plates of the analyser had radii of 2·5 and 3·8 cm. respectively

The Faraday cylinder F was rigidly supported inside a copper shield by a small piece of quartz tubing Q, the copper case being attached to one end of the analyser. The lead B to the Faraday cylinder passed inside a metal shield H to a tungsten-glass seal The complete analysing system was supported within its glass envelope by two rigid copper rods R, which screwed into the two plates and were hard-soldered to 1 mm. tungsten wires at the other end.

In order to assemble the apparatus, the analyser was passed through the large ground joint, and when approximately in position the rods R were screwed tightly into the plates. The analyser was then firmly supported by the thick tungsten leads L in such a position that the plane through the axis of rotation of the gun and the front slit of the analyser was perpendicular to the front end of the analyser The glass was then sealed on to the two tungsten leads

The electrical connections were the same as in fig 1B of I. The slit S_2, the copper plates on the two sides of the analyser, the Faraday cylinder case, and the metal shield H were all connected together electrically and earthed. A suitable potential was usually placed between the slits S_2 and S_1 in order to accelerate electrons entering the analyser to such a velocity that the earth's field had no appreciable effect on the path of the electrons in the analyser. A retarding potential of a few volts was placed between the Faraday cylinder and its case in order to reject slow secondary electrons from the slit of the Faraday cylinder case and elsewhere. The number of stray secondary electrons was reduced by sooting all surfaces with which electrons were likely to come into contact. The current collected by the Faraday cylinder was measured by the rate of drift of a Compton electrometer working at the comparatively low sensitivity of 500 divisions per volt.

The apparatus was connected, as shown in fig 1, through a short length of 5 cm. tubing to a large steel liquid air trap placed immediately over a four-stage mercury pump backed by a Hyvac oil pump The liquid air trap was designed so as to permit maximum pumping speed consistent with the maintenance of a low pressure of mercury vapour in the apparatus With this arrangement it was possible to use pressures of gas as high as 10^{-2} mm. Hg in the scattering chamber, while the analyser could be maintained at a pressure of less than 10^{-5} mm. Hg

The whole system—scattering chamber and analyser—was enclosed in a pyrex vessel, and the whole apparatus, with the exception of the ground joint, could be baked at a temperature of 450° in order to remove mercury vapour and outgas the metal parts of the apparatus.

The dimensions of the slits in the apparatus and their separations were such that the angular resolution was higher than that obtained in the previous apparatus, while the velocity resolution of the analyser was approximately the same.

The procedure was essentially the same as described in I and the same tests were made on the working of the apparatus. In particular the test of proportionality of the scattered current to the pressure of the gas was repeated carefully, since the absence of gas in the analyser permitted a more satisfactory test to be made.

Results.

The investigations consisted of measurements of the angular distribution of scattered electrons which have lost a discrete amount of energy in raising the atom or molecule to the most probable excited state The main inelastic losses in hydrogen, helium, and argon correspond to energy losses of 12·6, 21·1 and 11·6 volts respectively.

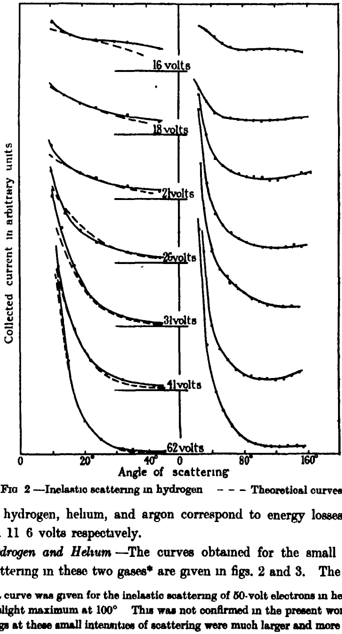

FIG 2 —Inelastic scattering in hydrogen - - - Theoretical curves

(*a*) *Hydrogen and Helium* —The curves obtained for the small and large angle scattering in these two gases* are given in figs. 2 and 3. The scattered intensity falls off very rapidly with increasing angle at the higher velocities, and so cannot conveniently be plotted on the same scale over the entire angular range investigated Theoretical curves are also shown for purposes of comparison, the two sets of curves being arbitrarily fitted together at one point

---

* In I, a curve was given for the inelastic scattering of 50-volt electrons in helium which showed a slight maximum at 100° This was not confirmed in the present work in which the readings at these small intensities of scattering were much larger and more accurate.

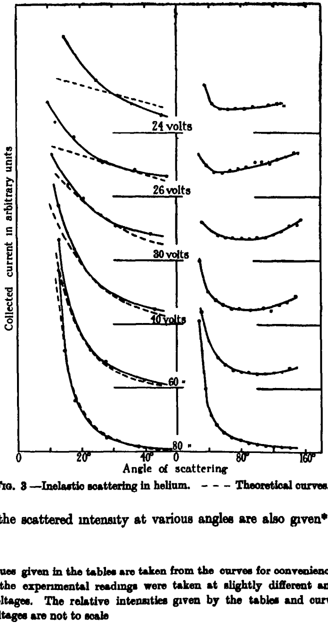

FIG. 3 —Inelastic scattering in helium. - - - Theoretical curves.

Values of the scattered intensity at various angles are also given* in Tables I and II.

---

* The values given in the tables are taken from the curves for convenience in tabulation, since the experimental readings were taken at slightly different angles at the different voltages. The relative intensities given by the tables and curves for the different voltages are not to scale

Table I.—Hydrogen.

Angle	16 volts	18 volts.	21 volts.	26 volts	31 volts	41 volts	62 volts.
°							
10	100	100	100	100	100	100	100
15	65	65	60	52	49	38	30
20	54	53	50	32	25	19	10 7
25	53	45	35	21	14	9 9	4 7
30	51	38	30	15	8 0	5 8	2 3
40	48	26	18	8 1	3 7	2 7	1 96
50	38	19	14	5 8	3 0	1 72	0 84
60	32	17	11	4 4	2 5	1 23	0 56
70	29	15	10	3 5	2 0	0 88	0 37
80	28	14	9	2 8	1 7	0 70	0 24
90	28	14	8	2 4	1 4	0 56	0 16
100	27	14	8	2 1	1 2	0 50	0 14
110	27	14	8	1 9	1 0	0 47	0 13
120	27	14	7	1 9	1 0	0 45	0 12
130	27	15	8	2 0	1 0	0 49	0 12
140	26	16	9	2 1	1 0	0 60	0 12
150	26	17	10	2 1	1 0	0 80	0 12

Table II.—Helium.

Angle	24 volts	26 volts	30 volts.	40 volts.	60 volts	80 volts.
°						
10	100	100	100	100	100	100
15	79	77	74	67	62	43
20	57	58	57	44	31	19
25	43	45	45	28	19	9 6
30	32	37	33	20	12	5 2
40	20	27	24	12	4 5	2 2
50	14	23	21	9	3 0	1 4
60	13	22	18	7	2 2	1 0
70	13	23	17	6	1 8	0 78
80	13	26	17	6	1 6	0 60
90	14	28	17	6	1 5	0 48
100	14	29	18	6	1 4	0 37
110	15	31	18	7	1 4	0 32
120	16	33	19	7	1 5	0 27
130	16	35	21	8	1 6	0 25
140	—	38	25	9	1 8	0 22
150	—	40	29	—	2 0	2 22

The form of the curves for hydrogen agrees quite well with that given by Hughes and McMillen (*loc. cit.*) for electrons of 25-, 35- and 50-volts energy, although there are slight differences at the smaller angles of scattering.

(*b*) *Argon.*—Angular distributions of electrons scattered inelastically in argon are illustrated in fig. 4 for small angles, and in fig. 5 for large angles of scattering, while the corresponding curves for the elastic scattering are also given for comparison. In addition, theoretical curves are given in fig. 4, and values of the observed scattered intensity at different angles in Table III. Hughes and McMillen* have given curves for the inelastic scattering of 100-volt and 50-volt electrons in argon for angles between 5° and 30°; their curves are less steep than ours. As pointed out in I, it is possible to explain the similarity between the elastic and inelastic scattering at large angles on the basis of double collisions, in which a large angle elastic collision is followed by a small angle inelastic collision with a second atom, or *vice versa*. This point

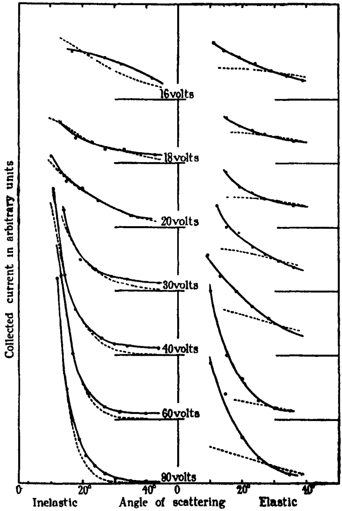

FIG. 4.—Small angle scattering in argon. - - - Theoretical curves.

---

* 'Phys. Rev.,' vol. 39, p. 585 (1932).

was tested more thoroughly with the present apparatus, since the tests were not complicated by the presence of gas in the analyser. The occurrence of double scattering may be disproved by showing proportionality of collected current to gas pressure. Tests were carried out at 110° for the inelastic scattering of 40-volt electrons. No departure from single scattering was found for pressures as high as eight times the pressure at which the angular distributions were obtained (about $0 \cdot 4 \times 10^{-3}$ mm. Hg.). Further, the ratio of the intensities at the maximum and minimum, at 110° and 85° respectively, remained exactly the same when the pressure was increased to the value referred to above

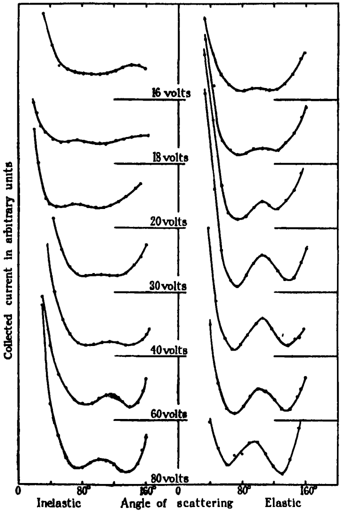

Fig. 5.—Large angle scattering in argon.

Table III —Argon.

Angle	16 volts.	18 volts.	20 volts.	30 volts.	40 volts	60 volts.	80 volts.
°							
10	100	100	100	100	100	100	100
15	94	60	62	53	40	33	25
20	88	41	47	27	19	12	9·2
25	80	28	37	17	10·5	5·8	3·7
30	71	24	23	12	6·5	3·9	1·9
40	47	17	13	6·3	3·3	2·4	0·85
50	31	15	11	3·7	1·9	1·4	0·52
60	25	15	11	2·1	1·1	0·98	0·27
70	22	16	13	1·4	0·64	0·66	0·18
80	21	16	13	1·1	0·45	0·54	0·18
90	21	15	12	1·2	0·45	0·54	0·22
100	21	14	11	1·3	0·51	0·71	0·27
110	22	14	12	1·3	0·57	0·82	0·25
120	23	15	13	1·2	0·58	0·82	0·22
130	25	16	16	1·3	0·49	0·61	0·14
140	27	18	20	1·6	0·42	0·44	0·14
150	27	19	24	2·3	0·52	0·57	0·23
160	—	19	—	3·5	0·89	1·30	0·50

(about 3 × 10^{-3} mm Hg). If there had been any trace of multiple scattering at the lower pressures, the ratio of the intensity at the maximum to that at the minimum would have increased towards the much greater value obtained for the elastic scattering curve Again, since the rise in the 40-volt inelastic curve near 160° is of about the same magnitude as the rise in the elastic curve, then, if the former were due to multiple scattering, the maximum at 110° would also be of the same magnitude as in the elastic curve. These arguments seem to indicate that the results for the inelastic scattering are due entirely to single scattering in the gas.

Discussion.

In discussing the results in the light of theory, it is convenient to treat the small and the large angle scattering separately since different effects are involved in each.

In the figures, the small angle scattering is compared with that obtained theoretically by the use of Born's formula * It is seen that the agreement with the experimental inelastic scattering curves is quite close at small angles, and even at voltages near the excitation potential. The small angle elastic

---

[*] To obtain these theoretical curves for hydrogen and helium, the well-known atomic wave functions were used (Massey and Mohr, 'Proc Roy. Soc.,' A, vol 132, p. 605 (1931)), while for argon approximate wave functions for the initial and final states were obtained by the use of simple rules given by Slater ('Phys. Rev.,' vol. 36, p. 57 (1930).

scattering curves in argon, however, are very much steeper than predicted by the simple Born formula. This effect has previously been pointed out for the elastic scattering in helium* and in argon† by Hughes and McMillen, they have shown that agreement with Born's formula is reached only for electron energies of over 400 volts This is in strong contrast to the inelastic scattering.

At large angles, Born's theory gives an angular distribution falling off monotonically to smaller and smaller values. As we have seen, however, the angular distributions exhibit maxima and minima for the heavier elements, or are fairly flat for hydrogen and helium, the cause of both effects being the same.

The similarity between the inelastic and elastic angular distributions may be explained on the basis of double collisions with the *same* atom, thus an 80-volt electron passing through argon may undergo an inelastic collision with an argon atom, being in all probability little deviated by the process, this electron, now possessing 68·4-volts energy, may be diffracted before it has left the field of the atom as if it were an incident electron of 68·4-volts energy Since the velocity of the incident electrons is large compared with the excitation potential of the atom, the large angle elastic scattering of the electrons by the excited atom will be similar to that by the normal atom, since the scattering comes mainly from the inner shells, as was shown in II. Now the reverse process may also take place in which the large angle elastic collision occurs before the small angle inelastic collision with the same atom The distribution of the inelastic scattering of 80-volt electrons at large angles would thus show the characteristics present in the distributions both of 80-volt and 68·4-volt electrons scattered elastically in argon.

At lower velocities, however, the energy lost in exciting the atom is comparable with the energy of the incident electrons, and the scattering by the normal and by the excited atom is no longer similar, the outer shell of the atom now being effective in the scattering, the diffraction effects in the inelastic angular distributions therefore begin to differ from those appearing in the elastic angular distributions.

This idea of double collisions with the same atom also accounts for the fact that the angular distribution of the elastic scattering is much steeper at small angles than that expected from the Born theory. The incident electron first makes an inelastic collision (probably with little deviation) in which the atom is raised to an excited state: the atom then returns to its normal state and the energy is transferred back to the electron before it leaves the atom. The electron thus leaves the atom with its original energy, but the distribution of the scattering of such electrons at small angles will be similar to that for the inelastic scattering, and will thus be steeper than that given by Born's formula for the elastic scattering This explanation has a theoretical basis.* In short, one may say that the initial and excited states of the atom are closely coupled together, so that the inelastic and elastic angular distributions tend to follow each other at all angles.

---

* 'Phys. Rev.,' vol. 41, p. 154 (1932).

† 'Phys. Rev.,' vol. 39, p. 585 (1932).

The results for hydrogen and helium are of special interest for theory, as these light atoms are, of course, most easily treated It has been found† that the effect of electron exchange is of fundamental importance in explaining certain peculiarities—in particular, the appearance of a pronounced minimum—which occur in the angular distribution of the elastic scattering in helium at quite low voltages. Similar calculations‡ for the case of the inelastic scattering of 33-volt electrons in helium reveal peculiarities in the angular distribution if exchange is taken into account, but if the effect of exchange is not introduced, the angular distribution obtained is more nearly like that obtained experimentally. This seems to indicate that the effect of exchange on inelastic collisions is over-estimated by the present theory, this is further evident from the fact that the calculations indicate too large values for inelastic cross-sections at low velocities, especially for the cross-section for triplet excitation which can occur only by electron exchange While the theory is admittedly not very accurate at such low velocities, in any case it seems likely on general grounds that if the contribution to inelastic scattering due to exchanged electrons is comparable with that due to non-exchanged electrons, peculiarities will appear in the angular distributions of slow inelastically scattered electrons just as they do for the elastic scattering The fact that the observed angular distributions for electrons with energies close to the excitation potential do not reveal any peculiar features seems to indicate that electron exchange probably does not play any important part in inelastic scattering for the excitation of optically allowed levels.

A puzzling feature, however, is that while the distribution of the inelastic scattering at small angles (between 10° and 30°) is given fairly well by Born's formula and is *larger* than predicted by the latter at large angles, the observed total cross-section is *smaller* than that given by Born's formula at low velocities. This might be accounted for if the inelastic scattering at even smaller angles (less than 10°) were much less than given by Born's formula Alternatively, it is possible that the absolute magnitude of the observed scattering is less than that given by the theory, although the form of the curves is the same at small angles.

---

* Massey and Mohr,' 'Proc. Roy. Soc.,' A, vol. 140, p. 613 (1933).

† *Eadem*, 'Proc. Roy Soc.,' A, vol. 136, p. 289 (1932).

‡ *Eadem*, 'Proc. Roy. Soc.,' A, vol. 139, p. 187 (1933).

Experiments are in progress with other gases.

In conclusion, it is a pleasure to thank Lord Rutherford and Dr J. Chadwick for their interest in the work.

Summary.

An apparatus has been constructed, similar to that described in a previous paper, but specially designed for work with electrons whose energies lie within a few volts of the excitation potential. Results have been obtained for the inelastic scattering of electrons in hydrogen, helium, and argon, the results covering an angular range of 10° to 155° and a range of seven voltages between about 80 volts and about 3 volts above the excitation potential.

The curves for the inelastic scattering in argon show diffraction effects at large angles which are similar to those which appear in the elastic scattering, but which disappear as the energy of the electrons approaches the excitation potential of the gas. The curves for hydrogen and helium do not exhibit any unusual features for low velocity electrons, and the significance of the curves is discussed. Unlike the elastic scattering, the inelastic scattering at small angles (between 10° and 30°) is seen to agree in form fairly well with that given by the Born formula down to relatively low velocities.

An X-Ray Study of p-*Diphenylbenzene.*

By Lucy W. Pickett, M.A., Ph.D.

(Communicated by Sir William Bragg, O.M., F.R.S.—Received June 2, 1933.)

There have been very few complete structure determinations of aromatic compounds which contain more than one benzene nucleus. Robertson[*] has recently presented conclusive evidence that the anthracene molecule is a planar configuration of carbon atoms 1.41 A apart. Dhar[†] has shown that the molecule of diphenyl consists of two planar hexagons of carbon atoms of a spacing of 1·42 A with a probable distance of 1.48 A. between the nuclei. The present paper describes the analysis of a compound containing three benzene nuclei, *p*-diphenylbenzene ($C_{18}H_{14}$).[‡] No data by other investigators upon the crystal form or structure of this compound have been found.

Experimental.

p-diphenylbenzene, a colourless substance melting at 211°, was obtained from the Eastman Kodak Company and purified[§] by repeated crystallization from benzene and spectroscopically pure hexane. It crystallizes from benzene in thin plates and from alcohol in minute monoclinic tablets which exhibit {001}, {110} and occasionally {201} forms. The following angles were measured with the reflecting goniometer :—

$$(110) \cdot (1\bar{1}0) = 69^\circ\ 30'$$
$$(001) : (110) = 88^\circ\ 51'$$
$$(001) : (201) = 71^\circ\ 34'$$

Examination with the polarizing microscope showed that the crystal is biaxial and optically positive. The (010) plane contains the optic axes; the acute bisectrix which is the vibration direction of the slow ray, is in the direction now known to be that of the length of the molecule.

A well-formed crystal weighing 0·035 mg. was used for most of the X-ray measurements. The following dimensions of the unit cell were determined from rotation photographs taken with copper radiation which was calibrated with mica of known spacing

---

[*] 'Proc. Roy. Soc.,' A, vol. 140, p. 79 (1933).

[†] 'Indian J. Phys.,' vol. 7, p. 43 (1932).

[‡] Pickett, 'Nature,' vol. 131, p. 513 (1933).

[§] The material used was purified by Miss Gertrude Walter of Mount Holyoke College and crystallized by Dr. Gilchrist of this laboratory.

$$a = 8{\cdot}08 \text{ A.} \qquad b = 5{\cdot}60 \text{ A.} \qquad c = 13{\cdot}59 \text{ A.}$$
$$\beta = 91^\circ\ 55'.$$

The density of 1·213, measured by a flotation method, confirmed the number of molecules in the unit cell as two (calculated value 1·987) Although reflections of other planes up to and including the indices $h = 6$, $k = 5$, $l = 10$ were observed, no reflections ($h0l$) where h is odd or ($0k0$) where k is odd were found This indicates that the space group is $P\,2_1/a$ of the monoclinic prismatic class.

The photographs which were used for intensity measurements were taken by means of a Weissenberg camera with the use of filtered copper radiation. The intensity of the reflections thus obtained was measured upon the integrating photometer designed by Dr Robinson[*] By these means the integrated intensities, on a relative scale, of all the measurable reflections for the three principal zones of the crystal and some of those from general planes were obtained. The small size of the crystal increased the accuracy of these measurements in that errors due to absorption of the radiation in the crystal were minimized but was a disadvantage in that it was not possible to get reflections of measurable intensity from the very weak planes. Some photographs were taken with the very intense beam from the X-ray tube with a rotating target designed by Dr. Muller[†] The accuracy of the intensity data is considered to be about 10% although it is probable that it is greater than this for reflections of moderate intensity and less for those of very large or very small values

Determination of Structure.

The analogy between this compound and diphenyl, whose structure as determined by X-ray methods has been published by Dhar (*loc cit*) is apparent not only in form, optical properties and unit cell dimensions but also in the intensities of corresponding reflections This suggested that a similarity of structure exists in the two compounds. Dhar based his analysis upon the results of Krishnan[‡] who showed from magnetic susceptibility measurements that the molecules are tilted at angles of + and − 59° from the plane

---

[*] 'J. Sci. Intruments' (*in the press*).

[†] 'Nature,' vol 124, p. 128 (1929); 'Brit. J. Radiology,' vol. 4, p 127 (1931).

[‡] 'Nature,' vol. 130, p. 313 (1932); 'Phil. Trans.,' A, vol. 231, p. 235 (1933).

of symmetry and 20·1° from the *c* axis. Dhar demonstrated that by placing planar molecules in the *bc* plane with their centres at the co-ordinates (0, 0, 0) and ($\frac{1}{2}$, $\frac{1}{2}$, 0) and rotating them 32° about the *c* axis and 20° about the *b* axis he obtained a structure whose calculated structure factors agreed with the experimental ones The molecule lies in the obtuse angle between the *a* and *c* axes

With diphenylbenzene it was obvious that the molecule lies in the acute angle both from the very great strength of the (201) reflection and from the fact that the (*h*0*l*) reflections of the one compound are comparable to the ($h0\bar{l}$) reflections of the other In order to test the analogy a planar molecule of *p*-diphenylbenzene was assumed and placed in a position corresponding to that occupied by diphenyl. The agreement between the calculated and observed structure factors while not perfect did indicate that the position could not be far from the correct one

A systematic study of the structure possibilities of *p*-diphenylbenzene was then begun. The chemical formula shows three benzene rings joined in the para position The analysis of hexamethylbenzene by Mrs. Lonsdale* and of anthracene† has established the fact that the benzene ring in these compounds is planar Diphenyl‡ also has been shown to be planar and in the absence of contrary evidence the assumption that the benzene nuclei in this compound are planar was considered to be justified. The question then arose as to the orientation of the three nuclei with respect to each other. Space group considerations limit the possible configurations to those which are centrosymmetrical.§ Hence there are three possibilities. the molecule is planar, the two end rings are rotated about the line of centres with respect to the middle ring or the line of centres is bent The distance between the carbon atoms of the nucleus might be safely assumed to be 1·42 A, but the distance between the nuclei was uncertain. The positions of the molecule as a whole were not known but if their centres were at the symmetry centres (0, 0, 0) and ($\frac{1}{2}$, $\frac{1}{2}$, 0) all possible orientations in space could be covered by a combination of successive rotations about three perpendicular directions

The preliminary analysis described above showed that the molecule was not likely to be greatly different in form or position from that first postulated. Furthermore, the comparison of the axial lengths of diphenyl, *p*-diphenylbenzene and *p*-diphenyldiphenyl* showed that each added phenyl group increased the *c* axis by 4·1 A. Since this distance must represent the projection of the length of one benzene ring on the *c* axis it would follow that the molecule is inclined at an angle of 15°–20° to this axis.

---

* 'Proc. Roy. Soc.,' A, vol. 123, p. 494 (1929).

† Robertson, *loc. cit.*;

‡ Dhar, *loc. cit.*

§ Astbury and Yardley, 'Phil. Trans.,' A, vol. 224, p. 221 (1924).

The method of analysis used in the work was as follows. A certain configuration of the molecule was assumed tentatively. This was placed in the (100) plane with its length parallel to the *c* axis and its co-ordinates noted. It was then rotated through an angle of θ about the *c* axis with the direction *b* to *a* taken as positive, next through an angle of ϕ about the *b* axis (direction *a* to *c* considered positive) and finally through an angle ψ about the perpendicular to the (100) plane (*c* to *b* as positive). The successive changes of the co-ordinates in these transformations may be represented by the following equations :—

For rotation of θ about *c*

$$x_1 = x \cos \theta + y \sin \theta$$
$$y_1 = y \cos \theta - x \sin \theta$$
$$z_1 = z.$$

For rotation of ϕ about *b*

$$x_2 = x_1 \cos \phi - z_1 \sin \phi$$
$$y_2 = y_1$$
$$z_2 = z_1 \cos \phi + x_1 \sin \phi.$$

For rotation of ψ about direction normal to (100) plane

$$x_3 = x_2$$
$$y_3 = y_2 \cos \psi + z_2 \sin \psi$$
$$z_3 = z_2 \cos \psi - y_2 \sin \psi.$$

These equations may be combined for convenience. The results were then transformed from rectangular to axial co-ordinates by the use of the relations

$$x_4 = x_3/\sin \beta$$
$$y_4 = y_3$$
$$z_4 = z_3 - x_3 \cot \beta$$

followed by division by the respective axial lengths.

---

* Pickett, *loc. cit.*

The structure factor for the space group under consideration has been simplified to the form

$$F = 4\Sigma\, F_C \cos 2\pi\left(hx + lz + \frac{h+k}{4}\right) \cos 2\pi\left(ky - \frac{h+k}{4}\right),$$

where F_C represents the scattering power of carbon The effect of the hydrogen atoms was ignored The summation was carried out over one crystal unit which consists of half a molecule or nine carbon atoms. Allowance was made for the decrease in the scattering power of carbon with increase in the angle of reflection according to the F curve constructed by Mrs Lonsdale from that observed in graphite The factors calculated in this way for assumed positions of the molecule were compared with those obtained from experimentally measured intensities through the relation

$$AF = \left(I \div \frac{1+\cos^2 2\theta}{\sin 2\theta}\right)^{\frac{1}{2}},$$

where I is the intensity and A is a constant

A planar molecule was tentatively adopted Inasmuch as the different orders of the (h00) planes are affected only by the first two rotations, agreement for these planes was first sought If h is even, $F/4 = F_C\,\Sigma \cos 2\pi hx$. The values of $\cos 2\pi hx$ were calculated for a variation of θ, ϕ being held constant, and for ϕ, θ being held constant These values are shown in graphical form in figs. 1 and 2 together with horizontal lines which for the (200) and (600) planes represent experimental values and for the (400), for which no reflection was observed, the upper possible limit It is obvious that the factors of these planes vary markedly with changes in ϕ and only slightly with changes of θ within a range of 15°, and that only two values of ϕ are probable, namely, at 15° and 21°. The latter figure was easily eliminated by a consideration of other planes.

The effect upon this position of maximum probability of varying the other factors such as the shape of the molecule and the distance between the rings was small.

The most favourable value of ψ was found by a similar method, using the planes (210) and (120), to be 0°. Less striking changes resulted from a variation of θ in the case of any of the planes studied. The value 34° was selected as giving the best agreement for a number of planes. In this way the angles chosen as representing the position of the molecule were $\theta = 34°$, $\phi = 15\cdot3°$ and $\psi = 0°$.

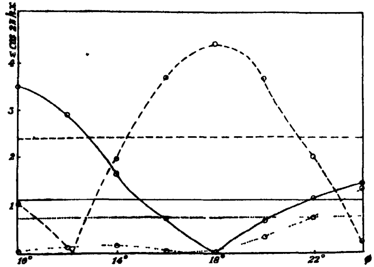

FIG 1 —— 200 plane ; . . 400 plane ; - - - 600 plane.

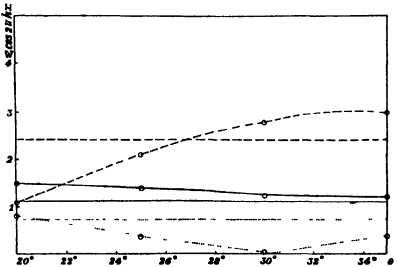

FIG. 2 —Variations of calculated structure factors with θ. —— 200 plane, ... 400 plane ; - - - 600 plane. Horizontal lines represent experimental values.

[FIGS. 1 and 2 —These diagrams illustrate the observed (relative) and calculated values of structure factor of the (200), (400) and (600) planes. The horizontal lines show the observed values except that in the case of (400), where the intensity was too small to measure, it represents the maximum below which the true value must lie. The corresponding curves show the calculated factors assuming various values for the angular tilt of the molecule Fig 1 shows that the variation with ϕ, the angle between the axis of the molecule and the c axis, is very marked and agrees with the observed values near 15°. Fig. 2 shows that the variation with θ is slight and that the values are within the limit of experimental error through a large range.]

In the early stages of the work it had been observed that the distance between the benzene nuclei most markedly affected the relative values of the structure factors of the (006) and (007) planes. These are accordingly thought to be sensitive tests of this difference and the placing of the molecule had purposely been accomplished by a very different set of planes, namely, those in the *hk*0 zone which were quite insensitive to this variation. The structure factors of these test planes calculated for internuclear distances of 1·54, 1·48 and 1·42 A were at this point compared with the experimental values. These results are given in Table I; it is seen that the distance which gives the relative values observed is 1·48 A.

Table I.—Values of $\Sigma \cos 2\pi lz$.

	(006).	(007)
Measured	2 72	3 35
Calculated—		
$> c - c < = 1\ 42$	2 13	3 29
$> c - c < = 1\ 48$	2 46	3 04
$> c - c < = 1\ 54$	2 75	2 64

The structure factors for all of the planes whose intensity had been measured were then calculated for a structure consisting of a planar molecule with distances of 1·42 A. between the carbon atoms of the ring and 1 48 A. between the rings, the position of the rings being defined by the angles given above. The results are tabulated in Table II and illustrated in fig. 3. The agreement

Table II —Measured and Calculated Values of the Structure Factors.

hkl	sin θ	F (obs.).	F (calc.)
001	0 056	13–16	+21 6
002	0 113	15–21	−24 1
011	0 148	<2 4	− 1 1
003	0·169	25–35	+41 0
012	0 178	<2 7	+ 2 5
013	0·219	11 6	−11 5
004	0 226	5 0	− 4 7
014	0 262	3 8	− 3 7
020	0 275	13 3	−11 0
021	0 281	<3 4	− 1·7
005	0 282	13 1	+11·4
022	0 297	6·1	+ 4 8
015	0·314	<3 7	0
023	0 322	28·5	−30·9
006	0 339	25 9	−23·6
024	0 355	17·5	−18 7
016	0·367	8 7	+ 4 9

Table II.—(continued).

hkl	sin θ	F (obs).	F (calc)
025	0 393	6 5	+ 8 0
007	0 396	27 4	−24 6
031	0 414	<4 5	0
017	0 418	15 6	+11 7
032	0 428	<4 6	− 0 4
026	0 436	6 4	− 6 4
033	0 445	<4·8	+ 1 7
008	0 452	5 4	+ 4 9
034	0 470	<5 0	+ 0 6
018	0 472	6 7	− 3 1
027	0 481	<5 1	+ 4 6
035	0 500	<5 2	0
009	0 508	<4 7	− 2 1
019	0 525	6 2	+ 5 7
028	0 528	<5 4	− 4 8
036	0 535	<5 4	− 1 0
040	0 550	12 2	+11 5
041	0 554	<5 5	+ 1 0
042	0 562	<5 6	− 0 3
0010	0 565	<5 6	− 2 9
037	0 571	<5 7	− 2 2
029	0 576	6 4	+ 6 1
043	0 577	7 5	− 5 9
0110	0 580	19 1	+20 6
044	0 594	<5 9	− 6 0
0210	0 626	23 9	+23 2
200	0 190	18 4	+19 4
$20\bar{1}$	0 197	14 8	−15 2
201	0 200	50–80	+89 0
$20\bar{2}$	0 219	20 7	+20 8
202	0 224	<5	+ 1 4
$20\bar{3}$	0 250	5 2	− 6 1
203	0 261	<5 6	− 0 9
$20\bar{4}$	0 290	10	−10 7
204	0 300	<6	− 5 0
$20\bar{5}$	0 332	23 2	−20 8
205	0 346	<6 5	− 8 9
400	0 380	<6 9	+ 2 9
$40\bar{1}$	0·383	12	−14 5
401	0 385	<7	− 1 7
$20\bar{6}$	0 386	33 7	−29 9
206	0 395	<7 1	+ 7 5
$40\bar{2}$	0 393	12	−14 5
402	0 399	<7 2	− 6·5
$40\bar{3}$	0·409	<7 3	+ 1 4
403	0 422	<7 5	+ 1 8
$40\bar{4}$	0 433	<7 6	− 9 0
$20\bar{7}$	0 435	7 6	+ 5 8
207	0 447	9 4	−10 3
404	0·447	<7 7	+ 0 5
$40\bar{5}$	0 463	<7 9	− 6·3
405	0 480	21·8	−24·3
$20\bar{8}$	0 484	<8 1	− 3·5
208	0 496	<8 2	− 1·3
$20\bar{9}$	0 537	12 4	−16 1
600	0 563	13	−15·0
$60\bar{1}$	0·568	13	−18·9
110	0·167	44–61	+69·8
210	0 238	12·9	−12·0

Table II—(continued).

hkl	sin *θ*	F (obs.)	F (calc.)
120	0·290	17·9	+18·6
310	0·318	6·0	+ 5·1
220	0·334	<5·5	+ 1·3
320	0·395	9·8	+ 8·3
410	0·406	10	+ 9·0
130	0·422	7·5	−11·5
230	0·452	<6·5	+ 2·1
420	0·470	<6·8	− 5·0
510	0·492	<7·0	− 1·4
330	0·501	<7·4	− 2·6
150	0·694	12·5	+19·8

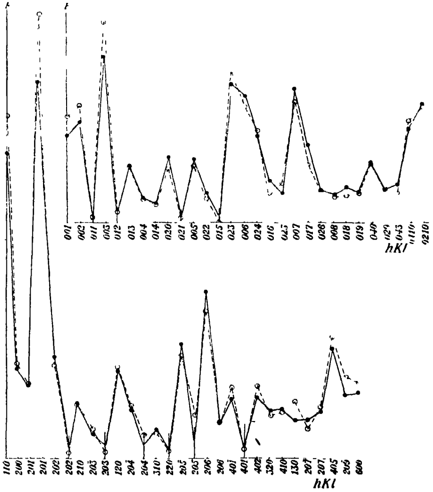

FIG. 3.—● observed; ○ calculated.

is considered to be within the limit of experimental error in all cases with the exception of the five strongest reflections which were noticeably low for the well-formed crystal used for most of the measurements. Photographs of poorer crystals yielded similar results for weaker planes and much larger values for these reflections Thus it is obvious that there are very appreciable extinction effects even in these minute crystals but that they become important only in the case of these five strong reflections The values as given are not corrected for this factor. It is not of particular consequence in the structure analysis because in the trial and error method the calculated structure factors for the planes in question are most insensitive to changes in the position of the molecules while in the Fourier analysis calculations showed that the contour lines were hardly affected.

Fourier Analysis of Results

A projection of the scattering matter of the unit cell upon a plane perpendicular to the a axis was then obtained through the method of the double Fourier series which has been developed and described by Bragg* The density of scattering matter per unit area, $\rho\,(y, z)$ for the projection along this axis is

$$\rho\,(y, z) = 1/bc \sum_{-\infty}^{+\infty} \sum_{-\infty}^{+\infty} \mathrm{F}\,(0kl) \cos 2\pi\,(ky/b + lz/c)$$

Table III gives the values and signs of the F terms used while Table IV gives the sums, $\mathrm{F}(0kl) \cos 2\pi(ky/b + lz/c)$, for a series of points approximately 0·2 A apart covering the area of projection of one crystal unit or one-half molecule. The contour lines for this portion are shown in fig. 4.

Table III.—Values of F $(0kl)$.

When k is even, $\mathrm{F}\,(0kl) = \mathrm{F}\,(0k\bar{l})$.

When k is odd, $\mathrm{F}\,(0kl) = -\,\mathrm{F}\,(0k\bar{l})$

	4	3	2	1	*k* 0	−1	−2	−3	−4
0	+12·2	—	−13·3	—	x	—	−13·3	—	+12·2
1	—	—	—	—	+12·8	—	—	—	—
2	—	—	+6·1	—	−15·6	—	+6·1	—	—
3	−7·5	-	−28·5	−11·6	+25·1	+11·6	−28·5	—	−7·5
4	—	—	−17·5	−3·8	−5·0	+3·8	−17·5	—	—
l 5	—	—	+6·5	—	+13·1	—	+6·5	—	-
6	—	—	−6·4	+8·7	−25·9	−8·7	−6·4	—	—
7	—	—	—	+15·6	−27·4	−15·6	—	—	—
8	—	—	—	−6·7	+5·4	+6·7	—	—	—
9	—	—	+6·4	+6·2	—	−6·2	+6·4	-	—
10	—	—	+23·9	+19·1	—	−19·1	+23·9	—	—

---

* 'Proc. Roy Soc.,' A, vol. 123, p. 537 (1929).

Table IV.—Projection along *a* axis.

$S(y, z) \times 10^{-1}$.

			b/4				*x*		*b*/4				
	15	13	10	7	5	4	5	8	13	20	26	31	35
	25	20	14	8	3	0	1	5	12	21	21	30	47
	39	33	25	16	10	5	4	6	13	19	28	41	44
	45	10	35	29	36	21	18	16	12	17	20	23	26
	36	35	35	36	37	38	35	30	24	18	12	8	7
	20	22	28	32	39	43	43	38	29	18	10	1	3
	8	9	14	20	30	36	36	33	26	15	7	1	1
	6	5	5	9	13	20	22	19	13	8	5	4	5
	10	6	4	5	8	11	13	11	7	3	1	4	7
	10	7	6	7	11	16	19	15	11	5	2	3	6
	5	5	7	13	22	27	31	22	24	15	10	8	9
c/2	1	3	8	16	26	36	41	40	35	29	24	21	21
	7	7	10	17	25	33	38	39	38	35	30	35	38
	24	20	18	17	18	21	24	26	28	31	36	42	48
	42	35	26	18	13	11	9	9	13	19	27	36	43
	49	40	30	20	11	5	1	1	3	8	15	23	29
	40	34	26	18	11	5	1	0	1	5	11	14	18
	24	21	17	12	8	5	3	4	6	10	16	18	20
	16	14	10	7	3	2	2	6	11	18	25	30	34
	21	18	13	7	3	0	1	6	13	22	31	40	46
	33	29	23	16	10	6	5	9	15	23	30	39	45
	41	38	33	28	21	18	17	16	17	21	23	27	30
	37	36	36	35	36	32	30	27	25	20	18	14	12
	24	26	29	32	35	37	36	32	26	19	14	6	3
	13	14	17	21	26	30	30	28	22	16	12	6	4
	8	7	7	9	15	16	18	17	16	10	8	9	10
	9	5	3	3	4	7	8	8	6	4	3	8	12
	9	5	2	2	4	7	8	7	4	1	0	4	8

The usefulness of this diagram is limited in two ways: first, the fact that the absolute values of the terms are not known makes the values of the contour lines of no significance although their positions are not affected; secondly, the definition of the individual atoms is not sharp and there is a considerable overlapping of the projections. The outer atoms of the molecule are quite indistinguishable from those of the reflected molecule halfway along the *a* axis while owing to the double tilt of the molecule some of the outer atoms are sufficiently near the centre ones to affect their contours

In spite of these disadvantages the analysis is thought to give evidence upon these points; that the line of centres of the molecule is projected upon the *c* axis, *i e.*, that $\psi = 0$; and that the projections of the centre and end benzene rings are of equal width, which in combination with similar evidence from a projection along the *b* axis shows that the three nuclei are coplanar. Furthermore, the *z* co-ordinates of the atoms may be calculated since the overlapping outer atoms of the two molecules have the same *z* co-ordinates. The values of *z* of the atoms estimated from the Fourier diagram are shown in comparison with the ones selected in the trial and error analysis.

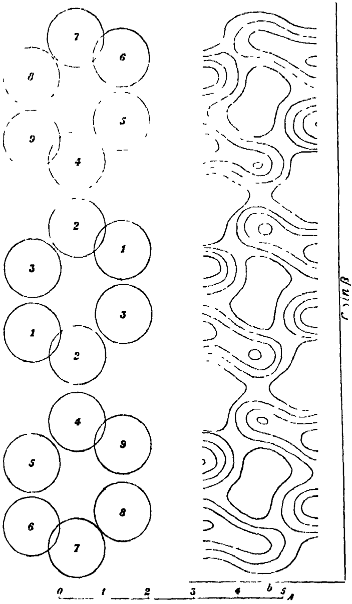

Fig. 4.—The measured contour lines for electron density over the area of projection of one molecule on a plane normal to the *a* axis are here shown together with a diagrammatic representation of the corresponding positions of the carbon atoms

Atom	Trial and error	Fourier analysis
1	0 064	0 065
2	0 100	0 100
3	0 035	0 037
4	0 204	0 205
5	0 269	0 267
6	0 369	0 367
7	0 403	0 400
8	0 339	0 340
9	0 240	0 237

The value for the distance between the nuclei as estimated from the Fourier diagram is 1·48 A. Thus the results of this analysis give evidence that this distance is intermediate between the length of the purely aliphatic and purely aromatic bond This is in agreement with the results obtained by Dhar. It has been pointed out* that the energy value of this bond, calculated from heats of combustion, is intermediate between the values of an aromatic and an aliphatic bond The distance of closest approach between the centres of carbon atoms of adjacent molecules is 3·92 A between the standard and reflected molecule and 3 99 A between the ends of the standard molecule and the reflected molecule removed by one translation along the *c* axis.

Although the electron density cannot be calculated from these results it is apparent that the density is appreciably less for the end carbon atom than for those nearer the centre. A similar phenomenon has been noted for anthracene although its cause is a matter for speculation

A Fourier analysis of the (010) zone showed the projection of the molecule as masses containing three atoms each whose individual contours were indistinguishable. The width and position of these masses was in harmony with the structure described.

I wish to express my thanks to the Managers of the Royal Institution for the privilege of working in the Davy Faraday Laboratory; to the American Association of University Women for the grant of the A.A.U.W. European Fellowship during the tenure of which this work was completed; to Sir William Bragg and the workers of the laboratory, past and present, not only for much timely assistance but for placing at my disposal the very important tools of apparatus and method evolved after much careful investigation; and especially to Mrs. Lonsdale whose constant interest and many helpful suggestions were of great value.

---

* Clopatt, 'Acta Soc. Sci. fenn.,' vol. 6, p. 23 (1932).

Summary.

p-diphenylbenzene crystallizes in the monoclinic prismatic class with two molecules in the unit cell whose dimensions are $a = 8\ 08$ A, $b = 5{\cdot}60$ A., $c = 13\ 59$ A, $\beta = 91° 55'$ The space group is $P\,2_1/a$.

The results of a structure analysis by trial and error and by Fourier analysis give evidence that the molecule is planar in form; that it consists of regular hexagons of carbon atoms 1·42 A apart with a probable distance of 1 48 A. between the hexagons; and that its position may be defined by two successive rotations of 34° and 15·3° about the *c* and *b* axes from an original position in the (100) plane parallel to the *c* axis

Probable positions for the thirty-six atoms of the unit cell are (x, y, z); $(\overline{x, y, z})$, $(\tfrac{1}{2} + x, \tfrac{1}{2} - y, z)$; $(\tfrac{1}{2} - x, \tfrac{1}{2} + y, \bar{z})$, where

1	$x = +0\ 059$	$y = +0\ 182$	$z = +0\ 064$
2	$-0\ 046$	0	$+0\ 100$
3	$-0\ 105$	$-0\ 182$	$+0\ 036$
4	$-0\ 094$	0	$+0\ 204$
5	$-0\ 036$	$+0\ 182$	$+0\ 268$
6	$-0\ 082$	$+0\ 182$	$+0\ 368$
7	$-0\ 187$	0	$+0\ 402$
8	$-0\ 246$	$-0\ 182$	$+0{\cdot}339$
9	$-0\ 200$	$-0\ 182$	$+0\ 239$

Analysis of the Long Range α-Particles from Radium C′ by the Magnetic Focussing Method.

By Lord RUTHERFORD, O M , F R S , W. B. LEWIS, B.A., and
B. V. BOWDEN, B A.

(Received August 23, 1933)

In our last paper[†] we gave an account of an annular ring magnet capable of focussing groups of α-particles after they have traversed a semicircle of 40 cm. radius. By this method the velocities of a number of important groups of α-particles were measured with a relative accuracy, it is believed, of 1 in 5000. Preliminary measurements were described of the two long range groups from thorium C′ and of two from radium C′.

In a previous paper[‡] we had shown by means of counting methods that the long range groups of α-particles from radium C′ were much more complicated than those from thorium C′, and consisted of at least nine distinct groups. This older method, however, had not sufficient resolving power to separate completely a number of these groups, and the annular ring magnet was constructed primarily to make a more complete analysis of this α-ray spectrum. It is hardly necessary at this stage to emphasize the importance of accurate measurements of the energies of these groups, for they give us direct information of the energy levels of the α-particle in an excited nucleus, which is of fundamental importance in considering the question of the origin of the γ-rays from radium C′ [§]

Experiments

The general arrangements for measuring the number and velocity of the particles in each group were similar to those described in our first paper, with one or two minor technical improvements A large number of experiments was made to determine the distribution of α-particles over the whole of the spectrum, which includes α-particles of ranges between 7 cm. and 12 cm., corresponding in our experiments to a change of field from 10,000 to 12,000 gauss

---

[†] Rutherford, Wynn-Williams, Lewis and Bowden, 'Proc. Roy Soc ,' A, vol. 139, p. 617 (1933)

[‡] Rutherford, Ward and Lewis, 'Proc. Roy. Soc.,' A, vol. 131, p. 684 (1931).

[§] Rutherford and Ellis, 'Proc. Roy. Soc ,' A, vol. 132, p. 667 (1931)

Special arrangements were made to obtain the strong sources of α-rays needed for the experiments. The active matter was deposited on the sides of a narrow " V " groove in a piece of stainless steel ground to form a conical stopper, as illustrated in fig 1. During exposure the whole of the emanation, about 250 mg, was introduced into the cavity between the " V " groove and the inner wall of the outer glass container. By this method of preparation the active deposit obtained on the source was over 50% of the total yield from the emanation.

The main difficulty in the analysis of these long range groups lies in their weak intensity. Apart from the strong group of particles of mean range 9·0 cm few of the other groups exceed one in a million of the main group of 7 cm. α-particles. The maximum solid angle over which the particles were counted in our experiments did not exceed 1 in 20,000, and even with a strong source of radium C′, corresponding to 100 mg radium, the total number of particles in a relatively strong group, containing one in a million in the main group, was only 11 per minute. The maximum number of particles counted was further reduced by the width of the counter slit to about half of this. Special precautions were taken to obtain a very clean counting chamber, in which the number of " natural " particles counted did not exceed one in 10 minutes under the experimental conditions.

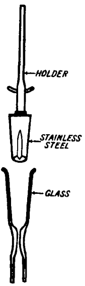

FIG 1

Five sources were used in the examination of the weakest group of which we are certain, namely, that of highest energy. We counted 34 particles in the group in a total counting time of an hour and a half. On either side of the group we counted 18 particles in a similar time. The number to be expected in the time owing to the natural effect was 10. It will at once be apparent that it would be exceedingly difficult to detect such a group if it occurred in the tail on the low velocity side of another larger group, owing to the inevitable probability fluctuations in the number counted. In fact we are unable to claim absolute certainty for our measurement of the group† at H = 10750 gauss on the very large " tail " of the 9 cm. group. This investigation is further complicated by the fact that the number of retarded particles forming the " tail " is extremely variable, differing not only from source to source, but also increasing in an uncertain manner as a given source decays.

---

† The group of excess energy 12·83 × 10^6 electron volts.

Results.

Our results, shown in fig 2, indicate the presence of 12 groups, the distribution of which[†] is in very good accord with that found previously by the range method (*loc cit.*) The 9 cm group, which is by far the most prominent, and which contains about 20 particles per million in the main group, has been investigated in some detail It appears to be a homogeneous group of velocity

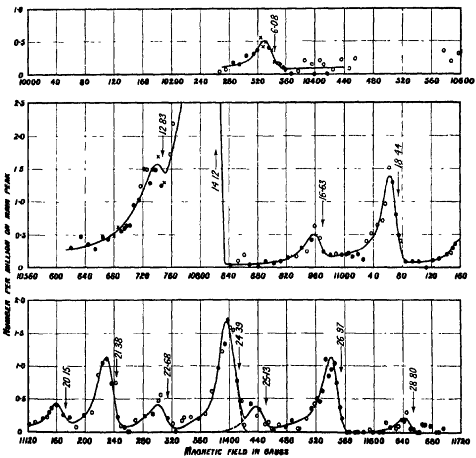

Fig. 2.

[†] The systematic differences in energy between our present results and those given before for corresponding groups are due to the use of an incorrect extrapolated curve to obtain the velocities from the ranges. We subsequently made accurate measurements of the ranges and velocities of a number of groups of particles, and obtained the curve given in fig. 10 of our last paper, *q.v.*

1·0862 in terms of the velocity V_0 of the main group. The energy of disintegration giving rise to such particles exceeds that of the *normal disintegration* by $14·12 \pm 0·03 \times 10^5$ electron volts. As theory indicates that the appropriate excess energy is the most important quantity characterizing a group, we shall use it to identify the groups, as will be seen in the figures and tables

The 7·8 cm group also completely resolved by the range method, was readily detected, but owing to the small number of particles in this group, several experiments were necessary to determine its position with precision We counted in all 320 particles in this group, and believe that the energy excess is $6·08 \times 10^5$ electron volts, with a probable error of less than $0\ 05 \times 10^5$ electron volts.

The analysis of the results of the range measurements above the 9 cm group was carried out by assuming the minimum necessary number of groups, and we now find that the spectrum is slightly more complex than our previous analysis suggested Between the groups of energy excess 26·97† and 24 39 (which correspond to groups Nos 7 and 8 in our previous paper) there is a small group of energy excess 25·13 In place of the two groups Nos 5 and 6 we find three groups of energy excess 20·15, 21 38 and 22 68. Groups Nos 3 and 4 are identified with the groups of energy 16·63 and 18·44 respectively.

In our previous experiments using direct counting methods we found that no α-particle group containing more than 0·02 particles per million in the main group can exist with range greater than 12 cm., *i e*, with energy excess greater than 31·5, nor can any group exist which contains as many as 0·1 per million with energy excess greater than 29·6, which was the limit of exploration in our present experiments. Further, we found that there cannot be any group containing more than 0·1 per million of the main group between ranges 8·0 and 8·6 cm. or energies 7·6 to 11·5. For this reason we have not re-explored this region, since we could not hope to detect the presence of groups of such weak intensity.

The peaks drawn through the experimental points are of the same shape as the main peak, which was carefully determined for each source, when it had decayed sufficiently. The probable error in fitting a peak to the experimental points varies according to the size and position of the peak, and our estimate of this error is indicated in the table for each group.

The results are collected in Table I. In the first column of the table are given the values of "Hρ" corresponding to the groups which are shown in fig. 2, in the second column are the velocities of the α-particles in terms of V_0, the velocity of the main group; the third and fourth columns give the energy of the α-particles and the corresponding energies of disintegration, which include the energy of recoil of the nucleus. The energy excess (the difference between the energy of disintegration of the excited nucleus and the normal disintegration) is given in the fifth column. This energy excess is used to identify the groups as already mentioned. The last column gives the number of α-particles emitted in the long range groups for every million normal disintegrations

---

† For simplicity all levels and α-particle groups are referred to in the sequel by their energy excess expressed in units of 10^5 electron volts.

Table I —Long Range α-particle Groups.

Hρ of α-particle group gauss cm × 10^{-5}	V/V_0	Energy of α particle *e* volts × 10^{-6}	Energy of disintegration (corrected for recoil) *e* volts × 10^{-6}	Energy excess of excited level above normal level *e* volts × 10^{-5}	Probable error *e* volts × 10^{-5}	Number of α-particles per million disintegrations.
3 9930	1 0000	$7\ 683_0$	$7\ 829_3$	0	—	10^6
$4\ 145_2$	1 0380	8 280	8 437	6 08	±0 04	0 43
$4\ 308_6$	1 0785	8 941	9 112	12 83	±0 1	(0 45)
$4\ 338_8$	1 08616	$9\ 068_3$	$9\ 241_6$	14 12	±0 03	22
$4\ 397_2$	1 1008	9 315	9 493	16 63	±0 07	0 38
$4\ 438_8$	1 1111	9 492	9 673	18 44	±0 04	1 35
$4\ 477_9$	1 1209	9 660	9 844	20 15	±0 07	0 35
$4\ 506_1$	1 1279	9 781	9 968	21 38	±0 06	1 06
$4\ 535_2$	1 1351	9 908	10 097	22 68	±0 07	0 36
$4\ 573_6$	1 1447	10 077	10 269	24 39	±0 04	1 67
$4\ 590_6$	1 1488	10 149	10 342	25 13	±0 1	0 38
$4\ 630_7$	1 1589	10 329	10 526	26 97	±0 04	1 12
$4\ 670_9$	1 1689	10 509	10 709	28 80	±0 1	0 23

Correlation of α-particles with γ-rays

It is natural to suppose that all the observed groups of long range particles are emitted by atoms of radium C′ which have been formed in an excited state by the emission of a β-particle from the parent body radium C. On this view, the energy of the α-particles constituting each of these homogeneous groups is a measure of the energy levels which exist in the excited nucleus. In the course of a very short interval the excited atom reverts to the normal state, and the excess energy of the α-particle is believed to be emitted in the form of γ-radiation, either as a single quantum or as successive quanta, in which case the excited atom passes through one or more transition energy levels.†

† In order to account for the complexity of the radium C′ spectrum compared with that of thorium C′, it has been suggested by Fowler and by Gamow that proton excitation may be important in radium C′ There is no experimental evidence on this point but if proton excitation occurs some of the observed α-ray levels may be a measure of the combined energy of excitation of an α-particle and a proton in the nucleus.

As mentioned in an earlier paper, the excess energy of the α-particle in the group of range 7·8 cm., viz., $6{\cdot}08 \times 10^5$ electron volts, is in excellent agreement with the energy of the strongest γ-ray observed, of energy determined by Ellis as $6{\cdot}07 \times 10^5$ electron volts. Similarly there is a very close accord between the excess energy of the α-particle in the predominant group of energy excess $14{\cdot}12 \times 10^5$ volts, and the equivalent strong "γ-ray" of energy found by Ellis to be $14{\cdot}14 \times 10^5$ volts. It is clear that in both these cases the α-particle falls direct to the normal level, emitting its energy in a single quantum. No such simple explanation can be found for the other strong γ-rays from radium C′, viz., 11·21, 17·61, and $21{\cdot}98 \times 10^5$ volts, for no energy levels of excess energies corresponding to these values have been found. Similarly the excess energies of many of the α-ray levels we have observed do not correspond with the strong β-ray groups in the high energy part of the β-ray spectrum. In searching for a correlation between the β- or γ-ray spectrum and the α-ray spectrum it is necessary to consider more complicated transitions between the energy levels in which the excited atom may emit its surplus energy in successive stages. This involves some consideration not only of numerical coincidences between the energies of observed β- and γ-ray lines with differences of energies between possible levels, but also of the intensities of the β-ray lines and of the α-ray groups. Great caution must be exercised in interpreting the results, for a number of important factors are involved on which our information is very indefinite. Some of these factors will be discussed later in some detail, but a few words of explanation may be given at this stage. In the first place it is necessary to emphasize the great distinction between the types of transition which take place from the 6·07 and from the $14{\cdot}14 \times 10^5$ volts excess energy levels. It is generally believed that a "radiationless"† transition takes place from the "14·14" level, the excess energy being directly communicated to one of the electron groups of the outer atom. If a γ-ray appears at all, the experimental evidence shows that it must be very weak. The time for this radiationless transition must be very long compared with the time for a direct "radiation" transition such as gives rise to the 6·07 γ-ray. For this reason by far the strongest group of α-particles corresponds to a level which is very rarely excited, only about once in 1000 disintegrations, while, on the other hand, the 6·07 level is excited 600 times in 1000 disintegrations. If such radiationless transitions occurred for one or more of the levels of greater energy where the rate of escape of the α-particle is very fast, we might observe a comparatively strong α-particle group where the corresponding line in the β-ray spectrum is weak or quite undetectable. There is at the moment no obvious way of deciding whether one or more of the higher energy groups of α-particles may be attributed to this abnormal type of disintegration

---

† Fowler, 'Proc. Roy. Soc.,' A, vol. 129, p. 1 (1930).

There is another important point which must be carefully considered. It is now believed that the γ-rays emitted from radium C′ may be divided into two distinct classes which have been called dipole and quadripole The intensity of the β-ray line corresponding to a quadripole transition is about three times stronger than that for a similar dipole γ-ray, and this factor varies with the energy of the γ-ray. While a number of the stronger γ-rays have been classified as belonging to one or other of these two types, from Ellis and Aston's measurements of internal conversion coefficient, we have no such information about the types of transition which give rise to the β-ray lines which are not associated with strong γ-ray lines In addition, recent theory indicates† that the rate of emission of the α-particle depends not only on its energy, but also very markedly on the quantum number associated with the energy level under consideration, so that the intensity of an α-ray group gives no clear indication of the intensity of the γ-ray which may arise from it For example, the α-ray group of highest energy, although the weakest group observed, is believed to be connected with the emission of the strong γ-rays of energies 11·21 and 17 61 × 10^5 volts

Taking into account these factors as far as possible, we have provisionally selected the group of energy levels shown in fig 3 in order to account for the origin of the stronger γ-rays In this scheme are included five of the observed α-ray levels, and in addition four hypothetical levels which seem to be necessary, and which correspond to the energies of γ-rays found by Ellis It will be shown later on general theoretical grounds that we should not expect to observe the presence of α-ray groups corresponding to these levels. It will be seen that the small group of energy excess 28·80 × 10^5 volts corresponds to the combined energies of the γ-rays 11·21 and 17·61. It is probable that these γ-rays arise in successive transitions to the ground state from this high energy level. The origin of the other strong γ-rays can be explained in a similar way (see fig. 3) and there is no systematic difference between the energies determined by these entirely independent measurements.

We have been guided in the construction of the scheme by the necessary condition that the number of transitions into a level can never exceed the number of transitions from that level. For instance there are two important transitions into the 17·61 level, which occur 0·06 and 0·21 times† per disintegration from the 26·97 and 28·80 levels respectively The 17·61 γ-ray is emitted 0·26 times per disintegration, so it seems clear that the nucleus is seldom if ever excited directly into this level, a conclusion which has been used by Ellis and Mott‡ in their explanation of the natural β-ray spectrum of radium C.

---

† Gamow, 'Nature,' vol. 131, p 433 (1933).

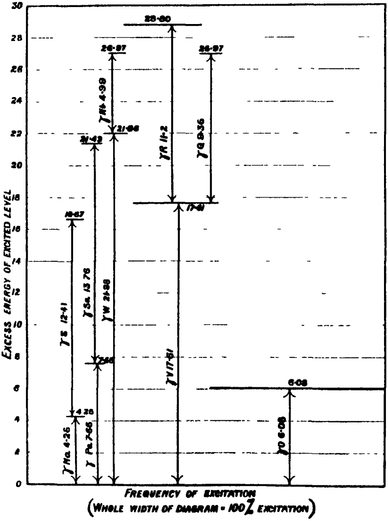

FIG. 3.

---

† It seems probable as was suggested by Ellis and Aston ('Proc. Roy. Soc.,' A, vol 129, p. 181 (1930)) that all the estimates of intensity given above may be too high by about 20%

‡ 'Proc. Roy. Soc.,' A, vol. 141, p 502 (1933)

We have not included the 14·12 level in this scheme, as there is no evidence that it is correlated by transitions with any of the stronger γ-rays. As already mentioned there seems to be no doubt that the excitation of this level is relatively a rare occurrence.

A more detailed scheme is given in Table II. This includes all the levels from which α-particles are known to be emitted together with the transition levels required by the intensity considerations mentioned above. All the possible differences between the energy levels are shown. Those in bold type correspond (within 0 07 × 10^5 volts) with γ-rays which have been deduced from the β-ray spectrum. γ-rays are included wherever a line which would result from their conversion in the K level of the atom is observed in the β-ray spectrum. Out of 136 numbers appearing in the table, 65 are correlated with γ-rays.

Table II. Detailed Level Scheme for Radium C′, showing all Energy Differences between Levels.

j	4	2	2	1	1	2	1	1	1	2	1	0	1	1	1	1
Energy level	28 80	26 97	25 13	24 39	22 68	21 98	21 38	20 15	18 44	17 61	16 63	14 12	12 83	7 66	6 08	4 26
28 80																
26 97	**1 83**															
25 13	3 67	1 84														
24·39	4 41	2·58	0 74													
22 68	**6 12**	**4 29**	**2 45**	1 71												
21 98	**6 82**	**4 99**	3 15	**2 41**	0 70											
21 38	7 42	5 59	3 75	3 01	**1 30**	0 60										
20 15	8 65	**6 82**	**4 98**	**4 24**	**2 53**	**1 83**	1 23									
18 44	10 36	8 53	**6 69**	5 05	**4 24**	3 54	2·94	1 71								
17 61	**11 19**	**9 86**	7 52	**6 78**	5 07	4 37	3 77	**2 54**	0 83							
16 63	12 17	**10 34**	**8 50**	7 76	**6 05**	**5 35**	4 75	3 52	1 81	0 98						
14 12	14·68	12 85	11 01	10 27	8 56	7 86	7 26	**6 08**	**4 32**	**3 49**	**2 51**					
12 83	**15 97**	**14 14**	**12·30**	**11 56**	**9 85**	9 15	8 55	7 32	5 61	4 78	**3 80**	1 29				
7 66	**21 14**	**19 31**	17 17	**16 73**	**15 02**	**14 32**	**13 72**	12 49	10 78	**9 95**	8 97	6 46	5 17			
6 08	**22 72**	20 89	19 05	**18·31**	**16 60**	**15 90**	**15 30**	**14 07**	**12 36**	**11 53**	10 55	8 04	8 75	**1 58**		
4 26	24 54	**22 71**	20 87	**20 13**	**18 42**	**17 72**	**17 12**	**15 89**	**14 18**	**13 35**	**12 37**	9 86	9 57	**3 40**	1 82	
0	**28 80**	26 97	25 13	**24 39**	**22 68**	21 98	21 38	**20 15**	**18 44**	**17 61**	16 63	**14 12**	**12 83**	**7 66**	**6 08**	**4 26**

Some of these correlations are probably due to fortuitous numerical coincidences, owing to the large number of γ-rays, and to the fact that some tolerance has to be allowed in fitting on account of experimental error. Nevertheless, the number of coincidences is considerably more than can be attributed to chance as we have verified by constructing a number of arbitrary "α-ray levels." The most remarkable feature of the scheme is the number of differences that occur two, three, or more times. This is far more than can be attributed to chance, and indicates that there is a simple numerical relation between the energy levels. In fact all the energy levels in the scheme, both observed and postulated, except the 7·66 level, can be represented to a close approximation by the formula

$$E = p \times 4{\cdot}26 + q \times 1{\cdot}82$$

or

$$E = 14{\cdot}14 + p \times 4{\cdot}26 + q \times 1{\cdot}82,$$

where "p" and "q" are integers, while the differences between several of the higher levels appear to be nearly equal to integral multiples of $1{\cdot}82 \times 10^5$ electron volts.

We hope later to discuss these relations in more detail and to consider their possible significance.

It seems probable that the proposed level scheme, which includes all the observed α-particle groups, together with four transition levels, must form the basis of any complete scheme of the energy levels of the excited radium C′ nucleus.

Discussion

We have already referred briefly to the new and important advance in classifying the γ-rays into quadripole and dipole. This is based on the experimental measurement by Ellis and Aston of the internal conversion coefficients of γ-rays, coupled with the mathematical theories of Hulme,† and of Taylor and Mott.‡ Quadripole radiation is associated with a change of azimuthal nuclear quantum number of 0 or 2 ($j = 0 \rightarrow j = 0$ forbidden) whereas dipole radiation corresponds to a change of quantum number of one. Of the prominent γ-rays from radium C′ they have found that γO = 6·07, γPa = 7·66, γSa = 13·8 are dipole, while γQ = 9·33, γR = 11·2, γS = 12·4, γV = 17·61, and γW = 21·97 are quadripole.

It is therefore natural to attempt to assign quantum numbers to the nuclear levels,§ as has already been done by Ellis and Mott‖ for nuclei of the thorium series.

Assigning quantum number $j = 0$ to the ground state, the 6·08 and 7·66 levels must have quantum number $j = 1$, and similarly the levels 17·61 and

---

† 'Proc. Roy. Soc.,' A, vol. 138, p. 643 (1932).

‡ 'Proc. Roy. Soc.,' A, vol. 138, p. 665 (1932).

§ Gamow has suggested a level scheme for the radium C′ nucleus ('Nature,' *loc. cit.*). His method of assigning quantum numbers is based on the levels for an α-particle in a reflecting box, and does not appear to agree with the levels experimentally found.

‖ 'Proc. Roy. Soc.,' A, vol. 139, p. 369 (1933).

21·98 must have $j = 2$. A quantum number $j = 0$ has been assigned to the anomalous 14 12 level. The selection rule which forbids transitions $j = 0 \rightarrow j = 0$ would account for the absence of a corresponding γ-ray produced by direct transition to the ground state It must be considered remarkable that no transitions to other lower levels occur during the comparatively long time during which the atom must remain in this level before it emits an α- or β-particle. Transitions into this level are notably rare, and there must be some fundamental difference between it and the ground state, to which we have also assigned the quantum number $j = 0$

While the 6 07 level is excited 0·66 times per disintegration we have seen that it gives rise to a very weak α-particle group We should not therefore expect to observe the α-particle group corresponding to the 7 66 level, which is excited only about one-tenth as often, as the difference in energy of the two levels is too small for the rate of emission of the α-particles to differ much in the two levels No α-particle groups are observed corresponding to the 17·61 and 21·98 levels for which $j = 2$, although these levels are frequently excited. On the other hand, α-particle groups are observed corresponding to the less frequently excited levels of similar energy Two possible explanations suggest themselves either the α-decay constant is abnormally small for these levels, or the optical transition probability is abnormally large It is not possible to decide between the alternatives, but the latter seems more likely, since it would suggest that the optical transition probability is greater for quadripole than for dipole transitions, which is in agreement with theoretical predictions based on certain nuclear models.† The assumption that this phenomenon is associated with "j" even is consistent with our observations and with the proposed level scheme

The detailed consideration of the level schemes involves assumptions concerning the probability of α-particle escape, and of γ-ray transitions from the excited nuclear states The information available on these points is too indefinite to hazard more than tentative conclusions at this stage

Following Rutherford and Ellis,‡ we have made estimates of the value of the α-ray disintegration constants of the excited states by using the formula of Gamow and Houtermans § We have adjusted the values of the constants appearing in this formula to fit the normal disintegration, for which we have assumed the value $\lambda = 10^4$ consistent with the recent determinations of

---

† Taylor and Mott, *loc. cit*, p. 692.

‡ 'Proc. Roy. Soc.,' *loc. cit*

§ 'Z. Physik,' vol. 52, p. 496 (1929).

Jacobsen. Though it is assumed that the "radius" of the nucleus is unaltered by the excitation it seems probable that this procedure is more reliable than a simple extrapolation of the empirical Geiger-Nuttall relation between λ and the energy of the escaping α-particle We have further assumed, as Gamow† suggests, that the probability of α-particle escape from the excited states of high quantum number is reduced in the ratios 1 · 1·3 4 · 16 : 105, for quantum numbers $j = 0, 1, 2, 3, 4$ The disintegration constant has been calculated from Gamow and Houtermans' formula for $j = 0$

It is assumed that for dipole radiation, the γ-ray emission probability varies as

$$\nu^3 \left[\int x\psi\psi^* \, d\tau\right]^2,$$

where ν is the frequency of the emitted radiation and

$$\int x\psi\psi^* \, d\tau$$

is an integral throughout space which involves the product of the wave functions defining the states between which the transition occurs Mott‡ informs us that for quadripole radiation the probability varies as

$$\nu^5 \left[\int x^2\psi\psi^* \, d\tau\right]^2.$$

It is impossible in general to say how these integrals vary, but we have assumed that for transitions to the same state involving the same type of radiation, the integral will not vary very markedly. We have calculated, on these assumptions, the number N_α of α-particles in the groups corresponding to levels for which the frequency of excitation can be derived from the associated γ-rays. This will be given by the relation

$$N_\alpha = P \frac{\lambda_\alpha}{g},$$

where N_α is the number of α-particles emitted per disintegration, P, is the excitation probability, or the number of times the level is excited per disintegration, λ_α is the disintegration constant for α-particle disintegration, and

---

† 'Nature,' *loc. cit.*

‡ We wish to express our thanks to Mr. Mott for assisting us in discussions on this subject.

g is the total probability per unit time of radiative transition from the excited state. The results are given in Table III and the bearing of these calculations on a few of the more important energy levels will now be considered.

The 17·61 level, which emits quadripole radiation on transition to the ground state, does not emit an α-particle group corresponding to as many as one in 5×10^6 disintegrations. From this we may calculate that the maximum number of α-particles to be expected from the 21·98 level is 0·12, which is again below the limit of observation, whereas the group from the 26·97 level may be as large as 0·9. Actually we find no trace of a group at 21·98, but find a relatively strong group of 1·12 per million in the main peak at 26·97. The excitation probability of this level is derived by assuming that transitions from it to the 17·61 and 21·98 levels give rise to the γ-rays, $\gamma Q = 9{\cdot}33$ and $\gamma N = 4{\cdot}98$. It is surprising that no γ-ray corresponding to the transition from the 26·97 level to the ground state is observed. The weakness of the γ-ray could be accounted for if a quantum number $j = 4$ were assigned to the level, but it would be then difficult to account for the strong group of α-particles observed, taking into account the reduction of α-particle escape due to the high quantum number. Moreover, the neighbouring 28·80 level appears to be more frequently excited, and gives rise to a weaker α-particle group, which is consistent with the allocation of the quantum number $j = 4$ to this higher level, which also gives no measurable γ-ray by direct transition to the ground state. A quantum number $j = 2$ has also been assigned to the 25·13 level.

A quantum number $j = 1$ has been assigned to all the other nuclear levels from which α-particle groups have been observed in order to account for the weak intensity of the γ-rays emitted by direct transitions to the ground state.

The intensities of the γ-rays have been calculated from the β-ray intensities using the internal conversion coefficients calculated by Hulme for dipole radiation. The values of g given in the table have been calculated from the formulæ already given, using the value of g determined for the 6·07 group, for which the γ-ray and α-particle intensities are known with some accuracy.

It will be seen that the ratio of the calculated to the observed number of α-particles increases with the energy of the level. This variation is very small compared with the variation in λ (of the order of 10^4), and can be attributed either to a change in

$$\int x\psi\psi^* \, d\tau$$

or to a correction term to be applied in the extrapolation for λ_a by the Gamow and Houtermans formula.

Excited energy level.	Number of α-particles per disintegration × 10⁶.	λ_a from Gamow and Houtermans' formula sec⁻¹	Dipole.			Quadripole.		
			P† From β-ray intensity and internal conversion coefficient.	$\frac{g}{x\,r^3}$	Expected number of α-particles per million disintegrations $=\frac{P\ \lambda_a}{1\cdot 3g}\times 10^6$	P†	$\frac{g}{x\,r^3}$	Expected number of α-particles per million disintegrations $=\frac{P\ \lambda_a}{4g}\times 10^6$
4·26	<0·06	$2\cdot1 \times 10^5$	0·010 probably low Ellis	$1\cdot86 \times 10^{11}$	0·009	[0·002]	$>3\cdot40 \times 10^{11}$	j = 2 [<0·00031]
6·08	0·43	$5\cdot5 \times 10^5$	0·55	$5\cdot42 \times 10^{11}$	(0·43)	—	—	—
7·66	<0·2	$1\cdot4 \times 10^6$	0·065	$1\cdot09 \times 10^{12}$	0·06	[0·022]	$>3\cdot55 \times 10^{12}$	[<0·0022]
12·83	(0·45)	$2\cdot7 \times 10^7$	0·043	$5\cdot10 \times 10^{12}$	0·18	[0·015]	$>3\cdot55 \times 10^{13}$	[<0·0028]
14·12	22	$5\cdot5 \times 10^7$	—	—	—	—	—	—
16·63	0·38	$2\cdot1 \times 10^8$	0·06 max.	$1\cdot12 \times 10^{13}$	0·86	[0·095]	$>1\cdot31 \times 10^{14}$	[<0·038]
17·61	<0·2	$3\cdot4 \times 10^8$	—	$1\cdot33 \times 10^{13}$	—	0·41 max [0·22 min]	$>1\cdot74 \times 10^{14}$	(<0·2)
18·44	1·35	$5\cdot1 \times 10^8$	(0·15 max)	$1\cdot54 \times 10^{13}$	3·8	—	—	—
20·15	0·35	$1\cdot2 \times 10^9$	0·03	$1\cdot98 \times 10^{13}$	1·4	[0·027]	$>3\cdot40 \times 10^{14}$	[<0·027]
21·38	1·06	$2\cdot2 \times 10^9$	0·025	$2\cdot38 \times 10^{13}$	1·78	[0·08]	$>4\cdot61 \times 10^{14}$	[<0·095]
21·98	<0·25	$2\cdot9 \times 10^9$	—	—	—	0·047 min 0·21 max	$>5\cdot30 \times 10^{14}$	<0·064 min. <0·29 max.
22·68	0·36	$4\cdot1 \times 10^9$	0·126 max	$2\cdot82 \times 10^{13}$	14 max	[<0·3]	$>6\cdot17 \times 10^{14}$	[<0·5]
24·39	1·67	$8\cdot7 \times 10^9$	0·24 max 0·04 min	$3\cdot53 \times 10^{13}$	45 max 7·6 min.	[<0·3]	$>8\cdot88 \times 10^{14}$	[<0·74]
25·13	0·38	$1\cdot2 \times 10^{10}$	[<0·015]	$3\cdot83 \times 10^{13}$	[<3·61]	<0·046	$>1\cdot04 \times 10^{15}$	<0·13]
26·97	1·12	$2\cdot7 \times 10^{10}$	[>0·16]	$4\cdot79 \times 10^{13}$	[>69·4]	0·64 min 0·25 max	$>1\cdot47 \times 10^{15}$	<0·283 min. <1·14 max.
28·80	0·23	$5\cdot8 \times 10^{10}$	—	$5\cdot84 \times 10^{13}$	—	$0\cdot17_5$ min	$>2\cdot04 \times 10^{15}$	j = 4 <0·04 min.

[ ] the alternative (dipole or quadripole) is adopted for this level.
' ; very uncertain values.
( ) values adopted as standard for calculation of g
: ; not adopted for calculation

† Owing to ambiguity in the correlation with γ-rays, few excitation probabilities are uniquely determined.

Conclusion.

When we consider in broad terms the data which have been accumulated, there can be no doubt that there is a high correlation between the α-particle levels which have been observed and the emission of γ-rays. In more important cases the numerical agreement is well within the experimental error of measurement, while the relation between the intensity of the α-ray groups and the γ-rays associated with them is of the right order of magnitude to be expected on general theoretical grounds. In other cases the agreement is very uncertain, and more definite information on the γ-rays is required to make the deductions trustworthy. It is unfortunate that we have been unable to detect the α-particle groups corresponding to certain postulated levels, *e.g.*, for the 17·61 level. In order to settle the presence or absence of these levels, using our experimental method, much stronger sources of α-rays would be required. No doubt many additional weak α-ray levels would be brought to light if we were able to employ clean sources of 10 grams instead of the 100 milligrams usually employed in our experiments. Such an extension of the experiment would, however, not be easy even if a sufficiently great quantity of radium were available. In any case we hope that the data which we have obtained in these measurements will serve as a useful guide in developing still further the theories concerning the excitation of the α-particles and thus throw further light on the nuclear disturbances of a heavy atom.

In conclusion we wish to express our thanks to the Department of Scientific and Industrial Research for grants to two of us. We are also indebted to Dr. Wynn-Williams for his assistance with the counting devices, and to Mr. G. R. Crowe for his help in the preparation of the radium sources.

Summary.

The velocities of the long range groups of α-particles from radium C′ have been measured with accuracy by the annular ring magnet previously described. The α-ray spectrum has been analysed into 11 distinct groups, which have thus been separated for the first time. The corresponding energy levels of the excited nucleus have been deduced with certainty. All the prominent γ-rays may be correlated with these levels if four other levels which do not correspond with observed α-particle groups are postulated. The relative intensities of the α-ray groups and the γ-rays show marked variations, which suggests the importance of dividing the γ-rays into the two types dipole and quadripole, and quantum numbers have been tentatively assigned to the levels.

Spectrum of the Afterglow of Carbon Dioxide.

By A. Fowler, D.Sc., F.R.S., Yarrow Research Professor, and A. G Gaydon, B.Sc., Research Student, Imperial College.

(Received July 15, 1933)

[Plate 4]

Introductory.

When compounds of carbon and oxygen are excited to luminosity in vacuum tubes, they give rise to a large number of band systems, depending upon the conditions of electrical discharge Most of these systems have been discussed by various authors, and on the basis of the theory of band spectra have been attributed to transitions between different states of the molecule CO Details of these systems, including those ascribed to the ionized molecule CO^+, have been conveniently summarized by Jevons[*] and by Kayser and Konen [†]

Another band system (Deslandres' second negative) which occurs under favourable conditions has been attributed by Bair,[‡] and by Fox, Duffendack and Barker[§] to the triatomic molecule CO_2, since the bands appear most strongly in CO_2, and are especially developed when a stream of this gas is passing through the discharge tube. The suggested CO_2 origin of these bands appears to be supported by Smyth's partial analysis of their structure [||]

Quite recently, still another set of bands has been observed by Mlle. Marie Kaczyńska[¶] in the spectrum of the afterglow of the discharge through CO_2. The observations were made by drawing gas from the discharge tube into a side tube, as in the well-known similar procedure for observations of the afterglow of nitrogen The afterglow was stated to be blue-grey in colour and to be most persistent at a pressure of about 2 mm. of mercury. As the pressure was increased, the intensity of the luminescence was increased and the colour became blue, but its extent and duration diminished rapidly. Increased intensity was also obtained by frequent renewals of the gas in the discharge tube. With an alternating current of 60 mA., the luminescence was observed to a distance of about 40 cm. and its duration was 8 seconds. The brightest part of the spectrum of the afterglow was found to extend from λ 3850 to λ 4836, and to be quite free from the Ångström bands of CO, which were the most prominent feature in the spectrum of the exciting discharge. No further details of the spectrum, however, were given.

---

[*] 'Report on Band Spectra of Diatomic Molecules,' p. 286, The Physical Society (1932).

[†] "Handbuch der Spectroscopie," vol. 8, p. 302 (1932).

[‡] 'Astrophys. J.,' vol. 52, p. 312 (1920).

[§] 'Proc. Nat. Acad. Sci.,' vol. 13, p. 302 (1927).

[||] 'Phys. Rev.,' vol. 38, p. 2000 (1931).

[¶] 'Bull. Int. Acad. Polonaise,' A, vol. 1A, p. 16 (1931).

The present investigation of the spectrum of the CO_2 afterglow was undertaken in connection with work in progress on the spectrum of the flame of carbon monoxide. This flame spectrum has been found to have nothing in common with the spectra of oxides of carbon which have been observed in vacuum tubes, and it seemed possible that a further investigation of the CO_2 afterglow might aid in its interpretation. It has been found, in fact, that apart from slight differences in relative intensities, the bands of the CO flame spectrum are identical with those of the CO_2 afterglow, at least in the region λ 3500 to λ 4850. As observed in the flame with considerable dispersion, the spectrum is extremely complex and the constitution of the emitting molecule cannot yet be certainly stated. The general experimental evidence, however, is in favour of the supposition that the bands of the afterglow and of the CO flame originate in molecules of CO_2

Experimental

Attempts to observe the afterglow by drawing gas from the discharge tube into a side tube did not give very satisfactory results, and another device (due to A. G G) was adopted. The main feature of this was the use of a mercury break with a shutter adapted so as to cut off the light from the spectrograph when the discharge was passing and to allow it to pass in the intervals between the discharges when the afterglow was visible The mercury break was of the usual form, driven by an electric motor, but some of the plates were removed so that contact was made and broken only twice in each complete revolution A rectangular flap of brass, blackened so as not to reflect light, was secured to the vertical spindle of the break and was adjusted between the discharge tube and the slit of the spectrograph so as to permit no light from the direct discharge to pass.

An 18-inch induction coil was used, and it was found necessary to introduce a fairly long spark gap in series with the discharge tube. The adjustment of the gap in order to obtain the best results was somewhat critical, but with due care the arrangement was found to work quite satisfactorily.

The discharge tube used in these experiments was 50 cm. in length and 7 mm.

in internal diameter, and of the form shown at T in fig 1. To facilitate collimation, the main part of the tube was mounted with its axis vertical, and the upper end was closed with a quartz window, G. The electrodes consisted of stout aluminium rods, FF, with a suitable clearance between them and the walls of the tube. Of the many discharge tubes which were tried, those of about the dimensions stated were found to give the most satisfactory results. The discharge tube, and the side tube, A, for preparing the gas, were made of pyrex glass, while the remainder of the system was of ordinary glass, joints being made with red sealing wax where necessary. No rubber tube was used, except in the short lead to the pump.

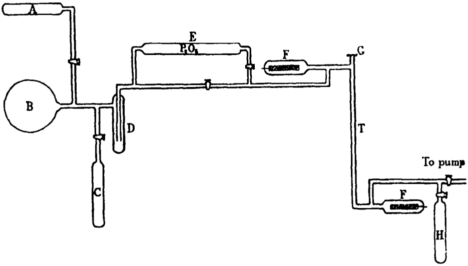

Fig. 1.

The carbon dioxide was prepared by heating magnesium carbonate in the side tube, A, and was stored in the litre flask, B. The gas was condensed in the side tube, C, by freezing with liquid air, and it was then possible to pump out any air or other impurity liberated by the heating of the tube A for the preparation of CO_2. On removing the liquid air from the trap, C, the carbon dioxide volatilized first, leaving most of the water vapour in C, which was closed as soon as sufficient gas had entered the storage flask, B The trap shown at D was further introduced to remove water vapour by applying either solid carbon dioxide or a mixture of alcohol and liquid air. After leaving the reservoir, B, the gas passed through a phosphorus pentoxide drying tube, E, into the discharge tube. The whole system was first evacuated by a good mechanical pump, giving a pressure estimated at 0·001 mm, and a charcoal-liquid air trap, H, was used further to improve the vacuum.

Light from the discharge tube passing through the window, G, was reflected by a small speculum mirror through a right angle, to render the beam of light horizontal and in coincidence with the collimator of the spectrograph A quartz lens placed near the mirror formed an image of the discharge on the rotating shutter, and a second quartz lens focussed the light from this image on the slit of the spectrograph. Care was taken that full illumination of the collimating lens was secured.

Occurrence of the Afterglow

The afterglow, as noted by Mlle. Kaczyńska, was observed to be of a bluish-grey colour, but it was always very feeble, so that long exposures were necessary for photographs of the spectrum. Under favourable conditions, it was observed to persist for about two seconds when the experiment was made in a darkened room A powerful discharge was found to be necessary for its production. Experiments with a condensed discharge, however, were not very successful on account of the intense heating of the discharge tube; the afterglow was still present, but was less blue in colour, and the spectrum was the same as that obtained when the uncondensed discharge was used.

The afterglow was better observed the more completely the CO_2 was dried, but although the "water vapour" bands at λ 3064 did not appear in the spectrum of the discharge itself, they were always present in that of the afterglow.

As possibly having some bearing upon the interpretation of the afterglow and its spectrum, observations were also made with the same apparatus when CO was substituted for CO_2 in the discharge tube, the CO being prepared by dropping formic acid into pure sulphuric acid. In the first experiments, a very feeble afterglow was observed but this disappeared completely when water vapour was removed by the use of the liquid air trap D, (fig. 1) Under these conditions, with the gas at various pressures, exposures of 10 hours duration, using a small spectrograph and a wide slit, yielded no trace of an afterglow spectrum. The admission of a trace of water vapour, however, caused the reappearance of a feeble afterglow, and this was again extinguished when a larger quantity of water vapour was introduced. A photograph obtained when the afterglow was present, though rather weak, was sufficient to show that the spectrum was the same as that obtained when the gas in the discharge tube was CO_2. No afterglow at all was observed when water vapour alone was passed through the discharge tube.

Spectrum of the Exciting Discharge.

A photograph of the spectrum of the discharge which appeared to be most effective in generating the afterglow is reproduced, together with that of the afterglow, in Plate 4, Nos. 1 and 2. The main features of the spectrum of the discharge are the Ångstrom bands of CO and the so-called "Third Positive" bands of this gas, all of which are of great intensity. Bands which have been attributed to CO_2, among which are bands degraded towards the red, having their heads at λλ 3247, 3370 and 3503, were entirely absent. In the further ultra-violet the bands appearing in the discharge tube (out of range in Plate 4) were those of the "Fourth Positive" system of CO The bands of Deslandres' "First Negative" group, which require much greater energy for their production, and are now attributed to CO^+, were entirely absent

It should be noted further that the spectrum of the discharge gave no indications of either molecular or atomic carbon, and no evidence of the presence of atomic oxygen. Since the CO shown in the spectrum of the discharge tube has been derived from CO_2, oxygen must also have been present, and in view of the absence of the well-known bands due to ionized oxygen molecules (O_2^+), it must be concluded that the oxygen liberated under the conditions of the present experiments was in the form of neutral oxygen molecules. The most characteristic bands of such molecules, however, have been observed only in absorption, and no direct confirmation of their presence was given by the spectra obtained.

The phenomena observed in the afterglow would accordingly appear to depend upon the interaction between neutral oxygen molecules and excited neutral molecules of carbon monoxide.

Spectrum of the Afterglow.

On account of the feeble luminosity of the afterglow, photographs of the spectrum could be obtained only with instruments of small dispersion. Several photographs were taken with a Hilger small quartz spectrograph (E3) and others with a large-aperture glass spectrograph giving about 2½ times the dispersion in the blue and nearly twice the rapidity.

The character of the spectrum, as depicted with small dispersion, will be gathered from Plate 4, No. 2. In agreement with Mlle. Kaczyńska, it appears

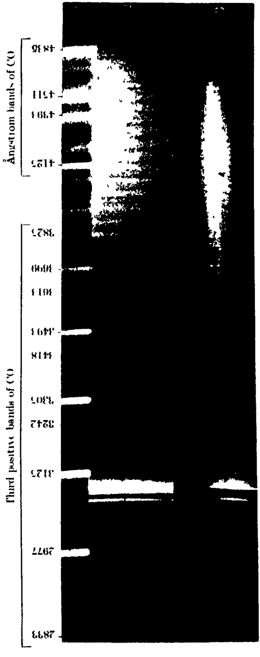
Ångstrom bands of CO
4835
4511
4393
4125
Third positive bands of CO
3825
3699
3613
3493
3418
3305
3242
3125
2977
2833

Fig. 1

quite conclusively that the spectrum of the afterglow has nothing in common with that of the exciting discharge. The spectrum consists of a succession of narrow bands of various intensities, following each other at short intervals, and the bands are not clearly degraded either towards the red or the ultra-violet. The bands could not be identified with any of the numerous band systems of CO or with the known bands of CO_2, but, in due course, it was recognized that the spectrum was closely similar to that of the flame of CO burning in air or oxygen. The similarity of the two spectra will be gathered from the comparison of spectra Nos. 2 and 3 in Plate 4. There are slight differences in the relative intensities of some of the bands, and in contrast with the CO flame the afterglow is comparatively free from continuous spectrum, so that the characteristic bands are more clearly displayed. On account of the much greater brightness of the flame, the true character of the spectrum can at present be more completely investigated by observations of the flame than of the feeble afterglow.

Numerous experiments have been made with vacuum tube discharges of various forms in the hope of obtaining a brighter source of the afterglow bands, but so far they have not been successful.

Spectrum of the Flame of CO.

An extended series of observations of the flame spectrum of CO under varied conditions was made in Professor Bone's laboratory a few years ago by Weston.* His papers on the subject included a description of the spectrum by one of the present authors (A. F.) and approximate measures of 52 of the principal bands in the region λ 3911 to λ 5555 These measures were made on a plate taken with a Hilger E2 quartz spectrograph, and in view of the ill-defined character of the bands they were believed to be subject to errors amounting to at least 2 or 3 Ångströms. It was concluded that "the CO flame bands constitute a characteristic spectrum which is quite distinct from the more familiar oxy-carbon bands which have been observed in vacuum tubes."

Among numerous other results, it was found by Weston that when the gas was burnt in air at reduced pressure, the banded part of the spectrum became more distinct, while the continuous part became less intense. By the kind permission of Professor Bone, one of the photographs taken under these conditions (No. 15 on Plate 1 of Weston's first paper) is reproduced in No. 3, Plate 4, for comparison with the afterglow spectrum, No. 2; this represents the flame of CO burning in oxygen at a pressure of 100 mm. In this photograph the bands occupy precisely the same positions as those of CO burning in air at ordinary pressure, and a careful comparison has shown that they are also in complete agreement with the bands of the afterglow

---

* 'Proc. Roy. Soc.,' A, vol. 109, pp. 176, 523 (1925).

An important observation made by Weston was that when the CO was well dried, the water vapour bands, which are prominent when the undried gas is burnt, were almost absent from the spectrum, while the continuous and banded parts of the spectrum were apparently unchanged. The characteristic features of the flame spectrum thus appeared to be independent of the presence or absence of water vapour

The conclusion reached by Weston, with the support of Professor Bone, was that "in the flame of pure (undried) carbon monoxide, two sets of independent interactions occur simultaneously, namely, (*a*) direct interactions between carbon monoxide and oxygen, exciting radiations which give rise to the continuous and banded parts of the spectrum, and to the characteristic blue colour of the flame, and (*b*) interactions between CO and OH_2 molecules, which originate the '*steam lines*' *in the spectrum.*" There was, however, no evidence at that time to show whether it was molecular or atomic oxygen that was concerned in the interaction of carbon monoxide with oxygen

The spectrum of the CO flame has also been investigated by Kondratjev* over the region λ 2800 to λ 5000 In these experiments, a mixture of CO and O_2 in combining proportions was passed through a quartz tube which was heated in an electric furnace to temperatures of 600°–750° C, the pressure of the mixed gases ranging from 20 mm to 60 mm. From the reproduction of the spectrum and the tabulated wave-lengths of the bands measured, it seems clear that the spectrum obtained in this way did not differ materially from that of the CO flame in air or oxygen. Kondratjev gave several reasons for attributing the characteristic bands to CO_2, but did not consider that this conclusion was finally established.

The afterglow spectrum, as photographed with small dispersion, has an appearance of simplicity which is not maintained when its analogue in the CO flame spectrum is photographed with the larger dispersion of Hilger's quartz spectrographs E2 and E1. With these instruments the spectrum has been found to be extremely complicated, consisting of a great number of narrow bands of various intensities, many of them being double. A few bands are possibly shaded to the red, but the majority of them are not clearly degraded in either direction. Some progress has been made in the analysis of the structure of the spectrum, but the results are still far from complete. The complicated system of bands, however, strongly suggests that the origin of the spectrum is something more complex than a diatomic molecule.

---

* 'Z. Physik,' vol. 63, p 322 (1930)

Summary and Conclusions.

The more important results of the experiments which have been mentioned above may conveniently be summarized as follows —

(1) The spectrum of the afterglow of CO_2 is different from any known spectrum given by oxides of carbon in vacuum tubes, but has been found to resemble that given by the flame of CO burning in air or oxygen

(2) The spectrum of the exciting discharge indicates that the afterglow is generated by the interaction of excited neutral molecules of CO with neutral molecules of oxygen. Under the conditions which gave rise to the afterglow, there was no evidence of dissociation of the CO_2 other than into neutral molecules of CO and O_2.

(3) The characteristic bands of the CO flame spectrum are independent of the presence of water vapour in the CO undergoing combustion (Weston).

(4) The HO bands which occurred in the spectrum of the afterglow probably originated in interactions between excited CO or O_2 molecules and water vapour which was present in quantities too small to reveal its presence in the exciting discharge.

These observations appear to be entirely in favour of the view that the bands of the CO_2 afterglow, and of the CO flame, are produced by the direct combination of CO and O_2, without dissociation into atoms of carbon and oxygen or molecules of carbon.

The probability that the characteristic bands of the afterglow represent CO_2 molecules is also strongly suggested by the great complexity which is revealed by the use of spectrographs of adequate resolving power.

DESCRIPTION OF PLATE.

Fig. 1.—Spectrum of CO_2 discharge by which the afterglow shown in No 2 was generated. Exposure 6 seconds. The Ångström and Third Positive bands of CO are very conspicuous. The Fourth Positive CO bands were also present but are out of range in the reproduction.

Fig. 2.—Spectrum of the CO_2 afterglow. Exposure 12 hours.

Fig. 3.—Spectrum of the flame of CO burning in oxygen at a pressure of 100 mm. (Weston).

Beryllium and Helium. I.—The Helium Contained in Beryls of Varied Geological Age.

By Lord Rayleigh, For. Sec., R.S.

(Received July 19, 1933.)

§ 1. *Introduction*

Many years ago I found[*] that the mineral beryl (composition $Al_2Be_3(SiO_3)_6$) contains much more helium than can be accounted for by the small traces of radioactive matter of the uranium and thorium series present in it. The same ground has been partly gone over again by other workers[†] but it cannot be said that their papers contain any further advance towards determining definitely the origin of the helium found.

Recently, on reconsidering the subject, it appeared that there was one outstanding point at least which was reasonably accessible to investigation, namely, the relation of helium content to the geological age of the specimen. If helium has accumulated in the mineral as the result of atomic disintegration continued through long geological periods, we should expect large helium content to be found only in beryls coming from ancient formations. If, on the other hand, it had been trapped in some way when the mineral was formed, or if its presence were due to the rapid disintegration of a comparatively short-lived parent such as radium or ionium originally present in the mineral, we should expect to find more helium in the beryls of younger formations, since the opportunities for its escape have been less.

Recent commercial interest in the production of beryllium has led to a more intensive search for beryl,[‡] and the continued labours of geological surveys in different parts of the world have also brought many fresh occurrences to light. It has, therefore, been possible to examine a much wider variety of samples than would have been obtainable in 1908.

The large majority of occurrences are in pegmatite or coarse grained granite. It not infrequently happens that veins of pegmatite, which is considered to represent the last phase in the consolidation of granite* represent offshoots from large granite "batholiths" and when such veins cut and bake sedimentary rocks of known geological horizon, there can be no doubt that they are younger than the latter. In other cases, as in the "basic complex" of the African continent, the pegmatites definitely underlie the sedimentary rocks, and are therefore older. The geological evidence is often far from being as definite as might be wished, but practically there is little doubt about the broader classifications of age, on which the main conclusion will depend. In most cases it will be enough to cite the opinions of geological authorities without going into their reasons in detail; but in a few critical cases of special importance some detail may usefully be given.

---

[*] 'Proc. Roy. Soc.,' A, vol. 80, p. 587 (1908); see also vol. 84, p. 195 (1910).

[†] Piutti, 'Rend. Acc. Lincei,' vol. 22, pp. 140, 671 (1913); Sasaki, 'Bull. Chem. Soc., Japan,' vol. 1, p. 253 (1926); Paneth and Peters, 'Z. phys. Chem.,' B, vol. 1, p. 170 (1928).

[‡] *Cf.* a pamphlet, "Beryllium (Glucinum) and Beryl," compiled by the Imperial Institute (H.M. Stationery Office, 1931).

By far the majority of the known occurrences of beryl are in the oldest formations. The reason for this may be sought in the fact that the beryl-bearing granites and pegmatites are "plutonic" rocks formed by the consolidation of rock magmas at great depths under the earth's surface. In the case of younger formations, time has often been lacking for the exposure of these by erosion of the overlying material In the present work, specimens from the younger rocks have been diligently sought, but only a limited number have been obtainable. Nevertheless, they seem to be enough to allow of a definite conclusion.

§ 2 *Experimental*

In the older work, helium was extracted from the beryls by heat. I have not been content with this simple method, which gives no adequate security that all the helium has been extracted. It has been thought necessary to break down by chemical decomposition the crystal structure in which the helium is held

Silicates are ordinarily decomposed for analysis by alkaline carbonate in a platinum vessel at a high temperature This is technically difficult to carry out when the gas evolved has to be collected quantitatively. The advantages of using a soft glass vessel are obvious, but any reagent capable of attacking a silicate will necessarily attack the glass also. This objection has not in practice been found to be serious. In order to eat away completely a grain of the powdered material, it is only necessary that the reagent should remove a layer of depth equal to the radius of the grain. By fine powdering, this radius may be made very small; and if the resistance of the glass walls to attack is at all of the same order as that of the mineral under investigation, the thickness of glass corroded away during the experiment will not be important.

---

* On this subject, see especially "Geology of the Pegmatites and Associated Rocks of Maine," by Edson S. Bastin, 'U.S. Geol. Surv. Bull. No. 445,' (1911); also "Rare-element Minerals of Canada," by H. V. Elsworth, pp. 111–130, 'Geol. Surv. Can., Economic Geology Series No. 11,' Ottawa (1932).

In practice it has been found that caustic potash at 300° C. quickly decomposes finely powdered beryl, without much destructive action on the glass vessel. The shape of the latter is as shown in the figure and it is enclosed in an electrically heated asbestos oven as shown by the dotted lines. The slope of the exit tube is necessary to prevent the water which is always contained in commercial sticks of caustic potash from condensing and running back into the vessel; this would almost certainly cause a crack. The condensed water runs forward into a drying tube containing broken stick potash. The gas is taken off through a Topler pump.

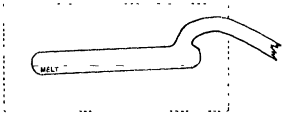

FIG 1 ½ actual size

In making a determination, 1 to 5 grams of beryl was finely powdered in an agate mortar, and introduced into the tube with about five times its weight of commercial stick potash. It was sealed into the pumping system and exhausted. Oxygen was then admitted to about 10 cm. pressure, so as to prevent undue frothing, and the oven was heated up. The potash fused at about 200° C., and at a rather higher temperature began to act vigorously on the beryl. This process could be watched through a mica window in the lid of the oven. As the temperature rose, water began to come over, the effervescing mass became pasty, and ultimately solid. At this stage the temperature had risen to about 300° or 310° C, and the action was over.

To make sure that decomposition was complete the residue was washed with water and all soluble or flocculent matter poured off. The residue was then warmed with dilute acid and this was in turn poured off. After further washing, the residue, if any, consisted of separated silica, soluble in warm caustic potash solution. No undecomposed beryl remained. After testing several residues in this way with satisfactory results, complete decomposition was usually taken for granted.

To return, however, to the method of dealing with the evolved gas. This along with the added oxygen was taken off through the Töpler pump, and introduced into a gas burette, where it was exploded. There was always a considerable quantity of hydrogen present in it The amount varied, and no particular note was taken of it, but it may perhaps have often been about 15 c.c. per gram of beryl The decomposition vessel (still kept hot) was washed out with more oxygen, and this in turn was added to the gas in the burette and exploded; this was continued till oxygen was in excess. The gas was then sparked over caustic potash to remove nitrogen. When contraction was over or nearly so, the excess oxygen was removed with phosphorus. The small residue from this operation, measuring perhaps 0·1 c.c., was introduced through the gas burette into the apparatus for final purification and measurement.

This final purification was by means of charcoal cooled in liquid air. The gaseous residue was allowed first to stand in contact with 1 gram of cooled charcoal, connection being open to the measuring apparatus, and to a second charcoal vessel, also containing 1 gram, but not yet cooled. After standing for some time (say, 30 minutes) in contact with this, the first charcoal was shut off and the second one brought into action. The measurement was carried out in an arrangement similar to a McLeod gauge, though it was, of course, used in this case primarily for measuring volume, not pressure. The cylindrical bulb of the gauge was of about 300 c.c. capacity, thus its volume was large compared with the charcoal bulbs and connections. To a first approximation the gas in this bulb might be taken as representing the whole quantity of helium. The necessary correction was determined as will be explained presently.

The gas was allowed to stand for some time in contact with the second charcoal. Owing to the rapid diffusion at low pressures this gave quite satisfactory purification throughout the volume of the complex tube system, uniform composition being reached almost instantaneously. After, say, 30 minutes, the residual gas was compressed into the measuring tube of the gauge, and its volume determined at some suitable pressure, chosen according to the quantity of helium present. As a check on purity, the spectrum of the residual gas was examined in the measuring tube itself. For this purpose a wire twisted once round the top of the tube was connected to one terminal of a small induction coil, the other terminal going to the mercury. The gas pressure was lowered to 1 cm. or less, and the discharge examined through a direct vision prism. If all had been done rightly, the helium lines stood out brilliantly on a dark background. Indeed, unless the quantity was exceptionally small the yellow colour of the discharge was reassuring even without the prism.

The measuring tube used had a volume of 1·526 c.mm. per millimetre length. Taking into account the range of pressure allowed for, the arrangements were convenient for measuring quantities of helium between 100 c.mm. and 0·05 c.mm. at N.T P.

As already mentioned, it was necessary to correct for helium remaining in the charcoal and connecting tubes. To determine this correction an arbitrary quantity of pure helium was trapped in the measuring tube and its volume measured. The charcoal tubes and connections up to the gauge were then washed out with a little air, and exhausted so that no helium remained in them. The mercury was then lowered in the gauge, so as to allow some of the helium to flow into the charcoal vessels, which were cooled in turn, as in the standard procedure described above. On measuring the helium volume again, it was, of course, less than before, a fraction of it remaining in the charcoal vessels and connecting tubes. The ratio of volumes was 1·154, and this factor was applied to the measured volume in each case, so as to allow for the helium remaining in the charcoal vessels and connecting tubes The volume was further reduced to N.T.P.

§ 3. *Tabulated Results.*

In giving the results, a broad classification into Archæan, Palæozoic, Mesozoic, and Tertiary, will be adopted in the first instance. In many cases the geological evidence does not really justify more than this, if indeed so much. After a preliminary survey, the more significant cases will be dealt with in greater detail.

In the following lists the first column gives the locality, and the second the source of my geological information. This is often simply the statement of the director of a geological survey or other competent authority who has kindly written on the matter In many cases it is to them that I owe the material. Such information is entered as p.c. (private communication). In other cases printed sources are cited. The results of the older investigation are incorporated in these lists.

§ 4. *Discussion.*

In examining these lists, it will be obvious that beryls of a given geological epoch may have almost any helium content over a wide range. Indeed, it cannot be said that there is any clear indication of an upper limit. The test

Archæan.

Locality of specimen.	Authority for geological age.	Helium content, c.mm. per gram.
Bangalore-Kankanhalli Road, Mysore, India.	Dr. L. L. Fermor (p.c)	77·6
Panchratan Hill, 4½ miles N W. of Goalpara, Assam, India.	„ „	31·9
Leydsdorp District, Transvaal (from Beryl Mining Co., Johannesburg).	Du Toit, 'Geology of S. Africa.' Map	29·2
Lakshinarayana Mine, Nellore District, Madras.	Dr L L Fermor (p.c.)	16·4
Kosumbah Central Provinces, Bhandra District, India.	„ „	16·0
Lyndoch Quarry, Renfrew Co., Ontario, Canada	H. V. Ellsworth, "Rare Minerals of Canada," pp. 168, 228.	14 8
Bihar Mica Belt, India	Dr. L. L Fermor (p.c.)	14 0
Tilana Village, Ajmer State, Rajputana, India.	„ „	13·3
Minas Geraes, Brasil	B. von Freyberg, "Ergebnisse Geologische Forschungen in Minas Geraes" (1932)	13·1
Cape Province, 30 miles N.W. of Steinkopf, Bushman Land	Du Toit, 'Geology of S Africa ' Map	11 5
S. Nigeria, between Ede and Offe River	"Bull. Geol. Surv , Nigeria," No 2, p 17 (1922)	10·7
Balingup, W. Australia	"Geological Map of Australia," by F W. Edgeworth David, Sydney, 1932 Also explanatory Notes to same, p. 32	9 64
Kamrup District, Assam	Dr L. L. Fermor (p.c.)	8·59
Ukeria Mica Mine, Mahaisri, Monghyr District, Bihar and Orissa.	„ „ ..	8·11
Amari, Nigeria ...	"Bull. Geol Surv , Nigeria," No. 5, p. 31.	7·79
12 to 16 miles N N E of Olary, S. Australia.	"Edgeworth David's Map of Australia," Sydney, 1932	6 98
Somaliland, lat 10° N., long. 45° E.	"First Report on Geology and Mineral Resources of British Somaliland," pp. 10, 39 (1924).	5·55
Nakop, S. Africa	Du Toit, "Geology of S. Africa." Map	4·80
Norway No locality given	Probably Archæan	4·75
Kalkfontein, S. Africa	Du Toit, "Geology of S. Africa." Map	4·14
Kahn Mine, Arandis	„ „ „	3·93
Govind Sagar, Kishengarh State, Rajputana.	Dr L. L. Fermor (p c)	3 49
Pur Gwalior State, within Udaipur State.	„ „	3·23
Knarwa, Ajmer, Rajputana	„ „	3·05
Kenya Colony (no locality given)	F R C. Reed, "Geology of British Empire," p. 27 (1921)	2·66
W. of Muchail, Padar, Kashmir	Doubtful. Probably Archæan Dr. L. L. Fermor (p.c).	2·40
Egypt, lat. 24° 40′ N., near Red Sea coast.	F. R. C. Reed, "Geology of British Empire" (1921)	0·934
Deadwood, S Dakota, U.S.A.	'U.S. Geol. Surv Bull. No. 507,' p. 38 (1912).	0 824
Tittamalai Village in Govichettypalayam Taluk, Coimbatore District, Madras.	Dr. L. L. Fermor (p.c.)	0·656
Kalichedu Mica Mine, Nellore District, Madras.	„ „	0·425
Konigswarte, Bohemia	F. Kratzer, "Geologie von Böhmen Prague," (1892). Map.	0·0550

Palæozoic.

Locality of specimen.	Authority for geological age.	Helium content, c mm. per gram.
Acworth, New Hampshire, U.S.A.	See below, p. 378	16·8
Hebron, Maine, U S.A.	"	7·92
Chester, Pennsylvania	"	6·80
Litchfield, New Hampshire, U.S.A.	"	5·77
New Hampshire (no detail)	"	3·45
Amelia, Co. Virginia	Dr. W. C Mendenhall (p.c.)	3·32
Massachusetts (no detail)	See below, p 378	3·20
Madagascar	Lacroix, " Mineralogie de Madagascar," (1923) Passim.	1·85
Galicia, Spain	Don Luis de la Peña y Braña (p c)	1·47
Australia, Emerald (probably from Emmaville, N S. Wales.)	" Mineral Resources of N.S. Wales," by E A. Pittman, p. 406 (1901).	0·557
Massachusetts (no detail)	See below, p. 378	0·525
Massachusetts, aquamarine	"	0·480
Hurum, Oslo District, Norway	Professor J Schetelig (p.c.)	0·317
Branchville, Connecticut (Rose beryl)	See below, p. 378	0·281
Donegal, Ireland	Cole and Halissy, " Geology of Ireland," pp. 6, 7.	0·277
Guarda, Portugal	Imperial Institute. Monograph on Beryllium and Beryl, p 18 (1931).	0·244
Siberia (Urals)	Dr. S. J. Tomkeieff (p.c.)	0·225
Siberia (Urals) (emerald)	" "	0·0925

Latah, Co. Idaho, U.S.A.	See below, p 379	2·27
Temecula, California	See below, Pala, California	0·818
Columbia (emerald)	" Encyclopædia Britannica " (article " Emerald ").	0·459
Byengzi Peak, Jamettim District, Burma.	Dr L. L. Fermor (p.c.)	0·157
Suebo Sunn, Tavoy, Burma	" "	0·120
Pala, California	" Report 14, State Mineralogist, California," p. 640 (1913–14). F. H. Hudson, University of California, ' Pub. Geol. Sci ,' vol. 13, p. 175 (1922).	0·0361
Sirwigh, Lutkup, Chitral, N.W. Frontier Province, India.	Dr. L. L. Fermor (p.c.)	0·0327

Tertiary.

Bergell Alp	See below, p. 380 ..	0·384
Lundy Island (Bristol Channel)	Probably tertiary. Professor W. T. Gordon (p.c.).	0·110
Clear Creek, Chaffee Co., Colorado	Dr. W. C. Mendenhall (p.c.)	0·0872
Mourne Mountains, Ireland (aquamarine)	Professor W. W. Watts (p.c.) ..	0·0758
Brown's Gulch, Coffee Co , Colorado	Dr. W. C. Mendenhall (p.c.)	0·0545
Mourne Mountains, Ireland ..	Professor W. W. Watts (p.c.)	0·0451
Elba	" Encyclopædia Britannica " (article " Elba ").	0·0182

of many further specimens would probably reveal examples in each of the four epochs with considerably more helium than any here examined, but my own effort in this direction is exhausted

In spite of the fact above mentioned, it is also apparent that beryls of archæan age contain in general far more helium than beryls of tertiary age. Indeed, if the archæan and tertiary were arranged together in a single list, in order of helium content, there would be little overlapping. We see, then, how very sharply this contrasts with what would be expected if the helium had been present at an early stage in the history of each specimen For in that case the tertiary specimens should contain more helium than the others, having had less opportunity to lose it

In general, each epoch tends to show smaller helium content than its predecessor We may compare the maxima in each list, but this is somewhat arbitrary, depending too much on exceptional specimens which might easily have been missed in obtaining the material Even the arithmetic means for each period are too much affected by these exceptionally rich specimens, and the medians, or values half-way down each list, are more representative. The values (cubic millimetres helium per gram) stand thus :—

	Archæan.	Palæozoic.	Mesozoic	Tertiary
Maximum ...	77·6	16·8	2 27	0·384
Median	6·98	1·47	0·157	0 0758

In view of these results, it seems safe to consider that the correlation with geological age is established, in the sense that increased age tends to bring increased helium content.

Great variability is found, however, in specimens of the same age, even in localities geologically similar and not very far apart geographically. The cause of this variability requires attentive consideration. Having regard to the definiteness of beryl as a mineral species, and the comparatively small variability of composition, it is probable that one specimen of unweathered beryl can, *cæteris paribus*, retain helium as well as another ; and, if so, the variability of helium content at a given age would most naturally be attributed to the temperature variations which the specimens have undergone during their past history. The temperature will in any case have varied according to the depth below the earth's surface at which they may have been at different periods of geological time ; and other and more violent agencies have probably intervened. Some specimens of beryl crystals are visibly bent, and in view of the experimental fact that moderate heating drives out much of the helium, it would scarcely be expected that the gas would be retained under such vicissitudes.

Accordingly the question put at the beginning of this paper is answered in the sense that helium is continuously generated in beryl throughout geological time. Sometimes it is largely retained, sometimes not, according to circumstances. This view is consistent with the facts, in that the older beryls contain considerable quantities of helium, while, so far as the data go, the younger ones never do so.

The evidence, taken as a whole, allows us to make the above assertion. Unfortunately, the possibility that helium may in individual cases have been lost, prevents the relation being of much use to the geologist, for determining the age of a given sample from the helium content.

Special importance attaches to the case when a specimen contains more helium than any of the contemporary or than any of the younger specimens. These cases which head the several lists given on pp. 375, 376, and constitute the maxima collected on p. 377 are the most informing, if we wish to approximate as nearly as may be to the total quantity of helium which has been generated in beryl since a given geological epoch. They may usefully be recapitulated with a fuller statement of the geological evidence, which for some of the specimens is fairly definite.

Archæan.—By far the largest helium content (77·6 c.mm. per gram) is found in beryl from pegmatite on the Bangalore-Kankanhalli Road, Mysore, India. This belongs to the basic archæan platform of India. There has been some difference of opinion as to whether these granites and pegmatites are to be placed in the earliest sub-division of all, or not.[*]

Palæozoic.—Nothing has been found in the present work richer than the specimen of beryl from Acworth, New Hampshire, U.S.A., containing 16·8 c.mm. helium per gram, which is described in the earlier investigation. Other specimens from this locality are not equally rich. The age is late Silurian or Devonian.

The granites of the New England States and their associated pegmatites are all considered to be of nearly the same age. This is on the ground of the general similarity of character, and of the nearly continuous extension over long distances bridged in some cases, by areas intensely intruded with granite. The age is best indicated in the Perry region on the eastern border of Maine. "In the Silurian rocks of this region no granite pebbles are found, but such pebbles, plainly derived from the main granite masses of this region, occur abundantly in the conglomerate of the Perry formation, which is of late Devonian age. The granite of the Perry region is therefore late Silurian or Devonian in age. Evidence confirmatory but less complete is found in the Vinalhaven region, where the granite intrudes surface volcanics of Niagaran age."*

---

[*] See "Geology of the British Empire," by F. R. C. Reed, pp. 264–265 (1921).

Mesozoic.—Beryl from Latah County, Idaho, U S.A , contains 2 27 c mm helium per gram Age, late Jurassic or early Cretaceous A statement of the geological evidence for this has been kindly drawn up for me by Dr. W Q Kennedy, of the Geological Survey of Great Britain. The following is slightly compressed from his account †

The pegmatite dykes from which the beryl is obtained belong to a class of dykes, some of which cut the plutonic rocks (quartz-monzonites) of the district, and belong to the same period of intrusion as the latter, which are to be classed with the main mass of the Idaho batholith The beryl-bearing rocks are therefore of the same general age as the Idaho batholith, which, on the following grounds is referred to a late Jurassic or early Cretaceous period of intrusion.

(1) The batholith is much older than the miocene, for the miocene volcanic rocks of the Colombia plateau rest on the eroded surfaces of the granitic rocks.

(2) In the Salmon River region, the batholith intrudes and alters rocks of Permian and Triassic age, and belongs therefore to a period of intrusion later than the Triassic

The above direct evidence points to a post-Triassic and pre-Miocene age for the batholith The following indirect evidence, however, may be adduced in favour of a late Jurassic or early Cretaceous age.

(3) In Eastern Oregon, granitic rocks, closely similar to the Idaho batholith, and presumably of the same age, are known to belong to a post-Triassic and pre-Upper Cretaceous period of intrusion

(4) The Nelson batholith in British Columbia is correlated with the Idaho batholith, and is believed to be a Northern continuation of the latter, although the two masses are not actually connected at the surface The Nelson batholith is younger than the carboniferous strata, but older than the upper Cretaceous. It is related to orogenic movements which took place in Jurassic times, and most probably dates from a late Jurassic or early Cretaceous epoch.

---

* G. O. Smith, "Bull. U.S Geol. Surv , No. 313," p. 11 (1907).

† The sources of information are . D. B. Sterret, "The Mica Deposits of the United States," 'Bull. U.S. Geol Surv ,' No 746, p. 86 (1923) ; A. L. Anderson, "Mica Deposits of Latah Co.," 'Idaho Bur. Min. Geol.,' pamphlet No. 14 ; C. T. Ross, "Tertiary Granitic Rocks in Idaho," 'J. Geol.,' vol. 36, p. 673 (1928).

(5) Tetiary and late Cretaceous igneous rocks are known from various parts of Idaho, and in all cases they are younger than the Idaho batholith.

From the direct evidence, therefore, the granitic rocks (and by inference the beryl-bearing pegmatites) of Idaho are of post-Triassic and pre-Miocene age. The indirect evidence, however, points most strongly to a late Jurassic or early Cretaceous age for these rocks.

Tertiary.—Beryl from the Bergell Alp contains 0·384 c mm. helium per gram. Age, Middle or Lower Miocene. The evidence[*] for this has been summarized for me by Dr. Kennedy as follows —

(1) Within the Bergell region there are representatives of the three great Pennine Nappes, the Great St. Bernard Nappe, the Monte Rosa Nappe, and the Dent Blanche Nappe. The granite cuts across and bakes the different members of the superimposed masses, and in addition sends innumerable veins and apophyses into the rocks. These cut across folds and planes of dislocation in all directions so that the intrusion of the granite is subsequent to the alpine folding.

(2) The granite does not show any cataclastic effects such as shearing, and the formation of mylonites, and the primary jointing (invariably destroyed by earth movements) is still preserved.

(3) At various localities, masses of known Trias and Lias, together with other mesozoic rocks are enclosed in and contact-metamorphosed by the granite.

(4) A lower age limit for the granite is given by the presence of Bergell granite boulders in the Upper Miocene "Nagelfluh" of the Southern Alps.

The granite was therefore intruded at some period later than the main alpine orogenic movements (*i.e.*, later than the oligocene), but earlier than the formation of the Nagelfluh in Upper Miocene times. Its age is therefore either Upper or Middle Miocene.

§ 5. *Acknowledgments.*

For material, I have to thank the kindness of Mr. T. Crook (Principal, Mineral Resources Department, Imperial Institute), Dr. L L Fermor (Director, Geological Survey of India), Professor W. T. Gordon, Mr. E. Hopkins, Professor A. Hutchinson, F.R.S , Messrs. Johnson and Matthey, Professor J. Joly,

---

[*] See A. Heim, "Geologie der Sweiz," Leipzig, vol. 2, pp. 61–65 (1922); R. Staub, 'Vjschr. naturf. Ges. Zurich,' p. 1 (1918); On the Occurrence of Beryl, see R. Staub, 'Schweiz. min. petrogr. Mitt.,' vol 4, p. 364 (1924).

F.R S., Sir Henry Lyons, F.R S, and Mr W F. Hume (Egyptian Survey), Dr. W. C Mendenhall (Director, U.S Geological Survey), Professor R. L. Parker, of Zurich, and Dr. Hirschi, of Spiez, Don Luis de la Peña y Braña (Director, Geological Survey of Spain), Sir Joseph Petavel, F R S, and Professor J Schetelig (Mineralogical Museum, University of Oslo).

Many of the above have also given helpful information, so also have Sir John Flett, F R S., Dr L J Spencer, F R S, and Dr. S J. Tomkeieff. I must also specially thank Dr. W Q Kennedy, of the Geological Survey of Great Britain, whose notes have been largely used in the text of this paper.

My assistant, Mr R Thompson, has given efficient assistance in the experimental work.

§ 6 *Summary and Conclusion*

The helium content of upwards of 60 specimens of beryl has been determined These, though predominantly Archæan in age, include a considerable number from later geological formations

Helium could readily be detected and measured in all of them* using as a rule only 1 gram of material. The following are the largest quantities of helium (cubic millimetre per gram of beryl) found in this work in the various geological groups, and also the median quantities which may be taken as typical for each group —

	Archæan.	Palæozoic.	Mesozoic	Tertiary.
Maximum	77·6	16·8	2·27	0·384
Median	6·98	1·47	0·157	0·0758

It is clear, therefore, that large helium content is limited to specimens of great geological age. It has never been found in the younger specimens.

The conclusion is that the helium has accumulated in beryl during geological time, and was not present in it initially, nor generated during the first few millennia by decay of any relatively short-lived radioactive constituent such as ionium or radium, which may have been initially present. It is also known from the author's earlier work not to be due to uranium or thorium.

A preliminary discussion of the origin of this helium was given in a letter to 'Nature.'† It is hoped to discuss it more fully in a sequel to this paper, in connection with further experimental work.

---

* One isolated specimen which did not show it proved ultimately not to be beryl at all

† Vol. 131, p. 724, May 20th (1933).

The Influence of the Underlying Surface on the Cataphoretic Mobility of Adsorbed Proteins.

By A. Dummett and Philip Bowden, Laboratory of Physical Chemistry, Cambridge.

(Communicated by T M. Lowry, F R S —Received April 10, 1933)

Our knowledge of the structure of the electrical double layer at the interface between a solid and a liquid is so indefinite that it is difficult to give a precise definition or to make an exact measurement of electrokinetic potential. In the liquid in the immediate vicinity of the solid surface, there will be an excess of ions of opposite charge to that on the surface, forming an electrical double layer which is approximately a molecular diameter in thickness All the potential drop, however, is not confined to this first double layer , the excess ions in the solution are not rigidly held to the surface, they are able to break away and to form a diffuse layer which extends some distance into the solution. Experience has shown that gentle stirring of the solution can influence the distribution of these ions, and it is probable that the diffuse layer extends as far as 10^{-5} to 10^{-4} cm. from the solid surface It is this diffuse layer of more or less loosely held ions which is responsible for the electrokinetic properties of liquids in contact with solid surfaces.

No exact relation has been established connecting the diffuse, or electrokinetic potential, with the total potential drop between a solid and a liquid. Usually they are of the same sign, but there is evidence that the potential drop across the diffuse layer can even be opposite in sign from the main potential, indicating a twofold double layer The presence of polar molecules adsorbed at the interface may have a profound effect on the distribution of the diffuse layer without sensibly affecting the total potential difference Further work on the relationship between these quantities would be valuable.*

Although electrokinetic measurements can give information only about the diffuse layer, and not about the total potential across an interface, they can be of considerable use in explaining or predicting the behaviour of colloidal and electrolyte systems Thus the electrokinetic potential of an amphoteric electrolyte is a minimum when the electrolyte is at its isoelectric point, and many of the chemical and physical properties of colloidal solutions show an optimum value when the electrokinetic potential, as measured by endosmosis or cataphoresis, shows a change of sign The rate of coagulation, the osmotic pressure and the viscosity of colloids are all at a maximum when the electrokinetic potential is a minimum.

---

* See Frumkin, ' Z. phys. Chem.,' vol. 164, p. 121 (1933)

Measurements of cataphoretic mobility have been widely used to determine the isoelectric point and electrokinetic properties of important proteins. When the protein particle is visible in the ultra-microscope, its movement in an electric field can be followed directly, but when dissolved, the protein molecule is too small to be visible The device of adsorbing the protein on to inert particles large enough to be seen, was used by Loeb,* who observed the motion of small collodion particles suspended in a gelatine solution The collodion particles showed a modified cataphoretic mobility which was characteristic of gelatine. Freundlich and Abramson† found that the mobility of zinc and quartz particles through gelatine and egg albumen solutions was independent of the nature of the suspended particle, provided the concentration of the protein exceeded 10^{-4} grams per litre They measured the mobility of the particles in solutions of egg albumen at different hydrogen ion concentrations, and found that the particles showed no movement at p_H 4·7 This agreed well with the results of Svedberg and Tiselius‡ obtained by the moving boundary method, and gave a value for the isoelectric point identical with that obtained independently from titration curves. Abramson§ also adsorbed serum proteins on to quartz particles and oil drops, and found that the p_H-mobility curve for the adsorbed serum was identical for both suspensions, and gave an isoelectric point which closely resembled that obtained from the titration curve for serum albumen Abramson has carried out an extensive series of experiments in this field. Using serum proteins, egg albumen and gelatine adsorbed on to particles of glass, quartz, menthol, tyrosine, cystine, camphor, agar, charcoal, zinc oxide, oil droplets and air bubbles, he found that the mobility was independent of the size, shape and nature of the particle and depended only on the nature of the protein He showed|| that, for gelatine and egg albumen adsorbed on quartz, the p_H-mobility curve was coincident with the titration curves of Simms,¶ and the streaming potentials of Briggs,** and concluded that "All these observations indicate that the process of

---

* 'J Gen. Physiol,' vol. 6, p. 116 (1923), vol 5, p. 395 (1922).

† 'Z phys Chem,' vol 128, p 25 (1927).

‡ 'J Amer. Chem. Soc,' vol 48, p 2272 (1926)

§ 'J. Gen. Physiol.,' vol. 13, p. 169 (1929)

|| 'Proc. Soc. Exp Biol Med.,' vol 36, p. 689 (1929).

¶ 'J. Gen. Physiol.,' vol 9, p. 629 (1928).

** 'J. Amer. Chem. Soc.,' vol. 50, p. 2358 (1928).

adsorption of the proteins mentioned does not appreciably change the ionisation of the adsorbed protein at the protein-water interface "*

Experiments described in this paper show that this is certainly not true for all proteins. Measurements have been made of the cataphoretic mobility of both oxy- and carboxy-hæmoglobin adsorbed on to suspended particles of fresh quartz, old quartz, carbon, evacuated carbon, copper and paraffin oil drops, all suspended in aqueous solution. All these substances gave excellently reproducible results and (with the exception of the oil drops) showed good adsorption maxima. The cataphoretic mobility and the apparent isoelectric point, were, however, very different for each adsorbing surface. The reason for this is discussed.

Apparatus

The measurement of the cataphoretic velocity of suspended particles is complicated by the fact that endosmotic effects cause a movement of the solution along the walls of the cell. For this reason the internal geometry of the cell is important. A cell of circular cross-section has the advantage that the flow of the liquid is symmetrical and easily calculable. The cell used in these experiments was a modified form of that described by Mattson† and is shown in fig 1.

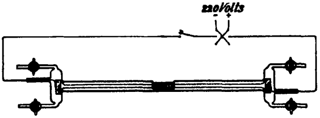

FIG. 1

It consisted of a piece of wide bore capillary tubing 2 5 mm. in internal diameter and 25 cm long. In the centre of this, two flat surfaces at right angles were ground out and optically polished, these served as windows for the Tyndall beam and the objective of the microscope respectively. The ends of the capillary tube were fused into small chambers about 1·5 cm. in diameter and 5 cm. long fitted with outlet tubes and accurately ground greaseless taps. These chambers contained the cylindrical platinum black electrodes 1 cm. long by 0·5 cm. in diameter which were fitted close against the ends of the capillary tube The circular cross-section of the tube gave symmetrical endosmotic flow, and a large potential gradient could be applied without causing turbulence or convection currents due to heating. The length of the capillary tube and the short time necessary for an experiment prevented any contamination of the protein in the centre of the tube by oxygen or hydrogen discharged at the electrodes The current densities employed were too low to permit any evolution of gas-bubbles at the electrodes A potential of 220 volts was applied directly to the two electrodes, with a reversing switch and tapping key in the circuit The light for the ultra-microscope was supplied by a small automatic arc, and passed through a filter of copper sulphate solution to absorb the heat, before being condensed in the capillary tube The microscope for observing the particles was fitted with a × 20 eyepiece and an objective with a working distance of 0 5 cm The whole microscope could be racked up and down in the vertical plane and its position read on a vernier so that the particles could be observed at different depths in the tube

---

* 'J. Gen. Physiol.,' vol. 13, p. 169 (1929).

† 'J. Phys. Chem,' vol 32, p. 1532 (1928).

Experimental

The proteins used in the early experiments were Kodak ash-free gelatine, and hæmoglobin prepared from ox blood by Mr. G. S. Adair. With the hæmoglobin it was found that, unless bacteria were rigidly excluded, sufficient change took place in the protein to vitiate all results. The final solution was therefore diluted to a stock strength of about 1% (estimated optically), filtered through a sterile candle and stored at 0° C All the vessels, pipettes, &c., were sterilized before use by steaming out.

The oxyhæmoglobin was converted to carboxyhæmoglobin by saturating the solutions with carbon monoxide The buffer solutions employed were acetic acid potash and potassium dihydrogen phosphate potash, the solutions always being made up so as to be N/200 to the anion. Measurements made in the two buffer solutions at the same p_H showed the mobility to be independent of the nature of the buffer at these concentrations.

The protein was adsorbed on to the following surfaces .—

(*a*) Quartz particles prepared by grinding a clear crystal of natural quartz in an agate mortar with a little water, making into a milky liquid, and rejecting and regrinding all that settled out. The resultant suspension was quite stable for some hours when diluted to a strength convenient for observation in the cell.

(*b*) Particles of active blood charcoal separated out by settling, as for quartz. These particles have very small air bubbles filling the pores and adhering to the surface. A further suspension of "evacuated charcoal" was prepared by evacuating under a filter pump and then admitting the solution.

(c) A copper suspension prepared by arcing pure copper under distilled water, with a potential difference of 12 volts, until a brown suspension was obtained.

(d) Paraffin oil drops prepared by shaking together vigorously equal volumes of medicinal paraffin and distilled water. This gave an emulsion stable for several hours

The best concentration of particles for maximum ease of observation in the ultra-microscope was determined by experiment, and this concentration was used throughout

The solutions were made up as follows:—A measured volume of the 1% stock solution was diluted until its strength was about ten times that finally required From 1 to 9 c c (depending on the p_H required) of potash were added to 10 c.c. of the N/20 buffer anion solution and diluted with 50 c c of water. Then 10 c c of the diluted stock and the requisite amount of suspension were added to this and the whole solution made up to 100 c.c. The solution was allowed to stand for half an hour until adsorption equilibrium was established.

The p_H of the solutions was measured with a quinhydrone electrode. For the dilute solutions used in these experiments, the errors due to salt and protein were negligible The p_H measurements were checked against a hydrogen electrode and in no experiment was the error greater than $\pm 0{\cdot}02$ p_H The p_H of the buffered solution was independent of the concentration of the protein over the range of concentration used (10^{-5} to 10^{-1} gm./litre).

The viscosities of the buffered protein solutions were measured in an Ostwald viscometer, but at the maximum concentration of protein used (10^{-2} to 10^{-1} gm /litre) the viscosity did not differ from that of distilled water.

It is essential that the walls of the cell be kept rigorously clean, and free from denatured protein. Strong chromic acid or alcohol are unsatisfactory as cleaning agents because they denature the protein which then adheres very strongly to the walls. It is better to clean with dilute caustic soda followed by distilled water

Measurement of Cataphoretic Mobility.

Since there is a diffuse electrical layer at the surface of the tube itself there will be a tangential movement of the liquid along the walls when a potential is applied along the tube. If the system is closed there will be a returning stream of liquid moving in the opposite direction down the centre of the tube.

The velocity of the liquid and the observed velocity of the suspended particles will therefore vary according to the level in the tube at which readings are taken. To determine the mobility of the particles through the *solution*, it is necessary to take a series of readings at different levels down the tube.

The apparent velocities of the particles were measured at different depths in the tube by racking down the microscope by successive turns of the vernier screw. Readings were taken of the time required by a particle to traverse a convenient number of divisions on a grid in the focal plane of the eyepiece, the grid being calibrated against a standard ruled grating Observations were made on several particles with the potential applied in alternate directions to compensate for minor variations among the particles and any slight general drift, due to thermal convection, which the solution may have. If t_1 and t_2 are the two average times of transit across n divisions of the grid with the potential applied in alternate directions, then $\frac{nl}{2}\left(\frac{1}{t_1}+\frac{1}{t_2}\right)$ = velocity in cm./sec., where l is the length in centimetres of one division of the grid For the calculation of the mobility it is sufficient to plot the "relative mobility" = $\frac{n}{2}\left(\frac{1}{t_1}+\frac{1}{t_2}\right)$ against the depth down the tube expressed in turns of the vernier screw. Table I shows typical results for carbon particles suspended in carboxyhæmoglobin solution at p_H 5·01.

Table I.

Turns from top.	n.	t_1	Mean	$1/t_1$	t_2.	Mean	$1/t_2$	$n/2\,(1/t_1 + 1/t_2)$.
8	2	4·0, 4·2	4·1	0·244	4·5, 4·7	4·6	0·217	0·461
16	3	3·5, 3·6	3·5	0·286	4·3, 4·5	4·4	0·227	0·770
20	4	4·3, 4·2	4·2	0·238	5·2, 5·3	5·3	0·189	0·854
24	4	4·0, 4·1	4·0	0·250	5·2, 5·1	5·2	0·192	0·884
28	4	4·2, 4·2	4·2	0·238	5·3, 5·4	5·4	0·185	0·846
32	4	4·7, 4·9	4·8	0·208	6·2, 5·9	6·1	0·164	0·744

Apparent diameter of tube = 48 turns, Temperature = 15·5° C., Charge +ve, Potential difference = 220 volts. Length of tube = 24·5 cm 1 div of grid = $2·64 \times 10^{-3}$ cm

The relative velocity of particles at different depths in the tube are plotted in fig. 2. Fig. 2 *a* is for bare quartz particles suspended in a buffer solution Fig. 2 *b* for quartz particles coated with gelatine (in a tube of smaller diameter) Both curves are smooth and parabolic and the centre of the parabole coincides with the geometric centre of the tube. The parabola for bare quartz particles, however, does not pass through the origin.

Smoluchowski* has derived an expression for the cataphoretic mobility in terms of the velocity observed at certain depths

Let V_s = observed velocity of the particle at a depth x in the tube
V_w = velocity of the liquid at a depth x in the tube
V_c = true cataphoretic velocity of the particle

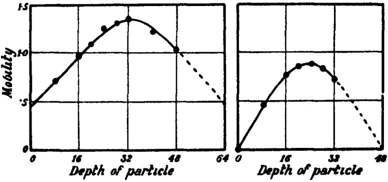

Fig 2

Therefore,

$$V_s = V_w + V_c,$$

or

$$\int_0^d V_s\,dx = \int_0^d V_w\,dx + \int_0^d V_c\,dx, \tag{1}$$

where d = diameter of the tube.

For a closed system $\int_0^d V_w\,dx = 0$, since no fluid is gained or lost therefore,

$$V_c = \frac{1}{d}\cdot\int_0^d V_x\,dx = \frac{1}{r}\int_0^r V_s\,dx, \tag{2}$$

where

$$r = \frac{d}{2}$$

$\frac{1}{r}\int_0^r V_s\,dx$ may be evaluated by graphical integration of the curve obtained by plotting V_s against x.

Smoluchowski has shown that, ideally, V_s is a parabolic function of x. If this is so, integration of (2) leads to

$$V_c = V_s \text{ when } x = r\left(1 \pm \frac{1}{\sqrt{3}}\right), \tag{3}$$

---

* "Handbuch der Electrizität und des Magnetismus," Leipzig, vol. 2, p. 366 (1921).

or

$$x = \frac{d}{5} \text{ approximately.}$$

Smoluchowski has also derived an approximation for V_e to be obtained by measurements at two widely different parts of the tube, namely,

$$V_e = \frac{3V_{d/6} + V_{d/2}}{4},$$

where $V_{d/6}$ = observed velocity of the particle at a depth equal to $d/6$, etc.

Thus, if the distribution of observed cataphoretic velocities is parabolic with respect to the depth at which the measurement is made,

$$V_e = V_{r\left(1 \pm \frac{1}{\sqrt{3}}\right)},$$

and approximately

$$V_e = V_{d/5}, \tag{4}$$

or

$$V_e = \frac{3V_{d/6} + V_{d/2}}{4} \tag{5}$$

The curves obtained bear out Smoluchowski's theory. Thus for figs. 2 *a* and 2 *b* we have, for the values of V_e (expressed as relative velocity)

	Graphical Integration.	$V_{r\left(1 \pm \frac{1}{\sqrt{3}}\right)}$	$V_{d/5}$	$\frac{3V_{d/6} + V_{d/2}}{4}$
Fig 2 *a*	0·940	0·922	0·898	0·960
Fig 2 *b*	0·556	0·561	0·544	0·554

All results used in this paper have been calculated from a graphical integration of the parabolic curve obtained by plotting V_a against x for varying values of x. A correction for change of viscosity with temperature was introduced and the true cataphoretic mobility calculated from the expression

$$\text{Cataphoretic Mobility}_{15^\circ} = \frac{Ll\eta_{t^\circ}}{E\eta_{15^\circ}} \times \text{Relative Mobility in cm./sec./volt./cm},$$

where L = length of tube in cm., l = length corresponding to one division on the grid in cm., E = applied potential in volts, and η_t = viscosity at t° C. For example, the cataphoretic mobility of quartz suspended in acetate buffer at p_H 4·67 is equal to

$$\frac{0{\cdot}940 \times 25{\cdot}1 \times 2{\cdot}64 \times 10^{-2} \times 10{\cdot}86}{220 \times 11{\cdot}45}$$

$$= 2{\cdot}686 \times 10^{-4} \text{ cm./sec./volt/cm.}$$

Significance of Position of Origin of the Parabola.

If V_E = endosmotic velocity of the solution at the wall of the tube, then V_0, the velocity of particles at the wall $= V_e - V_E$

On the theory of Helmholtz and Smoluchowski the cataphoretic mobility of a particle is given by

$$V_e = \frac{1}{4\pi}\frac{XD\zeta}{\eta},$$

where X = field strength, D = dielectric constant of the medium,

ζ = electrokinetic potential due to the double layer,

η = viscosity of the medium.

The theory predicts that V_e shall be independent of the size or shape of the particles and that $V_E = V_e$, when the electrokinetic potentials of the surfaces of the particle and the wall are the same.

Debye and Hückel* have derived a theory which predicts that though the Helmholtz-Smoluchowski formula holds for a cylinder, the cataphoretic mobility of a spherical particle is given by

$$V_e = \frac{1}{6\pi}\frac{XD\zeta}{\eta}$$

On this theory therefore $V_E = 1{\cdot}5\,V_e$ and V_e should be dependent on the size and shape of the particle. Abramson† has shown that these predictions do not hold for particles suspended in a protein solution.

The mobility curve for any given conditions in a cataphoresis cell can only pass through the origin if $V_E = V_e$. We found in these experiments that this occurred when the surfaces of the cell and of the particle were both saturated with protein. In fig. 2 *b* where both the quartz particles and the walls of the tube were saturated with protein the parabola passed through the origin. If either of the surfaces were unsaturated the readings became more variable and the parabolas did not pass through the origin. This is seen in fig 2 *a*, where one of the surfaces is quartz and the other glass, and no protein is present. A similar effect was observed for very dilute protein solutions, for protein at a weakly adsorbing interface, or for protein very near its isoelectric point.

When V_E was not equal to V_e, the ratio V_E/V_e had a variable value which depended upon the degree of saturation of the surfaces and it never became constant and equal to 1·5.

---

* 'Phys Z,' vol. 25, p. 49 (1924).

† 'J. Gen. Physiol.,' vol. 13, p. 657 (1930).

Rate of Adsorption of the Protein.

In order to determine the time required for adsorption equilibrium to be established between the dissolved protein and the adsorbing surface, measurements of mobility were made at different intervals of time after adding the protein.

The cell was filled with a solution of gelatine of concentration $1 \cdot 2 \times 10^{-2}$ gm./litre in a phosphate buffer at p_H 5·99 and allowed to stand for two hours This ensued that adsorption equilibrium had been established at the walls of the cell. This solution was then removed and quartz suspension added to the remainder of the solution which was shaken and quickly run into the cell. A series of readings were immediately taken at a depth in the tube corresponding to $r\left(1 - \frac{1}{\sqrt{3}}\right)$. The results are given in Table II

Table II.

Time in Minutes	Observed Velocity in cm./sec × 10^3.
3	0·89
5	0 91
7	0 90
15	0 90
30	0 91

Considering the roughness of the readings, the agreement is satisfactory, and shows that adsorption equilibrium with the suspended quartz particles was reached in a few minutes.

To determine the time necessary for adsorption equilibrium to be established at the glass walls of the cell, another series of readings was taken. A gelatine solution containing $1 \cdot 3 \times 10^{-3}$ gm. per litre was made up in phosphate buffer of p_H 5·89 and allowed to come to equilibrium with suspended quartz particles This was then run into the clean cell and a series of readings taken at various depths in the tube, sufficiently numerous to plot the parabola. The relative mobility was evaluated from it by graphical integration, and corrected for change of viscosity with temperature. The results are given in Table III.

The results for the mobility of the particles showed excellent agreement almost from the beginning, but the parabolas do not pass through the origin until between 20 and 40 minutes had elapsed. This showed that adsorption equilibrium with the glass was not established (in the dilute solution of 10^{-3} gm./litre) until after half an hour.

This gives a convenient method for measuring the rate of adsorption of proteins from solution In strong solutions the surface became saturated in a few seconds, but in very dilute solutions equilibrium was only reached after some hours

Table III

Time equilibrized in mins	Temp.	Observed Velocity in cm./sec. × 10^3	η_{t° × 10^3	Velocity, 15° C in cm /sec × 10^3.	Remarks
	°C				
0—20	11·5	0·85	12·55	0·89	Poor parabola.
20—40	11·7	0·81	12·48	0·89	Good parabola, not quite passing through zero
40—65	11·7	0·81	12·48	0·88	Good parabolas passing through zero.
75—95	12·0	0·80	12·39	0·87	

The procedure adopted was to make up the solution of protein in the buffer with the required amount of suspension and allow it to stand for half an hour. The clean cell was then filled with the solution and also allowed to stand for a half hour. This solution was then run out and the tube filled with the final solution on which the readings were made. Using this technique, readings were obtained which always gave good parabolas. The parabolas passed through the origin except when the protein concentration was less than that required to give saturation both on the suspension and on the walls of the cell A similar effect was observed for hæmoglobin very near its isoelectric point. The cataphoretic mobility was normal, and a good parabola was obtained, but it did not pass through the origin, indicating that the adsorption at the glass wall of the cell was weak when the protein was near its isoelectric point

The method was very sensitive to traces of impurity in the protein With hæmoglobin it was found that even minute traces of methæmoglobin or of denatured hæmoglobin made it impossible to get good parabolas or reproducible results. Bacteria were especially harmful, and it was essential that the solution of the protein should be kept sterile and stored below 0° C. The plotting of the whole parabola for each measurement of mobility gave a check on the conditions and showed up any irregularity or impurity in the solution or on the walls of the cell.

Adsorption Isotherms for Protein on Different Surfaces.

The relation between the concentration of a gelatine solution and the cataphoretic mobility of suspended quartz particles was determined. The mobility of the quartz was first affected when the concentration of the gelatine solution was ca. 10^{-7} gm./litre gelatine and reached a maximum when the concentration was 10^{-5} to 10^{-4} gm./litre This was in excellent agreement with Abramson's results, and indicated that at this concentration the surface of the quartz was completely saturated with protein.

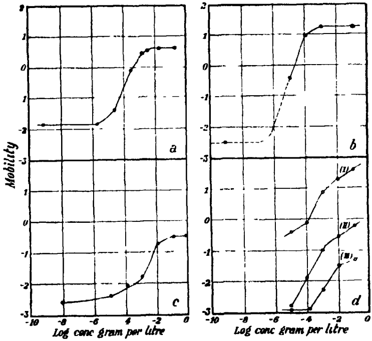

FIG. 3.—(*a*) Quartz surface, p_H 5·22, (*b*) carbon surface, p_H 4·97, (*c*) copper surface, p_H 7·28, (*d*) paraffin oil surface, (i) p_H 4·39, (ii) p_H 5·86, (iii) p_H 6·86

Adsorption isotherms for carboxyhæmoglobin on different surfaces are shown in fig. 3.

Fig. 3 *a* shows the adsorption of carboxyhæmoglobin on quartz at p_H 5·22. The mobility of the quartz was first affected at a concentration of 10^{-6} gm./litre and reached a saturation maximum at 10^{-3} to 10^{-2} gm./litre. Hæmoglobin is therefore less readily adsorbed than gelatine. The parabolas did not pass through the origin until the concentration of the protein was ca. 10^{-2} gm./litre.

This showed that the glass walls of the cell also became saturated with hæmoglobin, but at a somewhat higher concentration than that necessary to saturate the quartz particles. The adsorption of carboxyhæmoglobin on charcoal particles at p_H 4·97 is shown in fig. 3 *b*. The curve is very similar to that observed for quartz and shows a saturation maximum at 10^{-3} gm./litre.

The adsorption on suspended copper particles is shown in fig. 3 *c*. The protein was much less readily adsorbed on a copper surface and saturation was not reached until the concentration of the carboxyhæmoglobin was 10^{-2} to 10^{-1} gm./litre. The copper sol itself, though positively charged in water was negatively charged in a phosphate buffer solution of p_H 7·28. This may be due to preferential adsorption of the phosphate ions.

On a surface of paraffin oil, saturation was not reached at all, even at the highest concentrations used ($1 \cdot 15 \times 10^{-1}$ gm./litre). The curves showing the adsorption isotherms at different p_H's are shown in fig. 3 *d*. This incomplete covering of the surface made it impossible to determine the isoelectric point of the protein adsorbed on oil drops. The only indication of a possible value can be found from the curve at p_H 5·86. This shows that the charge at this p_H is likely to be positive and therefore that the isoelectric point would be at a p_H greater than 5·86.

Variation of Cataphoretic Mobility with p_H on different Adsorbing Surfaces.

The cataphoretic mobility of quartz particles coated with gelatine and suspended in solutions of different p_H is shown in fig. 4 *a*. All these measurements were made in protein solutions stronger than that required for surface saturation.

The points lie approximately on a straight line, and the particles have no mobility at p_H 4·79. This isoelectric point of p_H 4·79 for adsorbed gelatine agreed well with the isoelectric point of gelatine solutions found by other methods and showed that no change occurred in the isoelectric properties when the gelatine was adsorbed.

The measurements were then extended to oxy- and carboxy-hæmoglobin. The isoelectric point of oxyhæmoglobin has been determined by Michaelis and Davidson,* and of carboxyhæmoglobin by Michaelis and Bien,† using a qualitative cataphoresis method with small particles of the protein. They found that the isoelectric point of both proteins was about p_H 6·75.

---

* 'Biochem. Z.,' vol. 25, p. 49 (1912).

† 'Biochem. Z.,' vol. 61, p. 199 (1914).

Terroux titrated oxyhæmoglobin against a glass electrode in phthalate, acetate and phosphate buffers and found the isoelectric point to be p_H 6·79 ± 0·02. The generally accepted value from all sources is p_H 6 78. Geiger* observed that many hæmoglobins showed a wide isoelectric range, and by cataphoresis at a suitable hydrogen ion concentration he separated the hæmoglobins into two fractions possessing different isoelectric points He ascribed this result to the existence of two hæmoglobins in solution The results, however, were variable and the separated fractions scarcely seemed to be homogeneous in themselves In our early experiments we found that, at a p_H range near the isoelectric point, particles moved in both directions with different velocities in agreement with Geiger's observations As soon, however, as the technique of using the candle filter and sterilized vessels was adopted this effect vanished

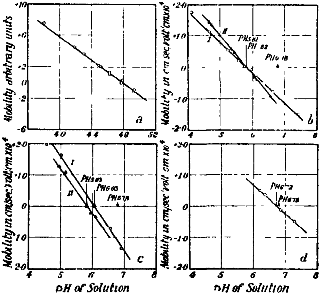

FIG 4 —(*a*) Gelatine on quartz, (*b*) △ Carboxyhæmoglobin on fresh quartz, × oxyhæmoglobin on fresh quartz, ○ carboxyhæmoglobin on old quartz, (*c*) carboxyhæmoglobin on carbon, (*d*) carboxyhæmoglobin on copper

The mobilities of quartz particles saturated with carboxyhæmoglobin in buffer solutions of different hydrogen ion concentrations are shown in Table IV, corrected for change of viscosity with temperature.

In fig. 4 *b*, curve I, the mobility is plotted against p_H. The points lie on a straight line and show an isoelectric point of p_H 5·82; this differs widely

---

* 'Proc Roy. Soc.,' B, vol. 107, p. 368 (1931).

Table IV.—Mobility of quartz particles in carboxyhæmoglobin at different p_H values. Dilution = 1 15 = 10^{-2} grams. per litre $\frac{Ll}{E\eta_{15^\circ}} = 2\cdot63 = 10^{-2}$.

	p_H	Temp	$\eta_{t^\circ} \times 10^3$	Rel. Mobility.	Mobility $\times 10^4$ 15° C	Remarks
		°C				
Acetate	4·09	15·3	11·36	+ 0·590	+ 1·766	Good parabola passing through origin.
,,	4·67	15·3	11·36	+ 0·372	+ 1·112	,, ,,
,,	5·22	see adsorption curve			+ 0·560	,, ,,
,,	5·44	15·3	11·36	+ 0·118	+ 0·354	,, ,,
Phosphate	5·44	16·8	10·93	+ 0·113	+ 0·324	,, ,,
,,	5·56	18·0	10·60	+ 0·065	+ 0·181	Fair parabola passing through origin.
Acetate	5·74	17·3	10·78	+ 0·009	+ 0·027	Fair parabola not passing through origin.
Phosphate	5·97	15·4	11·33	− 0·028	− 0·084	Fair parabola passing through origin.
,,	6·09	15·1	11·41	− 0·080	− 0·239	Good parabola passing through origin
,,	6·33	16·3	11·07	− 0·169	− 0·483	,, ,,
,,	6·64	16·4	11·04	− 0·273	− 0·794	,, ,,
,,	7·42	16·4	11·04	− 0·522	− 1·518	,, ,,

from the generally accepted value of p_H 6·78. The quartz suspension had been standing in distilled water for several days, and it was thought possible that the effect might be due to an "ageing" of the quartz. The experiments were repeated, using a suspension of freshly ground quartz. The results are shown in fig. 4 *b*, curve II. The slope of the line is slightly different, but the isoelectric point at p_H 5·81 is practically the same as that found on old quartz.

The experiment was repeated, using oxyhæmoglobin adsorbed on fresh quartz, the mobilities are plotted as ×'s on fig. 4 *b*, curve II. It will be seen that they lie on the same line as the carboxyhæmoglobin showing that there is no change in the electrokinetic properties of the protein on oxidation of the hæmatin. It is apparent that hæmoglobin adsorbed on quartz particles has very different electrokinetic properties from that of the protein in solution.

Hæmoglobin on a Charcoal Surface.

The mobility of a charcoal surface saturated with carboxyhæmoglobin is shown in fig. 4 *c*, curve I. The mobilities plotted against the p_H again gave an approximate straight line, but the isoelectric point at p_H 6·03 was again different from the normal and also different from that found on a quartz surface. The charcoal undoubtedly had air occluded in the pores and probably small bubbles adhering to the surface A sample of the charcoal was therefore evacuated under a water pump, to diminish the amount of air present, before adding the protein solution The mobility of the "evacuated charcoal" coated with protein is shown in curve II Evacuating the charcoal had a marked effect on the mobility and gave an apparent isoelectric point for the adsorbed protein at p_H 5 83

Hæmoglobin on a Copper Surface

The adsorption isotherm on copper showed that saturation of the surface was not reached until the concentration of the protein was ca 10^{-1} gm /litre. Fig. 4 *d* shows the variation of mobility with p_H in a solution of carboxyhæmoglobin of concentration $1 \cdot 3 \times 10^{-1}$ gm /litre The mobility is different from that observed on quartz or charcoal and gives an isoelectric point at p_H 6·72 This is in agreement with the value usually accepted for the hæmoglobin in solution but the agreement is probably fortuitous

Cataphoretic Mobility of the Bare Particles

The particles of quartz, carbon, copper, &c , when suspended in solutions free from protein will themselves possess characteristic mobilities. Measurements of the mobilities of the bare particles suspended in water and buffer solution are collected in Table V

Table V

Nature of Surface	Solution	Cataphoretic Mobility 15° C in cm /sec /volts/cm $\times 10^4$
Quartz	Buffer Solution p_H 4 6	− 2 48
	,, ,, p_H 5 9	2 66
	,, ,, p_H 6 9	− 3 39
Charcoal	Buffer Solution p_H 4 6	− 2 50
	,, ,, p_H 5 9	− 2 94
	,, ,, p_H 6 9	− 3 63
Copper	Distilled water	+ 1 14
	Buffer Solution p_H 7 3	− 2 50
Oil Drops	Distilled water	− 3 87
	Buffer Solution p_H 5 86	− 1 70
	,, ,, p_H 6 85	− 2 78

It will be seen that surfaces of bare quartz and charcoal had high and similar mobilities corresponding to a negative electrokinetic potential The copper surface had a positive potential in distilled water, but this became negative in a buffer solution of p_H 7 3 The mobility was, however, lower than that of quartz or charcoal at an equivalent p_H

Discussion

Measurements of the cataphoretic mobility of particles coated with adsorbed gelatine confirm the conclusions of other workers, that the electrokinetic properties and the isoelectric point of adsorbed gelatine are independent of the nature of the surface and are identical with those of the dissolved gelatine This is not true for all proteins and all surfaces Hæmoglobin adsorbed on various solid surfaces shows marked adsorption maxima, and the experimental reproducibility is good, but the mobility and the apparent isoelectric point are very different for each surface These are summarized below

Adsorbing Surface	Apparent isoelectric point for carboxyhæmoglobin
Fresh quartz	p_H 5 81
Old quartz	5 82
Evacuated Carbon	5 83
Carbon	6 03
Copper	6 72

These results show clearly that the mobility of particles coated with adsorbed protein is influenced by the nature of the underlying surface as well as by the ionizing properties of the protein. The effect of all the surfaces has been to shift the apparent isoelectric point of hæmoglobin in the acid direction. This is most marked for surfaces of an "acidic" type which have a high negative mobility themselves. The suspensions of quartz and evacuated charcoal, which, when naked have a high and similar negative charge, gave an isoelectric point at ca p_H 5·8. The hæmoglobin is more readily adsorbed on these surfaces. On unevacuated charcoal where much of the surface was air, the shift was less the isoelectric point was at p_H 6·0. The copper suspension was "basic" in distilled water (it had a positive cataphoretic mobility) but in the buffer solution used, it had a negative and smaller cataphoretic mobility. The adsorption was weaker on this, though it was quite definite and gave a saturation maximum The isoelectric point was shifted far less on this surface, the value being p_H 6·72.

It is only under special conditions that we should expect that a surface of adsorbed protein, should have the same electrokinetic properties as the protein itself. The conditions are :—

(i) The protein molecules should cover the surface completely.

(ii) The groups in the molecule which are attached to the surface should be different from the groups which are contributing to the ionization

(iii) The shape of the molecule should not be greatly changed on adsorption

If the first condition is not fulfilled, and part of the surface is exposed, the electrokinetic properties will be the sum of that due to the bare surface and that due to the adsorbed protein. If the protein is actually attached to the surface by the groups in the molecule which are responsible for the ionization, or even if these groups are near the surface, their properties will almost certainly be affected by the chemical nature of the surface. The degree of dissociation of these groups, and hence the isoelectric point and the cataphoretic mobility, will be different from that of the protein in bulk or in solution, and will vary from surface to surface If, for instance, the protein is attached to an acidic surface, it would be expected that the basic groups of the protein molecule would be more strongly held and the isoelectric point would be shifted in the acid direction The third possibility, that the shape of the large protein molecule may be changed by adsorption should not be neglected If, for instance, it could change from a spherical shape in solution to a fibre or sheet on the surface, its electrokinetic properties would be affected

For gelatine, these special conditions appear to be fulfilled , the surface is completely covered and the dissociating groups of the molecule are unaffected by adsorption For hæmoglobin this is not so ; the electrokinetic properties are dependent to a marked degree on the nature of the underlying surface. We must conclude for this latter substance either that the surface is not completely covered, or that the ionization of the protein is affected by adsorption. It is not easy to decide this with certainty, but the adsorption isotherms for quartz, carbon, and copper showed a definite saturation maximum This indicates that the surface is saturated, probably with a monomolecular layer * It is probable that quartz, carbon, and copper are all covered by a complete layer of hæmoglobin, but that the ionizing groups of the protein are very close to the surface. If the protein is attached to a negatively charged surface (*e.g.*, quartz, carbon) by its positive groups, and these are too strongly bound to ionize, the isoelectric point will be shifted in the acid direction.

---

* There is, of course, the possibility that only part of the surface can adsorb the protein and that this became saturated, leaving the remainder of the surface to contribute to the electrokinetic potential

For a less negative surface (*e g.*, copper) this shift will be less marked For a neutral surface (oil drops) very little adsorption will occur The oil drops showed only slight adsorption and no saturation maxima, in this case the surface was only partially covered and the resulting mobility was certainly the sum of that due to the protein and to the uncovered oil surface.

Proteins, such as gelatine and egg albumen, which show no change in isoelectric properties on adsorption, may cover the surface with a complete monomolecular layer so oriented that the ionizing groups are distant from, and unaffected by, the surface. It is quite probable, however, that they form polymolecular layers, so that the protein molecules on the outside of this relatively thick coating are unaffected by the underlying surface Taylor* found that in the serum precipitation reaction, though antibody and its homologous antigen react in the absence of inert serum protein, particulation does not occur unless such inert protein is present Chapman and Welsh† and others showed that the precipitate consisted essentially of serum protein. In these cases the antigen-antibody complex must have adsorbed serum protein as a polymolecular layer. Hæmoglobin apparently does not form polymolecular layers on the surface

Since oxy- and carboxy-hæmoglobin both give the same isoelectric point on quartz it is probable that any alteration of the isoelectric point on adsorption is a function of the globin of the hæmoglobin rather than of the hæmatin. If the hæmatin does contribute to the mobility its properties are not affected by oxidation or reduction.

We are very grateful to Mr. G S. Adair who supplied us with the pure hæmoglobin.

Summary.

Measurements have been made of the electrokinetic properties, in aqueous solution, of proteins adsorbed on to different surfaces. In gelatine, the cataphoretic mobility was independent of the nature of the underlying surface, which is in agreement with the results of other workers Experiments made on the rate of adsorption showed that surface equilibrium of the protein was reached in a few seconds in strong solutions (10^{-1} gm./litre), but took several hours in dilute solutions

---

* 'J. Hyg,' vol. 31, p. 56 (1931)

† 'Proc Roy Soc,' B, vol. 78, p 296 (1906)

Oxy- and carboxy-hæmoglobin showed a sharp adsorption maximum (indicating that the surface was saturated), but the cataphoretic mobility and apparent isoelectric point depended to a marked degree on the nature of the underlying surface. The reason for this is discussed

Both the oxyhæmoglobin and the carboxyhæmoglobin had identical electrokinetic properties when adsorbed, and no evidence was found for two forms of hæmoglobin possessing different isoelectric points

The Structure of Surface Films. Part XVIII *—The Effect of Alkalinity in the Underlying Solution on Films of Fatty Acids.*

By N K. Adam and J. G F Miller (From the Sir William Ramsay Laboratories of Physical and Inorganic Chemistry, University College, London, and Imperial Chemical Industries, Ltd)

(Communicated by F G. Donnan, F R S —Received June 1, 1933 Revised July 9, 1933)

Historical

It has been known for some time that extensive changes occur in monomolecular films of fatty acids on aqueous solutions, as the alkalinity or acidity is varied. These changes are of at least two kinds, changes in the packing of the molecules in the coherent types of film, and changes in the lateral adhesion between molecules have already been described Thus Adam* found changes in the packing of the molecules in the condensed films on changing from neutral to acid solution, and also† a change from condensed to gaseous or vapour expanded films, on changing from neutral to strongly alkaline solutions. The second of these effects was considered to be due to a decrease in the lateral adhesion between the molecules, caused by the development of similar electric charges on the end groups, through electrolytic dissociation of the carboxyl groups on alkaline solutions.

On alkaline solutions, it has previously been noted that the films contract spontaneously, Adam† called this "solution," but did not examine it in detail; Lyons and Rideal* believed it to be not a complete solution, but the formation of a bimolecular layer *two* molecules thick, Zocher and Stiebel,† by ultramicroscopic examination, concluded that this disappearance of the film was due to a partial collapse into thick, localized aggregates, not into a uniform bimolecular film

---

* 'Proc Roy. Soc,' A, vol 99, p. 336 (1921)

† *Ibid.*, vol. 101, p 522 (1922)

In the present investigation, we have examined, in considerable detail, films of the normal fatty acids containing from 12 to 22 carbon atoms, on solutions varying from dilute hydrochloric acid to twice normal caustic soda The principal points studied are (*a*) the lateral adhesion between the molecules, indicated either by the temperature at which expansion occurs, or by the form of the surface pressure—area relation with the expanded (or occasionally gaseous) films; (*b*) the packing in the condensed films, (*c*) the collapse of the films on alkaline solutions

Experimental

Measurements of surface pressure were made with the apparatus of Adam and Jessop‡, the films were frequently examined ultramicroscopically, using a cardioid condenser in the bottom of the trough, by the method of Zocher and Stiebel (*loc cit.*), with the simplifications employed by Adam § This ultramicroscopic examination is invaluable in detecting collapse and is very simple.

Strongly Alkaline Solutions.

Fig. 1 gives the principal results on solutions of caustic soda of various strengths The main curves show surface pressure plotted against area per molecule for the condensed films, which are only obtained with the 22 carbon acid (at room temperature). On 2N soda, the films are stable and do not collapse, they tend to a limiting area of about 31 sq. A, *i e.*, very much larger than that of closely packed long chains On N NaOH, the area tends to about 25 sq A. at no compression; there is a slow collapse on this solution On N/10 NaOH, there is rapid collapse; the surface pressure curves are therefore not very accurate, but correcting as nearly as possible for collapse, by taking observations at various times after the film was put on, the form of the curve at zero time could be approximately determined On this solution, the films appear to have the chains closely packed, the limiting area being about 20·5 sq A

---

* 'Proc. Roy Soc,' A, vol. 124, p. 349 (1929)

† 'Z. phys Chem,' A, vol. 147, p 421 (1930)

‡ 'Proc. Roy. Soc.,' A, vol. 110, p 423 (1926) Minor modifications made since are described in "The Physics and Chemistry of Surfaces," pp. 38–42 (1930)

§ 'Trans Faraday Soc,' vol 29, p. 91 (1933).

The lateral adhesion in the condensed films, indicated by the temperature at which the film was half expanded under 1 4 dynes per cm (referred to later as " half expansion temperature " or briefly as " expansion temperature ") was low, and constant throughout this range of concentrations. The expansion temperature was 10° ± 2 for the 20 carbon acid from 2N to N/10 NaOH.

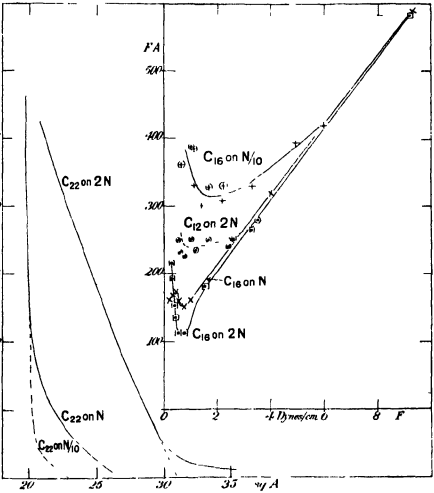

FIG. 1.—NaOH solutions
On left F —A curves for condensed films
Inset. FA —F curves for gaseous films

The curve inset in fig. 1 shows the product of surface pressure multiplied by area plotted against pressure, a method which shows clearly the degree of lateral adhesion between molecules in the gaseous film, the extent of dip below the line FA = 400, being a measure of the adhesional correction to the perfect gaseous state. There is a much smaller lateral adhesion in the dilute soda solutions than in the concentrated, with the gaseous films

On sodium carbonate, 2N strength, the films resemble closely those on 2N caustic soda, the expansion temperature and form of the surface pressure curve being practically the same, although the p_H is much smaller On N/10 sodium carbonate the expansion temperature is about 15° higher than on caustic soda, while on N/10 sodium and potassium bicarbonates it is nearly the same as on dilute hydrochloric acid. On all these N/10 solutions the pressure-area curve was approximately that of closely packed chains, with the condensed films

On 2N potassium carbonate and hydroxide, the condensed films showed a limiting area of 38 sq. A , *i.e* , decidedly larger than on soda of equivalent strength This indicates a very considerable swelling of the end groups, far the largest yet on record with monobasic fatty acids

Substitution of potassium for sodium appears to lower the temperature of expansion slightly in strong solutions, but accurate measurements were not made on this point

Some observations were also made on mixtures of sodium and potassium hydroxides with neutral salts of the same cations, the total strength being 2N, the hydroxyl concentration varying from 2N to 0·01 N The other anions used were Cl′, NO'_3, and CNS′ In all cases, the amount of collapse was negligible, no matter what the concentration of hydroxyl; the limiting area at no compression for condensed films was about 31 sq A. on the solutions containing sodium and 38 on those containing potassium It appears therefore that the total concentration of 2N is sufficient to prevent collapse, and that the cations rather than the anions determine the size of the end group. There were indications, though not accurately investigated, of slight changes in the lateral adhesion in the films when the anions were changed; these correspond probably to not more than five or ten degrees at most in expansion temperature With the chloride-hydroxide series, the lateral adhesion appeared to vary in an irregular manner, with minima at 1·9 N and at 0·5 N in hydroxyl, and maxima at 1·0 N and 0 01 N With the nitrate-hydroxyl series, there was a small steady rise in lateral adhesion as the hydroxyl concentration decreased. These changes require further investigation

The changes in the condensed films (usually determined on the 22 carbon acid) are summarized in Table 1.

Table 1

Solution	Area per molecule sq A	Expansion temperature for 20 carbon acid
N/10 NaOH	*ca* 20 (collapsing fast)	10° ± 3
N NaOH	25	10° ± 2
2N NaOH	31	10° ± 2
2N Na_2CO_3, or		
2N Na with various anions totalling 2N		approx 10°
2N KOH or K_2CO_3	38	—
N/10 Na_2CO_3	20·5	26 ± 3°*
N/10 $NaHCO_3$	*ca* 21	57 ± 5°*

* These experiments were done on the 16 and 18 carbon acids, the values for the 20 carbon acid being deduced by application of the usual rule that one additional carbon raises the expansion temperature by about 9° near 20° and 7° near 50°

The lowering of expansion temperature, with the 20 carbon acid, caused by changing the underlying solution from dilute acid to the first five of the above alkaline solutions, is about 48° This is presumably due to practically complete dissociation of the end groups, as the maximum lowering is reached even on 2N Na_2CO_3, of p_H about 11·2

Collapse of the films was rapid, with all chain lengths, on N/10 soda, much slower on N, and negligibly small, except with the shortest chains, on 2N. There was no reproducible area at which collapse could be said to have definitely ceased, it was unusual, however, for collapse to continue at an appreciable rate below an average of 6 sq A per molecule, and it quite frequently ceased somewhere near to 10 sq. A., on the other hand, the rate of collapse often slowed down to practical stoppage at areas greater than 12 sq A.* This frequent tendency for the collapse to cease not far from an area per molecule equal to half that occupied by a monomolecular film with closely packed chains is probably what led Lyons and Rideal to think that a bimolecular film was formed, it is by no means invariable, however, and we have found so little constancy in the final average area per molecule, that, on the ground of area alone, there seems little reason to suppose that the film is bimolecular.

Ultramicroscopic examination of the film during collapse always revealed the presence of numbers of small aggregates, distributed over the surface, the aggregates must be much more than two molecules thick and the surface is not homogeneous, hence the contraction of the film is certainly not due to a layer two molecules thick. This confirms Zocher and Stiebel's conclusion. The existence of apparent arrest points in the collapse is a phenomenon very frequently met with in surface films, and caution needs to be exercised in drawing conclusions from area measurements alone as to the structure of a film which has been contracting, even when several experiments indicate an apparent cessation of contraction at some particular area; there are frequently mysterious "passive resistances" to collapse in these films

---

* We are indebted to Mr. J. F. Danielli for numerous preliminary observations on the change of area with time during collapse.

It is difficult to say to what these passive resistances to collapses are due. The ultramicroscopic particles on to which the films collapse do not cover more than a small fraction of the surface, but they may sometimes be seen to interlock, forming a crude kind of two-dimensional gel Experiments on the rate of collapse on different solutions, including the more strongly alkaline borate buffers, have been made, without revealing any definite regularities, sometimes the rate of collapse first diminished, then increased after five minutes or so, finally diminishing again, often, however, the rate of contraction diminished steadily until it practically ceased Ultramicroscopic observation showed that there was a general tendency first for the formation of small particles, which later grew to larger particles, in some experiments the number of larger particles seemed to be smaller than the initial number of small ones, but we cannot say that it is a general rule that the number of particles diminishes As would be expected, the rate of collapse increases if the compression on the film is increased, it is also much greater with the shorter chain acids than with the longer chain, indicating perhaps that these aggregates are formed by a preliminary process of solution

Lower Alkalinities p_H 12 *to* 2.

To explore the phenomena in the intermediate region between strongly alkaline and acid solutions, four series of buffer salts were employed, containing borate, phosphate, citrate, and phthalate anions.* Clark and Lubs' series of borate mixtures, Sörensen's borate mixtures, Clark and Lubs' phthalate and phosphate mixtures, and Sorensen's citrate mixtures, were used Some experiments were also done on solutions containing the buffer salts, but outside the fully buffered range, using more acid or alkali than that recommended. In such experiments, the p_H given is only approximate, and tended to vary during the experiment.

---

* The solutions were made up to the strengths recommended by Clark, "The Determination of Hydrogen Ions" (1928), chap. 9, except where specifically mentioned.

Expansion Temperature.

Fig. 2 shows the principal variations in the expansion temperature over the whole range of p_H. Practically all the solutions show a gradual fall in expansion temperature on the alkaline side of neutrality, this was explored in detail only on the borate mixtures (curve II) At p_H 12, the 20 carbon acid has an expansion temperature about 29° on borate; this is a good deal higher than on twice normal sodium carbonate solution whose p_H is about 11·2. The borates are peculiar in showing a very marked maximum in expansion temperature at the neutral point, with a sharp fall at about 6 and 8 in p_H No difference was observed between the Clark and Lubs and the Sörensen series of borate mixtures; on diluting the former ten times, however, at p_H 9·0, the expansion temperature was raised considerably, about 20° (not accurately measured).

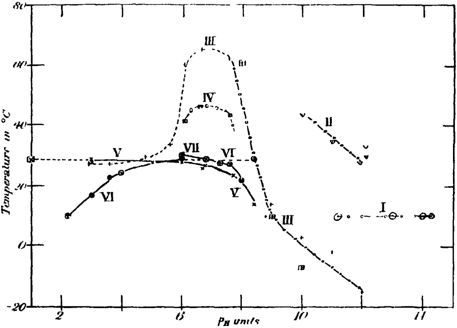

Fig. 2.—Half expansion temperatures under 1·4 dynes per cm.

I.—20 carbon acid on sodium hydroxide and sodium carbonate; II.—20 carbon on borate, III.—16 carbon on borate, IV.—14 carbon on borate, V.—16 carbon on citrate, VI.—16 carbon on phthalate, VII.—16 carbon on phosphate.

The plain dotted lines indicate solutions beyond the buffered range, the broken lines with rings indicate that the films were collapsing Full lines show stable films on buffered solutions

Phosphate and citrate solutions show an expansion temperature practically the same as on N/10 hydrochloric acid at all p_H values less than 6, and a slight lowering of expansion temperature between 6 and 8. Phthalates show a lowering of expansion temperature on the acid side of p_H 5, until at 2·2 it is about 18° lower even than that on dilute hydrochloric acid Diluting this buffer tends to raise the expansion temperature, about p_H 4

Stability of the Films

This depends mainly on the alkalinity With the 16 carbon acid, collapse is first perceptible about p_H 8, and its rate increases rapidly as the solutions become more alkaline. The 14 carbon acid is not fully stable even at p_H 6 5 The longer chain acids are somewhat more stable than palmitic, but all collapse readily at p_H 10 and upwards, up to N/10 alkali As pointed out above, collapse becomes less if the alkali is made very strong Collapse on the buffered solutions was always found to result in the formation of ultramicroscopic aggregates, not a uniform bimolecular film

States of Expanded and Condensed Films

The state of the expanded films, and the packing in the condensed films, depends mainly on the alkalinity, but there are minor specific differences between different buffers. In general, liquid-expanded films are formed on the acid side of the neutral point, vapour-expanded or gaseous films on the alkaline side, the lateral adhesion diminishing with increasing alkalinity

Borate Solutions (buffered p_H 12 to 7·6), fig. 3.

The condensed films have the chains closely packed, tending to a limiting area of 20·5 sq. A., on all solutions more alkaline than p_H 6·0. If more acid was added, bringing the p_H far beyond the buffered range, the condensed films became of the close-packed heads type below 15 dynes, very similar to those on dilute hydrochloric acid, with a limiting area of 24·5 ± 1 sq. A. Compression above 15 dynes causes the chains to pack closely The change in type of the films was fairly sudden, occurring about p_H 6.

Fig. 3, curves III to IX, show how the lateral adhesion between the molecules in the expanded state diminishes as the solution becomes more alkaline, with palmitic acid. At p_H 12, the film is gaseous with only moderately large corrections to the perfect gas laws. At p_H 8, it is vapour expanded, but with such large lateral adhesion that it closely approaches the liquid-expanded state.

Beyond the fully buffered region, on the acid side, the expanded films become liquid expanded at about p_H 7·6; between 7·6 and 6, the limiting area is about 40 sq. A , between 4·8 and 2·9, the limiting area is about 48 sq. A., the expanded films being indistinguishable from those on dilute hydrochloric acid.

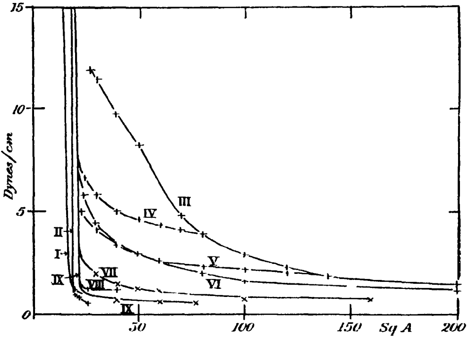

FIG 3

+ Sörensen × Clark and Lubs

Borate Solutions

I C_{20}, p_H 12·1, 16°,
II. C_{20}, p_H 10·0, 16°,
III. C_{16}, p_H 12·1, 18°,
IV. C_{16}, p_H 12·1, 8°,
V C_{16}, p_H 10·0, 17°,
VI. C_{16}, p_H 9·3, 16–17°,
VII C_{16}, p_H 9·0, 16–17°;
VIII C_{16}, p_H 8·5, 16–17°;
IX C_{16}, p_H 8·0, 16–17°.

Phosphate Solutions (buffered p_H 8·0 to 6·0), fig 4

Throughout the buffered range the condensed films of palmitic acid had the heads close packed with limiting area 24 ± 1 sq A. (curve III) below 15 dynes, above which pressure the chains pack closely The 20 carbon acid formed similar films of about 1 sq. A smaller area (curve II) Excess of alkali, bringing the p_H to about 8·6, caused the chains to pack closely at low pressures (curve I).

The expanded films are probably just liquid expanded at p_H 6·0, and definitely vapour expanded at p_H 8·0. Curves IV to VI and VII to X show how the 14 and 16 carbon acids change at low pressures, there is a marked increase in the tendency to cover large areas at low pressures, as the alkalinity is increased The change from liquid to vapour expanded occurs fairly close to p_H 6·5 The film of myristic acid (curve IV) on p_H 6·0 resembles that on dilute hydrochloric acid, except that the limiting area is 44 instead of 48 On p_H 6·8 a similar curve was obtained, except that the limiting area was 40

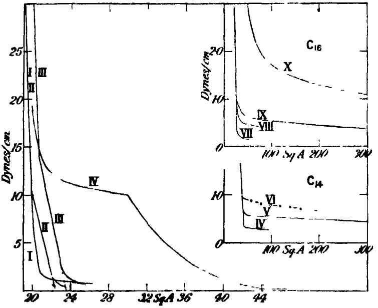

Fig 4 —Phosphate Solutions

I C_{18}, p_H ca 8·6, 18°.
II. C_{20}, p_H 6·8 to 8, ca 15°
III C_{16}, p_H 6 to 8, ca 15°
IV C_{14}, p_H 6·0, 18°
V C_{14}, p_H 6·8, 16°.
VI C_{14}, p_H 7·2, 14°.
VII C_{16}, p_H 6·0, 16°
VIII. C_{16}, p_H 7·2, 14°
IX. C_{16}, p_H 8·0, 8°
X C_{16}, p_H 8·0, 30°

There is a definite tendency for the limiting area of the liquid-expanded films to be slightly smaller, for a small range of p_H near the neutral point, than on more acid solutions

Citrate Solutions (buffered p_H 6·8 *to* 3·0).

On citrate solutions the expanded films were liquid expanded, and closely similar to those on dilute hydrochloric acid, in the buffered region. Addition of more alkali, bringing the p_H above 7, caused the films to become vapour expanded, the lateral adhesion decreasing with increasing alkalinity The condensed films in the buffered region were of the close-packed heads type, below 20 dynes per cm, above which pressure the chains became closely packed The 16 carbon acid gave areas extrapolated to no compression of about 25 sq. A., between p_H 6·7 and 3·0. The 20 carbon acid gave areas about 1 sq A smaller Closely packed chains at low pressures were not obtained till far beyond the alkaline side of the buffered region, probably not till about p_H 10, but here collapse was so rapid that measurements were not precise

Phthalate Solutions (buffered p_H *6·0 to 2·2).*

On phthalate solutions, fig 5, a new phenomenon appeared, the lateral adhesion both in the condensed and in the expanded states began to diminish about p_H 5·5 ($\pm$ 0·5), as the solution became more acid This appears in the lowering of expansion temperature shown in curve VI of fig 2; also in the expanded curves V to VII of fig 5 On p_H 6·0, the expansion temperature and the form of the expanded curve are nearly indistinguishable from those on dilute hydrochloric acid, for the 14 carbon acid. On p_H 3·6 and still more on 2·2, the films have become vapour expanded, and the expansion temperature has dropped appreciably. These phenomena were not found when the

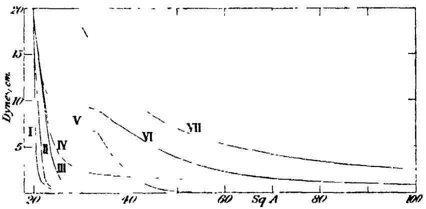

Fig 5 —Phthalate Solutions

I. C_{20}, p_H *ca* 8·4, 14°
II C_{20}, p_H *ca* 7·6, 11°,
III C_{16}, p_H 6 to 3, *ca* 15°,
IV C_{16}, p_H 2·2, *ca* 15°,
V C_{14}, p_H 6·0, 15°,
VI C_{14}, p_H 3·6, 15°,
VII C_{14}, p_H 2·2, 15°.

phthalate buffer was diluted a hundred times, e.g., on a buffer of p_H 3·8, M/2000 in phthalate, the films were indistinguishable from those on dilute acid or on the full strength buffer of p_H 6·0.

The condensed films in the buffered region were of the close-packed heads type below 18 dynes (curve III), tending to a limiting area 24·5 sq. A.; above 18 dynes the chains packed closely. No definite variation in the limiting area, within 1 sq. A., was found with p_H. If excess of alkali were added, bringing the p_H much above the buffered range, the films formed close packed chains at quite low compressions.

The decrease in lateral adhesion on the more acid solutions is probably due to adsorption of the bulky phthalic acid molecules at the surface. It was noticed that phthalic acid had a tendency to crystallize out at the surfaces in the M/20 solution of p_H 2·2.

The Principal Data between p_H 12 and 1 may be tabulated.

Buffer Salt	Condensed Films		Expanded Films		Remarks.
	p_H of change from close-packed heads to close-packed chains. ± 1 unit	Limiting area of close packed heads ± 1 sq. A. 16 carbon acid	p_H of change from vapour to liquid expanded ± 1 unit	Limiting area at no compression ± 3 sq. A.	
Borate	6	24·5	7·6	48 at $p_H < 5$ 40 at p_H 6 to 7·6	Very high expansion temps between p_H 6 and 8
Phosphate	8	24	6·5	44 at p_H 6·0 40 at p_H 6·8	
Citrate	(7·5 to 10)	25	7	48 at p_H 6·8	
Phthalate	7·5	24·5	ca 6·5 also ca 4·5	48 at p_H 6	Expansion temperature and adhesion in expanded films decrease at $p_H < 4$, on phthalate
HCl, N/10 to N/100	—	25	—	48	

Discussion.

The most marked effect of alkali is the diminution of lateral adhesion, both in the condensed and in the expanded states. There can be no doubt that this is mainly due to the development of similar electric charges on adjacent molecules, by ionization of the carboxyl groups. This fall in adhesion becomes apparent just on the alkaline side of the neutral point and reaches a maximum on very dilute caustic soda solution. p_H *alone*, however, does not fully determine the lateral adhesion on the alkaline side, *e.g.*, the adhesion is considerably greater on a borate solution of p_H 12 than on 2N sodium carbonate of p_H 11·2 The adhesion in condensed films of borate is very much higher near the neutral point than that of any other buffered solutions In general, the adhesion in the condensed films seems to run nearly parallel with that in the expanded films, though this rule is not of quite rigid application; *e g*, the expansion temperatures are practically identical on N/10 and 2N soda, although the adhesion in the expanded state is decidedly greater on 2N than on N/10

Complexes of a firm or loose character between the anions in buffer salts and the active groups in the films are presumably responsible for the specific effects of these salts on the adhesion, with borate, these appear to increase the adhesion, with phthalate, to diminish it It is possible that the diminishing effect on the adhesion, of the more acid phthalate solutions, is due, not to the formation of a definite complex, but simply to the phthalate ions becoming adsorbed at the surface, thus competing for the available space and causing the film molecules to adhere less strongly. Measurement of the surface tension of this phthalate buffer (p_H 2 2) at room temperature by the drop weight method, showed it to be 3 5 dynes per cm less than that of water, *i e.*, there is an appreciable adsorption at the air-liquid surface

Variations in alkalinity also bring about changes in the packing in the condensed state of the films, which are somewhat complex These are presumably due to changes in the size and shape of the end groups One of the most obvious of these changes is the enlargement of the end of the molecules on strongly alkaline solutions. On twice normal soda, the molecules pack to about 31 sq A at no compression, *i e*, about 50% larger area than that of closely packed chains, twice normal potash gives an even larger film, about 38 sq. A These changes are probably due to adsorption of the cations, potassium being larger than sodium Here it is the concentration of the cation rather than that of the hydroxyl group which determines the size of the end group, it is immaterial whether the twice normal solution of sodium contains mostly hydroxyl or mostly other anions, provided that some hydroxyl is present

Dilute alkaline solutions generally cause the films to pack with close-packed chains This packing persists, as the solutions become more acid, until a certain critical p_H, when there is a fairly sudden change to films giving compression curves in two portions, the lower portion reaching an area of 24 or 25 sq. A. (close-packed heads), the upper being the typical curve of close-packed chains. This change was first noticed by one of us in 1921; Lyons and Rideal thought the change was gradual, but on the solutions which we have most carefully examined, we have always found it to be complete in one or at most two units of p_H We agree with them, however, that the p_H of this critical point, at which the packing changes from close-packed heads to close-packed chains under low compressions, is different on different buffer solutions, it is usually between p_H 6 and 8

This change cannot be due to repression of ionization of the end group, as it occurs wholly within a range of p_H in which the ionization is probably small, and is changing but little There is no evidence for the theory sometimes advanced, that it is due to hydration of the end group increasing its size, it might be due to sterochemical alteration in the shape of the end group; or, as was suggested in 1921, not to any change in the size of the end groups, but to the influence of some forces between the end groups and the water causing all the end groups, naturally larger than the chains in cross-section, to come nearly or completely into one plane on the acid side of the point of change of packing, on the alkaline side, adjacent molecules might be packed at slightly different heights, so that the rather bulkier heads might tuck away into recesses formed by the zigzags in the chains, the result being close-packed chains. If this is the correct picture of what is happening, again there is no obvious reason why the change should occur abruptly, except that we know that most changes in the internal structure of crystals and other aggregations of molecules do commonly occur suddenly, *e g*, melting, or transition from one allotropic form to another.

A few scattered observations have hinted that the limiting area of the close-packed heads form of film may be smaller with chains of 20 or 22 carbons than with 16 carbons, this requires confirmation before it can be considered established

The spontaneous contraction on alkaline solutions is unquestionably a partial collapse of the films to localized aggregates of very much greater thickness than the films themselves There is no evidence that it is to a bimolecular film The rate of this collapse appears to increase *pari passu* with the extent of ionization, commencing at an alkalinity where a considerable proportion of the end groups are probably ionized It is, however, entirely prevented by considerable concentrations of sodium or potassium ions, an effect which, superficially at least, resembles "salting out" Collapse thus occurs when we should expect solution to take place, and may, indeed, be a secondary result of solution; possibly the molecules in the film are drawn a little way into the interior of the solution, and then aggregate into small groups which may be allied to McBain's "neutral colloid" form of soap There is, however, no proof of this connection.

We thank Dr G. Jessop for some preliminary observations on the more alkaline solutions. The cost of the ultramicroscopic apparatus was defrayed by a grant from the Government Grant Committee

Summary.

Monomolecular surface films of fatty acids have been studied in detail over the complete range of acidity between strong alkali and dilute acid, especially on the alkaline side

Electrolytic dissociation, progressively increasing from neutral to alkaline solutions, causes a very marked decrease in lateral adhesion both in condensed and in expanded films Minor specific effects of buffer salts on this adhesion are also found

Collapse occurs, to ultramicroscopic aggregates, on the more alkaline solution, but this is prevented if strong concentrations (2N) of salt are present Bimolecular films are not formed. Concentrations of salt sufficient to retard collapse on alkaline solutions tend to increase the size of the end groups, probably by adsorption of cations.

The change in packing of the condensed films from close-packed chains (the form found on alkaline solutions) to close-packed heads, usually occurs within a small range of p_H, the exact value of which depends somewhat on the buffers present

The Structure of Surface Films. Part XIX.—Influence of Alkaline Solutions on Films with Various End Groups.

By N. K. Adam and J. G. F. Miller. (From the Sir William Ramsay Laboratories of Physical and Inorganic Chemistry, University College, London, and Imperial Chemical Industries, Ltd.)

(Communicated by F. G. Donnan, F.R.S.—Received June 1, 1933. Revised July 9, 1933.)

In this paper, the effect of alkalinity of the underlying solution on substances with end groups other than carboxyl is studied. Surface pressure measurements only were made.

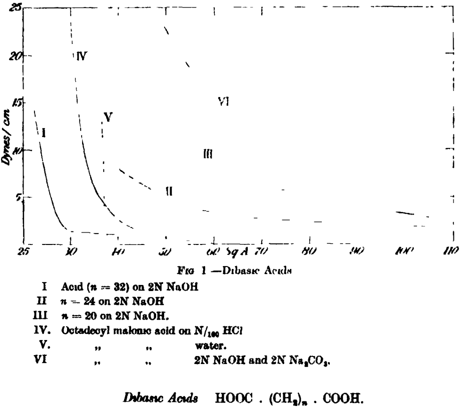

Fig. 1.—Dibasic Acids.

I.	Acid ($n = 32$) on 2N NaOH.
II.	$n = 24$ on 2N NaOH.
III.	$n = 20$ on 2N NaOH.
IV.	Octadecyl malonic acid on $N/_{100}$ HCl.
V.	" " water.
VI.	" " 2N NaOH and 2N Na_2CO_3.

Dibasic Acids. HOOC . $(CH_2)_n$. COOH.

Fig. 1, curves I to III, show the pressure-area relations found with three members of the series on twice normal caustic soda. The acid with $n = 32$

is condensed at 20°, tending to an area at no compression of about 30 sq A., this figure is not very accurate, owing to collapse of the films; the area is nearly the same as with the films of monobasic acids on this solution. The condensed films of these dibasic substances, with a polar group at each end of the chain, were shown in Part IX* to be oriented upright with one soluble group only in the water On 2N soda, the acids with $n = 24$ and 20 are both gaseous at the lowest temperature attainable (3°), the acid ($n = 20$) being naturally the more perfectly gaseous film

On dilute hydrochloric acid, the last two acids are half expanded under 1·4 dynes per cm. at temperatures of 57° and 38° respectively. It is probable that the half expansion temperature of the acid ($n = 24$) would be at least as low as $-5°$, perhaps very much lower, judging from curve II obtained at 3° It may safely be said that the strong soda solution lowers the expansion temperature of these dibasic acids at least as much as and probably more than, that of the monobasic acids

None of the films was very stable even on soda, but the collapse was much less rapid than with these dibasic acids on water Collapse occurs more rapidly with condensed than with gaseous films. It is easy to see why collapse should readily occur, in the condensed films the molecules are closely packed, nearly upright, with one carboxyl at the top of the film as well as one in the water below This upper carboxyl is exposed and serves as a nucleus on which collapse can easily occur

Octadecyl Malonic Acid $C_{18}H_{37}$ CH $(COOH)_2$

On dilute hydrochloric acid† and on water the films are condensed, on 2N sodium hydroxide or carbonate, they are gaseous at 20°. The film on water was not expanded even at 48°. There is thus a large decrease in lateral adhesion on sodium hydroxide or carbonate.

On water, the area tended to about 37·5 sq. A. at no compression, on dilute acid it was about 54 sq. A., the film spreading out considerably below 5 dynes per cm. There is only one chain in the molecule, so that evidently the two carboxyl groups attached to the end of the chain require, as would be expected, a considerable space on the surface

---

* 'Proc Roy. Soc,' A, vol. 112, p. 376 (1926).

† We are indebted to Mr. J. F. Danielli for determining the curve on dilute HCl That on water was determined by one of us in 1924, using the older apparatus with air jets, it is not very accurate, and in some experiments smaller areas were obtained

p — *Alkyl Phenols* $C_nH_{2n+1}C_6H_4OH$

Fig 2 shows the pressure-area curves obtained on water and on various alkaline solutions Curve I is the condensed curve previously obtained on water for the phenols with chains of 12 or more carbon atoms in the condensed state * Curve II, that with dodecyl phenol on water in the liquid expanded state, ending at about 39 sq A Dodecyl phenol is half expanded at 19° on water under 1 4 dynes The effect of alkali is twofold, twice normal caustic soda lowers the expansion temperature so that dodecyl phenol is a gaseous film at 19° (curve VII); hexadecyl phenol (curve V) is gaseous only below 6 dynes per cm at 21°—the half-expansion temperature under 1 4 dynes is about 14°, octadecyl phenol is condensed at 3°, but the area tends to about 29 sq. A per molecule (it is 24 on water). On water, the half-expansion

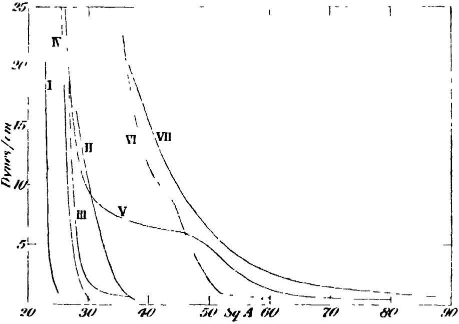

FIG 2 —Phenols

I Condensed films on water
II 12 carbon phenol on water, 30° (expanded)
III 18 carbon phenol on 2N NaOH, 3°
IV 16 carbon phenol on 2N Na_2CO_3, 16°
V 16 carbon phenol on 2N NaOH, 21°
VI 12 carbon phenol on 2N Na_2CO_3, 16°
VII. 12 carbon phenol on 2N NaOH, 19°

---

* 'Proc. Roy Soc,' A, vol 103, p 676 (1923), vol. 117, p. 532 (1928)

temperature of hexadecyl phenol is about 55°, hence the lowering of the expansion temperature caused by the twice normal caustic soda is about 40°, i e, appreciably less than with a carboxylic acid There appears to be some increase in size of the end group on the strong soda

On twice normal sodium carbonate, dodecyl phenol is expanded but not gaseous (curve VI) at 16°, hexadecyl phenol is condensed (curve IV) but tends to the area at no compression of 28 5 sq A On this solution, therefore, increase in area of the end group caused by the strong alkali is practically the same as with caustic of equal strength, but the diminution in lateral adhesion is considerably less than on caustic The carboxylic acids gave nearly the same diminution in lateral adhesion on twice normal carbonate as on caustic, the difference between the phenols and the carboxylic acids here is doubtless due to the much higher dissociation constant of the carboxylic acid

On a solution 1 5 N in sodium hydroxide and 0 5 N in sodium nitrate, the half-expansion temperature is about 15°, i e, practically the same as on 2N NaOH, on 0·5 N NaOH and 1 5 N $NaNO_3$ it is 23°. Thus the maximum lowering of lateral adhesion is not reached till a strength of hydroxyl nearly twice normal is reached, perhaps not even then

Stearyl Resorcinol $C_{17}H_{35}CO\,C_6H_3(OH)_2$ (1 3 4)

Fig 3 curves I and II, are on water at 13° and 45° respectively * With this class of compounds, no sudden expansion is found on raising the temperature. Curves III and IV are on twice normal caustic soda, at 3° and at 20°, respectively There is much less lateral adhesion than on water, but the diminution in adhesion cannot be estimated exactly as before owing to the absence of a definite temperature of expansion. Palmityl resorcinol, with two fewer carbons in the chain, gave a curve on water at 45° very close to II Since curve III lies well to the right of curve II, it is clear that there is much less lateral adhesion between the molecules in the film of the longer chain stearyl resorcinol at 3° on 2N soda, than in that of the palmityl resorcinol on water at 45° The effect of the strong caustic soda is thus to reduce the lateral adhesion at least as much as with the simple phenols described above, and probably more

Methyl Palmitate.

This ester forms a condensed film on water and acid, expanding to a vapour-expanded film at 25°. On alkaline solutions there is little if any change in the form of the condensed film or the temperature of expansion until strong alkalies are reached, when hydrolysis begins. On 2N caustic soda, the films increase rapidly in area, becoming gaseous, till they have nearly the same area as films of palmitic acid This is obviously due to hydrolysis of the ester group, at 19° it is half completed in approximately 3 minutes. The hydrolysis appears to be retarded by increasing the surface pressure It is very similar to the hydrolysis of γ-stearolactone, recently described by one of us.*

---

* Cf., Part XI, 'Proc. Roy Soc,' A, vol 119, p 630 (1928)

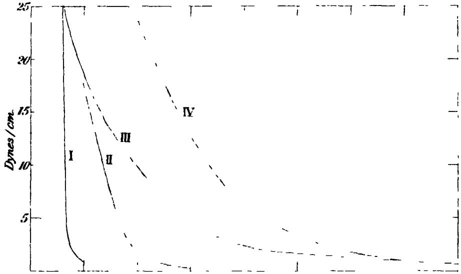

FIG 3 —Stearyl resorcinol

I —on water, 13°, II —on water, 45°, III —on 2N NaOH, 3°; IV —on 2N NaOH, 20°.

Nitriles. R. CN

Some measurements on films on various nitriles indicated no appreciable change, either in the form of the condensed or expanded curves or in the temperature of expansion, on 2N caustic soda, from the well-known films on water or dilute acid.

Discussion

A marked diminution in lateral adhesion occurs whenever the water-soluble end groups are likely to be ionized, but does not occur when no ionization is possible. The fatty acids described in the preceding paper, with a single carboxyl group, suffered a lowering of expansion temperature of nearly 50°

---

* 'Proc Roy. Soc.,' A, vol. 140, p 223 (1933)

on sodium carbonate (2N) and on all strengths of caustic soda. The more weakly ionized phenols suffer a slightly smaller lowering of expansion temperature, even on twice normal alkali, than the acids; and the maximum lowering with phenols is not reached till the strongest alkali is used. These changes in lateral adhesion in the condensed films are no doubt due to the development of similar electric charges by ionization on adjacent molecules, the phenols requiring stronger alkali before the ionization is complete, than the acids.

In addition to the experimental evidence in this paper, it may be noted that surface films of the alcohols* have the same surface pressure on N/10 caustic soda, water and dilute acid. Films of the amines have much less lateral adhesion on acid solutions, when they may be expected to be ionized, than on alkaline solutions †

There is probably some connection between the changes in lateral adhesion in these monomolecular films at an air-water interface, and the changes in interfacial tension between benzene solutions of various organic compounds, and aqueous solutions of varying alkalinity, studied especially by Peters.‡ He found a very marked diminution in interfacial tension, with benzene solutions of acids, as the aqueous solution became more alkaline, and a similar diminution with benzene solutions of amines, when the aqueous solution became acid Esters showed some diminution in interfacial tension, when the aqueous solution became strongly alkaline The parallelism is not, however, exact, as quite different quantities are being observed in the two sets of experiments Assuming, as is probably nearly correct, that the air-liquid surface tensions of the aqueous and benzene solutions used by Peters are practically the same throughout, the diminution of interfacial tension must be equal to the increase in adhesion between the two liquids, perpendicular to the interface. Any change in composition tending to start chemical reaction between the two liquids would increase this adhesion, it need not necessarily be an electrolytic dissociation. In our experiments, it is the lateral adhesion between the molecules in the surface film which is measured, and the electrolytic dissociation is the principal factor concerned in altering this. Peters' very marked fall in interfacial tension found with the ionizable substances under conditions when the end groups would be ionized is again an increase in perpendicular adhesion between the liquids, but is here presumably a secondary effect of the dissociation of the end groups.

---

* Adam and Dyer. 'Proc. Roy. Soc.,' A, vol. 106, p. 696 (1924).

† Adam. 'Proc. Roy Soc.,' A, vol. 126, p. 526 (1930).

‡ 'Proc. Roy. Soc.,' A, vol. 133, p. 140 (1931).

Summary

Monomolecular films of numerous substances with ionizable end groups show a marked decrease in lateral adhesion, when the alkalinity of the solution is changed so as to ionize the end groups Substances with non-ionizable end groups do not show this effect

Strong soda solutions tend to increase the size of carboxyl or phenolic groups at the end of the molecule

Films of methyl palmitate are fairly rapidly hydrolysed on 2N caustic soda

---

The Reflection of X-Rays from Anthracene Crystals

By B. WHEELER ROBINSON, Davy Faraday Laboratory, The Royal Institution, London, W 1

(Communicated by Sir William Bragg, O M , F R S —Received June 2, 1933)

[PLATE 5]

The importance of absolute, as opposed to relative, intensity measurements in X-ray crystal analysis has often been stressed,* and such measurements may lead, with compounds where one sort of atom is of dominant importance, to a direct and unequivocal determination of the structure Their value in the analysis of organic compounds, where usually no atoms are predominant in X-ray scattering power, is perhaps not so immediate, nevertheless, the absolute X-ray reflection of a given substance is at least as important a constant as, say, its thermal conductivity, and its determination is a necessary preliminary to any detailed study by the X-ray method

Hitherto such absolute measurements have been confined to inorganic substances, *e g* , rock-salt, usually occurring in large crystals It seemed to be worth while to make a determination of the absolute reflecting power of a typical organic crystal in conditions similar to those employed in the analysis of such crystals, *i e* , using a small crystal completely bathed in a monochromatic pencil of X-rays A very suitable substance for such a measurement is *anthracene*, since it is easily obtained pure and in crystals which are reasonably permanent and simple to adjust, but more particularly because its structure is already known in considerable detail and relative intensity measurements have been made on it with accuracy.* It is hoped that the measurements described in this paper will enable workers with other crystals to standardize series of relative intensity measurements with the minimum of labour, by comparing directly one of their observed reflections with the (001) reflection from a small weighed crystal of anthracene. The comparison can be made without difficulty, either photographically using an integrating microphotometer or by the ionization method on an ordinary spectrometer.

---

* Bragg and West, 'Z Kristallog.,' vol. 69, p 118 (1928).

We must admit in such an absolute determination two separate steps: first, the measurement of the X-ray intensity reflected in a given direction by a given crystal when exposed to a radiation field of known intensity, and second, the deduction from this result of the absolute reflecting power of an ideal crystal of the substance. The first part of the problem is a purely experimental one; the second involves in addition certain theoretical assumptions about the passage of X-rays through the crystal.

The intensity of reflection of X-rays from a small crystal has been investigated theoretically by several writers.† If we make the following assumptions: that a small crystal mosaic (*i.e.*, one in which the mis-orientation of the component blocks is sufficient to nullify the effects of extinction) is uniformly illuminated by an X-ray beam of intensity I, then the total energy E reflected by the crystal as it turns through a reflecting position with angular velocity ω is given by

$$\frac{\mathrm{E}\omega}{\mathrm{I}} = \mathrm{Q}d\mathrm{V},$$

where

$$\mathrm{Q} = \left(\mathrm{N}\,\frac{e^2}{mc^2}\,\mathrm{F}\right)^2 \lambda^3\,\frac{1+\cos^2 2\theta}{2\sin 2\theta}.$$

Here dV is the volume of the crystal, N the number of scattering units per unit volume, λ the wave-length, θ the angle of reflection, and F the structure factor for the set of planes considered. F includes the effects of temperature agitation of the atoms, and represents the extent to which for these planes the atoms find themselves on the average removed from the concentrated thin sheets of scattering matter in which the simplest picture imagines them to lie. In addition we assume that the incident radiation is non-polarized, and that the effects of non-coherent scattering can be neglected.

---

* Robertson, 'Proc. Roy. Soc.,' A, vol. 140, p. 79 (1933).

† Darwin, 'Phil. Mag.,' vol. 43, p. 800 (1922). 'Phil. Mag.,' vol. 27, pp. 315, 675 (1914). Compton, "X-rays and Electrons."

How far this equation is applicable in practice seems to be a difficult matter to decide The general opinion is that Darwin's "primary" extinction is not a cause of serious error for imperfect crystals—in which class we may place the majority of organic crystals. Experimental correction must be made for secondary extinction, but as we shall see later the correction is not large for the crystals which have been used in the experiments to be described here The normal absorption of the X-ray beam in the crystal, apart from extinction, causes a serious error for the longer wave-lengths ($\lambda = 1\ 539$ A) if it is neglected

The present paper describes measurements employing this equation on single crystals of anthracene for the planes (001), using two different wave-lengths, viz, $\lambda = 1\ 539$ A and $\lambda = 0 \cdot 709$ A., derived from copper and from molybdenum targets respectively We shall deal first with the method of measurement and the apparatus used, then we shall investigate certain necessary corrections, in particular the correction for extinction in the crystals, and finally present and discuss the final values for the absolute reflection of the (001) planes

Section A —The Experimental Method

Imagining the crystal to be mounted about a suitable axis in a homogeneous pencil of monochromatic X-rays, our problem is to compare the total intensity corresponding to a given crystallographic plane reflected by the crystal with the intensity of the radiation field at the crystal The simplest procedure is to rotate the crystal at a uniform angular rate through its reflecting position, measuring meanwhile the integrated intensity, then a small diaphragm of known area is substituted for the crystal, and the total energy passing through it in a given time is also observed

The energies may be measured with an ionization chamber or with a photographic plate, both methods have been employed with success, though the present paper includes only results obtained with the ionization chamber. In either method reliance is placed on the constancy of the X-ray beam through the experiment. The difficulties lie first in the obtaining of a monochromatic radiation field of sufficient uniformity, intensity and constancy, and next in the comparison of two quantities so different in magnitude as the direct beam through the diaphragm and the reflected beam from the crystal. This second difficulty is implicit in many physical measurements, it is usually overcome by reducing the variables to be determined to terms of such quantities as length, electrical resistance, time, etc, which can be measured very accurately without much trouble In the present experiments, using the photographic emulsion as indicator, the time factor may be used to obtain on the plate two blackened areas of nearly equal intensities for comparison on a photometer, using the ionization chamber, the electrical properties of the amplifying system may be invoked to provide the requisite range of comparison

The apparatus employed is shown diagrammatically in fig 1, its component parts will now be briefly discussed

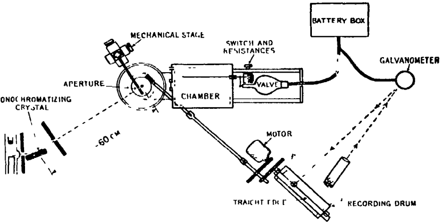

Fig 1 —General arrangement of apparatus.

(1) *The X-ray Source* –This was a sealed-off line focus tube with either copper or molybdenum target, the permissible loadings being $\frac{1}{2}$ or $1\frac{1}{2}$ kilowatt respectively Current at voltages up to 50 kilovolts was supplied from a 5-kilowatt transformer at 50 cycles, with biphase rectification and a reservoir condenser of 0·2 microfarads across the output No perceptible ripple at twice the supply voltage could be seen on an X-ray photograph taken on a rapidly moving plate The current passing through the tube could be adjusted to 0·2%, as could the voltage applied, the latter was measured in terms of the current passing to earth through an oil-immersed wirewound resistance of 20 meghoms, made to the design of Mr. R. E. Clay from the "sphagetti" wire now extensively used for high resistances in wireless sets It had a total length of 40 yards and was wound on a paxolin former; the temperature coefficient was negligible in the conditions of use The whole high-tension apparatus was enclosed in an earthed wire cage equipped with proper safety devices, and the apparatus would run steadily for hours at a time without attention beyond an occasional adjustment of the filament current of the X-ray tube. Fluctuations of the order of 1% in the supply voltage were

troublesome at times, they were sufficiently infrequent to make the observations possible without the use of any form of stabilization or automatic control.

Attached to the X-ray tube, and forming a unit with it, was mounted a monochromatizing crystal of rock-salt at a distance of some 10 cm. from the target, and equipped with slits and adjustments adequate to isolate the K_α lines of the radiation required By making this monochromator in one unit with the X-ray tube, the adjustment of the apparatus was greatly facilitated; the tube was so mounted that it could be turned about a vertical axis through the monochromatizing crystal The experimental crystal was 60 cm or more from the monochromatizing crystal, this large distance was found to be essential in order to secure, over an area several times that of the crystal, a radiation field uniform to 1%. The monochromatic beam could be traced on a fluorescent screen as far as the experimental crystal in a nearly dark room

(2) *The Aperture System*—Mounted on a mechanical stage giving three-dimensional motion was a brass strip carrying the apertures By a preliminary calibration of the mechanical stage, any aperture could be brought into coincidence with the centre of the crystal (the latter having been removed) to an accuracy of about 1/10 mm The apertures were round holes in platinum sheet 0·3 mm. thick, they were made by punching a small hole in the platinum with a needle point and enlarging it with watchmaker's broaches to the required size, the edges being bevelled with a small drill, and the holes carefully cleaned with a small splinter of wood dipped in alcohol. The areas were measured with a travelling microscope as carefully as possible, the smallest holes were, however, difficult to measure with an accuracy as great as 1%, and finally greater reliance was placed on areas deduced from measurements of transmission in a uniform X-ray field In this way the areas were "stepped up" until a size was reached which could be measured with confidence on the microscope Altogether four apertures were used, with areas varying from 0 04 to 0·15 sq. mm., and were compared with a larger aperture of area 0·6 sq mm

(3) *The Ionization and Recording Apparatus.*—The cylindrical ionization chamber was of steel, built to withstand a pressure of several atmospheres, and filled with argon. The window for the admission of X-rays was of cellophane, held in place by rubber gaskets and coated internally with thin aluminium leaf. The collecting electrode, protected by a guard ring in the usual manner, had quartz insulation, and was connected directly to the grid of a G.E.C. "electrometer" valve, which was shielded by a thick aluminium cylinder bolted to the ionization chamber. A flexible metal screening tube carried the necessary

leads to a metal box containing the batteries for valve and ionization chamber. The whole of the chamber and valve ensemble was carried on the arm of the ionization spectrometer, some of the weight being taken off the bearings by a vertical stretched spring.

The electrical connections are shown in fig 2 The high resistances R_1, R_2, R_3 were made according to Brewer's description* of a pencil line on amberoid rods, sealed with ebonite caps in glass tubes containing a drying agent They were brought into action by the selector switch indicated in the diagram, which could be operated from outside the screening tube, its contacts were of platinum on phosphor-bronze springs, and were worked by ebonite cams. A photograph of the switch assembly, showing the amberoid pillar carrying the grid lead, is shown in fig 3, Plate 5 A phosphorus pentoxide tube maintained the air inside the screening tube as dry as possible

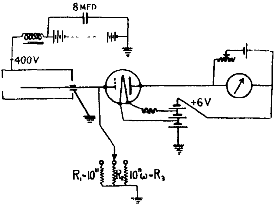

Fig 2 —Electrical connections

The indicating galvanometer was specially built for this apparatus; it was of the moving magnet type, Broca system, had high resistance coils (25,000 ohms), and was completely immersed in paraffin oil of suitable viscosity to give the requisite damping Its undamped period was of the order of $\frac{3}{4}$ second, and its sensitivity 300 mm. per microampere at 1 metre Since the quartz suspension in such an instrument can hardly be described as a "fibre," and the liquid damping gives practical immunity from mechanical shocks, the robustness of this simple galvanometer is extreme

The image of a crosswire reflected from the galvanometer mirror was received on a sheet of paper held in a roller (actually an old typewriter roller was used) which was geared through a shaft with universal joints to the traversing screw of the spectrometer, controlling the angular position of the crystal, and was turned at a slow speed by a small electric motor through a suitable clutch and gearing If the motion of the image be followed with a finely-pointed pencil pressed against a straight-edge fixed close to the paper, then as the crystal is turned through the reflecting position the reflection curve of the crystal is traced on the paper, assuming that the ionization chamber has been placed with wide open slit in such a position as to receive the reflected beam This apparatus for giving a continuous and permanent record of the behaviour of the crystal is easy to construct and instal It is superior to a more complicated automatic photographic arrangement, which of course would be quite feasible, because the observer can exercise his faculty of selection, he can hurry or retard the speed of recording at appropriate moments, and he can discount the effects of spurious disturbances, *e g*, caused by the emission of an alpha-particle in the chamber It is possible to make a complete record of a strong crystal reflection in about 1 minute, *i e*, within this time to draw the curve of reflected X-ray intensity plotted against angular position of the crystal over about 1° on either side of the reflecting position, a weak reflection must be recorded more slowly than this, as the time-lag of the grid circuit of the amplifier is appreciable if the highest value of shunt resistance is employed Nevertheless, even with the weaker reflections the process is quite speedy and is much to be preferred to the step-by-step plotting of the reflection curve in the usual manner On the curves as usually recorded, 10 cm corresponds to 1° of turning of the crystal, and the paper moves at rates varying from about 5 to $\frac{1}{2}$ cm in 10 seconds Using the highest value of shunt resistance (about 10^{11} ohms) each alpha-particle emitted in the chamber gives a sudden kick of some 2 cm, unfortunately owing to the general radioactive contamination of this laboratory it has not been possible to free the apparatus from these disturbances as well as might be wished

---

* 'Rev. Sci. Instr.,' vol. 1, p 325 (1930).

Section B —Necessary Corrections and Determinations

(1) *The Weight of the Crystal.*—This quantity enters directly into the equation we are using, and an essential feature of this investigation was the use of crystals of a considerable range of weights. A special microbalance was constructed of hollow fibres of fused Pyrex glass, the two sharp carborundum points about which the beam oscillated* being supported on a slab of plate glass. Inside

---

* McBain and Tanner, 'Proc Roy. Soc,' A, vol. 125, p. 579 (1929)

the beam on one side was enclosed a magnetized steel needle, at the other end a tiny balance pan of glass was hung from a V hook made of a glass fibre of small diameter The time of swing was about 2 seconds, a fine pointer at the end of the beam was observed in a microscope The whole balance in its protecting case was supported between two large Helmholtz coils giving a uniform magnetic field, the weighings were performed in terms of the current through these coils, which could be accurately adjusted by a system of rheostats, and the balance was calibrated by the use of a standard half-milligramme weight. No attempt was made to secure the extreme accuracy which is possible from a balance of this type, nevertheless, over a period of many months the sensitivity has remained unaltered, and weighings to an accuracy of 1/1000 milligram, which was adequate for the present research, were speedily performed. By further attention to screening against electrical, magnetic and thermal disturbances, there is no doubt that the accuracy could be improved by a considerable factor

(2) *The Performance of the Amplifier* —Small ionization currents flow to the grid of the valve from the ionization chamber In taking the deflections of the galvanometer as a true measure of these currents, we are in effect assuming (*a*) that the high resistances obey Ohm's law over the small voltage range employed, and (*b*) that the grid voltage anode current curve of the valve and the current. deflection curve of the galvanometer between them give a linear characteristic. The assumption (*b*) is easily checked by applying known potentials to the valve grid from a potentiometer system, it was found that the linearity of the apparatus was satisfactory over the range employed, with or without the galvanometer shunt (see next section) in use. The point (*a*) seems to have been implicitly assumed in the work of several experimenters who have used high resistances composed essentially of graphite * Some evidence in favour of the assumption was gained from the fact that the ratio between the values of the three graphite resistances in this apparatus (measured by using each resistance in turn and comparing the sizes of aperture in a uniform X-ray field necessary to give equal deflections on the galvanometer) was found to be independent of the intensity of X-rays used for the calibration. As the three resistances were of various shapes and thicknesses, this gives some evidence that Ohm's law was severally obeyed

Further evidence as to the electrical linearity of the apparatus was obtained by allowing an X-ray beam to enter the ionization chamber and observing the deflection as the current passing through the X-ray tube was raised, the voltage being kept accurately constant As the apparatus was being run at very low power, it is probable that the effects of ripple in the output voltage were negligible, and it is generally assumed that in these circumstances the X-ray output of a hot-filament tube is accurately proportional to the tube current A good straight line was obtained when galvanometer deflection was plotted against tube current

---

* *cf.* Rentschler and Henry, 'Rev. Sci Inst,' vol. 3, p. 91 (1932); and Brewer, *loc. cit.*

(3) *The High Resistances and Galvanometer Shunt.*—As has been said above, the values of the resistances were determined in terms of the size of aperture necessary to obtain equal deflections with each of them in turn in a uniform X-ray beam, to secure which the apertures and ionization chamber were removed to a distance of a couple of metres from the X-ray tube Plotted over a period of months, the value of the highest resistance (about 10^{11} ohms) shows a gradual rise as compared with the other two values, from day to day, however, its ratio was satisfactorily constant

Many of the best measurements were made using the same value of the high resistance throughout, but using a galvanometer shunt to secure the necessary extension of electrical range This was a shunt resistance of 1/4 G and a series resistance of 4/5 G (G representing the galvanometer resistance) both thrown into circuit by the operation of a switch, and in effect making the apparatus exactly 1/5 as sensitive as before The series resistance is essential, as otherwise the total resistance of the galvanometer combination (which is of the same order as that of the valve) is altered, and the valve would be caused to work on a different portion of its characteristic, leading to serious error

(4) *The Monochromatism of the Beam* —The radiation reflected by the monochromatizing crystal will not, of course, consist entirely of the desired wave-length λ; there will also be present radiation $\frac{1}{2}\lambda$, $\frac{1}{3}\lambda$, etc in amounts depending on the spectral distribution curve of the primary radiation and the relative intensity of reflection of the various orders of the planes of the crystal. There will also be general scattered radiation of various wave-lengths.

An analysis of the "monochromatic" beam was carried out both for the copper and the molybdenum X-ray tubes, using a large rock-salt crystal as analyser to secure the maximum possible intensity, and allowing the radiation to fall on it through a slit, the apparatus, screens, etc, being arranged exactly as was usual during the actual measurements Using the low resistance for the measurement of the area under the peak λ, a maximum value for the area under the remainder of the curve from approximately $\frac{1}{3}\lambda$ to 2λ was determined, using the highest resistance, *i.e.*, with the apparatus about 50 times more sensitive than before. It was found that practically all the unwanted radiation was of the wave-length $\frac{1}{2}\lambda$; and the following figures were adopted as the most probable after several separate determinations —

Unwanted radiation with the copper target = 1·6%
Unwanted radiation with the molybdenum target = 1·0%

In arriving at these figures, allowance must be made for the varying efficiency of reflection of the rock-salt analysing crystal as the wave-length diminishes. A calculation of this efficiency from the known structure of rock-salt would be rather hazardous, in view of the strong extinction which specimens of this crystal show for reflections from the cleavage plane, consequently an experimental determination of this efficiency was made. A monochromatic beam defined by a slit was allowed to fall on the crystal face, and the intensity of the main beam was compared with the total integrated intensity reflected by the face by just the methods which have been described for the anthracene crystals. The results of the measurements were —

$$\lambda = 1{\cdot}539\ \text{A} \quad \frac{E\omega}{I} = 2{\cdot}33 \times 10^{-4}$$

$$\lambda = 0{\cdot}709\ \text{A}. \quad \frac{E\omega}{I} = 4{\cdot}15 \times 10^{-4}$$

In addition, Bragg, James and Bosanquet* give the figure $5{\cdot}5 \times 10^{-4}$ for $\lambda = 0{\cdot}614$, Compton† $4{\cdot}4 \times 10^{-4}$ for $\lambda = 0{\cdot}709$, and Kirkpatrick and Ross‡ $1{\cdot}82 \times 10^{-4}$ for $\lambda = 0{\cdot}560$. The first two of these results are comparable with our own, being taken with a crystal with a ground surface, but the last one was with the freshly-cleaved surface of a particularly perfect specimen of rock-salt, and the value should therefore be multiplied by a factor of two or three times to bring it into line with the others. Though we may say from these figures that the efficiency of reflection at $\frac{1}{2}\lambda$ for Cu K_α is about twice that for λ, it is impossible to predict with any confidence the efficiency for $\frac{1}{2}\lambda$ for molybdenum rays; nor could the measurements be carried down to this wave-length, as no X-ray tube was available with a suitable anticathode. Failing other evidence, we have therefore assumed that the efficiency for Mo K_α radiation is the same at $\frac{1}{2}\lambda$ as at λ, *i.e.*, that the fall in Q, in the formula $\frac{E\omega}{I} = \frac{Q}{2\mu}$, as λ and θ diminish will be compensated by the diminution in μ

---

* 'Phil. Mag.,' vol. 41, p. 322 (1921)
† 'Phys. Rev.,' vol. 10, p. 95 (1917)
‡ 'Phys. Rev.,' vol. 43, p. 596 (1933).

Even if this assumption is far from the truth, the resulting error in the final measurements should not exceed about $\frac{1}{2}\%$.

In making this analysis, the difference in the absorption of the gas in the ionization chamber for the different wave-lengths must not be forgotten, but any error caused by incomplete absorption in the chamber is self-correcting, as it applies equally well to the main beam measurements with the anthracene crystals

Section C—General Procedure

The measurements were conducted as follows, a series of anthracene crystals was selected; the crystals employed in this research were all grown from amyl acetate solution They were weighed and then mounted with shellac on fine glass fibres The monochromator was adjusted to give the most intense and uniform beam possible, a fine pinhole was mounted on the mechanical stage and the uniformity of the field in the neighbourhood of the crystal was explored The ratios of the resistances in the amplifier were determined if necessary The experimental crystal was placed in position and the (001) reflection located A calibrated aperture of suitable size was adjusted to occupy the same position as the crystal, which was removed, this adjustment was made easier by the use of a brilliantly illuminated white strip attached to the monochromator slit, which could be viewed through the aperture The power of the X-ray tube was chosen to give a suitable maximum deflection, and the tube was run until conditions became quite steady Then the deflection given by the "main beam" passing through the aperture (the crystal being removed) was recorded several times, as was the reflection curve of the crystal (the aperture being removed), using the recording device which has been described, and altering the resistances or the galvanometer shunt as might be necessary Finally, the area under the recorded curves was measured with a planimeter

The main beam deflection when the aperture was in position was not of course perfectly steady, owing to various disturbances and (with the weaker beams) the probability fluctuations of the number of fast electrons liberated in the ionization chamber by the X-rays. The effects produced by an alpha-particle were usually clearly distinguishable, and were not recorded. To secure a proper time-average of these fluctuations, the roller carrying the paper was slowly turned while the galvanometer spot was followed with a pencil; then on the record afterwards the average could be made by eye or with a planimeter if the fluctuations were extreme A typical experimental record—actually the reflection curve of a small diamond which was used as a comparison standard—is shown in fig 4 Here the main beam has been measured three times and the reflection twice.

A usual difficulty of all careful measurements in crystal analysis is where to estimate the background—here, where to draw the base line of the curves A, B of fig 4 Fortunately owing to the highly monochromatic radiation used this is not a serious difficulty with a good crystal Several of the anthracene crystals tried were, however, so bad (*i e*, they reflected over so large an angular range) that base lines could not be drawn accurately Consequently measurements on these crystals were abandoned A representative series of reflection curves of the (001) planes from some of the crystals which were used is given in fig 5, the same angular scale being used throughout, their complicated and imperfect structure may be compared with the curve shown by the comparison diamond, which shows the α_1 and α_2 separated. Further reference will be made to these curves, which were taken in a nearly parallel X-ray beam for the purpose of evaluating the extinction corrections for the crystals (*cf.* next section)

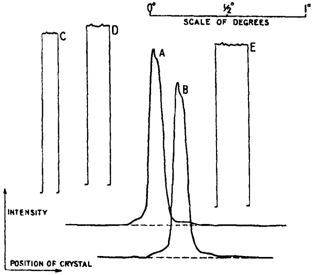

Fig 4—A typical record Diamond crystal λ = 0 709 A., area A = 12 45 sq. cm., B = 12 60 sq cm.; length C = 10 67 cm, D = 10 62 cm, E = 10 76 cm

The results of those measurements which were considered reliable are shown on the graphs, figs. 6 and 7, for the two wave-lengths employed. They represent, plotted against the weight of the crystal, the fraction of the incident radiation per unit area per second which the crystal would reflect from the

(001) planes if turned at 1 radian per second through the reflecting position. In these graphs a correction has been applied for absorption and extinction by the method to be described in the next section, allowance has also been made for the non-monochromatism of the beam.

It will be seen that the proportionality between weight and integrated reflection is quite good for the smaller crystals, but with the larger crystals discrepancies appear which are presumably due to the inadequate operation of the correction factor for the absorption in the crystal It should perhaps be emphasized that each point plotted on these graphs represents the average of several measurements on that crystal, each of several possible (001) reflections, always mutually consistent to a far greater degree than is indicated by the "scatter" of these points on the graph. The previous measurements of Sir William Bragg* led him to conclude that using rhodium radiation the reflection from anthracene crystals is proportional to their weight over quite a large range, these figures show that for intensity measurements with longer wave-lengths crystals not much larger than 1/10 milligram should be used.

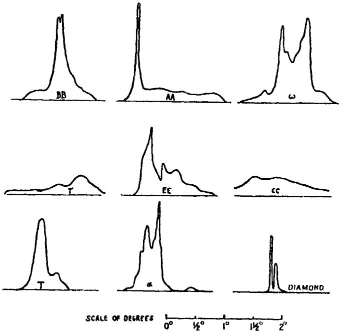

FIG 5.—Reflection curves of various anthracene crystals.

---

* 'Proc Phys. Soc.,' vol. 33, p. 304 (1921).

Section D.—Correction for Absorption and Extinction.

The fundamental formula $\frac{E\omega}{I} = QdV$ is only applicable without modification if we can assume that all the diffracting atoms are exposed to a radiation field of the same intensity. This is not permissible in practice, even for a very small crystal. The X-ray beam in traversing the crystal loses energy in two ways : (1), which we shall refer to as " absorption," from photo-electric emission and non-coherent scattering, which is a purely volume effect independent

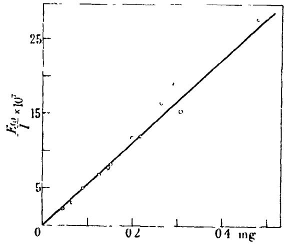

FIG. 6.—Reflected intensity-weight (corrected), λ = 1·539 A.

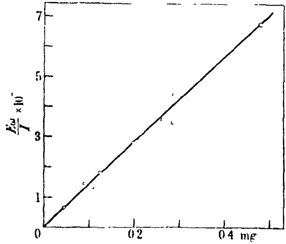

FIG. 7.—Reflected intensity-weight (corrected) ; λ = 0·709 A.

of the precise orientation of the crystal; and (2), which we shall refer to as "extinction," from the coherent reflection from the crystal lattice which is only appreciable in certain orientations of the crystal Darwin, in a well-known paper*, divides the extinction into two parts, the primary extinction, *i e*, the loss within a perfect micro-crystalline block, does not seem ever to have yielded to experiment, the effects of secondary extinction, *i e*, the shielding of lower blocks by the reflection of X-rays from the blocks lying above them, have several times been successfully overcome

The normal absorption of X-rays in a crystal can be easily found, either by direct measurement or by calculation from the known absorption coefficients of the component atoms On turning the crystal through the reflecting position, a sudden increase of absorption is apparent at the reflecting angle, and it might at first sight be thought that a measurement of this increased absorption coefficient, together with a knowledge of the geometrical shape of the crystal, would make possible a calculation of the complete effects of absorption plus extinction for that crystal This is not so, however, since the measurement can never be made with truly parallel X-rays Only part of the slightly divergent beam employed traverses the crystal at the reflecting angle, and the derived figure for the total effective absorption coefficient is too low

A separate correction for extinction has been made in these experiments in the following manner —

The effect of primary extinction has been neglected, it being assumed that in so soft and imperfect a crystal as anthracene those component blocks or units which may be regarded as perfect crystals are small enough to make the effect inappreciable Now let c be the average volume of these blocks, and taking some arbitrary reference direction in the crystal let $f(0)\,d0$ be the number of blocks, in any particular crystal, which have their planes within $d\theta$ of some angle 0 measured from this direction. Then we may draw a graph, fig 8, showing the angular distribution of blocks in the crystal, if the volume of the crystal is V, the area under the graph is

$$\int_0^\infty f(\theta)\,d\theta = \mathrm{V}/c,$$

the total number of blocks Now let us make the further assumption, which is justified by theory,† that each little block has a reflection curve similar to that of fig. 9, *i.e.*, it reflects uniformly over a small angle $1/a$ radians, $1/a$

---

* *Loc. cit*, 1922.

† Compton, "X-rays and Electrons," p. 140 (1926).

being very small compared, for example, with the angular spread of the blocks in the crystal Each such block would give an integrated reflection of Qc, *i.e.*, if allowed to remain *stationary* in its reflecting position it would reflect a fraction Qca of the radiation per unit area to which it was exposed

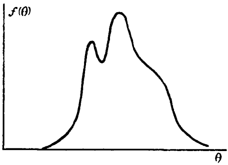

FIG 8

Now consider the path of a beam of X-rays traversing the crystal at the angle θ with the reference direction In unit element of path, length dx, it meets with a number $dx \,.\, \frac{f(\theta)\ 1/a}{V}$ of blocks having their planes lying within the angle $1/a$ of θ, *i.e.*, lying in a position to reflect, and each such block in

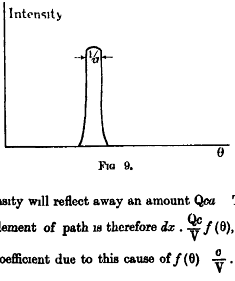

FIG 9.

a field of unit intensity will reflect away an amount Qca The total loss from the beam in this element of path is therefore $dx \,.\, \frac{Qc}{V} f(\theta)$, leading to a value of the extinction coefficient due to this cause of $f(\theta)\ \frac{c}{V} \,.\, Q = m$, say.

But in this expression $f(\theta)$ is the ordinate and V/c is the area of the curve of fig. 8, we can therefore deduce the correct extinction coefficient for any value of θ, *i.e.*, for any orientation of the crystal, by dividing the corresponding ordinate of fig 8 by the area of the curve, *i.e.*, by recalibrating the vertical axis. We have implicitly assumed in the above that the curve is drawn to a horizontal scale of 1 radian = 1 unit

We can however draw another curve for the same crystal, fig 10, the curve of reflected intensity against angular position, the crystal being supposed to be rotated in a parallel beam of X-rays If now we may assume that the effective length of path l traversed by the X-rays in the crystal is known, we may for any ordinate of fig 10 read off the corresponding extinction coefficient m from fig. 8, divide the ordinate by e^{-ml}, and replot the ordinate; leading to a new graph shown dotted in fig 10 which represents as a function of angle the intensity which would have been reflected by the crystal had extinction not been present The area under this dotted curve is thus the total integrated reflection, and the ratio of the original area of fig 10 to this new area is the required correction factor which must be applied to the measured values of total reflection to correct them for the effects of extinction.

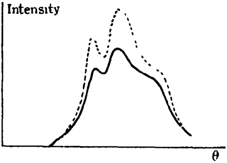

FIG 10.

Now as to the practical realization of this correction factor. The graph of fig 8 is not available to us, that of fig. 10 is, however, since we can plot experimentally the reflection curve of the crystal in a sensibly parallel beam of X-rays—parallel, that is, in comparison with the angular width of figs. 8 and 10. The *corrected* curve of fig. 10 should, however, be identical, except for its (arbitrary) vertical scale, with fig. 8, for presumably at any angular position of the crystal the number of blocks which are in a position to reflect, fig. 8, is proportional to the intensity, corrected for extinction, which actually is reflected, fig. 10. The difference between the dotted and the full curves of fig. 10 is, however, not great in practice for a small crystal; and to a first approximation this full curve—the experimental curve of reflection—may be regarded as a substitute for the curve of fig. 8. If we carry out the calculation as outlined above with this curve, then our result will be an approximation to the required answer; if we repeat the process with the new curve, our answer will be still nearer; and so by this successive approximation we can approach the desired result—the proper correction factor for extinction in the crystal—to any required accuracy.

The actual process of calculation is not as alarming as this description might suggest, since for anthracene the extinction factors, even for the best crystals, are quite small Let $y_1, y_2, y_3,$ be equally spaced ordinates of the experimental curve, the distance between them being $1/b$ Then if A is the area under this curve, $A = \frac{1}{b}\Sigma y$

The ordinates of the corrected curve, $Y_1, Y_2, Y_3,$, will be obtained by multiplying the y's by e^{ml} where m is the appropriate extinction factor and l the effective path through the crystal Let us now for the moment assume that the experimental curve is also the $f(\theta) - \theta$ curve of fig 6 In this case m equals Q times the ordinate divided by the area of the curve, i e, $m = Qy/A$.

Also if ml is less than $1/10$, as was found always to be so for the crystals measured, then we can with an error of less than ½% write

$$e^{ml} = 1 + ml = 1 + \frac{Ql}{A}y$$

The new ordinate Y therefore equals

$$y\left(1 + \frac{Ql}{A}y\right),$$

and clearly the fractional increase of area of the redrawn curve will be

$$\frac{Ql}{A}\Sigma y^2 \div A = \frac{Ql}{A^2}\Sigma y^2.$$

If therefore we list the y's and sum their squares, multiplication by the appropriate constants, involving the area (most simply found as the sum of the y's), will give the extinction correction for the crystal. As has been suggested, a single application of this process was usually enough to give the correction to the required accuracy. The corrections for the normal absorption in the crystal were made separately, they were of a different order of importance, as will be seen from the table on p. 443.

There are two possible objections to this process which require further discussion. The first is whether the phrase "effective length" of path of X-rays in the crystal has any meaning. It is of course true that the various diffracted rays do not traverse the same lengths of path, also a complete analysis of the problem would certainly average e^{ml} rather than ml itself, if any average were taken at all, nevertheless, owing to the shape of the crystals and the small value of the reflection angles concerned (about 5° for $\lambda = 1.539$ A.) a good approximation can be made graphically. The crystals are usually in shape of flat six-sided tables, fairly thick in relation to their width; and it is clear that the majority of the rays reflected from such a crystal at small glancing angles from the main face will traverse the same thickness of crystal. The estimation of the mean path was made in the following way, a careful picture of each crystal was drawn, and dimensioned by means of a microscope with eyepiece scale. On squared paper to a much magnified scale a series of cross-sections of the crystal by horizontal planes perpendicular to the axis of rotation was drawn, equally spaced vertically, and on each of these cross-sections a number of possible paths for the X-rays was plotted at close regular intervals. Owing to the favourable shape of most of the cross-sections it was not a great task to draw up for each crystal a list of perhaps 500 representative paths, and to average them with sufficient accuracy. An attempt to represent this process is given in fig. 11, where a typical anthracene crystal is drawn, also its cross-sections by five equally spaced horizontal planes, the path of a diffracted ray for $\lambda = 1.539$ A being indicated.

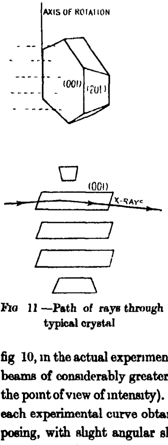

Fig. 11.—**Path of rays through typical crystal.**

The next objection which may be raised is that whereas these calculations are performed on curves measured with nearly parallel X-rays, fig. 10, in the actual experiments in which the absolute reflections were measured beams of considerably greater divergence were used (a practical necessity from the point of view of intensity). This objection is immaterial, since we may regard each experimental curve obtained in divergent radiation as the result of superposing, with slight angular shifts, many curves each similar and belonging to some particular nearly parallel radiation beam. If we imagine the above correction applied to each of these component curves, the total area of the corrected components would obviously not differ from the result of applying

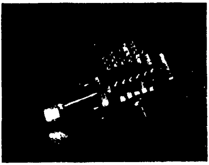

Fig 3

the correction factor in one step to the area of the original divergent curve, which is what we have proposed.

We may now recapitulate the steps necessary for the evaluation of the extinction correction for each crystal as follows

(*a*) the crystals were mapped and the mean paths through them determined as outlined above ;

(*b*) the normal linear absorption of anthracene for the two wave-lengths used was measured For this purpose a monochromatic beam defined by a fine pinhole was passed through several crystals, usually normal to the (001) planes, the crystals being selected as having parallel sides and an easily measurable thickness The absorption of each crystal was measured using the ionization chamber In addition to the crystals, several small blocks of anthracene, made by compressing the powdered substance in a powerful hydraulic press, were measured. After the measurements, the densities of the materials were determined, using the method of flotation, with the results given in Table I.

Table I.—Density of Crystals

—	Density
Crystal—	
No 1	1 205
No 2	1 202
No 3	1 205
No 4	1 226
No 5	1 237
No 6	1 235
Block—	
No. 1	1 247
No 2	1 230
No 3	1 245

Crystals 1 to 3 were rather opaque large crystals such as would not have been chosen for intensity measurements, but their geometrical shape was suited to the present purpose. Numbers 4 and 5 were very thin and perfectly transparent flakes ; number 6 was a remarkably perfect crystal of large size. The theoretical density of anthracene (from X-ray data) is 1·258 ; it will be seen that the compressed blocks approach this value more closely than any of the natural specimens. As the crystals used in the intensity measurements were all picked for transparency and perfection of faces in the first instance, it was considered probable that the group Nos. 4 to 6 above most nearly resembled them on the average ; the absorptions were therefore corrected to a mean density of 1 233, the average of these three crystals. The final values obtained and used in the subsequent calculations were .—

Absorption coefficient per millimetre, $\lambda = 0\ 709$ A, $\mu = 0\ 081$, $\lambda = 1{\cdot}539$ A, $\mu = 0{\cdot}503$

It is interesting to compare these values with the values found by calculation from the tables of absorption coefficients, though these tables do not seem to be very consistent as regards the lighter elements. Thus the International Critical Tables give for Cu K_α, $\mu/\rho = 4{\cdot}90$ for carbon and no value for hydrogen, for Mo K_α either $0{\cdot}63$ or $0{\cdot}55$ for carbon, and $0{\cdot}401$ for hydrogen, whereas the new International Tables* of crystal structure constants, now in the course of preparation, give for Cu K_α, $\mu/\rho = 5{\cdot}50$ for carbon, for Mo K_α $0{\cdot}70$ for carbon, the values for hydrogen being apparently about $0{\cdot}15$ in either case Adopting these latter values we get $\mu = 0{\cdot}650$ and $0{\cdot}092$ for molybdenum and copper radiation respectively, for anthracene of density 1 233, while if we take the lowest of the values, of the International Critical Tables we get values $0{\cdot}597$ and $0{\cdot}067$ (all expressed per millimetre) Our experimental values lie within these limits for the molybdenum value, but are decidedly low for the copper radiation

(*c*) As the next step, the reflection curve of each crystal in turn was determined, using nearly parallel X-rays. The molybdenum tube was used with a zirconium filter, and situated about 220 cm. from the crystals, a slit close to the target limited the divergence of the beam, which did not exceed 1½ minutes of arc for the largest crystals. Fig. 5 gives a series of the curves thus obtained, the diamond comparison crystal shows the separation of the alpha-doublet, but no attempt was made to allow for the presence of these two wave-lengths in the "monochromatic" radiation, for as will be seen even the best of the anthracene crystals gave reflection curves extending over a much wider angular range than this.

(*d*) Finally, series of ordinates to these reflection curves were measured off, and the calculation of the correction factor was made, as has been already outlined.

In Table II is given a list of all the crystals, measurements from which were incorporated in the final results. Combined with the curves of fig. 5, this list will show that the range both of size and of crystal "goodness" is considerable. The separate correction factors for absorption and for extinction are listed; it will be seen that extinction plays but a small part in the final result.

---

* I have to thank Dr. Lonsdale for access to the proofs of these tables. The references there given are Jonsson, "Dissertation Upsala" (1928), and Walter, 'Fortsch. Röntgenstr.,' vol. 35, pp. 929, 1308 (1927)

Table II.—Constants of Anthracene Crystals.

Name of crystal.	Path (mm.)	Weight (mg.).	Correction factors, $\lambda = 1\cdot539$ A.		$E\omega/I$.	Correction factors, $\lambda = 0\cdot7097$ A.		$E\omega/L$.
			Extinction.	Absorption.		Extinction.	Absorption.	
ψ	0·307	0·044	0·966	0·857	0·237	0·990	0·977	0·65
α	0·431	0·064	0·981	0·805	0·322	0·995	0·968	—
T	0·465	0·090	0·956	0·791	0·516	0·989	0·965	1·45
θ	0·422	0·099	0·969	0·819	—	0·991	0·968	1·29
L	0·478	0·104	0·958	0·794	—	0·989	0·964	1·30
U	0·412	0·124	0·985	0·813	0·706	0·995	0·969	1·80
ζ	0·395	0·146	0·980	0·819	0·797	0·985	0·970	—
EE	0·325	0·151	0·972	0·849	0·846	0·993	0·976	2·40
τ	0·550	0·199	0·952	0·758	1·212	0·987	0·959	2·80
η	0·557	0·212	0·945	0·769	—	0·986	0·958	2·89
V	0·432	0·218	0·936	0·805	1·221	0·983	0·968	3·30
BB	0·598	0·265	0·947	0·740	1·703	0·986	0·956	3·60
CC	1·123	0·288	0·960	0·568	2·004	0·989	0·918	3·48
ϵ	1·507	0·289	0·973	0·787	—	0·993	0·962	4·42
β	1·574	0·303	0·964	0·763	—	0·991	0·957	4·43
σ	1·732	0·308	0·952	0·692	1·58	0·987	0·946	3·97
AA	1·637	0·397	0·980	0·726	2·04	0·995	0·953	5·18
ω	1·013	0·482	0·943	0·600	2·90	0·984	0·926	6·74

Section E.—Discussion of Results.

The figures of Table II are represented on the graphs, figs. 6 and 7. In computing a mean value for $E\omega/I$, it was decided to give equal weights to the observations made with each crystal, *i.e.*, to take a simple average of the results for $E\omega/I$ per milligram for each crystal. The reason for this was that though the measurements with the larger crystals are likely to be more accurate owing to the greater intensity available, with the smaller crystals the extinction correction—probably the chief source of error—is proportionately smaller. The average values (indicated by the straight lines on the graphs) are:—

$$E\omega/I \text{ per milligram} = (5\cdot61 \pm 0\cdot106) \times 10^{-6} \text{ for } \lambda = 1\cdot539 \text{ A.}$$
$$E\omega/I \text{ per milligram} = (1\cdot392 \pm 0\cdot020) \times 10^{-6} \text{ for } \lambda = 0\cdot709 \text{ A.}$$

The plus and minus signs indicate the probable error evaluated by the ordinary least squares formula. It is interesting to note that the values obtained by allotting to the measurements on each crystal a weight proportional to the mass of the crystal are almost identical with those above.

Returning now to the original formula

$$Q\,dV = \frac{E\omega}{I} = dV\left\{N\,\frac{e^2}{mc^2}\,F\right\}^2 \lambda^3\,\frac{1+\cos^2 2\theta}{2\sin 2\theta},$$

and taking $\frac{e^2}{mc^2} = 2{\cdot}816 \times 10^{-13}$, and for anthracene, $a = 8{\cdot}58$, $b = 6{\cdot}02$, $c = 11{\cdot}18$, $\beta = 125°$, and density $= 1{\cdot}258$, we find

$$Q = 7{\cdot}582\,F^2 \times 10^{-6} \quad \text{for } \lambda = 1{\cdot}539\text{ A.}$$

and

$$Q = 1{\cdot}630\,F^2 \times 10^{-6} \quad \text{for } \lambda = 0{\cdot}709\text{ A.}$$

and hence finally

$$F = 30{\cdot}50 \pm 0{\cdot}29 \quad \text{for } \lambda = 1{\cdot}539\text{ A.}$$

$$F = 32{\cdot}76 \pm 0{\cdot}23 \quad \text{for } \lambda = 0{\cdot}709\text{ A.}$$

In this calculation N, the number of scattering units, was taken as the inverse of the volume of the unit cell, *i e*, the "F" above refers to the contents of the unit cell, and is comparable with the values quoted by Robertson (*loc. cit*).

The quantity F, the structure factor, is not, of course, a function of wavelength according to the picture of the crystal commonly used in structure analysis, it is a geometrical function of the mean positions of the atoms, and is presumably independent of the particular radiation with which we view them. If we may assume that the above figures are free from systematic error, then a real discrepancy appears, the chances are for example over 400 to 1 against both of the true experimental values for F differing from those quoted by as much as three times the probable error, and even this unlikely event would not suffice to bring the values into coincidence. There are, however, several ways in which error might have affected the results, leading to a systematic difference between the copper and the molybdenum values. These may be summarized as follows :—

(*a*) If the copper "monochromatic" beam were non-homogeneous to a much greater extent than has been assumed, the difference would be explained. Particular attention has, however, been paid to this point (*cf.* Section B).

(*b*) If the extinction, but more particularly the absorption, correction were incorrectly applied the values with copper radiation would be considerably altered. As Table II shows, very large corrections for absorption are necessary for some of the crystals, and a choice of a higher value for the linear absorption coefficient might remove the difference between the results A rough calculation shows that a value of $\mu = 0\cdot74$ per millimetre for copper radiation would bring about an approximate agreement, the experimentally found value was 0·50, and as we have already seen there is no justification based on the published values of μ/l for a figure higher than 0·65

(*c*) We have entirely neglected primary extinction in our calculations and corrections, possibly its effects are manifest in this difference between the F values

(*d*) A further possibility is that the effective size of the apertures used in the measurements is different with the different radiations owing, for example, to penetration of the edge of the aperture, or considerable scattering from this edge which might differ in the two cases A short calculation, knowing the absorption coefficient of platinum and the approximate profile of the edge of the aperture, shows that penetration can have no appreciable influence, and it is difficult to see how any scattering effect could account for as much as the necessary difference of about 14% Further evidence was given from the fact that the ratios of the effective areas of the four apertures used were the same, whether measured with soft radiation (tube potential not exceeding 8 kilovolts), or with quite hard radiation (tube potential 35 kilovolts, and radiation filtered through 2 mm. of aluminium).

If on the other hand we admit that satisfactory corrections have been made for systematic error, and that there is a genuine difference between the F values as determined with radiations of different wave-length, fundamental issues are raised. It is as if the hills and valleys of electron-density which we see by the light of $\lambda = 1\cdot539$ A in Robertson's contours would look slightly different by the light of $\lambda = 0\cdot709$ A —as indeed an actual landscape gives a different photograph on the modern infra-red plates It does not seem that theoretical writers have paid much attention to the problem of crystal reflection from the quantum mechanics standpoint, the general treatments of Wentzel and Waller* lead to expressions for the coherent radiation scattered from a single atom which are identical with the classical Thomson formula, and hence should lead to the same formula as that which we have used here for the total intensity for a small crystal.

---

* Wentzel, 'Z. Physik,' vol. 43, pp. 1, 779 (1927), Waller, 'Phil. Mag.,' vol 4, p. 1228 (1927).

It is, I think, impossible to admit this difference without further experimental work designed (*a*) to make the application of the extinction and absorption corrections more certain, as indicated by the "scatter" of the values for each crystal round the mean, until this scatter is reduced to the general level of experimental accuracy (say a variation of 1 or 2 per cent.) it is after all certain that these corrections have been unsatisfactorily applied, our fundamental formula states definitely that the total reflection from a crystal is proportional to its weight, whatever is the value of F And (*b*) to determine the value of F at some wave-length other than those used here. Good agreement has been found between the F values for rock-salt measured with rhodium and with molybdenum characteristic radiation*; but in these experiments the wave-length interval is hardly sufficient to show up a small variation if it exists. In the experiments of Wyckoff† F is found to vary near an absorption limit, but no such limit is concerned here Further measurements will not be easy, since there is no suitable target material available between the wave-lengths $\lambda = 1\cdot539$ A and $\lambda = 0\cdot709$ A., while for greater wave-lengths the error due to misapplication of the absorption correction becomes large Nevertheless, the problem seems an important one worth pursuing, if the difficulties can be satisfactorily overcome Meanwhile the value for F (001) for anthracene $= 32\cdot8$, taken with the molybdenum rays, should be quite reliable enough for the standardization of the majority of intensity measurements in organic crystal structure analysis

My thanks are due to the Managers of the Royal Institution and to Sir William Bragg for the facilities afforded me for the carrying out of the work here described; to my fellow-workers in the Davy-Faraday Laboratory for much helpful discussion and criticism, and to Mr. Ralph Dawton in particular, who has been responsible in many ways for experimental improvements and for the confirmation of results contained in this paper.

Summary

The absolute intensity of reflection of X-rays from anthracene crystals for the (001) planes has been measured for two wave-lengths ($\lambda = 1\cdot539$ A. and $\lambda = 0\cdot709$ A.), using small crystals up to $0\cdot5$ mg. in weight, bathed in a uniform monochromatic beam. The intensity measurements were made with a recording ionization spectrometer using valve amplification, which is described.

---

* Bragg, James and Bosanquet, *loc. cit.*, and 'Phil. Mag,' vol. 42, p. 1 (1922); James and Firth, 'Proc. Roy. Soc.,' A, vol. 117, p. 62 (1927).

† 'Phys. Rev.,' vol. 36, p. 1116 (1931).

Errors due to non-monochromatism of the beam and to extinction and absorption in the crystal are investigated, and a method of applying the extinction correction to small crystals is developed. The final values of the structure factor F for the (001) planes are 30·5 and 32·8 respectively for the two radiations; and the significance, if any, of this difference is discussed. The values found may be used for the determination by comparison of absolute values for other organic crystals, thus avoiding the labour of making absolute measurements afresh in each case

---

Exchange of Energy between Inert Gas Atoms and a Solid Surface.

By J. M. Jackson, Department of Mathematics, University of Manchester, and A. Howarth, Department of Mathematics, Municipal College of Technology, Manchester

(Communicated by D R Hartree, F R S —Received June 7, 1933)

§ 1. *Introduction.*—When a gas and a solid surface exchange energy, the transfer of energy from the one to the other is determined by the magnitude of the thermal accommodation coefficient α If a group of gas atoms with mean energy corresponding to the temperature T_2 are incident on a solid surface at temperature T_1, the gas atoms, after collision with the surface, will have mean energy corresponding to the temperature T'_2, where T'_2 lies between T_1 and T_2. The accommodation coefficient α is then defined by the limiting process

$$\alpha = \mathrm{Lim}_{T_1 \to T_2 \to T} (T'_2 - T_2)/(T_1 - T_2).$$

According to this definition α depends only on the nature of the gas and solid atoms, their interaction and the temperature T

A theory of the accommodation coefficient has been given by one of us† for two types of interaction between the gas and the solid, (i) the potential energy of the gas atom when outside the surface of the solid is zero and when inside the surface it is C, a constant, (ii) the potential energy at a normal distance y from the surface is Ce^{-ay}. Both these theories ignore any possible effects of the lattice structure of the solid. It was also assumed that the thermal oscillations of the solid atoms were all of the same frequency, as in Einstein's theory of the specific heat of solids. The first of these two potential fields was fairly successful in explaining the experimental results of Roberts† for the accommodation coefficient of helium on a clean surface of tungsten, whilst the second gave good agreement with experiment for the value of the exponential index

---

† Jackson, 'Proc. Camb. Phil. Soc.,' vol. 28, p. 136 (1932); Jackson and Mott, 'Proc. Roy. Soc.,' A, vol. 137, p. 703 (1932).

$$a = 9 \,.\, 10^8 \text{ cm}^{-1}.$$

The object of the present paper is to examine the modifications produced in the theory by removing the restriction that all the solid atoms should oscillate with the same frequency, and to obtain the average accommodation coefficient of the solid for its normal modes of vibration It is found that good agreement with the experiments of Roberts can be obtained, provided we choose the value of the exponential index a to be $4 \,.\, 10^8$ cm $^{-1}$

§ 2 *Calculation of the Average Value of the Thermal Accommodation Coefficient over the Normal Modes of the Solid*—The solid will be treated ideally as a simple cubic crystal containing N atoms, and therefore with 3N normal modes of vibration As N becomes very large the frequency spectrum of normal modes‡ tends to become continuous,

$$f(\nu)\, d\nu = 3\text{F}\nu^2\, d\nu \qquad \text{F, constant,} \tag{1}$$

being the number of normal modes lying within the range $d\nu$ about the frequency ν. If all the solid atoms were oscillating in a particular normal mode of frequency ν, the exchange of energy and the accommodation coefficient $\alpha(\nu)$ might be calculated as in the simple theory in which thermal oscillations of only one frequency were considered. The chance that the solid is oscillating in a particular normal mode of frequency lying between ν and $\nu + d\nu$ is

$$\frac{\text{F}}{\text{N}}\, \nu^2 d\nu.$$

The average accommodation coefficient $\bar{\alpha}$ can therefore be written as

$$\bar{\alpha} = \int_0^{\nu_m} \frac{\text{F}}{\text{N}}\, \nu^2\, \alpha(\nu)\, d\nu,$$

where the upper limit ν_m of the frequency range is chosen so that

$$3\text{N} = \int_0^{\nu_m} 3\text{F}\nu^2\, d\nu = \text{F}\nu_m{}^3,$$

---

† 'Proc. Roy. Soc.,' A, vol. 129, p. 146 (1930); vol. 135, p. 192 (1932).

‡ Born, "Atomtheorie des festen Zustandes," p. 587.

as in Debye's† theory of the specific heat of solids. ν_m is the Debye frequency of the solid, determined from specific heat data or otherwise. The average thermal accommodation coefficient can therefore be written as

$$\bar{\alpha} = \frac{3}{\nu_m{}^3}\int_0^{\nu_m} \nu^2\,\alpha(\nu)\,d\nu \tag{2}$$

The average accommodation coefficient per atom of the solid will be three times the above result, since if there are N atoms in the solid there are 3N normal modes. The average accommodation coefficient which has been calculated in this paper is the average over the normal modes (as in equation (2).) By changing the variable of integration in (2) we may write it in the more convenient form

$$\bar{\alpha} = \frac{3}{\Theta^3}\int_0^{\Theta} \theta^2\,\alpha(\theta)\,d\theta, \qquad \text{where} \qquad \theta = h\nu/k. \tag{3}$$

Θ is the Debye characteristic temperature of the solid. This method of averaging the accommodation coefficient over the normal modes of the solid is legitimate provided we can show that the exchange of energy between the gas atom and the solid takes place as if the gas atom exchanged energy with a particular normal mode independently of its energy exchange with the other normal modes.

§ 3. *Independence of the Probabilities of Energy Exchange with the different Normal Modes of the Solid.*—The Hamiltonian of the whole system gas atom and crystal may be written

$$\mathrm{H} = \tfrac{1}{2}\mathrm{S}_l \sum_x \mathrm{MU}_x{}^{l2} - \tfrac{1}{2}\mathrm{S}_{ll'} \sum_{xy} \phi_{xy}{}^{l-l'} u_x{}^l u_y{}^l + \tfrac{1}{2}m\dot{\mathbf{r}}_g{}^2 + \mathrm{S}_l\,\Phi\,(\mathbf{r}_g - \mathbf{r}^l) \tag{4}$$

The notation is that of Born‡ and Waller§. M is the mass of an atom of the crystal and m that of a gas atom. S_l denotes a summation over the lattice points l of the crystal; l is short for l_1, l_2, l_3. The displacement of the lattice point l from its equilibrium position is the vector $\mathbf{u}^l$, components $u_x{}^l, u_y{}^l, u_z{}^l$. Taking the potential energy of the crystal to be zero when the atoms are in their equilibrium positions, the second term represents the potential energy of the crystal when the displacements of the lattice points are $\mathbf{u}^l$. $\phi_{xy}{}^{l-l}$ depends on the the law of force between the solid atoms. The position vector of the gas atom referred to the same set of axes as we use for the crystal is $\mathbf{r}_g$

---

† Born, *loc. cit.*, p. 640.

‡ "Atomtheorie."

§ "Uppsala Universitets Årskrift," vol. 2 (1925).

and $S_l \Phi(\mathbf{r}_g - \mathbf{r}^l)$ is the potential energy of the gas atom in the field of force of the crystal atoms.

If we introduce the normal co-ordinates Q_i of the crystal lattice by means of the linear transformation

$$\mathbf{u}^l = \sum_{i=1}^{3N} \mathbf{U}^{li} Q_i, \tag{5}$$

where the components U_x^{li}, U_y^{li}, U_z^{li} of the vectors $\mathbf{U}^{li}$ satisfy the relations

$$\sum_{i=1}^{3N} U_x^{li} U_y^{l'i} = \delta_{ll'} \delta_{xy}$$

and

$$\sum_{i=1}^{3N} 4\pi^2 \nu_i^2 U_x^{li} U_y^{l'i} = -\phi_{xy}^{l-l'},$$

ν_i is the frequency of the ith normal mode, the first two terms of (4), viz., the Hamiltonian of the crystal becomes

$$H_c = \tfrac{1}{2} \sum_{i=1}^{3N} M Q_i^2 + 2\pi^2 \sum_{i=1}^{3N} M \nu_i^2 Q_i^2,$$

and we may write (4) in the form

$$H = \sum_{i=1}^{3N} \tfrac{1}{2} M (Q_i^2 + 4\pi^2 Q_i^2) + \tfrac{1}{2} m \dot{\mathbf{r}}_g^2 + S_l \Phi(\mathbf{r}_g - (l\mathbf{a}))$$
$$+ \sum_{i=1}^{3N} Q_i S_l \mathbf{U}^{li} . \operatorname{grad} \Phi(\mathbf{r}_g - (l\mathbf{a})) + \tag{6}$$

In this expression the potential energy of the gas atom in the field of the crystal has been expanded as a Taylor series in terms of the displacement components of the crystal atoms and these displacement components have in turn been replaced in terms of the normal co-ordinates of the crystal lattice defined in (5). Only the first two terms of the Taylor series have been taken in (6). This will be sufficiently accurate for a first order perturbation theory provided that the crystal is not too hot. The last term in (6) is the interaction energy between the gas and the solid.

The wave equation for the problem is therefore

$$\Big[-\frac{h^2}{8\pi^2 M} \sum_{i=1}^{3N} \frac{\partial^2}{\partial Q^2_i} + \sum_{i=1}^{3N} 2\pi^2 M \nu_i^2 Q_i^2 - \frac{h^2}{8\pi^2 m} \nabla_g^2 + S_l \Phi(\mathbf{r}_g - (l\mathbf{a}))$$
$$+ \sum_{i=1}^{3N} Q_i S_l \mathbf{U}^{li} . \operatorname{grad} \Phi(\mathbf{r}_g - (l\mathbf{a})) + \frac{h}{2\pi i} \frac{\partial}{\partial t} \Big] \Psi = 0. \tag{7}$$

Ignoring the interaction energy this wave equation is separable and the zero order approximation wave functions may therefore be written

$$\Psi_0 = \prod_{i=1}^{3N} \psi_i (Q_i) \chi_g e^{-\left(\frac{2\pi i}{h}\right)\left[\sum_{i=1}^{3N}(n_i+\frac{1}{2}) h\nu_i + W_g\right] t}, \tag{8}$$

where $\psi_i (Q_i)$ are the usual oscillator wave functions, corresponding to the normal co-ordinate Q_i and the normal mode of frequency ν_i, and χ_g is the wave function of the gas atom in the field of force of the crystal, the solid atoms being in their equilibrium positions Each of these wave functions is normalized to unity

The transition probability per collision that the system changes from a state specified by the quantum numbers n_1, n_2, , n_{3N} to the state n'_1, n'_2, , n'_{3N} of the normal modes of the solid with a corresponding change in the energy W_g of the gas atom is obtained by the variation of parameters as in the simple theory given previously † The only alteration required is that the element $B_n{}^m$, of the interaction matrix must be replaced by the element $B_{n_i}{}^{n'_i}$, where n_i stands for the set of oscillator quantum numbers, n_1, n_2, .., n_{3N}

$$B_{n_i}{}^{n'_i} = \prod_{i=1}^{3N} \int dQ_i \tilde{\psi}_{n'_i} \psi_{n_i} \int \sum_{j=1}^{3N} Q_j S_l U^{lj} \;\; \text{grad}\, \Phi (\mathbf{r}_g - (l\mathbf{a})) \tilde{\chi}_{W^*_g} \chi_{W_g} \, dx\, dy\, dz, \tag{9}$$

where the appropriate normalized wave functions are inserted in the product and where

$$W^*_g = W_g + \sum_{i=1}^{3N} (n_i - n'_i) h\nu_i$$

On account of the orthogonality of the oscillator wave functions ψ_{n_i}, ψ'_{n_i}, the summation over j reduces to a single term and

$$B_{n_j}{}^{n'_j} = \int dQ_j \tilde{\psi}_{n'_j} Q_j \psi_{n_j} \int S_l U^{lj} \,.\, \text{grad}\, \Phi (\mathbf{r}_g - (l\mathbf{a})) \tilde{\chi}_{W^*_g} \chi_{W_g} \, dx\, dy\, dz,$$

the other quantum numbers n_i, $i \neq j$, remaining unchanged.

$\int dQ_j \tilde{\psi}_{n'_j} Q_j \psi_{n_j}$ is, however, just that integral which appears in the selection rule of the one-dimensional oscillator‡ and is zero unless $n'_j = n_j \pm 1$.

Out of the aggregate of quantum numbers n_i specifying the state of the solid, only one, n_j, can change at once, and to the degree of approximation considered in this theory it can only change to $n_j \pm 1$. Thus

$$B_{n_j}{}^{n_j \pm 1} = \left(\frac{n_j + \frac{1}{2} \pm \frac{1}{2}}{8\pi^2 M h\nu_j / h^2}\right)^{\frac{1}{2}} \int S_l U^{lj} \;\; \text{grad}\, \Phi (\mathbf{r}_g - (l\mathbf{a})) \tilde{\chi}_{W^*_g} \chi_{W_g} \, dx\, dy\, dz. \tag{10}$$

---

† Jackson, *loc. cit.*, pp. 142–144.

‡ Sommerfeld, "Wellenmechanischer Ergänzungsband," p. 61.

The form of this result shows that the gas atom exhanges energy with the normal mode of frequency ν_j independently of the other normal modes. This approximation will be valid provided that the crystal is not too hot and the interaction energy between the gas and the solid is such that the first term in the Taylor series represents the major portion of the interaction energy These conditions are satisfied in the experiments of Roberts and for the exponential field for the interaction energy which we must take to fit the experimental values.

As we do not know the exact wave functions of a gas atom in the crystal potential field, but only the approximate wave functions for a one dimensional exponential field,† we have replaced the integral in (10) by the corresponding one involving the approximate wave functions The results obtained for the transition probabilities and therefore for the accommodation coefficient are the same as if all the atoms of the crystal were oscillating in the normal mode of frequency ν_j. The calculation of the average accommodation coefficient over the normal modes can therefore be made as in § 2

§ 4 *Numerical Results.*—The theory has been compared with the experiments of Roberts on the temperature variation of the accommodation coefficient of helium on a clean surface of tungsten. These results are

$$295^\circ \text{ K}, \alpha = 0{\cdot}057, \qquad 195^\circ \text{ K}, \alpha = 0{\cdot}046, \qquad 79^\circ \text{ K}, \alpha = 0{\cdot}025.$$

The accommodation coefficient for a particular normal mode of the crystal of frequency‡ ν is

$$\alpha(\nu) = \tfrac{2}{3}\mu^3 (e^\mu - 1)^{-1} \frac{m\Upsilon^2}{\mathrm{M}a^2} \int_0^\infty \frac{\sinh \frac{\Upsilon}{a}(\mathrm{E}+1)^{\frac{1}{2}} \sinh \frac{\Upsilon}{a}\mathrm{E}^{\frac{1}{2}} \;\; e^{-\mu\mathrm{E}}\, d\mathrm{E}}{\left[\cosh \frac{\Upsilon}{a}(\mathrm{E}+1)^{\frac{1}{2}} - \cosh \frac{\Upsilon}{a}\mathrm{E}^{\frac{1}{2}}\right]^2}, \qquad (11)$$

where $\gamma^2 = 32\pi^4 mh\nu/h^2$ and $\mu = h\nu/k\mathrm{T}$. The method used to calculate $\bar{\alpha}$ was to obtain $\alpha(\nu)$ as a function of T for a set of values of ν and then to evaluate the integral for $\bar{\alpha}$ in equation (2) numerically for various values of T. The calculations were made for two values of the exponential index a, viz., $a = 9$ and $4 \cdot 10^8$ cm $^{-1}$. The values of $\alpha(\nu)$ were obtained partly by numerical integration and partly by an analytical method. It is found that the transition probabilities per collision† are almost linear functions of the energy E, $p_1(\mathrm{E})$ tending asymptotically to the straight line

---

† Jackson and Mott, *loc. cit.*, p. 709, equation (21)

‡ Jackson and Mott, *loc. cit.*, p. 713.

$$p_1(\mathrm{E}) = 4\frac{m}{\mathrm{M}}\mathrm{E} + \frac{m}{\mathrm{M}}\left(2 - \frac{1}{12}\frac{\Upsilon^2}{a^2}\right), \tag{12}$$

for large values of the energy E. For small values of ν the main contribution to the integral in $\alpha(\nu)$ comes from large values of E where the above linear approximation for $p_1(\mathrm{E})$ may be used without serious error. On the contrary for large values of ν the main contribution to the integral comes from small values of E for which the use of the above linear approximation is not justified. In the former case

$$\left.\begin{aligned} \alpha(\nu) &= \frac{8}{3}\frac{m}{\mathrm{M}}\frac{\mu}{e^{\mu}-1}(1 + c\mu), \\ \text{where}\qquad c &= \tfrac{1}{4}\left(2 - \frac{1}{12}\frac{\Upsilon^2}{a^2}\right) \end{aligned}\right\}. \tag{13}$$

The curves for $\theta = h\nu/k = 51{\cdot}25^\circ$ K. were calculated from this result. The curves for $\theta = 102{\cdot}5^\circ$ and $153{\cdot}5^\circ$ K. were obtained by dividing the range of integration into two parts and evaluating the integral over the first part numerically and over the second analytically. The curve for $\theta = 205^\circ$ K. was obtained entirely by numerical integration. If we make ν tend to zero in (13) we find that $\alpha(0) = \frac{8}{3}m/\mathrm{M}$, this is also the asymptotic value of $\alpha(\nu)$ when T becomes very large. The curves obtained are shown in fig. 1 in which $\alpha(\theta)$ is shown as a function of T, the values of θ being $51{\cdot}25^\circ$, $102{\cdot}5^\circ$, $153{\cdot}5^\circ$ and 205° K. and the value of a being $4 \cdot 10^8$ cm.$^{-1}$. The curves obtained with the exponential index $a = 9 \cdot 10^8$ cm^{-1} are similar to those shown in fig. 1 but closer together. For a given value of T, $\alpha(\nu)$ decreases as ν increases. This is because it is less probable for a gas atom of given energy to exchange energy in large quanta rather than in small quanta. That is, those solids with high characteristic temperatures will give a low accommodation coefficient and therefore a large proportion of perfectly elastic reflection of gas atoms at the surface. This result is confirmed qualitatively by the experiments of Estermann and Stern‡ on the molecular ray diffraction of hydrogen and helium. They found the intensity of elastically reflected molecules of these gases was relatively greater from a crystal of lithium fluoride, $\Theta = 440^\circ$, than from a crystal of sodium chloride, $\Theta = 234^\circ$ K.

---

† Jackson and Mott, *loc. cit.*, equation (25.1) and fig. 3.

‡ 'Z. Physik,' vol. 61, p. 106 (1930).

The value of $\bar{\alpha}$ was now calculated using equation (3) and the integral $\frac{3}{\Theta^3}\int_0^{\Theta} \theta^2\alpha(\theta)\,d\theta$ was evaluated numerically using the curves shown in fig. 1. The value of Θ was taken to be 205° K., it is the value of the characteristic temperature of tungsten as determined by Lindemann's melting-point formula The values of $\bar{\alpha}$ found in this way for the two fields $a = 4$ and $9 \, . \, 10^8$ cm. $^{-1}$

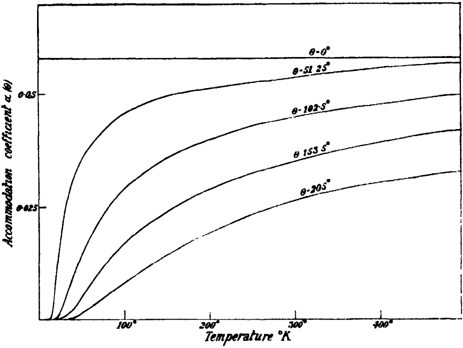

FIG 1.—The temperature variation of the thermal accommodation coefficient for tungsten and helium for various normal modes of the solid. If the frequency of a normal mode is ν, the characteristic temperature for this normal mode is $\theta = h\nu/k$. The interaction energy of the gas and solid is taken to be exponential $\sim e^{-ay}$, the curves given here were calculated for the value $a = 4 \, . \, 10^8$ cm.$^{-1}$.

are shown in fig 2 (curves 1 and 2). These two curves for $\bar{\alpha}$ were fitted to the experimental curve at T = 205° K, by multiplying by suitable constant factors, for, since the absolute value of the accommodation coefficient is uncertain owing to the roughness of the surface, and we have used the approximate one-dimensional wave functions instead of the exact three-dimensional wave functions, this will be the best way of comparing the theory with experiment. These fitted curves for $\bar{\alpha}$ are marked 3 and 4 in fig. 2. No account has been taken of two-quantum transitions; to the degree of approximation considered in

§ 3 they are forbidden. The effect of the attractive field of the solid has been ignored. The method of including this has been given by one of us† elsewhere. It will not affect the results greatly.

Comparing curves 3 and 4 in fig 2 with the experimental points, marked with a cross, we see that the field $a = 4 \ 10^8$ cm $^{-1}$ gives better agreement with experiment than the curve for $a = 9 \ 10^8$ cm.$^{-1}$ With the previous theory in which only one normal mode of the solid was considered the reverse was the case. The reduction of the value of the exponential index from 9 to $4 . 10^8$ cm.$^{-1}$ is very satisfactory, as the latter value is more in accord with the value we should expect from other sources. Slater‡ gives the repulsive potential energy of a pair of helium atoms in the ground state as depending on the exponential index $4 \cdot 6 . 10^8$ cm.$^{-1}$. An investigation by Born and Mayer§ on the properties

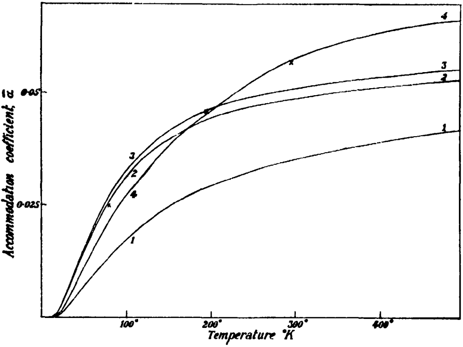

Fig. 2 —The temperature variation of the thermal accommodation coefficient averaged over the normal modes of the solid. The interaction energy of the gas and the solid is taken to be exponential $\sim e^{-ay}$ Curve 1, $a = 4 . 10^8$ cm $^{-1}$, curve 2, $a = 9 . 10^8$ cm.$^{-1}$; curve 3, $a = 9 . 10^8$ cm $^{-1}$, fitted to the experimental curve at T = 205° K, curve 4, $a = 4 . 10^8$ cm.$^{-1}$, fitted to the experimental curve at T = 205° K.

---

† Jackson, *loc. cit.*, p. 156.

‡ 'Phys. Rev.,' vol. 37, p. 696 (1931).

§ 'Z. Physik,' vol. 75, p. 1 (1932).

of the alkali halides, taking the intrinsic repulsive fields to be exponential instead of inverse *n*th power fields, showed that the repulsive fields of the alkali halides were characterized by the exponential index $3 . 10^8$ cm.$^{-1}$. On account of the relation of the alkalis and the halogens to the corresponding inert gases, we should expect that the intrinsic repulsive fields of the inert gases would be characterized by the same value of the exponential index. The value of the exponential index for helium suggested by the present theory of the accommodation coefficient is $4\ 10^8$ cm $^{-1}$ This lies between the values of Born and Slater. If the attractive field of the solid were included it would result in a decreased curvature in curves 3 and 4 in fig. 2. This would mean that better agreement could be obtained by taking a lesser value of the exponential index The difference would, however, not be large and it is probable that the value of the exponential index is not less than $3 . 10^8$ cm.$^{-1}$.

Summary

The theory of the thermal accommodation coefficient previously given by Jackson and Mott, for a one-dimensional exponential field is extended by averaging over the normal modes of vibration of the solid. Good agreement is obtained with the experiments of Roberts on temperature variation of the accommodation coefficient of helium on tungsten for the value $4 . 10^8$ cm.$^{-1}$ of the exponential index a. This is of the same order of magnitude as that suggested by the work of Born and Slater

A Comparison of the Catalytic Activity of Liquid and Solid Surfaces. The Decomposition of Methanol on Solid and Liquid Zinc.

By E W. R. Steacie and E M. Elkin, Physical Chemistry Laboratory, McGill University, Montreal.

(Communicated by H T Barnes, F R S —Received June 1, 1933)

Introduction

On account of its importance from the theoretical and practical standpoints, there has been a great deal of speculation regarding the nature of catalyst surfaces There is a considerable body of experimental evidence which has led to the assumption that catalyst surfaces are not uniformly active * The main lines of evidence which have led to this conclusion are (*a*) the ease with which the activity of a catalyst is destroyed by heating , (*b*) the poisoning of catalysts by the adsorption of amounts of foreign materials which are not sufficient to cover more than a fraction of the surface , (*c*) the fact that heats of adsorption vary with the amount of material adsorbed

The above evidence makes it highly probable that in *some* reactions on *certain* catalysts the surface is not uniformly active As a result a number of theories have been proposed which assign the activity of a solid catalyst to some one limited portion of the surface. The most important of these are the original theory of Taylor† in which the " active centres " are identified with peaks or extra-lattice atoms on the surface, and that of Schwab‡ which assigns the activity to crystal boundaries and microcrystalline imperfections

There is obviously no excuse for assigning the activity of *all* catalysts in *all* reactions to some one specified portion of the surface Specific effects must come into play in different cases, and hence the above theories, in addition to being entirely *ad hoc*, are also of limited applicability.

It was therefore considered to be of interest to compare the smooth surface of a pure metal, which will nevertheless possess the normal number of imperfections, crystal boundaries, etc., with a surface of the same metal which was free from all peaks, crystal boundaries, or imperfections. In the present investigation this has been accomplished by comparing the catalytic activity of pure zinc above and below its melting point

---

* No bibliography is given here since the subject has been frequently reviewed See especially the reports of the Committee on Contact Catalysis, and Schwab, " Katalyse vom Standpunkt der chemischen Kinetik," Berlin, 1931.

† 'Proc. Roy Soc ,' A, vol. 108, p. 105 (1925), etc

‡ 'Z. Elektrochem ,' vol. 35, pp. 135, 573 (1929) ; 'Z. phys. Chem.,' B, vol 1, p 385 (1929) ; B, vol. 2, p. 262 (1929).

If active centres come into play in catalytic reactions on solid zinc, it would naturally be expected that there would be a sudden very large drop in activity at the melting point. The absence of such a drop would seem, on the other hand, to be a conclusive proof that the entire surface was uniformly active.

As far as we are aware, there is only one reference in the literature which has any bearing on the present problem Hartman and Brown* have studied the hydrogenating activity of cadmium from the reduced oxalate and hydroxide Both catalysts give maximum yields at 319 5 ± 1° C (cadmium melts at 320 9° C.). The catalyst still retains its activity above the melting point A supporting material is used, which appears to prolong the activity of the catalyst by retarding the coalescence of the cadmium droplets There is no indication of any abrupt change in catalytic activity at the melting point No very definite conclusions can be drawn from this investigation, however, since the extent of the surface is not known, and the presence of the support is very objectionable

Experimental Method

The experimental requirements of the problem are .—

(1) a metal catalyst whose melting point is neither too low nor too high for the rate of the reaction to be measurable ,

(2) a reaction of a simple nature, whose products are not likely to introduce complications, and whose velocity is moderate at the temperature at which the catalyst melts ,

(3) a reaction vessel, the walls of which will have no appreciable effect on the rate of reaction.

The first requirement has been met by zinc It has a convenient melting point (420° C.). It may be obtained in comparatively pure form, and may be purified still further *in situ* by distillation *in vacuo*, and reduction with hydrogen.

The reaction chosen was the thermal decomposition of methyl alcohol This reaction may proceed either by dehydrogenation or by dehydration.† In the first case, we have

$$CH_3OH = H_2 + H\,CHO$$
$$HCHO = H_2 + CO,$$

---

* 'J. Phys. Chem.,' vol. 34, p. 2659 (1930)

† Sabatier, "Catalysis in Organic Chemistry," New York, 1922

in the second case

$$2CH_3OH = H_2O + CH_3OCH_3$$

In general, zinc favours dehydrogenation, and dehydration is inappreciable In the present investigation, the reaction has been followed by the pressure change As only relative rates were required, no attention has been paid to the mechanism of the reaction

The demand for an inert reaction vessel has been met by Pyrex glass In preliminary blank trials it was found that no appreciable decomposition of methyl alcohol takes place in Pyrex vessels up to 500° C. Furthermore, on solidification zinc does not adhere to the glass, and hence the metal may be melted and solidified without breaking the reaction vessel

Apparatus

The rates of reaction were followed by admitting the reactant, at a constant pressure of about 12 cm., to a heated Pyrex bulb, and observing the rate of pressure increase at constant volume by means of a capillary manometer The apparatus was similar to one which has been previously described * The reaction vessel was heated by means of an electric furnace, the temperature being controlled by the hand regulation of rheostats. It could be maintained constant to within about 1° C Temperatures were measured with a chromel-alumel thermocouple in conjunction with a thermocouple potentiometer

Methyl alcohol was treated with lime, and fractionally distilled, the middle third being retained.

To free the zinc from oxide, it was subjected to vacuum distillation. The zinc was placed in a heavy walled Pyrex bulb, which was connected by heavy walled capillary tubing to the reaction vessel The bulb containing the zinc was heated on a sand bath to about 630° C, while a hand torch was played on the connecting tubing. The reaction bulb and connecting tubing were heated to 500°–600° C for several hours previous to the distillation to remove adsorbed gases. The metal was then distilled into the reaction bulb while the system was under a vacuum of about 0·0001 mm. On completing the distillation the distilling bulb was sealed off from the reaction vessel and removed. The metal was then carefully melted off the walls of the reaction bulb on to the bottom. It had the form of a spheroidal drop, and had a very clear metallic lustre.

In a number of cases, especially between series of runs, the catalyst was subjected to reduction with hydrogen. The evacuated apparatus was filled with hydrogen at atmospheric pressure, and the temperature raised to 500° C. In most cases this treatment lasted for at least 24 hours.

---

* Steacie, 'Canadian J. Res.,' vol. 6, p. 265 (1932).

The temperature range used was from 360° to 440° C. This gave a satisfactory temperature interval on each side of the melting point. Below 360° the rate was too slow for convenience. Above 440° the rate was rather high for accurate measurements In addition small quantities of carbon were deposited if the temperature were too high.

Experimental Results.

In some preliminary series of runs zinc foil and shot were used without purification other than a superficial cleaning. It was found, however, that the results were untrustworthy on account of the presence of zinc oxide In all further runs, therefore, the zinc was purified by vacuum distillation as previously described

The results which follow are not highly reproducible, since on melting, or even on standing at a high temperature, some change in the surface area will occur. However, this is not serious since we are only interested in relative results, and if only a certain type of surface were effective we would expect such a sharp drop in catalytic activity at the melting point that any effects due to a small variation in total surface would be negligible.

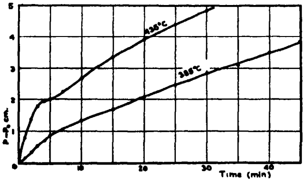

Fig. 1.—Typical pressure-time curves

The reaction has been followed by observing the rate of change of pressure with time Some sample pressure-time curves are given in fig 1 As will be seen from the curves, at the lower temperatures the pressure increases regularly with time. At higher temperatures there is a break in the curve, due to the fact that the reaction really takes place in stages. At all temperatures, however, the rates are satisfactorily reproducible on a given catalyst. Throughout this investigation the times for various arbitrary fractional pressure increases have been used as a measure of the rate of reaction, and hence as a measure of the activity of the catalyst.

The condensed data for several series of runs follow.

Series I.—The zinc used was purified by vacuum distillation, but was not reduced with hydrogen *in situ*. The surface area of the zinc was approximately 0·5 cm^2. Successive experiments were performed in order of increasing temperature. The results are given in Table I.

Table I

Temperature, °C	T_{20}, minutes	T_{25}, minutes	T_{30}, minutes
382	24·5	30·5	38·0
407	10·6	16·0	18·0
429	5·1	6·9	9·4
453	1·65	2·65	—
474	1·05	1·30	1·85
504	0·75	1·05	1·37

In fig. 2, $\log_e T_n$ is plotted against the reciprocal of the absolute temperature. The strict parallelism of the curves for T_{20}, T_{25} and T_{30} shows that we are justified in using the pressure increase as a measure of the rate of reaction. The curves are not quite linear, as required by the Arrhenius equation, but this is hardly to be expected since some change in area must take place on fusion, and on standing for considerable periods of time. The most noteworthy point is the complete absence of any sharp break in the curves at the melting point of zinc. In this, and in all subsequent series of runs, no visible change in the catalyst occurred with use. It always preserved a clear metallic lustre throughout.

Series II.—These experiments were made to show the effect of oxidation and of reduction on the activity of the catalyst. The zinc was purified by vacuum distillation as before. Its surface area was *ca*. 0·25 cm^2. Three runs were made on the liquid at 436° C. :—

(*a*) With the catalyst in its original state the value of T_{25} was 16·5 minutes.

(*b*) After 12 hours reduction with hydrogen at 500° C., it was found that $T_{25} = 19·0$ minutes.

(*c*) After contact with air for 3 minutes at 436° C., T_{25} decreased to 4·1 minutes.

Thus reduction with hydrogen has a very small effect on the activity of the catalyst, which is of the order of magnitude of the experimental error. Oxidation, on the other hand, causes a definite increase in activity It is therefore essential that the material be freed from traces of oxides, and in all subsequent runs the metal was left in contact with hydrogen at 500° C for at least 24 hours before being used This fact, together with the general reproducibility of the results, makes it certain that we are dealing with catalysis by metallic zinc, and not by traces of zinc oxide

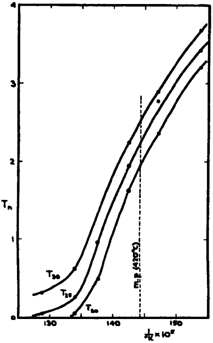

FIG 2 —Series I

Table II.

Temperature, ° C	366	395	416	430
T_{25}, minutes	29·5	10·5	5·95	4·6

Series III.—The zinc was distilled and reduced with hydrogen for 24 hours. The metal was in the form of a " button " 2 cm. in diameter and 0·5 cm. thick. The runs were made in order of increasing temperature. The results are given in Table II.

Series IV.—On the completion of the experiments in series III, the metal was again reduced with hydrogen for 24 hours. The results are given in Table III

Table III

Temperature, ° C	361	401	429
T_{25}, minutes	35·1	9·2	3·7

Series V.—The same sample was again used, with a further reduction with hydrogen for 24 hours It was used for runs above the melting point only, without solidification of the zinc after the reduction The results are given in Table IV.

Table IV

Temperature, ° C	424	424
T_{25}, minutes	3·75	3·75

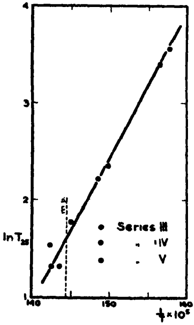

FIG. 3.—Series III, IV, and V

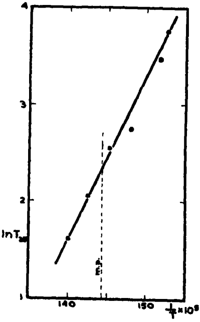

FIG 4—Series VI

The results from series III, IV and V are all given together in fig. 3 in the form of a $\log_e T_{25} - 1/T$ plot All the points lie on the same straight line. As in fig. 2, there is absolutely no indication of a break at the melting point of zinc.

Series VI.—Here the usual order was reversed, the first run being made at the highest temperature on the molten metal, with succeeding runs at consecutively lower temperatures. As before the zinc was vacuum distilled. It was reduced with hydrogen for 72 hours at 500° C before use. The surface area was about 0·5 cm^2. The results are given in Table V.

Table V.

Temperature, ° C	441	441	429	415	402	382	386
T_{33}, minutes	5·0	5·3	7·75	12·8	15·5	42·0	32·2

The results are plotted as before in fig. 4. There is again no indication of a break at the melting point.

Discussion.

The existing theories of the nature of catalyst surfaces postulate that only a fraction of the total surface is active, the remainder being relatively, or even totally, inactive. The original theory of Taylor was developed primarily in connection with hydrogenation reactions. Since then there has been a tendency to apply it to all reactions.

The investigation described here was attempted in order to test these theories. The catalyst has been used in bulk form, and with a limited, reasonably definite surface. This contrasts sharply with the general practice of using highly dispersed contact agents with a vastly extended surface. The treatment of the catalyst has been controlled with the object of obtaining as smooth a surface as possible, as opposed to the general practice where the main object is to create a surface of irregular character by means of some violent treatment.

Even if the surface of the catalyst used here were free from the extra-lattice peaks postulated by Taylor, it still possesses the crystal boundaries and microcrystalline cracks to which Schwab assigns catalytic activity. All these irregularities must disappear when the crystal lattice disappears on fusion of the metal.

It would therefore be expected that the activity of the catalyst would drop sharply on melting. No such discontinuity has been found, as is seen in figs 2, 3 and 4. We are therefore forced to the conclusion that the surface of the catalyst is free from active patches, or in other words that the whole surface of the metal is uniformly active. It is, of course, probable that in certain reactions the catalytic activity is not uniform over the entire surface. The field of force in which an adsorbed molecule finds itself will naturally differ according to whether we consider a plane surface or a crystal edge. We would therefore expect, merely by chance, that for some reactions one part of the surface would be more active than another

It should be emphasized that the investigations which have led to the idea of "active patches" are all of an indirect type The present investigation furnishes the most direct evidence which has yet been obtained as to the uniformity or otherwise of catalytic surfaces It therefore casts considerable doubt on the idea that the entire catalytic activity is to be ascribed to one definite limited part of the solid surface

Further investigations on catalysis by liquid metals are in progress

Summary

The effect of varying temperature on the rate of decomposition of gaseous methyl alcohol over solid and liquid zinc has been investigated from 360° to 440° C With constant surface the catalytic activity of the metal is directly dependent on the temperature, there being no discontinuity at the melting point of zinc It is therefore concluded that the entire surface of the metal is uniformly active, and that it is not in general justifiable to assign the whole catalytic activity of a solid to some one limited part of the surface.

The Emission Constants of Metals in the Near Infra-Red.

By C. Hurst, D.Phil., Christ Church, Oxford.

(Communicated by F. A Lindemann, F R S.—Received June 7, 1933.)

In the far infra-red, the reflecting power, R, of a metal at a wave-length, λ, is connected with its specific resistance, ρ, by the Hagen-Rubens relation,

$$1 - R = k\sqrt{\frac{\rho}{\lambda}},$$

where k is a constant with the value 0·365 when λ is measured in μ, and ρ is the resistance of a rod of the metal 1 metre in length and 1 sq mm in cross-section. The relation has only a restricted range of validity; for it is based theoretically on the electromagnetic theory, which does not embody the modern conceptions of the electron theory, and a restriction for a lower wave-length limit is made in the deduction of the formula itself.

Hagen and Rubens*† have subjected the formula to a rigid test by a series of emission measurements. At wave-lengths of 25·5 and 8·85μ, the calculated and observed emissivities‡ agreed usually to within about 10%. Further experiments at the same wave-lengths showed, moreover, that the emissivity changed with temperature in the manner demanded by the relation. It follows that the emissivity of a metal at sufficiently long wave-lengths is roughly proportional to the square-root of its absolute temperature.

It is frequently stated that in the visible region of the spectrum the temperature coefficient of the reflecting power of metals is zero. The evidence which has led to this belief is, however, not at all conclusive; of the experiments supporting the statement, many were performed at an early date and a number

---

[*] 'Ber. deuts. chem Ges.,' p 410 (1903).

[†] 'Ber. deuts. chem Ges.,' p 478 (1909).

[‡] Since the notation is by no means standardized, it is necessary to explain the sense in which the terms *emissivity* and *emissive power* will be used in the following pages.

If $e_\lambda\,\delta\lambda$ is the radiant energy between wave-lengths λ and $\lambda + \delta\lambda$ which is given out per second by unit surface of a body, then e_λ is defined to be the *emissive power* of the body for the wave-length λ and the temperature at which it is radiating.

The *emissivity* or *relative emissivity* of the body is the ratio of its emissive power to the emissive power of a perfectly black body for the same wave-length and temperature. This quantity is frequently called the *absorptive power* or the *absorptivity* of the body; and for bodies, such as metals, which, in sufficiently thick layers, transmit none of the radiation, is equal to $(1 - R)$, where R is the *reflecting power*.

of the later ones have since been controverted. Nevertheless, it can be stated without doubt that the variation of metallic emissivity with temperature is considerably less in the visible than it is in the region of validity of the Hagen-Rubens relation

The near infra-red, then, is a particularly interesting region in which to carry out emission experiments, since, somewhere between the visible and 8μ, there must be a transition, which may be more or less gradual, between the "optical" emission coefficients of the visible region and the "electrical" emission coefficients of the far infra-red

Unfortunately, a direct attempt to measure the relative emissivities of metals in the near infra-red is difficult The method of rest-strahlen cannot be employed and spectral resolution must be carried out by means of a spectrometer, with the result that the energy received can be measured only when the metals are heated to a very high temperature or when receiving instruments of high sensitivity are employed. Accordingly, the distribution of energy in the heat emission spectra of the metals has been directly investigated for only a few of the more easily treated Some metals, like copper, which have a low melting point, or suffer a surface deterioration when heated to a high temperature, have hitherto been left severely alone

The experimental difficulties arising from the fact that the emitted energy in general is so minute in quantity can be avoided by the use of a reflection method, in which it is the reflecting power of the metal, rather than its emissivity, which is directly determined. This type of experiment is not very accurate, however A simple example will make this clear The emissivity of copper at a wave-length of 3μ and a temperature of 850° C. is about 4·5%, an error of 1% in the *measured* reflecting power would therefore appear as an error of the order of 20% in the emissivity *calculated* from the reflecting power. Since the emissivity can be measured *directly* by an emission experiment with an error of only a few per cent., this method is to be preferred to a reflection method, whether "direct" or "polarimetric"

Owing to the fact that the study of metallic emission in the near infra-red has lagged behind the corresponding investigations beyond 10μ and in the visible, it has hitherto proved impossible to test the validity of Kronig's* quantum theory of dispersion in metallic conductors, the perfection of which should shed further light on the phenomena concerning interaction between matter and radiation

---

* 'Proc. Roy. Soc.,' A, vol 124, p. 409 (1929); vol. 133, p. 255 (1931).

The experiments described here have been undertaken to remedy to some extent the deficiencies in experimental data. The emissivity of copper has been determined directly over a wave-length range extending from 1·5μ to 5μ for two temperatures, viz., 700° and 850° C., that of nickel between the limits 1μ and 6·5μ for the temperatures, 850° C and 1000° C The probable error in the emissivity in each case is only a few per cent.

Experimental.

General Description, and Advantages of the Method.

The method employed possesses the great advantage that the emissivity of the metal under investigation is measured directly the energy of a given wave-length emitted by a certain area of the metal, radiating at a given temperature, is compared with the energy of the same wave-length emitted by an equal area of a black-body slit cut in the metal itself and radiating, therefore, at the *same* temperature. Such a comparison method does away with the need of measuring the temperature of the hot metal to a high degree of precision and removes the necessity of applying those numerous corrections which are essential in order to reduce the observed energy curves to "normal" curves when the black-body radiation is calculated rather than measured; absorption by the water-vapour and carbon dioxide of the air, and reflection losses at the surfaces of mirrors need not be taken into account; for although affecting the measured values of the metallic and black-body radiations at a given wave-length, they cannot influence the *ratio* between these two energies, *i.e.*, the emissivity of the metal.

Hagen and Rubens* and McCauley† have previously applied an emission method to a few metals in the region between the visible and 6μ. For each metal, the black body curves were computed, and it was essential that the temperature of emission should be measured with a high degree of precision. One feels that much more reliance could have been placed in their results had direct measurements been made on the black body emission under the proper conditions of temperature and geometry. In addition, the particular method adopted by Hagen and Rubens suffers from the disadvantage that emissivities cannot be measured in absolute units; only the change of emissivity with temperature can be found at each wave-length investigated. They measured temperatures above 800° C. by an optical pyrometer, the observed black-body temperatures being corrected to surface temperatures by using Holborn and Henning's* results for the visible emissivities—results which have been adversely criticized by Worthing.† At lower temperatures, deflections of only a few millimetres were obtained, and it is hard to see how the accuracy of a few per cent. claimed by the authors for all their results can be justified. McCauley admits that, as his black-body curves were computed from a knowledge of the emissivities of the metals at a part of the spectrum where bolometric measurements are uncertain to as much as 10%, his values of the reflecting power are apt to be in error. His results have also been criticized by Coblentz,‡ who likewise objects to the indirect method of obtaining the data.

---

* 'Ber. deuts chem Ges.,' p. 467 (1910).

† 'Astrophs. J.,' vol 37, p 164 (1913).

It is obvious that the direct method of the present research possesses many advantages over these former methods. An account of the individual features of the apparatus will be presented in succeeding sections. Here a brief outline of the method will be given.

Fig. 1 shows the general arrangement of the apparatus. The metal radiator, in which was cut a V-shaped slot, was heated *in vacuo* to the desired

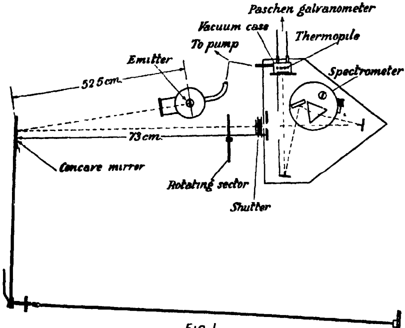

FIG. 1.

---

* 'Ber. deuts. chem. Ges.,' p. 311 (1905).

† 'Phys. Rev.,' vol. 10, p. 377 (1917).

‡ 'Bull. Bur. of Stand.,' vol. 14, p. 115 (1918).

temperature. By rotating an auxiliary mirror, the image of the slot and the image of a closely adjacent portion of the metal surface could be focussed in turn on an infra-red spectrometer The energy emerging from the exit slit was measured by means of a thermopile and galvanometer The ratio between the two was the emissivity of the metal at the wave-length indicated by the spectrometer drum

The Emitter

A composite type of emitting element was designed which would provide, in addition to the metallic radiation under investigation, black-body radiation of the same temperature. It consisted of three parts—an inner heating element; a surrounding thin walled silica tube for insulation purposes, and an outer metal cylinder.

The heating element consisted of a coil of 200μ tungsten wire wound in a spiral thread of small pitch, which was ground in a silica rod, 6 cm long and 5·5 mm. diameter

Outer metal radiators of various patterns have been used. Fig 2 illustrates the most successful design, which is a development of the Mendenhall wedge

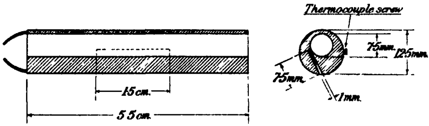

Fig 2

From a solid rod of the metal under investigation, 5·5 cm. long and 1·25 cm in diameter, a cylindrical portion, 0·75 cm in diameter, was drilled out (to take the heating coil and its surrounding insulator) with its axis parallel to, and 1·5 mm from, the axis of the rod. A saw-cut was made in the metal along its whole length, 1 mm. wide and 7·5 mm. deep, the plane of cut being inclined at as small an angle as circumstances would allow to the plane containing the generator of cut and the axis of the rod. A rectangular parallelipiped of the metal, of the same dimensions as the saw-cut, was made to fit tightly into it. The central portion (1·5 cm. in length) of this strip was filed into the shape of a wedge, *i.e.*, a triangular prism, 1·5 cm. long, 7·5 mm × 1 mm. base, so that, when the strip was hammered into the saw-cut in the emitter and riveted into position, a cavity with the shape of a Mendenhall wedge, 1·5 cm long, 1 mm. broad at the orifice and 7·5 mm. deep, was formed. The angle of the wedge was therefore 7° 36′. A rough file was used on the sides of the V-cavity in order to reduce the reflection coefficient of the walls by the formation of scratches parallel to the length of the cavity, each of which would blacken the radiation by internal reflection.

Calculations, which were borne out by experiment, showed that the temperature gradients in the emitter were quite negligible.

A ray is reversed in a wedge of angular opening 7° 36′ after about 24 reflections. If, in the near infra-red, a reflecting power of 0·8 is assumed for the rough-filed walls of the cavity, the effective absorbing power of the wedge becomes $1-(0\cdot 8)^{25}=0\cdot 996$ — that is, the radiation from the V-cavity is 99·6% black.

"Commercially pure" copper was employed. Previous researchers, *e.g.*, Tool,* have found the use of chemically pure copper impossible for work of the present nature owing to the fact that it is too full of flaws to allow of the preparation of a satisfactory reflecting or emitting surface. For the investigation on nickel, a rod of their pure nickel (nickel content, 99·5%) was obtained from Messrs. Johnson, Matthey and Company.

The temperature of the radiating metal was measured thermo-electrically, a platinum, platinum-10% rhodium element being employed. The e.m.f. generated was balanced by a potentiometer system which allowed temperatures to be estimated to the nearest degree, and since the method is one of comparison, the temperature only being measured to determine the *change* of emissivity with temperature, this accuracy is sufficient. The radiating metal itself was used as the hot junction. The thermocouple wires were attached by means of 10 B.A. binding screws tapped into the radiator, very fine saw-cuts were made in the heads of the screws, the wires inserted therein and the screw-heads compressed tightly over them.

The emitter was enclosed in a vessel of the shape shown in fig. 3. It was suspended with its V-cavity opposite a fluorite window. Four lead-in tubes—two for the heating current and two for the thermocouple—were sealed in to the top portion of the vessel, which was joined to the pumping system with its window at the same height from the bench as the spectrometer slit. To prevent radiation being reflected back on to the emitter, the interior surface of the lower portion of the vessel was coated with a layer of an absorbing

---

* 'Phys. Rev.,' vol. 31, p. 1 (1910).

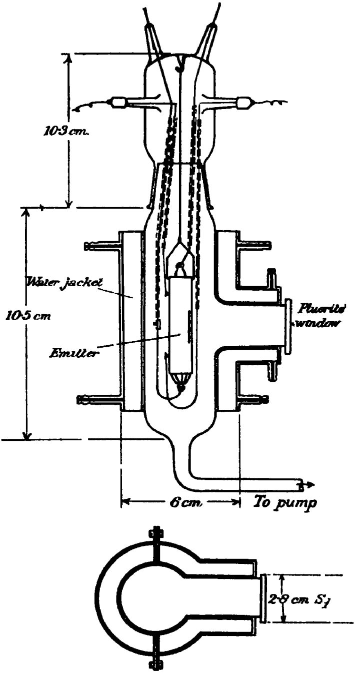
10·3 cm.
Water jacket
10·5 cm
Fluorite window
Emitter
6 cm
To pump
2·8 cm S_1

Fig. 3.

material. During the course of the work on copper, a dull black paint, drying with a matt surface, was used. This paint, supplied by British Drug Houses, Ltd., is chiefly composed of an extract of lampblack in turpentine. After the application of the paint, the turpentine was driven off by gentle heating in a current of air The carbon content of the paint rendered it unsuitable for use while nickel was under investigation. It was replaced by platinum black, which was deposited on thin copper foil fixed to the walls of the container

The window was of good quality and possessed a very high polish. Owing to the fact that, hitherto, but little work involving vacuum technique has been done in the infra-red beyond 3μ, little attention has been paid to the problem of producing easily a vacuum-tight joint between glass and fluorite or rock-salt. While carrying out tests on various cements which seemed suitable, "Durofix," a celluloid cement made by the Rawlplug Company, Ltd., was tried. This proved to be admirable, and can be thoroughly recommended for this purpose The two surfaces to be joined should be previously ground plane and the apparatus should not be exhausted until a few hours have elapsed after the application of the cement

When the emitter was in use, a fast 3-stage mercury-vapour pump, backed by an oil pump, was kept in operation and a mercury-vapour trap between the pump and the vessel housing the emitter was surrounded by liquid air. Under these conditions, the pressure in the apparatus was about 10^{-4} mm.

The emitter was heated from A C mains, rheostats in series being used to keep the current at the required value of an ampere or so.

The Thermopile

The thermopile consisted of 8 copper-constantan elements in series. The constantan wire was of 47 gauge, the copper of 50 gauge. The junctions, about 1 mm. square, were of silver foil 8μ thick. The instrument was balanced and was very insensitive to extraneous temperature fluctuations.

By using an extremely small quantity of solder, the heat-capacity of the junctions was kept low, and the period of the thermopile was only about 6 seconds. Its resistance was 11·7 ohms and was therefore very close to the resistance of the galvanometer (12 ohms) in conjunction with which it has been used. The other requirements of the theoretical investigation of Johansen* on "rationally constructed" thermopiles were also met as far as possible.

---

* 'Ann. Physik,' vol. 33, p. 517 (1910).

To avoid fluctuations, it is necessary to work with a thermopile either *in vacuo* or in an airtight casing. Since a pump had already been installed as a necessary part of the apparatus little complication was introduced by adopting the former alternative, in addition, a slight increase in sensitivity was obtained (about 30%) and all corrosive action of the atmosphere on the fine thermopile wires was eliminated

A special brass casing, provided with slides to take the adjustable spectrometer slits, was made for the thermopile. It was fitted with a rock-salt window on its front face, while the thermopile leads were taken through the back in thin glass tubes. The case was made vacuum-tight and mounted in place of the ocular fitting provided with the spectrometer. Round it was placed a wooden box, provided with a lid, which was packed with cotton wool as a heat insulator. When placed *in vacuo* behind a slit, 10 × 1 mm, at a metre from a candle, the thermopile developed an e m.f. of 4 microvolts

The Galvanometer.

A Paschen galvanometer was used in conjunction with the thermopile A modern suspension, consisting of two groups of 3 cobalt steel magnets, was supplied and fitted by courtesy of the Cambridge Instrument Company. With a sensitivity of 10^{-10} amps. per mm., scale distant 1 metre, the period was 6 seconds.

The galvanometer was supported on a wooden baseboard which was mounted on Sorbo sponges at its four corners. These, in turn, rested on a stone pier whose foundations were in the basement of the laboratory Not the slightest trouble was experienced from vibration; only when exceptionally heavy traffic passed on the road outside the laboratory was a slight tremor visible in the spot of light reflected from the galvanometer mirror.

The galvanometer was surrounded by a heavy soft-iron shield Nevertheless, the high sensitivity employed rendered it necessary to take all readings between the hours of 11 p.m. and 6 a.m. owing to magnetic disturbances—due chiefly to traffic outside the laboratory. A sensitivity of $4\ 10^{-11}$ amps per mm. was essential for the lower temperatures at the extremes of the wave-length scales investigated. Owing to the fact that the galvanometer was then on the point of becoming unstable, serious zero-creep frequently set in and several hours' work were sometimes necessary in order to obtain a single set of satisfactory readings. Where possible, therefore, a sensitivity of not more than 10^{-10} amps. per mm. was used in order to expedite the work.

The linearity of the galvanometer scale was tested for each new setting of the control magnets by means of a potentiometer system. With few exceptions, it was found that, so long as the deflection did not exceed about 15 cm., it was accurately proportional to the current passing through the galvanometer.

Optical System, Sectors, etc

The infra-red spectrometer was a Hilger No 1 instrument with a 60° rock-salt prism and a Wadsworth mirror, which, with the prism, formed a constant deviation system The slit width used was ½ mm The makers' calibration was confirmed by means of the sodium D lines and by plotting the emission spectrum of the bunsen burner in the neighbourhood of 4·4 μ. The instrument was enclosed in a wooden housing in order to keep off draughts and to enable a dry atmosphere to be maintained round it. As a precaution against stray radiation, the interior of the case was painted black

A front-silvered concave mirror, of good optical quality, 12 inches in focal length and 4 inches in diameter, was employed to form an image of the radiating metal on the collimating slit of the spectrometer A remote control was fitted to the mirror so that the small rotation about its vertical axis, necessary to concentrate the slit radiation and the metal radiation in turn on the spectrometer, could be brought about by the rotation of a knob situated near the galvanometer scale The geometry of the control mechanism was such that one complete revolution of the control knob gave the image a lateral displacement of one millimetre The distances between infra-red source and mirror and between spectrometer slit and mirror were respectively 52·5 cm. and 73·0 cm so that the linear magnification of the image was about 1·5 and the solid angle of the cone of radiation entering the slit of the spectrometer was the same as the solid angular aperture of the instrument itself. The inclination of the beam of radiation to the axis of the subsidiary mirror was less than 4°, with the result that astigmatic errors were not present in the image, which was of excellent quality.

In order to avoid frequent changes in the galvanometer sensitivity, rotating sectored discs were used to reduce the intensity of the black-body radiation to a value comparable with that of the radiation from the metal. The sector was mounted on an arm, which could swing about a fulcrum situated in a line with the driving axis of the motor, and which could be clamped in position with the sector either in, or out of, the path of the heat radiation. The sector was driven by an elastic belt from a small A.C. motor, screened from the galvanometer by a soft-iron casing. When the motor was switched on or off, a deflection of a few centimetres was registered by the Paschen galvanometer, but while the motor was actually running no disturbing effect could be detected The coefficients of transmission of the sectors which were used were 5·94 and 18·30%

Immediately in front of the spectrometer slit was a pneumatically-operated shutter, consisting of four plates of brass, mounted parallel to each other on two short ebonite rods so that each plate was heat-insulated from its neighbours

The Preparation of the Radiating Surfaces

The emitter to be polished was mounted on a mandril and ground on emery papers of increasing fineness, the last used being a French 0000 paper.

In the past, it has been usual to complete the preparation of a metal surface by the process of " buffing " with a steel polishing rod or by the usual optical method of polishing with rouge. However, there seems little point in subjecting a surface which is to be subsequently annealed to a heavy polishing process. Indeed, the recent work of Lowery and Moore* shows that there is a definite decrease in the reflecting power of copper with increasing heaviness of polish, and even when the metal is not to be subjected to a later heat treatment, these investigators do not recommend burnishing The possibilities of polishing copper with rouge were, therefore, explored. A beautiful polish was obtained with ease, but, when the metal was first heated, numerous bright red specks were visible on the comparatively dark background of the greenish-hued copper and the surface showed traces of filming. It appeared impossible, therefore, to polish with rouge without at the same time working impurities into the surface of the metal.

A prolonged rubbing with soft chamois leather while the emitter was rapidly rotated in the lathe was found to effect a considerable improvement in the state of the emeried surface, especially if the metal had been heated previously to a high temperature *in vacuo* and if considerable pressure was brought to bear upon it Although such treatment left a few fine scratches on the surface, it was adopted for both the metals investigated; it is agreed that a surface film can cause a large change in the emissivity of a metal, whereas it is hard to see how a few scratches, which occupy a very small proportion of the area viewed and which are not sufficiently deep to blacken the radiation by internal reflection, can exert any appreciable effect. This view is supported by the fact that the scratches in the specimens used were invisible when they were incandescent.

---

* 'Phil. Mag.,' vol 13, p 938 (1932).

After polishing, the metal was well washed in alcohol to remove grease and moisture. It was mounted *in vacuo*, brought to a dull red heat, and any traces of an oxide film which might have formed during the polishing process were removed by the admission of about 1 mm of hydrogen into the apparatus Thereafter, the metal was kept *in vacuo* and cleaned up in hydrogen at intervals.

Besides possessing other advantages, an emission method is far less exacting as regards the perfection of the surface required than is a reflection method. This was apparent during the course of the work on copper, the surface of which, when heated to 900° C., frequently developed crystal facets, each of which retained its polish The effect on the emissive power was, however, very small—from 5 to 10%—in accordance with the fact that the recrystallization could not be observed when the copper was self-luminous, but was apparent when the surface was viewed by reflected light Whereas such crystal facets would certainly exercise a large effect on the *specular* reflecting power of the surface, the only error appearing in the direct emissivity determination would result from the departure from Lambert's cosine law

There still remains to be considered the possibility of the formation of a surface film (other than an oxide film) after polishing As was to be expected, the slight traces of hydrocarbons and other vapours of carbon, arising from the black paint and from tap-grease, caused no difficulty when working with copper. After a series of emissivity measurements extending over a period of many weeks, the metal was as bright as when it was first set up—confirmed by the fact that no progressive increase in the values of the emissivity was observed.

The reverse was found when experimenting on nickel A slow progressive change was noticeable in its surface condition when this metal was maintained incandescent at temperatures below about 700° C., even though every effort had been made to exclude all traces of carbonaceous vapour and the pump had been kept in operation for several days prior to the heating Presumably the change was due to the formation of nickel carbonyl. As a result, measurements were made only at higher temperatures and the metal was heated and cooled quickly (the latter by the admission of hydrogen) between series of readings. In this way reproducible results have been obtained and filming and loss of polish was avoided.

The Cosine Law of Emission.

According to Lambert's cosine law, the apparent brightness of the different elements on a self-luminous surface is the same, no matter what angle the normal to the element makes with the straight line joining the element to the eye, but theory shows that the law can be rigorously true only for the black body For metals, when the refraction of the emerging radiation is taken into account, its intensity is reduced in accordance with Fresnel's formulæ and a more complicated distribution is obtained for the surface brightness

Because, hitherto, no observations seem to have been made on the deviations from the cosine law for infra-red radiation, some rough, preliminary measurements were carried out for copper and nickel, radiating at 850° C, for a wave-length of $3 \cdot 5\ \mu$. As in the visible, the deviations found were in the sense of the computed deviations which are obtained when surface refraction is taken into account, but were greater, and of a different order of magnitude Beginning with normal emission, the brightness increased until it reached a maximum (about $1 \cdot 4$ times the normal) at about 80° and then decreased rapidly again. This deviation from the cosine law is considerably greater than the discrepancies which have been observed in the visible region of the spectrum

The emissive power in the present work has been so limited as to refer only to that radiation which leaves the surface normally or nearly so. So long as the angle of emission was not greater than 20°, it was found that the error arising owing to a departure from the cosine law was not more than 1%; while an angle of emission as large as 30° led to an error of only about 3% The emitters employed were so designed and oriented that the angles of emission for the metallic radiation arising from the portions of the surface closely adjacent to the black-body slit were less than 10°.

The Measurement of the Emissivities of Copper and Nickel.

Experimental Procedure.—After a period of pumping of about half an hour the heating current was switched on and the emitter brought to the required temperature. The image of the slit in the radiator was focussed on to the spectrometer slit and the rotating sector was swung into position in the path of the radiation. Operating the shutter by its pneumatic release, ten or six galvanometer deflections (according to the high or low sensitivity employed) were taken. Next, the mirror control was rotated through a pre-determined number of revolutions until the image of that portion of the metal from which the radiation was to be received was focussed on the slit As stated previously, it was so arranged that normal, or nearly normal, radiation was received from that part of the surface which was distant not more than a few millimetres from the black-body slit, and tests were made prior to a series of observations to verify that this condition was satisfied The sector was then removed from the path of the beam The energy received by the thermopile was measured as before

It was often very difficult when working at the extremes of the wave-length scale to obtain deflections of a few centimetres, with the energies available, and at the same time a satisfactory zero stability; frequently, indeed, it was impossible to complete a set of readings when the galvanometer was pushed almost to its point of instability owing to a serious zero-creep setting in after the set had been commenced. On many nights it was not possible to take readings at the highest sensitivities.

Results

Copper —The results of the emissivity measurements on copper at the two temperatures, 700° and 850° C , are summarized in Table I —

Table I.—Emissivities, in per cent

Wave-length, in μ	1 5	1 75	2 0	2 5	3 0	3 5	4 0	4 5	5 0
Temperature, 700° C	6 1	5 6	5 05	4 5	4 2	3 9	3 8	3 6	3 55
Temperature, 850° C	5 8	5 3	5 0	4 65	4 5	4 3	3 9	4 0	4 0

For 700° C , each value given is the mean of 10 independent determinations , these showed no tendency to increase progressively with time and were in remarkably good agreement with one another , not one of them deviated by more than 5% from the means displayed in the table.

After the work at 700° C had been completed, a prolonged attempt was made to measure the emissivities of copper at about 1000° C , in order to obtain conclusive data about the transition from " electrical " to " optical " emission constants. It became apparent, however, that this course was impossible owing to crystallization of the surface, which took place whether the metal was heated *in vacuo* or in a hydrogen atmosphere Although the effect on the emissivity was small, about 5 or 10%, the fact that a temperature increase from 700° to 1000° C. would be expected to cause a variation of the same order of magnitude rendered it imperative to avoid the formation of crystal facets. The deposition of a film of copper on the fluorite window owing to evaporation from the surface of the copper when it was operated at 1000° C. was also a difficulty

The second series of results was taken therefore at 850° C Even so, the surface crystallized frequently and in consequence, fewer measurements were made at each wave-length than at 700° The first five results in the last line of Table I are the means of three or four determinations, while only a single determination was made at each of the four remaining wave-lengths In the course of obtaining them, it was necessary to repolish the emitter twice. Fortunately, the greater energy available at 850° C reduces the probable experimental error so that the few observations made at this temperature are more reliable than they would be for a lower temperature.

Fig 4 shows the emissivity at 700° plotted against the wave-length

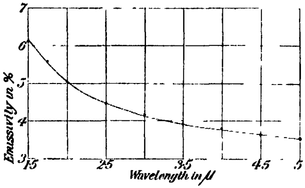

FIG. 4

Nickel.—For reasons already stated, it has been possible to obtain accurate values of the emissivity of nickel only at comparatively high temperatures. The final results at 850° and 1000° C. are shown in Table II. Each value of the emissivity is the mean of four or five consistent determinations There was no sign of a progressive increase with time, although many hours separated successive individual determinations at any given wave-length.

Table II.—Emissivities, in per cent.

Wave-length, in μ	1·0	1·25	1·5	1·75	2·0	2·5	3·0	3·5	4·0	4·5	5·0	6·5
Temperature, 850° C	—	23·4	21·1	19·5	18·2	16·2	14·5	13·0	11·8	10·8	10·2	9·0
Temperature, 1000° C	26·0	23·1	21·0	19·6	18·5	16·6	14·9	13·5	12·3	11·4	10·7	9·7

The emissivity at 1000° C. is plotted against wave-length in fig. 5.

Theoretical.—Drude[*] was the first to discover theoretical relations between the optical constants of a metal and its electrical conductivity. If n is the index of refraction of the metal, k its extinction coefficient, this classical theory leads to the results

$$\left.\begin{aligned} n^2 &= \tfrac{1}{2}\left(\sqrt{\epsilon^2+\frac{4\sigma^2}{\nu^2}}+\epsilon\right) \\ k^2 &= \tfrac{1}{2}\left(\sqrt{\epsilon^2+\frac{4\sigma^2}{\nu^2}}-\epsilon\right) \end{aligned}\right\}, \qquad (1)$$

where ϵ is the dielectric constant and σ the electrical conductivity of the metal transmitting electro-magnetic waves of frequency ν.

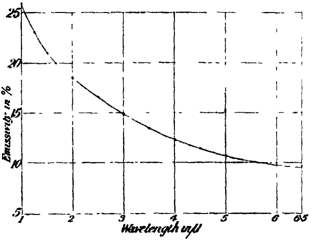

FIG. 5

By the electromagnetic theory, the reflecting power of a metal from vacuo is, for perpendicular incidence,

$$R = \frac{(n-1)^2+k^2}{(n+1)^2+k^2}.$$

Substituting for n and k from the above equations, we obtain

$$R = \frac{\sqrt{\epsilon^2+\frac{4\sigma^2}{\nu^2}}+1-\sqrt{2\left(\sqrt{\epsilon^2+\frac{4\sigma^2}{\nu^2}}+\epsilon\right)}}{\sqrt{\epsilon^2+\frac{4\sigma^2}{\nu^2}}+1+\sqrt{2\left(\sqrt{\epsilon^2+\frac{4\sigma^2}{\nu^2}}+\epsilon\right)}}.$$

---

[*] "Physik des Aethers," 1st Edn., p. 574 (1894).

For good conductors, for long wave-lengths,

$$\varepsilon \ll 4\sigma^2/\nu^2$$

Therefore,

$$n = k = \sqrt{\frac{\sigma}{\nu}},$$

and R may be expanded in the form

$$\mathrm{R} = 1 - 2\sqrt{\frac{\nu}{\sigma}} + 2\frac{\nu}{\sigma} - \quad ,$$

which becomes

$$1 - \mathrm{R} = 0\cdot365\sqrt{\frac{\rho}{\lambda}} - 0\cdot067\frac{\rho}{\lambda} +$$

if σ is replaced by the specific resistance, ρ, in $\left(\frac{\text{ohm, mm}^2}{\text{metre}}\right)$, and ν is replaced by the wave-length, λ, expressed in μ. The first two terms alone are of importance for $\rho/\lambda <$ about 1/3.

From about 12μ on there is a close agreement between the above theoretical result and experiment At shorter wave-lengths, however, differences between observed and calculated results become apparent, and the theory breaks down entirely for visible light. Its failure is due to the fact that it presupposes that the dielectric constant and the electrical conductivity are indepdenent of the frequency.

Krönig, *loc cit*, has attempted to remove this restriction by adopting the Bloch theory of metallic conduction as a basis for an ingenious quantum theory of dispersion. He has shown that, for sufficiently high frequencies, when the collisions of the electrons with the metallic lattice may be neglected, the behaviour of the electrons in an elementary lattice cube may be represented mathematically by assigning to them a sharp resonance line of frequency zero and practically continuous absorption bands From about $1\cdot5\mu$ onwards into the infra-red, the metal may be treated as though it had only the pseudo-resonance frequency at $\nu = 0$, and the effect of the collisions of the electrons with the lattice may be introduced by discussing the broadening which this line undergoes thereby. Calling δ the half-breadth of the representative line, $\nu = 0$, the expressions,

$$\sigma = \frac{\sigma_0}{u^2 + 1}, \qquad \varepsilon = 1 - \frac{2\sigma_0 u}{\nu(u^2 + 1)},$$

where σ_0 is the electrical conductivity for constant fields and $u = \nu/\delta$, are obtained for the electrical conductivity and for the dielectric constant at frequency ν. Krönig introduces these expressions for σ and ϵ into the usual equations for n and k (1, above) and, after further simplification, obtains

$$n^2 = \frac{\sigma_0}{\nu}\left(\frac{1}{\sqrt{u^2+1}} - \frac{u}{u^2+1}\right), \qquad k^2 = \frac{\sigma_0}{\nu}\left(\frac{1}{\sqrt{u^2+1}} + \frac{u}{u^2+1}\right), \tag{2}$$

and thence

$$\mathrm{R} = 1 - 2\sqrt{\frac{\nu}{\sigma_0}}\sqrt{\sqrt{u^2+1} - u},$$

which, for small values of u, *i.e.*, in the far infra-red, goes over into the classical expression of Drude.

It is shown by Krönig that the product $\sigma_0\,\delta$ depends solely upon the periodic field of potential of the Bloch conduction theory, and is therefore independent of the temperature. Hence, to a first approximation, the breadth of the resonance line is directly proportional to the absolute temperature. Owing to lack of data on the temperature dependence of the reflecting power in the near infra-red, the inferences to be drawn from this last conclusion were not discussed by Krönig. The results of the present research are of importance in this connection, and show that drastic modifications are necessary in the theory, as will be pointed out in the next section.

Krönig calculates σ_0 and δ for room temperature for copper, silver, gold, platinum and iridium from equations (2) and the measurements of Forsterling and Frédericksz* on n and k for these metals. The values of σ_0 and δ (which, for any one metal, should be independent of wave-length) are of the same order of magnitude at the various wave-lengths, although the former shows a tendency to increase progressively with the wave-length and the latter appears to decrease with wave-length. The values calculated for σ_0 and averaged over wave-length are less than the values of the conductivities determined by direct measurement, the ratios between the two for the various metals investigated varying between the extremes of 2 and 100. This result, Krönig suggests, may be due to the fact that the optical constants depend upon the properties of a thin surface layer of the metal, in which layer it is possible that the conductivity is diminished on account of the distortion of the lattice. The disagreement between calculated and measured values of σ_0 is, however, a defect in the theory; for, since the Krönig equations must merge into the classical equations for sufficiently long wave-lengths, the limiting value attained by the calculated values of σ_0 must be identical with the conductivity of the material in bulk, this latter being the conductivity which is always inserted into the Drude equations. Hence σ_0 must continue to increase with wave-length even in the region remote from the influence of the optical absorption bands

---

* 'Ann. Physik,' vol 40, p. 201 (1913).

It is unfortunate that, in order to test the theory at room temperature, it is necessary to refer to polarimetric measurements which, in the infra-red, are not accurate owing to the facts that the angles of polarization observed change but little with wave-length and that use is made of formulæ of the type

$$\sqrt{n^2 + k^2} = \tan\phi, \qquad \frac{2kn}{n^2 - k^2} = \tan 4\psi,$$

which, for large values of Φ, may lead to large errors in n and k. Although the reverse is stated by Krönig, reflecting powers calculated from the values of n and k due to Försterling and Fréedericksz are not in good agreement with reflecting powers directly measured by Hagen and Rubens

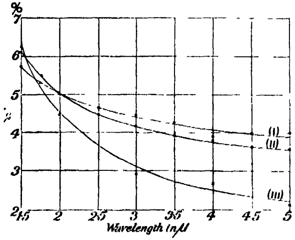

Fig 6.—Illustrating the transition from the electrical coefficient of the infra-red to the optical coefficient of the visible. (i) Emissivity 850° C.; (ii) emissivity 700° C.; (iii) room temperature absorptivity (Hagen and Rubens).

Discussion of Results.

Copper.—Fig. 6 incorporates the experimental curves of the present research and also the reflection measurements of Hagen and Rubens* on copper at room temperature. It will be observed that, whereas at a wave-length of 5μ the high temperature emissivities are almost twice as great as the absorptivity at room temperature, there is little difference between the emissivities and the absorptivity for wave-lengths less than about 2μ. Thus is demonstrated the gradual transition from the "electrical" emission constant of the far infra-red to the "optical" constant of the visible region.

---

* 'Ann. Physik,' vol 11, p. 873 (1903).

For the time being, attention will be concentrated on the emissivities at 700° C in order to show that the quantum theory of Kronig fits the facts less well than does the classical theory of Drude The theoretical values of the emissivities at 700° C will be calculated —

(*a*) on the assumption that the Drude theory is valid throughout the wave-length range investigated,

(*b*) on the assumption that the Kronig theory is valid.

(*a*) According to measurements of Northrup,* the specific resistance of copper at 700° C, measured in $\left(\frac{\text{ohm, mm}^2}{\text{metre}}\right)$, is $6 \cdot 9 \times 10^{-2}$ Thence, according to the Hagen-Rubens relation, the emissivity of pure copper at 700° C. should be 4·2% at a wave-length of 5μ The measured value is nearly 20% lower than this calculated value Any impurities present in the actual specimens of copper used in the research would tend to increase this discrepancy.

The divergence between calculated and observed figures is not surprising in view of the fact that the theoretical formula is derived for radiation of greater wave-length than those actually used. Even at longer wave-lengths, precisely similar results have been observed by Hagen and Rubens (*loc. cit*, 1909, 1910).

Table III contains the experimental values of the emissivity at 700°, and the values calculated on the assumption that the Hagen-Rubens relation is valid

Table III —Temperature, 700° C

Wave-length, in μ	5	4	3	2	1·5
Observed Emissivity, in %	3·55	3·8	4·2	5·05	6·1
Emissivity calculated from H.-R relation	4·2	4·7	5·4	6·6	7·5

(*b*) The equation for the emissivity derived by Kronig, *loc cit.*, is

$$e = 2\sqrt{\frac{\nu}{\sigma_0}}\sqrt{\sqrt{u^2+1}-u}, \tag{3}$$

where σ_0 is the electrical conductivity (in e.s.u) of the surface layers of the metal, and $u = \nu/\delta$, where δ is the half-breadth of the resonance line, $\nu = 0$, in the equivalent spectrum of the electrons. It is reasonable to suppose, as Kronig suggests, that σ_0, and hence κ, changes with temperature in the same way as does the conductivity of the bulk of the material. According to Northrup, *loc. cit.*, the specific resistance of copper at 700° C. is 3·9 times its specific resistance at room temperature. It follows that, for any given wave-length, the values of σ_0 and of κ at 700° C. should be 1/3·9 times the values of these quantities tabulated by Kronig. Table IV contains, for the wave-lengths 4, 3, 2 and 1·5μ, the values of σ_0 and of κ for sputtered copper at room temperature assumed by Krönig, the values of these quantities calculated for 700° C. and the values of the emissivity calculated from the formula (3).

---

* 'J. Franklin Inst,' vol. 177, p. 1 (1914).

Table IV.

Wave-length in μ.	Krönig's room temperature values		Calculated values for 700° C.		$(\sqrt{\kappa^2+1}-\kappa)_{700}$	Calculated emissivity for 700° C. in %
	$\sigma_0\times10^{-17}$	κ	$(\sigma_0)_{700}\times10^{-17}$	κ_{700}		
4	1·12	6·20	0·29	1·59	0·29	5·5
3	0·86	8·33	0·22	2·14	0·22	6·3
2	0·62	7·21	0·16	1·85	0·25	9·7
1·5	0·48	7·60	0·12	1·95	0·24	12·6

Since the values of σ_0 and δ derived by Kronig should be, but, in fact, are not, independent of wave-length, it may be fairer to adopt as basis of calculation Krönig's *mean* values of σ_0 and δ (averaged over wave-length) rather than the *different* values of σ_0 and δ derived for each particular wave-length. The mean values at room temperature of σ_0 and δ for sputtered copper given by Kronig are respectively 0·82 × 10^{17} and 0·165 × 10^{14}. Thus, the values of these quantities at 700° should be $(\sigma_0)_{700} = 0{\cdot}21 \times 10^{17}$ and $\delta_{700} = 0{\cdot}644 \times 10^{14}$. The emissivities at 700° C. derived from (3) now become 7·1% at 5μ; 7·3% at 4μ; 7·4% at 3μ; 7·7% at 2μ, and 7·8% at 1·5μ.

In Table V are collected the experimental results of the research on copper at 700° C. and also the values calculated for the emissivities from the Hagen-Rubens relation and from the Krönig dispersion formula—(1) according to the "method of variable σ_0 and δ" and (2) according to the "method of average σ_0 and δ."

Throughout the whole wave-length range the values derived from Kronig's formula agree less well with experiment than do the values derived from the classical theory. The figures appearing for the longer wave-lengths in the last column are impossibly high, while the value in the preceding column for $1\cdot5\mu$ is so great that, were it correct, in order to obtain agreement with the measured emissivity of copper for red light, it would be necessary to assume (in opposition to all current ideas) that the emissivity decreases as the frequency increases between $1\cdot5\mu$ and the visible

Table V

Wave-length in μ	Emissivities in %			
	Observed	Calculated from H.-R. relation	Calculated from Krönig's formula	
			Method (1)	Method (2).
5	3·55	4·2	—	7·1
4	3·8	4·7	5·5	7·3
3	4·2	5·4	6·3	7·4
2	5·05	6·6	9·7	7·7
1·5	6·1	7·5	12·6	7·8

It might be argued that the results calculated above from the modern theory depend upon the accuracy of the dispersion measurements of Forsterling and Fréedericksz and that, were different values assumed for σ_0 and δ, the calculations might be brought into better agreement with the facts. It is not difficult to prove, however, on general grounds, that this is not so, even though the derived emissivities are very sensitive to slight changes in the values of σ_0 and δ

The proof assumes only that the surface conductivity is inversely proportional to the absolute temperature From the equation

$$\sigma_0\,\delta = \text{constant, independent of temperature,} \tag{4}$$

derived by Kronig, it then follows that δ is directly proportional to T. Let σ_1 be the surface conductivity at absolute temperature T_1 and u_1 be the value of ν/δ for this temperature and for a frequency ν. By hypothesis, the values of surface conductivity and of u for a higher temperature T_2 are then $\sigma_1 T_1/T_2$ and $u_1 T_1/T_2$. Thus the ratio of the emissivities at temperatures T_2 and T_1 is, by Kronig's formula,

$$\frac{e_2}{e_1} = \sqrt{\frac{T_2}{T_1}}\sqrt{\frac{\sqrt{\left(\frac{u_1 T_1}{T_2}\right)^2+1}-\frac{u_1 T_1}{T_2}}{\sqrt{u_1^2+1}-u_1}}$$

Since u_1 is positive and $\frac{T_2}{T_1} > 1$,

$$\sqrt{\left(\frac{u_1 T_1}{T_2}\right)^2 + 1} - \frac{u_1 T_1}{T_2} > \sqrt{u_1^2 + 1} - u_1.$$

Therefore, for all frequencies to which the formula is applicable,

$$\frac{e_2}{e_1} > \sqrt{\frac{T_2}{T_1}}. \tag{5}$$

When $u = 6$ and $T_2/T_1 = 4$, for example,

$$\frac{e_2}{e_1} = 1 \cdot 9 \sqrt{\frac{T_2}{T_1}}$$

The conclusion (5) may in fact be reached without making use of equation (4) if it is assumed that the surface conductivity is inversely proportional to T and that the width of the resonance line increases with temperature The latter is no new assumption, it is fundamental to the derivation of the dispersion theory in the near infra-red.

The theory implies, therefore, that in the region extending from about 1·5 μ to the domain of validity of the Hagen-Rubens relation the emissivity should increase considerably more rapidly with temperature than it does in the latter region. There is little doubt, however, that in the near infra-red the change of emissivity with temperature is *less*, and not *more*, rapid than is given by the square-root law: fig. 6 certainly supports this latter conclusion.

In order to conserve the Kronig theory and yet to derive from it results in agreement with experience, it would be necessary to assume not only a high value for the resistance of the surface layers of the metal, but also to assume that this resistance increases with temperature considerably less rapidly than does that of the metal in bulk. Such an hypothesis does not seem plausible. Moreover, the postulation of a new law connecting surface conductivity and temperature increases materially the number of adjustable quantities in the formula for the emissivity and destroys almost completely the *raison d'être* of the theory.

A number of simplifying hypotheses were made by Kronig, but in view of the fact that the theory is based on Bloch's theory of conduction, which does not pay sufficient attention to the mutual repulsion of the electrons in the metal, it seems unlikely that mere refinements will bring about that drastic change in the calculated reflecting power which this research proves to be necessary. The influence of the free electrons on one another must be comparable with the interaction of the ions of the atomic lattice on these electrons, and it seems unreasonable to expect a theory which neglects the mutual potential energy of the electrons to be in quantitative agreement with experiment Not until a solution of the fundamental Thomas-Fermi equation for a 3-dimensional lattice has been obtained does there seem much hope of formulating a satisfactory quantum-mechanical theory of the optical properties of metals in the near infra-red

Nickel—The gradual transition from an emission constant increasing with temperature in the far infra-red to one which is practically independent of temperature near the visible region is again made manifest by a comparison of the high temperature emissivities measured in the present research with the reflecting powers of nickel at room temperature and at 300° C, measured by Hagen and Rubens (*loc cit*, 1910) by their multi-reflection method Owing to lack of reliable data about the resistance of pure nickel at temperatures above 400° C, it is not possible to enter into a detailed discussion such as was given for copper From the figures available, however, it appears that, at a wave-length of $6 \cdot 5\mu$, the observed values of the emissivity do not differ from those calculated from the Hagen-Rubens relation by more than about 20%, and that the main conclusions of the discussion on copper hold also for nickel

As that of copper, the experimental curve at the higher temperature is less steep to the wave-length axis than is the curve for the lower temperature and the two cross at some wave-length between 1 and 2μ The temperature coefficient of emissivity between 1 and 2μ appears to be very small, as is seen by comparing these results with those of Hagen and Rubens Their evidence of a change from a positive to a negative temperature coefficient in this region is strengthened by the present results

For copper, at a wave-length of $1 \cdot 5\mu$, the emissivity at 850° appears to be about 6% less than that at 700° C. Even though the results at the former temperature are few in number, the smoothness of the curve would indicate that the diminution is probably too great to be ascribed to experimental error. It is unfortunate that repolishing was necessary in order to obtain the results at 850° C., and the effect may be due, at any rate in part, to a changed condition of the surface of the metal.

As yet, nothing is known about the high temperature emissivities of metals between the visible and 1μ, and much additional work is necessary before it can be definitely stated whether or not the emissivity is dependent on the temperature in the visible region. It is hoped to extend the present observations up to, and into, the visible, using a spectrometer for the resolution of the energy and a photoelectric method of recording. Continuous curves showing high temperature emissivities plotted against wave-length should do much to remove the confusion which has resulted from the general practice of determining visible emissivities by photometric methods at a few discrete wave-lengths only.

In conclusion, I wish to thank Professor Lindemann, F.R S, for his help and for extending to me the facilities of his laboratory I am indebted also to Mr T C Keeley and to Mr. C H Collie for many helpful suggestions

Summary

The emmissivity of copper has been determined over a wave-length range extending from 1·5μ to 5μ at the two temperatures, 700° C and 850° C, and the emissivity of nickel over the range 1·25μ to 6·5μ at 850° C. and the range 1μ to 6·5μ at 1000° C.

The emissivity for a given wave-length was measured directly as the ratio between the energy received from a given area of the radiating metal and the energy received from an equal area of a black-body slot cut in the metal and radiating, therefore, at the same temperature as the metal.

The method possesses the following advantages.—

(1) The emissivities can be measured with a far greater accuracy than is possible by employing a reflection method

(2) The comparison black-body emission is measured, and not calculated from the laws of full radiation

(3) Since the metallic radiation and the black-body radiation are of the same temperature, it is not necessary to measure the temperature of the radiator with a high degree of precision, in fact, it was measured only because it was desired to investigate how the reflection coefficients varied with the temperature

The results have been compared with the values predicted by the classical theory of Drude and by the quantum-mechanical theory of Krönig; the latter theory is shown to fit the facts less well than the former. An argument based on general grounds has been advanced in support of this conclusion.

The Flow of Viscous Liquid Past Spinning Bodies

By T E. GARSTANG, M.Sc , University College, London

(Communicated by L N G Filon, F R S —Received June 8, 1933)

§ 1 Introduction.

The motion produced in a viscous liquid by a spinning sphere has been investigated for small values of the Reynolds' number, using Stokes' equations for slow motion, in which the inertia terms are neglected * By combining the solution for this problem with that given by Stokes† for the flow of a stream of viscous liquid past a fixed sphere, we obtain the solution for a stream flowing past a spinning sphere Oseen‡ introduced a modified system of equations, in which the inertia terms are partly taken into account, and obtained the solution for flow past a fixed sphere using these equations. The problem of the flow of viscous liquid past a fixed circular cylinder has been investigated by Lamb,§ using Oseen's equations, and the additional solution required if the cylinder is rotating has been given by Oseen.|| In the present paper the solution for flow past a spinning sphere is discussed, using Oseen's equations.

The flow of viscous liquid past a spinning body is physically equivalent to motion of the body through the liquid with combined translation and rotation. Now it is well known that in practice when a body moves through a liquid in such a manner, if there is rotation about an axis y perpendicular to the direction of motion x, then there is a lift on the body in a direction perpendicular to both x and y¶. In theoretical investigations, if we suppose that the motion is steady, we are restricted in three dimensions to a body rotating about an axis of symmetry, and in two dimensions to the circular cylinder. In these cases it is impossible to obtain a lift if we use Stokes' equations for slow motion. For since the equations are linear, the lift is the sum of the lifts due to the solution for flow past a fixed body and the solution for spin without flow, and these are both zero by symmetry. This argument does not apply to Oseen's

---

* Lamb, "Hydrodynamics," § 337.

† 'Trans. Camb Phil Soc.,' vol. 9, p 8 (1851).

‡ 'Ark. Mat. Astr. Fys.,' vol. 6, No 29 (1910).

§ 'Phil. Mag.,' vol. 21, p 112 (1911)

|| "Hydrodynamik," § 17 2.

¶ P. G. Tait, 'Scientific Papers,' vol 2, pp 356, 371 (Camb., 1898); 'Trans. Roy. Soc. Edin.,' vol. 37 and vol. 39.

equations, since we cannot have a solution for spin alone with no flow, the stream velocity being implied in the equations themselves. In the absence of a method for solving the complete hydrodynamical equations, it is therefore of interest to investigate the flow of viscous liquid past spinning bodies, using Oseen's equations, and particularly to find whether a lift is obtained

§ 2. *Summary of Results*

In discussing the rotating sphere, we have to consider separately rotation about an axis coinciding with the direction of the stream and about an axis perpendicular to this direction. These two rotations will be referred to as side spin and top spin respectively In each the known solution for flow past a fixed sphere is combined with a solution which is appropriate to the altered boundary conditions at the surface of the sphere These boundary conditions are satisfied to the same degree of approximation as in Oseen's solution for the fixed sphere, and a method of obtaining further approximations is indicated

Before discussing the results obtained concerning the lift, it must be understood that there are three different quantities involved First, there is the lift calculated from integrals at infinity, using a method first introduced by Filon, and extended to three dimensions by Goldstein , secondly, there is the lift calculated from integrals over the body , and finally, there is the experimental lift, of which the sign is in general in accordance with the Kutta-Joukowski theorem for a perfect fluid The first two would be the same if the solution related to the complete hydrodynamical equations, but in solutions using Oseen's equations they are found to differ

Considerations of symmetry show that there can be no lift on the sphere rotating with side spin When we come to investigate the lift on the sphere rotating with top spin, some unexpected results are found. On evaluating the lift by means of integrals at infinity, we obtain the value zero, but if we calculate the lift from integrals over the body, we obtain a force in the opposite direction to that given by the Kutta-Joukowski theorem.

By transforming the surface integrals used in the two calculations, we show that the difference in the results is a necessary consequence of the neglect of the inertia terms in the hydrodynamical equations On investigating the known solution for a rotating circular cylinder, a similar discrepancy in the values of the lift given by the two methods is found In this case, however, the calculation using integrals at infinity gives a value in agreement with the Kutta-Joukowski theorem, while the calculation by means of integrals over the body gives half this value Provided, however, the body is not spinning, the forces calculated from integrals at infinity agree with those calculated from integrals over the body

For the rotating sphere, we find on comparing the additional solutions for rotation with those obtained by using Stokes' equations for slow motion, that the distribution of velocity near the sphere is identical to our order of approximation From this we deduce that the couple opposing the rotation, calculated from integrals over the sphere, has the same value whichever equations are used. This value of the couple cannot be compared with that obtained from integrals at infinity, using Oseen's equations, since it has not yet been found possible to calculate the couple by the latter method. It is hoped that it will be possible to include this in another paper dealing with general theorems concerning the forces and couples on a body in a stream of viscous fluid.

§ 3 *The Solution for Flow past a Fixed Sphere.*

Since the solution for flow past a fixed sphere forms part of that for flow past a spinning sphere, we first give a short account of the former solution, following the method used by Lamb * We consider a stream of viscous liquid, of velocity U at great distances, flowing past a fixed sphere of radius a. We write $U + u, v, w$ for the velocity resolutes at any point of the fluid, so that u, v, w are the disturbance velocities Let p be the pressure, ρ the density, and ν the kinematic viscosity of the fluid. Then if the motion is supposed steady, and we neglect terms of the second order in u, v, w, the hydrodynamical equations assume the form adopted by Oseen, namely,

$$\left.\begin{aligned} U\frac{\partial u}{\partial x} + \frac{1}{\rho}\frac{\partial p}{\partial x} &= \nu\nabla^2 u \\ U\frac{\partial v}{\partial x} + \frac{1}{\rho}\frac{\partial p}{\partial y} &= \nu\nabla^2 v \\ U\frac{\partial w}{\partial x} + \frac{1}{\rho}\frac{\partial p}{\partial z} &= \nu\nabla^2 w \end{aligned}\right\}, \tag{3.1}$$

together with the equation of continuity

$$\frac{\partial u}{\partial x} + \frac{\partial v}{\partial y} + \frac{\partial w}{\partial z} = 0. \tag{3.2}$$

---

* "Hydrodynamics," § 340, or 'Phil. Mag,' vol 21, p. 112 (1911)

The solution of (3.1) and (3.2) is well known to be given by

$$p = \rho U \frac{\partial \phi}{\partial x}$$

$$(u, v, w) = - \operatorname{grad} \phi + (u', v', w'),$$

where ϕ is any harmonic function and u', v', w' are solutions of the equation

$$\left(\nabla^2 - 2k \frac{\partial}{\partial x}\right) \chi = 0, \tag{3.3}$$

satisfying

$$\frac{\partial u'}{\partial x} + \frac{\partial v'}{\partial y} + \frac{\partial w'}{\partial z} = 0. \tag{3.4}$$

It is convenient at this stage to introduce the following notation, r, θ, ω being spherical polar co-ordinates with the axis of x as polar axis.

$$F_n(kr) = \left(\frac{2}{\pi kr}\right)^{\frac{1}{2}} K_{n+\frac{1}{2}}(kr),$$

$$G_n = F_n(kr) P_n(\cos\theta),$$

$$G_n{}^m = F_n(kr) P_n{}^m(\cos\theta) \cos m\omega,$$

$$H_n{}^m = F_n(kr) P_n{}^m(\cos\theta) \sin m\omega.$$

$K_{n+\frac{1}{2}}$ is the Bessel function of imaginary argument, defined as in Watson's "Bessel Functions" (§§ 3.7, 3 71). $P_n{}^m$ is the associated Legendre function, defined by the equation

$$P_n{}^m(\mu) = (1 - \mu^2)^{\frac{m}{2}} \frac{d^m P_n(\mu)}{d\mu^m}.$$

The functions G_n, $G_n{}^m$ and $H_n{}^m$ are solutions of the equation

$$(\nabla^2 - k^2) V = 0,$$

while the functions $e^{kx}G_n$, $e^{kx}G_n{}^m$ and $e^{kx}H_n{}^m$ are solutions of the equation (3 3).

A solution of equations (3.3) and (3.4) is given by

$$u' = \frac{1}{2k}\frac{\partial \chi}{\partial x} - \chi, \qquad v' = \frac{1}{2k}\frac{\partial \chi}{\partial y}, \qquad w' = \frac{1}{2k}\frac{\partial \chi}{\partial z},$$

where χ satisfies (3.3)

In order to solve the problem of flow past a fixed sphere, we take the solution of (3.1) and (3.2) given by

$$\phi = \frac{\alpha_0}{r} + \frac{\alpha_1 \cos\theta}{r^2}$$

$$\chi = \beta e^{kx} G_0.$$

The boundary conditions $u = -U$, $v = 0$, $w = 0$ for $r = a$ are found to be satisfied approximately, when ka is small, provided

$$\alpha_0 = \tfrac{3}{2}Ua, \qquad \alpha_1 = \tfrac{1}{4}Ua^3, \qquad \beta = \tfrac{3}{2}Uka.$$

It is easily verified that to the same order of approximation, the distribution of velocity in the neighbourhood of the sphere is identical with that obtained using Stokes' equations for slow motion The drag on the sphere, calculated from the stresses as given by the flow in the neighbourhood of the sphere, has therefore the same value as on Stokes' theory, viz, $6\pi\mu a U$, where μ is the viscosity of the liquid If the drag is calculated from integrals at infinity, the same value is obtained

§ 4 *The Additional Solution for Side Spin.*

Suppose now that the sphere, instead of being fixed, is rotating about the axis of x with spin Ω_x The boundary conditions for $r = a$ are now

$$u = -U, \qquad v = -z\,\Omega_x, \qquad w = y\,\Omega_x$$

We have therefore to combine the solution for the fixed sphere with a solution satisfying the conditions for $r = a$

$$u = 0, \qquad v = -a\,\Omega_x \sin\theta \sin\omega, \qquad w = a\,\Omega_x \sin\theta \cos\omega \qquad (4\,1)$$

On referring to the discussion of the solution of Oseen's equations in § 3, we see that rotational solutions for the velocities involving v and w only, and associated with constant pressure are obtained by writing

$$u = 0, \qquad v = -\frac{\partial\psi}{\partial z}, \qquad w = \frac{\partial\psi}{\partial y},$$

where ψ satisfies (3.3)

Solutions suitable for our present purpose are given by

$$\psi = e^{kx}G_n$$

Using the recurrence formulæ for the $K_{n+\frac{1}{2}}$'s and the P_n's, we find that if $n \geqslant 2$,

$$v = -\frac{ke^{kx}}{2n+1}\left[H^1_{n-1} - H^1_{n+1}\right]$$

$$w = \frac{ke^{kx}}{2n+1}\left[G^1_{n-1} - G^1_{n+1}\right],$$

while if

$$\psi = e^{kx}G_1,$$

we have

$$v = \frac{ke^{kx}}{3}\,\mathrm{H}_2^1, \qquad w = -\frac{ke^{kx}}{3}\,\mathrm{G}_2^1,$$

and if

$$\psi = e^{kx}\mathrm{G}_0$$

$$v = ke^{kx}\mathrm{H}_1^1, \qquad w = -ke^{kx}\mathrm{G}_1^1$$

For a first approximation, we adopt the solution

$$\psi = \gamma e^{kx}\mathrm{G}_0$$

Using the relation

$$\left(\frac{2}{\pi kr}\right)^{\frac{1}{2}} \mathrm{K}_{\frac{3}{2}}(kr) = e^{-kr}\left(\frac{1}{kr} + \frac{1}{k^2r^2}\right), \tag{4 2}$$

and retaining only the terms of lowest order in ka, we find that for $r = a$

$$v = \frac{\gamma \sin\theta \sin\omega}{ka^2}, \qquad w = -\frac{\gamma \sin\theta \cos\omega}{ka^2} \tag{4 3}$$

It follows from (4 1) and (4 3) that the boundary conditions are satisfied to this order of approximation provided $\gamma = -ka^3\,\Omega_x$

If we started with the solution

$$\psi = \gamma_0 e^{kx}\mathrm{G}_0 + \gamma_1 e^{kx}\mathrm{G}_1$$

in which case we should have two arbitrary constants at our disposal, a better approximation could be obtained in which we retain terms of the next order in ka. By starting with a sufficient number of terms in ψ, we could satisfy the boundary conditions to any desired degree of approximation, although the calculations involved would soon become very laborious It does not seem to be worth while proceeding beyond the first approximation, since subsequent results lead to the conclusion that Oseen's equations are not a suitable basis for the investigation of flow past spinning bodies

It is of some interest to compare our solution with the solution for a rotating sphere which is obtained if we use Stokes' equations for slow motion. In this case the boundary conditions are satisfied exactly, and the solution is given by

$$u = 0, \qquad v = -\frac{a^3\Omega_x z}{r^3}, \qquad w = \frac{a^3\Omega_x y}{r^3},$$

together with constant pressure. It is easily verified that to the order of approximation used in our solution, the distribution of velocity in the neighbourhood of the sphere is the same in the two cases. Now considerations of symmetry show that the solution for the fixed sphere will not contribute anything to the couple on the sphere opposing the rotation. Thus it follows that this couple has the same value, namely, $8\pi\mu a^3 \Omega_x$, as is given by the solution using Stokes' equations.

We now proceed to determine whether the additional motion of the fluid due to the side spin has any effect on the drag, which is given by

$$X = \iint_{r=a} (l'\widehat{xx} + m'\widehat{xy} + n'\widehat{xz})\, dS$$

$$= \iint_{r=a} \left\{ -l'p + \mu \left[2l' \frac{\partial u}{\partial x} + m' \left(\frac{\partial v}{\partial x} + \frac{\partial u}{\partial y} \right) + n' \left(\frac{\partial u}{\partial z} + \frac{\partial w}{\partial x} \right) \right] \right\} dS,$$

l', m', n' are here the direction cosines of the outward-drawn normal to the sphere, so that

$$l' = \cos\theta, \qquad m' = \sin\theta\cos\omega, \qquad n' = \sin\theta\sin\omega$$

In the additional solution p is constant and u does not appear, so that if X_1 is the contribution of the additional solution to the drag, we have

$$X_1 = \mu \iint_{r=a} \left(m' \frac{\partial v}{\partial x} + n' \frac{\partial w}{\partial x} \right) dS$$

$$= \mu a^2 \int_0^{\pi} \int_0^{2\pi} \left(m' \frac{\partial v}{\partial x} + n' \frac{\partial w}{\partial x} \right) \sin\theta \, d\omega \, d\theta,$$

where $v = \gamma k e^{kx} H_1^1$, $\qquad w = -\gamma k e^{kx} G_1^1$

We find that

$$\frac{\partial v}{\partial x} = \tfrac{1}{3}\gamma k^2 e^{kx} (3H_1^1 - H_2^1) \tag{4.4}$$

$$\frac{\partial w}{\partial x} = -\tfrac{1}{3}\gamma k^2 e^{kx} (3G_1^1 - G_2^1). \tag{4.5}$$

Using (4 4) and (4.5), we see that in each term in the expression for X_1 the integral with respect to ω vanishes. Thus the drag is unaffected by the rotation of the sphere.

§ 5. *The Additional Solution for Top Spin.*

We now consider the case in which the sphere is rotating about an axis perpendicular to the direction of the stream. If we suppose that the sphere has a spin Ω_y about the y-axis, the boundary conditions for $r = a$ are

$$u = -U + z\Omega_y, \qquad v = 0, \qquad w = -x\Omega_y.$$

We must therefore combine with the solution for a fixed sphere a solution satisfying the conditions for $r = a$

$$u = a\,\Omega_y \sin\theta \sin\omega, \qquad v = 0, \qquad w = -a\,\Omega_y \cos\theta \tag{5.1}$$

Rotational solutions for the velocities involving u and w only, and associated with constant pressure, are obtained by a method similar to that used in § 4 In this case we write

$$u = -\frac{\partial\psi}{\partial z}, \qquad v = 0, \qquad w = \frac{\partial\psi}{\partial x},$$

where ψ again satisfies (3 3).

Suitable solutions are obtained if we take

$$\psi = e^{kx}G_n,$$

in which case we find that if $n \geqslant 2$,

$$u = -\frac{ke^{kx}}{2n+1}\left[H^1_{n-1} - H^1_{n+1}\right]$$

$$w = -\frac{ke^{kx}}{2n+1}\left[nG_{n-1} - (2n+1)\,G_n + (n+1)\,G_{n+1}\right],$$

while if

$$\psi = e^{kx}G_1,$$

we have

$$u = \frac{ke^{kx}}{3}\,H^1_2, \qquad w = -\frac{ke^{kx}}{3}\left[G_0 - 3G_1 + 2G_2\right],$$

and if

$$\psi = e^{kx}G_0,$$

$$u = ke^{kx}\,H^1_1, \qquad w = ke^{kx}\left[G_0 - G_1\right].$$

For a first approximation we write

$$\psi = \delta e^{kx}G_0$$

Using equation (4 2) and also the relation

$$\left(\frac{2}{\pi kr}\right)^{\frac{1}{2}} K_{\frac{1}{2}}(kr) = \frac{e^{-kr}}{kr},$$

and retaining only the terms of lowest order in ka, we find that for $r = a$

$$u = \frac{\delta \sin\theta \sin\omega}{ka^2}, \qquad w = -\frac{\delta\cos\theta}{ka^2} \tag{5.2}$$

We see from (5.1) and (5.2) that to this order of approximation the boundary conditions are satisfied provided $\delta = ka^3\,\Omega_y$.

Further approximations could be obtained if desired as explained in § 4, but for the reason given there it does not seem to be worth while going beyond the first approximation.

We now come to consider the effect of the top spin on the drag. If X_2 is the contribution to the drag of the additional solution, then since in this solution p is constant and v does not appear, we have

$$X_2 = \mu \iint_{r=a} \Big[2l' \frac{\partial u}{\partial x} + m' \frac{\partial u}{\partial y} + n' \Big(\frac{\partial u}{\partial z} + \frac{\partial w}{\partial x}\Big)\Big] dS$$

$$= \mu a^2 \int_0^\pi \int_0^{2\pi} \Big[2l' \frac{\partial u}{\partial x} + m' \frac{\partial u}{\partial y} + n' \Big(\frac{\partial u}{\partial z} + \frac{\partial w}{\partial x}\Big)\Big] \sin\theta \, d\omega \, d\theta,$$

where

$$u = \delta k e^{kx} H_1^1, \qquad w = \delta k e^{kx} [G_0 - G_1] \tag{5.21}$$

We find that

$$\frac{\partial u}{\partial x} = \frac{\delta k^2 e^{kx}}{3} (3H_1^1 - H_2^1) \tag{5.3}$$

$$\frac{\partial u}{\partial y} = -\frac{\delta k^2 e^{kx}}{6} H_2^2 \tag{5.4}$$

$$\frac{\partial u}{\partial z} = \frac{\delta k^2 e^{kx}}{6} (G_2^2 - 2G_0 + 2G_2) \tag{5.5}$$

$$\frac{\partial w}{\partial x} = \frac{\delta k^2 e^{kx}}{3} (4G_0 - 6G_1 + 2G_2) \tag{5.6}$$

Using equations (5.3) to (5.6) it is easily seen that in every term in the expression for X_2 the integral with respect to ω vanishes, so that the top spin has no effect on the drag.

By comparing our solution as before with that obtained using Stokes' equations for slow motion, we see that the couple opposing the rotation has the same value as for side spin, if Ω_y is substituted for Ω_x.

§ 6. *The Lift on the Sphere Rotating with Top Spin*

We come now to the most important part of the investigation, namely, the calculation of the lift on the sphere rotating with top spin. In the case we have considered, the sphere is rotating about the axis of y, so that the lift is the force in the direction of the axis of z. If Z' is the value of this force calculated from integrals over the sphere, we have

$$Z' = \iint_{r=a} (l'\widehat{xz} + m'\widehat{yz} + n'\widehat{zz})\, dS$$

$$= \iint_{r=a} \Big\{ -n'p + \rho\nu \Big[l' \Big(\frac{\partial u}{\partial z} + \frac{\partial w}{\partial x}\Big) + m' \Big(\frac{\partial w}{\partial y} + \frac{\partial v}{\partial z}\Big) + 2n' \frac{\partial w}{\partial z}\Big]\Big\} dS.$$

The terms in u, v, w, p which make up the solution for a fixed sphere will not contribute anything to the lift, so that we have only to consider the additional solution for top spin. It follows that

$$Z' = \rho\nu \iint_{r=a} \left\{ l' \left(\frac{\partial u}{\partial z} + \frac{\partial w}{\partial x} \right) + m' \frac{\partial w}{\partial y} + 2n' \frac{\partial w}{\partial z} \right\} dS, \tag{6 1}$$

where u and w are given by (5 21)

We find that

$$\frac{\partial w}{\partial y} = \frac{\delta k^2 e^{kz}}{3} [- 3G_1^1 + G_2^1] \tag{6.2}$$

$$\frac{\partial w}{\partial z} = \frac{\delta k^2 e^{kz}}{3} [- 3H_1^1 + H_2^1], \tag{6.3}$$

while the values of $\partial u/\partial z$ and $\partial w/\partial x$ are given by (5 5) and (5.6) On substituting these values into (6 1) we see that the term $e^{kz}G_2^2$ in $\partial u/\partial z$ contributes nothing to Z', since the integral with respect to ω vanishes

In order to evaluate the other integrals which occur, it is convenient first to consider the integral

$$T_n = \iint_{r=a} F_n(ka)\, e^{ka\mu} [\alpha P_{n-1}(\mu) + \beta P_{n+1}(\mu)]\, dS,$$

where α and β are arbitrary multipliers Here and throughout this section, μ is used to denote $\cos\theta$

We proceed to obtain an approximate expression for T_n, retaining only the most important term. By using the expansion*

$$e^{kr\mu} = \sum_{m=0}^{\infty} \left(\frac{\pi}{2kr}\right) (2m + 1)\, I_{m+\frac{1}{2}}(kr)\, P_m(\mu),$$

we find that

$$\int_{-1}^{1} e^{kr\mu} P_n(\mu)\, d\mu = 2 \left(\frac{\pi}{2kr}\right)^{\frac{1}{2}} I_{n+\frac{1}{2}}(kr). \tag{6.31}$$

It follows that

$$T_n = 4\pi a^2 F_n(ka) \left(\frac{\pi}{2ka}\right)^{\frac{1}{2}} \{\alpha I_{n-\frac{1}{2}}(ka) + \beta I_{n+\frac{1}{2}}(ka)\}$$

Now we have†

$$K_{n+\frac{1}{2}}(ka) = \left(\frac{\pi}{2ka}\right)^{\frac{1}{2}} e^{-ka} \sum_{m=0}^{n} \frac{(n+m)!}{m!\,(n-m)!\,(2ka)^m}, \tag{6.32}$$

---

* Goldstein, 'Proc. Roy Soc.,' A, vol. 123, p. 225 (1929).

† Watson, "Bessel Functions," §§ 3.7, 3 71.

and

$$\mathrm{I}_n(ka) = \sum_{m=0}^{\infty} \frac{(\tfrac{1}{2}ka)^{n+2m}}{m!\,\Gamma(n+m+1)},$$

whence

$$\left(\frac{\pi}{2ka}\right)^{\frac{1}{2}} \mathrm{I}_{n+\frac{1}{2}}(ka) = \sum_{m=0}^{\infty} \frac{(ka)^{n+2m}}{(2n+2m+1)(2n+2m-1)\quad(2m+1)(2m)!}. \tag{6.33}$$

Using (6.32) and (6.33) we find that, retaining only the most important term,

$$\mathrm{T}_n = \frac{4\pi\alpha}{k^2} \tag{6.4}$$

The integral

$$\mathrm{T}_0 = \iint_{r=a} \mathrm{F}_0(ka)\, e^{ka\mu}\ \beta \mathrm{P}_1(\mu)\, d\mathrm{S},$$

is seen to be negligible compared with the general value of T_n.

Using (6.4) and the formula

$$(2n+1)\,\mu \mathrm{P}_n(\mu) = n\mathrm{P}_{n-1}(\mu) + (n+1)\,\mathrm{P}_{n+1}(\mu), \tag{6.41}$$

we find that to our order of approximation

$$\iint_{r=a} e^{kx} l' \mathrm{G}_n\, d\mathrm{S} = \frac{4\pi n}{(2n+1)k^2} \tag{6.51}$$

Also using the formulæ

$$(2n+1)(1-\mu^2)^{\frac{1}{2}} \mathrm{P}_n^1(\mu) - \mathrm{P}_{n+1}{}^2(\mu) - \mathrm{P}_{n-1}{}^2(\mu)$$
$$= n(n+1)\,[\mathrm{P}_{n-1}(\mu) - \mathrm{P}_{n+1}(\mu)],$$

we find that

$$2\,(2n+1)\,m'\mathrm{P}_n^1(\mu)\cos\omega = n\,(n+1)\,[\mathrm{P}_{n-1}(\mu) - \mathrm{P}_{n+1}(\mu)]$$
$$-\,[\mathrm{P}_{n-1}{}^2(\mu) - \mathrm{P}_{n+1}{}^2(\mu)\,]\cos 2\omega \tag{6.52}$$

It easily follows from (6.4) and (6.52) that

$$\iint_{r=a} e^{kx} m' \mathrm{G}_n^1\, d\mathrm{S} = \frac{2\pi n\,(n+1)}{(2n+1)\,k^2}. \tag{6.53}$$

Similarly we have

$$\iint_{r=a} e^{kx} n' \mathrm{H}_n^1\, d\mathrm{S} = \frac{2\pi n\,(n+1)}{(2n+1)\,k^2}. \tag{6.54}$$

By means of equations (6.51), (6.53) and (6.54) we find that

$$Z' = -\frac{8\pi\rho\nu\delta}{3},$$

and since $\delta = ka^3 \Omega_y$, we finally obtain

$$Z' = -\tfrac{4}{3}\pi\rho a^3 \mathrm{U}\, \Omega_y \tag{6.6}$$

Now it is a fact of observation that a sphere moving with under spin through air experiences a lifting force,* which, in regard to sign, is in accordance with the Kutta-Joukowski formula for two-dimensional motion of a perfect fluid. This requires that, treating U as essentially positive, Z' and Ω_y should have the same sign in the case we have considered in which a stream flows past a rotating sphere. We see, however, from (6.6) that Ω_y and Z' must have opposite signs. This must not be taken to imply a complete disagreement between observation and theory, since, so far as the author is aware, the experimental evidence relates to Reynolds' numbers far larger than those to which the present approximation applies.

We now proceed to calculate the lift on the sphere by Filon's method, employing integrals over a large sphere Σ whose radius r is ultimately made infinite. The calculation is simplified by using a formula given by Goldstein.† If Z is the value of the lift given by this method, Goldstein's formula takes the form

$$\mathrm{Z} = -\rho \mathrm{U} \iint_{\Sigma} l' w \, d\Sigma,$$

where, in the present case, w is given by (5.21).

Consider now the integral

$$\begin{aligned} \mathrm{L}_n &= \iint_{\Sigma} e^{kz} l' \mathrm{G}_n \, d\Sigma \\ &= 2\pi r^2 \mathrm{F}_n (kr) \int_{-1}^{1} e^{kr\mu} l' \mathrm{P}_n (\mu)\, d\mu. \end{aligned}$$

Using (6.31) and (6.41), we have

$$\mathrm{L}_n = 4\pi r^2 \frac{\mathrm{F}_n (kr)}{2n+1} \left(\frac{\pi}{2kr}\right)^{\frac{1}{2}} [n\mathrm{I}_{n-\frac{1}{2}} (kr) + (n+1)\, \mathrm{I}_{n+\frac{1}{2}} (kr)].$$

With the help of (6.32) and the formula‡

$$\mathrm{I}_{n+\frac{1}{2}} (kr) = \frac{1}{(2\pi r)^{\frac{1}{2}}} \left[e^{kr} \sum_{m=0}^{n} \frac{(-1)^m (n+m)\,!}{m\,!\ (n-m)\,!\ (2kr)^m} \right.$$
$$\left. + (-1)^{n+1} e^{-kr} \sum_{m=0}^{n} \frac{(n+m)\,!}{m\,!\ (n-m)\,!\ (2kr)^m} \right],$$

---

* Tait, *loc. cit.*

† 'Proc. Roy. Soc.,' A, vol. 131, p. 198 (1931).

‡ Watson, *loc. cit.*

we find that

$$\lim_{r\to\infty} \mathrm{L}_n = \frac{2\pi}{k^2}.$$

This formula holds for all values of n, including zero.

Since L_n is independent of n, it follows at once that Z vanishes.

Thus our two calculations of the lift do not agree The explanation of this result is to be found in the neglect of the terms $u\dfrac{\partial u}{\partial x}$, etc., in the hydrodynamical equations The further discussion of the significance of the discrepancy is deferred to § 9

§ 7. *Comparison of Forces on a Body, calculated from Integrals at Infinity, and from Integrals over the Body.*

The discrepancy between the values of the lift found from integrals at infinity and integrals over the body is so remarkable that it is desirable to confirm the result by another method. This we are able to do by means of the following transformation of the integrals involved, for which I am indebted to Professor Filon

Let S be the surface of a solid of any shape and Σ a large surface which is everywhere at a great distance from S Then if X, Y, Z are the forces exerted by the fluid on the solid S, we have the following formula for X, due to Goldstein*

$$\mathrm{X} = \iint_\Sigma \left\{-l'p + \mu\left[2l'\frac{\partial u}{\partial x} + m'\left(\frac{\partial u}{\partial x} + \frac{\partial v}{\partial x}\right) + n'\left(\frac{\partial u}{\partial z} + \frac{\partial w}{\partial x}\right)\right]\right\} d\Sigma$$
$$- \rho\iint_\Sigma (\mathrm{U} + u)\left[l'(\mathrm{U} + u) + m'v + n'w\right] d\Sigma$$

Goldstein has shown that the integrals of products of u, v, w tend to zero when Σ is made indefinitely large. Further, $\iint_\Sigma l'\mathrm{U}^2\,d\Sigma$ vanishes identically, and if (u, v, w) are such that they give no total expansion of the fluid, then

$$\iint_\Sigma (l'u + m'v + n'w)\,d\Sigma = 0.$$

Hence we have

$$\mathrm{X} = \iint_\Sigma \left\{-l'p + \mu\left[2l'\frac{\partial u}{\partial x} + m'\left(\frac{\partial u}{\partial y} + \frac{\partial v}{\partial x}\right) + n'\left(\frac{\partial u}{\partial z} + \frac{\partial w}{\partial x}\right)\right]\right\} d\Sigma$$
$$- \rho\mathrm{U}\iint_\Sigma l'u\,d\Sigma.$$

---

* *Loc. cit.*, p 220 (1929).

Also, if X′, Y′, Z′ are the forces calculated directly from the tractions on the body, we have

$$X' = \iint_S \left\{ - l'p + \mu \left[2l' \frac{\partial u}{\partial x} + m' \left(\frac{\partial u}{\partial y} + \frac{\partial v}{\partial x} \right) + n' \left(\frac{\partial u}{\partial z} + \frac{\partial w}{\partial x} \right) \right] \right\} dS$$

If now J denotes the space between S and Σ, it follows that

$$X - X' = \iiint_J \left\{ - \frac{\partial p}{\partial x} + \mu \left[2 \frac{\partial^2 u}{\partial x^2} + \frac{\partial^2 u}{\partial y^2} + \frac{\partial^2 u}{\partial z^2} + \frac{\partial^2 v}{\partial x \, \partial y} + \frac{\partial^2 w}{\partial x \, \partial z} \right] \right\} dx \, dy \, dz - \rho U \iint_\Sigma l'u \, d\Sigma.$$

Making use of (3 1) and (3 2), we have

$$\begin{aligned} X - X' &= \rho U \iiint_J \frac{\partial u}{\partial x} \, dx \, dy \, dz - \rho U \iint_\Sigma l'u \, d\Sigma \\ &= - \rho U \iint_S l'u \, dS \end{aligned}$$

Similarly, we find that

$$Y - Y' = - \rho U \iint_S l'v \, dS$$

$$Z - Z' = - \rho U \iint_S l'w \, dS$$

Now suppose that the body S is rotating with spins Ω_x, Ω_y, Ω_z. It may be remarked that it is necessary for steady motion that the rotation should be about an axis of symmetry The boundary conditions over S are then

$$\begin{aligned} u &= - U + z \Omega_y - y \Omega_z \\ v &= x \Omega_z - z \Omega_x \\ w &= y \Omega_x - x \Omega_y \end{aligned}$$

Thus we have

$$X - X' = \rho U \iint_S l' (y \Omega_z - z \Omega_y) \, dS$$

$$Y - Y' = \rho U \iint_S l' (z \Omega_x - x \Omega_z) \, dS$$

$$Z - Z' = \rho U \iint_S l' (x \Omega_y - y \Omega_x) \, dS.$$

If the body S is a sphere of radius a, we easily find that

$$\begin{aligned} X - X' &= 0 \\ Y - Y' &= - \tfrac{4}{3} \pi \rho a^3 U \, \Omega_z \\ Z - Z' &= \tfrac{4}{3} \pi \rho a^3 U \, \Omega_y \end{aligned}$$

This confirms the discrepancy found by calculating Z and Z′ separately. Also it is now clear that the discrepancy arises from the use of the equations of motion (3.1), in which the inertia terms are neglected.

We see that if the body S is not rotating, in which case the restriction to axial symmetry is unnecessary, the forces calculated from integrals at infinity agree with those calculated from integrals over the body.

§ 8. *The Solution for a Circular Cylinder*

The flow of viscous liquid past a fixed circular cylinder has been discussed by Lamb,* using Oseen's equations. Since the solution obtained forms part of the solution for flow past a rotating cylinder, it is convenient to give a brief summary of the results.

Oseen's equations in two dimensions are satisfied by

$$u = -\frac{\partial\phi}{\partial x} + \frac{1}{2k}\frac{\partial\chi}{\partial x} - \chi, \qquad v = -\frac{\partial\phi}{\partial y} + \frac{1}{2k}\frac{\partial\chi}{\partial y},$$

and

$$p = \rho U \frac{\partial\phi}{\partial x},$$

provided

$$\nabla^2\phi = 0$$

and

$$\left(\nabla^2 - 2k\frac{\partial}{\partial x}\right)\chi = 0$$

Lamb assumes as the appropriate solution

$$\phi = \alpha_0 \log r + \alpha_1 \frac{\partial}{\partial x} \log r$$

$$\chi = \beta e^{kx} K_0(kr)$$

It is found that the boundary conditions $u = -U$, $v = 0$, $w = 0$ for $r = a$ are satisfied approximately provided

$$\beta = \frac{2U}{\frac{1}{2} - \gamma - \log\left(\frac{1}{2}ka\right)}, \qquad \alpha_0 = -\frac{\beta}{2k}, \qquad \alpha_1 = \tfrac{1}{4}\beta a^2,$$

where γ is Euler's constant.

The drag on the cylinder per unit length is found to be

$$\frac{4\pi\mu U}{\frac{1}{2} - \gamma - \log\left(\frac{1}{2}ka\right)}$$

---

* "Hydrodynamics," § 343, or *loc. cit.* (1911).

The additional solution required if the cylinder is rotating has been given by Oseen.* In this case there is a solution of the equations giving irrotational velocities which satisfy the boundary conditions exactly, and the corresponding pressure supplies a lift in the direction required by observation If the cylinder is rotating with spin Ω, the boundary conditions to be satisfied by the additional solution for $r = a$ are

$$u = -\,\Omega y, \qquad v = \Omega x$$

The appropriate solution is given by

$$\phi = -\,a^2\Omega\theta$$

$$u = -\,a^2\,\Omega\,\frac{\sin\theta}{r}, \qquad v = \frac{a^2\Omega\cos\theta}{r}$$

$$p = \rho a^2 \mathrm{U}\,\Omega\,\frac{\sin\theta}{r},$$

r and θ being polar co-ordinates with the axis of x as initial line

If I is the circulation round the cylinder, we have

$$\mathrm{I} = 2\pi a^2\,\Omega$$

The lift Y per unit length of the cylinder, calculated from integrals at infinity, is easily shown to be given by

$$\mathrm{Y} = -\,2\pi\rho a^2 \mathrm{U}\,\Omega = -\,\rho \mathrm{UI}$$

in agreement with the general theorem due to Filon † On the other hand, if Y′ is the force calculated from integrals over the cylinder, we find that

$$\mathrm{Y}' = -\,\pi\rho a^2\mathrm{U}\,\Omega = -\,\tfrac{1}{2}\rho\mathrm{UI},$$

which is in accordance with Oseen's formula, having regard to the fact that he considers a cylinder moving through fluid at rest at infinity.

On applying the method of § 7 to a cylinder S of any shape we find as before that

$$\mathrm{X} - \mathrm{X}' = -\,\rho\mathrm{U}\int_{\mathrm{S}} l'\,u\,d\,\mathrm{S}$$

$$\mathrm{Y} - \mathrm{Y}' = -\,\rho\mathrm{U}\int_{\mathrm{S}} l'\,v\,d\,\mathrm{S}$$

If we now suppose that the cylinder is rotating with spin Ω, it is necessary for steady motion that the cylinder should be circular Using the boundary conditions

---

* "Hydrodynamik," § 17.2

† 'Proc Roy Soc,' A, vol 113, p. 7 (1926)

$$u = -U - y\Omega$$
$$v = x\Omega$$

we have, if a is the radius,

$$X - X' = 0$$
$$Y - Y' = -\pi\rho a^2 U\Omega$$

This confirms the discrepancy obtained by separate calculation of Y and Y'

§ 9 *Conclusion*

It remains to consider the bearing of the results obtained on the question as to whether Oseen's equations can justifiably be used at the boundary of the solid The use of the equations in this way seems to lead to fairly satisfactory results in some cases Thus we have seen that provided the body is not spinning, the forces calculated from integrals over the body agree with those calculated from integrals at infinity Also it is known that the theoretical values of the drag for the sphere and cylinder agree with experiment for small values of ka The agreement must, however, be regarded as somewhat accidental, since there is no more justification for neglecting $u\dfrac{\partial u}{\partial x}$, etc, in the neighbourhood of the body, than for neglecting $U\dfrac{\partial u}{\partial x}$, which is retained.

The results here obtained show that if the equations are used to determine actual coefficients at the boundary of a spinning solid, we are faced with the difficulty that the two methods of calculating the lift give different results Now it is clear that it is at a great distance from the solid that Oseen's equations are most likely to give a good approximation to the motion We must therefore take the value of the lift given by integrals at infinity as being more probably the correct one In fact we might hope, by obtaining the coefficients in this way, to get a solution which is a good approximation to the motion at infinity, even though it does not accurately represent the motion near the solid. But the fact that, for the sphere rotating with top spin, the calculation using integrals at infinity does not give a lift at all, seems to indicate that the method cannot even be relied upon to give a good approximation to the motion at infinity.

Finally, I wish to express my thanks to Professor Filon, both for the original suggestion of the problem of flow past a spinning sphere, and for the great interest which he has shown in the matter

Summary

The flow of viscous liquid past a spinning sphere is investigated by means of Oseen's approximate equations, it being assumed that these equations can be used to determine coefficients from boundary conditions The known solution for flow past a fixed sphere is combined with a solution which is appropriate to the altered boundary conditions at the surface of the sphere These boundary conditions are satisfied approximately, as in Oseen's solution for the fixed sphere When the sphere is rotating about an axis y perpendicular to the direction x of the stream, observation requires that there should be a lifting force on the sphere perpendicular to both x and y, the sign being in general in accordance with the Kutta-Joukowski theorem for a perfect fluid On calculating this force from integrals over the sphere we obtain a force in the opposite direction to that given by the Kutta-Joukowski theorem If we calculate the lift from integrals at infinity, we obtain the value zero The discrepancy between the two values is verified by a transformation of the surface integrals On investigating the known solution for a rotating circular cylinder a similar discrepancy in the values of the lift given by the two methods is found In this solution, however, the calculation using integrals at infinity gives a value in agreement with the Kutta-Joukowski theorem, while the calculation by means of integrals over the body gives half this value The cause of the discrepancy lies in the neglect of the inertia terms $u\dfrac{\partial u}{\partial x}$, etc which in the neighbourhood of the solid are of the same order as $U\dfrac{\partial u}{\partial x}$, which is retained The discrepancy and the disagreement of the results with observation show that if Oseen's equations are used to determine coefficients from boundary conditions, we cannot rely upon obtaining a good approximation to the motion either near the solid or at infinity

The Scattering of Electrons by Metal Vapours. II.—Zinc

By E. C. CHILDS, Ph.D., Exhibition of 1851 Senior Student, Clare College Cambridge, and H. S. W. MASSEY, Ph.D., Exhibition of 1851 Senior Student, Trinity College, Cambridge

(Communicated by Lord Rutherford, O.M., F.R.S.—Received June 9, 1933.)

In a previous paper* the importance of experimental investigations of the scattering of electrons by metal vapours was pointed out. It appears probable that the diffraction effects which occur in the elastic collisions of electrons with gas atoms are mainly determined by the ratio of the wave-length of the incident electrons to a certain atomic distance r_0. This distance is such that the potential energy of the electron in the atomic field at this distance is comparable in magnitude with its initial kinetic energy. If this be correct the determination of atomic and molecular fields by scattering experiments can be readily carried out by comparative methods and it is therefore important to test the validity of such an interpretation of the diffraction process. This can only be done by a wide series of investigations of electron scattering by atoms with a great variety of electron structures. As only the rare gases can be investigated in the gaseous state it is essential to develop methods of measuring the scattering from metal vapours. In Paper I a technique suitable for such measurements was described. With its use cadmium vapour was investigated and the comparison of the results with those obtained in mercury vapour confirmed the idea outlined above. With the electron energies used (4–48 volts) the scattering should be due to the outermost shells of the atoms. These are of very similar dimensions and electron density for mercury and cadmium and hence very similar angular distributions are expected and were in fact observed. In the present paper the investigations are extended to zinc vapour for a range of electron energies from 4 – 143 volts, and the results obtained throw further light on the applicability of the general method of viewing the phenomena outlined above.

1. *Description of Apparatus and Experimental Procedure.*—The apparatus used was identical in essentials with that described in Paper I. A homogeneous beam of electrons was fired through a cloud of metal vapour issuing from a

---

[*] 'Proc. Roy. Soc.,' A, vol. 141, p. 473 (1933). This paper will be referred to as Paper I in the following.

circular aperture in an oven and the scattering was measured by a Faraday collector. The variation of intensity with angle of scattering was measured by rotating the source about an axis coincident with that of the oven. Owing to the smallness of the scattering volume the vapour pressure of the metal may be taken as constant over the volume.

Difficulty was experienced in the collecting system of this apparatus owing to condensation of metal vapour. This deposition caused a pad of metal to build up on the ion-repelling electrode, which eventually became connected to the outer case. It was then impossible to make use of this electrode to prevent the collection of positive ions when working at electron energies above the ionization energy of the vapour. For this reason the ion-repelling electrode was eliminated and ions were rejected by maintaining the outer case at a small positive potential (up to 3 volts) above the rest of the scattering space. This procedure has been used previously* and is known to have a negligible disturbing effect for the electron energies for which its employment is necessary. In practice, for electron energies greater than 80 volts it was not possible to reject all the ions. Under these conditions the positive ion current alone was also observed at each angle by preventing the collection of electrons with a suitable retarding potential on the Faraday cylinder. In this way the correction necessary to the observed electron currents could be determined. As the ion current was small compared with the electron current except in the region of a diffraction minimum at a large angle, this procedure leads to satisfactory results.

Owing to the higher temperature (600° C.) required for the evaporation of zinc, the oven heaters were wound with molybdenum wire of 0.3 mm. diameter.

Specially pure zinc was employed and, before introduction into the oven, was outgassed by melting *in vacuo*. The oven having previously been maintained *in vacuo* at a bright red heat for 8 hours, the zinc was then introduced and the apparatus rebaked to 400° C. for a further 8 hours. Evaporation of the zinc proceeded in the same way as cadmium, and the experimental procedure adopted was the same as described in Paper I. Similar precautions were taken to maintain constancy of vapour pressure during measurements and to prevent contamination with mercury. Control readings were also taken with argon.

Results and Discussion.—Angular distribution curves were obtained for 4, 8, 13, 18, 23, 28, 38, 48, 58, 78, 118 and 143 volt electrons and are reproduced in figs. 1, 2, 3 and 4. The variation of intensity of scattering at 60° with electron energy is illustrated in fig. 5. This curve enables the angular distributions to be reduced to the same scale, a procedure rendered necessary by slight variations of vapour pressure and slit widths during the complete experiment.

---

* Bullard and Massey, 'Proc. Roy. Soc.,' A, vol. 130, p. 579 (1931).

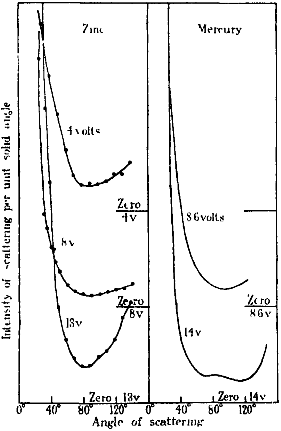

FIG. 1.—Angular distribution curves for 4, 8 and 13 volt electrons scattered by zinc vapour. For purposes of comparison corresponding curves for mercury vapour measured by Arnot are also shown.

The variation of the cross-section for elastic scattering between angles of 20° and 140° with electron energy, obtained by graphical integration of the angular distributions, is illustrated in fig. 6. This curve is compared with the corresponding curve obtained by Brode* for the total cross-section by direct measurement with a Ramsauer type of apparatus. Exact agreement of the two curves is not to be expected as Brode's cross-section includes scattering at all angles and also inelastic collisions However, the main features of Brode's curve are reproduced It is of interest to notice that the maximum in the cross-section in the region of 60 volts is to be expected from the theory of Allis

---

* 'Phys. Rev.,' vol. 35, p. 504 (1930).

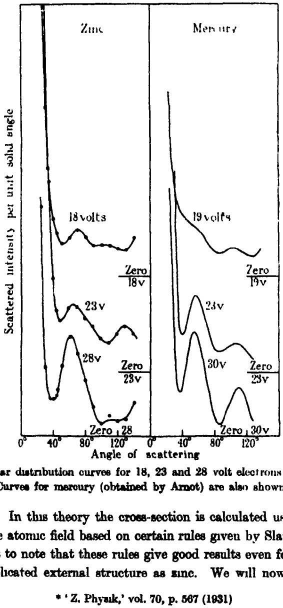

Fig 2.—Angular distribution curves for 18, 23 and 28 volt electrons scattered by zinc vapour. Curves for mercury (obtained by Arnot) are also shown

and Morse* In this theory the cross-section is calculated using a simplified model for the atomic field based on certain rules given by Slater† and it is of some interest to note that these rules give good results even for an atom with such a complicated external structure as zinc. We will now show that the

---

* 'Z. Physik,' vol. 70, p. 567 (1931)

† 'Phys Rev,' vol 36, p 57 (1930)

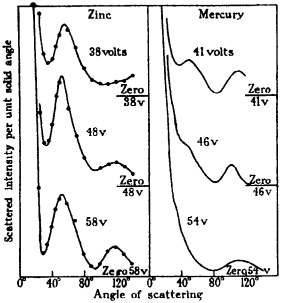

FIG. 3.—Angular distribution curves for 38, 48 and 58 volt electrons scattered by zinc vapour. Curves for mercury (obtained by Arnot) are also shown.

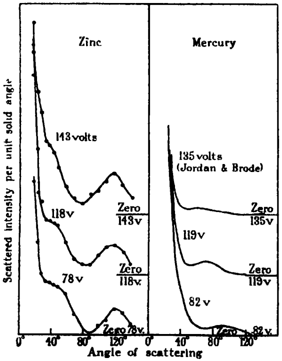

FIG. 4.—Angular distribution curves for 78, 118 and 143 volt electrons scattered by zinc vapour. Curves for mercury are also shown.

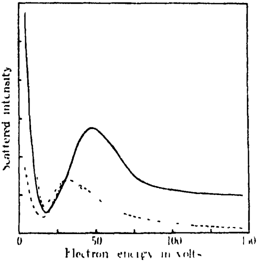

FIG. 5.—Variations of intensity of scattering at 60° with electron energy ——— zinc —·—·— cadmium, - - - - mercury (Arnot's observations).

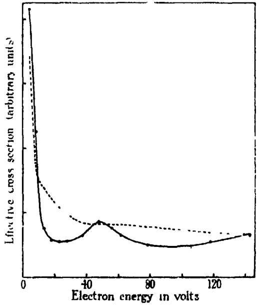

FIG. 6.—Variation of cross section of zinc atoms for electron scattering as a function of electron energy ——— obtained by integrating angular distributions between 20° and 140° - - - - total cross section observed by Brode.

angular distributions may also be calculated with fair accuracy using an atomic field based on a slight modification of these rules.

The number of electrons scattered per unit solid angle by an atomic field of potential $- \mathrm{V}(r)$ is given by*

$$\mathrm{I}(\theta) = \frac{1}{4k^2}\left|\Sigma_n \left(e^{2i\delta_n} - 1\right)(2n+1)\,\mathrm{P}_n(\cos\theta)\right|^2, \tag{1}$$

where $2\pi/k$ is equal to the wave-length of the electrons and the phases δ_n are defined in terms of the solutions of the equation

$$\frac{d^2u}{dr^2} + \left\{k^2 + \frac{8\pi^2m}{h^2}\mathrm{V} - \frac{n(n+1)}{r^2}\right\}u = 0 \tag{2}$$

The solution which is zero at the origin has the asymptotic form

$$u \sim \sin\left(kr - \tfrac{1}{2}\pi n + \delta_n\right) \tag{3}$$

It is not possible to solve (2) analytically for any atomic field and it is therefore necessary to resort either to direct numerical integration of the equations (2) for various values of n, or to an approximate method. Such a method has recently been introduced by Henneberg† and by Massey and Mohr ‡ According to this method we may take

$$\delta_n = \int_{r_n}^{\infty}\left\{k^2 + \frac{8\pi^2m}{h^2}\mathrm{V} - \frac{n(n+1)}{r^2}\right\}^{\frac{1}{2}} dr - \int_{e_n}^{\infty}\left\{k^2 - \frac{n(n+1)}{r^2}\right\}^{\frac{1}{2}} dr$$

where r_n, e_n are the greatest positive zeros of the respective integrands, provided δ_n is > 1 (that is to say, for small values of n) For large n such that $\delta_n < 0{\cdot}5$, we may use Born's approximation

$$\delta_n = \frac{\pi}{2}\,\frac{8\pi^2m}{h^2}\int_0^{\infty} r\mathrm{V}\left\{\mathrm{J}_{n+\frac{1}{2}}(kr)\right\}^2 dr$$

The phases for intermediate values of δ_n may then be obtained by interpolation This method has already been applied to the calculation of the scattering of 135, 480 and 800 volt electrons in mercury vapour by Henneberg (*loc cit*), good agreement with the curves observed by Arnot§ being obtained, and it is accurate provided the electron energy is not too low By comparison with the results of Holtsmark's exact numerical integrations for argon‖

---

* Faxen and Holtsmark, 'Z. Physik,' vol 45, p 307 (1927)

† 'Naturwiss,' vol 30, p. 561 (1932)

‡ 'Nature,' vol 130, p. 276 (1932).

§ 'Proc Roy. Soc,' A, vol 130, p. 655 (1931)

‖ 'Z Physik,' vol 55, p 437 (1929)

it was found that the method should give results of sufficient accuracy provided the electron energy is greater than 30 volts

It remains to determine the form to be used for V(r) for zinc. For $r < r_0$ where r_0 is the radius of the M shell of zinc given by Slater's rules the Fermi-Thomas* values for V were used For $r > r_0$ the Fermi-Thomas field is inaccurate while Slater's rules are not applicable to the N electrons of zinc as they do not predict the correct ionization potential The value of the effective nuclear charge in which the N electrons move was therefore adjusted to give this potential correctly. It was then found that the radius of the outer shell is 2·1 A. and the effective nuclear charge Z_{eff} acting on the N electrons is 3 8 With this value of Z_{eff} the potential of the atomic field given by Slater's rules agrees with that given by the Fermi-Thomas model at $r = r_0$ so the field for $r > r_0$ was obtained by smoothly extrapolating the Fermi-Thomas potential for $r = r_0$, to a value of zero at $r_0 = 2 \cdot 1$ A

The calculations were carried out for 30, 54 and 122 volt electrons and the comparison between observed and calculated curves is illustrated in fig 7 The comparison has been affected by adjusting the ordinates of the observed and calculated 30 volt curves so that the heights of the first maxima of the two are equal. It will be seen that the general agreement obtained is very satisfactory The chief discrepancy consists in an angular displacement between the two curves at small angles This is undoubtedly due to underestimation of the atomic field at large distances

A striking feature of the observations is the similarity of the curves obtained for zinc below 50 volts with those obtained for mercury vapour by Arnot (*loc cit.*) (see figs 1, 2, 3) The similarity between cadmium and mercury at all voltages investigated (up to 50 volts) has already been remarked in Paper I In that paper this similarity was shown to be a consequence of the similar electronic structure of the outer shells of the mercury and cadmium atoms and would be expected to persist to quite high energies of impact. With zinc it may be shown in a similar way that the resemblance should be apparent at low voltages, for which the scattering arises mainly from the outer portion of the atomic field, but should disappear when the electron energy becomes comparable with 100 volts This behaviour may be observed in figs. 3 and 4 For the lower voltages (less than 25 volts) the behaviour of mercury more closely resembles that of zinc than cadmium, as may be seen by comparsion of figs. 1 and 2 of this paper with figs. 1 and 2 of Paper I, and also by reference to fig 5 This result is to be expected from the values of the ionization potentials of the three atoms, that (10·4 volts) of mercury being more nearly equal to that of zinc (9·4 volts) than that (8·9 volts) of cadmium, and it has also been observed by Brode* in the absorbing cross-sections of the atoms for slow electrons. The curves given in this paper and in Paper I should make possible a more precise determination of the fields of the zinc and cadmium atoms at large

---

* 'Z Physik,' vol. 48, p. 73 (1928).

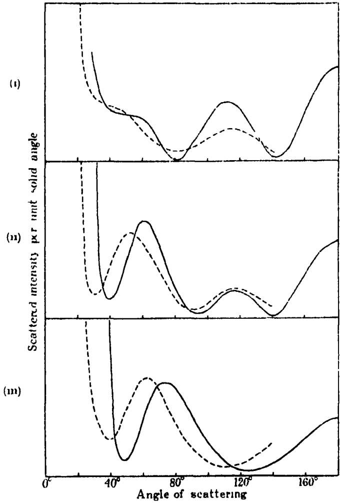

FIG 7 —Comparison of observed and calculated angular distribution of 30, 54 and 122 volt electrons elastically scattered by zinc atoms.

(i) ——— Calculated 122 volts, – – – – observed 118 volts (ii) ——— Calculated 54 volts, – – – – observed 48 volts (iii) ——— Calculated 30 volts, – – – – observed 28 volts distances. However, as the form of this field is most effective in determining the shape of the angular distribution curves for such low velocity electrons that the approximate method used in the above calculations is no longer accurate, no attempt has yet been made to carry out the necessarily lengthy calculations required

---

* 'Phys Rev,' vol 35, p 504 (1930)

It is a pleasure to express our thanks to Lord Rutherford and Dr J Chadwick for the interest they have taken in these experiments

Summary.

Measurements of the angular distributions of 4, 8, 13, 18, 23, 28, 38, 48, 58, 78, 118 and 143 volt electrons scattered elastically in zinc vapour are described The resulting curves are compared with theoretical curves calculated by the use of a modified Fermi-Thomas field for zinc and Faxèn and Holtsmark's theory of scattering, good agreement being obtained The relation of the scattering curves observed for zinc to those observed for cadmium and mercury is also discussed

---

The Exchange of Energy between Gas Atoms and Solid Surfaces
III.—*The Accommodation Coefficient of Neon.*

By J K Roberts, Ph D., Moseley Student of the Royal Society

(Communicated by Lord Rutherford, O.M , F R S —Received June 10, 1933)

In two earlier papers* experiments have been described on the measurement of the accommodation coefficient of helium with a tungsten surface free from films of adsorbed gas Similar experiments have now been carried out with neon.

The experimental technique was exactly the same as with helium and has been fully described in the second of the earlier papers The values of the accommodation coefficient of neon at 79°, 195°, and 295° K are given in the table together with the values for helium, and are plotted as a function of the temperature in fig. 1 The same wire was used as in the helium experiments so that the results for both gases will be equally affected by any roughness of the surface The results have been confirmed using a second wire

---

* Roberts, 'Proc Roy Soc,' A, vol. 129, p 146 (1930), vol 135, p. 192 (1932)

Temperature	Accommodation coefficient of neon	Accommodation coefficient of helium
°K		
295	0·07	0·057
195	0·08	0·046
79	0·08	0·025

The value 0·07 for neon at room temperature may be compared with the older values of about 0·6 obtained with ordinary surfaces covered with adsorbed films. Similar high values were obtained in the present experiments if the surface of the wire was not cleaned by flashing.

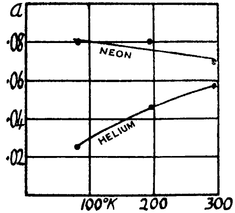

Fig. 1.

Comparison with Elastic Sphere Theory

Developing the earlier approximate methods of Jackson and of Zener, Jackson, and Mott* have given an accurate one dimensional theory of the interchange of energy between monatomic gas atoms and the atoms of a solid surface, assuming that the attractive forces between the solid and the gas atoms are negligibly small. If the potential energy due to repulsive forces of a gas and a solid atom separated by a distance r is given by $Ce^{-\lambda r}$, where C and λ are constants, the theory shows that the accommodation coefficient for gas and solid atoms of given masses depends on the value of λ and increases as λ increases.

---

* Jackson, 'Proc. Camb. Phil. Soc.,' vol 28, p 136 (1932); Zener, 'Phys. Rev.,' vol 37, p 557 (1931); vol. 40, pp 178, 335 (1932); Jackson and Mott, 'Proc. Roy. Soc.,' A, vol 137, p 703 (1932).

If the atoms behave as elastic spheres, the theory shows that the ratio of the accommodation coefficients at a given temperature of two monatomic gases with a given solid should be the same as the ratio of the atomic weights, that is, the accommodation coefficient of neon should be about five times that of helium. Experiment shows that at room temperature the ratio is only about 1·2.* We may therefore conclude that the atoms do not behave as elastic spheres.

The theory accounted satisfactorily for the type of temperature variation observed in helium, and the helium results alone suggested that the atoms do not behave as elastic spheres, but they were not quite conclusive on this point owing to the unknown factor of the roughness of the surface. Actually the values given by the theory for elastic spheres agreed reasonably with the experimental values for helium, but it must be remembered that the theory gives values for a plane surface, while the actual surface of any wire is almost certainly rough. The effect of this roughness is that an appreciable fraction of the molecules leaving the solid will strike it again in another place before finally escaping. The true value of the accommodation coefficient for a smooth surface will therefore always be less than the measured value. General considerations as to the likely appearance that a surface built up of micro-crystals would present to a gas molecule in its neighbourhood would lead us to expect a factor of about 1·5 or 2 for this effect, and, if we assume such a factor, the helium results do not agree with the theory for elastic spheres, but suggest that λ for helium and tungsten is about 4 or 6 $\times 10^{8}$ cm^{-1}.

Repulsive and Attractive Forces.

The interpretation of the neon results is complicated by the fact that the attractive force exerted by a tungsten surface on a neon atom at a given distance is much greater than that on a helium atom at the same distance. The presence of some such complicating factor is indicated immediately by a comparison of the curves for helium and neon in fig. 1, which shows that the temperature variation is quite different for the two gases. The difficulty in interpretation is that, while the theory given by Jackson and Mott for the case when attractive forces are absent is exact, only approximate methods have been developed for taking into account the effect of attractive forces In consequence of this no great reliance can be placed on the numerical values of the force constants obtained, but the comparison between theory and experiment carried out below shows that, if an accurate theory were available, the experimental results would enable us to determine the force constants within reasonably narrow limits

---

* We shall consider later the effect of attractive forces, and shall see that their effect is to increase the accommodation coefficient. Attractive forces will be more important for neon than for helium, so that for elastic spheres with attractive forces the ratio of the accommodation coefficient of neon to that of helium would be greater than five.

As a result of the attractive force the potential energy V of a gas atom at a distance x from the solid surface is given by a curve of the type shown in fig 2 The approximate theories of the effect of the attractive forces of Jackson and of Zener* both give the effect in terms of the quantity indicated in fig 2 by ϕ, which is a measure of the energy of adsorption Using Jackson and Mott's theory modified by Jackson's methods to take into account the effect of the attractive forces, the theoretical values† for the accommodation coefficient of neon shown in fig 3 are obtained (these values are *not* corrected for roughness) The curves for a given value of the repulsive force constant λ are all shown under each other, and the value of ϕ corresponding to

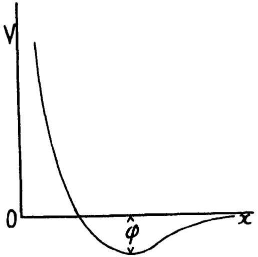

FIG 2

---

[*] Jackson, 'Proc Camb Phil Soc,' vol 28, p 156 (1932), see also Jackson and Mott, *loc cit*, p 713, Zener, 'Proc. Camb Phil. Soc,' vol. 29, p 136 (1933).

[†] The only transitions of the oscillator (solid) that have been included in the calculations are those in which the quantum number changes by one, but Jackson and Mott have shown that the errors introduced by neglecting other transitions are small

each curve is written on the curve. ϕ is measured in calories per gram molecule

It will be seen from the figure that, if we assume a roughness factor of 1·5, a repulsive force constant $\lambda = 2 \cdot 07\ 10^8$ cm^{-1} and an energy of adsorption of 2460 calories per gram molecule would give an almost constant observed accommodation coefficient of 0·075 which agrees with what is obtained experimentally For higher values of λ than this the theoretical curves, when a value of ϕ is taken sufficient to give a theoretical result of the right order at room temperature, all fall off too rapidly with temperature The theoretical results must give both the correct value for the accommodation coefficient and the correct shape for the curve showing the temperature variation These two conditions enable both λ and ϕ to be fixed within limits

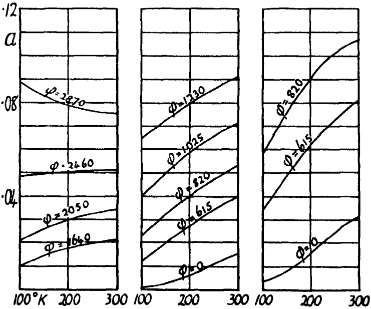

(a) (b) (c)

FIG 3—(a) $\lambda = 2\ 07\ 10^8$ cm^{-1}, (b) $\lambda = 3\ 30\ 10^8$ cm^{-1}, (c) $\lambda = 4\ 13\ 10^8$ cm^{-1}

The above considerations will also explain the rise in the accommodation coefficient of hydrogen as the temperature falls below room temperature which has been observed in the experiments of Blodgett and Langmuir and of Rowley and Bonhoeffer,[*] but the detailed application of the theory to a diatomic gas would be difficult.

[*] Blodgett and Langmuir, 'Phys Rev,' vol 40, p 78 (1932), Rowley and Bonhoeffer 'Z. phys Chem.,' B, vol 21, p 84 (1933)

Upper Limit to Repulsive Force Constant

The curve in fig 4 shows the value of the accommodation coefficient for neon and tungsten at 300° K for different values of λ obtained by neglecting the attractive force altogether, so that the accurate theory of Jackson and Mott can be used * We have seen that the effect of the attractive force is to increase the accommodation coefficient above that which would be obtained if only the repulsive force were present An upper limit to the value of λ can therefore be obtained by finding the point on the curve which corresponds to the measured value of the accommodation coefficient at room temperature If we take the measured value 0 07, the value of λ from the curve is 5 9 10^8 cm $^{-1}$,

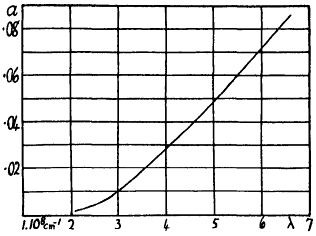

FIG 4

and, if we assume a roughness factor of about 1·5, so that the measured value for a smooth surface would be about 0 047, the value of λ from the curve is about 5 10^8 cm $^{-1}$ We therefore conclude that for neon and tungsten the value of the repulsive force constant λ must be less than 5 or 6 10^8 cm.$^{-1}$

In conclusion I should like to thank Lord Rutherford and Professor R H. Fowler for their continued interest in the progress of this work

Summary

The accommodation coefficient of neon with a tungsten surface free from adsorbed films has been measured and found to be 0·07 at 295° K and to

---

* It should be mentioned that as $\lambda \to \infty$ the curve would approach a constant value of 0 25 for the accommodation coefficient.

vary very little with temperature down to 79° K The value obtained with an ordinary surface covered with adsorbed films is 0 6.

From the accurate one dimensional theory of Jackson and Mott and these results it is possible to draw the following conclusions —

(1) From the ratio of the accommodation coefficients at room temperature of helium and neon the repulsive forces between tungsten atoms and the gas atoms are not similar to the forces between elastic spheres.

(2) If the potential energy due to the repulsive force between a tungsten atom in the solid and a neon atom at a distance r is given by $Ce^{-\lambda r}$, where C and λ are constants, λ is not greater than 5 or 6 $\times 10^8$ cm^{-1}

The experimental results are compared with an approximate theory taking into account the attraction between the solid and the gas atoms and it is shown that the results enable us to choose within limits the repulsive and attractive force constants, and it is pointed out that we need a more accurate theory of the effect of attractive forces in order to obtain from the experimental results reliable values for these constants

The Kinetics of the Reaction between Hydrogen and Nitrous Oxide —I

By H W. MELVILLE

(Communicated by J Kendall, F R S —Received June 10, 1933)

Until about five years ago, the theoretical treatment of the mechanism of the oxidation of simple molecules had been comparatively neglected. Prior to this, however, considerable progress had been made in the study of the kinetics of thermal and photochemical gas reactions That knowledge has now been successfully applied and extended to solve some of the major problems in combustion chemistry, and thereby has given rise to the development of the theory of thermal chain reactions Hitherto, the investigation of these reactions has been confined almost entirely to oxidations by molecular oxygen * It is known,† however, that many gases ignite in nitrous oxide at about the same temperature as they do in oxygen, and it might be anticipated that here, too, a chain process is in operation. The object of studying the interaction of hydrogen and nitrous oxide was to determine whether it is a chain reaction, and if so, to make a detailed analysis of its mechanism by the kinetic method

---

* Exceptions are the Cl_2, Br_2 and HBr sensitized decomposition of O_3, Bodenstein, Padelt and Schumacher, 'Z. phys Chem.,' B, vol 5, p 209 (1929), Lewis and Feitknecht, 'J Amer. Chem. Soc.,' vol 53, p 2910, p 3565 (1931)

† Dixon and Higgins, 'Proc Manc. Phil. Soc ,' vol. 71, p. 17 (1927)

One of the first criteria in looking for the possibility of the propagation of chains in a gaseous mixture is that the reaction must be exothermic This condition is amply fulfilled in the present instance, for 75 k cal are liberated per mole of water formed Indeed, the reaction is even more exothermic than the formation of one mole of water from hydrogen and oxygen, when only 50 k cal are evolved. This greater exothermicity is due to the fact that 45 k.cal. are required to dissociate 1 mole of N_2O into N_2 and O, whereas the production of 1 mole of O atoms from O_2 requires about 60 k cal.

There was another important reason for choosing N_2O as one of the participants in the reaction Recently, the kinetics of the decomposition have been very thoroughly worked out,* and it is now thought probable that the first step in the thermal decomposition is the formation of a nitrogen molecule and an oxygen atom from an excited molecule, the necessary energy of activation being derived from a collision between molecules of a sufficiently high energy content In addition, experiments have shown what effect inert gases exert on the rate of production of these activated molecules

Several other interesting points arise out of the use of the N_2O molecule, for example, there is only one oxygen atom available and the nitrogen molecule may, in suitable circumstances, play the part of an energy scavenger. Hydrogen was chosen as the other reactant for the reason that since the kinetics of the H_2–O_2 reaction have been worked out in some detail, they might prove helpful in elucidating the mechanism of the H_2–N_2O reaction It is hoped, however to extend the experiments to the reactions of other simple molecules with nitrous oxide.

The H_2–N_2O reaction has been studied on the surface of a platinum filament by Cassel and Gluckauf† at low pressures and with an excess of hydrogen, under these conditions there is a complete change in the mechanism as the temperature of the catalyst is increased beyond 775° C Similarly Hinshelwood‡ found at high pressures that the kinetics of the reaction differed depending upon whether the N_2O or the H_2 were in excess The possible bearing of these observations on the results to be described below will be discussed later.

---

* Volmer and Kummerow, 'Z phys Chem ,' B, vol 9, p 141 (1930), Nagasako and Volmer, *ibid*, vol. 10, p. 414 (1930), vol 11, p 420 (1931), Volmer and Froelich, *ibid*, vol. 19, pp 85, 89 (1932), Musgrave and Hinshelwood, 'Proc. Roy. Soc ,' A, vol 135, p. 23 (1932), *ibid.*, vol 137, p. 25 (1932).

† 'Z phys Chem.,' B, vol. 19, p 47 (1932).

‡ 'Proc Roy. Soc.,' A, vol. 106, p 292 (1924)

When hydrogen was sealed up with nitrous oxide at about atmospheric pressure in a Jena glass bulb, Hinshelwood* noticed that the rate of formation of water was no faster than the rate of decomposition of nitrous oxide at about 700° C It was suggested that the first stage in the reaction was the decomposition of nitrous oxide into nitrogen and oxygen molecules, the oxygen thereafter being quickly removed by combination with hydrogen, since the H_2–O_2 reaction is very rapid at this temperature The net rate is determined by the slowest process, namely, the decomposition of the nitrous oxide It is to be observed, however, that at the lower temperatures used in these experiments, the rate of H_2O formation was somewhat faster than that of the decomposition of N_2O

In sharp disagreement with these experiments are the results of Dixon and Higgins (*loc cit*), who found that a jet of hydrogen inflamed spontaneously in an atmosphere of nitrous oxide at about 550° C, or 150° below the temperature of Hinshelwood's experiments, where the rate of decomposition of N_2O is very small The temperature of ignition depended on pressure and was preceded by an induction period In this latter dynamic method the composition of the mixture could, of course, vary within wide limits It is one of the objects of this paper to determine, if possible, the reason for this discrepancy

The question of the mechanism of this reaction can be most logically approached by considering the possible ways in which it might occur -

(1) Heterogeneous reaction, exclusively on the walls of the reaction tube

(2) Homogeneous bimolecular reaction, $H_2 + N_2O \rightarrow H_2O + N_2$

(3) Decomposition of N_2O followed by rapid oxidation of H_2, *i e*,

$$N_2O + N_2O = 2N_2 + O_2$$
$$2H_2 + O_2 = 2H_2O$$

(4) Chain reaction various mechanisms

While the possible types of reaction have been separately classed above, the chain process may include 1, 2 and 3 since (*a*) initiation of the chain may be homogeneous or heterogeneous, (*b*) similarly, termination may occur in the gas or at the walls, and (*c*) propagation probably involves a series of bimolecular encounters.

---

* 'Proc Roy. Soc.,' A, vol 106, p. 292 (1924)

The first point to be settled about this reaction is, therefore, the class to which it belongs, the second, by extending the experiments in suitable directions, to determine, as far as the present method will allow, the nature of the individual processes leading to the final products, which appear to be mainly N_2 and H_2O

Experimental

Consideration of the equation $H_2 + N_2O = N_2 + H_2O$ shows at once that there is no pressure change during reaction, and therefore it would appear that the convenient and sensitive manometric method could not be employed for measuring the velocity By withdrawal of the water by absorption with P_2O_5 or $CaCl_2$, the resultant decrease in pressure may be used as a measure of the extent of reaction

The apparatus consisted of a silica reaction bulb placed in an electric furnace The bulb was provided with a wide neck (1 7 cm diameter) and a silica-glass ground joint so that a porcelain boat containing P_2O_5 or $CaCl_2$ could be inserted in the neck just outside the mouth of the furnace The volume of the "cold" parts of the reaction bulb system was reduced to less than 5% of the total by packing with glass beads In order to ensure rapid and thorough mixing of the reactants, the gases were lead from the reservoirs directly into the middle of the bulb by a silica tube 3 mm in diameter as is shown in fig. 1. Neglect of these precautions led to the variation of the kinetics with the order of addition of the gases to the reaction tube owing to the time required for interdiffusion. Such a variation was exaggerated to some extent for, as will be seen below, the rate of reaction is nearly independent of the concentration of hydrogen and directly dependent on that of nitrous oxide. In some bulbs there was fused to the neck a wide side tube which could be immersed in a CO_2/ether bath at − 80° C. The bulb was connected to a mercury condensation pump for

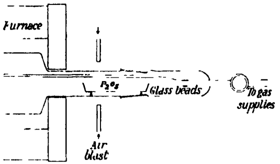

FIG 1

evacuation and to a number of gas reservoirs A capillary mercury manometer served as a pressure gauge The temperature of the furnace was manually controlled to within 1° C in the range 500°–800° C, using a Pt/Pt-Rh thermocouple and millivoltmeter Nitrous oxide was obtained from a cylinder and contained not more than 0·2% air. This gas was first dried by slow passage over P_2O_5, then collected in a liquid air trap and fractionated. The hydrogen was electrolytic and was freed from traces of oxygen by palladized asbestos and dried with P_2O_5. Argon and nitrogen were freed from traces of oxygen by passing over a tungsten filament at 2000° C

The absorbing agent has to be situated just outside the furnace and therefore the water vapour requires a short time to diffuse to the $CaCl_2$. Such a time lag between production and removal leads to the establishment of a "stationary" concentration of water vapour in the reaction tube.

The first problem to be solved was the determination of this stationary concentration, and the second, to find if the variation in p_{H_2O}, as must inevitably occur during the progress of the reaction, had any measurable effect on the kinetics A reaction tube 10 cm. long and 2·5 cm. in diameter was fitted with a side tube 7 cm. from the centre of the reaction tube itself. 100 mm. of a 1 . 1 H_2 N_2O mixture were passed into the tube and the reaction allowed to go for several minutes at 660° C The water was then condensed out by cooling the side tube and the pressure of the residual H_2-N_2O-N_2 mixture determined. A similar experiment was then made except that the side tube was kept cool from the start After making due allowance for the cooling of the side tube on the pressure of the non-condensable gases, it was found that 13·5 mm. H_2O were produced in 6 min. when H_2O was allowed to accumulate while 16·5 mm. were obtained if H_2O was removed continuously Water vapour is therefore an inhibitor at these pressures Similar results were obtained with a 7 cm. bulb, in these experiments the gases were removed for analysis by a Topler pump. The rate of reaction, on allowing the H_2O to accumulate, was smaller than that in which the H_2O was removed at intervals and the gas mixture readmitted to the reaction bulb

An approximate estimate of the stationary concentration may be made in the following way. If R is the rate of reaction (millimetres per second) and T the time in seconds required for an H_2O molecule to diffuse to the absorbing agent, the pressure of H_2O (p_{H_2O}) in millimetres will be given by

$$R \, . \, T = p_{H_2O}.$$

T can be calculated from the Einstein equation $x^2 = 2D\ T$ where x is the distance the molecule diffuses through a gas of diffusion coefficient D. Taking the above example, D for 100 mm of H_2 N_2O at 1000° K is about 12 cm ^{2}/sec. The temperature of the gas from the centre of the bulb to the H_2O absorbent is not uniformly at 1000° K and hence D may be reduced to 10 cm ^{2}/sec. Although the $CaCl_2$ boat was 5 cm. from the centre of the bulb, x will be assumed to have a value of 7 cm as the time for diffusion is proportional to the square of the distance On substituting $T = 2 \cdot 5$ sec, $R = 16 \cdot 5$ mm /360 sec, p_{H_2O} is 0·11 mm, which is insufficient to retard the reaction to any appreciable extent or to affect the manometer readings In the experiments to be described below, the rate did not exceed 0·2 mm /sec, nor did the pressure exceed 300 mm., in which circumstances p_{H_2O} would be 1 mm and the retardation would not exceed 2% The manometer would therefore indicate the pressure of H_2, N_2O and N_2, in the most adverse case, to within 1 mm. or 0·3%, which is within the limits of experimental error

To make absolutely certain that the variation in this small stationary concentration of H_2O did not influence the reaction, a bulb was set up with a somewhat longer neck so that the $CaCl_2$ boat could be situated at a distance from the mouth of the furnace A run was then made with the boat at the furnace (position I) and a second run with the boat placed 5 cm from its previous position (position II) In the second position the molecules would therefore require to diffuse a further 5 cm. through a *cold* gas mixture; the time of diffusion would increase about 10 times and with it the value of p_{H_2O} As can be seen from an examination of Δp (pressure decrease) in Table I, no diminution occurs in the rate with the boat in the second position. The

Table I

Temperature 655° C 2·5 cm diameter reaction tube

Time	Position I			Position I.			Position II.		
	p_{H_2}	p_{total}	Δp	p_{H_2}	p_{total}	Δp.	p_{H_2}	p_{total}	Δp
min	mm	mm							
0	51·0	102·0	0	52·5	103·5	0	52·0	105·0	0
1	—	100·5	1·5	-	102·0	1·5	—	103·5	1·5
2	-	97·0	5·0	-	98·5	5·0	—	100·5	4·5
3	—	93·5	8·5	—	95·5	8·0	—	96·5	7·5
4	—	90·5	11·5		92·5	11·0	-	93·0	12·0
6	-	88·5	16·5		87·5	16·0	—	88·5	16·5
8	—	81·5	20·5	—	84·5	19·0	—	84·5	20·5
10		79·0	23·0	—	81·5	22·0	—	81·0	24·0

reaction exhibits an induction period which is characteristic if the hydrogen is admitted to the reaction tube before the nitrous oxide.* Experiments were also made to see if any difference in results was obtained by using P_2O_5 or $CaCl_2$ as H_2O absorbent, but no variation in rate could be detected.

The method is therefore suitable for a study of the reaction provided, (*a*) the total pressure of the mixture does not exceed half an atmosphere, (*b*) the rate does not exceed 0·2 mm./sec., (*c*) the absorbing agent is close to the reaction bulb.

Results

Comparison of Rate of Reaction with the Decomposition Rate of N_2O.—In view of the observation of Hinshelwood† that the rate of H_2O formation was no faster than the rate of decomposition of N_2O it was of importance to determine if this occurred in the present experiment. In Table II the first experiment is a run with a 1 : 1 H_2-N_2O mixture and the second a decomposition run for N_2O at a somewhat higher pressure.

Table II

Temperature 645° C. 5 cm. tube

H_2-N_2O			N_2O alone		
t	*p*	*Δp*	*t*	*p*	*Δp*
0	97·0	–	0	295·4	
0·5	93·2	3·8	5	298·0	2·4
1·0	88·8	8·2	10	300·2	4·8
1·5	84·8	12·2	15	302·4	7·0
2	81·6	15·4	20	305·0	9·6
3	77·0	20·0	25	307·4	12·0
4	73·4	23·6	30	309·0	13·6
5	71·2	25·8	35	311·4	16·0
6	68·8	28·2			
7	66·2	30·8			

On reducing the rate of decomposition of N_2O to 48·5 mm., assuming a bimolecular reaction in this pressure range, the initial rate of decomposition would be 0·026 mm./min. compared with 8·5 mm./min. of the H_2-N_2O reaction; the latter is 325 times faster than the former. In a long spiral of silica tubing, 0·4 cm. in bore, at 630°, the rate of the H_2–N_2O reaction was

---

* This is caused by the long neck, since the nitrous oxide requires a short time to diffuse into the reaction zone.

† 'Proc. Roy. Soc.,' A, vol. 106, p. 292 (1924).

1·5 mm /min., while that for N_2O was 0·017, the ratio being 90 Using a 7 cm bulb at the same temperature, the respective values were 22 0 and 0 044 mm /min or 500 1 (The smaller rate of N_2O decomposition in the spiral was due to part of its being close to the mouth of the furnace and therefore at a somewhat lower temperature, and to the volume of the tubing leading to the Topler pump being comparable with that of the spiral itself) It will be observed that the rate of the H_2-N_2O reaction relative to that of N_2O is rather greater in wider vessels As the N_2O reaction is homogeneous at these pressures, the increase must be due wholly to the H_2-N_2O reaction

Packing Experiments —The effect of packing a reaction tube with the same material of which it is made provides a great deal of information about the nature of a gas reaction If packing increases the rate, the reaction is predominantly heterogeneous, if there is no change in velocity, the reaction is probably homogeneous On the other hand, if packing retards the rate, it may be assumed that the process involves some kind of chain mechanism, since inhibition by surfaces has been shown to be a definite characteristic of chain reactions

A restriction is placed upon the method of carrying out the packing, for the diffusion of H_2O out of the tube must not be impeded Silica tubes 5 cm long and 1 cm. and 0 7 cm external and internal diameter were employed, their axes being set parallel to that of the reaction tube itself On packing a 5 cm. diameter tube, 10 cm. long, half-full with 20 of these tubes and so increasing the silica surface about 3·5 times, the results in Table III were obtained In experiment 225, the tube was empty, in 226 and 230 packed, and 231 empty

Table III

Temperature 660° 1 1 mixture

t	225		226		230		231	
	p	Δp	p	Δp	p	Δp	p	Δp.
0	101 0	—	103 2	—	102 0	—	100 5	—
0 5	97 0	4 0	—	—	—	—	97 0	3 5
1	93 0	8 0	100 5	2 8	99 0	3 0	93 0	7 5
2	87 0	14 0	96 2	7 0	94 5	7 5	86 0	14 5
3	82 5	18 5	92 5	10 7	90 5	11 5	80·0	20 5
4	77 5	23 5	90 2	13 0	87 0	15 0	75 5	25 0
5	—	—	—	—	—	—	72 0	28 5
6	72·5	28 5	85 8	17 5	83 0	19 0	—	—
8	69 0	32 0	82 0	21 2	78 5	23 5	—	—

again. Additional experiments (Table IV) were also made with a 2·5 cm tube packed completely with similar tubes thus increasing the surface about twice. In both tubes, there is a most marked inhibiting effect on packing the tube. In experiment 246 the rate is reduced to 0·4 of its value in 243 and 247. The method of packing in this case really amounted to reducing the diameter to 0·7 cm. Consequently, if it is assumed, according to the chain theory, that the rate is proportional to the square of the diameter the rate should decrease 13-fold. The reason for this wide discrepancy will be discussed below.

Table IV

t	243 Empty		246 Packed		247 Empty	
	p	Δp	p	Δp	p	Δp
0	102·5	—	103·0	—	102·0	—
1	95·0	7·5	100·0	3·0	94·0	8·0
2	88·0	15·5	98·0	5·0	88·0	14·0
3	83·0	19·5	95·5	8·5	83·0	19·0
4	80·0	22·5	93·0	10·0	78·5	23·5
6	72·5	30·0	87·0	16·0	72·0	30·0
8	69·5	33·0	84·5	18·5	68·0	34·0
10	67·0	35·0	82·5	20·5	66·0	36·0

The results could be reproduced within about 10% over a period of several weeks; in individual series, better agreement could be obtained. It may be added, however, that on first putting into use a tube which had not been employed for some time, the reaction velocity for the first run was consistently smaller (in some experiments as much as 50%) than that of the next run, after which it remained sensibly constant, although the tube was baked out in a vacuum of 10^{-5} mm.

Effect of Total Pressure.—A 1 : 1 mixture was employed for these experiments and the total pressure did not exceed 300 mm. as is required by the calculations made above. The initial rate (R) of reaction is nearly proportional to the pressure (p) as is shown in Table V by the constancy of the value of R/p. Unimolecular constants (k) were therefore calculated for each run; the figures obtained are reasonably constant, at least during the first half of the reaction. When making these calculations, a slight correction was applied since, if the $\Delta p - t$ (Δp = pressure decrease, t = time) curves are plotted the reaction exhibits a slight induction period of about 5 sec. The times used to calculate k were therefore reduced by 0·1 min. Similarly R was

Table V

Temperature 628° 5 cm tube

138				139			
t	p	Δp	k (sec^{-1} × 10^{3})	t	p	Δp	k
0	254 0	—	—	0	200 0	—	-
0 5	251 0	3 0	—	0 5	197 6	2 4	—
1 0	247 0	7 0	1 04	1 0	194 2	5 8	1 11
1 5	242 8	11 2	1 30	2 0	187 2	12 8	1 22
2	238 0	16 0	1 19	3	181 0	19 0	1 22
3	229 6	24 4	1 21	4	171 4	25 6	1 27
4	221 4	32 6	1 28	5	168 6	31 4	1 30
5	214 2	39 8	1 29	6	163 4	36 6	1 25
6	207 2	46 8	1 31	8	155 0	45 0	1 27
8	196 4	57 6	1 28	10	148 4	51 0	1 23
	R 8 5 mm /min				6 6		
	R/p 0 034				0 033		

140.				134			
t	p	Δp	k	t	p	Δp	k
0	148 0	—	-	0	99 4	—	—
0 5	146 2	1 8	–	1	96 0	3 4	—
1 0	143 2	4 8	1 28	2	92 4	7 0	1 30
1 5	140 4	7 4	1 27	3	89 4	10 0	1 38
2	137 8	10 2	1.22	4	86 8	12 6	1 25
3	132 6	15 4	1 32	5	84 4	15 0	1 23
4	128 0	20 0	1 30	6	83 0	16 4	1 14
5	124 0	24 0	1 34	8	79 8	19 6	1 07
6	120 8	27 2	1 30	10	77 4	22 0	0 95
8	115 0	33 0	1 30	12	76 0	23 4	0 90
10	112 0	36 0	1 13				
	R 5 4				3 4		
	R/p 0 037				0 034		

163			
t	p	Δp	k
0	51 0	—	—
1	49 0	2 0	1 33
2	46 8	4 2	1 40
3	45 0	6 0	1 49
4	43 0	8 0	1 57
5	41 8	9 2	1 50
6	41 0	10 0	1·39
8	39 6	11 4	1 24
10	30 2	12 8	1 17
	R 2 2		
	R/p 0 043		

obtained by measuring the slope of the tangent to the $\Delta p - t$ curve extrapolated back to $\Delta p = 0$.

Effect of Nitrous Oxide and of Hydrogen.—In order to determine the effect of the gases separately, the following experiments were made (*a*) p_{H_2} varying from 25–200 mm., for $p_{N_2O} = 50$ and for $p_{N_2O} = 200$ (Tables VI and VII); (*b*) p_{N_2O} varying from 25–150 mm. for $p_{H_2} = 50$ and for 150 mm., Table VIII and fig. 4, respectively. Fig. 2 shows how the initial rate varies with hydrogen pressure. When p_{N_2O} is 50 mm., there is only a small increase from $p_{H_2} = 25$ to 50, and thereafter R is very nearly constant. On the other hand, if $p_{N_2O} =$ 200, the rate increases quite rapidly to a maximum which is reached at a higher value of p_{H_2}, viz., 100 mm.

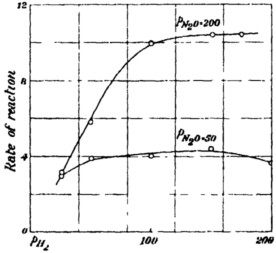

Fig. 2

In fig. 3 it is observed that R is almost proportional to p_{N_2O} except that at higher pressures there is a tendency for the R — p_{N_2O} curve to bend over. That the results for the 1 : 1 mixture conform closely to a unimolecular equation is thus mainly due to the nitrous oxide. In Tables VI and VII, the value of k has been calculated on the assumption that the kinetics of the reaction are given accurately by the equation $-dp_{N_2O}/dt = kp_{N_2O}$. In accordance with the effect of H_2 when p_{N_2O} is 200 mm. (fig. 3), it will be seen that in Table IV the value of k decreases rapidly in runs 142 and 143, whereas in 144–146 the decrease is less marked. Further, the initial value of k increases until p_{H_2} reaches 100 mm. and then remains constant. When p_{N_2O} is small as in Table VII, the effect of p_{H_2} is also small and k remains fairly constant in an individual run and throughout the series.

Effect of Nitrogen and of Argon.—Since the value of k in Table V does not change during the course of the reaction, nitrogen must have practically no influence on the rate Separate experiments were, however, made with nitrogen and with argon in order to confirm this supposition As the results in Table IX demonstrate, no measurable effect could be detected. The absence of inhibition incidently provides evidence for the validity of the method of observation, for although the inert gas impedes the diffusion of H_2O from the

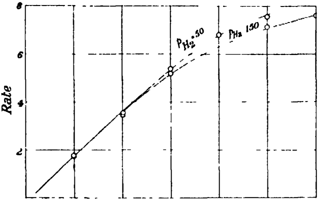

Fig 3

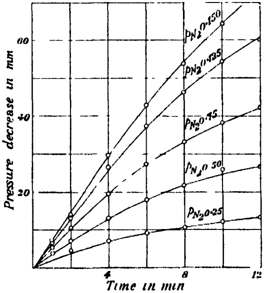

Fig 4

Table VI

Effect of p_{H_2} (p_{N_2O} = 200 mm.) 615° 5 cm. tube

	142			143		
	p_{H_2} 25 0, p_{N_2O} 199 4			p_{H_2} 50 0, p_{N_2O} 201 8		
t	p	Δp	k	p	Δp	k
0	224 6	–	—	251 8	—	–
1	221 6	3 0	2 81	246 4	5 4	5 28
2	218 0	6 6	2 91	240 0	11 8	5 75
3	224 0	10 6	3 11	233 0	18 8	5 86
4	212 0	12 6	2 77	228 0	23 8	5 53
5	209 8	14 8	2 66	223 4	28 4	5 32
6	—	—	-	220 2	31 6	4 93
7	206 4	18 2	2 33	—	—	—
8	205 2	19 4	2 14	215 2	36 6	4 36
10	204 0	20 6	1 82	212 2	39 6	3 75
12	203 2	21 4	1 61	210 4	41 6	3 20

	144			145		
	p_{H_2} 99 4, p_{N_2O} 202 2			p_{H_2} 150 8, p_{N_2O} 202 2		
t	p	Δp	k	p	Δp	k
0	301 6	—	—	351 0	—	—
1 0	294 2	7 4	8 88	344 2	6 9	—
1·5	289 0	12 6	8 92	339 0	12 0	8 43
2 0	283 2	18 4	9 08	334 2	16 8	8·52
2 5	277 4	24 2	9 73	328 8	22 2	8 78
3 0	271 6	30 0	9 42	323 8	27 2	8 88
4 0	261 0	40 6	10 20	314 0	37 0	9 08
5 0	253 0	48 6	9 75	304 8	46 2	9 18
6 0	245 0	56 6	9 67	297 0	54 0	9 07
7 0	239 2	62 4	9 16	289 0	62 0	9 10
8 0	234 0	67 6	8 31	281 2	69 8	9 14
10 0	227 2	74 4	7 88	269 2	81 8	8 95

	146		
	p_{H_2} 178 4, p_{N_2O} 200 8.		
t	p	p	k.
0	379 2	—	—
1 0	371 8	7 4	—
1 5	367 2	12 0	8 54
2 0	361 2	18 0	9 25
2 5	356 6	22 6	9 07
3	350 0	29 2	9 68
4	341 0	38 2	9 51
5	331 4	47 8	9 62
6	322 8	56 4	9 63
7	314 0	65 2	9·77
8	307 0	72 2	9 67
10	288 6	85 6	9·69

Table VII.

	129.			130.			131		
	p_{N_2O} 50 0, p_{H_2} 202 0			p_{N_2O} 50 6, p_{H_2} 150 0.			p_{N_2O} 50 0, p_{H_2} 100 2		
t.	*p.*	*Δp.*	*k.*	*p*	*Δp*	*k.*	*p*	*Δp*	*k*
0	252·0	—	—	200 8	—	—	150 2	—	—
1	248 4	3 6	1 37	196 6	4 2	1 62	144 6	5 6	1 95
2	244 8	7 2	1 35	192 4	8 4	1 58	141 2	9 0	1 74
3	241 8	10 8	1 40	189 0	11 8	1 53	138 0	12 2	1 60
4	238 0	14 0	1·40	186 0	14 8	1 47	135 0	15 2	1 54
6	231 8	20 2	1 45	181 4	19 4	1 36	130 4	19 8	1 42
8	227 8	24 2	1 39	178 0	22 8	1 36	127 0	23 2	1 31
10	223 8	28 2	1 36	175 2	25 6	1 17	124 4	25 8	1 21
12	—	—	—	173 2	27 8	1 10	122 8	27 4	1 11

	132.			133		
	p_{N_2O} 50 6, p_{H_2} 50 4			p_{N_2O} 50 0, p_{H_2} 25 0.		
t.	*p*	*Δp*	*k*	*p*	*Δp*	*k*
0	101 0	—	—	75 0	—	—
1	97 2	3 8	1 34	72 4	2 6	0 98
2	93 2	7 8	1 45	69 0	6 0	1 11
3	90 4	10 6	1 33	66 6	8 4	1 06
4	87 6	13 4	1 31	64 0	11 0	1 06
6	83 8	17 2	1 17	60 0	15 0	1 01
8	80 6	20 4	1 19	58 0	17 0	0 88
10	78 4	22 6	1 00	55 4	19 6	0 84
12	76 4	24 6	0 93	54 0	21 0	0 76

Table VIII.

Effect of p_{N_2O} (p_{H_2} = 50 mm). 615°.

	147.		148.		153	
	p_{H_2} 50 0, p_{N_2O} 25 2.		p_{H_2} 50 2, p_{N_2O} 49 8.		p_{H_2} 50 4, p_{N_2O} 75 2	
t.	*p.*	*Δp*	*p*	*Δp*	*p.*	*Δp*
0	75 2	—	100 0	—	125 2	—
1	74 2	1 0	97 0	3 0	121·4	3 8
2	72 4	2 8	93 6	6 4	115 8	9 4
3	71 2	4 0	90 0	10 0	110 2	15 0
4	69 4	5·8	86 2	13 8	106·0	19 2
5	68·0	7 2	84 0	16 0	101·8	23·4
6	66·8	8 4	81 4	18 6	97·6	27 6
8	65 0	10 2	78 0	22·0	91·2	34·0
10	63·2	12 0	75·0	25 0	87 0	38·2
12	62·0	13 2	73·2	26 8	83·4	41·8

Table VIII—(continued)

	149		152	
	p_{H_2} 50·4, p_{N_2O} 100·6		p_{H_2} 50·2, p_{N_2O} 124·8	
t.	*p*	*Δp*	*p*	*Δp*
0	151·0	—	174·8	—
1	146·0	5·0	169·0	5·8
2	139·2	11·8	161·4	13·4
3	131·2	19·8	154·2	20·6
4	126·4	24·6	147·8	27·0
5	120·8	30·2	142·6	32·2
6	116·2	34·8	139·0	35·8
8	110·0	41·0	134·8	40·0
10	107·0	44·0	132·2	42·6
12	105·4	45·6		

Table IX

Effect of N_2 615°. 1 . 1 Mixture.

p_{mix} p_{N_2}	100·2 0	99·8 90·0	99·6 50·2	100·2 25·8
t	*Δp*	*Δp*	*Δp*	*Δp*
1	3·2	3·0	3·2	3·4
2	8·0	6·8	7·4	7·4
3	11·4	9·8	11·8	11·2
4	15·0	13·0	14·2	14·2
5	17·2	15·6	16·8	17·2
6	19·4	17·8	19·0	19·6
8	23·0	20·8	22·8	23·0
10	25·4	23·6	25·6	25·8
12	27·4	25·8	—	27·8

Effect of Argon 615°. 1 : 1 Mixture.

p_{mix} p_A	99·4 —	98·8 152·2	101·6 80·4	100·4 40·0
t.	*Δp*	*Δp*.	*Δp*	*Δp*
1	3·4	2·8	3·0	3·4
2	7·0	6·0	7·2	7·0
3	10·0	9·0	12·2	10·2
4	12·6	11·6	14·8	13·0
5	15·0	14·6	16·2	15·4
6	16·4	16·2	18·8	17·4
8	19·6	19·4	22·0	20·4
10	22·0	22·0	25·0	23·0
12	23·4	24·0	27·0	—

reaction zone to the P_2O_5 and so increases the stationary concentration of H_2O, the increase is not sufficient to retard the reaction appreciably. This is to be expected from the rough calculations made previously

Temperature Coefficient.—It has been shown in Table II that the rate of the H_2–N_2O reaction at 645° is considerably faster than the rate of decomposition of the nitrous oxide. The relative rates of the two reactions would only remain the same at different temperatures if their temperature coefficients are identical. It was consequently of importance to determine the temperature coefficient of the H_2–N_2O reaction The apparent energy of activation (E) was calculated from the approximate equation $d\ ln\ R/dT = E/RT^2$. The value of E, viz., 32·5 k.cal., is much smaller than that for the decomposition of N_2O which is 54 k.cal. As the temperature is raised, therefore, the relative rates of the H_2–N_2O and the N_2O reaction will decrease and at some high temperature may eventually become equal

Explosions.—Inflammation of the mixture could readily be obtained if the pressure or the temperature were sufficiently raised For example, taking the results in Table X, at 700°, on increasing the pressure beyond 200 mm., the mixture exploded provided the gases were admitted quickly, on slow admission, no explosion could be obtained probably because of the rapid disappearance of H_2 and of N_2O. Similarly, explosions could be observed in the following way The reaction tube was attached to another bulb (volume two or three times that of the tube) which could be filled with mercury thus increasing the pressure in the tube. If, during the course of a run (*e g*, similar to experiment 110) the mercury was suddenly admitted to the bulb, explosion occurred. On the other hand, if compression were gradual no such explosion took place. Indeed, it appeared that the condition for explosion depended on the reaction rate exceeding a certain value. The limit it thus quite different from that in the H_2–O_2 reaction where the transition from an

Table X

Temperature coefficient 1 : 1 Mixture Total pressure 200 mm.

Experiment	Temp	R
	° C	
110	700	25
111	638	13
112	597	5·1
113	540	1·0
	E 32·5 k.cal	

extremely slow reaction to explosion is comparatively abrupt Attempts were also made to discover the existence of an upper limiting pressure for explosion, adopting the methods employed in the H_2–O_2 reaction, but no indication of this phenomenon could be observed

Discussion of Results and Mechanism of the Reaction.

The first decision to be made from these experiments concerns the class to which the mechanism of the reaction belongs That the reaction consists of the decomposition of N_2O followed by oxidation of H_2 (No 3, p 526) must be excluded since the observed rate of production of water is much faster than the decomposition rate of N_2O. The inhibitory influence of surfaces rules out the possibility of the bimolecular reaction. Further, a bimolecular reaction having an energy of activation of 30 k cal. would be measurable at a temperature of 300°–400° instead of about 600° The inhibition by surfaces likewise eliminates the purely heterogeneous reaction. There remains, then, the chain mechanism, but although the present reaction is placed in this class by a process of elimination, there is definitely positive evidence of chain characteristics In a chain reaction, the first three types may be incorporated for (*a*) initiation may be the result of a heterogeneous* or of a homogeneous reaction† as is the case in the H_2–O_2 reaction, (*b*) termination may take place in the gas or at a surface, (*c*) propagation most likely involves a series of bimolecular encounters but the possibility of ternary collisions may also require to be taken into account

The best evidence for the chain hypothesis is the increase in rate in wider vessels The explosive nature of the reaction also points to the chain hypothesis being the correct one to employ. Before any quantitative scheme can be constructed, the nature of the carriers must be known. While direct evidence is, in most cases, extremely difficult to obtain, there are usually only a small number of possibilities when dealing with a comparatively simple reaction such as the one under discussion.

One of the simplest schemes is as follows :—

$$H + N_2O \rightarrow OH + N_2 + 75{\cdot}5 \text{ k.cal}$$
$$OH + H_2 \rightarrow H_2O + H,$$

---

* Alyea and Haber, 'Z. phys. Chem.,' B, vol. 10, p. 193 (1931), Alyea, 'J. Amer. Chem. Soc.,' vol. 53, p. 1324 (1931), Melville and Ludlam, 'Proc. Roy. Soc.,' A, vol. 135, p. 315 (1932).

† Haber and Oppenheimer, 'Z. phys. Chem.,' B, vol. 16, p. 443 (1932); Taylor and Salley, 'J. Amer. Chem Soc ,' vol. 55, p. 96 (1933).

the carriers being H and OH as in the H_2–O_2 reaction, H or OH being generated by some primary reaction It is known that hydrogen atoms attack nitrous oxide* with the eventual production of water; there is thus evidence for the first step. Proof of the second is not so direct, but there is a considerable body of opinion in favour of OH reacting with H_2,† especially at high temperatures, as papers on the H_2–O_2 reaction demonstrate. OH radicals occur in the flame of H_2 burning in N_2O‡ but this, of course, is not a proof but only an indication that they may occur in the stable reaction If a stationary concentration of OH be set up, it should be possible by the use of a dynamic method to sweep these radicals out of the reaction tube and so obtain hydrogen peroxide in a cooled trap §

There is now the question of initiation to be considered. In the corresponding H_2-O_2 reaction, homogeneous initiation seems to require so much activation at temperatures below 560°, it appears that a surface reaction is responsible for the provision of reaction centres || With H_2–N_2O mixtures, there is a source of O atoms in the gas on account of the unimolecular decomposition of N_2O, and, as O atoms react with H_2 readily at 600°,¶ initiation may occur as follows —

$$\left.\begin{array}{lll} N_2O + N_2O & \rightarrow N_2O' + N_2O \\ N_2O' & \rightarrow N_2 + O \end{array}\right\} k_1$$

or

$$\left.\begin{array}{lll} H_2 + N_2O & \rightarrow N_2O' + H_2 \\ N_2O' & \rightarrow N_2 + O \end{array}\right\} k_2$$

followed by

$$O + H_2 \rightarrow OH + H \qquad k_3$$

k_1, k_2 and k_3 being velocity coefficients. Activation by hydrogen is included since H_2 may behave similarly to other inert gases in this respect If the collisions of H_2 with N_2O are particularly efficient in activating N_2O, as is the

---

* Taylor, 'Trans Faraday Soc,' vol 21, p 560 (1926)

† Cf in particular, Bonhoeffer and Haber, 'Z phys Chem,' vol. 137, p. 337 (1928), Frankenburger and Klinkhardt, *ibid*, B, vol 15, p 421 (1932)

‡ Fowler and Badami, 'Proc Roy Soc.,' A, vol. 133, p. 325 (1931)

§ Pease, 'J. Amer Chem. Soc.,' vol. 52, p. 5106 (1930); vol 53, p 3188 (1931); Bates and Salley, *ibid.*, vol. 55, p. 110 (1933).

|| Alyea, *loc. cit.*, also Goldman, 'Z. phys Chem.,' B, vol. 5, p. 316 (1929).

¶ Harteck and Kopsch, 'Z. Electrochem.,' vol 36, p. 714 (1930), 'Z. phys. Chem,' B, vol 12, p. 327 (1931).

case with many other unimolecular reactions,* it may be that initiation is wholly dependent on this encounter.

The termination of the chains may occur by $H + H \rightarrow H_2$, $OH + OH \rightarrow H_2O_2$, or $H + OH \rightarrow H_2O$, these processes requiring the presence of a third molecule or a surface That surface combination does not wholly control termination is shown by the comparatively small influence of packing. Consequently, most of the termination occurs in the gas. Setting up the equations for the stationary concentrations of H and of OH, then,

$$\frac{d[H]}{dt} = I + k_5[OH][H_2] - k_4[H][N_2O] - k_6[H]^2[X] - k_7[H][OH][X] = 0,$$

$$\frac{d[OH]}{dt} = I + k_4[H][N_2O] - k_5[OH][H_2] - k_8[OH]^2[X] - k_7[H][OH][X] = 0,$$

where I is the rate of initiation, X is a third molecule Surface combination has been neglected for a first approximation. Solution of these equations would be extremely difficult since they are both quadratic. A great simplification can be made if it be assumed that $k_5 \gg k_4$, in which case the stationary concentration of H atoms would greatly exceed that of OH, $k_7[H][OH][X]$ could then be neglected Further, according to Bonhoeffer and Pearson† instead of

$$OH + OH + X \rightarrow H_2O_2 + X,$$
$$OH + OH \rightarrow H_2O + O$$

which would be followed by

$$O + H_2 \rightarrow OH + H$$
$$OH + H_2 \rightarrow H_2O + H$$

and the chain would not be terminated by the disappearance of two OH radicals in this way. $k_8[OH]^2[X]$ could also be neglected Therefore

$$[H] = (2I/k_6[X])^{\frac{1}{2}} \text{ and } [OH] = I/k_5[H_2] + \frac{k_4[N_2O]}{k_5[H_2]}\left(\frac{2I}{k_6[X]}\right)^{\frac{1}{2}},$$

$$\frac{d[N_2O]}{dt} = k_4[N_2O](2I/k_6[X])^{\frac{1}{2}},$$

if the chains are long $I = [N_2O]\{k_1[N_2O] + k_2[H]\}$ Since nitrogen and argon have no effect, it will be supposed that compared with N_2O and H_2 they are inefficient in promoting the stability of the newly formed H_2 molecule.

---

* *Cf* Rice, 'Chem. Rev,' vol 10, p. 127 (1932).

† 'Z. phys. Chem.,' B, vol. 14, p. 1 (1931).

This absence of inhibition may in part be due to the inert gas impeding the diffusion of H atoms to the walls and so tending to increase the rate. To a first approximation, it will be assumed that $[X] = [N_2O] + [H_2]$, so that the equation expressing the kinetics of the reaction becomes

$$-\frac{d[N_2O]}{dt} = k_4\,[N_2O]\left(\frac{2[N_2O]\{k_1[N_2O] + k_2[H_2]\}}{k_6\{[N_2O] + [H_2]\}}\right)^{\frac{1}{2}}.$$

An inhibiting influence of N_2O might also occur in virtue of the reaction $H + H + N_2O \rightarrow H_2O + N_2 + 180$ k cal for, owing to the production of two molecules after the reaction, the 180 k cal. might be equally divided between the two and would therefore be insufficient to dissociate the H_2O molecule into H and OH This latter process requires some 103 k cal

Some information about the relative magnitudes of k_1 and k_2 may be obtained from the effect of hydrogen on the rate $k_1 \neq k_2$ as H_2 would then have no effect. In order to account for the rate reaching a maximum which maximum is attained at a lower pressure of H_2 when N_2O is small, k_1 must be considerably less than k_2 From the results of Volmer and Bogdan* on the variation of the efficiency of activation collisions with mass in the monatomic gas series, it might be expected that the collisions between H_2 and N_2O would be about as effective as those between N_2O molecules themselves k_2 would then be 2·5 times that of k_1 on account of the greater collision frequency of the partners H_2 and N_2O

The same result could be obtained if it be assumed that $k_1 = k_2$ and that N_2O is much more efficient in participating in ternary collisions than is H_2 There is, however, no reason to suppose that this is the case; in fact, on making the calculations for the number of ternary collisions of $H + H + N_2O$ and of $H + H + H_2$, it was found that the latter was about 20% greater than the former.

When $[H_2]$ is so great that the rate becomes independent of it, the order with respect to $[N_2O]$ is 3/2 and thus is slightly higher than the observed order of unity

If termination had occurred mainly by the combination of two OH radicals in a ternary collision then the kinetic equation would have become

$$-\frac{d[N_2O]}{dt} = k_5[H_2]\left(\frac{2\,[N_2O]\{k_1[N_2O] + k_2[H_2]\}}{k_3\{[N_2O] + [H_2]\}}\right)^{\frac{1}{2}},$$

which is definitely not in agreement with observation

---

* 'Z phys. Chem,' B, vol. 21, p. 271 (1933)

According to this interpretation, the relative rate of the H_2–N_2O reaction to that of the N_2O decomposition does not represent exactly the chain length For a 1 1 mixture the ratio would require to be reduced by 3 5 in view of the rate of activation due to H_2 As each O atom is responsible for the initiation of two chains, the reduction factor would amount to 1/7

Since the rate of the H_2–N_2O reaction increases with the first power of the pressure (for a 1 1 mixture) and the rate of starting of the chains with the square of the pressure, the chain length will decrease as the total pressure increases. The reaction has thus been studied virtually in a region above the upper limit of a chain explosion Had such an explosion been possible, then on reducing the pressure inflammation should have resulted, but no indication of this phenomenon was observed.

The mechanism of the reaction, as suggested by these experiments, can be summarized in broad outline as follows The reaction is of the chain type initiated by O atoms derived from the thermal dissociation of N_2O molecules and propagated by H atoms and OH radicals Termination occurs mainly in the gas by combination of H atoms, but some may take place on the walls

The author wishes to thank Dr E B Ludlam for his encouragement, the Carnegie Trustees for a scholarship and the Moray Fund Committee of the University of Edinburgh for a grant for silica apparatus.

Summary

The kinetics of the reaction between hydrogen and nitrous oxide have been investigated at pressures from 50–400 mm. and temperatures from 550°–700° C. in silica bulbs.

The rate of reaction is much faster than that of the decomposition of nitrous oxide The products are mainly N_2 and H_2O. The rate is directly proportional to the pressure of nitrous oxide and nearly independent of that of H_2 except when the pressure of N_2O is high The reaction goes faster in wider vessels, but the increase is not proportional to the square of the diameter The apparent energy of activation is 32 k cal. Nitrogen and argon have no effect.

The chain mechanism suggested to explain these results is :—

(*a*) Initiation—

$$\begin{aligned} N_2O + N_2O &\rightarrow N_2O' + N_2O, \\ N_2O + H_2 &\rightarrow N_2O' + H_2, \\ N_2O' &\rightarrow N_2 + O, \\ O + H_2 &\rightarrow OH + H. \end{aligned}$$

(*b*) Propagation—

$$\mathrm{H} + \mathrm{N_2O} \rightarrow \mathrm{OH} + \mathrm{N_2},$$
$$\mathrm{OH} + \mathrm{H_2} \rightarrow \mathrm{H_2O} + \mathrm{H}$$

(*c*) Termination—

$$\mathrm{H} + \mathrm{H} + \mathrm{X} \rightarrow \mathrm{H_2} + \mathrm{X},$$

X being a third molecule or a wall.

Explosions may also occur if the pressure and temperature are high enough, but no sharp explosion limits could be obtained, such are characteristic of chain reactions

---

On the Two-Dimensional Steady Flow of a Viscous Fluid Behind a Solid Body.—I.

By S Goldstein

With an Appendix by A Fage.

(Communicated by L N. G Filon, F R S —Received June 15, 1933)

1 *Introduction*

1.1 The purpose of this paper is to exhibit, for reasons given below, calculations of the velocity distribution some distance downstream behind any symmetrical obstacle in a stream of viscous fluid, but particularly behind an infinitely thin plate parallel to the stream, the motion being two-dimensional. For a slightly viscous fluid, Blasius* worked out the velocity distribution in the boundary layer from the front to the downstream end of the plate, and in a previous paper,† I calculated the velocity in the wake for a distance varying from 0·3645 to 0·5 of the length of the plate from its downstream end (according to distance from its plane) In these calculations the fluid was supposed unlimited, and the undisturbed velocity in front of the plate was taken as constant The viscosity being assumed small, the work was carried out on the basis of Prandtl's boundary layer theory, with zero pressure gradient in the direction of the stream. The velocity is then constant everywhere except within a thin layer near the plate, and in a wake which must gradually broaden out downstream. (The broadening of the wake just behind the plate is so gradual that it could not be shown by calculations of the accuracy obtained in I). Pressure variations in a direction at right angles to the stream are negligible, and so is the velocity in that direction.

---

* 'Z. Math. Phys,' vol 56, p 1 (1908).

† 'Proc. Camb. Phil. Soc.,' vol. 26, p. 18 (1930), subsequently quoted as I.

Later, Tollmien attacked the problem from the other end, and found a first asymptotic approximation for the velocity distribution in the wake at a considerable distance downstream.* He simplified the Prandtl equations by assuming that the departure from the constant velocity, U_0, of the main stream is small, and neglecting terms quadratic in this departure In other words, he applied the notion of the Oseen approximation to the Prandtl equations. His result for the velocity is

$$U = U_0\{1 - aX^{-\frac{1}{2}} \exp(-U_0Y^2/4\nu X)\}$$

Here Y is distance from the plane of the plate, and X distance parallel to it from an origin in its neighbourhood whose exact position is unknown. (Necessarily so, since the formula is only a first approximation for large X, and a change of origin would therefore not affect it) ν is the kinematic viscosity of the fluid. a is a constant of integration, whose value, determined by considerations of momentum, is

$$D/(2\pi^{\frac{1}{2}}\rho\nu^{\frac{1}{2}}U_0^{3/2}),$$

where D is the drag on the plate per unit breadth, and ρ the density of the fluid. D is known from Blasius's calculations, and so a is found Apart from the substitution for D, the work applies to any symmetrical laminar wake. Tollmien asserts that for the wake behind the flat plate, the formula given is valid if $X > 3l$, where l is the length of the plate, but he gives no justification of the statement, and does not state the position of the origin from which he has measured X In any case, there is a region in which neither the asymptotic formula nor my previous calculations are valid, and in this region Tollmien found the velocity by graphical interpolation.

In paragraph 2 below, I have set out the derivation of this first approximation, found the second approximation, and shown that a third approximation cannot be found by the same methods Up to this point the work applies to a laminar wake behind any symmetrical obstacle, and the formulæ and symbols special to the case of the plate have not yet been introduced. This is done in paragraph 3, and for this special case, it is found that if the origin from which X is measured is taken at a distance of $0 \cdot 52l$ upstream from the rear end of the plate, then if we draw two graphs of velocity against distance behind the plate, for $Y = 0$, the one from the formulæ found here, and the other from the previous calculations set out in I, these two graphs join up smoothly. The position of the origin is thus determined. For values of Y other than zero, there are regions where the velocity can be determined only by graphical interpolation. This has been done, and on pp. 558, 559 and 560, the ratio, u, of the actual velocity to U_0, is tabulated for various values of x_1/l and y, where x_1 is distance parallel to the stream from the rear end of the plate, and y is $Y\,(U_0/4\nu l)^{\frac{1}{2}}$. The values are derived partly from the previous calculation, partly from the present one, and partly from interpolation. (The reader who wishes to know which values are found by calculation and which by interpolation is referred to p. 558.

---

* 'Handbuch der Experimental Physik.,' vol. 4, Part 1, p. 269 (1931).

1.2 For the plate parallel to the stream, the velocity has, then, been approximately calculated all over the field. In order that the calculations should be everywhere valid, three conditions must be fulfilled. The viscosity must be small enough for the Prandtl equations to apply, the method used to find the first and second approximations to the motion at a considerable distance downstream, based on the application of the notion of the Oseen approximation to the Prandtl equations, must give satisfactory results, and, lastly, the motion must be steady. It is with the discussion of this last condition that we are concerned here; we shall return to the other two later. In the first place, it is known that if the velocity of the stream and the length of the plate are large enough, then at a certain distance downstream from the front of the plate, the flow in the boundary layer along the plate becomes turbulent. But the Reynolds' number, $U_0 l/\nu$, at which the transition to turbulent motion takes place, is large, and there is a wide range of Reynolds' numbers in which the Prandtl equations apply and the flow along and just behind the plate is steady. It is with this range that we are concerned, and the question immediately arises—if the flow in the wake is steady immediately behind the plate, does it become turbulent further downstream? For any given distance behind the plate, the graph of the velocity against Y has a point of inflection, and its shape certainly suggests instability in the absence of sufficient damping,* so that in such cases turbulence is to be expected. Preliminary experiments by Fage and Falkner, which enabled measured and calculated distributions of velocity to be compared for $U_0 l/\nu$ equal to $0\cdot536 \,.\, 10^5$ and $2\cdot01 \,.\, 10^5$, at $x_1/l = 0\cdot20$ and for $U_0 l/\nu$ equal to $0\cdot540 \,.\, 10^5$ and $1\cdot825 \,.\, 10^5$ at $x_1/l = 0\cdot512$, strongly suggest that, whilst the flow immediately behind the plate at these Reynolds' numbers is steady, that is no longer true at half the length of the plate downstream from the rear end.[*] If it be granted that the transition to turbulence does take place, the next questions that arise are how and when does the transition take place, and how does the manner and place of the transition depend on Reynolds' number, and what, if any, is the lowest Reynolds' number at which it does take place ? These are, in the first place, suitable matters for experiment, and the answers are all the more interesting since the theoretical investigation of the stability of the flow does not appear impossible, and would be facilitated by the experimental results

---

* The reader may compare certain calculations by Lord Rayleigh, 'Scientific Papers,' vol. 1, p. 482 (1899).

For any symmetrical cylindrical obstacle other than a plate parallel to the stream, the complete calculation of the velocity field is not possible , but the formulæ of paragraph 2 should apply for the velocity in the wake at a considerable distance downstream if the three conditions above are fulfilled It is doubtful, however, if the motion is ever steady at a sufficient distance downstream when ν is small—or, more accurately, when U_0d/ν is large, where d is a representative length of the obstacle For a slender, stream-line, body, the motion in the wake, even if steady just behind the body, probably becomes turbulent further downstream (these, too, are matters for experimental investigation) , whilst for a bluff body the motion in the wake is definitely not steady, but is quasi-periodic or turbulent, when U_0d/ν is large.

One last question remains to be considered here. To what extent do the formulæ of paragraph 2 apply when the motion at a considerable distance downstream in the wake is turbulent or quasi-periodic ? The second approximation will not then apply at all , the first approximation will apply, as Filon has pointed out,[†] to motion which is steady on the average, if we can neglect the *average* value of terms quadratic in the departure of the velocity from that of the main stream The distance downstream required for this will usually be enormous.

1 3 *List of Symbols*

ν, ρ . the kinematic viscosity and density of the fluid
U_0 the undisturbed velocity of the stream.
l the length of a plate parallel to the stream
d . a representative length for any obstacle, taken as $4l$ for the plate.
X, Y rectangular Cartesian co-ordinates with the axis of X in the direction of the undisturbed stream. The origin is on the

---

[*] It should be noticed that for these comparisons, both the calculated distributions required depend mostly on the previous calculations, and only slightly on the present ones and the graphical interpolation. *Cp.* p. 558.

[†] 'Proc. Roy Soc ,' A, vol. 113, p. 7 (1926–27).

line of symmetry for a symmetrical obstacle. It is in the neighbourhood of the obstacle, but its exact position is unknown *a priori* For the plate it is calculated to be $0\cdot 52l$ upstream from the rear end.

p, U, V · the pressure and the components of velocity in the wake.

$u = \mathrm{U}/\mathrm{U}_0$

$v = \left(\frac{\mathrm{U}_0 d}{\nu}\right)^{\frac{1}{2}} \frac{\mathrm{V}}{\mathrm{U}_0}$

$x = \mathrm{X}/d$

$y = \left(\frac{\mathrm{U}_0 d}{\nu}\right)^{\frac{1}{2}} \frac{\mathrm{Y}}{d}$ In paragraph 3, d is put equal to $4l$ in these definitions of u, v, x, y.

$\eta = \frac{y}{(2x)^{\frac{1}{2}}} = \left(\frac{\mathrm{U}_0}{2\nu\mathrm{X}}\right)^{\frac{1}{2}} \mathrm{Y}$

$w = 1 - u$

w_1, v_1, w_2, v_2, w_3, v_3 first, second and third approximations respectively to w and v.

β . a numerical constant, approximately $0\cdot 33204$.

D the drag per unit breadth on any cylindrical obstacle, equal to $4\beta\rho\nu^{\frac{1}{2}}\mathrm{U}_0^{3/2}l^{\frac{1}{2}}$ for the plate

k_{D} : a drag coefficient, equal to $\mathrm{D}/\rho\mathrm{U}_0^2 d$

A a constant of integration, equal to $\mathrm{D}/(2\pi^{\frac{1}{2}}\rho\nu^{\frac{1}{2}}\mathrm{U}_0^{3/2}d^{\frac{1}{2}})$ or $\frac{1}{2\pi^{\frac{1}{2}}}\left(\frac{\mathrm{U}_0 d}{\nu}\right)^{\frac{1}{2}} k_{\mathrm{D}}$, in general, and equal to $\beta/\sqrt{\pi}$ for the plate.

x_1 : distance parallel to the stream from the rear end of the plate.

c . a constant, equal to $(\mathrm{X} - x_1)/l$, taken as 0 52 on p 24.

2. *Asymptotic formulæ for flow in a symmetrical wake.*

2.1. ***The first approximation.***—Consider the two-dimensional flow of an incompressible fluid of unlimited extent and of small viscosity past a fixed cylindrical body. Assume that the section of the cylinder is symmetrical about a line parallel to the velocity of the stream, and let the notation be as in paragraph 1.3. Then, as explained more fully in the next paper, in paragraph 1.1, when we are considering the motion in the wake, the respresentative Reynolds' number is $\mathrm{U}_0\mathrm{X}/\nu$, and when this is large the assumptions of the boundary layer theory apply. The width of the wake will be found to be of the order of $(\nu X/U_0)^{\frac{1}{2}}$. Hence, in the wake, $Y(U_0/\nu X)^{\frac{1}{2}}$ will be finite; that is, $yx^{-\frac{1}{2}}$ or η will be finite. The approximate equations for determining a steady motion are then

$$\left.\begin{aligned} U\frac{\partial U}{\partial X} + V\frac{\partial U}{\partial Y} &= -\frac{1}{\rho}\frac{\partial p}{\partial X} + \nu\frac{\partial^2 U}{\partial Y^2} \\ 0 &= -\frac{\partial p}{\partial Y} \\ \frac{\partial U}{\partial X} + \frac{\partial V}{\partial Y} &= 0 \end{aligned}\right\} \qquad (1)$$

Moreover, the fluid being unlimited, at a considerable distance downstream we can neglect $\partial p/\partial X$ as being of a higher order in X^{-1} than will be required for our approximations.* (When the obstacle is a flat plate, $\partial p/\partial X$ will vanish with ν.) From the second of equations (1) it then follows that to our order of approximation p is constant

In order to make the quantities non-dimensional, we let d be a representative length of the obstacle, and define u, v, x and y as in paragraph 1.3 The equations (1) then become

$$\left.\begin{aligned} u\frac{\partial u}{\partial x} + v\frac{\partial u}{\partial y} &= \frac{\partial^2 u}{\partial y^2} \\ \frac{\partial u}{\partial x} + \frac{\partial v}{\partial y} &= 0 \end{aligned}\right\} \qquad (2)$$

We now assume that when x is large, u is nearly equal to 1 and v is small We write $u = 1 - w$, and for the first approximation (w_1, v_1), we neglect terms in the equations (2) that are quadratic in w and v. The result is

$$\left.\begin{aligned} \frac{\partial w_1}{\partial x} &= \frac{\partial^2 w_1}{\partial y^2} \\ \frac{\partial w_1}{\partial x} &= \frac{\partial v_1}{\partial y} \end{aligned}\right\} \qquad (3)$$

The boundary conditions are that w must tend to zero as x tends to infinity, and must tend to zero exponentially as y tends to infinity. Also, from symmetry, w must be an even function and v an odd function of y, so that $\partial w/\partial y$ and v must be zero when y is zero. Moreover, because of considerations of momentum, we must have

$$D = \rho_0 U \int_{-\infty}^{\infty} (U_0 - U)\, dY = 2\rho\nu^{\frac{1}{2}} U_0^{3/2} d^{\frac{1}{2}} \int_0^{\infty} w\, dy, \qquad (4)$$

---

* For a verification, see p. 567 of the next paper.

where D is the drag per unit length on the obstacle, and the integral is along a line at right angles to the line of symmetry at an infinite distance downstream. (This equation expresses one of the main results of Filon's first paper.*)

To find an appropriate solution of the first of equations (3) for w_1, write

$$\eta = y/(2x)^{\frac{1}{2}} \tag{5}$$

$$w_1 = f_1(\eta)/x^{\frac{1}{2}} \tag{6}$$

Then

$$f''_1 + \eta f'_1 + f_1 = 0 \tag{7}$$

One solution of this equation is $e^{-\frac{1}{2}\eta^2}$ Write

$$f_1 = e^{-\frac{1}{2}\eta^2} g_1 \tag{8}$$

Then

$$g''_1 - \eta g'_1 = 0$$

$$g_1 = \mathrm{A} + \mathrm{B}\int^{\eta} e^{\frac{1}{2}\eta^2}\, d\eta,$$

and in order that w_1 should tend to zero exponentially with y, B must be zero It should be specially noted that the same condition ensures that g_1, and, therefore, f_1 and w_1, are even functions of η. To determine A we use equation (4) This gives

$$\mathrm{D}/(2\rho\nu^{\frac{1}{2}}\mathrm{U}_0^{3/2}\, d^{\frac{1}{2}}) = x^{-\frac{1}{2}}\int_0^{\infty} f_1(\eta)\, dy = 2^{\frac{1}{2}}\int_0^{\infty} \mathrm{A}e^{-\frac{1}{2}\eta^2}\, d\eta = \mathrm{A}\pi^{\frac{1}{2}},$$

or

$$\mathrm{A} = \mathrm{D}/(2\pi^{\frac{1}{2}}\rho\nu^{\frac{1}{2}}\mathrm{U}_0^{3/2}\, d^{\frac{1}{2}}) \tag{9}$$

Then

$$w_1 = \mathrm{A}x^{-\frac{1}{2}}\, e^{-\frac{1}{2}\eta^2}, \tag{10}$$

and from equation (3)

$$\frac{\partial v_1}{\partial y} = \frac{\partial w_1}{\partial x} = \frac{\partial^2 w_1}{\partial y^2},$$

so that, since v_1 vanishes with $\partial w_1/\partial y$ at $y = 0$,

$$v_1 = \frac{\partial w_1}{\partial y} = -\frac{\mathrm{A}}{2^{\frac{1}{2}}x}\,\eta e^{-\frac{1}{2}\eta^2}. \tag{11}$$

2.2 *The second approximation.*—To find a second approximation, write

$$u = 1 - w_1 - w_2, \qquad v = v_1 + v_2. \tag{12}$$

Then w_2 will be of order x^{-1}, and v_2 of order $x^{-3/2}$. To find the second approximation we must retain terms of order x^{-2} in the equation. The first of equations (2) then becomes

---

* 'Proc. Roy. Soc.,' A, vol 113, p. 7 (1926–7).

$$\frac{\partial^2 w_2}{\partial y^2} - \frac{\partial w_2}{\partial x} = v_1 \frac{\partial w_1}{\partial y} - w_1 \frac{\partial w_1}{\partial x}$$

$$= \frac{A^2}{2x^2} e^{-\eta^2}. \tag{13}$$

We require a particular integral, such that w_2 vanishes exponentially when η tends to infinity, and $\partial w/\partial y$, or $\partial w/\partial \eta$, vanishes when η is zero. We therefore write

$$w_2 = x^{-1} f_2 (\eta). \tag{14}$$

Then

$$f''_2 + \eta f'_2 + 2f_2 = A^2 e^{-\eta^2} \tag{15}$$

Put

$$f_2 = e^{-\frac{1}{2}\eta^2} g_2 \tag{16}$$

Then

$$g''_2 - \eta g'_2 + g_2 = A^2 e^{-\frac{1}{2}\eta^2}. \tag{17}$$

One complementary functon of this equation is η. Hence, put

$$g_2 = \eta h_2, \tag{18}$$

so that

$$w_2 = x^{-1} \eta e^{-\frac{1}{2}\eta^2} h_2. \tag{19}$$

Then

$$\eta h''_2 + (2 - \eta^2) h'_2 = A^2 e^{-\frac{1}{2}\eta^2},$$

or

$$\frac{d}{d\eta} (\eta^2 e^{-\frac{1}{2}\eta^2} h'_2) = A^2 \eta e^{-\eta^2} = -\frac{d}{d\eta} (\tfrac{1}{2} A^2 e^{-\eta^2}),$$

and

$$h'_2 = -\tfrac{1}{2} A^2 \eta^{-2} e^{-\frac{1}{2}\eta^2} + C\eta^{-2} e^{\frac{1}{2}\eta^2}, \tag{20}$$

where C is a constant of integration. In order that w_2 should vanish exponentially when η tends to infinity, C must be zero. Therefore

$$h_2 = -\tfrac{1}{2} A^2 \int_0^\eta \eta^{-2} e^{-\frac{1}{2}\eta^2} d\eta$$

$$= \tfrac{1}{2} A^2 \eta^{-1} e^{-\frac{1}{2}\eta^2} + \tfrac{1}{2} A^2 \int_0^\eta e^{-\frac{1}{2}\eta^2} d\eta + D, \tag{21}$$

by a partial integration, D being a constant. In order that w_2 should be an even function of η, h must be an odd function, and D must vanish. Also if

$$\operatorname{erf} \eta = \frac{2}{\pi^{\frac{1}{2}}} \int_0^\eta e^{-\eta^2} d\eta,^* \tag{22}$$

---

* This function is tabulated in Dale's "Mathematical Tables."

then

$$\int_0^\eta e^{-\frac{1}{2}\eta^2}\,d\eta = (\tfrac{1}{2}\pi)^{\frac{1}{2}}\,\mathrm{erf}\,(\eta/\sqrt{2}), \tag{23}$$

and

$$w_2 = \frac{A^2}{2x}\left[e^{-\eta^2} + (\tfrac{1}{2}\pi)^{\frac{1}{2}}\,\eta\, e^{-\frac{1}{2}\eta^2}\,\mathrm{erf}\,(\eta/\sqrt{2})\right] \tag{24}$$

To determine v_2 we use the second of equations (2). This gives

$$\frac{\partial v_2}{\partial y} - \frac{\partial w_2}{\partial x} = \frac{\partial^2 w_2}{\partial y^2} - \frac{A^2}{2x^3}\,e^{-\eta^2}, \tag{25}$$

from (13), so that, since v_2 vanishes with y, and $y = (2x)^{\frac{1}{2}}\,\eta$,

$$\begin{aligned} v_2 &= \frac{\partial w_2}{\partial y} - \frac{A^2}{2x^2}\int_0^y e^{-\eta^2}\,dy \\ &= \frac{1}{(2x)^{\frac{1}{2}}}\frac{\partial w_2}{\partial \eta} - \frac{A^2}{(2x^3)^{\frac{1}{2}}}\int_0^\eta e^{-\eta^2}\,d\eta \\ &= -\frac{A^2}{(2x)^{3/2}}\left[(\tfrac{1}{2}\pi)^{\frac{1}{2}}(1-\eta^2)\,e^{-\frac{1}{2}\eta^2}\,\mathrm{erf}\,(\eta/\sqrt{2}) - \eta e^{-\eta^2} - \pi^{\frac{1}{2}}\,\mathrm{erf}\,\eta\right] \end{aligned} \tag{26}$$

Collecting our results, we find, correct to the second approximation,

$$\left.\begin{aligned} u &= 1 - Ax^{-\frac{1}{2}}e^{-\frac{1}{2}\eta^2} - \frac{A^2}{2x}\left[e^{-\eta^2} + (\tfrac{1}{2}\pi)^{\frac{1}{2}}\,\eta e^{-\frac{1}{2}\eta^2}\,\mathrm{erf}\,(\eta/\sqrt{2})\right] \\ v &= -\frac{A}{2^{\frac{1}{2}}x}\,\eta e^{-\frac{1}{2}\eta^2} + \frac{A^2}{(2x)^{3/2}}\left[(\tfrac{1}{2}\pi)^{\frac{1}{2}}(1-\eta^2)\,e^{-\frac{1}{2}\eta^2}\,\mathrm{erf}\,(\eta/\sqrt{2})\right. \\ &\qquad\qquad\qquad\qquad\qquad\qquad \left. - \eta e^{-\eta^2} - \pi^{\frac{1}{2}}\,\mathrm{erf}\,\eta\right] \end{aligned}\right\}, \tag{27}$$

where

$$\left.\begin{aligned} u &= \frac{U}{U_0}, \qquad v = \left(\frac{d}{\nu U_0}\right)^{\frac{1}{2}} V \\ x &= \frac{X}{d}, \qquad y = \left(\frac{U_0}{\nu d}\right)^{\frac{1}{2}} Y, \qquad \eta = \frac{y}{(2x)^{\frac{1}{2}}} = \left(\frac{U_0}{2\nu X}\right)^{\frac{1}{2}} Y \end{aligned}\right\} \tag{28}$$

A is given by equation (9), so that if we define a drag coefficient k_D by

$$k_D = D/\rho U_0^2 d, \tag{29}$$

then

$$A = \frac{1}{2\pi^{\frac{1}{2}}}\left(\frac{U_0 d}{\nu}\right)^{\frac{1}{2}} k_D \tag{30}$$

Note that the first approximation to v tends to zero exponentially as y, or η tends to infinity, but that, since erf η remains finite, the second approximation remains finite. It is a general feature of solutions of boundary layer equations that v remains finite when y tends to infinity, and, in general, this introduces an error of the order of the reciprocal of the square root of the representative Reynolds' number. (We shall find, however, that v remains finite in the same way as here according to Filon's equations also; so that, on this account, there should be no difference between the solution here found and Filon's solution See II, p 563.)

Again, for a flat plate, k_D is of the order of $(\nu/U_0 d)^{\frac{1}{2}}$, and A remains finite when ν tends to zero. But for a bluff obstacle, k_D in general remains finite when ν tends to zero, because of the separation of the boundary layer from the surface of the obstacle, and the suction in the rear A is then of the order of $(U_0 d/\nu)^{\frac{1}{2}}$, and the asymptotic formulæ in (27) will be valid only when ν is small and νx is large, so that x must be very large For a bluff obstacle, however, the motion in the wake is not steady when $U_0 d/\nu$ is large, but quasi-periodic or turbulent The second approximation will not then apply at all, the first approximation will apply, as Filon has pointed out in his first paper, to motion which is steady on the average, if we can neglect the *average* value of terms quadratic in the departure of the velocity from that of the main stream. This can be expected to be valid only at very large distances; for this reason also, therefore x must be very large for the first approximation to be valid

2 3 *Unsuccessful attempt at a third approximation.*—To seek for a third approximation, write

$$u = 1 - w_1 - w_2 - w_3, \qquad v = v_1 + v_2 + v_3 \tag{31}$$

Then w_3 will be of order $x^{-3/2}$, and v of order x^{-2}. We must then retain terms of order $x^{-5/2}$ in the equation. The first of equations (2) then becomes

$$\begin{aligned}\frac{\partial^2 w_3}{\partial y^2} - \frac{\partial w_3}{\partial x} &= v_1 \frac{\partial w_2}{\partial y} + v_2 \frac{\partial w_1}{\partial y} - w_1 \frac{\partial w_2}{\partial x} - w_2 \frac{\partial w_1}{\partial x} \\ &= \frac{e^{-\frac{1}{2}\eta^2}}{2x^{5/2}} \mathrm{F}(\eta),\end{aligned} \tag{32}$$

where

$$\mathrm{F}(\eta) = \tfrac{1}{2}\mathrm{A}^3 \left[3e^{-\eta^2} + (2\pi)^{\frac{1}{2}} \eta \, e^{-\frac{1}{2}\eta^2} \operatorname{erf}(\eta/\sqrt{2}) + \pi^{\frac{1}{2}} \eta \operatorname{erf} \eta \right]. \tag{33}$$

Put

$$w = x^{-3/2} f_3(\eta). \tag{34}$$

Then

$$f''_3 + \eta f'_3 + 3 f_3 = e^{-\frac{1}{2}\eta^2} \mathrm{F}(\eta). \tag{35}$$

Put

$$f_3 = e^{-\frac{1}{2}\eta^2} g_3. \tag{36}$$

Then

$$g''_3 - \eta g'_3 + 2g_3 = \mathrm{F}(\eta). \tag{37}$$

One complementary function of this equation is $1 - \eta^2$. Therefore, put

$$g_3 = (1 - \eta^2)\, h_3, \tag{38}$$

so that

$$w_3 = x^{-3/2}\, e^{-\frac{1}{4}\eta^2}\, (1 - \eta^2)\, h_3 \tag{39}$$

Then

$$(1 - \eta^2)\, h''_3 - (5\eta - \eta^3)\, h'_3 = \mathrm{F},$$

or

$$\frac{d}{d\eta}\, [e^{-\frac{1}{4}\eta^2}\, (1 - \eta^2)^2\, h''_3] = \mathrm{F}e^{-\frac{1}{4}\eta^2}\, (1 - \eta^2)$$

Now $\partial w_3/\partial\eta$ must vanish when η vanishes, and therefore $(1 - \eta^2)\, h'_3$ must vanish when η vanishes Hence

$$e^{-\frac{1}{4}\eta^2}\, (1 - \eta^2)^2\, h'_3 = \int_0^\eta \mathrm{F}e^{-\frac{1}{4}\eta^2}\, (1 - \eta^2)\, d\eta \tag{40}$$

When the upper limit becomes infinite, the integral on the right is finite, and equal to $-\frac{1}{3}\mathrm{A}^3\, (\pi/6)^{\frac{1}{2}}$. Hence, when η tends to infinity, h'_3 is of order $e^{\frac{1}{4}\eta^2}\, \eta^{-4}$, and therefore h_3 is of the order $e^{\frac{1}{4}\eta^2}\, \eta^{-5}$ and w_3 of order η^{-3}. Hence w_3 does not tend exponentially to zero when η tends to infinity. This result is on a different footing from the finiteness of v_2 for large values of η For whereas, when A is finite, the latter makes V of order $(\nu \mathrm{U}_0/d)^{\frac{1}{2}}$, so that V vanishes with ν, the former makes U differ from U_0 by a quantity of order η^{-3} which does not vanish with ν

We have assumed, without proof, that w may be expanded in the form

$$\frac{f_1(\eta)}{x^{\frac{1}{2}}} + \frac{f_2(\eta)}{x} + \frac{f_3(\eta)}{x^{3/2}} + \ \ldots,$$

so that we can draw no conclusions from the failure of the calculations to give results of the type we anticipated. The case of the flat plate seems, anyway, to shut out any possible physical basis for the result. Most probably the method of approximation tried is at fault; for a second approximation we ought to have found an exact solution of the equation

$$(1 - w_1)\frac{\partial w}{\partial x} + v_1 \frac{\partial w}{\partial y} = \frac{\partial^2 w}{\partial y^2},$$

and so on. Since the second approximation we did find is a solution of this equation correct to the order x^{-1}, it is probably valid.

3. *Numerical results for the case of the flat plate.*

For a flat plate of length l, the drag D is given by the formula*

$$D = 4\beta\rho\nu^{\frac{1}{2}}U_0^{3/2}l^{\frac{1}{2}}, \tag{1}$$

where†

$$\beta = 0\cdot33204. \tag{2}$$

Hence, if we take

$$d = 4l, \tag{3}$$

equation 2 (9) gives

$$A = \beta/\sqrt{\pi}. \tag{4}$$

Then 2 (27) gives

$$u = 1 - \frac{f_1(\eta)}{x^{\frac{1}{2}}} - \frac{f_2(\eta)}{x}, \tag{5}$$

where

$$\left.\begin{aligned} f_1(\eta) &= \frac{\beta}{\sqrt{\pi}}\, e^{-\frac{1}{2}\eta^2} \\ f_2(\eta) &= \frac{\beta^2}{2\pi}\left[e^{-\eta^2} + (\tfrac{1}{2}\pi)^{\frac{1}{2}}\eta e^{-\frac{1}{2}\eta^2}\operatorname{erf}(\eta/\sqrt{2})\right] \\ u = \frac{U}{U_0}, \quad x = \frac{X}{4l}, \quad y &= \tfrac{1}{2}\left(\frac{U_0}{\nu l}\right)^{\frac{1}{2}} Y, \quad \eta = \frac{y}{(2x)^{\frac{1}{2}}} = \left(\frac{U_0}{2\nu X}\right)^{\frac{1}{2}} Y \end{aligned}\right\} \tag{6}$$

$f_1(\eta)$ and $f_2(\eta)$ are tabulated against $\eta/\sqrt{2}$ in Table I

Table I

$\eta/\sqrt{2}$.	$f_1(\eta)$	$f_2(\eta)$	$\eta/\sqrt{2}$	$f_1(\eta)$	$f_2(\eta)$.
0	0·1873	0·0176	1·3	0·0347	0·0076
0·1	0·1855	0·0176	1·4	0·0264	0·0062
0·2	0·1800	0·0175	1·5	0·0197	0·0049
0·3	0·1712	0·0174	1·6	0·0144	0·0038
0·4	0·1596	0·0173	1·7	0·0101	0·0029
0·5	0·1459	0·0169	1·8	0·0073	0·0022
0·6	0·1308	0·0164	1·9	0·0051	0·0016
0·7	0·1148	0·0156	2·0	0·0034	0·0011
0·8	0·0987	0·0146	2·1	0·0022	0·0008
0·9	0·0834	0·0133	2·2	0·0015	0·0006
1·0	0·0689	0·0120	2·3	0·0009	0·0004
1·1	0·0558	0·0105	2·4	0·0006	0·0002
1·2	0·0444	0·0090	2·5	0·0004	0·0002
			2·6	0·0002	0·0001

Now, if x_1 is distance behind the rear end of the plate, as in I then $X = x_1 + lc$, where c is a constant previously unknown Hence

$$x = \tfrac{1}{4}\left(\frac{x_1}{l} + c\right). \tag{7}$$

---

* Blasius, *loc. cit.*, p. 13.

† The numerical value is taken from I, p. 19.

The values of u for $\eta = 0$ or $y = 0$, as calculated from (5), were plotted against x. The values of u in I for $y = 0$ were plotted against $x_1/4l$, and it was found that the two curves joined up smoothly if c was taken equal to 0·52.

With this value of c the value of u was then calculated from (5) for various values of x_1/l and y. The results are shown in Table II. For a given value of x_1/l, x was first found from (7), with $c = 0{\cdot}52$; u was then calculated from (5) and Table I for those values of y which are obtained by multiplying the values of $\eta/\sqrt{2}$ in Table I by $2\sqrt{x}$ (since $y = (2x)^{\frac{1}{2}}\eta$), and the values of u for other values of y were found by graphical interpolation.

Table II

y \ x_1/l	0·5	0·6	0·7	0·8	0·9	1·0	1·2	1·4	1·6	1·8	2·0	2·2
0	0·560	0·583	0·603	0·621	0·636	0·650	0·673	0·693	0·709	0·724	0·736	0·747
0·1	0·564	0·586	0·605	0·623	0·638	0·652	0·675	0·694	0·710	0·725	0·737	0·747
0·2	0·574	0·596	0·614	0·630	0·645	0·658	0·680	0·699	0·714	0·728	0·739	0·749
0·3	0·592	0·611	0·627	0·642	0·656	0·668	0·689	0·706	0·720	0·732	0·743	0·753
0·4	0·615	0·631	0·646	0·658	0·670	0·680	0·699	0·715	0·728	0·739	0·750	0·760
0·5	0·643	0·654	0·669	0·679	0·688	0·695	0·712	0·726	0·738	0·749	0·759	0·767
0·6	0·675	0·682	0·694	0·701	0·708	0·716	0·728	0·740	0·749	0·759	0·768	0·775
0·7	0·709	0·711	0·720	0·725	0·731	0·737	0·745	0·755	0·764	0·771	0·778	0·784
0·8	0·744	0·744	0·749	0·752	0·754	0·759	0·765	0·771	0·778	0·784	0·789	0·796
0·9	0·780	0·779	0·778	0·779	0·780	0·782	0·786	0·789	0·793	0·798	0·802	0·806
1·0	0·813	0·810	0·806	0·806	0·806	0·805	0·806	0·807	0·809	0·812	0·815	0·817
1·1	0·844	0·840	0·834	0·833	0·829	0·828	0·826	0·825	0·826	0·827	0·830	0·831
1·2	0·873	0·866	0·860	0·855	0·850	0·850	0·846	0·844	0·842	0·842	0·843	0·844
1·3	0·898	0·890	0·884	0·879	0·874	0·870	0·863	0·862	0·860	0·858	0·857	0·856
1·4	0·920	0·912	0·906	0·900	0·895	0·890	0·881	0·878	0·875	0·872	0·869	0·868
1·5	0·939	0·931	0·924	0·918	0·912	0·908	0·899	0·894	0·889	0·886	0·883	0·881
1·6	0·953	0·948	0·940	0·934	0·928	0·924	0·915	0·908	0·903	0·899	0·895	0·892
1·7	0·966	0·960	0·954	0·947	0·942	0·938	0·928	0·921	0·916	0·912	0·908	0·905
1·8	0·976	0·971	0·965	0·959	0·954	0·950	0·941	0·934	0·928	0·923	0·919	0·915
1·9	0·983	0·978	0·974	0·969	0·964	0·960	0·952	0·945	0·939	0·934	0·930	0·926
2·0	0·988	0·984	0·981	0·976	0·972	0·969	0·962	0·955	0·949	0·944	0·940	0·935
2·1	0·992	0·989	0·986	0·982	0·979	0·976	0·970	0·963	0·957	0·953	0·948	0·943
2·2	0·995	0·993	0·990	0·987	0·984	0·982	0·977	0·971	0·965	0·961	0·956	0·951
2·3	0·996	0·995	0·993	0·991	0·988	0·986	0·982	0·977	0·972	0·967	0·963	0·958
2·4	0·997	0·996	0·995	0·994	0·992	0·990	0·987	0·982	0·977	0·973	0·969	0·964
2·5	0·998	0·998	0·996	0·995	0·994	0·993	0·990	0·986	0·982	0·978	0·974	0·970
2·6		0·998	0·997	0·996	0·996	0·995	0·992	0·989	0·986	0·982	0·979	0·975
2·7		0·999	0·998	0·997	0·997	0·996	0·994	0·992	0·989	0·985	0·983	0·980
2·8			0·998	0·998	0·998	0·997	0·996	0·994	0·992	0·989	0·986	0·983
2·9			0·999	0·998	0·998	0·998	0·997	0·996	0·994	0·991	0·989	0·986
3·0				0·999	0·999	0·999	0·998	0·997	0·995	0·993	0·991	0·989
3·1						0·999	0·999	0·998	0·996	0·995	0·993	0·991
3·2							0·999	0·998	0·997	0·996	0·995	0·993
3·3								0·999	0·998	0·997	0·996	0·995
3·4								0·999	0·998	0·998	0·997	0·996
3·5									0·999	0·998	0·997	0·996
3·6										0·999	0·998	0·997
3·7											0·998	0·998
3·8											0·999	0·998
3·9												0·999

For any value of y other than zero, there are values of x_1/l for which u must be found by graphical interpolation. A table of values of u embodying the results of the calculations here, and of those in I, and of the graphical interpolation, is given on pp. 558, 559 and 560 (Table III). In this table, the results for x_1/l between 0 and 0·3645 inclusive are from the previous calculation for all values of y*; the results for x_1/l equal to 0·5 are from the previous calculation for values of y between 0 and 0·5 inclusive. From $x_1/l = 2\cdot 2$ onwards, the results are from the formula (5) above for all values of y. For smaller values of x_1/l, the results are partly from (5) and partly from interpolation. For example, for $x_1/l = 1\cdot 0$, the results are from (5) for $y \leq 0\cdot 4$ and $y \geq 2\cdot 0$. The manner in which the interpolated values join on to the calculated ones may be seen by comparing Tables II and III.

I have not thought it worth while to tabulate u for $x_1/l > 2\cdot 8$. The computation from formula (5) and Table I is easy.

Table III.

y \ x_1/l	0	0·0005	0·004	0·0135	0·032	0·0625	0·108	0·1715
0	0	0·061	0·123	0·183	0·243	0·302	0·359	0·413
0·1	0·066	0·101	0·146	0·199	0·255	0·311	0·366	0·419
0·2	0·133	0·166	0·201	0·242	0·288	0·338	0·388	0·437
0·3	0·199	0·233	0·266	0·300	0·337	0·378	0·421	0·463
0·4	0·265	0·298	0·331	0·362	0·394	0·428	0·463	0·499
0·5	0·330	0·373	0·395	0·425	0·453	0·482	0·512	0·545
0·6	0·394	0·426	0·457	0·486	0·513	0·538	0·562	0·584
0·7	0·456	0·487	0·517	0·544	0·570	0·593	0·614	0·630
0·8	0·517	0·547	0·555	0·601	0·624	0·645	0·662	0·675
0·9	0·575	0·603	0·630	0·654	0·676	0·694	0·707	0·717
1·0	0·630	0·656	0·681	0·704	0·723	0·739	0·751	0·760
1·1	0·681	0·706	0·729	0·749	0·766	0·780	0·790	0·797
1·2	0·729	0·752	0·772	0·791	0·806	0·817	0·826	0·830
1·3	0·772	0·793	0·811	0·827	0·840	0·850	0·857	0·860
1·4	0·812	0·830	0·846	0·860	0·871	0·879	0·884	0·886
1·5	0·846	0·862	0·876	0·888	0·897	0·904	0·908	0·909
1·6	0·876	0·890	0·902	0·911	0·919	0·925	0·928	0·928
1·7	0·902	0·913	0·923	0·931	0·937	0·942	0·944	0·944
1·8	0·923	0·933	0·941	0·947	0·952	0·955	0·957	0·957
1·9	0·941	0·949	0·955	0·960	0·964	0·966	0·967	0·967
2·0	0·956	0·962	0·967	0·971	0·974	0·975	0·976	0·976
2·1	0·967	0·972	0·976	0·979	0·981	0·982	0·982	0·982
2·2	0·976	0·980	0·983	0·985	0·986	0·987	0·987	0·987
2·3	0·983	0·985	0·988	0·989	0·990	0·991	0·991	0·991
2·4	0·988	0·990	0·991	0·993	0·993	0·994	0·994	0·994
2·5	0·992	0·993	0·994	0·995	0·995	0·996	0·996	0·996
2·6	0·994	0·995	0·996	0·997	0·997	0·997	0·997	0·997
2·7	0·996	0·997	0·997	0·998	0·998	0·998	0·998	0·998

---

* Except that 1 has been added to the last digit for $y = 1\cdot 2$, $x_1/l = 0\cdot 256$ and $0\cdot 3645$; 2 has been added for $y = 1\cdot 0$ and $1\cdot 1$, $x_1/l = 0\cdot 256$; and 4 has been added for $y = 1\cdot 0$ and $1\cdot 1$, $x_1/l = 0\cdot 3645$.

Table III—(continued).

y \ x_1/l	0	0·0005	0·004	0·0135	0·032	0·0625	0·108	0·1715
2·8	0·997	0·998	0·998	0·999	0·999	0·999	0·999	0·999
2·9	0·998	0·999	0·999	0·999	0·999	0·999	0·999	0·999
3·0	0·999	0·999	0·999	0·999	1·000	1·000	1·000	1·000
3·1	0·999	1·000	1·000	1·000	1·000	1·000	1·000	1·000
3·2	1·000	1·000	1·000	1·000	1·000	1·000	1·000	1·000
3·3	1·000	1·000	1·000	1·000	1·000	1·000	1·000	1·000
3·4	1·000	1·000	1·000	1·000	1·000	1·000	1·000	1·000
3·5	1·000	1·000	1·000	1·000	1·000	1·000	1·000	1·000
3·6	1·000	1·000	1·000	1·000	1·000	1·000	1·000	1·000
3·7	1·000	1·000	1·000	1·000	1·000	1·000	1·000	1·000
3·8	1·000	1·000	1·000	1·000	1·000	1·000	1·000	1·000
3·9	1·000	1·000	1·000	1·000	1·000	1·000	1·000	1·000

y \ x_1/l	0·256	0·3645	0·4	0·5	0·6	0·7	0·8	0·9	1·0
0	0·464	0·511	0·524	0·555	0·581	0·603	0·621	0·636	0·650
0·1	0·469	0·515	0·528	0·558	0·584	0·605	0·623	0·638	0·652
0·2	0·484	0·527	0·540	0·569	0·593	0·613	0·631	0·645	0·658
0·3	0·505	0·545	0·556	0·582	0·605	0·624	0·642	0·656	0·668
0·4	0·533	0·567	0·576	0·598	0·619	0·637	0·653	0·668	0·680
0·5	0·568	0·592	0·600	0·618	0·636	0·652	0·666	0·680	0·692
0·6	0·603	0·624	0·632	0·645	0·662	0·674	0·686	0·697	0·707
0·7	0·644	0·659	0·665	0·676	0·688	0·698	0·707	0·716	0·724
0·8	0·686	0·695	0·700	0·708	0·715	0·722	0·729	0·736	0·742
0·9	0·725	0·732	0·736	0·740	0·745	0·750	0·754	0·759	0·764
1·0	0·766	0·770	0·773	0·776	0·779	0·782	0·785	0·788	0·791
1·1	0·801	0·803	0·804	0·806	0·809	0·811	0·813	0·815	0·816
1·2	0·832	0·832	0·833	0·834	0·835	0·836	0·837	0·837	0·838
1·3	0·860	0·860	0·860	0·860	0·860	0·860	0·860	0·860	0·860
1·4	0·886	0·886	0·886	0·886	0·886	0·886	0·885	0·884	0·883
1·5	0·909	0·909	0·909	0·908	0·907	0·906	0·904	0·902	0·900
1·6	0·928	0·928	0·928	0·926	0·924	0·923	0·922	0·920	0·918
1·7	0·944	0·944	0·944	0·943	0·942	0·940	0·938	0·936	0·934
1·8	0·957	0·957	0·957	0·956	0·955	0·954	0·952	0·950	0·948
1·9	0·967	0·967	0·967	0·966	0·965	0·964	0·963	0·961	0·959
2·0	0·976	0·976	0·976	0·975	0·975	0·974	0·973	0·971	0·969
2·1	0·982	0·982	0·982	0·982	0·982	0·981	0·980	0·978	0·976
2·2	0·987	0·987	0·987	0·987	0·987	0·986	0·986	0·984	0·982
2·3	0·991	0·991	0·991	0·991	0·991	0·991	0·990	0·988	0·986
2·4	0·994	0·994	0·994	0·994	0·994	0·994	0·993	0·992	0·990
2·5	0·996	0·996	0·996	0·996	0·996	0·996	0·995	0·994	0·993
2·6	0·997	0·997	0·997	0·997	0·997	0·997	0·996	0·996	0·995
2·7	0·998	0·998	0·998	0·998	0·998	0·998	0·997	0·997	0·996
2·8	0·999	0·999	0·999	0·999	0·999	0·999	0·998	0·998	0·997
2·9	0·999	0·999	0·999	0·999	0·999	0·999	0·998	0·998	0·998
3·0	1·000	1·000	1·000	1·000	1·000	1·000	0·999	0·999	0·999
3·1	1·000	1·000	1·000	1·000	1·000	1·000	0·999	0·999	0·999
3·2	1·000	1·000	1·000	1·000	1·000	1·000	1·000	0·999	0·999
3·3	1·000	1·000	1·000	1·000	1·000	1·000	1·000	1·000	0·999
3·4	1·000	1·000	1·000	1·000	1·000	1·000	1·000	1·000	1·000
3·5	1·000	1·000	1·000	1·000	1·000	1·000	1·000	1·000	1·000
3·6	1·000	1·000	1·000	1·000	1·000	1·000	1·000	1·000	1·000
3·7	1·000	1·000	1·000	1·000	1·000	1·000	1·000	1·000	1·000
3·8	1·000	1·000	1·000	1·000	1·000	1·000	1·000	1·000	1·000
3·9	1·000	1·000	1·000	1·000	1·000	1·000	1·000	1·000	1·000

Table III—continued.

y \ x_1/l	1·2	1·4	1·6	1·8	2·0	2·2	2·4	2·6	2·8
0	0·673	0·693	0·709	0·724	0·736	0·747	0·757	0·765	0·773
0·1	0·675	0·694	0·710	0·725	0·737	0·747	0·757	0·765	0·773
0·2	0·680	0·699	0·714	0·728	0·739	0·749	0·759	0·767	0·775
0·3	0·689	0·706	0·720	0·732	0·743	0·753	0·753	0·770	0·778
0·4	0·699	0·715	0·728	0·739	0·750	0·760	0·769	0·775	0·783
0·5	0·710	0·726	0·738	0·748	0·759	0·767	0·775	0·781	0·788
0·6	0·724	0·738	0·749	0·759	0·768	0·775	0·782	0·788	0·794
0·7	0·738	0·750	0·761	0·770	0·778	0·784	0·790	0·794	0·801
0·8	0·754	0·765	0·774	0·782	0·789	0·795	0·800	0·805	0·809
0·9	0·773	0·782	0·790	0·796	0·802	0·806	0·810	0·814	0·818
1·0	0·796	0·801	0·806	0·810	0·814	0·817	0·820	0·823	0·825
1·1	0·819	0·822	0·824	0·827	0·829	0·831	0·833	0·835	0·837
1·2	0·839	0·840	0·841	0·842	0·843	0·844	0·845	0·846	0·847
1·3	0·859	0·859	0·858	0·858	0·857	0·856	0·856	0·857	0·858
1·4	0·879	0·877	0·875	0·873	0·869	0·868	0·868	0·868	0·868
1·5	0·896	0·892	0·889	0·886	0·883	0·881	0·879	0·878	0·878
1·6	0·913	0·908	0·903	0·899	0·895	0·892	0·890	0·889	0·888
1·7	0·928	0·921	0·916	0·912	0·908	0·905	0·902	0·900	0·898
1·8	0·941	0·934	0·928	0·923	0·919	0·915	0·912	0·909	0·907
1·9	0·952	0·945	0·939	0·934	0·930	0·926	0·922	0·919	0·916
2·0	0·962	0·955	0·949	0·944	0·940	0·935	0·931	0·928	0·925
2·1	0·970	0·963	0·957	0·953	0·948	0·943	0·939	0·936	0·933
2·2	0·977	0·971	0·965	0·961	0·956	0·951	0·947	0·944	0·941
2·3	0·982	0·977	0·972	0·967	0·963	0·958	0·954	0·951	0·948
2·4	0·987	0·982	0·977	0·973	0·969	0·964	0·961	0·958	0·955
2·5	0·990	0·986	0·982	0·978	0·974	0·970	0·967	0·964	0·961
2·6	0·992	0·989	0·986	0·982	0·979	0·975	0·972	0·969	0·966
2·7	0·994	0·992	0·989	0·986	0·983	0·980	0·977	0·974	0·971
2·8	0·996	0·994	0·992	0·989	0·986	0·983	0·981	0·978	0·975
2·9	0·997	0·996	0·994	0·991	0·989	0·986	0·984	0·981	0·979
3·0	0·998	0·997	0·995	0·993	0·991	0·989	0·987	0·985	0·982
3·1	0·999	0·998	0·996	0·995	0·993	0·991	0·989	0·987	0·985
3·2	0·999	0·998	0·997	0·996	0·995	0·993	0·991	0·989	0·987
3·3	0·999	0·999	0·998	0·997	0·996	0·995	0·993	0·991	0·989
3·4	0·999	0·999	0·998	0·998	0·997	0·996	0·994	0·993	0·991
3·5	1·000	0·999	0·999	0·998	0·997	0·996	0·995	0·994	0·993
3·6	1·000	0·999	0·999	0·999	0·998	0·997	0·996	0·995	0·995
3·7	1·000	1·000	0·999	0·999	0·998	0·998	0·997	0·996	0·996
3·8	1·000	1·000	1·000	0·999	0·999	0·998	0·997	0·997	0·997
3·9	1·000	1·000	1·000	0·999	0·999	0·999	0·998	0·998	0·997

APPENDIX

By A. FAGE.

About a year ago, Mr. Falkner and myself had occasion, in connection with some work undertaken for Prof. Taylor, to measure the velocity distribution in the wake behihd a thin flat plate mounted with its plane in the direction of the oncoming stream. The results obtained were unsuitable for the purpose in mind and accordingly they were not published. They have, however, a direct bearing on the theoretical analysis given in Dr. Goldstein's paper and for this reason they are now prepared for publication.

The experiments were made in a 1-foot open-jet tunnel of the double return type. The plate was made of thin sheet aluminium, with very sharp leading and trailing edges. The downstream length (l) of the plate was 5 inches The cross-stream breadth was sufficient to allow the plate to extend beyond the boundary of the jet. Velocity explorations were made across the wake behind the median section of the plate at a distance $0 \cdot 02l$ beyond the trailing edge for the two wind speeds (U_0) 20·46 and 76·8 feet per second, and also at a distance $0 \cdot 512l$ for the speeds 20·6 and 69·7 feet per second The corresponding values of the Reynolds' number (U_0l/ν) for the plate are 0·54 and $2 \cdot 01 \times 10^5$ ($x_1 = 0 \cdot 02l$), and 0·54 and $1 \cdot 83 \times 10^5$ ($x_1 = 0 \cdot 512l$)

The velocity results plotted in a form suitable for comparison with Goldstein's predictions are given in fig 1 The velocity distributions measured close behind the trailing edge of the plate ($x_1 = 0 \cdot 02l$) are given by the full-lines in fig 1*a*, and that predicted by Goldstein by the dotted line. The measured distributions are seen to be in close agreement with the predicted distribution. The flow along and just behind the plate appears therefore to be laminar at the Reynolds' numbers at which the measurements were made. Further, the curves of fig 1*b* show that at the greater distance $0 \cdot 512l$ behind the plate there is little resemblance between the measured and predicted velocity distributions, especially near the axis ($y = 0$). The experimental wakes are also considerably wider than the theoretical wake The differences exhibited are so great, that the only possible explanation would seem to be that at this distance behind the plate the laminar motion has definitely broken down. It will also be observed that the two velocity distributions measured at $x_1 = 0 \cdot 512l$ differ appreciably, a fact which indicates that the distance behind the plate at which the breakdown occurs depends on Reynolds' number

Summary.

The calculation of the velocity distribution in the wake behind an infinitely thin plate parallel to a stream, which had been begun in a previous paper, is completed. Prandtl's boundary layer equations will apply to the flow in the wake of fluids of small viscosity; and these equations are solved by successive approximation for the flow at a considerable distance downstream, by assuming that the velocity there is nearly equal to the undisturbed velocity. The first and second approximations are set out, and it is shown that a third approximation cannot be found by the same methods. The results of the second approximation are then joined up with the results from the previous paper,

which give the velocity distribution from the rear end of the plate to a short distance downstream. In this way the velocity has been approximately calculated all over the field. The calculated velocity distribution is such as strongly to suggest that the steady motion will be unstable some distance behind the plate, and experiments by Fage and Falkner have confirmed this.

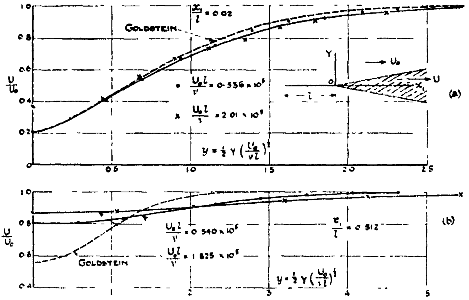

FIG 1.

The formulæ for the velocity at a considerable distance downstream apply to the wake behind any symmetrical obstacle in a stream, for two-dimensional steady motion, though the numerical evaluation is carried out for the flat plate only.

On the Two-Dimensional Steady Flow of a Viscous Fluid Behind a Solid Body.—II.

By S. GOLDSTEIN

(Communicated by L. N. G. Filon, F.R.S.—Received June 15, 1933.)

1. *Introduction*

1.1. One reason for carrying out the calculations of the previous paper was to provide material for an experimental study of the transition to turbulence in the wake behind a plate parallel to the stream. A second reason was to compare the results with certain results due to Filon, who has calculated both the first and second approximations to the velocity at a considerable distance from a fixed cylindrical obstacle in an unlimited stream whose velocity at infinity is constant.* He also uses the notions of the Oseen approximation, that is to say, he assumes that the departures from the undisturbed velocity are small, and neglects terms quadratic in these departures for the first approximations, etc., but he does not assume that ν is small and does not use the Prandtl equations. Thus the formulæ of Paper 1, paragraph 2, should be limiting forms, for small ν, of Filon's formulæ for a symmetrical wake. This is verified in paragraph 2 below, and the calculations in Paper 1, paragraph 2, other than the attempt at a third approximation, may be regarded as a simplified form of Filon's calculations.

The direct simplification of Filon's results gives the formulæ 2 (31) (p. 569), for the velocity at a sufficient distance downstream in any symmetrical wake provided that the motion is steady, whether ν is small or not. These formulæ differ only in the last terms from the formulæ 2 (27) on p. 553 of Paper 1, obtained from the Prandtl equations, and these terms are negligible, compared with the others, when ν is small. (For the meaning of the symbols, see paragraph 1.3 of Paper 1.) Thus the first asymptotic approximation is exactly the same here as in the previous paper; in the second approximation the more accurate results of this paper contain extra terms, which it is shown on p. 567 arise entirely from the previous neglect of the pressure gradient in the direction of the stream.

The wake broadens out downstream, and becomes infinitely broad when X is infinite, so that if the basic hypothesis of the Prandtl theory is expressed, as it sometimes is, by saying that the velocity differs from its value in the main stream, and the velocity gradient is large, only within a narrow layer, then it may seem surprising, at first sight, that the theory applies at all some distance downstream. But, more accurately expressed, the hypothesis is that δ/L should be small, with U_0L/ν large, where δ is the width of the layer, and L a representative length of the system. In the wake the correct representative length is X (the distance from some point in the neighbourhood of the obstacle), and although δ is of the order of $(\nu X/U_0)^{\frac{1}{2}}$, and increases like $X^{\frac{1}{2}}$, δ/X is of the order $(\nu/U_0X)^{\frac{1}{2}}$, and decreases like $X^{-\frac{1}{2}}$ In fact, δ/X is of the order of the square root of the reciprocal of the representative Reynolds' number, $U_0 X/\nu$, in accordance with general theory. Moreover, the representative Reynolds' number increases, and the theory gives a closer and closer approximation, as X increases, in the application to the plate, the theory will not give correct results immediately behind the rear end of the plate, as we can also see from the occurrence there of a mathematical singularity in the solution (The same remarks apply also, of course, to the flow along the plate Blasius's solution will not apply in the immediate neighbourhood of the front edge, it becomes a better and better approximation the further we go along the plate, the representative length being, not the length of the plate, but the distance from the front edge *)

---

* 'Proc. Roy. Soc.,' A, vol. 113, p. 7 (1926); 'Phil. Trans.,' A, vol. 227, p. 93 (1928).

1 4 To the end of paragraph 2 we are concerned entirely with flow in a symmetrical wake, in paragraph 3 we are concerned with an asymmetrical wake In his second paper, Filon came to the conclusion that the second approximation he had obtained was invalid, and that Oseen's equations could not be used as a basis for approximations after the first He came to this conclusion because, after expressing the torque on the cylinder in terms of an integral round a circle of large radius, with an integrand involving the formulæ he had found for the velocities, the integral for the torque did not tend to a finite limit as the radius of the circle tended to infinity, but became infinite like a multiple of the logarithm of the radius The objection does not apply when the obstacle and wake are symmetrical, when this is not the case, there is a circulation round any contour embracing the cylinder, and it is shown in paragraph 3 that it might have been expected that Oseen's equations would not be a suitable basis for further approximations in this case, and that

---

* The approximations of the boundary-layer theory usually introduce an error of the order of the square root of the reciprocal of the representative Reynolds' number. (See 'Proc. Camb. Phil. Soc.,' *loc. cit.*, p. 3.) The special circumstances of the present problem are such that this does not hold here. *Cp.* p. 563 of the previous paper.

the expression for the couple, formed on this basis, would necessarily have an infinite term of exactly the amount found by Filon

2 *Direct Simplification of Filon's results*

2 1 ***First Approximation*** —For the first approximation, Filon's results, in the case of a symmetrical wake, are (equations (F 3 6) (F 3 7))*

$$U = U_0 + U' + U'', \qquad V = V' + V'', \tag{1}$$

where

$$\left.\begin{aligned} U' &= \frac{\alpha_0}{k^2}\frac{\cos\theta}{r} + \sum_{n=1}^{\infty}\frac{nc_n\cos(n+1)\theta}{r^{n+1}} \\ V' &= -\frac{\alpha_0}{k^2}\frac{\sin\theta}{r} + \sum_{n=1}^{\infty}\frac{nc_n\sin(n+1)\theta}{r^{n+1}} \end{aligned}\right\} \tag{2}$$

$$\left.\begin{aligned} U'' &= \frac{e^{kX}}{k}\sum_{n=1}^{\infty} a_n\left[K_n(kr)\cos n\theta + K_{n+1}(kr)\cos(n+1)\theta\right] \\ V'' &= \frac{e^{kX}}{k}\sum_{n=1}^{\infty} a_n\left[K_{n+1}(kr)\sin(n+1)\theta - K_n(kr)\sin n\theta\right] \end{aligned}\right\}, \tag{3}$$

and

$$k = U_0/2\nu, \tag{4}$$

K_n is the Bessel function usually so denoted, a_n, c_n are arbitrary constants such that

$$\alpha_0 = \sum_{n=0}^{\infty} a_n, \tag{5}$$

and, according to the main results of Filon's first paper,

$$D = -2\pi\rho U_0\alpha_0/k^2, \tag{6}$$

where D is the drag on the obstacle per unit length, so that

$$\frac{\alpha_0}{k^2} = -\frac{k_D}{2\pi}U_0 d, \tag{7}$$

where d is a representative length of the obstacle, and k_D the drag coefficient. Also, r and θ are polar co-ordinates corresponding to our Cartesian co-ordinates X, Y In the wake θ is small, we may replace $\cos\theta$ by 1, $\sin\theta$ by Y/X, and r by X The first approximations to U′ and V′ are therefore

$$\left.\begin{aligned} U' &= -\frac{\alpha_0}{k^2X} = \frac{k_DU_0d}{2\pi X} \\ V' &= -\frac{\alpha_0Y}{k^2X^2} = \frac{k_DU_0dY}{2\pi X^2} \end{aligned}\right\} \tag{8}$$

---

* The notation has been slightly changed. References with F are to Filon's second paper.

When kr is large,

$$K_n(kr) \sim \left(\frac{\pi}{2kr}\right)^{\frac{1}{2}} e^{-kr} \tag{9}$$

Hence, if the a_n fall off sufficiently rapidly, the first approximation to U″ is

$$\begin{aligned} U'' &= 2\,\frac{e^{-k(r-X)}}{k}\left(\frac{\pi}{2kr}\right)^{\frac{1}{2}} \Sigma a_n \\ &= \frac{(2\pi)^{\frac{1}{2}}\, \alpha_0 e^{-k(r-X)}}{k^{3/2} r^{\frac{1}{2}}} \end{aligned} \tag{10}$$

Again, $r - X$ is equal to $r(1 - \cos\theta)$, and is approximately $\frac{1}{2}X\,\theta^2$ or $Y^2/2X$ Hence

$$U'' = -\frac{k_D U_0\, d k^{\frac{1}{2}}}{2\pi X^{\frac{1}{2}}}\, e^{-kY^2/2X} \tag{11}$$

Similarly

$$\begin{aligned} V'' &= 2\,\frac{e^{-k(r-X)}}{k}\left(\frac{\pi}{2kr}\right)^{\frac{1}{2}} \Sigma\, a_n \cos\left(n + \tfrac{1}{2}\right)\theta \sin\tfrac{1}{2}\theta \\ &= \frac{\alpha_0 e^{-kY^2/2X}}{k}\left(\frac{\pi}{2kX}\right)^{\frac{1}{2}} \frac{Y}{X} \\ &= -\frac{k_D U_0\, d k^{\frac{1}{2}}}{(2\pi X)^{\frac{1}{2}}}\, \frac{Y}{2X}\, e^{-kY^2/2X} \end{aligned} \tag{12}$$

If we now put

$$\left.\begin{aligned} u &= \frac{U}{U_0}, \qquad v = \left(\frac{d}{\nu U_0}\right)^{\frac{1}{2}} V, \qquad x = \frac{X}{d}, \\ y &= \left(\frac{U_0}{\nu d}\right)^{\frac{1}{2}} Y, \qquad \eta = \frac{y}{(2x)^{\frac{1}{2}}} = \left(\frac{U_0}{2\nu X}\right)^{\frac{1}{2}} Y = \frac{k^{\frac{1}{2}} Y}{X^{\frac{1}{2}}} \end{aligned}\right\}, \tag{13}$$

as before, we find, for the simplified form of Filon's first approximation

$$\left.\begin{aligned} u &= 1 - A\left[x^{-\frac{1}{2}} e^{-\frac{1}{2}\eta^2} - \left(\frac{\nu}{\pi U_0 d}\right)^{\frac{1}{2}} x^{-1}\right] \\ v &= -\frac{A}{\sqrt{2}}\left[x^{-1}\eta e^{-\frac{1}{2}\eta^2} - 2\left(\frac{\nu}{\pi U_0 d}\right)^{\frac{1}{2}} \eta x^{-3/2}\right] \end{aligned}\right\}, \tag{14}$$

where

$$A = \frac{1}{2\pi^{\frac{1}{2}}}\left(\frac{U_0 d}{\nu}\right)^{\frac{1}{2}} k_D, \tag{15}$$

as in 2 (30) of the previous paper (p. 553).

The first terms here are the same as in 2 (27) of the previous paper (p. 553). The terms neglected here in u are of order $x^{-3/2}$.

The variable part of the pressure is seen from Lamb's form of the solution of Oseen's equations* to be given by

$$p = -\rho U_0 U' \tag{16}$$

Hence

$$\frac{p}{\rho U_0^2} = -\frac{k_D d}{2\pi X} = -\frac{k_D}{2\pi x}, \tag{17}$$

and

$$\frac{1}{\rho U_0^2}\frac{\partial p}{\partial x} = \frac{k_D}{2\pi x^2} = \left(\frac{\nu}{\pi U_0 d}\right)^{\frac{1}{2}}\frac{A}{x^2} \tag{18}$$

This is the term neglected in the reduced equations of motion 2 (2) on p 550 of the previous paper. It is of order x^{-2} The terms omitted in calculating it are of order x^{-3}

If we retain this term in the reduced equations 2 (2) of Paper 1, it will affect the second approximation found in paragraph 2 2 We should add

$$-\frac{1}{\rho U_0^2}\frac{\partial p}{\partial x}$$

to the right side of 2 (13) on p 552, and

$$-\left(\frac{\nu}{\pi U_0 d}\right)^{\frac{1}{2}}\frac{A}{x}$$

to w_2 Also we should add

$$\left(\frac{\nu}{\pi U_0 d}\right)^{\frac{1}{2}}\frac{Ay}{x^2} = \left(\frac{2\nu}{\pi U_0 d}\right)^{\frac{1}{2}}\frac{Ay}{x^{3/2}}$$

to v_2. These are exactly the second terms in (14) above

2.2 *Second approximation*—For the second approximation, Filon finds that we must add to U and V the terms U_2 and V_2 respectively, where

$$U_2 = -\frac{\partial\psi_2}{\partial Y} \qquad V_2 = \frac{\partial\psi_2}{\partial X} \tag{19}$$

and, for the symmetrical wake,

$$\psi_2 = -\frac{4\pi\alpha_0^2}{k^3 U_0}\left[\left\{E(\eta) + \tfrac{1}{2}e^{-\frac{1}{2}\eta^2}\int_0^\eta e^{-\frac{1}{2}\eta^2}\,d\eta\right\}\xi^{-1} - \pi^{\frac{1}{2}}\cos\tfrac{1}{2}\theta/4\,(kr)^{\frac{1}{2}}\right]. \tag{20}$$

((F 8 1) and (F 5.43).) ξ and η are parabolic co-ordinates such that

$$\left.\begin{aligned} \xi + i\eta &= 2k^{\frac{1}{2}}(X + iY)^{\frac{1}{2}} \\ \xi^2 &= 2k\,(r+X) \\ \eta^2 &= 2k\,(r-X) \end{aligned}\right\} \tag{21}$$

---

* "Hydrodynamics," p. 582 (1924).

and

$$\left.\begin{aligned} U_2 &= -\frac{1}{2r}\left[\eta\frac{\partial\psi_2}{\partial\xi} + \xi\frac{\partial\psi_2}{\partial\eta}\right] \\ V_2 &= \frac{1}{2r}\left[\xi\frac{\partial\psi_2}{\partial\xi} - \eta\frac{\partial\psi_2}{\partial\eta}\right] \end{aligned}\right\} \tag{22}$$

(See F 4) Also ξ is to be taken positive in the (X, Y) plane,

$$\left.\begin{aligned} E(\eta) &= \int_\eta^\infty e^{-\eta^2}\,d\eta \qquad (\eta > 0) \\ &= \int_\eta^{-\infty} e^{-\eta^2}\,d\eta \qquad (\eta < 0) \end{aligned}\right\}, \tag{23}$$

so that E (η) is an odd function, and in (20) we must take θ from 0 to 2π and not from $-\pi$ to π As a result, ψ_2 and its relevant derivatives are continuous, and U_2 is an even function of Y, V_2 an odd function We shall therefore find U_2 and V_2 for $Y \geqslant 0$

In the wake, when X is large,

$$\xi = 2\,(kX)^{\frac{1}{2}}, \qquad \eta = \frac{k^{\frac{1}{2}}Y}{X^{\frac{1}{2}}}, \tag{24}$$

so that η is the same quantity as defined above in (13).

Consider first the part of ψ_2 explicitly involving ξ and η For this part

$$\begin{aligned} \frac{\partial\psi_2}{\partial\eta} &= \frac{4\pi\alpha_0^2}{k^3U_0\xi}\left[\tfrac{1}{2}e^{-\eta^2} + \tfrac{1}{2}\eta e^{\ \frac{1}{2}\eta^2}\int_0^\eta e^{-\frac{1}{2}\eta^2}\,d\eta\right] \\ &= \frac{k^{\frac{1}{2}}U_0\,d^2k_D^2}{4\pi X^{\frac{1}{2}}}\left[e^{-\eta^2} + (\tfrac{1}{2}\pi)^{\frac{1}{2}}\,\eta e^{-\frac{1}{2}\eta^2}\operatorname{erf}(\eta/\sqrt{2})\right], \end{aligned} \tag{25}$$

(see (7) and (24) above, and 2 (23) on p 553 of Paper 1), and

$$\frac{\partial\psi_2}{\partial\xi} = \frac{U_0\,d^2k_D^2}{8\pi X}\left[2E(\eta) + (\tfrac{1}{2}\pi)^{\frac{1}{2}}\,e^{-\frac{1}{2}\eta^2}\operatorname{erf}(\eta/\sqrt{2})\right]. \tag{26}$$

Hence, for this part, U_2 and V_2 are approximately given by

$$U_2 = -\frac{kU_0d^2k_D^2}{4\pi X}\left[e^{-\eta^2} + (\tfrac{1}{2}\pi)^{\frac{1}{2}}\,\eta e^{-\frac{1}{2}\eta^2}\operatorname{erf}(\eta/\sqrt{2})\right], \tag{27}$$

and (since

$$E(\eta) = \tfrac{1}{2}\sqrt{\pi}\,(1 - \operatorname{erf}\eta) \tag{28}$$

for $\eta > 0$)

$$V_2 = \frac{k^{\frac{1}{2}}U_0\,d^2k_D^2}{8\pi X^{3/2}}\left[\pi^{\frac{1}{2}}(1 - \operatorname{erf}\eta) + (\tfrac{1}{2}\pi)^{\frac{1}{2}}(1 - \eta^2)\,e^{-\frac{1}{2}\eta^2}\operatorname{erf}(\eta/\sqrt{2}) - \eta e^{-\eta^2}\right]. \tag{29}$$

In the same way, we find that the term in (r, θ) in ψ_2 gives a contribution to U_2 which is of order X^{-2}. Its contribution to V_2 is

$$V_2 = -\frac{k^{\frac{1}{2}} U_0 d^2 k_D^2}{8\pi^{\frac{1}{2}} X^{3/2}}. \tag{30}$$

This just cancels the first term in (29), and from (13) and (15) it follows that the contributions to u and v from Filon's second approximation are

$$\left.\begin{aligned} u &= -\frac{A^2}{2x}\left[e^{-\eta^2} + (\tfrac{1}{2}\pi)^{\frac{1}{2}}\,\eta e^{-\frac{1}{2}\eta^2}\operatorname{erf}(\eta/\sqrt{2})\right] \\ v &= \frac{A^2}{(2x)^{3/2}}\left[(\tfrac{1}{2}\pi)^{\frac{1}{2}}\,(1-\eta^2)\,e^{-\frac{1}{2}\eta^2}\operatorname{erf}(\eta/\sqrt{2}) - \eta e^{-\eta^2} - \pi^{\frac{1}{2}}\operatorname{erf}\eta\right] \end{aligned}\right\}.$$

From (14) it now follows that the values of u and v correct to the second approximation are

$$\left.\begin{aligned} u &= 1 - Ax^{-\frac{1}{2}}e^{-\frac{1}{2}\eta^2} - x^{-1}\Big[\tfrac{1}{2}A^2\{e^{-\eta^2} + (\tfrac{1}{2}\pi)^{\frac{1}{2}}\,\eta e^{-\frac{1}{2}\eta^2}\operatorname{erf}(\eta/\sqrt{2})\} \\ &\qquad\qquad - A\left(\frac{\nu}{\pi U_0 d}\right)^{\frac{1}{2}}\Big] \\ v &= -\frac{A}{\sqrt{2x}}\,\eta e^{-\frac{1}{2}\eta^2} + x^{-3/2}\Big[\frac{A^2}{2^{3/2}}\{(\tfrac{1}{2}\pi)^{\frac{1}{2}}\,(1-\eta^2)\,e^{-\frac{1}{2}\eta^2}\operatorname{erf}(\eta/\sqrt{2}) \\ &\qquad\qquad - \eta e^{-\eta^2} - \pi^{\frac{1}{2}}\operatorname{erf}\eta\} + A\left(\frac{2\nu}{\pi U_0 d}\right)^{\frac{1}{2}}\eta\Big] \end{aligned}\right\} \tag{31}$$

These formulæ should give the velocity components in any symmetrical wake for sufficiently large values of x whenever the motion is steady.

When ν is small, the last terms are negligible compared with the others. Apart from them, the formulæ are the same as those in Paper 1, 2 (27), p. 553.

3. *On the Calculation of the Torque on an Asymmetrical Obstacle.*

If the immersed cylindrical body is not symmetrical, then the wake is not symmetrical, and there is circulation round any circuit enclosing the cylinder. If we assume that at a large distance from the cylinder the first approximation to the velocity satisfies Oseen's equations, then, as in 2 (1), this first approximation is given by

$$U = U_0 + U' + U'', \qquad V = V' + V'', \tag{1}$$

where U'' and V'' are insensible outside the wake, and

$$U' = \frac{\partial\phi}{\partial X}, \qquad V' = \frac{\partial\phi}{\partial Y}, \tag{2}$$

the leading terms in ϕ being*

$$\phi = \mathrm{C} \log r + \mathrm{D}\theta + \ldots \tag{3}$$

According to (3) the terms (U′, V′) give an outflow across a large circuit equal to 2π C. The terms (U″, V″) must give an equal inflow These terms are sensible only in the wake. The inflow in the wake due to (U″, V″) is therefore 2π C. The inflow in the wake due to (U′, V′) is negligible, since (U′, V′) are of order r^{-1}, and the width of the wake is of order $r^{\frac{1}{2}}$ Hence, apart from the constant velocity U_0, the total inflow in the wake is 2π C

Again, according to (3), there is a circulation 2π D round any large circuit, due to the terms (U′, V′) If the circuit cuts the wake at right angles, this is the whole of the circulation, the contribution from (U″, V″) being negligible For this contribution is

$$\int \mathrm{V}'' \, d\mathrm{Y}, \tag{4}$$

along a line X = constant across the wake V″ consists of two parts, one of which is an odd function and the other an even function of Y (see (F 3·72)). The odd function has been considered in paragraph 2, and shown to be of order $\mathrm{Y}e^{-k\mathrm{Y}^2/2\mathrm{X}}/\mathrm{X}^{3/2}$. The even function is easily seen to be of order Y/X compared with this Since Y is of order $\mathrm{X}^{\frac{1}{2}}$ in the wake, the even part of V″ is of order $\mathrm{X}^{-3/2}$, and the contribution of (4) to the circulation of order X^{-1}

Let us now take a large contour cutting the wake at right angles The pressure and viscous stresses over this contour have a moment, and the couple exerted by the fluid on the solid must be equal to this moment, minus the rate of outflow of angular momentum. Filon found that when the contour is a large circle of radius R, the couple as thus calculated became infinite with R like $-4\pi\rho$ CD log R We shall show that this result is to be expected. It is easier to take a rectangle, Y = ± ∞, X = ± constant, when Filon's result is that the couple becomes infinite like $-4\pi\rho$ CD log X.

In the accurate equations of motion there are terms representing the convective rate of change of the velocity; and in the equation for the vorticity, there are terms representing the convective rate of change of the vorticity. In Oseen's approximation, the velocity of convection is assumed to be (U_0, O). When there is a circulation 2π D round the obstacle, this velocity differs appreciably from the correct value not only in amount, but also in direction, since in the wake there is a velocity D/X at right angles to U_0. The wake is really displaced from the symmetrical position, where it is according to Oseen, through a distance Y, such that approximately

---

* C and D are used instead of Filon's $-\alpha_0/\kappa^2$ and $-d_0$ respectively.

$$\frac{dY}{dX} = \frac{D}{U_0 X}, \qquad Y = \frac{D}{U_0} \log X + \text{constant}. \tag{5}$$

Now consider the rate of outflow of angular momentum through the rectangle mentioned above Let us suppose that this rate of outflow has been calculated by the use of the first approximations to the velocities, as given by equation (1) (p 569); when calculated on this basis, the result is finite (F paragraph 20). Now suppose that, instead of calculating out at length the second approximations to the velocities, and recalculating the rate of outflow of angular momentum using them, we simply allow for the most important part of the error of the first approximation by moving the whole wake through a distance $(D/U_0) \log X$ parallel to the axis of Y, and calculate the effect of this displacement of the wake on the rate of outflow of angular momentum. Only along the side $X =$ constant of the rectangle mentioned above will the displacement of the wake produce an effect The rate of outflow of angular momentum is

$$\rho \int U(VX - UY)\, dY, \tag{6}$$

where the integral is along the side $X =$ constant Only the part of the integrand containing Y need be considered here, and if we write

$$U = U_0 + U' + U''$$

as in equation (1) (p. 569), then only the terms containing U'' are affected by the displacement of the wake, and we proceed to calculate the effect of the displacement on the most important of these terms, namely,

$$-2\rho U_0 \int U'' Y\, dY. \tag{7}$$

U'' is sensible only in the wake. The displacement of the wake through a distance $(D/U_0) \log X$ parallel to the axis of Y in the positive direction, therefore increases the term in (7) by

$$-2\rho U_0 (D/U_0) \log X \int U''\, dY. \tag{8}$$

Now $-\int U''\, dY$ is the inflow in the wake due to (U'', V''), and is therefore $2\pi C$. The displacement of the wake therefore increases the rate of outflow of angular momentum by $4\pi\rho$ CD log X from the value as given by the first approximation to the velocities, and the couple is decreased by the same amount from its value given by the first approximation to the velocities. If, therefore, we calculated the couple on the solid cylinder by considerations of angular momentum, according to the first Oseen approximation for the velocities at a large distance, and then allowed for the displacement of the wake in the actual flow from the symmetrical position, we should find exactly the infinite term which Filon found from the second approximation.

Some very helpful criticism by Professor Filon, to whom I am very much indebted for it, led me to rewrite part of the preceding paragraph, and also to consider another point which might be mentioned At a large distance downstream in the wake, the most important part of U″ is an even function of Y and is approximately given by

$$-(2\pi k)^{\frac{1}{2}}\,\mathrm{C}\mathrm{X}^{-\frac{1}{2}}e^{-k\mathrm{Y}^2/2\mathrm{X}}.\text{*} \tag{9}$$

This is of order $\mathrm{X}^{-\frac{1}{2}}$ in the wake. The part of U″ which is an odd function of Y is of order Y/X or $\mathrm{X}^{-\frac{1}{2}}$ compared with this, and is therefore of order X^{-1}. Also U′ is of order r^{-1}, or of order X^{-1} in the wake. If we now suppose that when the second approximation is found, this adds on a term U_2 to U, then, in the asymmetrical wake, the most important term in U_2 is, in Filon's notation

$$\mathrm{L}_1\eta e^{-\frac{1}{4}r^2}\log(\xi/2)/8k^3r\mathrm{U} \tag{10}$$

(See F 19.1.†) If we transfer to the notation here used, and keep only the most important part, we get

$$-\frac{(2\pi k^3)^{\frac{1}{2}}\,\mathrm{CDY}e^{-k\mathrm{Y}^2/2\mathrm{X}}\log\mathrm{X}}{\mathrm{U}_0\mathrm{X}^{3/2}}, \tag{11}$$

which is of order $\mathrm{X}^{-1}\log\mathrm{X}$ in the wake, and is therefore larger than any other term in $\mathrm{U}-\mathrm{U}_0$ except (9). Hence (9) and (11) together give the most important part of $\mathrm{U}-\mathrm{U}_0$ in the wake, as far as the second approximation. Together, they give

$$-(2\pi k)^{\frac{1}{2}}\,\mathrm{CX}^{-\frac{1}{2}}e^{-k\mathrm{Y}^2/2\mathrm{X}}\left\{1+\frac{k\mathrm{D}}{\mathrm{U}_0\mathrm{X}}\mathrm{Y}\log\mathrm{X}\right\}. \tag{12}$$

Now (12) is exactly what its first term, or (9), becomes when we substitute

---

* This is the same as the value in equation (10) (p. 566) or equation (11) (p. 566) with the notation adapted in this section. See the footnote on p. 570.

† This term is quoted from a formula for the radial velocity, not for the velocity parallel to the axis of X. But it is easy to see that to our order of approximation the radial and axial velocities may be taken equal in the wake.

$Y + (D/U_0)\log X$ for Y, and approximate, considering Y large compared with $\log X$. (Since, in the integral for the rate of outflow of angular momentum, a factor Y in the integrand introduces a factor of order $X^{\frac{1}{2}}$ in the integral, this is justified.) In other words, the second approximation for the velocity in the wake is the same function of $Y + (D/U_0)\log X$ as the first approximation is of Y. But this statement is exactly the same as saying that the wake is displaced through a distance $(D/U_0)\log X$ parallel to the axis of Y. Since it was exactly the term in (10) that led to the infinite term for the couple in Filon's work, and since this term also accounts for the displacement of the wake, we see that it is exactly because the first approximation does not take account of the displacement of the wake, and the second approximation does, that the infinite term in the couple arises. In order to proceed correctly by successive approximation it would therefore be necessary to take account of the displacement of the wake in the first approximation.

Summary

The general formulæ of the previous paper, for the velocity at a considerable distance downstream in the wake behind a symmetrical obstacle, in a two-dimensional steady stream of viscous fluid, are compared with the results of some calculations made by Filon, in which he calculated the velocity in the wake behind a cylindrical obstacle by the method of successive approximation, but without the approximations of the boundary layer theory. It is shown that for a symmetrical wake Filon's formulæ reduce, for small viscosity, to those here found; and the additional terms, when the viscosity is not small, are given in simplified form.

For an asymmetrical obstacle, Filon came to the conclusion that his second approximation was invalid, because the calculation of the torque on the obstacle, from this second approximation and from considerations of angular momentum, led to an infinite result. It is shown that this infinite term is entirely accounted for if allowance is simply made for the effect of the circulation round the asymmetrical obstacle in displacing the wake, in the actual motion, from the symmetrical position which it occupies according to the first approximation.

Some Intensity Measurements on the Band Spectrum of Helium (He_2).

By R. C. Johnson, M A., D.Sc. and R. C. Turner, B Sc., King's College, London.

(Communicated by O W Richardson, F R S —Received July 1, 1933)

Introduction.

The Summation Rule of Burger and Dorgelo in the hands of R. H Fowler, Mulliken, Dieke and others, has led to the rapid development of theoretical intensity relations For some time only qualitative data were available, but with the development of intensity measurement technique, quantitative data are accumulating to test the theoretical predictions

Work of a quantitative nature on the band spectrum of Helium has been carried out by Childs,* Fujioka,† and Read,‡ who have made measurements on the 4650 band, the "decoupling bands," and the λ 6400 band respectively.

In the present paper the five bands λλ 4650, 3676, 3356, 3206, and 3120 have been examined and the intensities in each band studied in detail. These bands are the first five members of the main "line series" of Helium. ($np\pi\,{}^3\Pi \rightarrow 2s\sigma\,{}^3\Sigma$.)

Experimental.

(1) *Excitation of the Helium Bands.*—The tube used was 50 cm. in length with a cross section of 1·5 cm. having aluminium electrodes A quartz window at one end and a mirror at the other were affixed with sealing wax. Bulbs containing P_2O_5 and KOH, and a Palladium regulator were fused on the sides.

The tube was excited with a condensed discharge produced by an alternator and transformer, the secondary of which was shunted by a condenser of a few thousand cm. capacity, a small spark gap being placed in series with the tube.

The bands λ 4650 and λ 3676 were photographed in the first position (λ 8000 — λ 3200) and the bands λ 3676, λ 3356, λ 3206 and λ 3120 in the second position (λ 4200 — λ 2800) of a Hilger E1 Quartz spectrograph. The intensity of each line of the common band λ 3676 was obtained in the first and in the second position, and the ratio of the intensities in the two positions, for each line, obtained. The mean of these ratios was taken as the correlation factor, by which all the intensities in the bands λ 3356, λ 3206 and λ 3120 were multiplied.

---

* 'Proc Roy. Soc.,' A, vol. 118, p. 296 (1927).

† 'Z. Physik,' vol. 63, p. 175 (1930).

‡ 'Proc. Roy Soc,' A, vol. 134, p. 643 (1932).

(2) *Photometric technique*.—The intensities were measured by observations on the densities of the images produced on the photographic plate. A set of calibration marks, using a step slit and standard lamp, was obtained on each plate, care being taken to ensure that the times of exposure for both spectrum and calibrations were kept identical.

A large number of plates were obtained and of these, seven were microphotometered. Photometric records for both spectrum and calibration marks were obtained on the photo-electric recording micro-photometer kindly placed at our disposal by Professor A. Fowler, of the Imperial College of Science.

Blackening-intensity curves for four points over each band were constructed and from these curves the intensity of each line determined. These intensities were corrected for energy-wave-length distribution of the standard lamp, and for the dispersion of the instrument, and brought to the same scale formed by taking the strongest line of the strongest band (Q5 of band 4650) as intensity = 1000.

Ilford special rapid panchromatic plates were used throughout, as the grain of these plates is much less pronounced than that of faster plates.

Experimental Results.

The corrected intensities on the 1000 scale are given in Tables I to V. The wave-lengths are taken from a paper by Curtis and Long.*

Table I.—Band near λ 4650.

	P Branch.			Q Branch			R Branch.		
J	λ air	ν vac	I	λ air	ν vac	I.	λ air	ν vac	I
1	—	—	—	4649 78	21506 4	967†	4642 38	21534·7	528
3	4658 79	21458 8	—	4650 65	21502 3		4637 34	21558 1	580
5	4666 83	21421 8	491	4651 00	21494 8	1000	4633 18	21577·4	566
7	4675 67	21381 3	717	5653·32	21484 0	960	4629 91	21592 7	412
9	4685·31	21337 4	616	4656 35	21470·1	863	4627·53	21603·8	266
11	4695·70	21290·1	403	4660·06	21453 0	796	—	—	429†
13	4706 82	21239 9	254	4664 46	21432 8	401	—	—	
15	4718·61	21186 8	150	4669 52	21409·5	210	—	—	
17	4731 02	21131 2	80	4675 14	21383·8	108	—	—	

† Unresolved lines.

---

* 'Proc. Roy. Soc.,' A, vol. 108, p. 513 (1925).

In figs. 1 to 5 the intensities, all on the same scale, are plotted against J′ values for each branch of each band. Perturbed lines are indicated by the letter *p*.

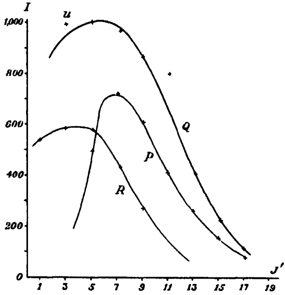

FIG 1 —Band λ 4650 *u* — unresolved lines.

Table II —Band near λ 3676.

	P Branch			Q Branch.			R Branch		
J	λ air	ν vac	I	λ air	ν vac	I	λ air	ν vac	I
1	—	—	—	3676 49	27192·1	240†	3672 77	27219 7	115
3	3683 02	27143·9	43	3677 11	27187·5		3669 86	27241 3	164
5	3688·29	27105 1	65	3678 22	27179 4	300	3667 74	27257 0	168*
7	3694 31	27061 0	179*	3679·84	27167 4	270	3666 02	27269 8	112
9	3700 66	27014 5	156	3682·17	27150 2	137*	—	—	200†
				3681·29	27156 7	62*			
11	3707 68	26962 6	106	3684 43	27133·5	156	—	—	
13	3715 46	26906 9	74	3687 47	27111 2	112	—	—	
15	3723 66	26847 7	45	3690 96	27085·6	77	—	—	
17	3732·38	26785·0	20	—	—	—			

* Perturbed intensity. † Unresolved lines

The following general conclusions have been arrived at by Mulliken‡ with regard to the intensities in the λ 4650 band.

---

‡ 'Phys. Rev,' vol. 29, p. 391 (1927).

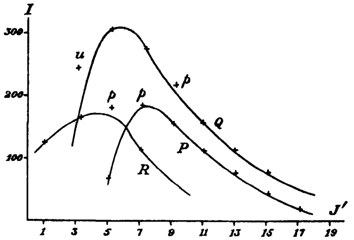

FIG. 2 —Band λ 3676 *u* — unresolved lines ; *p* = perturbed lines.

Table III.—Band near λ 3356.

	P Branch			Q Branch			R Branch.		
J	λ air	ν vac	I	λ air	ν vac	I	λ air	ν vac	I.
1	—	—	--	3356 48	29784 6	32	3353 46	29811·5	35*
3	3362 02	29735 5	16	3357 04	29779 6	60	3351 09	29832·5	37
				1 ⎧3357 85	29772 4	15*			
5	3366 47	29696 2	29				3349 52	29846 5	40
				2 ⎩3358 25	29768 9	65*			
7	3371 60	29650 5	33	3359·39	29758 8	66	—	—	—
9	3377·38	29600 3	16	3361 16	29743 1	44	—	—	—
11	3383·63	29545·6	10	3363 37	29723 6	28	—	—	—
13	3390·31	29487 4	6	3365 99	29700 4	14	—	--	—
15	—	—	—	3368 97	29674 2	7	-	—	—

* Perturbed intensity

Table IV.—Band near λ 3206

	P Branch.			Q Branch			R Branch		
J.	λ air	ν vac	I.	λ air	ν vac	I.	λ air	ν vac	I.
1	—	—	—	3206 37	31179 1	9	3203 74	31204 6	13
3	3211·52	31129 0	5	3206 87	31174·1	19	3201 97	31221·8	19
5	3216 02	31085·4	10	3207 72	31165·8	26	3200·96	31231·6	20
7	3221 16	31035 8	13	3209 02	31153·2	24	—	—	—
9	3227·00	30979·6	7	3210·69	31137 0	17	—	—	—
11	3233·39	30918·4	5	3212 68	31117 7	12	—	—	—
13	3240·24	30853·1	3	3215 14	31093·9	9	—	—	—
15	—	—	—	3217·92	31067·1	6	—	—	—

1. The Q branch is always the strongest and its maximum intensity should be twice as strong as that of the P or R branches

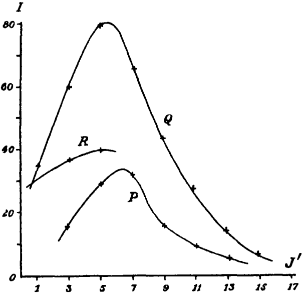

FIG. 3.—Band λ 3356.

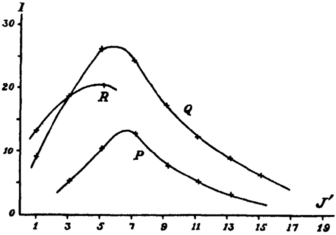

FIG. 4.—Band λ 3206.

That the Q branch is the strongest may be seen immediately from figs. 1 to 5, but the prediction that its maximum should be twice as strong as that of the P or R branches is not verified. We find that in the λ 4650 band the relation of the maximum intensity of the Q branch to that of the P branch is

Table V.—Band near 3120.

	P Branch			Q Branch			R Branch		
J.	λ air	ν vac	I.	λ air	ν vac	I.	λ air	ν vac	I.
1	—	—	—	3122 55	32015 9	—	3120 18	32040 2	2
3	3127 60	31964 2	3	3123 02	23011 0	3	3118 78	32054·5	6
5	3132 10	31918 2	7	3123 85	32002 6	16	3118 13	32061·3	11
7	3137 34	31864·9	10	3125 07	31990 0	15	—	—	—
9	3143·15	31806 0	7	3126 65	31973 8	11	—	—	—
11	3149·43	31742 6	3	3128 61	31953 8	8	—	—	—
13	3156 08	31675 1	1	3130 91	31930 4	6	—	—	—

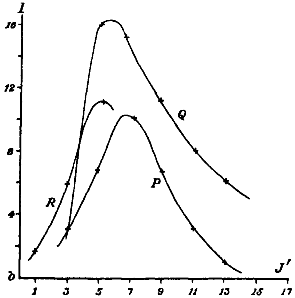

Fig 5.—Band λ 3120.

100 : 72, which agrees very well with the ratio of 100 . 70 found by Childs (*loc. cit.*).

2. The values of J′ for the strongest line in each branch should be in the order P > Q > R and should be of the same order for all the bands

This is well borne out by our results, the maxima being in the correct order P > Q > R, and being nearly equal for all the bands, as evidence the agreement between the effective temperatures calculated for the bands from J'_{MAX}, Table VI.

3. The R branch is always markedly stronger than the P branch for small

J′ values, while for large J′ values the two branches are asymptotically about equal in intensity.

This conclusion is borne out by figs. 1 to 5.

Perturbations.

Curtis and Long (*loc. cit.*) have noted six perturbations in this series of bands. They are :—

Band 3676	Band 3356.
R 5.	R 1.
P 7.	P 3.
Q 9.	Q 5.

Of these, Q 9 of band 3676 and Q 5 of band 3356 were noted as being split up into two components. Dieke* has advanced an explanation of this effect.

In our observations on these bands, the above perturbations were observed, and for the lines Q 9 and Q 5 the summed intensity of the two components was measured. This value of intensity was found to be the value predicted from the curves in figs. 2 and 3, for the respective lines.

The line Q 11 of band λ 4650 has abnormal intensity, as has been found by Childs. This seems to be due to its coincidence with some foreign line not yet identified.

Determination of Effective Temperatures

Two methods are available for the determination of effective temperatures from the line intensities in a band.

Method 1.—Considering the intensity distribution in a single branch of a band, we have the temperature T given by :—

$$T = \frac{J_m \quad (J_m + 1) \,.\, h^2}{4\pi^2 \quad I \quad k}, \tag{1}$$

where J_m = the rotational quantum number for the initial state of the line of maximum intensity.

I = moment of inertia of emitter in initial state

$$= \frac{h}{8\pi^2 \,.\, B \,.\, c}. \tag{2}$$

h = Planck's constant = $6{\cdot}55 \times 10^{-27}$.

k = Boltzmann constant = $1{\cdot}37 \times 10^{-16}$.

$c = 3 \times 10^{10}$.

B = rotational term constant.

---

* 'Nature,' vol. 123, p. 446 (1929).

The values of I were calculated, using the values of B given by Jevons.*

The value of J_m for each branch of each band was determined by inspection of curves in figs. 1 to 5, and the temperatures calculated from equation 1.

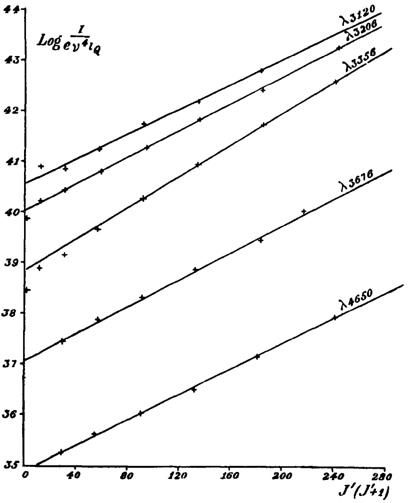

FIG. 6.—Q branches.

The temperatures thus obtained are tabulated in Table VI

Method 2.—For the intensity of any line in a band we have :—

$$\text{Intensity I} = C \,.\, i \,.\, \nu^4 \,.\, e^{-\frac{E'_r}{k\theta}} = C \,.\, i \,.\, \nu^4 \,.\, e^{-\frac{B' \;\; J' \;\; (J'+1)}{0\cdot 7\theta}},$$

---

* "Report on Band Spectra."

Table VI.—Calculated temperature in °Abs.

	P Branch		Q Branch.		R Branch.	
Band.	T from J_{MAX}	T from i_P	T from J_{MAX}.	T from i_Q.	T from J_{MAX}.	T from i_R.
λ 4650	785	788	759	769	785	794
λ 3676	781	783	755	771	755	760
λ 3356	692	669	729	720	754	752
λ 3206	717	682	754	753	779	794
λ 3120	681	667	779	768	779	—

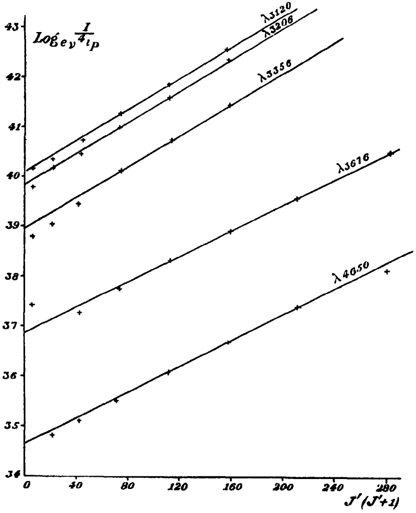

Fig. 7.—P branches.

where i = the appropriate intensity factor,

= statistical weight of the level × probability factor.

θ = temperature in degrees absolute,

i.e.,

$$\log_e \frac{\mathrm{I}}{\nu^4 \,.\, i} = \log_e \mathrm{C} - \frac{\mathrm{B}' \;\; \mathrm{J}'(\mathrm{J}'+1)}{0{\cdot}7\theta}, \tag{3}$$

where J′ refers to the initial state of the molecule.

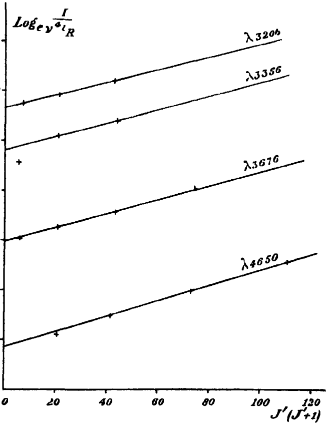

FIG 8 —R branches

The values of the intensity factor "i" for various types of band have been derived by Honl and London,* and the appropriate values for the bands under consideration are given by Mulliken (*loc cit*). They are :—

$$i_{\mathrm{P}} = a \,.\, (\bar{\mathrm{J}} - 1).$$
$$i_{\mathrm{Q}} = 2a \,.\, \mathrm{J}'$$
$$i_{\mathrm{R}} = a \;\; (\bar{\mathrm{J}} + 1).$$

---

* 'Z. Physik,' vol. 33, p. 803 (1925).

where

a = constant,

$\bar{J}$ = mean of J′ for initial state and J″ for final state.

The values of $\log_e \frac{I}{\nu^4\, i}$ and of J′ (J′ + 1) were calculated for each line of each branch and $\log_e \frac{I}{\nu^4\, i}$ plotted against J′ (J′ + 1) as in figs. 6, 7 and 8. The resultant graphs should be straight lines of slope $-\frac{B'}{0{\cdot}7\theta}$.

As will be seen from the figs. 6, 7 and 8, approximate straight lines are obtained and from the slopes, the values of θ for each branch were calculated, using the values of B′ given by Jevons. A slight distortion of the curves is apparent for low J′ values indicating that either the measured intensities are too low or that the values of "i" for low J′ values are too big.

As the phenomenon is observed in all of the bands, and has been recorded independently by Childs (*loc. cit.*) for the λ 4650 band, we are of the opinion that the intensity factors are responsible for the effect

The temperatures were calculated from the linear part of the curves and are given in Table VI, together with the values from Method 1.

The effective temperatures computed from the two methods show remarkable agreement, the maximum variation being only 5%. The mean effective temperature found for these bands is thus 750° A. which is in close agreement with the values of 750° A. and 785° A. found by Childs (*loc. cit.*) and Read (*loc. cit.*) for the 4650 band and the 6400 band respectively.

The conclusion of Childs that a higher temperature is obtained from the Q branch than from the P and R branches, is not borne out by our results.

These effective temperatures as is usually the case, are much higher than the true temperatures of the source. While it seems evident that they must bear some relation to the true temperature, no such relation has as yet been found.

Fall of Intensity down the Series.

Since the bands of the "main line series" of Helium are distributed according to a line series formula, it is of interest to compare the fall of intensity down the bands with the fall of intensity down the Balmer series.

For this purpose, it is necessary to take the intensity of a band as $\Sigma \frac{I}{\nu^4}$ for all the lines of the band.

Bongers* has measured the Balmer series and has found that his results are represented by —

$$\frac{I}{\nu^4} = \frac{c \quad (n - n_0)^3}{n^{12}}, \tag{4}$$

where n and n_0 are the principal quantum numbers for the initial and final states respectively

The analogues of n and n_0 will be the principal quantum numbers n' and n'' respectively of the bands under consideration. They are —

$n' = 3, 4, 5, 6, 7$, for the bands at 4650, 3676, 3356, 3206 and 3120 respectively,

while $n'' = 2$ for all the bands.

A relation of the form equation 4 was assumed, namely —

$$\Sigma \frac{I}{\nu^4} = \frac{c \quad (n' - n'')^x}{n'^{12}}, \tag{5}$$

where c is a constant, and $\Sigma \frac{I}{\nu^4}$ is as defined above

Table VII

Band	$\Sigma \frac{I}{\nu^4} \times 10^{-17}$	$\log \Sigma \frac{I}{\nu^4}$	$12 \log n'$	$\log \Sigma \frac{I}{\nu^4}$ $+ 12 \log n'$	$\log (n' - n'')$
λ 4650	5190 40	$\overline{14}$ 7152	5 7252	− 7 56	0
λ 3676	635 80	$\overline{15}$ 8033	7 2252	− 6·97	0·3010
λ 3356	92 60	$\overline{16}$ 9664	8 3880	− 6 65	0 4771
λ 3206	22 80	$\overline{16}$·3579	9 3384	− 6 31	0 6021
λ 3120	10 10	$\overline{16}$ 0025	10 1412	− 5 88	0·6990

Equation (5) may be written —

$$\log \Sigma \frac{I}{\nu^4} + 12 \log n' = \log c - x \,.\, \log (n' - n'')$$

The values of $\log \Sigma \frac{I}{\nu^4} + 12 \log n'$ and of $\log (n' - n'')$ were calculated and plotted as in fig 9.

It is interesting to note that the first four members of the series lie precisely

---

[*] 'Dissertation,' Utrecht, 1927.

on a straight line, the fifth member showing slight deviation from the linear relation. The slope of the line :—

$$\frac{\log \Sigma \frac{I}{\nu^4} + 12 \log n'}{\log (n' - n'')} = x$$

It seems significant that measurement of the slope gives the value of x as exactly $= 2$

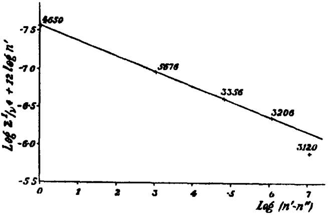

FIG 9

Thus the fall of intensity down the first four members of the principal series may accurately be represented by .—

$$\Sigma \frac{I}{\nu^4} = \frac{c\,.\,(n' - n'')^2}{n'^{12}}.$$

The values of $\log \Sigma \frac{I}{\nu^4}$, $12 \log n'$, and of $\log (n' - n'')$ are given in Table VII.

On the scale adopted the value of $c = 6 \cdot 44 \times 10^{-8}$

The above formula is in striking contrast with that of Bongers which gives the power 3 to $(n' - n'')$.

Summary.

Line intensity measurements on the first five members, λλ 4650, 3676, 3356, 3206 and 3120, of the main line series of Helium bands are given.

The predicted distribution is of the correct type, but agreement with observation is not complete. Notably the P and R branches are much stronger, relative to the Q branch, than the theory indicates.

An expression of the form, i.e. $i\,e^{\frac{E}{kT}}$, where "i" is a linear function of J′, is sufficient to describe the observed distribution

As with many other bands, the temperatures obtained by assuming Maxwell-Boltzmann distribution are much higher than the true temperature of the source. A temperature of approximately 750° A is found for all the bands.

The temperatures obtained from intensity factor considerations are in close agreement with the values found from the position of the maximum intensity in the branches

The fall of intensity down the series is examined and it is found that the relative intensities of the bands are given by a formula which is similar in some respects to that found by Bongers for the Balmer Series

The Change in the Absorption Spectrum of Cobalt Chloride in Aqueous Solution with increasing Concentration of Hydrochloric Acid.

By Owen Rhys Howell and Albert Jackson, The College of Technology, Manchester

(Communicated by Eric K Rideal, F R S —Received July 4, 1933)

Introduction

The red and blue colours of the cobaltous compounds and the change from one to the other have attracted much attention As the result of an investigation of the absorption spectra of a number of red and blue cobalt pigments of known crystal structure and also of a number of red and blue cobaltous compounds in solution, it has been suggested* that both in the crystal and in solution the cobalt atom is in association with six other atoms or groups when the colour is red and with four when the colour is blue. Subsequent determinations† of the crystal structures of a variety of compounds have confirmed this view ‡

---

* Hill and Howell, 'Phil. Mag,' vol 48, p. 833 (1924). A fairly full bibliography of previous work will be found in this paper.

† See 'Ann. Rep. Chem Soc.,' vol. 24, p. 288 (1927).

‡ There has been one apparent exception, viz, the blue anhydrous cobalt chloride in which the cobalt is surrounded by six chlorine atoms. The structure, however, is of the layer type and the compound is being further investigated.

The red colour of an aqueous solution of cobalt chloride is attributed to the ion $[Co(H_2O)_6]^{\cdot\cdot}$ and the blue colour with the same substance in presence of concentrated hydrochloric acid to the ion $[CoCl_4]''$ The transition from red to blue has been followed by measuring the densities,* viscosities*, refractive indices†, surface tensions† and electrical conductivities‡ of a series of solutions containing the same amount of cobalt chloride with increasing concentration of hydrochloric acid and of an exactly similar series containing no cobalt The differences for corresponding members show marked inflection at the same concentration of acid (about 5N) for all the properties (except surface tension, since the concentration in the surface is different from that in the bulk), and clearly indicate that the change is practically complete when the concentration of acid is about 9N The present investigation confirms these earlier observations and the general conclusions drawn from them, and throws much new light on the changes occurring in solution.

The absorption spectra of a series of solutions containing the same amount of cobalt chloride with increasing concentration of hydrochloric acid have now been measured and it has thus been possible to follow quantitatively the conversion of the cobalt from red to blue grouping, and to determine its dependence on the environment.

The absorption spectrum of cobalt chloride in concentrated hydrochloric acid solution has been determined by a number of observers§ chiefly for purposes of general comparison with other blue solutions but a very accurate investigation by Brode‖ has shown the existence of seven bands · (*a*) 695 $m\mu$, (*b*) 679 $m\mu$, (*c*) 666 $m\mu$, (*d*) 648 $m\mu$, (*e*) 626 $m\mu$, (*f*) 610 $m\mu$ and (*g*) 595 $m\mu$. Of these, however, only four, viz., (*a*) 695, (*c*) 666, (*e*) 626 and (*f*) 610 are clearly defined by the spectrophotometer with readings at intervals of 5 $m\mu$, and we have therefore confined our attention to these.

Experimental.

Solutions.—It was found by trial that the concentration of cobalt necessary to give a blue solution of suitable intensity in the thinnest cell available (0·1 cm.) was secured by using 12 grams per litre of $CoCl_2$ $6H_2O$. Two solutions were prepared with this amount of Kahlbaum's pure salt, free from iron and nickel, one in pure water and the other in pure hydrochloric acid solution so that the whole solution was exactly 10 N with respect to the acid All the intermediate solutions were prepared by taking x c c. of one of these and $100 - x$ c c. of the other, both at 18°, and after mixing and cooling again to 18°, making up to 100 c c with water at this temperature. The more concentrated solutions were made up individually. The concentrations of all the solutions were checked by titration against standard sodium carbonate solution and against standard silver nitrate solution.

---

* Howell, 'J. Chem. Soc.,' p. 158 (1927).

† *Ibid*, p. 2039.

‡ *Ibid*, p. 2843.

§ Russell, 'Proc. Roy. Soc.,' vol. 32, p. 258 (1881) , Hartley, 'Trans. Roy Soc. Dublin,' vol. 7, p. 253 (1909); 'J. Chem. Soc.,' vol. 83, p 401 (1903); Jones and Uhler, 'Amer. Chem. J.,' vol. 37, p. 126 (1907); Hill and Howell, *loc cit.*

‖ 'Proc. Roy. Soc.,' vol. 118, p. 286 (1928).

An exactly similar series of solutions for use as compensating blanks in the other beam was prepared from water and 10 N hydrochloric acid only.

Apparatus.—All measurements were made with the latest model of the Hilger-Nutting spectrophotometer, readings being taken every 5 $m\mu$ from 720 $m\mu$ to 420 $m\mu$.

The cells were specially made* and were ground accurately to length to within 0·0003 mm. Those from 10 cm. to 2 5 cm. were of the usual type, consisting of a tube provided with glass plates held in screw caps, those from 1 cm. to 1 mm consisted of square plates of glass, bored, ground on both faces and closed with glass plates held by clips or rubber bands.

Since the colour of the solution is dependent on temperature, it was essential to maintain this constant for all the observations The cells were therefore immersed in a thermostat placed immediately in front of the photometer windows The thermostat was a small box 13·5 × 10·5 × 10 cm made of brass and fitted at the ends with glass windows 4 0 cm. wide and 8·0 cm. high It was lagged with asbestos sheet The thermostat liquid was water heated by a small spiral of resistance wire immersed in it and stirred by means of a small glass stirrer driven mechanically The spiral was fed from a 4-volt accumulator through a thermo-regulator. Since the available space was so small, this regulator had to be very compact, further, with the low voltage applied, it was possible to make it direct-acting instead of using it to operate a relay. A description of it may therefore be of interest It is shown in fig. 1, and consists of a length of ¼-in. copper tubing A, bent as shown, and provided at one end with a glass tap B and at the other with a glass U-tube CC′, both sealed in with Faraday wax. With tap B open, sufficient mercury is placed in CC′ so that the surface lies in the capillary of C and in the bulb of C′. A little glycerin is placed on the surface in C to reduce sparking. The tube D has sealed into the end a piece of platinum wire with which contact is made in the usual way by means of a stout copper wire through mercury. Permanent contact is made with the mercury in C′ by means of a similar tube E. D is fastened to C, and E to C′, by means of rubber tubing. The polarity of D and E is important to secure a sharp make and break The regulator is placed in the bath and the necessary connections made; when the desired temperature has been attained, D is adjusted until the platinum wire just touches the mercury and tap B is closed.

---

* Messrs. Bellingham and Stanley, London.

The working temperature throughout was 20° ± 0 01°.

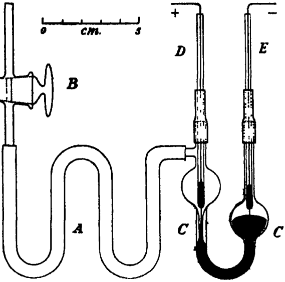

Fig. 1.

Results.

The instrument readings give the density, and this divided by the thickness of the solution is the Bunsen extinction coefficient. The values of the extinction coefficient were plotted against the wave-length for each solution. Typical curves for the red, blue and transitional solutions are shown in fig. 2.

The values of the extinction coefficient at each of the four principal band maxima, 695*, 666, 626 and 610 mμ were read from the curves and these are given in Table I for each concentration of acid. They are plotted against the normality of the acid in fig. 3.

---

* Actually, with a reading interval of 5 mμ, the first maximum is at 688 mμ, but Brode's nomenclature is retained.

Discussion

The curves, fig. 3, are very remarkable. The first point of interest is that until a considerable concentration of acid is reached, no blue constituent is formed

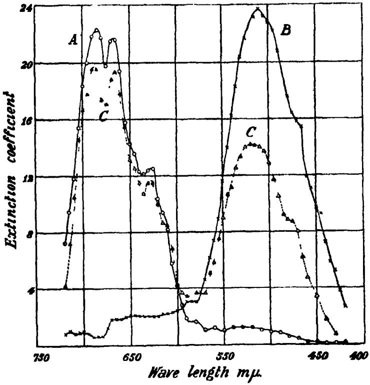

Fig 2

Curve A	Cobalt chloride in 9 0 N HCl	Scale as shown.
Curve B	Cobalt chloride in water only	Scale · multiply by 0 01.
Curve C.	Cobalt chloride in 6 0 N HCl	Scale · multiply by 0 03

Yet some change has occurred over this range, since the solutions become "muddy" in appearance and are much more readily converted to blue by increase of temperature. Moreover, it has been shown* by measurement of the physical properties (densities, viscosities and electrical conductivities) of one such solution (4 N with respect to hydrochloric acid) at a series of temperatures, that the conversion to blue on warming occurs quite continuously, in contrast to that resulting from increasing the concentration of acid. It is therefore apparent that the effect of adding hydrochloric acid up to this point is to replace two of the six water molecules by chlorine atoms, no change of colour resulting since the cobalt atom still maintains a six grouping.

---

* Howell, 'J Chem Soc.,' p. 162 (1929).

Table I.

Thickness.	Conc. HCl N	Bunsen extinction coefficient			
		695 *mμ.*	666 *mμ.*	626 *mμ.*	610 *mμ.*
cm.					
10 0	0	0 008	0 018	0·020	0 022
	1 00	0 001	0 010	0 016	0 018
	2 50	0 007	0 009	0 010	0 018
5 0	3 75	0 025	0 024	0 043	0 051
	4·50	0 038	0 036	0 032	0 031
2 5	5·00	0 060	0 055	0 060	0 068
	5 50	0 260	0 240	0 180	0·170
	6·00	0 590	0 580	0 345	0 255
	6·25	1 035	1 00	0 690	0 485
1 0	6·75	2 54	2 24	1 46	0 96
0 5	7 00	3 26	3 20	2 24	1 50
	7 25	4 60	4 40	2 84	1 80
0·25	7 40	5 32	4 60	3 12	2 00
	7 50	6 60	6 08	3 81	2 52
	7·75	7 92	7 25	4·80	3 10
0·1	8 00	11 2	10 8	7·10	4 50
	8 25	13 6	13 0	8·20	5 65
	8 50	16 9	16 0	10 0	6 55
	8·75	20 0	18 7	10 8	7 1
	8 90	21 4	20 3	11·8	8 0
	9 00	22 0	21 6	12 6	8 2
	9 25	21 9	21 4	13·9	8 7
	10 00	21 9	21 6	15 2	9 8
	11·10	21 9	21 6	16 2	10 9
	12 05	22·0	21 7	16 3	11 6
	13 10	22 0	21 6	16 3	11 8

First stage $[Co(H_2O)_6]^{\cdot\cdot} \rightarrow [Co(H_2O)_4Cl_2]$

With increasing concentration of acid beyond 5 0 N, the curves begin to rise sharply and eventually become linear. The linear portion on projection strikes the axis of concentration at 7·10 N.

The change beginning at 5·0 N, resulting in the formation of a blue constituent, necessitates a reduction of the number of groups around the cobalt atom from six to four. It will appear that this occurs by introduction of another chlorine atom and elimination of three water molecules.

Second stage. $[Co(H_2O)_4Cl_2] \rightarrow [Co(H_2O)Cl_3]'$

The linear change beginning at 7·10 N is complete at 9·0 N. It is seen from the curves for the bands 695 and 666 $m\mu$ that the change ceases abruptly at this point. Conversion to the four grouping is complete and further increase in the concentration of acid produces absolutely no effect. The curves for the bands 626 and 610 $m\mu$, however, show that a further change of different character proceeds beyond this point and this will be discussed below.

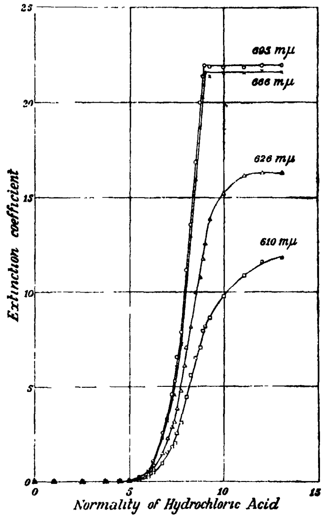

FIG. 3.

The change over the linear portion is evidently the completion of the replacement of water molecules by chlorine atoms.

Third stage : $[Co(H_2O)Cl_3]' \rightarrow [CoCl_4]''$

The ratios of the relative concentrations of chlorine atoms to water molecules for the three critical concentrations, 5·0 N, 7·1 N and 9·0 N, are calculated in Table II. It is seen that the relative concentrations of chlorine atoms, 2 : 3 : 4, are the same as for the number of chlorine atoms in the three complexes successively produced.

Table II

—	Concentration of HCl		
	5·0 N	7·1 N	9·0 N
Normality of chlorine.			
(*a*) From HCl	5·00	7·10	9·00
(*b*) From $CoCl_2$	0·01	0·01	0·01
Normality of Cl	5·01	7·11	9·01
Molality of water			
Weight of 100 c.c. of solution	108·65	111·84	114·63
HCl present	18·25	25·21	32·85
$CoCl_2$	0·65	0·65	0·65
H_2O	89·75	85·98	81·13
Molality of H_2O	49·9	47·8	45·1
$\frac{\text{Number of chlorine atoms}}{\text{Number of water molecules}}$	0·100	0·149	0·200
Ratios	1	1·49	2·00
Ratios of Cl atoms in the complexes	1	1·5	2

Evidently, therefore, the factor determining the state of the cobalt atom is the environment. The relative concentrations of the constituents of the medium alone determine the constitution of the complex, the relative concentration of cobalt to the other constituents is of no account.

This is clearly seen from Table III where the extinction coefficients at the two principal maxima (695 and 666 $m\mu$) of a series of solutions all 6 N with respect to hydrochloric acid but containing varying amounts of cobalt are given. The extinction coefficient is directly proportional to the concentration of cobalt over this wide (sixfold) range.

Indeed in the previous work, already mentioned, on the physical properties of solutions of cobalt chloride and hydrochloric acid, the concentration of cobalt was ten times that in the present experiments, yet the differences curves all indicate that the change is complete at about 9 N and all exhibit inflexion at about the same concentration of acid as that at which it is now seen that the blue constituent begins to be formed. In the absence of any information, apart from the appearance of the solution (which is deceptive), regarding the actual amounts of red and blue constituents present, it was suggested that at this point equal numbers of the doubly positively and doubly negatively charged ions were present; it is now seen, however, that at this point no blue form is present and the electrical neutrality is accounted for by the fact that the cobalt atom is present wholly as the uncharged complex $[Co(H_2O)_4Cl_2]$. In particular, the very pronounced minimum at 5 N acid on the conductivity differences curve receives a full explanation.

Table III

Conc. $CoCl_2$	Thickness	Extinction coefficient 695 $m\mu$	$\frac{\text{Ex coeff}}{\text{Conc}}$	Extinction coefficient 666 $m\mu$	$\frac{\text{Ex coeff}}{\text{Conc}}$
gm /litre	cm				
3	10	0·150	0·050	0·140	0·047
6	5	0·305	0·051	0·296	0·049
12	2·5	0·590	0·049	0·580	0·048
18	2·5	0·924	0·051	0·896	0·050

The curves for the maxima 626 and 610 $m\mu$, fig. 3, are markedly different from those for 695 and 666 $m\mu$ in one respect, namely, that beyond 9·0 N the extinction coefficient does not remain constant but continues to increase.

The fact that the extinction coefficient for the 695 and 666 $m\mu$ bands remains perfectly constant with increasing concentration of acid above 9·0 N shows that the whole of the cobalt must be completely converted to the four grouping at this point; it is therefore suggested that the continued increase in the extinction coefficient for the 626 and 610 $m\mu$ bands is due to the depression of the ionization of the complex $[CoCl_4]''$ with increasing concentration of acid. With this divalent ion one of the hydrogen ions should be more readily associated than the second. It is seen that the extinction coefficient increases much more rapidly for the 626 $m\mu$ maximum than for the 610 $m\mu$.

It would therefore appear that these four principal bands in the spectrum are due to the four valences between the cobalt atom and the four groups associated with it, the bands 695 and 666 $m\mu$ being due to the two principal valences and the bands 626 and 610 $m\mu$ to the two auxiliary valences.

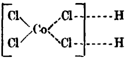

This would account for the facts (1) that the two bands 695 and 666 $m\mu$ develop simultaneously and are both fully complete at the same concentration of acid, since the two chlorine atoms attached by principal valences are already present before the four grouping begins, (2) that the intensity of the bands 626 and 610 $m\mu$ continues to increase with increasing concentration of acid (after the other two have reached their full value), since it is only the two chlorine atoms attached by auxiliary valences which are affected by depression of ionization, and (3) that the increase in intensity after the linear stage is over proceeds at different rates for the two bands, since the degree of dissociation of the two ionizable hydrogens will be different.

Attention has been devoted to the blue constituent to the exclusion of the red, because the absorption of the one extends into the region of the other, this is of small account so far as the blue is concerned, since the absorption of the red is so feeble and no correction has been made for it. Although the absorption of the blue constituent is relatively small in the region of the principal band of the red constituent, the correction for it would be enormous compared with the total absorption, since the intensity of the blue is so very large compared with the red. The extinction coefficient for the principal band when the solution is wholly red (see fig. 2) is only 0·238 and for the principal band when the solution is wholly blue, with the same concentration, of cobalt, it is 22 0, which is 92·5 times as great

Summary

1. The absorption spectra of a series of solutions containing a fixed amount of cobalt (12 grams of $CoCl_2 6H_2O$ per litre) with increasing concentration of hydrochloric acid have been measured and plotted.

2. The extinction coefficients at the maxima of the four principal bands, 695, 666, 626 and 610 $m\mu$, have been plotted against the concentration of acid.

3. These curves show that no blue constituent is formed until a critical concentration of acid (5·0 N) is reached

4. The amount of the blue constituent then increases rapidly with increasing concentration of acid, the relation soon becoming linear. The linear relation

begins at 7·1 N acid and, for the 695 and 666 $m\mu$ bands, it is complete at 9·0 N acid.

5 The ratio of the relative numbers of chlorine atoms to water molecules at these three critical concentrations of acid is 2 3 4

6 The mechanism of the change as suggested by previous work is —

$$\underset{\text{Red}}{[Co(H_2O)_6]^{\cdot\cdot}} \rightarrow \underset{\text{Red}}{[Co(H_2O)_4Cl_2]} \rightarrow \underset{\text{Blue}}{[Co(H_2O)Cl_3]'} \rightarrow \underset{\text{Blue}}{[CoCl_4]''}$$

The relative number of chlorine atoms in the complexes at the three stages is also 2 3 . 4

7. The state of the cobalt atom is therefore determined only by the environment and is independent of the relative concentration of the cobalt to the other constituents This has been demonstrated by measuring the absorption spectra of solutions containing varying amounts of cobalt in the same concentration of acid , the extinction coefficient for each band is directly proportional to the concentration of cobalt

8 For the bands 626 and 610 $m\mu$, the extinction coefficient continues to increase with increasing concentration of acid beyond 9·0 N. This is explained by the depression of ionization of the complex , the suggestion therefore follows that the two major bands, 695 and 666 $m\mu$, relate to the principal valences and the two minor, 626 and 610 $m\mu$, to the two auxiliary valences, which alone are affected by further increase in the concentration of acid.

9. The intensity of absorption of the blue complex ion is 92·5 times that of the red

The Transmission of Infra-red Radiation by a Thin Layer of Horn.

By H. J. Taylor, Ph D., B.Sc.

(From the London Clinic and Institute of Physical Medicine.)

(Communicated by Sir Leonard Hill, F R S —Received July 6, 1933.)

The layer of horn used for this research was peeled in relatively large sheets off the skin after the subject had been exposed to an arc lamp. Microscopic sections of it showed several layers of hornified cells. The sample was free from holes, and the average thickness was 0 022 mm. A sample of the same origin had been used in a research by Angus and Taylor* on the transmission of visible and ultra-violet rays The present paper completes the study of the transmission and is of interest in regard to the penetration of rays, from various sources of heat, through the outer horny layer of the skin.

Apparatus and Method

As a source of infra-red radiation shorter than 2·8 μ a 100-watt tungsten filament gas-filled lamp was used, and for radiation longer than 2·8 μ a small electric resistance made by Gerdes of New York. The pre-heater of a Nernst filament is very often used as a source, but owing to the nature of the experiments to be described the emission of this source was found to be too low for the Paschen galvanometer which could not be used at the high sensitivities of which it was capable. The dispersive system was a Hilger infra-red spectrometer (small model) with a collimator slit, collimator mirror, rock-salt prism, Wadsworth mirror, telescope mirror and telescope slit behind which the thermopile was mounted. The prism table was rotated by a wave-length drum An apparatus of this sort does not lend itself to exceptionally refined measurements, but for the work to be described its accuracy was more than sufficient. The thermopile used in the early experiments, when the skin sample was placed in front of the collimator slit of the instrument, to determine its transmission, was a Hilger linear thermopile. In subsequent experiments a surface thermopile with a sliding adjustable slit, kindly loaned by Professor A. V. Hill, was used. With this combination the transmission of a material could be determined by reading the galvanometer deflection with the instrument set to the wave-length required, then placing the material whose transmission was required, in front of the collimator slit and again measuring the deflection. The comparison of these readings gives the fractional transmission for the wave-length used This procedure was repeated throughout the whole range of spectrum required

---

* 'Proc. Roy. Soc.,' B, vol. 109, p. 309 (1931)

The sources used were always allowed to run for a considerable time, never less than half an hour, before an experiment was carried out, so that the emissions were constant The voltage applied to the source was also controlled for mains fluctuations by an assistant The results are given in Table I.

Table I.

Wave-length (μ)	% transmission	Wave-length (μ)	% transmission
0 8	9	2 7	9 8
0 9	9 2	2 8	5 2
1 0	10 4	2 9	2
1 1	10 5	3 0	Nil
1 2	10 6	3 1	Nil
1 3	10 8	3 2	Nil
1 4	11 1	3 3	Nil
1 5	10 8	3 4	Nil
1 6	11 4	3 5	Nil
1 7	11 8	3 75	1 6
1 8	11 8	4 0	3 0
1 9	11 8	4 25	9 3
2 0	11 5	4 5	2 0
2 1	12	4 75	9 3
2 2	12 1	5	10 9
2 3	12 3	5 25	13 1
2 4	12 4	5 5	13 5
2 5	13	5 75	5
2 6	12 4	6 0	Nil

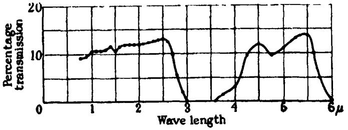

FIG 1 —Transmission of horny layer by first method.

Losses in transmitted radiation due to scatter had then to be considered They were fully discussed by Angus and Taylor (*loc. cit.*) and will only be briefly referred to here. There are two ways in which loss due to scatter may be overcome :—

(*a*) By using such a scattering source of radiation so that no reduction in intensity due to scatter by the horny layer could take place ; and (*b*) By placing the horny layer so close to the thermopile that no scattered radiation is lost

An attempt had been made with Angus to use method (*a*); a scattering source being obtained by the use of two frosted rock-salt plates. But it was found that however well the surfaces of the plates were frosted their scattering power in the infra-red region was comparatively low, and method (*b*) was therefore tried

It was impossible to place the horny layer actually in contact with the thermopile surface since the latter would have been damaged by this procedure. A thin piece of stiff cardboard with a rectangular orifice over which the horny layer could be mounted was therefore fixed to two cork supports which fitted into spaces between the thermopile itself and its mount. This was constructed to give a clearance for the horny layer when mounted of 0·75 mm.

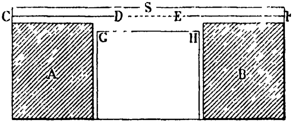

FIG 2

A and B are the cork supports for the mount CD, EF, whilst DE represents the horny layer and GH the thermopile surface. S represents the slit.

The adjustable slit S was set to a standard width (0·01-inch) by means of engineers' "feelers." This method of setting the slit lends itself to quite accurate determinations since in six trial settings of the slit no difference in galvanometer deflections could be obtained

An experimental determination was carried out as follows. The thermopile was placed so that the dispersed radiation was focussed on it by the telescope mirror.

A mercury vapour lamp was set up in front of the telescope slit of the spectrometer, and the wave-length drum of the instrument set for the line λ 5460 in the mercury spectrum. The thermopile was then adjusted until this line by visual observation was coincident with the slit. This procedure was repeated with the line λ 5790. The wave-length drum was then set for the line λ 10200 and adjustments made to the thermopile if necessary so that a maximum galvanometer deflection was obtained. This line was then focussed on the slit. This procedure was carried on until each of these lines in turn could be focussed in the thermopile slit by movement of the wave-length drum only. Any wave-length marked on the drum could then be focussed on the thermopile slit. The mercury vapour lamp was then removed and the infra-red source to be used placed in position in front of the telescope slit. The 100-watt tungsten filament lamp was placed at a distance of 1 metre from this slit, the voltage across it being controlled by a small resistance and a voltmeter

With the mount, but without the horny layer, fixed in position in front of the thermopile, deflections on the galvanometer were obtained for wave-lengths 0 8 μ to 2 8 μ

The connection from the thermopile to galvanometer was then broken, the slit opened and the horny layer placed in position in the mount in front of the thermopile. The horny layer was fixed to its mount by a little gum on its edges The slit was then closed to width of 0 01 using the feelers, as before, and the thermopile placed in its correct position using the radiation from the mercury vapour lamp as a standard, also as before. The deflections on the galvanometer for wave-lengths 0·8 μ to 2 8 μ were then obtained The determinations were repeated both without and with the horny layer in position The mean deflection for each wave-length determined in each series was found. From this the fractional and therefore the percentage transmissions could be found. For wave-lengths longer than 2·8 μ the small electric heating resistance coil was used A series of experiments for these wave-lengths and with this source was carried out in a similar manner to that for wave-lengths 0·8 μ to 2·8 μ when the tungsten filament lamp was used.

It should be noted that the galvanometer should be on a low sensitivity so that no alteration of sensitivity need be made during a series of experiments Under these circumstances a rapid swing of the galvanometer system was obtained. It was thought that this rapidity of determination might help to eliminate the effect on the thermopile of any warming of the horny layer by absorption of radiation, but this was found by an experiment, to be described later, to be negligible

If the material, the transmission of which is to be found, is non-scattering then one can tell if the heat generated by absorption of radiation affects the thermopile by moving the material to a certain distance from the thermopile and comparing deflections. This cannot, however, be done with the horny layer owing to scatter. An experiment was, however, carried out on a piece of cellulose acetate material of thickness 0·03 mm. This is a clear non-scattering material which has a transmission curve (in the infra-red) similar

Table II.

Wave-length in μ.	Mean deflections.		Percentage transmissions.
	Horny layer in	Horny layer out	
0·8	5	8	62
0·9	9	14	64
1·0	12	20	60
1·1	16	27	59
1·2	28	41	68
1·3	32	48	67
1·4	41	56	73
1·5	45	62	73
1·6	48	66	73
1·7	48	69	69
1·8	44	69	64
1·9	41	66	62
2·0	44	63	70
2·1	43	60	72
2·2	37	56	66
2·3	31	48	65
2·4	29	44	66
2·5	25	37	68
2·6	19	29	65
2·7	13	21	62
2·8	80	176	45
2·9	35	176	20
3·0	18	182	10
3·1	9	178	5
3·2	5	175	3
3·3	Nil	179	Nil
3·4	Nil	170	Nil
3·5	12	165	7
3·6	37	165	22
3·7	55	167	33
3·8	64	160	40
3·9	64	150	42
4·0	64	152	49
4·1	75	117	64
4·2	64	100	64
4·3	64	88	73
4·4	59	94	63
4·5	59	98	60
4·6	55	98	56
4·7	59	91	55
4·8	46	85	54
4·9	38	80	48
5·0	45	76	60
5·1	37	71	52
5·2	33	65	51
5·3	37	60	62
5·4	29	54	54
5·5	21	48	44
5·6	12	40	30
5·7	5	32	16
5·8	1	20	5
5·9	0·5	16	3
6·0	Nil	12	Nil

to that of horny layer. The transmission of this material for wave-lengths between 0·8 μ and 6 μ was found by placing it in front of the collimator slit of the spectrometer, and comparing galvanometer deflections with and without it in position, in the usual way. For comparison the cellulose acetate material was then placed near the thermopile surface in the position occupied by the horny layer in the previous experiment, and its transmission determined for some wave-lengths. As shown in Table III the results are comparable showing that the effect on the thermopile of any heating of the sample by absorption of radiation may be neglected. One then assumes that the same holds good for the horny layer.

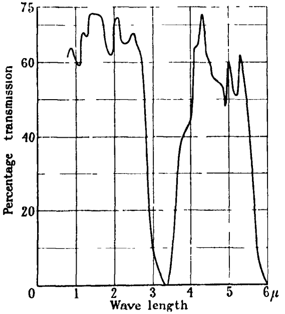

FIG 3.—Transmission of thin horny layer, thickness 0 022 mm.

In addition to the factor of rapidity in the swing of the galvanometer and the resultant small time the horny layer is exposed, the small area of horny layer exposed compared with its total area allows any heat generated to be rapidly dissipated. (Slit width 0·01-inch, width of skin sample 0·375-inch.)

The transmission curve for the horny layer shows marked absorption in the region 2·75–3·75 μ and beyond 6 μ. Water, water vapour and substances containing the hydroxyl group show absorption bands in the region of 3 μ whilst a large number of organic substances have absorption bands between 3 μ and 3·5 μ a shift occurring with the type of carbon linkage. Inorganic carbonates also show marked absorption in the region of 3·5 μ. Owing to the complex chemical nature of the horny layer an accurate analysis of the absorption bands is impossible.

For a sample of the whole skin of a rat, dried in the air, 0·41 mm. thick, absorption was found to be complete beyond 3 μ. If it could have been studied in a moist condition it is probable that absorption would have been

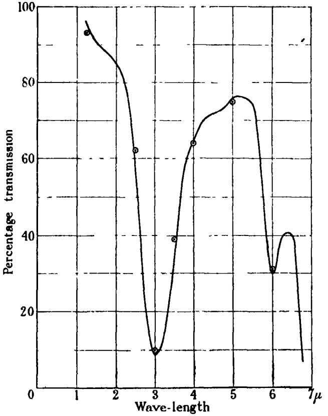

FIG 4.—Transmission of cellulose acetate material, 0·03 mm thick. ⊙ Material near thermopile.

complete at a somewhat shorter wave-length. The transmission curves shown confirm the work of Sonne.* He compared the effect on the body of the radiation from an incandescent lamp with that of a resistance coil heated to just below visibility. The former gives most of its radiation in the region of wave-lengths shorter than 3 μ where skin transmission is high and the latter gives high emission at 3 μ where skin surface absorption is high.

---

* 'Acta. med. scand.,' vol. 54, p. 335 (1921)

Table III

The Transmission of Cellulose Acetate.

Wave-length in μ	Mean deflections		Percentage transmission	Percentage transmission with sample near thermopile
	Material in.	Material out		
1·25	19	20	95	93
1·5	70	77	91	—
1·75	135	153	88	—
2·0	72	85	85	—
2·25	80	100	80	—
2·5	54	99	60	62
2·75	19	85	22	—
3·0	8	90	9	10
3·25	15	95	16	—
3·5	37	104	36	39
3·75	58	103	56	—
4·0	59	92	64	64
4·25	75	107	70	—
4·5	77	107	72	—
4·75	72	98	73	—
5·0	69	90	76	75
5·25	61	80	76	—
5·5	42	56	75	—
5·75	12	23	52	—
6·0	4	14	30	31
6·25	12	30	40	—
6·5	10	25	40	—
6·75	2	28	7	—
7·0	Nil	30	Nil	—

I am indebted to Sir Leonard Hill for help and to Professor A. V. Hill for the loan of one of the thermopiles used.

Summary

A method is described for measuring the transmission in the infra-red region of the spectrum of a thin layer of horn, 0·022 mm. thick. Marked absorption was found in the region of 3·4 μ, and also in the region beyond 6 μ

Power Loss Phenomena in Liquid Dielectrics.

W. Jackson, M.Sc., Electrical Engineering Dept., College of Technology, Manchester.

(Communicated by M Walker, F R S—Received July 8, 1933)

Introduction.

While attention has been devoted to the behaviour of liquid dielectrics under constant applied voltage, the effect of prolonged steady voltage application on the power loss exhibited by such dielectrics in alternating electric fields does not appear to have been studied. The present paper describes an analysis of this effect in a series of dielectric loss measurements on samples of several liquid hydrocarbon derivatives—benzene, toluene, chlorbenzene and nitrobenzene—over the frequency range 2×10^5 to 2×10^6 cycles per second, before and after the application of D C. voltage

The scope of the measurements may be summarized under the following heads —

(1) Investigation of the variation of the dielectric loss, as shown in the equivalent series resistance of a test condenser containing the dielectric, with frequency at constant temperature.

(2) Investigation of the variation of the loss resistance with temperature at constant frequency.

(3) Investigation of the behaviour of the dielectric under steady potential and following prolonged steady voltage application.

Method of Measurement.

The method which has been used most frequently for condenser loss resistance measurements at radio frequencies is a Substitution Method, the validity of which rests on the assumption of zero loss in some standard condenser with which the test condenser is compared. In the circuit of fig. 1, L is a self inductance, $C_\times$ the condenser to be tested, C a standard condenser and A a current measuring device. This circuit is loosely coupled through L to a source of continuous oscillations of the requisite frequency. The procedure consists in adjusting C and $C_\times$ so that they are equal and give circuit resonance at this frequency. The total circuit resistance is then measured with $C_\times$

inserted and afterwards remeasured with C_x replaced by the standard condenser C On the assumption that the standard C is devoid of energy loss, the unknown loss resistance R_x of the test condenser follows at once as the difference between the two measurements.

This supposition of zero loss is not justified, however, for even the best commercial air condensers, and three methods have been devised to overcome this limitation. Dye* developed a special condenser in which the whole of the losses were regarded as concentrated in the insulating material supporting the insulated plate This condenser he applied successfully to the determination of the loss in high-grade condensers of power factor of the order of 50×10^{-6} over a frequency range from 5×10^4 to $1 \cdot 5 \times 10^6$ cycles per second Moullin† has adopted a somewhat reverse procedure in developing a method for use at frequencies of the order of 4×10^6 cycles per second, by employing coils L of accurately calculable high-frequency resistance in the form of long narrow single layer rectangles, thus avoiding the need for a standard condenser The author‡ has also attempted to eliminate this need by making use of a variable mutual inductance, but in the latter small self and mutual capacities introduce unavoidable inaccuracies.

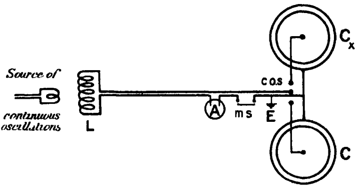

FIG 1 —C_x, test condenser, C, air condenser, C O S, change-over switch, m s, mercury switch for insertion of resistance

In the present work the substitution method has been retained, but in order to avoid any assumptions regarding zero loss in the standard condenser and at the same time to allow for any residual loss in the test condenser not arising from the inserted dielectric, two continuously variable condensers of identical form were constructed, one to act as the standard C, the other representing C_x and carrying the dielectric under test

---

* 'Proc Phys. Soc.,' vol. 40, p 285 (1928).

† 'Proc. Roy. Soc.,' A., vol. 137, p 116 (1932)

‡ Jackson, 'J. Inst Elect. Eng.,' vol. 68, p 296 (1930).

The details of these condensers are shown in fig. 2. Each consisted of a thick circular brass disc mounted inside a shallow cylindrical brass container.

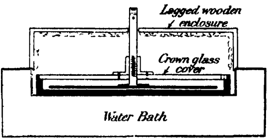

FIG 2 – Scale 1 cm — 2¼ in (approx.)

The disc was provided with a long spindle, threaded at its lower end, and supported on this in a metal bush located at the centre of a thick circular crown glass plate which rested on the rim of the container. At the upper end of the spindle holes were drilled into which a long ebonite rod could be inserted for the purpose of rotating the disc and varying its distance from the bottom of the container In addition, a mercury cup was provided at the top of the spindle to permit of undisturbed connection of the condenser during capacitance variation Since the calibrated condenser available covered a range up to 800 micro-microfarads, the condensers were designed to give this capacitance value with air dielectric for a plate separation of about 0·5 mm The test condenser was nickel plated in order to guard against the possibility of the brass being attacked by the dielectrics to be inserted The frequency range of measurement from 2×10^5 to 2×10^6 c p s (1500 to 150 metres) was covered in steps by use of several low loss coils of different inductance value. Resonant adjustment was effected with each of these coils in circuit by coarse and vernier control of the oscillator frequency.

In view of the important effect which temperature exercises on dielectric loss, it was necessary to keep this constant throughout a series of measurements This was done by surrounding the condensers by a water bath of the form shown in fig. 2. The trough into which the condensers were inserted was only slightly deeper than the container, and the enclosure was completed by a lagged wooden cover through the top of which the condenser spindles protruded. The mass of water contained in the bath was such as to ensure that once the bath had been brought slowly to the desired region of temperature, either by addition of ice or by external heating, and the condenser temperature allowed to equalize itself, the temperature of the condensers remained steady over a sufficiently long period to enable a complete set of measurements over the frequency range to be carried out This arrangement also made possible an investigation of the effect of temperature on the dielectric loss in an ordered manner, since the temperature of the condensers could be raised or lowered at a very gradual rate. In view of the small thickness of liquid dielectric in the test condenser, provided that this temperature variation was carried out very slowly, no serious danger existed of a temperature gradient across the dielectric medium The container of each condenser was bonded to the copper water bath, and the latter connected to the earth point E of the measuring circuit.

Before commencing the dielectric loss measurements, the two condensers were adjusted to the same capacitance value, 800 micro-microfarads, and compared, each with air dielectric, over the whole frequency and temperature range to be covered in the measurements. In carrying out this comparison, the condensers were switched into the resonant circuit in turn and the current value for each noted. This was followed by measurement of the total circuit resistance with each condenser in circuit It was found that the condensers could be regarded as identical over the whole frequency range at temperatures from zero to 45° C Above 50° C the condenser used as $C_\times$ had a measurably greater loss than the normal air condenser, and at a temperature of 55° C. and a frequency of 5 5 × 10^5 had an excess loss resistance of about 0·02 ohm. These tests were followed by a comparison of the condensers when a known resistance was inserted in series, and when a known leak resistance was connected in parallel with one of them. The deduced values of the added series and leak resistances agreed with their previously known values.

The main difficulty with comparison methods of condenser resistance measurement arises in making the difference between the total circuit resistance with the test and air condensers in circuit a sufficiently large fraction of the total to permit of its accurate determination Where a vacuo thermo-junction proved unsuitable, this was facilitated by using a thermionic voltmeter to measure the voltage set up across a small coil included in the measuring circuit.

Before the insertion of a dielectric into the test condenser particular care was taken to purify the liquid and to ensure, as far as possible, freedom from moisture. The liquids were introduced through a hole provided near the edge of the crown glass cover, the filling process being carried out slowly, and with the condenser tilted, so as to avoid the trapping of air bubbles between the plates To make sure of this, it was usual to screw the movable plate into contact with the base of the container before the capacitance was finally adjusted to the desired value The dielectric was arranged always to cover the upper surface of the movable plate, and its temperature was measured on a thermometer dipping into the dielectric at the edge of the container and protruding through the wooden cover surrounding the condensers. All the important measurements were carried out at low temperatures to avoid the formation of a film of evaporated liquid on the under surface of the glass cover.

Dielectric Loss Measurements on Nitrobenzene.

The removal of the last traces of moisture from nitrobenzene during its preparation for test proved a matter of great difficulty, but this led to the interesting effects which were apparent following the prolonged application of D.C. voltage across this dielectric. Since the paper is concerned mainly with the behaviour of this liquid, it will be well to record the procedure adopted in its preparation.

A reasonably pure commercial product was washed twice with dilute caustic soda, followed by six washings with distilled water, with the lapse of one hour between washings. It was then allowed to stand overnight to permit of adequate separation of free water, and then shaken for two days over anhydrous calcium chloride, and filtered This prolonged shaking was twice repeated. The resulting liquid was distilled and then re-distilled with neglect of an appreciable amount of the early and late products of distillation.

The nitrobenzene was finally transferred from the collecting chamber to the test condenser, and the dielectric loss resistance measured, for a capacitance value of 1600 micro-microfarads, at a constant temperature of 21° C. over the frequency range from 2×10^5 to 2×10^6 cycles per second. The results of these measurements are shown in curve (*a*), fig. 3, where, for convenience in interpretation, the loss resistance has been plotted against the inverse of the square of the frequency.

The linear nature of this curve indicates that the behaviour is that of a perfect condenser with a leakage resistance which is constant and independent of frequency. This conclusion is based on an analysis of the simple system of fig. 4, in which c represents a loss-free condenser and r a constant leakage. The equivalent series resistance and capacitance of this system are, respectively :

$$\mathrm{R}_{\times} = \frac{r}{1 + r^2c^2\omega^2} \text{ and } \mathrm{C}_{\times} = \frac{1 + r^2c^2\omega^2}{r^2c\omega^2}.$$

If, however, r is large in comparison with $1/\omega c$, these simplify to the form

$$R_{\times} = \frac{1}{rc^2\omega^2} \quad \text{and} \quad C_{\times} = c.$$

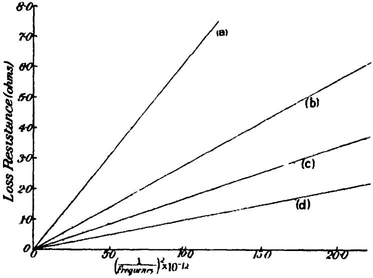

FIG 3 —(*a*) Temperature 21° C ; (*b*) 11° C , (*c*) 11° C , (*d*) modified form of curve (*b*) after 16 hours steady voltage application, and recovery for 8½ hours Frequency range 2×10^5 to 2×10^6 cycles/sec.

Within the range of frequencies employed no change of test condenser capacitance could be detected. This also is consistent with representing the loss by a constant shunt resistance, as indicated by the equation $C_{\times} = c$ above.

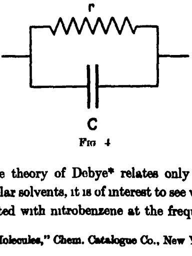

FIG 4

Although the dipole theory of Debye* relates only to dilute solutions of polar liquids in non-polar solvents, it is of interest to see whether any anomalous effect might be expected with nitrobenzene at the frequencies with which the measurements are concerned. The region of frequency in which anomalous dispersion and absorption occur is given by the following relation for the "characteristic frequency"

---

* "Polar Molecules," Chem. Catalogue Co., New York (1928)

$$f_0 = \frac{\mathrm{KT}}{8\pi^2 \ \eta \ a^3} \text{ cycles/sec.,}$$

where a is the radius of the equivalent molecular sphere

η is the coefficient of viscosity,
K is Boltzmann's constant ($1 \cdot 37 \times 10^{-16}$),
and T the absolute temperature.

At a temperature of 20° C. (T = 293), η and a may be taken as 0·0201 and $3 \cdot 43 \times 10^{-8}$ cm.* respectively, for which $f_0 = 6 \cdot 3 \times 10^8$ cycles per second It is not to be expected, therefore, that the effect would be noticeable in the present measurements

The leakage resistance which would account for the behaviour of curve (*a*), fig 3, is about 16,000 ohms, and it was at once apparent that greater precaution must be taken to avoid moisture content

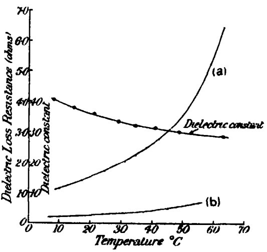

FIG. 5.—Frequency 6 25 × 10^5 cycles/sec.

Before carrying this into effect, however, the variation of loss resistance with temperature was investigated, and the results obtained at a frequency of $6 \cdot 25 \times 10^5$ cycles/sec. (480 metres) are shown in curve (*a*), fig. 5. A continuous increase of loss resistance with temperature, simultaneous with a rapid decrease of the dielectric constant, was found to occur. In order to permit of the dielectric loss results being related to constant capacitance and frequency, the test condenser was readjusted in sympathy with the variation of the dielectric constant. The increase of conductivity with temperature noted was observed again later, on the application of steady voltage across the dielectric. Curve (*b*), fig. 5, shows the results on a sample of nitrobenzene which had been subject to prolonged application of steady potential.

---

* Landolt and Bornstein, 'Phys. Chem. Tables.'

In order to guard against the danger of absorption of moisture during transfer of the nitrobenzene into the test condenser, the liquid was re-distilled, after a long period of shaking over anhydrous calcium chloride, directly into the condenser via a suitable collecting chamber Even this was not regarded as a sufficient safeguard unless all moisture was removed from both the distilling apparatus and the condenser. The distilling system was arranged, therefore, so that a current of air could be circulated continuously for a long period previous to the introduction of the liquid and the commencement of distillation, in such a way as to pass, at suitable points, over phosphorous pentoxide. The whole system was sealed except at such points as air outlets were necessary for safety during distillation, but these had access to the distilling circuit only through phosphorous pentoxide tubes Facility was provided for by-passing the early products of distillation from the collecting chamber, and for disconnecting the condenser from the system, without inlet of moist air, when the nitrobenzene had been transferred

Measurements on nitrobenzene prepared in this manner gave curve (*b*), fig. 3. It is seen that there is a marked decrease in loss resistance as compared with curve (*a*), though the nature of the variation over the frequency range is the same The nearest approach to complete removal of moisture by preparation of the nitrobenzene in the above manner, without the application of steady potential across the test condenser, is indicated by curve (*c*) The measurements recorded in curves (*b*) and (*c*) were carried out at a constant temperature of 11° C. Curve (*d*) shows the modified form of curve (*b*) after the application of a steady potential of 60 volts for 16 hours and a recovery period of 8½ hours following its removal.

Effects with Nitrobenzene Resulting from Steady Voltage Application.

Interesting effects were observed on the application of steady voltage across the dielectric medium. These measurements under D.C. potential consisted in recording the charging current during voltage application to the condenser, and in a study of the effect of this application on the loss resistance to high frequency currents at intervals of time after its removal. During the periods between successive measurements of loss resistance, the measuring circuit was kept closed so that the condenser was able to discharge through the circuit. During these times a micro-ammeter was introduced to measure any discharge current existing

(A) *Dielectric Recovery Following Voltage Removal*

The curve of fig. 6 shows the variation with time of the current entering the condenser under a steady potential of 60 volts suddenly applied at time $t = 0$. The condition of the dielectric previous to this application was that to which the results of curve (*b*), fig. 3, apply. Since it was not possible to commence current measurement until several seconds after voltage application, by which time the "normal" charging current will have ceased to flow, the curve of fig. 6 gives the sum of an "anomalous" current and the "steady" leakage. This latter may reasonably be taken as the current value of 105 micro-amperes after 16 hours voltage application.

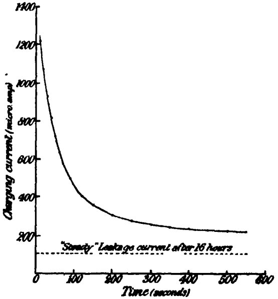

Fig. 6.—Capacity 1600 micro-microfarads, applied voltage = 60.

For alternating electric fields the conditions are such as correspond to very small values of t. It has been seen that the nitrobenzene samples tested behave as if the liquid has a constant conductivity. This should be equal to the initial conductivity under continuous voltage.*† Since the earliest current measurement recorded in the present work was after 10 seconds, it is not possible to check this conclusion effectively. At the time of 10 seconds, however, the equivalent leakage resistance is 49,000 ohms, a value which would be responsible for a loss resistance of 0·99 ohm at 663 metres, as compared with the value of 1·34 ohms measured immediately before application of steady voltage, and the value of 0·085 ohm which would be produced by the conductivity corresponding to the "steady" leakage current of 105 micro-amperes.

The manner in which the loss resistance of the dielectric varied with recovery time following the removal of the steady voltage, as measured at a frequency of $4\cdot5 \times 10^5$ cycles/sec (663 metres) is shown in fig. 7 Curve (*c*) relates to conditions after the application of 60 volts to the dielectric on which the results of curve (*b*), fig 3, and fig. 6 were obtained. The loss resistance at this frequency before the steady voltage application was 1·34 ohms Curves (*a*) and (*b*), fig 7, relate to a sample of nitrobenzene which had not been so well purified and which, therefore, had a somewhat higher initial loss, 1·75 ohms These curves show the behaviour of this liquid after the application of 60 volts for periods of ½ and 1½ hours respectively. Curves (*d*) and (*e*), fig 7, were taken on the same dielectric as curve (*c*), but after a further voltage application of roughly 40 and 80 hours duration. These latter periods are not stated

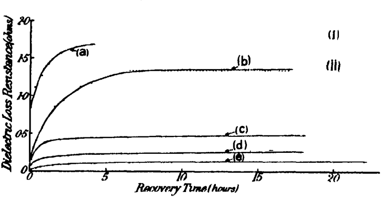

FIG. 7.—(i) Loss resistance before steady voltage application for (*a*) and (*b*); (ii) Loss resistance before steady voltage application for (*c*), (*d*), and (*e*). (*a*) and (*b*) After ½ and 1½ hours application respectively; (*c*) after 16 hours application, (*d*) and (*e*) after 40 and 80 hours further application. Frequency $4\cdot5 \times 10^5$ cycles/sec.; temperature, 11° C.

---

* Tank 'Ann. Physik.,' vol. 48, p. 307 (1915).

† Whitehead. 'Trans Amer Inst. Elect. Eng.,' vol. 50, p. 693 (1931).

precisely since additional tests were carried out on the dielectric at intervening times.

The effect of steady voltage application is thus to cause a decrease in the high frequency loss resistance to an increasing extent with increased time of application. The dielectric shows an approach to complete recovery of its original state after 4 hours under the conditions of curve (*a*), but for (*b*), (*c*), (*d*) and (*e*) no suggestion of ultimate recovery is apparent

Following a recovery period of 16 hours, the nitrobenzene on which the results of curve (*c*) were taken was removed from the condenser, and later replaced after the condenser had been thoroughly cleaned with acetone and dried The loss resistance measured just previous to removal was 0·48 ohm and after replacement 0·55 ohm, as compared with the original value of 1·34 ohms In view of the affinity of nitrobenzene for small quantities of moisture, the increase from 0·48 to 0·55 ohm is probably due to moisture absorption during the emptying and refilling process.

No nickel content could be discerned on testing the nitrobenzene with dimethyl glyoxime, so that direct attack on the electrodes could not have occurred.

During the recovery of the dielectric it was noticed that a small reverse current existed. The curve of fig. 8 shows the variation of this reverse current with time during the recovery conditions to which curve (*e*), fig. 7, relates. It is seen that the current passes through a maximum after about 1½ hours, and then decreases very slowly to zero

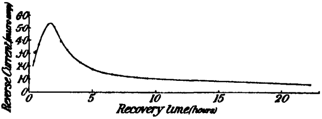

Fig 8.

(B) *Phenomena on Voltage Reversal.*

In analysing the causes of this behaviour the effect of sudden reversal of the applied steady potential is of interest and importance. The type of curve showing the current flow through the dielectric on voltage reversal, following the attainment of a " steady " state in the original direction is shown in fig. 9. It is noted that on voltage reversal the current reverses relatively slowly, reaches a maximum, which is many times greater than the initial steady current, after about 90 seconds and then decreases, in much the same manner as seen in fig. 6, to approach a stationary value in this reverse direction.

The changes in the state of the dielectric following voltage reversal were investigated by carrying out high frequency loss resistance measurements at different regions of the current reversal curve of fig. 9. These measurements were made on the dielectric to which curve (*d*) of fig. 7 relates after a recovery period of about 50 hours The loss resistance at the commencement of the measurements was 0·26 ohm. With the dielectric in this state a steady potential of 120 volts was applied between the condenser plates for 10 hours. The battery was then removed for a few minutes and the loss resistance measured as 0·03 ohm. The voltage was at once re-applied and 15 minutes later was suddenly reversed. As the reverse current was passing through the maximum —corresponding to the region A, fig. 9—the battery was removed and the loss resistance determined as 0·14 ohm. The reversed battery was then re-applied for 10 minutes—corresponding to the region B, fig. 9—at which point the loss resistance was 0·10 ohm. After 4 hours re-application the loss resistance had fallen to 0·05 ohm, suggestive of an approach to a steady conducting state in the reversed direction.

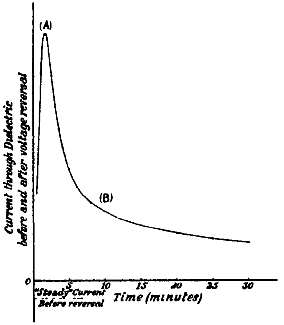

FIG. 9

The whole test, commencing with the same electrode polarities as before, was repeated some hours later, when it was found that the loss resistance in the region A, fig. 9, had fallen to the value of 0·07 ohm. Analagous with this reduction in loss resistance from the value of 0·14 ohm noted above, the reverse current maximum was reduced in roughly the same proportion.

Discussion

It is apparent that a small quantity of moisture remained in the nitrobenzene at the completion of the distillation processes The presence of this moisture is undoubtedly the main cause of conductivity. The results show clearly that an "electrical cleaning" action is occurring during the application of continuous voltage After removal of the potential, however, it is seen from fig 7 that the loss resistance, and therefore the effective conductivity, of the dielectric is not constant, but gradually increases to a constant value which is appreciably lower, by virtue of this electrical cleaning, than the original

It seems probable that the important electrode phenomena are of the same type as those occurring in electrolytic cells Thus, an accumulation, during charge, of the gaseous products of electrolysis of the moisture impurity present would result in the gradual formation of an obstructive film on the electrode surfaces. This would help to account for the slow decay in conductivity under steady potential, and for the slow rate of recovery during short circuit, although it could not account for the presence of a reverse current. Further, an accumulation of electromotively active impurity, in some form,* can occur at the electrodes. Since the amount of impurity in the nitrobenzene is small, the gradual withdrawal of a part of it from the mass of the dielectric, and its accumulation on or in the immediate vicinity of the electrodes, must show itself as a decrease in the conductivity of the medium When the voltage is removed, and the condenser shorted, this active material may be expected to diffuse into the dielectric medium to produce a gradual increase in conductivity. The rate of increase of conductivity will depend on the rate at which the disintegration of the accumulation at the electrodes proceeds. The application of continuous voltage for longer and longer periods should remove more and more of the active impurity completely from the dielectric, and reduce the extent of the possible recovery, as illustrated in the curves of fig. 7.

The presence and form of time variation of the reverse current, fig. 8, may be explained in terms of the active back e m.f. which results from this latter accumulation. The slow diffusion of the accumulated material must produce a decrease in the value of this e m f., simultaneous with the increase in conductivity of the dielectric medium These two actions tend to oppose each other in determining the magnitude of the reverse current, and may well produce the maximum observed

---

* Bowden, 'Proc Roy Soc.,' A, vol 126, p. 107 (1929).

The form of the conduction current curve on voltage reversal might be explained also on the basis of an accumulation of active material at the electrodes. The first effect of voltage reversal must be to cause the removal of this material from the surfaces of the respective electrodes, and the final effect to cause its re-accumulation, with some loss by discharge, at the opposite electrodes. Between the two limiting steady states a region of maximum conductivity should occur as shown in the curve of fig. 9

Results in Liquids other than Nitrobenzene

The same general procedure, as described for nitrobenzene, was adopted for chlorbenzene, but for a capacitance value of 800 micro-microfarads The performance observed under alternating and steady applied voltage was essentially similar to that recorded for nitrobenzene except that the conductivity and the high frequency loss resistance were of much smaller value. For a sample distilled directly into the condenser after the drying process described previously, but before the application of steady potential, the loss resistance did not exceed 0·10 ohm even at the lower limit of the range of frequency 4×10^5 to 2×10^6 cycles per second After prolonged application of steady voltage the loss was too small to measure

With toluene, the initial conductivity, as shown by the loss resistance of a purified sample, was still smaller, while with benzene it was not possible to notice any difference between the test and air condensers at any part of the frequency range.

The fact that the frequencies employed in these measurements are too low for the Debye effect to become apparent was demonstrated by preparing and testing similar solutions of para- and ortho-dichlorbenzene in purified toluene Since para-dichlorbenzene has no dipole moment, the dielectric constant of the former solution was the same as that of toluene, 2·38 at 14° C., whereas the dielectric constant of the ortho- solution was 3·15, at the same temperature. In neither liquid, however, was the dielectric loss greater than had been found for pure toluene.

Summary

The paper covers a series of dielectric loss measurements on samples of several liquid hydrocarbon derivatives—benzene, toluene, chlorbenzene and nitrobenzene—over the frequency range 2×10^5 to 2×10^6 cycles per second, before and after the application of steady voltage For this purpose a substitution method of condenser resistance measurement has been employed, in which two parallel plate condensers of identical construction, one with air and the other with liquid dielectric, have been compared. It has been found that the dielectric loss over this frequency range can be accounted for in terms of ionic conduction, and that the application of steady voltage materially affects the magnitude of this loss as the result of an "electrical cleaning" process which occurs. It is suggested that in association with the elimination by electrolysis of part of the moisture impurity present, an accumulation of electromotively active material occurs at the electrodes. On removal of the applied voltage, this material slowly diffuses into the dielectric medium with a consequent gradual increase in the dielectric loss to a value which is lower than the original to an extent depending on the duration of the steady voltage application. A small discharge current, which passed through a maximum value before decreasing slowly to zero, was found to exist during this recovery period, and its presence and mode of variation are accounted for in terms of this accumulation and diffusion.

On the Stability for Three-Dimensional Disturbances of Viscous Fluid Flow between Parallel Walls.

By H. B. Squire.

(Communicated by R. V Southwell, F R S —Received July 12, 1933)

Introduction

The turbulence problem is still unsolved, though a number of valuable papers have been published on it comparatively recently. But, since Hopf* and von Mises† proved that uniform shearing motion between two parallel planes was stable for infinitesimal disturbances, the view that viscous flow is stable for infinitesimal disturbances but unstable for disturbances of a finite size has become more and more widely held. Von Mises suggested that the roughness of the walls might be the determining factor, but the experiments of Schiller‡ have shown that the degree of roughness of the walls is of negligible influence on the critical value of Reynolds' number. He concluded that the breakdown of laminar flow depended primarily on the size of the initial disturbance, in agreement with Osborne Reynolds' view §

Important papers have been published by Noether‖ and Tollmien,¶ whose conclusions are in contradiction to one another. On the one hand, Noether, by a formal investigation of the asymptotic solutions of the equation governing the two-dimensional disturbances of flow between parallel walls, claims to have proved that all velocity profiles are stable for all values of Reynolds' number. On the other hand, Tollmien has determined a critical value of Reynolds' number for the flow past a flat plate placed edgeways to the stream. This value is in good agreement with the experimental results. There are, however, certain points in his analysis which are not clear and it would be useful to know if the method gave results in agreement with those derived more strictly.

Hitherto most investigations into the stability of flow between parallel planes by the method of small oscillations have been limited to disturbances of two-dimensional type. This has been done on grounds of simplicity and is partially justified by Osborne Reynolds' investigation* which indicates that those disturbances most likely to be unstable are two-dimensional. But Reynolds' method differs greatly from the method of small oscillations and it seemed useful to apply the latter to three-dimensional disturbances This is the object of the present paper, in which it is shown that the problem is analogous to the simpler one and that Reynolds' general conclusion holds precisely.

---

* 'Ann. Physik,' vol 44, p 1 (1914)

† 'Jahrb. deuts. Math. Ver,' vol. 21, p. 241 (1912).

‡ 'Z. angew. Math. Mech,' vol. 2, p 96 (1922)

§ 'Phil Trans,' vol. 174, p. 935 (1883) [Papers, vol 2, p 51]

‖ 'Z. angew Math Mech.,' vol. 6, p. 232 (1926)

¶ 'Nach. Ges. Wiss Gött.,' p. 21 (1929).

The Equations of Motion

We consider the steady two-dimensional flow of an incompressible viscous fluid upon which a disturbance is superposed. The origin O is taken at a point midway between the walls, the axis of x is in the direction of the flow and parallel to the walls, the axis of y is perpendicular to the walls, and the axis of z is parallel to the walls and perpendicular to the other axes. If $2b$ is the distance between the walls, these will coincide with the planes $y = \pm b$ The main flow is defined by

$$u = \mathrm{U}(y), \qquad v = 0, \qquad w = 0, \tag{1}$$

where u, v, w are the velocities in the directions Ox, Oy, Oz respectively. It will be assumed that $\mathrm{U}(y)$ is a continuous function of y which may be differentiated as often as required

If now a small disturbance be superposed on the main flow, the velocities will be given by

$$u = \mathrm{U}(y) + u_1, \qquad v = v_1, \qquad w = w_1, \tag{2}$$

where u_1, v_1, w_1 are small quantities whose squares may be neglected The expressions (2) must satisfy the Stokes-Navier equations,†

$$\left.\begin{aligned} \frac{\mathrm{D}u}{\mathrm{D}t} &= \mathrm{X} - \frac{1}{\rho}\frac{\partial p}{\partial x} + \nu\,\nabla^2 u, \\ \frac{\mathrm{D}v}{\mathrm{D}t} &= \mathrm{Y} - \frac{1}{\rho}\frac{\partial p}{\partial y} + \nu\,\nabla^2 v, \\ \frac{\mathrm{D}w}{\mathrm{D}t} &= \mathrm{Z} - \frac{1}{\rho}\frac{\partial p}{\partial z} + \nu\,\nabla^2 w, \end{aligned}\right\} \tag{3}$$

and the equation of continuity

$$\frac{\partial u}{\partial x} + \frac{\partial v}{\partial y} + \frac{\partial w}{\partial z} = 0. \tag{4}$$

---

* 'Phil Trans.,' A, vol. 186, p. 123 (1894). [Papers, vol. 2, p 535.]

† *Cf.* Lamb, "Hydrodynamics," 5th ed., p. 547.

In these equations p stands for the pressure, ρ the density, ν the kinematic viscosity; X, Y, Z are the external forces per unit mass and as usual

$$\frac{\mathrm{D}}{\mathrm{D}t}=\frac{\partial}{\partial t}+u\frac{\partial}{\partial x}+v\frac{\partial}{\partial y}+w\frac{\partial}{\partial z}.$$

We shall take the body forces to be zero except so far as they are necessary to keep up the main flow Substituting the values of u, v, w from (2) in (3) and (4), cancelling the terms arising from the main flow and neglecting the quadratic terms these equations become

$$\left.\begin{aligned}\frac{\partial u_1}{\partial t}+\mathrm{U}\frac{\partial u_1}{\partial x}+v_1\frac{d\mathrm{U}}{dy}&=-\frac{1}{\rho}\frac{\partial p}{\partial x}+\nu\nabla^2 u_1,\\ \frac{\partial v_1}{\partial t}+\mathrm{U}\frac{\partial v_1}{\partial x}\qquad\quad&=-\frac{1}{\rho}\frac{\partial p}{\partial y}+\nu\nabla^2 v_1,\\ \frac{\partial w_1}{\partial t}+\mathrm{U}\frac{\partial w_1}{\partial x}\qquad\quad&=-\frac{1}{\rho}\frac{\partial p}{\partial z}+\nu\nabla^2 w_1,\end{aligned}\right\}\tag{5}$$

and

$$\frac{\partial u_1}{\partial x}+\frac{\partial v_1}{\partial y}+\frac{\partial w_1}{\partial z}=0\tag{6}$$

Eliminating p between equations (5) we have*

$$\left.\begin{aligned}\left[\frac{\partial}{\partial t}+\mathrm{U}\frac{\partial}{\partial x}-\nu\nabla^2\right]\left[\frac{\partial w_1}{\partial y}-\frac{\partial v_1}{\partial z}\right]+\mathrm{U}'\frac{\partial w_1}{\partial x}\qquad\quad&=0, &(7)\\ \left[\frac{\partial}{\partial t}+\mathrm{U}\frac{\partial}{\partial x}-\nu\nabla^2\right]\left[\frac{\partial u_1}{\partial z}-\frac{\partial w_1}{\partial x}\right]+\mathrm{U}'\frac{\partial v_1}{\partial z}\qquad\quad&=0, &(8)\\ \left[\frac{\partial}{\partial t}+\mathrm{U}\frac{\partial}{\partial x}-\nu\nabla^2\right]\left[\frac{\partial v_1}{\partial x}-\frac{\partial u_1}{\partial y}\right]+\mathrm{U}'\frac{\partial w_1}{\partial z}-\mathrm{U}''v_1&=0 &(9)\end{aligned}\right\}$$

Assumption of a Periodic Disturbance.

It will be assumed that any disturbance can be broken up into a set of disturbances which are periodic with respect to x and to z For two-dimensional disturbances periodicity with respect to x is always assumed A proof that this is valid for uniform shearing motion has been given by Haupt† and it is natural to suppose that it could be extended to cover other types. Then we may take

---

* Equation (9) has been simplified by use of (6).

† 'SitzBer. bayer Akad. Wiss,' p. 289 (1912).

$$\left.\begin{aligned} u_1 &= u(y)\,.\,\exp i\,(jx + kz - \sigma t), \\ v_1 &= v(y)\,.\,\exp i\,(jx + kz - \sigma t), \\ w_1 &= w(y)\,.\,\exp i\,(jx + kz - \sigma t), \end{aligned}\right\} \tag{10}$$

where j and k are real and positive and σ is in general complex.

Substitution in the equations (6) to (10) gives

$$iju + \mathrm{D}v + ikw = 0, \tag{11}$$

$$[\nu(\mathrm{D}^2 - j^2 - k^2) + i\sigma - ij\mathrm{U}]\,[\mathrm{D}w - ikv] - ij\mathrm{U}'w = 0, \tag{12}$$

$$[\nu\,(\mathrm{D}^2 - j^2 - k^2) + i\sigma - ij\mathrm{U}]\,[iku - ijw] - ik\mathrm{U}'v = 0, \tag{13}$$

$$[\nu\,(\mathrm{D}^2 - j^2 - k^2) + i\sigma - ij\mathrm{U}]\,[ijv - \mathrm{D}u] - ik\mathrm{U}'w + \mathrm{U}''v = 0, \tag{14}$$

where D stands for d/dy.

These equations may now be reduced to a non-dimensional form by replacing y/b, jb, kb, σ/j, U/U_0 and $\mathrm{U}_0 b/\nu$ by y, α, β, $c\mathrm{U}_0$, V and R respectively. $2\pi/\alpha$ and $2\pi/\beta$ are then the wave-lengths of the disturbance in the directions x and z, R stands for Reynolds' number and U_0 is some velocity defining the magnitude of the main flow.* The equations become†

$$i\alpha u + \mathrm{D}v + i\beta w = 0, \tag{15}$$

$$\Delta\,[\mathrm{D}w - i\beta v] - i\mathrm{R}\alpha\,.\,\mathrm{V}'w = 0, \tag{16}$$

$$\Delta\,[i\beta u - i\alpha w] - i\mathrm{R}\beta\,.\,\mathrm{V}'v = 0, \tag{17}$$

$$\Delta\,[i\alpha v - \mathrm{D}u] - i\mathrm{R}\beta\ \ \mathrm{V}'w + \mathrm{R}\mathrm{V}''v = 0, \tag{18}$$

where Δ stands for the operator $\mathrm{D}^2 - (\alpha^2 + \beta^2) - i\mathrm{R}\alpha\,(\mathrm{V} - c)$.

The boundary conditions are that the disturbance shall vanish at the walls, i.e., for $y = \pm 1$ we have

$$u = v = w = 0. \tag{19}$$

Formulation of the Problem.

When the velocity profile V (y) of the main flow is given, equations (15) to (18) in conjunction with the boundary conditions are just sufficient to determine the value of c corresponding to given values of the independent quantities

---

* *E.g.*, for uniform shearing motion U_0 is equal to the relative velocity of the walls.

† One of these four equations is redundant and may be deduced from the other three.

R, α, β. This value will in general be a complex quantity, of which the imaginary part will certainly be negative for sufficiently small values of Reynolds' number, showing that the flow is stable for such values of R. If, on increasing R, c passes through a purely real value, the corresponding value of R is said to be a "critical" value, for, if this value be exceeded, the disturbance will increase without limit, indicating instability and a breakdown of the laminar flow

The only two cases which have been worked out in detail for two-dimensional disturbances are that of uniform shearing motion,* for which $V = y$, and that for which $V = y^2$.† In neither case does a "critical" value of R exist and hence these velocity profiles are stable for all values of Reynolds' number.

Determination of an Equation for v.

We now proceed to eliminate u and w from equations (15), (16), and (17) and to obtain a fourth order equation for v For the time being the possibility that any of the quantities u, v, w vanish will be excluded.

We note first that the commutative law for the operators D and Δ is

$$D\,.\,\Delta - \Delta\;\; D = - iR\alpha\,.\,V', \tag{20}$$

and also that

$$D\,.\,V' - V'\,.\,D = V''. \tag{21}$$

Making use of (20) equation (16) may be written

$$D\,.\,\Delta w - i\beta\Delta v = 0. \tag{22}$$

Eliminating u between (15) and (17) we have

$$i\,(\alpha^2 + \beta^2)\,\Delta w + \beta\,[\Delta\,.\,D + iR\alpha\,.\,V']\,v = 0. \tag{23}$$

Now w appears in (22) and (23) only in the form Δw and may be eliminated on substitution from (23) in (22) We obtain

$$[D\,.\,\Delta\,.\,D + iR\alpha\,.\,D\,.\,V']\,v = (\alpha^2 + \beta^2)\,\Delta v.$$

Making use of relation (20) the equation for v becomes

$$[\Delta\,.\,D^2 - iR\alpha\,.\,V'\,.\,D + iR\alpha\,.\,D\,.\,V']\,v = (\alpha^2 + \beta^2)\,\Delta v,$$

and applying (21),

$$[\Delta D^2 + iR\alpha\;\; V'']\,v = (\alpha^2 + \beta^2)\,\Delta v.$$

---

* Hopf, *loc. cit* The exact calculations of Southwell and Chitty, 'Phil. Trans.,' A, vol. 229, p. 205 (1930), agree with Hopf's results.

† Blumenthal, 'SitzBer bayer Akad Wiss.,' p. 563 (1913).

Replacing Δ by its value $D^2 - (\alpha^2 + \beta^2) - iR\alpha(V - c)$ we have finally

$$[D^4 - 2(\alpha^2 + \beta^2) D^2 + (\alpha^2 + \beta^2)^2] v = iR\alpha [(V - c) \{D^2 - (\alpha^2 + \beta^2)\} - V''] v. \tag{24}$$

Now the boundary conditions require that u, v, and w shall vanish on the walls $y = \pm 1$. It is clear from (15) that, for this to be possible, Dv must also vanish on the walls Hence v is completely determined by the fourth-order equation (24) and the four boundary conditions which it must satisfy.

If we further suppose v to have been determined by (24), w is then fixed by equation (23), which is of the second order, and by the conditions that it must vanish on $y = \pm 1$. When v and w are fixed u is given immediately by (15) and will vanish automatically on the walls since Dv and w vanish there

The discussion of the stability of the flow for a disturbance of this kind can thus be limited to an examination of equation (24) together with the boundary conditions which v must satisfy

Remarks on Equation (24).

Equation (24) is analogous to the equation obtained from a consideration of two-dimensional disturbances To complete the analogy we make the substitutions

$$\left.\begin{aligned} \alpha^2 + \beta^2 &= \bar{\alpha}^2, \\ R\alpha = \bar{R}\bar{\alpha} &= \bar{R}(\alpha^2 + \beta^2)^{\frac{1}{2}} \end{aligned}\right\} \tag{25}$$

Then equation (24) becomes

$$[D^4 - 2\bar{\alpha}^2 . D^2 + \bar{\alpha}^4] v = i\bar{R}\bar{\alpha} [(V - c)(D^2 - \bar{\alpha}^2) - V''] v, \tag{26}$$

which is exactly the equation satisfied by a two-dimensional disturbance of wave-length $2\pi/\bar{\alpha}$ when $\bar{R}$ is the value of Reynolds' number. The latter* may be derived immediately from equations (15) and (18) by putting β and w equal to zero and eliminating u. The boundary conditions are also identical in the two cases.

The analogy is now complete and we may conclude that the development of a three-dimensional disturbance as defined by (10) is exactly similar to that of a disturbance of two-dimensional type for which the wave-length is $2\pi/\bar{\alpha}$ and the value of Reynolds' number is $\bar{R}$. Since $\bar{R}$ is necessarily less than R† it follows that any instability which may be present for three-dimensional disturbances is also present for two-dimensional disturbances at a lower value of Reynolds' number. *For the study of the stability of flow between parallel walls it is sufficient to confine attention to disturbances of two-dimensional type.* We conclude also that for the two cases which have been worked out by Hopf and Blumenthal the flow is stable for all disturbances and, if Noether's conclusion is valid, all velocity profiles are stable for infinitesimal disturbances.

---

* First given in this form by Noether, 'Z angew. Math Mech.,' vol. 1, p. 125 (1921).

† This is obvious from the definition (25) of $\bar{R}$.

Case for which $v = 0$.

When v vanishes equations (16) to (18) reduce to

$$\Delta(u) \equiv [D^2 - (\alpha^2 + \beta^2) - iR\alpha(V - c)]u = 0; \tag{27}$$

the boundary conditions are

$$u = 0, \quad \text{for} \quad y = \pm 1.$$

It can be proved most simply that such a disturbance cannot be unstable by showing that, if c is real, no real value of $R\alpha$ can be found which satisfies these conditions.

In general to each real value of c will correspond a complex value of $iR\alpha$ and we may write

$$iR\alpha = \lambda + i\mu.$$

Then equation (27) becomes

$$\Delta(u) \equiv [D^2 - (\alpha^2 + \beta^2) - (\lambda + i\mu)(V - c)]u = 0. \tag{28}$$

Let $\bar{u}$ be the function conjugate to u, which then satisfies the equation

$$\bar{\Delta}(\bar{u}) \equiv [D^2 - (\alpha^2 + \beta^2) - (\lambda - i\mu)(V - c)]\bar{u} = 0, \tag{29}$$

and the same boundary conditions as u.

Multiply (28) by $\bar{u}$, (29) by u, subtract and integrate across the field. Then

$$0 = \int_{-1}^{1} [\bar{u}\,\Delta(u) - u\,\bar{\Delta}(\bar{u})]\,dy = -2i\mu \int_{-1}^{1} (V - c)\,u\,.\,\bar{u}\,dy, \tag{30}$$

performing the same operations and adding we have

$$0 = \int_{-1}^{1} [\bar{u}\,\Delta(u) + u\,\bar{\Delta}(\bar{u})]\,dy = -2\int_{-1}^{1} [\bar{u}'\,.\,u' + (\alpha^2 + \beta^2)\,u\,.\,\bar{u}]\,dy - 2\lambda \int_{-1}^{1} (V - c)\,u\,.\,\bar{u}\,dy, \tag{31}$$

after integrating by parts and making use of the boundary conditions. Now the first integral on the right-hand side of (31) cannot vanish since the integrand is essentially positive and hence

$$\lambda \int_{-1}^{1} (V - c)\, u \,.\, \bar{u}\, dy < 0\,;$$

it follows from (30) that μ is zero.

Therefore no real values of $R\alpha$ exist corresponding to real values of c and all profiles $V(y)$ are stable for disturbances of this degenerate type

Summary.

The stability of the flow of a viscous fluid between parallel walls for three-dimensional disturbances is discussed A fourth-order differential equation is derived and it is shown that, if any velocity profile is unstable for a particular value of Reynolds' number, it will be unstable at a lower value of Reynolds' number for two-dimensional disturbances. Further, all profiles are shown to be stable for disturbances of a certain degenerate type.

The Mechanism of the Oxygen Electrode.

By T. P. Hoar, University Chemical Laboratory, Cambridge.

(Communicated by Eric K Rideal, F R.S —Received July 15, 1933.)

1. *Introduction.*

It is well known that the so-called " oxygen electrode " does not behave in a thermodynamically reversible manner. The decomposition voltage of water has been calculated thermodynamically from various calorimetric and solubility data by Lewis,[*] Nernst and von Wartenberg,[†] Brönsted[‡] and Lewis and Randall.[§] The final critical value given by the last-named authors is 1·227 volt at 25° C., which should therefore be the e.m f. of a cell consisting of a reversible hydrogen electrode and a reversible oxygen electrode immersed in the same electrolyte, both gases being at 760 mm. pressure. In practice this value has never been obtained. Smale[||] found that the e.m.f. of the

---

[*] 'J. Amer Chem. Soc.,' vol. 28, p. 158 (1906)

[†] 'Z. phys. Chem.,' vol. 56, p. 534 (1906)

[‡] *Ibid.*, vol. 65, pp. 84, 744 (1909).

[§] 'J. Amer. Chem. Soc ,' vol. 36, p. 1969 (1914).

[||] 'Z. phys. Chem.,' vol. 14, p. 577 (1894).

hydrogen-oxygen cell, though independent of the p_H of the electrolyte, was only 1·07–1·08 volt Wilsmore[*] obtained a value of 1·07 volt, rising to 1·12 volt if the cell were allowed to stand for some days, while a similar result, 1·06 volt, was obtained by Crotogino.[†] More recently, Richards[‡] has reported 0·979 volt, and Furman[§] also obtains a value of about 0·98 volt.

Since it is well established that the hydrogen electrode behaves in a perfectly reversible manner in accord with thermodynamic laws, the discrepancy between the "theoretical" and experimental e.m f of the hydrogen-oxygen cell must have its origin in the oxygen electrode It is in fact experimentally found that oxygen electrodes, whether set up with bright or platinized platinum, (*a*) tend to be irreproducible, (*b*) do not obey the thermodynamic relation between electrode potential and partial pressure of oxygen, and (*c*) are readily polarized even by minute currents, thus failing to conform with any of the criteria of reversibility.

Various explanations have been put forward for the cause of the incomplete reversibility of the oxygen electrode. Tartar and Wellman[‖] suggest that it is due to the formation of hydrogen peroxide, for addition of hydrogen peroxide depresses the potential still further below the thermodynamic value.[¶] However, the formation of hydrogen peroxide appears to be very doubtful,[**] and the most widely held view is that oxides of platinum are formed on the electrode, which never becomes saturated with oxygen and thus never attains the reversible oxygen potential. Lorenz and his co-workers[††] and Grube[‡‡] found that the various platinum oxides gave electrode potentials very similar to that of a platinum electrode surrounded by oxygen. Again, by working at high temperatures where the oxides are unstable, using glass, porcelain, or fused alkali as electrolyte, Haber and his co-workers[§§] obtained e.m.f's of the hydrogen-oxygen cell very close to the calculated values. Richards[‖‖] considers his results are best explained on the oxide theory; furthermore, Bowden[*] has put forward evidence for the formation of platinum oxides at a platinum anode, although his view is questioned by Butler and Armstrong.[†]

---

[*] *Ibid.*, vol. 35, p. 291 (1900)

[†] 'Z. anorg Chem.,' vol. 24, p 258 (1900)

[‡] 'J Phys. Chem.,' vol. 32, p. 990 (1928)

[§] 'J. Amer. Chem. Soc.,' vol. 44, p 2685 (1922).

[‖] 'J Phys Chem.,' vol. 32, p. 1171 (1928)

[¶] Brislee, 'Trans. Faraday Soc ,' vol 1, p. 65 (1905), Wilsmore, 'Z. phys. Chem ,' vol 35, p 291 (1900), Fisher and Krönig, 'Z. anorg Chem.,' vol. 135, p. 169 (1924).

[**] Bornemann, *ibid.*, vol. 34, p 1 (1903).

[††] 'Z. anorg. Chem.,' vol. 51, p. 81 (1906), 'Z Electrochem.,' vol 14, p. 781 (1908); vol. 15, pp. 157, 206, 293, 349, 661 (1909)

[‡‡] 'Z. Electrochem.,' vol. 16, p. 621 (1910).

[§§] *Ibid.*, vol. 12, p. 415 (1906); 'Z. anorg. Chem.,' vol 51, pp. 245, 289, 356 (1906)

[‖‖] 'J. Phys. Chem.,' vol. 32, p. 990 (1928)

Besides having considerable theoretical interest, the oxygen electrode has been used for electrotitration,[‡] and it plays an important part in the corrosion of metals[§], it therefore appeared desirable to have more definite evidence as to the nature of the reactions involved In the present investigation, the kinetics of the dissolution and deposition of oxygen at several so-called "inert" electrodes have been examined, and a tentative mechanism of the irreversibility is put forward It has also been found possible to deduce an approximate value for the e.m.f. of the hydrogen-oxygen cell from electrical measurements, and the result, 1·20 ± 0·03 volt at 25° C., appears to be in closer agreement with the theoretical value of 1·227 volt than any previously obtained

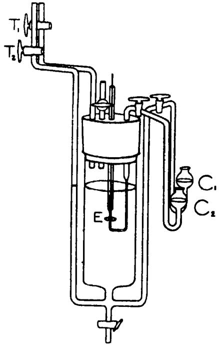

Fig 1

2 *Apparatus.*

The electrode vessel, fig 1, consisted of a cylinder 15 cm. high by 4 cm. diameter The electrode E under test was arranged centrally and horizontally, with the face on the underside, the back and edges being coated with an insulating layer of resistant wax, to ensure that the current-density was as uniform as possible. Polarizing current could be supplied to the test electrode via a half-cell making liquid contact in the cup C$_1$, while the electrode potential could be measured against a half-cell connected to C$_2$. Calomel or quinhydrone electrodes, being only slightly polarizable, were used indiscriminately for the current half-cell. The half-cell used for potential measurement consisted, in experiments where the electrolyte was of $p_H < 7$, of a quinhydrone electrode in the same electrolyte. In experiments in alkaline solution, where the quinhydrone electrode becomes inaccurate, a mercury/mercuric oxide alkali half-cell was used, the alkali being of the same concentration as the main electrolyte; this half-cell was standardized against a hydrogen electrode in the same alkali. All liquid junction P.D's were thus avoided, and the potential of the test oxygen electrode could be immediately found with reference to a hydrogen electrode in the same solution.

---

[*] 'Proc. Roy. Soc.,' A, vol. 125, p. 446 (1929).

[†] *Ibid*, vol 137, p. 604 (1932)

[‡] Furman, 'J. Amer Chem Soc,' vol. 44, p. 2685 (1922), Goard and Rideal, 'Trans. Faraday Soc.,' vol 19, p 740 (1924), Britton, 'J Chem Soc,' vol. 127, p. 1896 (1925).

[§] Aston, 'Trans Amer Electrochem. Soc,' vol. 29, p. 449 (1916); Evans, 'J Inst. Met.,' vol. 30, p 239 (1923), "Corrosion of Metals" (Arnold) (1926), Evans, Bannister and Britton, 'Proc. Roy. Soc.,' A, vol. 131, p 355 (1931); Evans and Hoar, *ibid.*, A, vol. 137, p. 343 (1932).

The apparatus was contained in a brass box immersed in a water thermostat, to avoid risk of electrical leakage which might occur if the apparatus were directly immersed in water The electrical leads were brought out through insulators in the lid of the box. The lid was heavily lagged with asbestos, to prevent loss of heat by radiation and convection, and a satisfactory temperature control of ± 0·1° C. within the box was obtained

Before a run, the electrode vessel and connecting tubes were swept out with purified oxygen admitted through tap T_1. Electrolyte, which had been boiled out under reflux and saturated with oxygen at the temperature of the experiment, was then introduced through tap T_2, until the electrode was immersed to a depth of 3·0 cm., preliminary experiments showed that this depth was immaterial. The connecting tubes and the cups C_1 and C_2 were also filled with electrolyte, as shown, and the half-cells were then inserted so that they made liquid junctions in C_1 and C_2 The arrangement of the liquid levels and the length of the connecting tubes effectively prevented any appreciable siphoning or diffusion in the system, and as an additional precaution all taps were kept closed.

The electrical lay-out is shown schematically in fig. 2. E.m.f. was measured by means of the valve electrometer of Evans and Hoar* which takes less than 5×10^{-13} ampere from the cell under measurement and is accurate to $\pm 0 \cdot 001$ volt; the voltmeter on which readings are obtained was checked against a standard Weston cell and a Cambridge Instrument Company potentiometer.

Current was supplied to the cell from a potential divider through a resistance box containing resistances ranging from 10,000 ohms to 10 megohms. This was constructed from radio resistances sealed into paraffin wax and was frequently calibrated; the resistances, though often 10–15% off the rated value, showed a satisfactory constancy. Current was measured by obtaining the potential drop across the resistance carrying it by means of the valve electrometer; the larger currents were sometimes measured on a Weston type 440 galvanometer or a Weston type 301 milliammeter.

---

* 'Proc. Roy. Soc.,' A, vol. 137, p. 343 (1932).

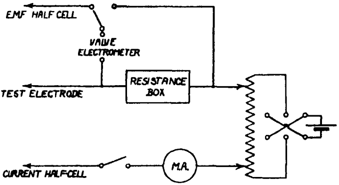

Fig. 2

3. *Preliminary Work.*

In the first experiments, the electrode was a circular piece of bright platinum foil 1·10 cm. diameter, prepared by alternate heating in a spirit flame and immersion while hot in concentrated hydrochloric acid. The electrolyte was N/10 sulphuric acid, saturated with oxygen at 25·0° C The potential difference between the electrode and the solution, referred to a hydrogen electrode in the same solution, which we shall henceforward shortly call the "potential," was initially about + 0·85 volt, well below the theoretical value of + 1·227 volt.

The unused electrode was made slightly cathodic, and a current-potential curve obtained over a current-density range of $2 \times 10^{-8} - 1 \times 10^{-6}$ ampere/cm.^{2}. The steady value of the potential for each applied current was reached rather slowly, but the reproducibility was moderately good. When, however, the anodic polarization curve was investigated, equilibrium was reached only after many hours even at fairly high (c. 5×10^{-7} ampere/cm.^{2}) current-density, while equilibrium points at lower anodic current-densities could not be obtained owing to the slow rise of the potential with time. These preliminary results made it clear that an irreversible process was occurring which prevented the equilibrium potential for a given anodic current-density being reached, and it was decided to investigate this in greater detail.

4 *Experiments at Constant Electrode Potential*

Since the "reversible" oxygen potential is somewhat more noble than the open-circuit potential adopted by an oxygen electrode, such an electrode must be polarized anodically in order to bring it to the reversible potential A bright platinum electrode 1·10 cm diameter prepared as in Section 3 was set up in oxygen-saturated N/10 sulphuric acid at 25·0° C, and the anodic current-density required to maintain it at the reversible potential, viz, + 1·227 volt, was measured at intervals It was found that the necessary current-density decreased with time, at first rapidly and finally very slowly, becoming after some hours of the order of $1-2 \times 10^{-8}$ ampere/cm^2 Similar results were obtained in N/10 sodium hydroxide (carbonate-free), though here the necessary current was, at the corresponding time, about half that required in N/10 sulphuric acid After a run of 400 minutes the polarizing current was removed, and the potential returned slowly to about + 0·98 volt for the acid and to about + 1·01 volt for the alkali. If the electrode were allowed to stand overnight on open circuit, and a similar current-time experiment carried out on the following day, a more rapid fall of the current was observed. A third repetition gave a still more rapid fall

A platinum electrode prepared by flaming in the manner described almost certainly possesses an oxide-film on the surface some molecules thick[*] Such a film may be expected to contain cracks and pores, pervious to the electrolyte, which therefore also comes into contact with exposed platinum metal The adsorbed oxygen on the film surface will render the film cathodic towards the exposed metal,[†] and current will therefore flow between film and metal, with cathodic dissolution of oxygen at the film surface and a consequent fall of its potential. The equivalent anodic reaction at the metal surface is probably oxygen-deposition, with subsequent formation of platinum oxide, though some platinum dissolution may perhaps occur, particularly in acid solutions Any platinum ions formed will, however, at once be precipitated by the cathodically produced hydroxyl ions migrating inwards through the pores. The net result will be the formation within the pores of platinum oxide or hydroxide at a rate equivalent to the current flowing.

If the reversible oxygen potential is to be maintained at the film surface, the current necessary for this irreversible oxide-formation within the pores must be supplied from elsewhere than the film, that is, from a separate cathode. Thus, an anodic current-density, of value such that the consequent fall of potential along the resistance of the pores is equal to the difference of potential between the film surface and the exposed metal surface, must be applied, and this is the current that has been measured.

---

[*] Jacobs and Whalley, 'Proc. Roy Soc.,' A, vol. 140, p. 489 (1933)

[†] Evans, 'J Chem Soc.,' p 92 (1929); Bannister and Evans, *ibid.*, p 1361 (1930). Müller, 'Mhft Chem,' vol. 52, p. 221 (1929)

Since the film surface is maintained at the reversible oxygen potential, and the exposed metal surface may be expected to show approximately the platinum/platinum oxide potential, not much affected by current polarization, the drop of potential E volts along the pores may be regarded as roughly constant. Thus if the applied current-density is i amperes/cm.^{2} at time t seconds, and the electrolytic resistance of the pores is R ohms per cm.^{2} of film,

$$iR = E = \text{constant}$$

But the pore-resistance, say initially R_0, must continuously increase as platinum oxide is deposited within the pores, and we shall assume that to a first approximation the increase of pore-resistance is proportional to the amount of oxide formed by the process, that is, to $\int_0^t i\,dt$. Then

$$i\left(R_0 + A\int_0^t i\,dt\right) = E, \quad \text{A being a constant,}$$

therefore

$$A\int_0^t i\,dt = \frac{E}{i} - R_0$$

or

$$Ai = -\frac{E}{i^2}\cdot\frac{di}{dt}.$$

Thus if the initial current-density is $i_0 = E/R_0$

$$t = \frac{E}{A}\int_{i_0}^{i} -\frac{di}{i^3}$$

$$= \frac{E}{2A}\left(\frac{1}{i^2} - \frac{1}{i_0^2}\right), \qquad (1)$$

an equation rather similar to one obtained by Muller and Konopicky* for somewhat different conditions. It has been shown experimentally that i_0 is large compared with values of i obtained even after a few minutes, and the equation thus reduces to

$$\frac{1}{i^2} = kt, \qquad (1\text{A})$$

where k is a constant.

---

* 'Mhft. Chem.,' vol. 50, p. 861 (1928).

In fig 3, $1/i^2$ is plotted against t, for bright platinum in N/10 sulphuric acid and N/10 sodium hydroxide. Excellent straight lines are obtained, the value of k being $7{\cdot}65 \times 10^{10}$ in the acid and $2{\cdot}50 \times 10^{11}$ in the alkali When, however, the $\frac{1}{i^2}\Big/t$ relation for the second experiment on an electrode is plotted, the gradient of the curve obtained is at first greater than k (since i falls more rapidly with t than with a fresh electrode), but eventually the curve approaches asymptotically to a straight line of gradient k which can be written

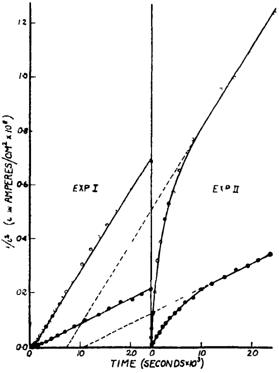

FIG. 3.

$$\frac{1}{i^2} = kt + l, \tag{1B}$$

Here l represents the constant term of equation (1), which cannot now be neglected, since the treatment of the electrode in the first experiment has greatly increased the initial pore-resistance The fact that the second experiments show early values of i much greater than those deducible from the straight part of the $\frac{1}{i^2}\Big/t$ curves probably indicates that the film has undergone a certain amount of spontaneous cracking while standing overnight between the two experiments.

The third experiments, not shown in the figure, gave results very similar to the second experiments

The curves given have been selected as typical of three concordant sets of experiments.

It is of interest to consider the extent of the irreversible process, which will be equivalent to $\int_0^t i\,dt$ coulombs per/cm ^{2} at time t seconds. Thus in a 400-minute run,

$$\text{Number of coulombs passed} = \int_0^{24,000} i\,dt$$

But $1/i^2 = kt$, i.e., $i = 1/k^{\frac{1}{2}}t^{\frac{1}{2}}$, and for N/10 sulphuric acid $k = 7\cdot65 \times 10^{10}$ Therefore

$$\text{Number of OH}' \text{ ions discharged} = \int_0^{24,000} i\,dt \times \frac{6\cdot06 \times 10^{23}}{96,500},$$

$$= \int_0^{24,000} \frac{dt}{(7\cdot65 \times 10^{10})^{\frac{1}{2}}t^{\frac{1}{2}}} \times \frac{6\cdot06 \times 10^{23}}{96,500},$$

$$= 7\cdot0 \times 10^{15}.$$

Similarly in N/10 sodium hydroxide, $k = 2\cdot50 \times 10^{11}$, and $3\cdot9 \times 10^{15}$ OH′ ions are discharged in a 400-minute run. These amounts would produce one or two molecular layers of oxide if distributed over the whole of an " apparent " cm ^{2} of the electrode surface, which for bright platinum has a " true " surface area of 2–3 cm.^{2} * But, if the initial pore-area of the oxide-film is only some 1/10 of the whole, it will be seen that the extra amount of oxide produced in a run is sufficient to close up the pores to a considerable extent, and cause a much increased pore-resistance, in harmony with the hypothesis developed above

Even if the above explanation of the irreversible process is incorrect or incomplete, it has been shown that the applied anodic current-density to which the process is equivalent rapidly becomes very small, being of the order of $1 - 5 \times 10^{-8}$ ampere per apparent cm ^{2} at the reversible potential after a few minutes. It therefore appeared desirable to study the main cathodic and anodic reversible reactions at considerably higher current densities where the irreversible reaction would be of relatively small extent.

---

* Bowden, 'Proc Roy. Soc ,' A, vol. 125, p. 446 (1929)

5. *The Relation between Current-density and Electrode Potential*

Cathodic and anodic polarization curves, for several electrodes in various electrolytes, with current-densities between about 10^{-7} and 10^{-4} ampere per apparent cm.^{2} of electrode surface, were obtained as follows The electrode system was set up and allowed to stand for about 1 hour, when the potential had become nearly constant The cathodic polarization of the electrode was then investigated over the range of current-density given above; the equilibrium potential at each fixed current-density was usually attained in 5–15 minutes. After this cathodic polarization, an anodic current-density of *c* 10^{-6} ampere/cm.^{2} was applied for some 18 hours, by which time the rate of the irreversible process had, as expected, become very small, for the potential and current-density were very nearly constant in time Further points on the anodic polarization curve could then be obtained, the equilibrium potential at each current-density being attained in 5–15 minutes A satisfactory agreement between points obtained with successively increasing and decreasing current-densities was achieved.

The following systems were studied, each electrolyte was saturated with oxygen and the temperature was 25 0° ± 0·1° C —

(1) Bright platinum in N/10 sodium hydroxide

(2) Bright platinum in M/15 sodium phosphate buffer, $p_H = 7\cdot0$.

(3) Bright platinum in N/10 sulphuric acid

(4) Black platinum in N/10 sodium hydroxide.

(5) Bright gold in N/10 sodium hydroxide

The results are shown in figs 4 and 5 as plots of electrode potential in volts referred to hydrogen in the same solution, V, against $\log_{10}$ (current-density, i_c or i_a, in amperes per apparent cm.^{2}) It will be seen that both the $\log_{10} i_c/V$ and $\log_{10} i_a/V$ curves, representing the cathodic and anodic processes respectively, are linear over a considerable range,[*] but begin to depart from linearity in opposite senses at low current-densities comparable to the rate of the irreversible process. The constants of the straight portions, and of two repeats of system (1) not shown in the figures for the sake of clarity, are given in Table I, columns 4–7.

---

[*] *Cf.* Tafel, 'Z phys. Chem,' vol 50, p 641 (1905); Bowden, 'Proc Roy Soc.,' A, vol. 126, p. 107 (1930).

6. *Deduction of the Reversible Oxygen Potential.*

The reversible oxygen potential is obtained thermodynamically on the assumption that the *net* electrode process at an oxygen electrode is

$$O_2 + 2H_2O + 4\epsilon \rightleftarrows 4OH'$$

It must, however, be remembered that this process undoubtedly takes place

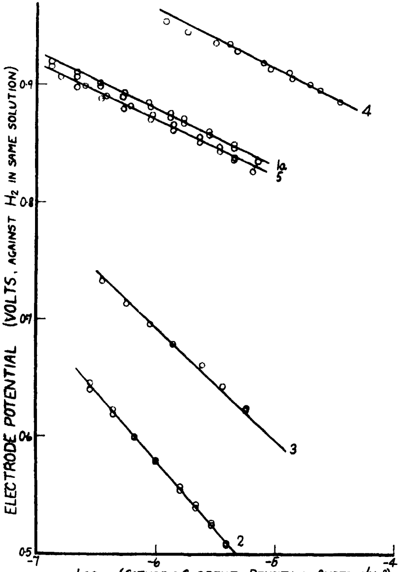

FIG. 4.

in a series of steps Thus, it is very possible that molecular oxygen is first adsorbed on the oxide-film by Van der Waals' forces, becoming subsequently chemi-adsorbed either as molecules or atoms, reaction with cations or discharged cations then takes place, the equivalent of hydroxyl ion eventually being formed The rate of the reaction will, of course, be limited by that of the slowest stage.

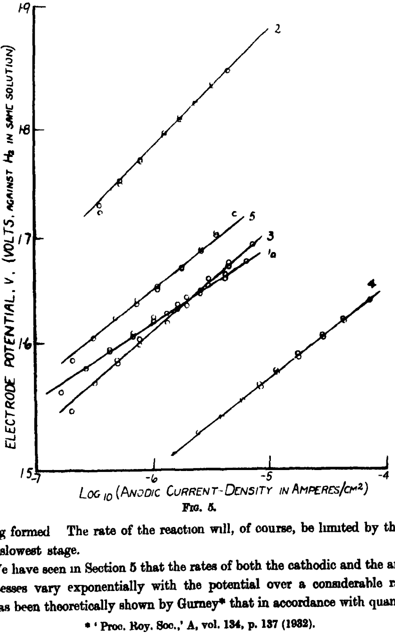

Fig. 5.

We have seen in Section 5 that the rates of both the cathodic and the anodic processes vary exponentially with the potential over a considerable range. It has been theoretically shown by Gurney* that in accordance with quantum-

---

* 'Proc. Roy. Soc.,' A, vol. 134, p. 137 (1932).

Table I.—Summary of Polarization Curves.

The linear portions of the curves may be represented as $V = A_c \log_{10} i_c + B_c$ and $V = A_a \log_{10} i_a + B_a$. Values of A_c, B_c, A_a and B_a are given for V in volts against hydrogen and i_c, i_a in amperes/cm.². The last two columns give the simultaneous solutions of the cathodic and anodic equations for V and $\log_{10} i$.

Electrode system	No. of system	Open-circuit potential (volts against H_2)	Cathodic constants		Anodic constants		$[\log_{10} i]_R$	V_R
			A_c	B_c	A_a	B_a		
Pt, bright, N/10 NaOH	1*a*	+0·988	−0·048	+0·592	+0·064	+2·01	$\overline{13}\cdot34$	+1·20
	1*b*	+0·982	−0·055	+0·513	+0·074	+2·10	$\overline{13}\cdot78$	+1·19
	1*c*	+0·973	−0·046	+0·615	+0·068	+2·03	$\overline{13}\cdot52$	+1·19
Pt, bright, M/15 phosphate buffer	2	+0·936	−0·118	−0·129	+0·101	+2·33	$\overline{12}\cdot53$	+1·22
Pt, bright, N/10 H_2SO_4	3	+0·828	−0·097	+0·111	+0·086	+2·13	$\overline{12}\cdot98$	+1·19
Pt, black, N/10 NaOH	4	+1·057	−0·046	+0·690	+0·078	+1·97	$\overline{11}\cdot68$	+1·17
Au, bright, N/10 NaOH	5	+1·099	−0·048	+0·586	+0·078	+2·12	$\overline{13}\cdot73$	+1·17
			Mean (omitting (4) and (5))					+1·20

mechanical principles, the rate of discharge of an ion at an inert electrode is an exponential function of the electrode potential. It would appear from his discussion that the rate of the reverse process, namely, the formation of an ion from a neutral molecule or atom, is also an exponential function of the potential, of course in the opposite sense. It is therefore very probable that the stage limiting the reaction rate is one involving electron transfer, quite possibly the chemi-adsorption stage.

In any case, if the rates of the charge and discharge processes (whatever they may be) are ρ_1 and ρ_2 gram-equivalents per second per cm.² of electrode surface, then

$$\text{total cathodic current-density on oxide-film surface} = (\rho_1 - \rho_2)\,F,$$

where F is Faraday's number. This is the sum of the applied cathodic current-density i_e and that due to the irreversible current flow through the pores of the oxide-film, say i_p. Therefore,

$$i_e + i_p = (\rho_1 - \rho_2)\,F \qquad (2)$$

ρ_2 quickly becomes quite negligible even at very small values of i_c, and at somewhat higher values i_p is also negligible. Here

$$i_c = \rho_1 F \tag{2A}$$

and the straight portion of an experimental $\log_{10} i_c/V$ curve, fig 4 is therefore equivalent to the exponential relationship between ρ_1 and V For smaller values of i_c, where i_p cannot be neglected,

$$i_c = \rho_1 F - i_p, \tag{2B}$$

in harmony with the fact that the $\log_{10} i_c/V$ curve here falls off from the straight line in the sense that i_c is too small for a given value of V

Similarly

total anodic current-density on oxide-film surface $= (\rho_2 - \rho_1)F$

The applied anodic current-density is equal to the sum of this and the anodic current-density supplied through the pores for the irreversible process, i_p

Therefore

$$i_a - i_p = (\rho_2 - \rho_1)F \tag{3}$$

At sufficiently high values of i_a, ρ_1 and i_p can be neglected. Hence

$$i_a = \rho_2 F, \tag{3A}$$

and the straight part of a $\log_{10} i_a/V$ curve, fig 5, therefore gives the exponential relation between ρ_2 and V

For smaller values of i_a,

$$i_a = \rho_2 F + i_p, \tag{3B}$$

in agreement with the fact that the $\log_{10} i_a/V$ curve here departs from linearity in the sense that i_a is too large for a given value of V.

At the thermodynamically reversible oxygen potential, the total reversible electrode reaction must be in dynamic equilibrium, and hence the rates of the charge and discharge processes must be equal, *i e.*,

$$\rho_1 = \rho_2.$$

The linear portions of the cathodic polarization curves of fig 4 are $\log_{10} \rho_1 F/V$ curves, while the linear parts of the anodic curves of fig. 5 give the $\log_{10} \rho_2 F/V$ relation. The reversible oxygen potential V_R is therefore obtained by putting $\rho_1 = \rho_2$ and solving the simultaneous equations representing the linear parts of corresponding cathodic and anodic curves for V. This is done in Table I, column 9, and graphically by extrapolating corresponding cathodic and anodic curves till they intersect, fig. 6. In all cases the result is in satisfactory agreement with the thermodynamically calculated value of + 1·227 volt. Systems (4) and (5) are less experimentally reliable than the remainder, and have been omitted in calculating the mean value of + 1·20 volt, with a calculated experimental error of ± 0·03 volt, at 25·0° C.

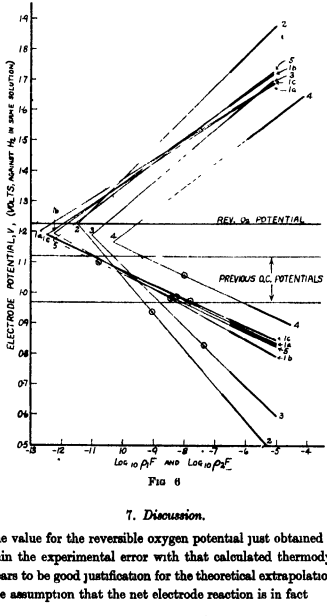

FIG 6

7. *Discussion.*

Since the value for the reversible oxygen potential just obtained is in agreement within the experimental error with that calculated thermodynamically, there appears to be good justification for the theoretical extrapolation involved, and for the assumption that the net electrode reaction is in fact

$$O_2 + 2H_2O + 4\epsilon \rightleftarrows 4OH'.$$

It may also be noted that we have tacitly assumed that the cathodic and anodic polarization curves obtained on any one electrode system are measures of the forward and reverse reaction velocities under identical catalytic conditions, although the electrode surface must have been somewhat changed by the irreversible process taking place during the two runs But if, as has been suggested, the surface is always covered almost completely with an oxide-film, and the irreversible process occurs merely at the small cracks in this, producing more oxide, the assumption is justifiable, for the cathodic and anodic processes both take place on a nearly complete oxide surface, which is sensibly the same for both. Furthermore, although the reaction *rates* found in the triplicate experiment on system (1) are not very closely reproducible owing no doubt to the general irreproducibility of a platinum surface, nevertheless the *equilibrium* potentials deduced are in very close agreement—alteration of the catalyst may change the rate but not the equilibrium

The range of potentials found by previous investigators for experimental oxygen electrodes on open-circuit is indicated in fig 6 The points marked with circles on the extrapolated $\log_{10} \rho_1 F/V$ curves at the potentials given by the various electrodes on open-circuit (Table I, column 3), accord with the previous work The corresponding open-circuit values of $\rho_1 F$ are of about the same order of magnitude, 10^{-8} ampere/cm.^{2}, as the applied anodic current-density necessary to maintain the electrode at the reversible potential as in Section 4 Since on open-circuit the applied current is zero, these values of $\rho_1 F$ represent the current-flow through the pores in the oxide-film from the cathodic film to the anodic base of the pores (see equation (2B)). An oxygen electrode on open-circuit is thus "*self-polarized*," and is undergoing a slow irreversible oxidation, the rate of which can be found by extrapolating the straight part of the cathodic polarization curve to the open-circuit potential

Furthermore, the equal values of $\rho_1 F$ and $\rho_2 F$ at the reversible potential, viz., about 10^{-13}–10^{-12} ampere/cm.^{2} for bright platinum (Table I, column 8, and fig. 6) are several orders of magnitude smaller than the open-circuit values of $\rho_1 F$ and the smallest value of i observed in the experiments of Section 4, viz., about 10^{-6} ampere/cm^2 after some hours. Even if the relation there found, $1/i^2 = kt$, holds up to very large values of t, which is unlikely, owing to spontaneous film-breakdown, calculation shows that it would take at least 10,000,000 years for i to descend even to the same order magnitude as $\rho_1 F$ and $\rho_2 F$ at the reversible potential, so it is not surprising that an oxygen electrode showing the reversible potential on open-circuit has never been prepared.

It appears that the low potentials given by the oxygen electrode are due not so much to the *presence* of the oxide-film as to its *permeability* to the electrolyte, which gives rise to self-polarization. A perfectly impermeable oxide-film should give the reversible oxygen potential, whereas a very porous film should give the lower metal/metal oxide potential.

Much of the previous experimental work falls into line with this hypothesis. The rise of the open-circuit potential with time, noted by many previous workers and confirmed in this investigation, is due to the gradual closing up of the pores by the self-polarizing process, the rate of which therefore continually decreases Lorenz's observation[*] that silver, nickel, copper, iron and zinc, when used as "inert" bases for oxygen electrodes, give potentials almost identical with those given by their oxides, is readily explained, since the oxide-films of these metals are known to be easily penetrated by electrolytes.[†] Again Richards[‡] found that increase of the concentration of the electrolyte produces a lowering of the potential of the ordinary platinum oxygen electrode, it would seem that the higher conductivity reduces the pore-resistance and so increases the self-polarization. Smale,[§] studying the effect of different electrolytes on the hydrogen-oxygen e.m.f, obtained lowest values (+ 0·88– + 0·96 volt) in hydrochloric acid and the alkali chlorides, and highest (+ 1·08– + 1·09 volt) in the alkali hydroxides. Now chloride ion is particularly effective in promoting oxide-film breakdown, while hydroxyl ion effects repair[||]; presence of chloride ion should therefore cause increase, and of hydroxyl ion decrease, of the self-polarization, which accords with Smale's results. Similarly, the depressing effect of hydrogen peroxide on the potential of the oxygen electrode may be due to decomposition of the peroxide at the platinum surface, with consequent mechanical disruption of the film by the oxygen gas produced.[¶]

There is thus a dual difficulty involved in the preparation of a reversible oxygen electrode. In the first place, the electrode reaction must perforce take place on an *oxide* surface. It is therefore not surprising that it is slow compared with, for example, the corresponding reaction at a hydrogen electrode, which takes place on the much more catalytically active *metallic* surface.* This slow reaction rate would not of itself depress the oxygen electrode potential, were it not that the porosity of the oxide-film allows the self-polarizing current to flow between the film and the underlying metal. Although the current is very small, it is yet large compared with the reaction rate at the reversible potential, and thus produces considerable self-polarization.

---

[*] 'Z Electrochem,' vol. 14, p 781 (1908)

[†] *Cf* Evans and Stockdale, 'J Chem Soc.,' p 2651 (1929), Bannister and Evans, *ibid.*, p 1361 (1930), Müller, 'Mhft. Chem,' vol. 52, p. 221 (1929); Hoar and Evans, 'J Chem Soc,' p 2476 (1932), Hoar and Evans, 'J. Iron and Steel Inst.,' vol 126, p. 379 (1932), Bengough, Lee and Wormwell, 'Proc. Roy Soc,' A, vol 134, p 308 (1931).

[‡] 'J. Phys. Chem,' vol. 32, p. 990 (1928)

[§] 'Z. phys Chem.,' vol. 14, p 577 (1894)

[||] Evans, 'J Chem Soc.,' p 1020 (1927), p. 92 (1929), Britton and Evans, *ibid*, p. 1773 (1930).

[¶] *Cf*. Hoar and Evans, 'J. Chem. Soc,' p. 2476 (1932), who found that hydrogen peroxide intensified the breakdown of the oxide-film on iron in chloride solution.

The criterion which a surface must satisfy in order to function as an inert basis for a reversible oxygen electrode is that it shall catalyse the reversible reaction at the reversible potential at a rate relatively rapid to the rate at which it allows electromotively active material to be removed by self-polarization, and with this criterion it appears at present impossible to comply.

The formation of an oxide surface, and the consequent very slow velocity of the cathodic dissolution of oxygen, at any metallic surface exposed to oxygen-containing electrolyte, has an important consequence in determining the velocity of metallic corrosion. As has been shown in previous work,† most metals on exposure to oxygen-containing electrolytes become anodic at those points where their initial air-formed oxide-film is weakest, and relatively cathodic at other points, particularly those best supplied with oxygen. Current therefore flows, with oxygen dissolution at the cathodes and metallic dissolution at the anodes. The basic potential at the anodes is determined by the nature of the metal and the solution, and is not much affected by current-polarization; but the cathodic potential is greatly affected, and tends to approach the anodic value. Even at such low values of cathodic potential, the rate of oxygen dissolution is very slow, and this limits the rate of corrosion.

Thus, while the slowness of the oxygen $\rightleftarrows$ hydroxyl ion reaction has the unfortunate academic consequence that the reversible oxygen electrode cannot be prepared, it nevertheless has the much more important practical effect of rendering the corrosion of metals in aerated electrolytes comparatively slow.

I am very grateful to the Master and Fellows of Sidney Sussex College, Cambridge, for a Research Studentship, and to the British Non-Ferrous Metals Research Association for a grant, which have made this investigation financially possible.

---

* *Cf.* Bowden, 'Proc. Roy. Soc.,' A, vol. 125, p. 446 (1929).

† Evans, "Corrosion of Metals" Arnold (1926); Evans, 'J. Franklin Inst.,' vol. 208, p. 45 (1929); Evans, Bannister and Britton, 'Proc. Roy. Soc.,' A, vol. 131, p. 355 (1931); Evans and Hoar, *ibid.*, A, vol. 137, p. 343 (1932).

My thanks are also due to Mr. W. J. Palmer for the loan of a hydrogen electrode, and especially to Dr U. R Evans for his kindly interest and stimulating suggestions throughout the progress of the work.

Finally, I am greatly indebted to Professor E K Rideal for his valuable advice and for communicating this paper

Summary

The kinetics of the processes which occur at the so-called "oxygen-electrode" have been investigated The results are consistent with the hypothesis that the total electrode process can be represented by the reversible reaction

$$O_2 + 2H_2O + 4\epsilon \rightleftarrows 4OH',$$

which takes place, no doubt in stages, on the surface of the oxide-film with which the inert electrode is covered Since the oxide-film contains pores pervious to the electrolyte, current flows between the film surface and the relatively anodic metal of the base of the pores, causing an irreversible removal of electromotively active material from the film surface, and a lowering of the potential. To maintain the reversible potential a small anodic current-density i is needed, this is shown to decrease with time t according to the relation

$$1/i^2 = kt,$$

which is theoretically justified on the assumption of further oxide formation within the pores

Cathodic and anodic polarization curves have been obtained for oxygen electrodes formed by platinum and gold in various oxygen-saturated electrolytes, and the logarithm of the current-density is shown to bear a linear relation to the electrode potential except at very low current-densities. By an extrapolation of the anodic and cathodic curves, involving certain reasonable assumptions, a value of $+1 \cdot 20 \pm 0 \cdot 03$ volt at 25·0° C. is obtained for the reversible oxygen potential referred to hydrogen in the same solution, in good agreement with the value of $+1 \cdot 227$ volt calculated from thermal data by Lewis and others.

The rate of the reversible process at the reversible potential is extremely slow, and reasons are given for the belief that it is consequently impossible to prepare a truly reversible oxygen electrode

The importance of the sluggishness of the oxygen $\rightleftarrows$ hydroxyl ion reaction in limiting the velocity of metallic corrosion is pointed out.

The Inelastic Scattering of Slow Electrons in Gases.—IV.

By F. H. Nicoll, M.Sc., Trinity College, Cambridge, 1851 Exhibitioner, University of Saskatchewan, and C. B. O. Mohr, Ph.D., Trinity College, Cambridge, 1851 Exhibitioner, University of Melbourne.

(Communicated by Lord Rutherford, O.M., F.R.S.—Received August 14, 1933.)

Introduction.

Recent investigations have shown that the inelastic scattering of electrons in gases exhibits some very interesting phenomena. In previous papers we have described the angular distribution of the scattering of electrons which have lost a discrete amount of energy. Papers I[†] and II[‡] described preliminary results which established the existence of diffraction effects at large angles in a number of gases. In Paper III[§] the measurements were carried out over a range of velocities lower than those previously studied, results being obtained for incident electron energies down to within a few volts of the excitation potential. Angular distributions were obtained for the inelastic scattering of electrons in hydrogen, helium, and argon between the angles 10° and 155°.

The present paper describes the extension of the measurements to methane, nitrogen, neon and mercury vapour.

Method.

The apparatus has already been described fully in Paper III, and consisted essentially of a collision chamber and an electrostatic analyser. The electrons, after being scattered at the centre of the collision chamber, passed into the analyser where electrons of the desired energy were focussed. The distribution in angle of the scattering was obtained by rotating the electron gun inside the scattering chamber by means of a ground glass joint. The pressure of the gas in the scattering chamber was maintained at a constant value less than 10^{-3} mm Hg, while the pressure in the analysing chamber was kept below 10^{-5} mm. Hg by means of a fast pump. The apparatus was connected to a mercury diffusion pump by a wide tube, and since liquid air could not be kept on the trap over night, it was found necessary to bake the apparatus to 450° C. before taking readings, in order to reduce the pressure of mercury vapour to a negligible quantity.

[†] 'Proc. Roy. Soc.,' A, vol. 138, p. 229 (1932).

[‡] 'Proc. Roy. Soc.,' A, vol. 138, p. 469 (1932).

[§] 'Proc. Roy. Soc.,' A, vol. 142, p. 320 (1933).

The gases used for investigation were obtained from cylinders, and were specified to be 98% pure. For the experiments on mercury vapour, a small bulb containing mercury was sealed on close to the collision chamber

Results

Methane.—Since the study of inelastic scattering has hitherto been confined to diatomic gases, it was thought that it might be of interest to investigate the inelastic scattering by a more complex molecule such as methane. A discrete energy loss of about 9 volts was found in this gas, but the resolving power of the analyser was not sufficiently high to enable one to be certain that this loss was due to excitation to a single level, although the loss was quite distinct from the ionization losses.

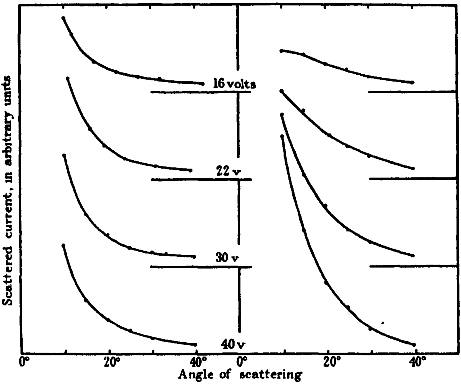

Fig 1.—Small angle scattering in methane

Angular distributions of inelastically scattered electrons are given in figs. 1 and 2 for small and large angle scattering respectively, and the corresponding curves for the elastic scattering are also given for purposes of comparison.

Curves are given for the scattering of electrons with incident energies of 40, 30, 22 and 16 volts

It is seen that the curves for the inelastic scattering at large angles are much flatter than the curves for the elastic scattering. The 40-volt and 30-volt

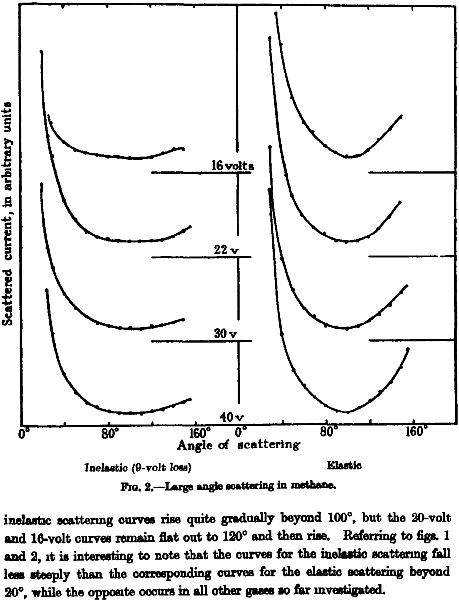

Inelastic (9-volt loss) Elastic

FIG. 2.—Large angle scattering in methane.

inelastic scattering curves rise quite gradually beyond 100°, but the 20-volt and 16-volt curves remain flat out to 120° and then rise. Referring to figs. 1 and 2, it is interesting to note that the curves for the inelastic scattering fall less steeply than the corresponding curves for the elastic scattering beyond 20°, while the opposite occurs in all other gases so far investigated.

Nitrogen.—The main loss in nitrogen† is the 12·8-volt loss which corresponds to excitation to the first singlet level of the molecule; a pronounced peak due to this loss was observed in the energy distribution of the scattered electrons. A less marked peak was also observed corresponding to a loss of

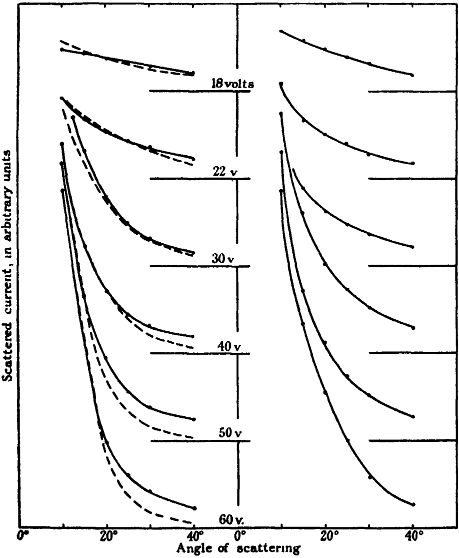

12·8-volt loss. 8·5-volt loss.

--- Theoretical

FIG. 3.—Inelastic scattering in nitrogen (small angles).

---

† Rudberg, 'Proc. Roy. Soc.,' A, vol. 129, p. 628 (1930).

about 8·5 volts.† Angular distributions are shown in figs. 3 and 4 for small and large angle scattering of electrons which have suffered these two losses. Curves are given for the scattering of electrons with incident energies of 60, 50, 40, 30, 22 and 18 volts.

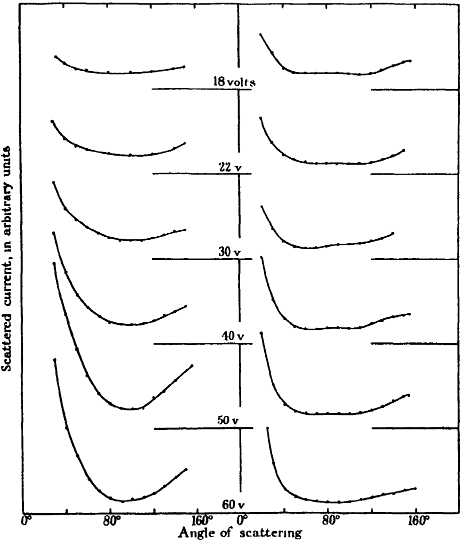

12 8-volt loss 8·5-volt loss

FIG. 4.—Inelastic scattering in nitrogen (large angles).

---

† Since this was written, a note has appeared by Brindley ('Nature,' vol. 132, p. 183 (1933)) on the energy losses in nitrogen. He obtains a loss at 8 6 volts, which is in agreement with our observations but not with the results obtained by Rudberg.

The small angle scattering curves for the two losses investigated are seen to be quite similar, although at the higher velocities the curvature near 25° is greater for the 12·8-volt loss. At large angles, however, the curves for the two losses are clearly of a different character. The curves for the 13-volt loss have a distinct minimum at about 100°, while the curves for the 8-volt loss are quite flat over a large angular range, with even a trace of a slight secondary maximum at 90°. The curves for the 13-volt loss resemble more closely the corresponding curves for elastic scattering,[†] but the rise at large angles is less pronounced

Neon.—The loss investigated in this gas[‡] was the 16·6-volt loss due to excitation to the $2\,^1P$ level. Inelastic scattering curves are given in fig. 5 for incident electron energies of 60, 40, 30, 26 and 22 volts, and the corresponding curves for the elastic scattering are also given purely for purposes of comparison. The inelastic scattering curves are seen to bear only a slight resemblance to the corresponding curves for the elastic scattering, except for the 60-volt curves.

Mercury Vapour —The main inelastic loss in mercury vapour is at 6·7 volts, and is due to excitation to the $1\,^1P_1$ level. Curves are shown in fig. 6 for the inelastic scattering at small and large angles for 30- 25- 20- 16- 12- and 10-volt electrons. The elastic scattering curves at large angles are also given for comparison purposes; these were obtained from a recent paper by Arnot.[§] The two sets of curves are drawn to arbitrary scales.

It was shown in Paper I that there is a close resemblance between the large angle elastic and inelastic scattering at higher voltages (above 55 volts). Turning now to fig. 6, we see that at 30 volts, the maximum which occurs at 50° in the elastic curve has disappeared from the inelastic curve, although a slight maximum still remains at 100° in the latter; at the lower voltages even this maximum has disappeared. However, the persistence of strong diffraction in the inelastic scattering at these lower voltages is shown by the marked rise which occurs beyond 130°. A striking feature of the inelastic curves between 30 volts and 16 volts is that they resemble a mean drawn through the undulations of the corresponding elastic curves.

Elastic Scattering of Slow Electrons in Mercury Vapour.—Although the elastic scattering of electrons in mercury vapour has now received considerable attention from numerous investigators, the measurements have not been extended below 10 volts except by Arnot (*loc. cit.*). In view of the peculiar shape of his low velocity curves and his mention of slight experimental difficulties below 10 volts, it was thought to be of interest to repeat the measurements with our apparatus. The results of our investigation are shown in fig. 7. Experimental values obtained by Jordan and Brode† for 10-volt electrons and by Childs and Massey for 4-volt electrons‡ are also shown in

---

[†] Bullard and Massey, 'Proc. Roy. Soc.,' A, vol. 133, p. 637 (1931)

[‡] Van Atta, 'Phys. Rev.,' vol. 38, p. 876 (1931).

[§] 'Proc. Roy. Soc.,' A, vol. 140, p. 334 (1933).

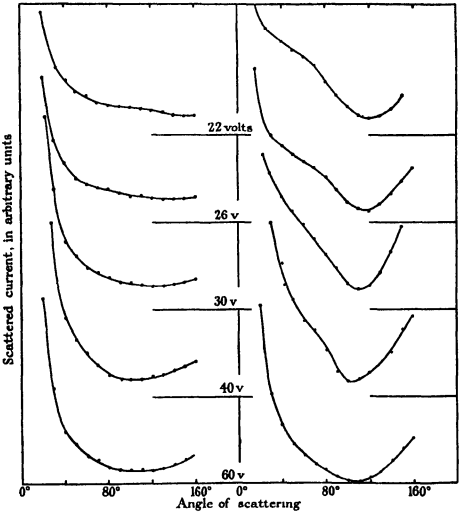

Fig. 5 —Scattering in neon.

---

† 'Phys. Rev.,' vol. 43, p. 112 (1933).

‡ Unpublished results.

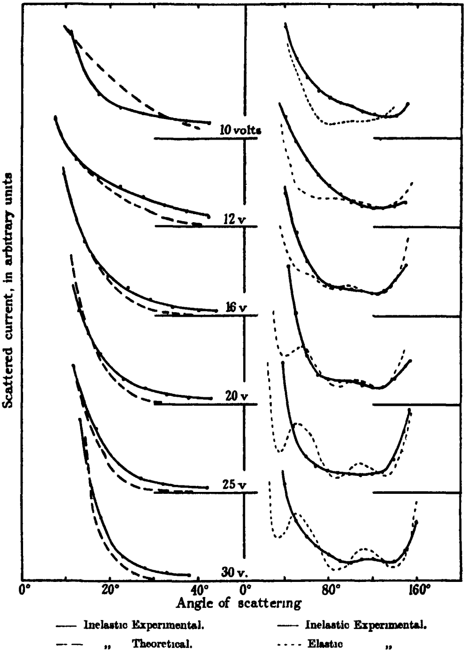

FIG. 6.—Inelastic scattering in mercury vapour (6·7-volt loss).

fig. 7. It will be seen that the curves agree reasonably well in form with ours, while those obtained by Arnot for 10- 6- and 4-volt electrons are entirely

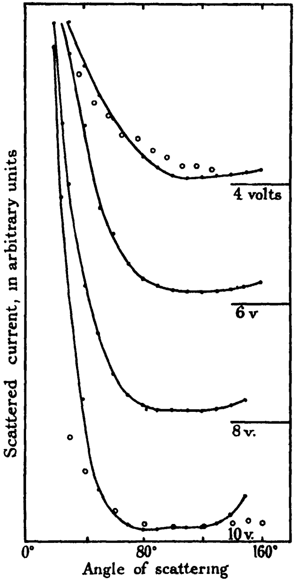

FIG. 7.—Elastic scattering in mercury vapour O Values obtained by other observers.

different, although there is some similarity in his 8-volt curve. The curves obtained here change gradually as the voltage changes from 10 to 4 volts.

Discussion.

A detailed theory of the inelastic scattering of slow electrons in gases has not yet been provided, although some progress has been made in explaining qualitatively certain aspects, such as the diffraction effects at large angles.

At sufficiently high velocities of impact, where diffraction effects are not present, the scattering should be given by Born's theory. As the velocity is decreased and diffraction effects appear, the scattering may still be given quite well at small angles by Born's theory, although the curve predicted by the latter will fall monotonically to smaller values than those obtained experimentally at large angles. For purposes of comparison, theoretical curves obtained by the use of Born's formula are given for the small-angle scattering in figs 3 and 6 for nitrogen and mercury vapour respectively. This formula is seen to give fairly well the steep fall which occurs between 10° and 20°, a result which was also obtained in Paper III for hydrogen, helium, and argon[†] As the velocity is raised to higher and higher values, the theoretical curves will be expected to fit the observed angular distributions out to larger angles of scattering. It would therefore clearly be of value to deduce a general formula for all atoms using Born's theory This may be done by the use of approximate atomic wave functions for the initial and excited states of the atom obtained from simple rules given by Slater[‡] There is no difficulty in showing[§] that the amplitude of the inelastically scattered electron waves is proportional to

$$\frac{1 + f(n)\,\mathrm{K}^2\mu^{-2} + }{\mathrm{K}\,(\mu^2 + \mathrm{K}^2)^m}\,, \tag{1}$$

where

$$\mathrm{K}^2 = k^2 + k'^2 - 2kk'\cos\delta,$$

δ is the angle of scattering, and $\frac{kh}{2\pi m}$, $\frac{k'h}{2\pi m}$ are the velocities of the incident and scattered electrons respectively Thus $k = 0{\cdot}272\sqrt{\text{volts.}}$ $f(n)$ is the quotient of two polynomials in n Also

$$m = n^* + (n+1)^*,$$

$$\mu = \frac{z - s}{n^*} + \frac{z - s'}{(n+1)^*}\,,$$

[†] It must be pointed out that the calculations for hydrogen and nitrogen refer only to the atom.

[‡] 'Phys. Rev.,' vol. 36, p 57 (1930).

[§] The method of procedure will be made clear by reference to 'Proc Roy. Soc.,' A, vol. 132, p. 605 (1931).

where $(z - s)$, $(z - s')$ are the effective nuclear charges and n^*, $(n+1)^*$ the effective quantum numbers for the normal and excited states of the atom respectively. Rules for determining these quantities are given by Slater (*loc. cit.*). For simplicity one may take only the first term in the numerator of the expression (1) as sufficiently accurate at small angles, since K/μ is small at small angles. Hence the angular distribution of the scattered intensity is given approximately by

$$\frac{1}{K^2(\mu^2 + K^2)^{2m}} \tag{2}$$

Some values of the constants μ and m are given in the following table :—

	μ	m
Nitrogen	2·48	5
Neon	3·60	5
Argon	2·81	6·7
Mercury vapour	1·31	8·3

Turning our attention to the diffraction effects which occur at large angles, we have noted in our previous papers that at higher velocities of impact there is a close resemblance between the inelastic and elastic curves, but that the resemblance gradually disappears as the velocity of impact is decreased to values such that the wave-lengths of the incident and outgoing electrons differ appreciably. We have previously discussed why this should be so, and the present results show more clearly how the diffraction effects disappear, while indicating also that a somewhat more detailed explanation is possible.

The results for methane and nitrogen are what might be expected in view of what has already been said, for the diffraction effects in these light gases are not at all complicated. For nitrogen, two separate losses have been studied, and it is noticed that the curves for the greater energy loss are slightly less complicated. Further, the scattering curves for still greater energy losses—for example, ionization losses—would be expected to become even more regular. Some preliminary results for the scattering of electrons which have ionized the atom indicate the extent to which diffraction effects disappear as the electrons lose more and more energy to the atom.

The curves for the inelastic scattering in neon below 40 volts are entirely different in form to those for the elastic scattering; in particular, the pronounced bulge appearing in the elastic curves in the neighbourhood of 70° is entirely absent in the inelastic curves which are almost flat beyond 60°. The significance of this will be clear from the discussion of the results for mercury vapour.

Let us turn now to the results for mercury vapour, in which there are well-marked diffraction effects in the elastic scattering. In general, the angular distribution of the scattering may be expressed in terms of an infinite series of spherical harmonics, and in Paper II we described how diffraction maxima and minima are due to the predominance of one (or more) of the harmonics of lower order. Now, for the voltages investigated, the wave-lengths of the incident and outgoing inelastically scattered electrons are appreciably different, and hence the interference of the two sets of waves (and their associated harmonics) smooths out the undulations. However, at the larger angles, since the predominant harmonics associated with the incident and outgoing electrons increase in magnitude towards the same value at 180°, the inelastic scattering will thus also tend to rise at large angles. The flatness of the curves and the rise at larger angles was also observed in Paper III for the inelastic scattering at low voltages in argon. At quite low velocities, however, as the energy of the incident electrons approaches closer to the excitation potential, the inelastic scattering curves for all gases are seen to become flatter and flatter at all angles

In conclusion, we have much pleasure in expressing our thanks to Lord Rutherford and Dr. J Chadwick for their interest at all times.

Summary.

The investigations on the angular distribution of inelastically scattered electrons, described in a previous paper, have been extended to other gases. The voltages used extended from a few volts above the excitation potential upwards, measurements being made in methane, nitrogen, neon, and mercury vapour over the angular range 10°–155°.

The inelastic scattering observed at small angles is discussed in relation to Born's theory, while the gradual disappearance of the diffraction effects at large angles at the lower voltages is investigated and discussed.

Fourier Analysis of the Durene Structure.

By J. MONTEATH ROBERTSON, M.A., Ph.D., D.Sc.

(Communicated by Sir William Bragg, O.M., F.R.S.—Received July 25, 1933.)

In a recent paper* the crystal structure of durene, 1 . 2 . 4 . 5 -tetramethyl benzene, has been described. The experimental work, including the measurement of the X-ray intensities, has been dealt with, and the structure deduced to within fairly narrow limits by trial and error methods. In order to obtain more precise information about the orientation and molecular structure of this benzene derivative, a double Fourier analysis has now been applied to the structure factors for the three principal crystallographic zones, and the results are set out below.

Crystal Data.

Durene.—$C_{10}H_{14}$. Melting point 80° C. Density 1·03. Monoclinic prismatic. $a = 11\cdot57$, $b = 5\cdot77$, $c = 7\cdot03$ A., $\beta = 113\ 3°$. Space group C_{2h}^5 ($P2_1/a$). Two molecules per unit cell. Molecular symmetry, centre. Molecular volume, 430 A^3. Total number of electrons per unit cell = F(000) = 148.

Fourier Analysis. (Formulæ, Tables, Description of Diagrams).

A crystal being essentially a periodic structure, the distribution of scattering matter in the unit cell may be represented by means of a Fourier series. It can then be shown that the coefficients in such a series are proportional to the structure factors for the various planes in the crystal.† In this analysis the Bragg double series are employed, which give the distribution of scattering matter as projected upon various planes in the crystal. By putting together the results of three such projections along different directions in the crystal, a fairly good representation of the structure in three dimensions is obtained.

The results which are given below differ from those previously described in that the density of scattering matter, ρ, is represented in the tables and contoured diagrams in absolute units, that is, as number of electrons per square Ångstrom unit. For this purpose the summation values have been divided by the area of the face upon which the projection is made. As these projections are all drawn upon planes normal to the monoclinic crystal axes, the formulæ for ρ are :—

---

* 'Proc. Roy. Soc.,' A, vol. 141, p. 594 (1933).

† See, for example, Compton, "X-rays and Electrons," p. 151 (1927); W. L. Bragg, 'Proc. Roy. Soc.,' A, vol. 123, p. 537 (1929).

$$\rho(y, z') = \frac{1}{bc \sin \beta} \sum_{-\infty}^{+\infty} \sum_{-\infty}^{+\infty} F(0kl) \cos 2\pi (ky/b + lz/c)$$

$$\rho(x, z) = \frac{1}{ac \sin \beta} \sum_{-\infty}^{+\infty} \sum_{-\infty}^{+\infty} F(h0l) \cos 2\pi (hx/a + lz/c)$$

$$\rho(x', y) = \frac{1}{ab \sin \beta} \sum_{-\infty}^{+\infty} \sum_{-\infty}^{+\infty} F(hk0) \cos 2\pi (hx/a + ky/b)$$

for the projections along the *a*, *b* and *c* crystal axes respectively, the origin being taken at a centre of symmetry in each case.

The contour lines in the diagrams are drawn at equal density increments of one or two electrons per square Angstrom unit, so that a definite meaning can be attached to each line in the diagrams.[*] This is of value for comparison purposes, for example, in estimating the amount of overlap of the atoms. It will be seen that the carbon atom in the benzene ring has a peak value of just over six electrons per square Ångstrom unit in the *b* axis projection, fig. 2 *a*, whereas the peaks of the methyl groups are somewhat lower, just failing to reach the value of six Where there is considerable overlap of the atoms, as in the *c* axis projection, the density rises to 10 or more electrons per square Ångstrom unit. The one electron line is dotted in each diagram. The slope is usually very gentle at this point, and the position of the line correspondingly uncertain.

The coefficients F(*hkl*) for the three series are given in Tables I to III. It is well known that only the magnitudes of these quantities can be derived from the experimental measurements ; the signs are taken from the results of the trial and error analysis which has already been given (*loc. cit.*). This is, of course, the fundamental weakness of the Fourier analysis method, but the agreements previously obtained seemed good enough to make sure of the signs of all but a few of the very weak reflections. The structure factors have now been entirely recalculated from the final values of the co-ordinates which are given in this paper (p. 671) and the only change of sign which has to be recorded is that the very weak (402) should probably be positive instead of negative. The concluding terms are generally small, presumably owing to

---

[*] It should be noted, however, that there is at present a slight uncertainty regarding the scale of absolute values. The measurements upon which the present values are based were made with copper radiation. In other experiments, Robinson ('Proc. Roy. Soc.,' A, vol. 142, p. 422 (1933)) found that with molybdenum radiation slightly higher values were obtained for the absolute scale than with copper radiation.

Table I.—Durene. Values and Signs of F (0*kl*).
When *k* is even, F (0*kl*) = F (0*k*$\bar{l}$).
When *k* is odd, F (0*kl*) = — F (0*k*$\bar{l}$).

l \ *k*	0	1	2	3	4	5	6
5	—	—	+ 4·5	—	—	—	—
4	—	—	+ 2		+2	—	—
3	−20	− 6	—		—	—	—
2	−37	−10	—	—	—	—	-
1	+38·5	+ 2·5	−5	—	−5	—	—
0	+148	—	−12·5	—	−4	—	+9
$\bar{1}$	+38·5	− 2·5	− 5	—	−5	—	—
$\bar{2}$	−37	+10	—	—	—	—	—
$\bar{3}$	−20	+ 6	—	--	—	—	—
$\bar{4}$	—	—	+2	--	+2	—	—
$\bar{5}$	—	—	+4·5	—	—	—	—

Table II.—Durene. Values and Signs of F(*h*0*l*)
***h* is always even.**

l \ *h*	0	2	4	6	8	10
5	—	—	+ 2	—	—	—
4	—	− 4	+ 9	+ 5·5	—	—
3	−20	− 5·5	+ 3·5	+11·5	—	—
2	−37	+ 5·5	− 2·5	—	+ 2·5	--
1	+38·5	+12·5	—	−18·5	− 3	—
0	+148	+28	− 9	−12·5	−10	--
$\bar{1}$	+38·5	+34	−17	+ 1·5	—	—
$\bar{2}$	−37	− 5	+ 6	− 9	—	− 3
$\bar{3}$	−20	−18·5	+ 9	−12	−14·5	--
$\bar{4}$	—	− 8	− 4	—	− 9	—
$\bar{5}$	—	—	− 4·5	+ 3	+ 6·5	—
$\bar{6}$	—	− 2·5	—	+ 3·5	+ 9·5	--

Table III.—Durene. Values and Signs of F(*hk*0).

When (h + k) is even, F(*hk*0) = F($\bar{h}\bar{k}0$)

When (h + k) is odd, F(*hk*0) = − F($\bar{h}\bar{k}0$).

	k	0	1	2	3	4	5	6
	9	—	2	—	—	—	—	—
	8	−10	−3	—	—	—	—	—
	7	—	−3·5	—	—	—	—	—
	6	−12·5	+4·5	+3	—	—	—	—
	5	—	—	+9·5	+8	−3·5	—	—
	4	−9	+10·5	+5·5	—	+3·5	−2	—
	3	—	+30·5	+14·5	−5	−6	—	—
	2	+28	+56·5	+14	—	—	−8	—
	1	—	+27	−13	—	+2	—	—
h	0	+148	—	−12·5	—	−4	—	+9
	$\bar{1}$	—	+27	+13	—	−2	—	—
	$\bar{2}$	+28	−56·5	+14	—	—	+8	—
	$\bar{3}$	—	+30·5	−14·5	−5	+6	—	—
	$\bar{4}$	−9	−10·5	+5·5	—	+3·5	+2	—
	$\bar{5}$	—	—	−9·5	+8	+3·5	—	—
	$\bar{6}$	−12·5	−4·5	+3	—	—	—	—
	$\bar{7}$	—	−3·5	—	—	—	—	—
	$\bar{8}$	−10	+3	—		—		—
	$\bar{9}$	—	−2	—	—	—	—	—

the high temperature factor for the crystal (melting point 80° C) so that the series are fairly rapidly convergent.

Tables IV, V and VI give the results of the summations, and figs. 1 *a* to 5 are the contoured diagrams obtained from them. Alongside are drawings on the same scale, figs. 1 *b* to 4 *b*, which show the relative positions of the atoms and how they are connected to form the durene molecules. In these drawings the circles which represent the atoms are half size in each case.

Table IV.—Projection along the *a* axis.

Density of scattering matter as number of electrons per square Ångstrom unit × 10.

↑	14	16	14	8	0	3	12	16	12	3	0	8	14	16	14
	13	15	15	8	3	5	13	17	12	4	0	7	13	14	11
	11	15	17	12	6	8	15	19	14	5	3	8	12	10	5
	15	20	23	19	12	12	17	20	15	8	6	11	13	9	4
	26	32	34	29	20	17	20	20	17	10	10	16	18	15	9
	43	47	48	41	30	24	25	26	21	15	16	23	27	25	20
	58	62	61	54	41	36	37	36	32	26	26	34	39	38	33
	68	72	72	64	54	50	53	53	47	41	41	48	53	50	46
c/2	69	75	78	72	64	61	65	66	61	56	56	63	66	63	56
	68	74	79	76	68	65	68	69	68	65	68	76	79	74	67
	63	71	77	74	65	59	60	61	63	65	73	84	89	84	76
	55	64	70	66	55	47	45	47	50	57	69	84	91	88	80
	45	53	59	54	42	33	31	33	37	44	59	76	84	81	74
	33	41	47	43	31	24	23	26	29	35	48	62	70	66	58
	25	33	38	36	27	21	22	24	25	28	35	48	51	48	39
↓	27	34	40	37	28	23	23	$\boxed{24}$	23	23	28	37	40	34	27

← *b*/4 → × ← *b*/4 →

Centre of symmetry

In the projection along the *a* axis, fig. 1, the molecules overlap to such an extent that the detail becomes very confused. The overlapping molecules are, of course, actually half a translation behind the centre one. The most notable feature is the large gap between the ends of the molecules, where the strong cleavage of the crystal occurs.

The projection along the *b* axis, fig. 2, is much the most interesting, because here every atom in the molecule is separately resolved, in spite of the fact that the plane of the molecule is actually inclined at about 50° to the plane of the paper. Most of the measurements given below are based on this projection.

Fig. 3 is the same projection showing, on a smaller scale, the mutual relations of six molecules as they are built together to form the crystal.

Table V.—Projection along the *b* axis.

Density as number of electrons per square Ångstrom unit × 10.

	6	5	3	4	8	13	14	14	15	17	17	14	10	8	9	10
	7	4	3	5	9	13	17	22	28	31	28	19	12	9	9	9
	7	5	3	5	7	12	21	34	44	45	36	23	13	9	8	7
	7	5	4	3	5	13	29	47	57	53	38	22	12	7	7	5
	7	7	5	2	5	18	37	54	59	50	34	20	11	7	6	5
	6	7	5	4	11	25	42	52	50	39	26	16	10	7	6	5
	7	7	8	12	23	36	44	42	34	25	17	12	9	6	7	6
	10	10	15	25	38	45	42	31	21	14	12	10	8	7	7	5
a/4	15	16	25	42	53	53	40	25	15	12	11	9	7	8	6	4
	24	24	36	53	63	56	42	27	19	15	12	9	8	7	6	2
	30	30	42	57	63	57	47	38	30	23	14	9	8	8	5	2
	33	31	40	50	55	56	54	50	41	28	16	10	10	8	5	2
	29	26	29	37	45	54	61	58	45	27	15	10	9	7	4	4
	22	17	18	24	38	53	62	57	41	23	12	9	8	6	4	4
	13	11	12	21	37	52	56	46	30	16	10	8	6	4	4	6
Centre of symmetry ×	$\boxed{10}$	11	17	28	42	48	44	31	19	12	9	6	3	2	5	5
	13	19	30	42	49	45	32	20	14	12	10	6	3	3	5	6
	22	32	46	56	54	40	25	17	17	16	12	7	4	5	6	4
	29	42	57	63	54	38	27	25	26	22	14	8	6	6	5	3
	33	46	59	60	51	41	37	37	34	25	15	9	8	6	3	2
	30	41	50	51	48	47	48	47	37	23	13	9	7	4	1	2
	24	30	36	40	45	52	55	48	33	17	10	7	5	1	0	2
	15	19	23	31	43	53	53	41	24	11	7	5	3	0	0	4
a/4	10	10	15	25	39	46	43	29	16	8	6	4	1	0	2	5
	7	7	12	21	31	34	28	18	12	8	6	4	2	1	4	6
	6	7	11	18	22	21	17	13	11	10	7	4	3	3	5	5
	7	8	11	13	13	12	11	11	12	10	7	4	4	4	5	5
	7	9	10	8	7	8	10	12	11	8	5	4	5	4	5	5
	7	8	7	5	5	9	12	13	9	6	5	6	6	5	6	7
	7	7	4	3	7	12	14	12	9	8	9	9	7	6	7	9
	6	5	3	4	8	13	14	14	15	17	17	14	10	8	9	10

← *c*/2 →

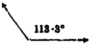

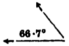

Table VI.—Projection along the *c* axis.

Density as number of electrons per square Ångström unit × 10.

6	11	16	20	22	16	7	2	7	16	22	20	16	11	6
11	17	21	24	25	18	5	0	4	12	17	15	11	6	2
15	27	32	33	31	19	5	$\bar{5}$	$\bar{2}$	5	9	8	6	1	$\bar{3}$
25	44	50	49	43	28	8	$\bar{4}$	$\bar{4}$	0	1	2	1	0	$\bar{3}$
39	62	69	65	57	39	15	1	$\bar{1}$	0	$\bar{1}$	$\bar{2}$	0	2	2
47	71	76	72	64	47	21	6	3	2	$\bar{2}$	$\bar{4}$	0	4	7
46	64	67	64	63	50	25	7	4	4	$\bar{2}$	$\bar{4}$	0	5	11
36	49	50	54	61	57	32	8	2	2	$\bar{3}$	$\bar{4}$	0	5	12
26	34	37	49	70	73	46	14	3	0	$\bar{3}$	$\bar{3}$	2	6	17
18	24	30	52	84	95	64	25	6	3	0	0	5	9	21
12	16	26	52	92	107	78	35	14	8	3	1	6	9	21
4	9	19	44	84	103	80	43	23	16	6	2	3	5	16
$\bar{2}$	2	9	28	63	86	75	50	38	29	12	0	1	2	8
$\bar{2}$	2	3	14	43	71	71	59	54	44	19	4	2	2	4
3	6	3	7	32	63	73	69	67	56	27	6	5	6	4
6	9	5	7	29	61	73	|73|	73	61	29	7	5	9	6

b/2

← *a*/4 × *a*/4 →

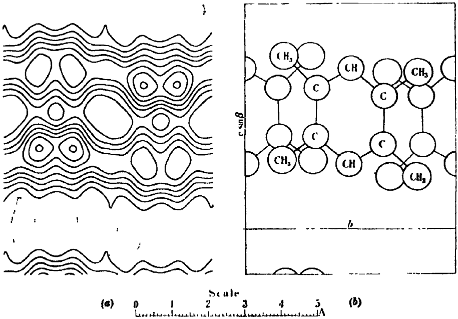

FIG. 1.—Projection along the *a* axis. Each contour line represents a density increment of one electron per A². The one electron line is dotted.

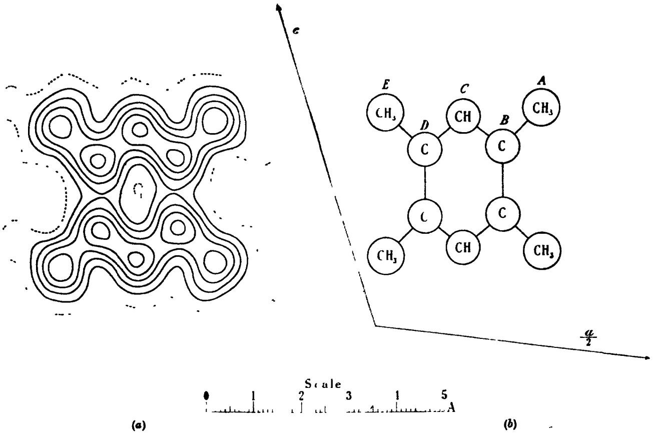

FIG 2 —Projection along *b* axis. Each contour line represents one electron per A². First line dotted.

The projection along the *c* axis, fig. 4, is somewhat disappointing. In spite of the fact that over 50 terms have been employed in this series, the scattering centres are not separately resolved, but only in groups of two. The projection does, however, give an accurate measurement of the inclination of the plane of the molecule to the *a* and *b* axes, information which is missing from the *b* axis projection in fig. 2.

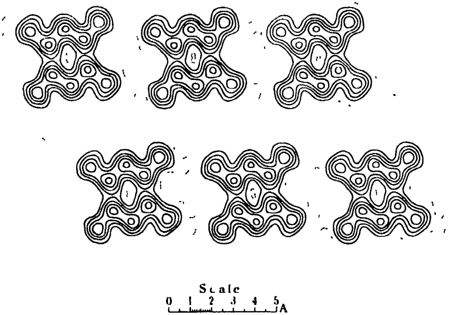

Fig 3.—Projection along *b* axis showing mutual relation of molecules.

Fig. 5 is still the *c* axis projection, showing on a smaller scale how the molecules are related in the crystal.

The Detailed Structure deduced from the Fourier Analysis. (Co-ordinates, etc.)

As mentioned above, the *b* axis projection, fig. 2, gives the most precise information concerning the structure of the molecule. The regularity of the central hexagon of carbon atoms is easily tested. Any two opposite sides are found to be parallel to and one-half the length of the line through the centre joining the other two corners, to a fairly good approximation. It seems very unlikely that anything other than a regular plane hexagon could give rise to this projection.

The distances between the centres of the atoms can be directly measured on fig. 2, and when these values are combined with the direction cosines given below, the model illustrated in fig. 6 is obtained. The carbon to carbon distance in the benzene ring is 1·41 A. at the sides, but at the centre the slightly smaller measurement of 1·38 A. is obtained. This result might indicate some slight distortion of the ring from the regular plane hexagon, but it is more likely a mismeasurement resulting from the difficulty of estimating the exact positions of the centres.

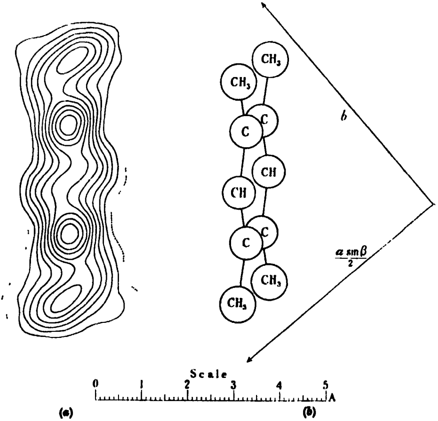

FIG. 4.—Projection along c axis. Each contour line represents one electron per A². First line is dotted.

The position of the methyl group is interesting. The centres appear to lie at a height of 1·50 A. above the horizontal axis, which is distinctly greater than the 1·41 A. of the benzene carbon. Yet the line joining the centres of the groups intersects the horizontal axis at only 1·23 A. from the benzene ring. The methyl groups thus appear to be displaced away from each other, towards

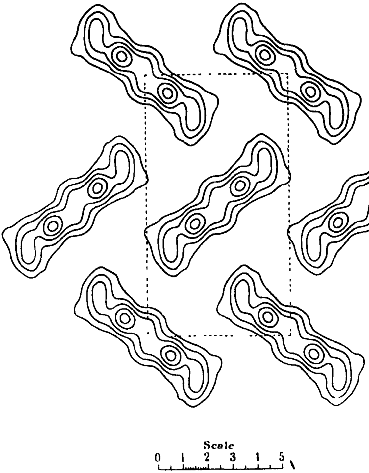

FIG. 5.—Projection along *c* axis showing mutual relation of molecules. Each contour line represents two electrons per A^2.

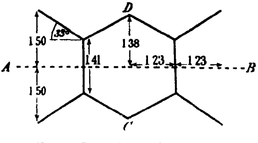

FIG. 6.—Dimensions of the molecule.

the unsubstituted positions of the benzene ring This is rather a small effect, but it appears to be quite distinct in this projection, the angle between the methyl group and the horizontal axis being 33° instead of the 30° required by a regular structure. The distance between the centre of the methyl group and the centre of the adjacent carbon atom in the benzene ring is 1·47 A., which it is interesting to note would be the distance from the centre of a sphere of 1·54 A. diameter (diamond carbon) to the centre of a sphere of 1 41 A. diameter (graphite carbon) in contact with each other.

These results regarding the positions of the methyl groups are not quite borne out by a study of the *c* axis projection, fig. 4. In this projection the line of centres of the unresolved methyl groups appears to lie at a somewhat greater distance from the benzene ring than would be expected from the above figures. This is probably due to lack of spherical symmetry in the methyl group, but the resolution obtained in this projection is not sufficiently good for reliable results.

With regard to the actual orientation of the molecule in the crystal, the apparent angle which the long axis (AB) makes with the *a* axis in the *b* projection, fig. 2, is 8·4° (mean of four lines). In the *a* projection, fig. 1, the overlapping is too complicated to yield a reliable result, but in the *c* projection, fig. 4, the angle with the projected *a* axis is estimated at 49·5°. Combining these measurements, we obtain for the actual angles χ, ψ and ω, which the long axis of the molecule makes with the *a*, *b* and *c'* axes (*c'* being perpendicular to the *a* and *b* axes),

$$\chi = 49{\cdot}1^\circ \qquad \cos\chi = 0{\cdot}655$$
$$\psi = 41{\cdot}4^\circ \qquad \cos\psi = 0{\cdot}750$$
$$\omega = 84{\cdot}5^\circ \qquad \cos\omega = 0{\cdot}097$$

The cross-axis (CD) is found to make an apparent angle of 83·2° with the *a* axis in the *b* projection (mean of five lines). In the *a* and *c* projections this axis of the molecule appears to be very nearly parallel to the *c* crystal axis. The most consistent results are, however, obtained when this cross-axis is put at a small angle of about 1·2° with the *c* axis in the *a* projection. With these figures we obtain for the real angles χ', ψ' and ω', which the cross-axis makes with the *a*, *b* and *c* crystal axes

$$\chi' = 96{\cdot}8^\circ \qquad \cos\chi' = -\,0{\cdot}118$$
$$\psi' = 91{\cdot}2^\circ \qquad \cos\psi' = -\,0{\cdot}021$$
$$\omega' = 6{\cdot}9^\circ \qquad \cos\omega' = 0{\cdot}993.$$

The real angle between the long and the cross-axis of the molecule is arc cos $(\cos\chi\cos\chi' + \cos\psi\cos\psi' + \cos\omega\cos\omega')$ and is equal to 89·8° when the above figures are employed. This is not, however, in the present instance, an entirely independent check on the regularity of the molecule, as some weight has been attached to this result in arriving at the small angle of 1·2° mentioned above which the cross-axis makes with the c direction in the a projection

It is interesting to note that the orientation given above only differs by about 2° from that reached in the trial and error analysis previously given (*loc. cit.*).

Ten out of 15 co-ordinates which determine this structure can be directly measured on fig. 2. The remaining five, the y co-ordinates, can be obtained from the orientation worked out above, based chiefly upon the b and c projections. The complete set is given in Table VII, the figures in bold type referring to separately resolved centres.

Table VII.—Co-ordinates. Centre of Symmetry as Origin. Monoclinic axes.

Atom *cf.* fig 2.	xA.	$2\pi x/a$	yA.	$2\pi y/b$.	zA.	$2\pi z/c$.
A	**2·18**	**67·6°**	1·81	113°	**1·88**	**96·3°**
B	**1·08**	**33·4°**	0·91	56·6°	**0·89**	**45·6°**
C	**0·43**	**13·2°**	−0·03	−1·8°	**1·49**	**76·5°**
D	**−0·64**	**−19·9°**	−0·94	−58·5°	**0·63**	**32·4°**
E	**−1·25**	**−38·9°**	−1·87	−117°	**1·36**	**69·9°**

Intermolecular Distances.

With the above values for the co-ordinates the distances of approach between atoms on neighbouring molecules can be obtained.* The shortest distance between the methyl groups on the standard and the reflected molecule is found to be 3·93 A., and between adjacent molecules on the b axis the corresponding distance is 3·87 A. The similarity of these figures is significant, showing that the molecules are poised in the crystal in such a manner that the minimum distance of approach between adjacent methyl groups is practically constant (These figures should also be compared with the anthracene results.* The corresponding figures for aromatic carbon atoms were then found to be 3·77 A. and 3·80 A.)

* 'Proc. Roy. Soc.,' A, vol. 140, p. 94 (1933).

Across the cleavage planes the gap is somewhat larger. The distance between the methyl groups on adjacent molecules on the c axis is 4·22 A., and between the standard and reflected molecule one translation along the c axis it is 4·15 A.

The Electron Distribution

The position of the methyl groups relative to the benzene ring has already been described, and it has been pointed out that the peak value of the electron density on the methyl groups is a little lower than on the benzene carbon atoms. The difference is perhaps too small to be significant, the density being about 5·9 on the methyl groups compared with about 6·4 electrons per square Ångstrom on the benzene carbon atoms. As well as showing this difference in density, the structure is somewhat more distended around the methyl groups, a result which might be expected from the fact that three hydrogen atoms are known to be associated with the structure at these points. Again, any oscillation of the molecule as a whole, about its centre, if it is quite a rigid structure, would have greatest effect at the outlying points

Any attempt at electron counting is necessarily difficult owing to the large overlap of the atoms even in the b axis projection. A count has been made, however, in the following way, which at least has the advantage of avoiding any arbitrary definition of the atomic boundaries The whole area of the b axis projection has been divided up into sections by drawing perpendiculars through the mid points of the lines joining each pair of atomic centres. The partitioning which results from this operation is shown in fig. 7. It will be seen that the scattering matter at each point on the projection is now attributed to the group nearest to that particular point.

When the scattering groups all have about the same radius the method should give reasonable results. With durene no allowance has been made for the somewhat larger radius of the methyl groups, so a deficiency may be expected for these groups. When the figures are summed over these areas the following results are obtained :—

A. Methyl group	$-CH_3$.	8·4 electrons	(9 required by chemical structure)
B. Single carbon	$\rightarrow C$:	6·4 ,,	(6 ,, ,,)
C. Carbon and hydrogen	$>CH$:	7·2 ,,	(7 ,, ,,)
D. Single carbon	$\rightarrow C$:	6·4 ,,	(6 ,, ,,)
E. Methyl group	$-CH_3$:	8·7 ,,	(9 ,, ,,)

The total of 37 electrons is necessarily the same as $\frac{1}{4}F$ (000), as a quarter of the whole area of the projection has been covered. But the variation in the number among the groups gives some evidence of the presence of the hydrogen atoms.

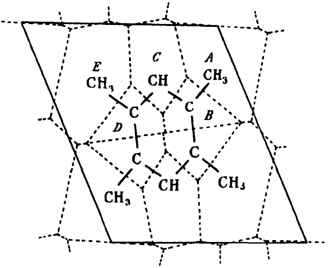

FIG 7.—Electron count in durene.

In conclusion, it gives me pleasure to acknowledge the help and encouragement received from my wife in the course of this work. I am indebted to Sir William Bragg, O.M., F.R S , and the Managers of the Royal Institution for the facilities afforded at the Davy Faraday Laboratory where this work was carried out

Summary

The results of the crystal analysis of durene, 1 . 2 . 4 . 5-tetramethyl benzene, already described, have been subjected to a double Fourier analysis about the zones of the three principal crystal axes The results are set out in five contoured diagrams drawn to an absolute scale. The detailed structure deduced from this analysis shows a regular plane hexagon benzene ring with the four methyl groups also in the plane of the ring, but slightly displaced (about 3°) towards the unsubstituted positions. The orientation of the molecule in the crystal is stated on p. 670, and the 15 parameters of the structure are given on p. 671. In one of the projections all the carbon atoms in the molecule are separately resolved.

The centre-to-centre distance in the benzene ring is about 1·41 A., but the centre of the methyl group lies at the somewhat greater distance of about 1·47 A. from the adjacent aromatic centre. The shortest distance between methyl groups in neighbouring molecules is of the order of 3·9 A.

The electron count shows the effect of the hydrogen atoms.

The Crystalline Structure of Naphthalene. A Quantitative X-Ray Investigation.

By J. Monteath Robertson, M.A., Ph.D., D Sc.

(Communicated by Sir William Bragg, O M , F R S.—Received August 16, 1933.)

Crystal Data.

Naphthalene.—$C_{10}H_8$. Melting point 80° C. Density 1·152 (calc. 1·172). Monoclinic prismatic, $a = 8·29$, $b = 5·97$, $c = 8·68$ A., $\beta = 122·7°$. Space group C_{2h}^5 ($P2_1/a$). Two molecules per unit cell. Molecular symmetry, centre. Molecular volume, 362 A^3 Total number of electrons per unit cell = F(000) = 136.

Experimental—Measurement of Intensities.

When a small single crystal is placed completely in an X-ray beam, the integrated reflection is proportional to the mass of the crystal, if the latter is sufficiently small. Although fairly large crystals of naphthalene can easily be obtained, the aim in this work has been to carry out the measurements on specimens small enough for this proportionality to hold good. With soft organic crystals of the hydrocarbon type, the size required for reliable results is found to be of the order of 0·1 milligrams.

A difficulty thus arises owing to the volatile nature of the compound. A naphthalene crystal of such a size changes rapidly in weight, and in fact will not last long enough for a complete record to be taken. The absolute measurements and most of the relative measurements of intensity were therefore carried out on specimens sealed off in very thin glass tubes, previously tested as regards uniformity and absorption, the whole technique being very similar to that described for the durene investigation, p. 659.

The absolute measurements were made on two selected naphthalene crystals by comparison with an anthracene standard, kindly lent by Dr. B W. Robinson. These two naphthalene crystals were then used as sub-standards to convert all relative intensity measurements into absolute values. All the measurements were carried out with copper radiation ($\lambda = 1 \cdot 54$ A.).

The photographic method was used in most of the relative intensity work. About twelve different crystal specimens of various sizes were employed altogether, and the various sets of measurements were in general correlated through the weaker reflections. The stronger reflections show a very marked falling off in intensity with the larger crystal specimens, as shown, for example, by the correlation given in Table I.

Table I.—Relative intensities, integrated (uncorrected).

hkl.	Crystal No. 4 about 1·0 mg.	Crystal No 8 about 0·2 mg	Crystal No 12 0·249 mg.
001	698	1850	2250
002	278	325	315
003	226	—	290
004	110	106	106
203	110	113	—
200	1083	2035	—
$20\bar{1}$	1303	2510	—
$20\bar{2}$	484	632	—

The true values for the strongest reflections remain a little doubtful, but cannot differ much from the highest values found. The large correction factors necessary for the glass tubes also tend to make the scale of absolute values rather less certain than the anthracene figures, for example, but quite consistent results were obtained in different experiments. A complete list of the measured structure factors is given in Table II.

The Structure by Trial and Error.

Ever since Sir William Bragg's pioneer work on organic crystals* it has been known that the crystal structure of naphthalene is very similar to that of anthracene. A complete determination of the latter structure has recently been given,† and these figures form a natural starting-point for the exact determination of the naphthalene structure. With a model based on the

* 'Proc. Phys. Soc.,' vol. 34, p. 33 (1921)

† 'Proc. Roy. Soc.,' A, vol. 140, p. 79 (1933).

Table II.—Measured and Calculated Values of the Structure Factor.

hkl.	sin θ Cu Kα.	F calc.	F measured.
200	0·221	+45	40
400	0·441	−3·5	5
600	0·662	−6·5	5·5
020	0·255	−13	14
040	0·510	+4	< 3·5
060	0·765	−2	< 3
001	0·106	+31	27·5
002	0·211	−15·5	15·5
003	0·317	+17	19
004	0·422	+13	14
005	0·528	−2·5	2
006	0·633	−4·5	< 2·5
007	0·739	−5·5	3
011	0·165	−6	6
012	0·246	−3	4
013	0·340	−4·5	5·5
014	0·441	−10	7·5
015	0·542	−3·5	< 3·5
016	0·645	+6·5	4·5
017	0·747	+5·5	< 3·5
021	0·275	−14·5	14
022	0·331	+3	5·5
023	0·405	+10·5	10
024	0·494	−5·5	4·5
025	0·586	+0·5	< 3·5
026	0·681	+11	6
031	0·395	+13	12·5
032	0·437	+8	8
033	0·497	+7	7·5
034	0·569	+11	7·5
035	0·652	+7·5	6
036	0·739	+3	< 3·5
041	0·520	−3·5	2·5
042	0·551	−2	< 3·5
043	0·599	+3·5	< 3·5
044	0·662	−6·5	5·5
045	0·733	−7·5	3
051	0·645	−3·5	< 3·5
052	0·671	−6·5	4·5
053	0·712	−2	< 3·5
207	0·881	−4·5	5
206	0·778	−6	5
205	0·676	−1	< 2·5
204	0·575	+7·5	6·5
203	0·476	+18	16
202	0·380	+4·5	5·5
201	0·293	−4·5	5
$20\bar{1}$	0·186	+41	40
$20\bar{2}$	0·206	−16·5	21·5
$20\bar{3}$	0·273	0	< 1·5
$20\bar{4}$	0·356	+9·5	8·5
$20\bar{5}$	0·450	−6·5	3
$20\bar{6}$	0·545	+1·5	< 2·5
$20\bar{7}$	0·648	+5	3
$20\bar{8}$	0·749	−1·5	< 2·5
404	0·761	+1·5	< 2
403	0·670	+4	2·5
402	0·584	+7	6
401	0·507	−3	< 2·5
$40\bar{1}$	0·395	+6	4
$40\bar{2}$	0·372	−5·5	7
$40\bar{3}$	0·380	0	< 2
$40\bar{4}$	0·415	+10	9·5
$40\bar{5}$	0·469	−6	5·5
$40\bar{6}$	0·540	+0·5	< 2·5
$40\bar{7}$	0·621	+18·5	14
$40\bar{8}$	0·710	+7·5	6
601	0·726	+1·5	< 2·5
$60\bar{1}$	0·612	−9	9·5
$60\bar{2}$	0·577	−4·5	4·5
$60\bar{3}$	0·558	+3	3·5
$60\bar{4}$	0·561	+12·5	13·5
$60\bar{5}$	0·580	+3·5	4·5
$60\bar{6}$	0·620	−3·5	< 2·5
$60\bar{7}$	0·673	+13	10·5
$60\bar{8}$	0·738	+14	10·5
$80\bar{3}$	0·760	+2	< 2
$80\bar{4}$	0·743	+6·5	5·5
$80\bar{5}$	0·743	+3·5	5·5
$80\bar{6}$	0·756	−1	4
$80\bar{7}$	0·785	+1	4
$80\bar{8}$	0·825	+7·5	7·5
110	0·168	+41	37
210	0·253	+29	30·5
310	0·353	+5	6
410	0·457	+15	14
510	0·563	−5·5	6
610	0·670	+1·5	< 4·5
120	0·277	+12·5	12·5
220	0·335	−8	8
320	0·416	+15	15·5
420	0·506	−3	< 4
520	0·604	+4	6·5
620	0·704	−2	< 4
130	0·397	−10	10·5
230	0·440	0	< 3·5
330	0·504	−4	4
430	0·581	0	< 4
140	0·521	−1·5	< 4
240	0·556	+2	< 4
340	0·606	0	< 4·5
440	0·670	−2	< 4·5

anthracene dimensions and orientation the structure factors were calculated and compared with the measured values. Although a good general agreement was obtained for all the strong reflections, a number of the weaker and high index reflections showed rather large discrepancies, indicating some change in the structure. The nature of this change was not at first obvious, but after a few trials it was found that the long axis of the naphthalene molecule is tilted further out of the (010) plane than that of anthracene. (In the previous notation, ψ is increased from 97° to about 103°.) The structure factors for all the planes were now calculated, and in this way the signs of the terms in the Fourier series were determined. From the results of the Fourier analysis, given below, the structure has been refined, and the structure factors have now been recalculated once more from the final values of the parameters given on p. 686. The agreement found between the measured and the calculated values is shown in Table II, and it may be noted that none of the structure factors have changed from the sign employed in the Fourier analysis (Tables III–V).

Table III.—Naphthalene. Values and signs of F (0*kl*).

		k					
		0	1	2	3	4	5
	7	− 3	—	—	—	—	—
	6	—	+ 4·5	+ 6	—	—	—
	5	− 2	—	—	+ 6	− 3	—
	4	+14	− 7·5	− 4·5	+ 7·5	− 5·5	—
	3	+ 19	− 5·5	+10	+ 7·5	—	—
	2	−15·5	− 4	+ 5·5	+ 8	—	− 4·5
	1	+27·5	− 6	−14	+12·5	− 2·5	—
l	0	+136	—	−14	—	—	—
	$\bar{1}$	+27·5	+ 6	−14	−12·5	− 2·5	—
	$\bar{2}$	−15·5	+ 4	+ 5·5	− 8	—	+ 4·5
	$\bar{3}$	+19	+ 5·5	+10	− 7·5	—	—
	$\bar{4}$	+14	+ 7·5	− 4·5	− 7·5	− 5·5	—
	$\bar{5}$	−2	—	—	− 6	− 3	—
	$\bar{6}$	—	− 4·5	+ 6	—	—	—
	$\bar{7}$	− 3	—	—	—	—	—

Table IV.—Naphthalene. Values and signs of F (*h*0*l*).

				h		
		0	2	4	6	8
	7	−3	−5	—	—	—
	6	—	−5	—	—	—
	5	−2	—	—	—	—
	4	+14	+6·5	—	—	—
	3	+19	+16	+2·5	—	—
	2	−15·5	+5·5	+6	—	—
	1	+27·5	−5	—	—	—
l	0	+136	+40	−5	−5·5	—
	$\bar{1}$	+27·5	+40	+4	−9·5	—
	$\bar{2}$	−15·5	−21·5	−7	−4·5	—
	$\bar{3}$	+19	—	—	—	—
	$\bar{4}$	+14	+8·5	+9·5	+13·5	+5·5
	$\bar{5}$	−2	−3	−5·5	+4·5	+5·5
	$\bar{6}$	—	—	—	—	—
	$\bar{7}$	−3	+3	+14	+10·5	—
	$\bar{8}$	—	—	+6	+10·5	+7·5

Table V.—Naphthalene. Values and signs of F (*hk*0).

			k		
		0	1	2	3
	6	−5·5	—	—	—
	5	—	−6	+6·5	—
	4	−5	+14	—	—
	3	—	+6	+15·5	−4
	2	+40	+30·5	−8	—
	1	—	+37	+12·5	−10·5
h	0	+136	—	−14	—
	$\bar{1}$	—	+37	−12·5	−10·5
	$\bar{2}$	+40	−30·5	−8	—
	$\bar{3}$	—	+6	−15·5	−4
	$\bar{4}$	−5	−14	—	—
	$\bar{5}$	—	−6	−6·5	—
	$\bar{6}$	−5·5	—	—	—

Fourier Analysis (Tables and Diagrams).

A double Fourier analysis of the experimental data has been carried out for the zones about the *a*, *b* and *c* crystal axes, and the results are expressed in figures which give the projection of the structure on planes normal to these axes. In these figures each contour line represents a density increment of either one or two electrons per square Ångstrom unit. The results are thus expressed in the same form as in the durene analysis (*loc. cit.*) and the same formulæ are applicable. The coefficients for the three series with their signs are collected in Tables III–V, and the results of the summation follow in Tables VI–VIII.

The projection along the *a* axis, fig. 1, shows one complete molecule overlapped by two others at the sides These overlapping molecules are actually situated half a translation along the *a* axis (perpendicular to the paper) from the centre one. After a large gap, corresponding to the cleavage plane in the

Table VI.—Projection along the *a* axis

Density of scattering matter as number of electrons per A² × 10.

↑	8	9	10	11	13	14	15	15	15	14	13	11	10	9	8
	6	6	6	9	12	15	16	14	10	9	9	10	12	12	11
	8	6	6	8	14	17	17	13	7	5	6	9	10	10	9
	14	10	8	10	17	26	29	25	18	14	12	12	11	9	7
	16	12	11	15	27	39	46	44	37	29	24	21	19	16	14
	16	15	16	23	36	49	56	55	46	39	35	35	35	35	34
	26	26	29	35	43	49	50	46	39	36	38	44	51	57	60
	42	45	49	51	50	44	35	27	23	26	35	48	59	68	73
c/2	56	60	62	60	50	36	22	13	12	20	31	43	55	62	65
	52	55	57	53	41	27	15	9	11	17	25	34	42	48	53
	34	36	38	35	27	18	12	11	12	15	18	25	35	47	55
	17	21	25	25	23	19	15	14	12	9	11	21	40	62	77
	12	19	28	35	35	31	25	18	11	6	9	25	52	81	100
	14	25	41	53	56	49	38	25	16	12	18	34	59	85	101
	23	34	51	63	65	58	44	33	27	29	36	48	59	70	76
↓	43	49	57	60	56	48	39	$\boxed{36}$	39	48	56	60	57	49	43

← *b*/4 —— × —— *b*/4 →

Centre of symmetry.

Table VII.—Projection along the *b* axis.
Density as number of electrons per $A^2 \times 10$.

	17	14	10	10	11	9	5	7	9	11	10	9	7	6	9	10
	16	14	9	9	9	8	7	7	11	14	14	10	6	7	10	10
	15	13	8	5	7	9	9	10	15	19	18	11	7	9	11	9
	14	13	7	4	6	10	13	17	23	25	20	13	11	12	12	10
	16	15	7	4	7	12	19	27	33	30	23	18	17	15	12	11
	22	17	9	6	9	16	29	41	42	34	27	26	23	17	12	13
	28	20	13	12	14	23	40	53	47	35	34	36	28	16	13	14
a/4	33	23	21	19	18	30	52	61	47	38	45	46	31	15	15	14
	34	27	31	26	21	36	60	60	44	44	57	52	29	14	15	11
	34	36	43	32	22	41	61	55	42	54	68	54	25	13	13	7
	35	40	54	32	21	41	56	46	45	66	74	48	20	11	10	3
	41	63	58	28	20	38	46	39	53	77	72	39	16	10	6	1
	53	74	55	22	18	33	35	39	64	82	63	30	12	7	2	2
	66	77	47	17	20	28	28	44	74	78	48	20	10	4	1	5
	78	72	37	18	23	24	27	54	78	66	34	15	9	2	2	7
centre of symmetry. ×	83	61	30	26	30	23	32	62	74	51	23	14	8	1	4	8
	78	48	31	39	37	25	38	65	63	35	16	12	6	1	6	7
	66	39	40	53	41	27	42	61	49	24	14	11	5	3	6	5
	53	37	53	63	42	28	42	51	36	18	13	10	5	4	5	2
	41	41	65	64	39	27	37	40	26	16	12	7	4	4	2	1
	35	49	66	58	31	23	29	28	20	13	8	5	5	3	0	3
	34	52	62	46	23	17	21	19	15	11	6	5	5	1	1	7
	34	49	49	30	15	12	13	13	12	8	5	5	3	1	2	11
a/4	33	40	32	18	11	9	9	10	9	6	5	5	3	0	6	14
	28	28	16	10	8	8	7	6	6	5	6	5	3	2	9	14
	22	17	9	8	9	8	5	4	5	7	8	5	3	5	11	13
	16	11	6	8	11	9	3	2	5	9	9	5	4	7	11	11
	14	10	8	10	12	9	4	2	7	11	8	5	6	9	9	10
	15	11	9	11	14	9	2	3	8	11	8	6	7	8	8	9
	16	14	11	12	14	9	4	5	9	11	9	8	7	6	8	10
	17	14	10	10	11	9	5	7	9	11	10	9	7	6	9	10

c/2

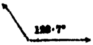

Table VIII —Projection along the *c* axis

Density as number of electrons per A^2 × 10.

↑	16	15	11	8	8	9	9	11	9	9	8	8	11	15	16
	14	15	12	9	7	6	7	9	12	11	8	7	10	15	17
	13	14	14	11	8	6	5	8	12	13	10	8	10	15	18
	12	15	16	15	11	8	7	10	13	13	10	7	10	15	18
	12	15	19	23	22	18	14	13	15	14	10	8	9	14	18
	11	17	25	33	37	35	29	22	19	16	11	8	10	15	17
	12	18	30	45	56	57	49	36	26	19	13	9	10	13	15
	13	19	35	59	78	83	72	53	35	22	15	11	10	12	14
b/2	14	21	41	70	97	107	94	69	43	26	17	13	11	11	11
	16	23	44	79	113	126	111	81	50	29	19	15	12	10	10
	17	22	45	84	121	135	119	86	52	31	21	17	12	10	9
	17	23	44	83	119	133	117	84	51	32	23	19	14	10	9
	17	21	41	77	110	122	106	75	48	33	27	22	16	11	10
	17	20	37	67	95	103	90	66	47	38	34	27	18	12	11
	15	18	31	56	77	83	72	57	49	48	45	35	22	13	12
↓	14	16	27	45	59	63	58	$\boxed{54}$	58	63	59	45	27	16	14

← *a*/4 × *a*/4 →

Centre of symmetry

crystal, the beginning of the next layer of molecules is shown. It will be noticed that four of the atoms in the molecule, forming the inner pairs, are separately resolved, but that the exact situation of the others is obscured by the overlap. The arrangement will be made clear by a study of fig. 1*b*, where the atoms are represented by circles drawn half size

These diagrams should be compared with the corresponding anthracene projections (*loc. cit.*). It will then be seen that the contour lines defining the ends of the molecules are of very similar appearance in the naphthalene and anthracene *a* axis projections, in spite of the widely different lengths of the two molecules. The shorter naphthalene molecule is tilted over at a larger angle, just sufficient to bring the end pair of atoms into almost the same relative position as that occupied by the end pair of anthracene atoms In other words, the x and y co-ordinates of the end pair of atoms are nearly the same in the two substances, only differing by about 0·1 A. at the most. It would seem that this particular configuration must be of some importance to the stability of the structure.

In the projection along the *b* axis, fig 2, the plane of the molecule is inclined at about 60° to the plane of the paper, yet a good resolution of the molecule as a whole and of four of the individual atoms is obtained These atoms show a very good spherical symmetry, allowing the position of their centres to be estimated very accurately It may be noted that this time the outer pairs

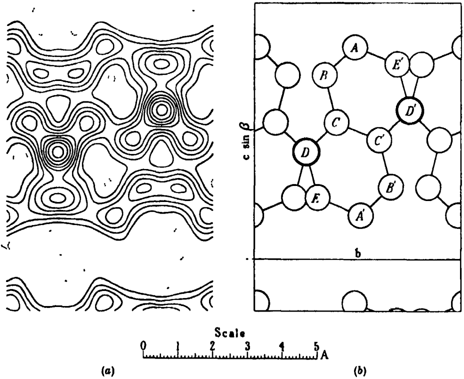

Fig. 1—Projection along the *a* axis. Each contour line represents a density increment of one electron per A³ The one electron line is dotted in all the diagrams

of atoms are resolved, so that by putting the *a* and *b* axis projections together we obtain a separate picture of every atom in the molecule, except one on each of the end pairs, which is always obscured by overlap.

Fig. 3 is again the *b* axis projection, showing on a smaller scale how the molecules are built together in the crystal. It should be borne in mind, however, that the centre molecules in this picture are really half a translation along the *b* axis (perpendicular to the paper) away from the others.

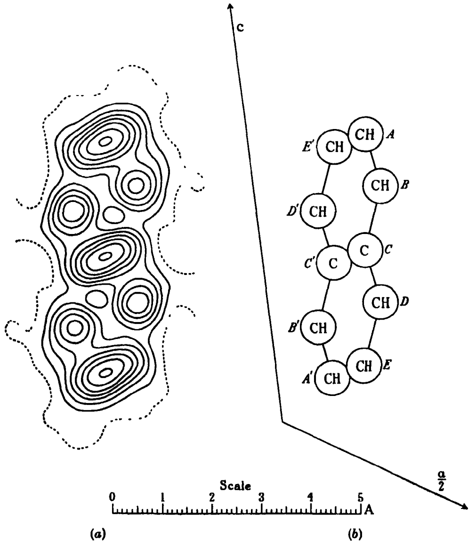

FIG. 2.—Projection along *b* axis. Each contour line represents one electron per A^2.

The complete structure will be made clear by comparison with fig. 4, which gives the end on view along the *c* axis. The relation of five molecules is shown, but as none of the individual atoms are resolved in this projection, it is not so useful as the others in elucidating the details of the structure.

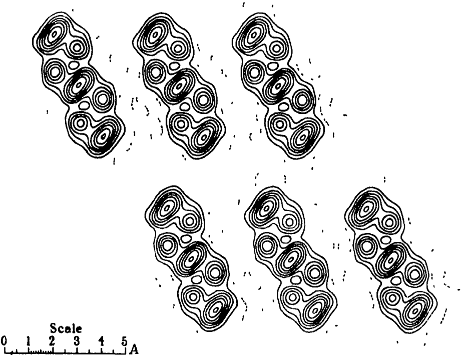

FIG. 3.—Projection along *b* axis showing mutual relation of molecules Each line represents one electron per A^2

The Structure Refined from the Fourier Analysis (Co-ordinates, etc.)

The deduction of the orientation and structure of the molecules follows closely that given for anthracene and durene (*loc. cit.*). Careful measurement of the diagrams shows that the carbon rings are almost certainly in the form of two regular plane hexagons.

The apparent angle which the long axis of the molecule makes with the *c′* (vertical) direction in the *a* axis projection is 14·0°, and in the *b* axis projection it is 26·0°. From these figures the actual angles χ, ψ and ω which the long axis of the molecule makes with the *a*, *b* and *c′* (perpendicular to *a* and *b*) axes are :—

$\chi = 115{\cdot}3°$ $\cos\chi = -\ 0{\cdot}428$

$\psi = 102{\cdot}6°$ $\cos\psi = -\ 0{\cdot}219$

$\omega = 28{\cdot}7°$ $\cos\omega = 0{\cdot}877.$

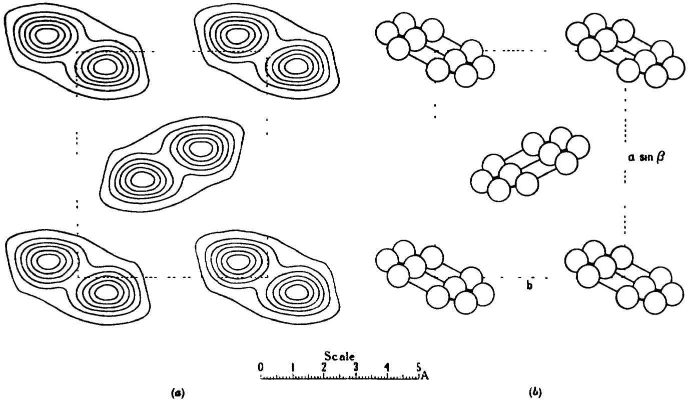

Fig. 4—Projections along *c* axis Each contour line represents two electrons per A².

Similarly, the cross axis (cc') makes an average apparent angle of 67·8° with the c' direction in the a axis projection, and 42·1° in the b axis projection, giving for the real angles :—

$$\chi' = 71\cdot2^\circ \qquad \cos\chi' = 0\cdot323$$
$$\psi' = 28\cdot8^\circ \qquad \cos\psi' = 0\cdot876$$
$$\omega' = 69\cdot1^\circ \qquad \cos\omega' = 0\cdot357.$$

The angle between the long and the cross axis of the molecule is 90·9° with the above figures This result provides an independent check on the regularity of the structure.

The distances between the atoms which are resolved in the projections can now be measured and combined with these direction cosines to give their real magnitudes. Owing to the overlap, the a axis projection is difficult to measure, but the carbon to carbon distance can be safely placed at between 1·40 and 1·44 A. The centre distance (cc') appears to have the larger of these values, but this may not be a reliable result. The b axis projection, on the other hand, is very easy to measure accurately, and the radius of the hexagons (measured as half the distance across the rings) is here 1·41$_2$ A., and the periodicity along the axis of the molecule is 1·22 A. These last figures are the same as the corresponding anthracene results.

The co-ordinates of the atoms can be worked out from these figures and the orientation angles, ten out of the fifteen values can also be obtained by direct measurement of the diagrams, and are given in bold type in Table IX.

Table IX.—Co-ordinates. Centre of Symmetry as Origin. Monoclinic Axes.

Atom, *cf.* fig 1.	xA.	$2\pi x/a$.	yA.	$2\pi y/b$	zA.	$2\pi z/c$
A	0·72	31·3	**0·09**	**5·1**	**2·85**	**118·0**
B	**0·94**	**41·0**	**0·97**	**58·5**	**1·88**	**78·0**
C	0·39	16·9	**0·62**	**37·3**	**0·30**	**12·5**
D	**0·62**	**26·8**	**1·50**	**90·5**	**−0·68**	**−28·2**
E	0·06	2·5	1·15	69·5	−2·25	−93·5

Intermolecular Distances.

The closest distance of approach between the centres of atoms on neighbouring molecules appears to occur between the standard and the reflected molecule, where a minimum distance of 3·60 A. has been obtained from the above co-ordinates. Between adjacent molecules on the *b* axis the minimum distance is 3·72 A. These figures are slightly less than the corresponding anthracene values (3·77 and 3·80 A) Between the ends of molecules lying along the *c* axis the minimum distance is about 3 95 A., and between the standard and the reflected molecule one translation removed along the *c* axis it is about 3 80 A.

The Electron Distribution.

The decrease in the peak values of the electron density on passing outwards from the centre of the molecule, which was so noticeable in anthracene, is not observed in the naphthalene *b* axis projection, fig. 2 The three pairs of unresolved centres rise to peaks of just over 8, while the separately resolved atoms are between 6 and 7 electrons per square Ångstrom unit In the *a* axis projection, fig. 1, the density at the central atoms marked C is also between 6 and 7 units, but on the end atom A it falls to just under 6 units. This result seems to be due, however, to the varying amount of overlap of the atoms in the *a* projection.

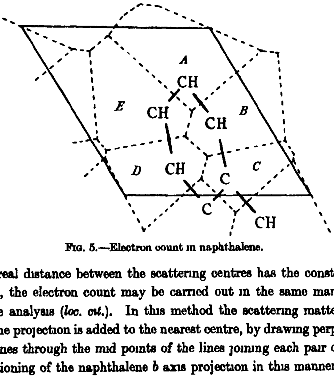

FIG. 5.—Electron count in naphthalene.

As the real distance between the scattering centres has the constant value of 1·41 A., the electron count may be carried out in the same manner as in the durene analysis (*loc. cit.*). In this method the scattering matter at each point on the projection is added to the nearest centre, by drawing perpendicular dividing lines through the mid points of the lines joining each pair of centres. The partitioning of the naphthalene *b* axis projection in this manner is shown in fig. 5.

When the figures are summed over these areas, the following results are obtained :—

A. > CH : 7·4 electrons (7 required by chemical structure)
B. > CH : 7·1 „ (7 „ „)
C. → C · 5·7 „ (6 „ „)
D. > CH · 7·0 „ (7 „ „)
E. > CH 6·9 „ (7 „ „)

These results seem to indicate that the hydrogen atoms are on the average located in the regions shown.

In conclusion, I again wish to thank Sir William Bragg, O.M., F.R.S., for his interest in this work, which has been carried out in the Davy Faraday Laboratory. I am indebted to Miss I. Woodward for assistance in converting the naphthalene and durene summation values to absolute units, and in recalculating some of the structure factors

Summary.

The crystal structure of naphthalene has been worked out in detail in a form parallel to the anthracene and durene determinations The measurement of the intensities is described, and the structure is first obtained by trial and error, starting from the orientation found for anthracene. These results are refined by a double Fourier analysis carried out for the zones of the three chief crystallographic axes, and the results are expressed in absolute units. The orientation is given on p. 684, and the 15 co-ordinates of the atoms on p. 686. The structure differs from anthracene chiefly in the larger inclination of the long axis of the molecule to the (010) plane

With the exception of one on each of the end pairs, all the carbon atoms in the molecule are separately resolved in the combined *a* and *b* axis projections. The interatomic distance of 1·41 A. is the same as in anthracene, and the closest distance of approach between the centres of atoms in adjacent molecules (3·60 A.) is also very nearly the same as in anthracene.

The electron distribution does not show any marked falling off in the peak values on passing out from the centre of the molecule as in anthracene, but the electron count is again in good agreement with the chemical structure.

Collisions of Neutrons with Light Nuclei.—Part II.

By N. Feather, Ph.D., Trinity College, Cambridge

(Communicated by Lord Rutherford, O M , F R S —Received October 4, 1933)

[Plates 6 and 7]

Introduction

In a previous paper* experiments were described in which collisions between neutrons and nitrogen nuclei had been investigated by stereoscopic photography of the tracks produced in an expansion chamber filled with nitrogen and traversed by the radiation from a source of polonium and beryllium placed at its centre. With this arrangement 1740 pairs of photographs were taken The method has since been extended to neutron-oxygen nucleus encounters, and a preliminary report of the results obtained in 1490 pairs of photographs has appeared.† In the present paper these results are presented in greater detail and more recent experimental material, provided by 1460 stereoscopic pairs belonging to an oxygen-hydrogen series of photographs and 2210 pairs to an acetylene-helium series, is given for the first time The analysis of this new material scarcely does more than provide preliminary data for the discussion of the general problem of the close collisions of neutrons with light nuclei, but its publication at this time may well be of interest

During the course of the work reports of similar experiments—in progress, or already productive of preliminary results—have been received from Auger‡, Meitner and Philipp§, Harkins, Gans, and Newson‖, Kurie¶, and Rieder ** Reference will be made to their results at a later stage It is necessary, however, to draw attention at the outset to a feature common to all such experiments, in which the expansion chamber is used Although individual events may be studied and the angles involved in their description be determined directly, the kinetic energies concerned may be deduced only from measurements of lengths of cloud track. However extensive the experimental material may be, we are very seriously handicapped in interpreting it by the inadequacy of our knowledge of the range-velocity relation, except for a very few types of atom Until recently the researches of Blackett and his co-workers provided the only data for use in this connection. Now range-velocity curves are also available for the recoil atoms of fluorine and (less accurately) of carbon, these having recently been investigated by the writer * Some of the earlier results must be reconsidered in the light of this new knowledge.

---

* 'Proc. Roy. Soc.,' A, vol. 136, p. 709 (1932), referred to as Part I

† 'Nature,' vol. 130, p 237 (1932).

‡ 'C. R. Acad. Sci. Paris,' vol 195, p 234 (1932), vol 196, p 170 (1933), Auger and Monod-Herzen, 'C R. Acad. Sci Paris,' vol 196, p. 1102 (1933)

§ 'Naturwiss,' vol. 20, p 929 (1932)

‖ 'Phys. Rev.,' vol. 43, p. 208 (1933), vol 43, p. 584 (1933), Harkins, 'Phys Rev.,' vol. 43, p. 362 (1933), 'Science,' vol. 77, p. 458 (1933).

¶ 'Phys. Rev,' vol. 43, p. 672 (1933), vol. 43, p 771 (1933)

** 'SitzBer. Akad. Wiss Wien,' vol. 142, p. 169 (1933).

Experimental Arrangement and the Gases Employed

A description of the apparatus employed in the work to be described has already been given.† For the oxygen-hydrogen series of photographs and for the first 740 photographs of the acetylene-helium series no change whatsoever was made—except that a new polonium source was used—whilst for the remainder of the work (1470 pairs of photographs with the acetylene-helium mixture), in addition to a second renewal of the source (in this case the polonium was deposited on a disk of silver 7·5 mm in diameter), a slight modification of the source container was also effected The additional absorber of lead previously surrounding the source box was removed, leaving a wall thickness of 0·75 gm /cm.^{2} of brass only, and the interior lower portion of the box was lined with beryllium-aluminium foil (70% beryllium by weight)‡ in an attempt to increase efficiency by using a greater fraction of the α-particles emitted by the polonium. The target of beryllium metal previously employed was, however, retained. Throughout the experiments the mean strength of the polonium source was about 25–30 millicuries

Concerning the gases employed, the principles of choice have likewise already been discussed § With the present apparatus it is not desirable that large expansion ratios be used, and initial pressures other than roughly atmospheric are entirely impracticable. Moreover, it is important in preliminary work never to have more than one type of atom present which is capable of disintegration under neutron bombardment. When it was desired, therefore, to investigate the inelastic collisions in oxygen at greater dilution,|| hydrogen

---

* 'Proc Roy Soc ,' A, vol 141, p 194 (1933).

† Part I, p 710

‡ I wish here to acknowledge the kindness and co-operation of the Western Electric Co., Ltd , in providing this material.

§ 'Proc. Roy. Soc ,' A, vol 141, p. 194 (1933)

|| 'Nature,' vol 130, p 237 (1932)

was added to the oxygen in the chamber A mixture of 60% hydrogen and 40% oxygen was used. The stopping power of this mixture at the instant of track formation was about 0·43, compared with 0·76 for the almost pure oxygen previously employed.

Acetylene was used in an attempt to observe inelastic collisions between neutrons and carbon nuclei.* Since all hydrocarbon molecules are polyatomic, any hydrocarbon requires the addition of an inert gas if "normal" expansion ratios are to be employed—and amongst the inert gases helium is here the obvious choice Furthermore, acetylene was chosen as being that gaseous hydrocarbon which, mixed with helium in the proportions necessary to give the mixture the characteristic diatomic ratio of specific heats, also provided the mixture with the greatest proportion of carbon atom stopping power. The proportions by volume finally adopted were helium 57 5%, acetylene 41·2%, hydrogen 1·3% At the time of track formation the calculated† stopping power of this mixture was 0 41, in terms of standard air. Acetylene was taken from a small cylinder (from solution in acetone), bubbled through a wash bottle containing water and collected The requisite amount was passed into the expansion chamber, which had previously been washed out with hydrogen and filled to the desired pressure with helium. In the latter operation crude helium, containing about 20% air, was passed slowly over charcoal cooled in liquid air before it entered the chamber.

Analysis of the Results.

Elastic Collisions.—The experimental results under this head will be treated first. They comprise measurements upon single recoil tracks and may be presented quite simply. Measurements upon paired disintegration tracks will then be considered.

Figs. 1, 2, and 3 give the integrated‡ range distribution curves for the recoil atoms produced by elastic collisions in oxygen, oxygen-hydrogen, and acetylene-helium mixtures, respectively. The reduced air range is employed throughout. Fig. 1 is derived from measurements on 47 recoil tracks (2 having lengths greater than 4 mm. of standard air), fig 2 from 97 tracks and fig. 3 from 213 tracks (16 and 57 longer than 10 mm. of standard air, as shown in figs. 2 and 3, respectively). In these two latter cases almost all the tracks classified as longer than 10 mm. of standard air were produced by particles starting in the

---

* These collisions having been thoroughly explored, those of fluorine may be studied using carbon tetrafluoride in the expansion chamber as the writer has already done in another investigation

† Mean α-particle stopping powers have been used throughout, for acetylene Bragg's value, 1·118, was adopted.

‡ Curves showing the number of particles with ranges greater than any given range.

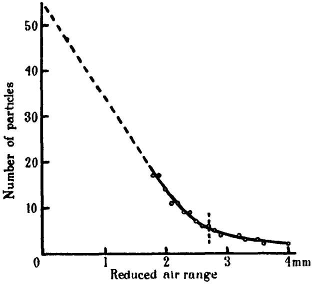

FIG 1

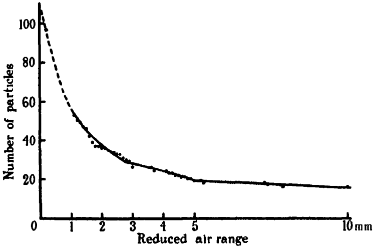

FIG 2

gas and passing out of sight of one or both cameras before being completely absorbed. Now in each experiment the air equivalent depth of chamber illuminated was somewhat in excess of 10 mm., whilst the transverse dimension

—radially from the source box to the chamber wall—was about 3 cm of standard air. It is probable, therefore, that the majority of the particles producing these longer tracks had reduced air ranges considerably greater than 1 cm. Only 2 tracks out of 16 in the one case and 6 out of 57 in the other had measured lengths between 1 cm. and 3 cm in terms of standard air.

In the region of short ranges the curves are shown dotted. This does not mean that no tracks were measured here; some were, in fact, measured, the lengths of which were found to lie within this region Other short tracks, however, were not measured, being classified as "apparently too short for accurate measurement." The number of these is included with that of the measured tracks in the initial points of the curves Where the curves are shown full, on the other hand, it is thought that no tracks are likely to have passed unmeasured owing to an unfavourable orientation producing the suggestion of shortness; they represent those regions in which a satisfactory precision in measurement could be attained.

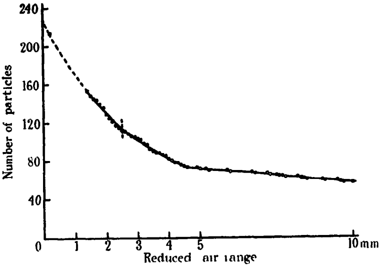

FIG. 3

In the original experiments with nitrogen in the chamber this limitation to the measurements was not sufficiently appreciated, nor were the conditions of photography sufficiently good to make evident beyond doubt the presence of a considerable number of very short recoil tracks The possibility of their presence was admitted in the course of the discussion,* but no explicit suggestion was made that the range distribution curve of fig 2*b* (Part I) might be incomplete in this region. However, there was definite evidence in this direction from the experiments of Dee * Assuming the proportions which he found (albeit from a small number of tracks), fig. 4 may be taken as representing the original nitrogen results so corrected as to be brought into line with the later results here presented.

---

* "The shortest nitrogen recoil tracks no doubt fail to be detected," I, p 717.

Figs 1 and 4 then become precisely comparable. The two curves are of very nearly the same form ; not many oxygen recoil atoms have ranges greater than 2·7 mm. nor nitrogen recoil atoms greater than about 2·8 mm. of standard air. Applying elastic collision relations and using the range-velocity data of Blackett and Lees† we may thus conclude (without inconsistency) that very few of the neutrons emitted from beryllium bombarded by the α-particles from polonium have energies greater than about 4·6 . 10^6 electron volts (from the oxygen results)—or 4·4 . 10^6 electron volts (from the nitrogen results). Rather, this is a conclusion to be accepted provisionally, always admitting that the assumption of collision radii varying but slowly with the velocity of the

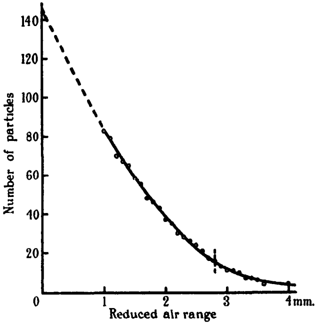

FIG 4

---

* 'Proc. Roy. Soc.,' A, vol. 136, p. 727 (1932).

† 'Proc Roy. Soc ,' A, vol 134, p 658 (1932)

neutron is involved. Only if interaction becomes rapidly less frequent as the velocity increases—or if it results chiefly in nuclear disintegration—can the majority of the neutrons have energies in excess of $4 \cdot 5 \,.\, 10^6$ electron volts. Now Curie and Joliot,[*] as also Chadwick,[†] find that the recoil protons projected by polonium-beryllium neutrons for the most part have energies less than this amount. The maximum range of the most prominent group, 43 mg /cm ^{2} of aluminium (28 cm. of standard air), found by Curie and Joliot would indicate an upper limit at $4 \cdot 5$ 10^6 electron volts, that of 24 cm of standard air, from the most recent work of Chadwick, a limit at $4 \cdot 1 \,.\, 10^6$ electron volts to the energy of the majority of the neutrons This measure of agreement with the present results suggests that a real feature of the energy spectrum of the emitted neutrons is in question. Yet there can be no further indication, solely on the basis of integrated distribution curves, such as figs 1 and 4 provide, whether this feature consists in a homogeneous group of neutrons of somewhat more than $4 \,.\, 10^6$ electron volts energy—or whether a continuous distribution with energy is involved. Measurements of angles as well as lengths in the original work on the nitrogen collisions provided some support for the latter alternative. On the basis of Chadwick's interpretation of his complete range distribution curve for recoil protons evidence of a prominent group of neutrons possessing all energies between $2 \cdot 5$ and $4 \cdot 1 \,.\, 10^6$ electron volts is to be expected

To proceed further it is necessary next to compare fig 2 with fig. 1. The maximum range of $2 \cdot 7$ mm, taken to be characteristic of the majority of oxygen recoil atoms, again appears ($2 \cdot 8$ mm. here), though less definitely—no doubt because oxygen recoil tracks are almost certainly less numerous than proton recoil tracks on the photographs from which the data of fig. 2 are derived. There are several arguments which may be adduced in support of this otherwise arbitrary statement First, the proportion of disintegration collisions was much less in the experiment with the oxygen-hydrogen mixture than in that in which pure oxygen was employed (*v. infra*). Secondly, the form of the distribution curve of fig. 2 is quite different from that of fig. 1 in the region 0–3 mm. of standard air. This can only be explained[‡] if a considerable number of proton tracks is represented in this region of fig. 2 and if their distribution in length is itself quite different from that of fig. 1. The proportion of very short proton tracks must, in fact, be much greater than fig. 1 shows the proportion of short oxygen recoil tracks to be. Finally, we may argue from previous knowledge of approximate collision radii. It is very likely that for neutrons of the energies here considered the target area for proton collisions is considerably greater than that effective in collisions with oxygen nuclei—and in the experiment under discussion there were 50% more hydrogen nuclei than oxygen nuclei present in the chamber. Certainly less than one-third of the observed recoil tracks, therefore, should be ascribed to the latter. The conclusion that a very large fraction (of the order of ½) of all the recoil protons (maximum range perhaps greater than 100 cm.) have ranges less than 1 cm. of standard air has already been reached by Auger (*loc. cit.*, 1932), and the results of Meitner and Philipp (*loc. cit.*) are in agreement with this conclusion. The present distribution curve suggests that these low energy particles have a maximum range of 5·0 mm. of standard air, or a maximum energy of 0·30 . 10^6 electron volts.* It is very probable that they are projected by the neutrons which are emitted in the resonance disintegration of beryllium by α-particles of about 1·4 . 10^6 electron volts energy.† However, the exact position of this resonance level, and so the exact energy of the corresponding neutrons, are matters of some uncertainty. Chadwick's (*loc. cit.*) observations lead to 0·5 . 10^6 electron volts for the most probable energy of the neutrons, but the general evidence from recoil protons suggests a somewhat smaller value‡ for the effective upper limit of energy of this group.

---

[*] 'J. Phys. Rad.,' vol. 4, p. 21 (1933)

[†] 'Proc. Roy Soc,' A, vol. 142, p. 1 (1933).

[‡] The suggestion that many more very short oxygen recoil tracks were recognized as such at the greater dilution receives little support when figs. 2 and 3 are compared—where the effective stopping power of the mixture was very nearly the same in the two cases

There remains, last of all, the interpretation of fig. 3. In the acetylene-helium series of experiments—neglecting the water vapour in the chamber—the relative numbers of nuclei present were hydrogen 37·4%, helium 25·7%, carbon 36·9%. It is necessary first to estimate roughly to what extent recoil tracks of these different types are represented in fig. 3. In the present state of knowledge this cannot be done with very great confidence. The scattering-absorption measurements of Dunning and Pegram,[*] for the radon-beryllium neutrons filtered through 4 cm. of lead, definitely refer to neutrons of higher energy than those here involved; they do suggest, however, a roughly monotonic relation between target area and atomic number, with a minimum target area for carbon nuclei. But there is no evidence how the position of this minimum depends upon the velocity of the neutrons. The matter is extremely complicated and little better than a guess is at present possible, but for the interpretation of fig. 3 we shall assume hydrogen : helium : carbon ratios of roughly 45 : 30 : 25 for the total recoil tracks. Carbon recoil tracks, on this assumption, account for only one-quarter of the total number, say, 55 tracks in all.

---

* The stopping power of hydrogen for protons (or for α-particles) varies so rapidly in the region of small velocities that considerable caution is necessary here. For reduced air ranges greater than 4 mm., however, and for the gas mixtures in question velocities may probably be estimated within 5% without any correction being applied.

† Although the majority of recoil protons are ascribed to neutrons of this resonance group it is not suggested that the relative abundance of the neutrons themselves is equally great. Chadwick (*loc. cit.*) has shown that the target area characteristic of neutron-proton collisions increases very rapidly as the velocity of the neutron is reduced below 2·5 . 10^9 cm./sec.

‡ Auger ('C. R. Acad. Sci. Paris,' vol. 196, p. 1102 (1933)) gives the range distribution of 81 short proton tracks, out of 93 used in an investigation of the angular distribution. The maximum range observed is 15 mm. of standard hydrogen—and the corresponding neutron energy 0·26 . 10^6 electron volts.

It is difficult from the curve to decide what is the true distribution of these tracks with range. The maximum velocity which a carbon atom may acquire as the result of nuclear collision with a neutron of $4 \cdot 1 \,.\, 10^6$ electron volts energy is $4 \cdot 34 \,.\, 10^8$ cm./sec. On the basis hitherto adopted in this work, the accepted range-velocity curve for nitrogen recoil atoms, together with the empirical relation of Blackett[†]

$$r = kmz^{-\frac{1}{2}} f(v),$$

it would be concluded that the maximum range of such a recoil atom was $2 \cdot 95$ mm. of standard air. However, the recent work of the writer[‡] leads to a somewhat different range-velocity curve for carbon recoil atoms, and in this particular case to a maximum reduced air range of about $2 \cdot 3$ mm. There is slight evidence for a fairly abrupt change of slope of the curve of fig. 3 somewhere between these two ranges, say, at $2 \cdot 5$ mm. range. Possibly this may be the feature under discussion. Recoil α-particles projected by neutrons of maximum energy $0 \cdot 3 \,.\, 10^6$ electron volts cannot have ranges greater than $1 \cdot 8$ mm. of standard air and cannot therefore be in question here. If the majority of carbon recoil atoms have ranges less than $2 \cdot 5$ mm., however, the number of tracks remaining with reduced lengths less than $4 \cdot 6$ mm. is too great to be ascribed to protons alone. Some of these tracks no doubt belong to the same group as that, of maximum range $5 \cdot 0$ mm., which is a feature of fig. 2, but the greater proportion must have another origin. We may examine in turn the suggestions that these tracks are produced by recoil atoms of helium and carbon, respectively. It may be that each type of recoil atom is responsible for some of the tracks.

---

[*] 'Phys. Rev.,' vol. 43, p. 497 (1933).

[†] 'Proc. Roy. Soc.,' A, vol. 107, p. 349 (1925).

[‡] 'Proc. Roy. Soc.,' A, vol. 141, p. 194 (1933).

Helium recoil atoms of maximum range 4·6 mm. of standard air require neutrons of $1 \cdot 1 \,.\, 10^6$ electron volts for their production by elastic impact. Now penetration of the beryllium nucleus by way of the upper resonance level—at $2 \cdot 5 \,.\, 10^6$ electron volts α-particle energy*—may be expected to give rise to neutrons of $1 \cdot 47 \,.\, 10^6$ electron volts energy † It is possible that we have here to do with recoil α-particles projected by neutrons belonging to this group. The corresponding recoil protons would have ranges of roughly 4·5 cm. ($1 \cdot 47 \; 10^6$ electron volts) or 2·9 cm ($1 \cdot 1 \; 10^6$ electron volts), and in either case would be outside the limits covered by the distributions of figs. 2 and 3. It is perhaps worthy of note that Auger (*loc cit.*) found very few proton tracks of lengths between 2 cm. and several decimetres of air. It may be that this evidence again suggests a value slightly lower than that at present accepted for the energy of the neutrons produced in this resonance disintegration

According to the second suggestion above made, carbon recoil atoms with reduced air ranges up to 4·6 mm. are projected by polonium-beryllium neutrons Then the energy spectrum of these neutrons must extend to $10 \cdot 1 \,.\, 10^6$ electron volts at least.‡ Evidence has steadily been accumulating in favour of an upper limit in this region. From the mass measurements of Bainbridge§ neutrons of $11 \cdot 9 \,.\, 10^6$ electron volts ought to be observed, unless some energy is always emitted in the form of a quantum of radiation—and their observation, in measurements of recoil track lengths, is obviously favoured when the bombarded nuclei are not easily disintegrable For, if disintegration by neutrons can take place at all, it is probably the faster neutrons which are the most efficient. Now carbon nuclei are not readily susceptible of disintregation as the present experiments show (*v. infra*).|| There is the greater chance, therefore, that any high energy neutrons present shall be observed by the elastic collisions which occur. Very little evidence for their presence can be obtained from the elastic collisions in oxygen and nitrogen (figs. 1 and 4). On the other hand, certain disintegrations have here been attributed to the

---

* Rasetti, 'Z. Physik,' vol. 78, p. 165 (1932); Curie and Joliot, 'C R. Acad. Sci. Paris,' vol. 196, p. 397 (1933); Chadwick, *loc. cit.*

† Chadwick, *loc. cit.*

‡ $9 \cdot 4 \,.\, 10^6$ electron volts, if the empirical range-velocity relation of Blackett be employed.

§ 'Phys. Rev.,' vol. 43, p. 367 (1933).

|| Harkins, using ethylene in the expansion chamber, finds this, also—report to the American Physical Society, Chicago meeting, June, 1933, concerning work in progress.

capture of high energy neutrons.* Evidence from recoil tracks, being more direct, is less open to doubt than that from the measurement of disintegration forks. It is important, therefore, to determine how far this direct evidence is established. For we might regard all the tracks of lengths between 2·5 and 4·6 mm. in fig. 3 as due either to hydrogen or to helium recoil atoms. Apart from statistical considerations the only appeal must be to individual tracks. It is profitable to enquire whether any reliance may be placed on such a procedure. We wish to be able to assign observed tracks to the atoms responsible for their production in the majority of cases, or, at least, to decide between various possibilities when a mixture of gases is employed.

The only possible criterion is one based upon differences in the linear density of ionization in the recoil tracks of different atoms, and, for reasons which will appear, the variation of ionization along the track is likely to provide a criterion in all respects more practicable than any which depends upon differences in absolute ionization density as between one track and another. Now we do not know how the linear density of ionization varies with the distance from the end of the recoil path of any atom, although we are able to deduce how the rate of loss of energy depends upon the residual range of the particle. This is obtained by differentiation of the corresponding range-energy curve. Curves I to IV of fig. 5 have been deduced from the accepted range-velocity curves for protons (in hydrogen-air, 1 : 1), α-particles (in air), carbon recoil atoms (in carbon tetrafluoride-helium, 1 : 4), and nitrogen recoil atoms (in air-hydrogen, 3 : 2). They show how the rate of loss of energy in each of the above cases depends upon the residual reduced air range of the recoil atom in question. It is probable that the corresponding ionization-distance curves will have roughly the same form.† Moreover, there is some evidence‡ to show that in a well-developed and heavily ionized cloud track the power of scattering light reaches a maximum where the initial ionization per centimetre of path is a maximum—if the connection between these quantities is not indeed closer

---

[*] Harkins, Gans, and Newson, 'Phys. Rev.,' vol 43, p. 1055 (1933), *ibid.*, vol. 44, p 236 (1933); Kurie, 'Phys. Rev.,' vol. 43, p 771 (1933).

[†] The mean energy per ion pair may not, however, remain constant when ionization is to any large extent due to capture and loss of electrons. Then, as the recoiling atom becomes slower, the most probable state of instantaneous ionization is a less heavily ionized one and the average amount of energy necessary to produce "loss" of an electron is smaller. The "ionization maximum" may in consequence occur nearer the end of the track than the "rate-of-loss of energy maximum" (*cf.* Blackett and Lees, 'Proc. Roy Soc.,' A, vol. 134, p. 658 (1932)).

[‡] Feather and Nimmo, 'Proc. Camb. Phil. Soc.,' vol. 24, p. 139 (1928).

than this. Curves I to IV may then suggest the manner in which the brightness of a track image depends upon the distance from the end of the track in the different cases. Without undue error these same curves may be assumed applicable to the recoil tracks of hydrogen, helium, and carbon* atoms in the acetylene-helium mixture employed in the present experiments. This, then, provides the desired criterion.

The examples reproduced, at a common magnification,† in Plate 6, quite definitely support this conclusion. Numbers 2 and 3 are from the oxygen-hydrogen series of photographs and represent tracks of lengths 2·97 and 5·25 mm. of air, respectively. Only curve I, fig. 5, can apply to these and the length of number 3 and the large deflection of number 2 provide additional reasons why both must be recoil tracks of hydrogen nuclei. The remaining examples of Plate 6 refer to the acetylene-helium series; hydrogen, helium, and carbon recoil atoms are thus involved. Number 1 is almost certainly the track of a

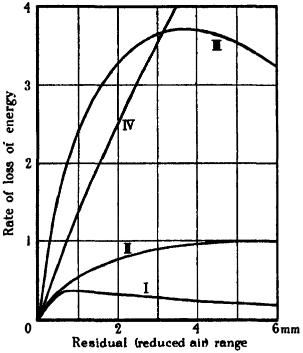

Fig. 5.

---

* If the range-velocity curve for carbon atoms is more accurately given by Blackett's relation, then curve III must be replaced by a curve of the same form as IV, fig. 5..

† × 3·3, in terms of standard air.

swift proton having its origin in the gas On account of the characteristic difference in the linear distribution of brightness (curves I and II, fig. 5), numbers 4 and 5 (reduced air lengths 12·14 and 9·00 mm , respectively) are here ascribed to protons and numbers 6 and 7, though equally long* (11·33 and 12·04 mm.), to α-particles. Now the maximum range of helium nuclei projected by neutrons of $4 \cdot 1 \,.\, 10^6$ electron volts energy is 15·3 mm., so that α-particle tracks of this length are to be expected Similarly numbers 8, 9, and 10 (7·23, 3·49, and 4·90 mm., respectively) show the α-particle intensity distribution , moreover, each has a sudden deflection which can only have been due to a nuclear encounter with a heavier atom. The possibility of ascribing number 9 to a recoil atom of carbon is thus excluded. It is believed, however, that this classification is correct for numbers 11, 12, 13, and very probably for number 14 also Reduced air ranges are as follow number 12, 3·39 mm. , number 13, 2·30 mm , number 14, 4·18 mm. If number 11 provides an example of elastic collision between similar atoms, as appears probable, then a carbon-carbon collision is much the most likely event, and the origin of this recoil track is fixed. The distribution† of brightness is very similar in the other three, 12, 13, and 14, and the common origin already assumed is in no way questioned. Finally, in a number of photographs, in addition to those here reproduced (numbers 12 and 14), these characteristics have likewise been found for tracks of reduced length greater than 2·5 mm. and less than about 5 mm. of air. This, then, is the extent of the direct evidence, from the recoil tracks observed in these experiments, for neutrons of high energy (about 10^7 electron volts) from beryllium bombarded by the α-particles of polonium.

Disintegration Collisions.—The eight examples of disintegration found with nearly pure oxygen in the chamber have already been briefly reported ‡ In three examples the length of the recoil track was very small and in a fourth the initial direction was difficult to determine with accuracy, so that for all these the plane of the visible fork was somewhat indefinite. Yet, considering the results as a whole, there appeared no reason to assume other than capture disintegration to be taking place. This was almost to be expected, since the most probable non-capture process—that which would result in carbon of mass 12 and an α-particle—requires that at least $5 \cdot 4 \,.\, 10^6$ electron volts energy be supplied.

---

* The maximum foreshortening on Plate 6, 25%, occurs with number 4.

† Assuming uniform conditions the absolute brightness of a well-developed carbon recoil track should be much greater than that of the other tracks observed, but conditions are not sufficiently uniform in practice to make this criterion at all trustworthy.

‡ 'Nature,' vol. 130, p. 237 (1932).

This decision, in favour of capture disintegration, is strictly of a qualitative nature, depending upon the condition of coplanarity The quantitative results given in the former note were calculated on the basis of the empirical range-velocity relation for carbon* recoil atoms. To an accuracy of 0·4% the product $mz^{-\frac{1}{2}}$ has the same value for the nuclei N^{14} and C^{13}. The experimental range-velocity curve for nitrogen recoil atoms was thus used without modification Now the formula of Blackett is intended to take account both of change of mass and of nuclear charge. There can be little doubt that the effect of the second factor is the more difficult to express simply. As far as concerns the former, simple mechanical principles lead to a rate of loss of energy independent of the mass (large compared with the electronic mass), and so to a range directly proportional to the mass, for a given value of the velocity. If the range-velocity curve for the recoil atoms C^{12} is known, that for the atoms C^{13} can, therefore, be confidently deduced

More recently the oxygen disintegrations have been recalculated on the basis of the approximate range-velocity curve for C^{12} recoil atoms obtained by the writer.† Comparison of the new results with the old in the matter of internal consistency may possibly indicate how far the meagre data for the range-velocity curve are to be trusted; it will certainly show what extreme caution is necessary in drawing conclusions from numerical results when there is still some doubt concerning the auxiliary data employed in the calculations. The accuracy of the measurements themselves is first in question. Here we shall be concerned entirely with the more satisfactory collisions, numbers 1 to 4 of the original table. Two independent sets of measurements were made on number 4. The results were as follow‡: length of track of new nucleus, 2·96 (3·02) mm., of disintegration particle, 7·72 (7·58) mm. of standard air. ω, 133·0° (131·4°); γ, 1·2° (5·0°); θ, 25·8° (24·9°); ϕ, 107·5° (106·7°), Δ, 9·5° (9·5°). Criterion of accuracy of measurement. ω (calculated), 133·3° (131·1°)—in sufficiently good accord with ω (observed). The results of the second set of measurements are shown in brackets throughout. It will be seen that the agreement is quite satisfactory. In Table I, for numbers 1,§ 2 and 4, are given in column I the measured values of θ, in columns II and V the kinetic energy* of the neutron responsible for the disintegration, calculated from the resultant momentum of the two final particles on the basis of the old and the new range-velocity curves, respectively, in columns III and VI the energy absorbed in the disintegration process, following these alternative calculations, and in columns IV and VII the corresponding values of θ′, the angle between the direction of the resultant momentum and the direction of motion of the recoil nucleus Any disintegration may be regarded as satisfactorily explained when θ and θ′ differ by less than the quantity Δ (column VIII), the angle subtended at the point of inelastic collision by half the diameter of the neutron source For numbers 1 and 2 there is better agreement when the old range-velocity curve is employed, for number 4 the new curve gives the greater consistency

---

* The nuclear reaction $O^{16} + n^1 \rightarrow N^{14} + H^3$ being endothermic, with energy absorption of about 10^7 electron volts, the reaction $O^{16} + n^1 \rightarrow C^{13} + He^4$ was regarded as the more probable, and calculations were made on that basis.

† 'Proc. Roy. Soc.,' A, vol. 141, p. 194 (1933).

‡ For the significance of the various symbols see Part I, pp. 714, 719.

§ Reproduced as number 15, Plate 7, also on previous occasions, *e.g.*, by Chadwick, Brit. J. Radiology,' vol. 6, p. 24 (1933).

Table I.

No.	I (θ)	II (E_1)	III (W_1)	IV (θ'_1)	V (E_2)	VI (W_2)	VII (θ'_2)	VIII (Δ)
	°			°			°	°
1	37·7	7·2	2·4	32·5	9·8	4·6	28·8	7·2
2	64·6	7·0	4·3	62·6	9·6	6·5	49·3	13·7
4	25·4	7·8	5·4	37·2	12·2	9·3	29·1	9·5

A curve lying roughly mid-way between these two is found to give satisfactory agreement in all three† cases, it will be convenient to employ this mean curve until more accurate data are available. Yet to adopt even so slight a modification in the auxiliary data is to change accepted energy values by as much as $2 . 10^6$ electron volts in some cases. The general trend is an increase in the calculated kinetic energy of the neutron, with frequently a roughly equal increase in the amount of energy found to be absorbed in the transformation process It is this latter aspect of the results which calls for some comment There is almost an exact balance of mass in the nuclear reaction

$$O^{16} + n^1 \rightarrow C^{13} + He^4.$$

If the present conclusions are correct, therefore, we must assume the emission of a quantum of high energy γ-radiation in each of the disintegrations so far observed Hitherto the only other disintegration of an oxygen nucleus reported in the literature is one* in which a neutron of $8 \cdot 3 . 10^6$ electron volts energy was effective and $0 \cdot 9 . 10^6$ electron volts of energy was absorbed. These values, presumably, were calculated on the basis of the empirical range-velocity relation generally employed, so that the energy of the quantum has been somewhat underestimated.

---

* Energy values in millions of electron volts

† Example number 3 of the original table has not been included in Table I since the recoil track is very short (~0·6 mm.), so that calculated values depend chiefly on the length and direction of the track of the disintegration particle.

Now experiment appears to show that the emission of energy in the form of radiation is a feature common to the different types of capture disintegration of light nuclei. If this radiation is always emitted (from the residual nucleus) after the particle disintegration has taken place, and if the state of excitation of the emitting nucleus depends only upon the structure of that nucleus and the amount of energy available, then the same γ-radiation should be observed whenever the final complex nucleus is the same,† provided the initial energy is sufficient. Subject to this condition, therefore, if our assumptions are correct, the same γ-radiation is to be expected as a result of the α-particle disintegration of boron (B^{10} affected, proton emitted), or the neutron disintegration of oxygen (α-particle emitted), or the neutron disintegration of nitrogen (if the mode in which H^2 is emitted does, in fact, occur), or the disintegration of the carbon nucleus C^{12} by capture of the less abundant hydrogen nucleus H^2.‡ Actually, the amount of energy available is very different in these four disintegrations, so that in some of them a portion only of the complete γ-ray spectrum may appear Concerning the third and fourth of these types of disintegration no data are at present available, for the first direct evidence so far is in favour of a single monochromatic γ-radiation.§ Moreover, the existence of the corresponding proton groups is a well-established fact.‖ In order to explain these observations an excited state of the nucleus C^{13} with $3 \cdot 0 . 10^6$ electron volts excess energy is postulated. Now, if the present results be broadly correct, higher excited states must equally be possible, and in that event, when the initial energy is sufficient, they should appear in the boron disintegration also. When α-particles of higher energy are employed, in addition to proton groups corresponding to the two already observed, other

---

* Meitner and Philipp, 'Naturwiss.,' vol. 20, p. 929 (1932)

† If the quantum is emitted first the interrelations here predicted would not be expected to hold, for it is hardly to be imagined that different particle changes would follow a common quantum emission.

‡ Lawrence, Livingston, and Lewis, 'Phys. Rev.,' vol. 44, p. 56 (1933); Lawrence, 'Science,' June 30, 1933 ('Science News ').

§ Becker and Bothe, 'Z. Physik,' vol. 76, p. 421 (1932).

‖ *E.g.*, Chadwick, Constable, and Pollard, 'Proc. Roy. Soc.,' A, vol. 130, p. 463 (1931).

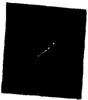

2

1

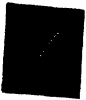

3

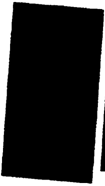

6

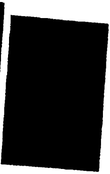

4

5

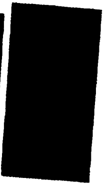

7

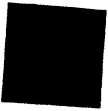

9

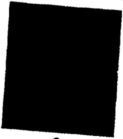

8

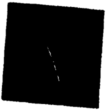

10

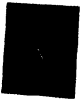

13

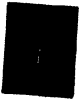

11

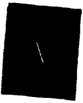

12

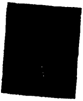

14

16

15

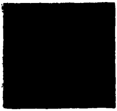

17

18

19

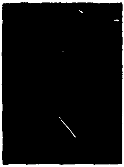

20

21

22

23

and shorter-range groups should be found.* The ability to sustain a high energy excited state, even for a short time, is an important property of any nucleus, deriving, as it must, from the nature of its intimate structure. To obtain further and more trustworthy evidence concerning the reality of these states is therefore essential.

In the experiments carried out with the oxygen-hydrogen mixture in the chamber only two additional examples of disintegration were recorded, numbers 18 and 19, Plate 7 Of these only the former was completely in view of both cameras, and even here the disintegration particle was not fully absorbed in the chamber However, it is fairly certain from the measurements that a neutron of about 8 10^6 electron volts energy was captured and that roughly $3 . 10^6$ electron volts of kinetic energy failed to reappear in the products of disintegration. In this calculation the " mean " range-velocity curve adopted above was employed , in the matter of consistency the new curve gave more satisfactory results than the old. Concerning the second example, the deflection near the end of the track of the disintegration particle was recorded on both films The measured deviation is 23°, the residual range at the point of deflection 2·7 mm. of standard air. Almost complete failure to detect any visible spur makes it possible to regard the disintegration particle as an H^2 nucleus rather than an α-particle. For an α-particle an oxygen recoil track of length 0·20 mm of standard air is to be expected, whereas for an H^2 particle the predicted length of spur is 0·12 mm. However, the range-velocity curve may well be in error for oxygen recoil atoms of this small speed, and the two examples recently published by the writer† of α-particle tracks showing sudden deflections and negligible spurs make it improbable that the present disintegration is different in type from the others previously discussed.

In the acetylene-helium series of experiments only three certain disintegrations were photographed, numbers 20, 21, 22, 23, Plate 7. It is natural to assume, in the absence of evidence to the contrary, that three instances of the disintegrations of the carbon nucleus are here in question. Already one example of a reversible nuclear reaction has been established, namely, that which is written

$$B^{11} + \alpha^4 \rightleftharpoons N^{14} + n^1.$$

---

* Evidence pointing to the occurrence of more than one excited state of the residue nucleus (Si^{30}) resulting from the capture disintegration of aluminium by fast α-particles has recently been obtained. The experiments of Haxel ('Z. Physik,' vol. 83, p. 323 (1933)) suggest a second, and those of Duncanson and Miller, carried out in the Cavendish Laboratory, a third excited state.

† 'Proc. Roy. Soc.,' A, vol. 141, p. 194 (1933), Plate 1, numbers 8 and 9.

Similarly, since the production of neutrons by the bombardment of beryllium by α-particles involves the formation of the nucleus C^{13}—if the incident particle is captured, inelastic collision between a neutron and a carbon nucleus may well result in the reverse reaction taking place. Formally, we should write

$$Be^9 + \alpha^4 \rightleftharpoons C^{12} + n^1.$$

It was natural to regard the three disintegration collisions observed as of this type.

The great difficulty in making calculations on the basis of the above assumption lies in our lack of knowledge of the range-velocity relation for the recoil atoms of beryllium Difficulties already encountered appear here in a much aggravated form In one case, however, number 23, Plate 7, the numerical result was found to be rather insensitive to the exact form of range-velocity relation adopted It is probable that a neutron of about 10^7 electron volts energy was captured and that roughly $7 . 10^6$ electron volts of kinetic energy disappeared in the process. Now it is known that the adverse balance of mass, expressed as an energy difference, is about $6 \cdot 8 \ 10^6$ electron volts[*] in the reaction with which we are concerned In this instance, therefore, it is unnecessary to assume the emission of energy in the form of radiation

Concerning the other two examples it may be said at once that they are not of the same type Whatever assumption is made it is obvious in each case that a relatively slow neutron was involved. In the first, number 20, Plate 7, disintegration of a nitrogen nucleus by a neutron of somewhat less than $4 . 10^6$ electron volts, with the simultaneous release of about 10^6 electron volts energy, is one possibility. (The measurements here are a little uncertain, since one camera only had a full view of the complete fork.) In the second case, numbers 21 and 22, Plate 7, which proved more suitable for measurement, if capture disintegration of a nitrogen nucleus be again assumed, then the effective neutron must have possessed about $4 \cdot 5 . 10^6$ electron volts energy, of which about $1 \cdot 5 . 10^6$ electron volts did not reappear as kinetic energy at the end of the process. On the other hand, it was not thought that any disintegrable "impurity" was present in these experiments, beyond the oxygen in the water vapour. However, it seems necessary to conclude that a slight leakage of air had, in fact, taken place. This explanation is the more credible because both anomalous disintegrations occurred in the first 740 photographs of the series.

---

[*] Neutrons of energy less than about $7 \ 4 . 10^6$ electron volts must therefore be incapable of causing this particular disintegration. The adverse energy balance is approximately twice as great in the disintegration $C^{12} + n^1 \rightarrow B^{11} + H^2$.

A new filling of the chamber was carried out before the remaining 1470 photographs were taken In these no anomalous disintegrations were observed. A fourth example, probably of disintegration, was, however, found, almost completely obscured (by the central source box) on one view of the event. It is very probable that this was another case of nuclear disintegration of carbon, similar to the first, a 10^7 electron volt neutron and a $7 \cdot 10^6$ electron volt absorption of energy being quite consistent with the (incomplete) observations.

The new experimental material having been analysed and discussed it remains to make brief reference to the old material concerning the nuclear disintegration of nitrogen—and to the interpretation of that material originally offered. During the past year the inadequacy of any empirical range-velocity relation of wide validity has been made abundantly clear For that reason alone, it must again be insisted, numerical results must be regarded with suspicion. At present no attempt will be made to amend the original results in this particular, the determination of range-velocity curves is a matter for future experiment—and it is a matter of some urgency. It is intended here merely to compare the results as they stand with those reported by other experimenters. Harkins, Gans, and Newson, and Kurie, have described disintegrations in which the effective neutron appeared to be of high energy. In the original results of the writer no such examples appeared. To some extent the discrepancy is more apparent than real. Evidence from nitrogen recoil tracks appeared to place an upper limit to the energy of the polonium-beryllium neutrons in the neighbourhood of $6 \cdot 4 . 10^6$ electron volts. This evidence has been rediscussed above Now one principle of analysis of the disintegration results was that—admitting certain limits of experimental error—the energy of the neutron necessary to explain the measurements in any case should not be greater than the maximum energy indicated by the recoil track measurements (Part I, p 719). It appears that this principle erred in being too conservative, based, as it was, upon a limited set of data. As a result of its application at least two examples were classified as non-capture disintegrations when all other conditions for capture appeared to be fulfilled. Reversing this verdict, a maximum neutron energy of about $12 . 10^6$ electron volts appears to be indicated. Just possibly, for other reasons similar to the above, there was an undue bias in favour of the non-capture interpretation throughout the results. It remains for further experiment to show how serious this bias may have been.

Finally, concerning the capture disintegrations themselves, this remark may be made. It appears likely, upon further consideration, that the disintegration

$$N^{14} + n^1 \rightarrow C^{13} + H^2,$$

was, in fact, observed. This possibility was left open in the previous account of the work It now appears that there is one case at least in which any other interpretation is very unlikely. If the present interpretation be correct, then a neutron of about 12 . 10^6 electron volts must have been captured and 8·5 . 10^6 electron volts of kinetic energy absorbed This need not be at all improbable, for the adverse balance of mass is equivalent to about 3·5 . 10^6 electron volts energy—well within the limits of kinetic energy available. Further experiment is obviously needed Only when sufficient disintegration photographs have been obtained in which the ends of both tracks are in view of both of the cameras will the true position become clear. Then it is possible that the distribution-of-brightness criterion above developed will be of use in establishing doubtful decisions.

It is unlikely that the multiplication of instances will be achieved without some new phenomenon appearing. Possibly we may find electron tracks—either singly, or as positive and negative pairs—associated with the tracks of the heavy products of disintegration. For, occasionally—it is not at present known how frequently—the quantum of radiation, the emission of which it has so often been necessary to assume, must suffer internal conversion in the atom of origin.

It is a pleasure again to acknowledge gifts of material as well as opportunities for discussion, all of which have contributed to the realization of the work here described. For material and funds I wish to thank Drs. Burnam and West and the Council of Trinity College, respectively; and for helpful advice Professor Lord Rutherford and Dr. Chadwick.

Summary.

A previous paper gave an account of cloud track photography of the collisions of neutrons with nitrogen nuclei. The same method has now been applied to neutron-oxygen nucleus encounters and further series of photographs have likewise been obtained of the tracks produced in oxygen-hydrogen and acetylene-helium gas mixtures, respectively. Range distribution curves are given for the single recoil tracks resulting from elastic collisions and an attempt is made to analyse the curves referring to the mixtures of gases. Evidence is adduced

for the presence of recoil protons due to neutrons produced in the resonance disintegration of beryllium and also for carbon recoil atoms due to neutrons of high energy A criterion based upon the distribution of photographic density in the track image is suggested for the purpose of identifying recoil tracks produced by different atoms

Disintegration collisions in oxygen have been observed, but it appears that carbon nuclei are not readily disintegrated by the neutrons from polonium-beryllium Only one such disintegration was found in more than 2000 photographs

Finally it is insisted that present knowledge of range-velocity relations for recoil atoms is quite inadequate for a full numerical investigation of the energy changes in the disintegrations observed. Further data are urgently needed

INDEX TO VOL. CXLII. (A)

Acids, fatty, films, effect of alkalinity in underlying solutions (Adam and Miller), 401.

Adam (N K.) and Miller (J G. F.) The structure of surface films XVIII —The effect of alkalinity on the underlying solutions on films of fatty acids, 401

Adam (N K.) and Miller (J. G F) The structure of surface films XIX —The influence of alkaline solutions on films with various end groups, 416

Alpha particles from radium C′, analysis by magnetic focussing method (Rutherford and others), 347.

Anthracene, reflection of X-rays from crystals (Robinson), 422

Bailey (C R.) and Cassie (A B D) Investigation in the infra-red region of the spectrum IX.—The absorption spectrum of chlorine monoxide (Cl_2O), 129

Bairstow (S.) and Hinshelwood (C N) The homogeneous catalysis of gaseous reactions by iodine. The decomposition of propionic aldehyde, and a general discussion, 77

Bakerian lecture, the neutron (Chadwick), 1.

Barium I, perturbations in spectrum (Langstroth), 286

Benzyl compounds electric moment (Fairbrother), 173.

Beryllium, helium content in beryls of varied geological age (Rayleigh), 370

Bismuth, behaviour in atomic hydrogen (Pearson and others), 275

Bowden (B V.) *See* Rutherford, Lewis and Bowden

Bowden (P) *See* Dummett and Bowden

Carbon dioxide, spectrum of after-glow (Fowler and Gaydon), 362.

Cassie (A. B. D) *See* Bailey and Cassie.

Catalysis, homogeneous of gaseous reactions by iodine (Bairstow and Hinshelwood), 77

Catalytic activity of liquid and solid surfaces (Steacie and Elkin), 457

Chadwick (J) The Bakerian lecture, the neutron, 1.

Charge, electric, collected by water drops falling through ionized air (Gott), 248.

Childs (E. C.) and Massey (H. S W.) The scattering of electrons by metal vapours. II.—Zinc, 509

Chlorine monoxide, absorption spectrum (Bailey and Cassie), 129

Cobalt chloride, change in absorption spectrum (Howell and Jackson), 587.

Corrosion, relation of oxygen electrode (Hoar), 628.

Crystals of anthracene, reflection of X-rays (Robinson), 422

Crystals with layer lattices, thermal expansion (Megaw), 198.

Davidson (P. M.) Quantization of the Kramers and Pauli model, 269.

Davidson (P M) *See also* Richardson and Davidson

Dielectrics, power loss phenomena in liquid (Jackson), 606

Diphenylbenzene, *p*-, an X-ray study (Pickett), 333.

Dummett (A.) and Bowden (P) The influence of the underlying surface on the cataphoretic mobility of adsorbed proteins, 382

Durene, Fourier analysis of structure (Robertson), 659.

Egerton (A.) and Pidgeon (L. M.) Absorption spectra of burning hydrocarbons, 26.
Electrons, inelastic scattering of slow (Nicoll and Mohr), 320, 647.
Electrons, scattering by metal vapours (Childs and Massey), 509.
Elkin (E. M.) *See* Steacie and Elkin.
Emission constants of metals in the near infra-red (Hurst), 466.
Energy exchange between gas atoms and solid surfaces (Roberts), 518.
Energy exchange between gas atoms and a solid surface (Jackson and Howarth), 447
Evans (W. M.) *See* Richardson and Davidson.
Expansion apparatus, a new type (Wilson), 88.

Fairbrother (F) The estimation of electric moment in solution by the temperature coefficient method. I.—Experimental method and the electric moments of some benzyl compounds, 173.
Feather (N.) Collisions of neutrons with light nuclei—II, 689.
Films, influence of alkaline solutions (Adam and Miller), 401, 416
Films, structure of surface (Adam and Miller), 401, 416
Flow, viscous fluid, stability of three-dimensional disturbances between parallel walls (Squire), 621
Flow of a viscous fluid, steady two-dimensional, behind a solid body (Goldstein), 545, 563.
Flow of viscous liquid past spinning bodies (Garstang), 491
Fowler (A.) and Gaydon (A. G.) Spectrum of the afterglow of carbon dioxide, 362

Gamma rays, internal conversion (Taylor and Mott), 215
Garstang (T. E) The flow of viscous liquid past spinning bodies, 491.
Gaydon (A. G) *See* Fowler and Gaydon.
Gold, first spark spectrum (Raghavendra Rao), 118.
Goldstein (S) On the two-dimensional steady flow of a viscous fluid behind a solid body—I, II, 545, 563.
Gott (J. P.) On the electric charge collected by water drops falling through ionised air in the vertical electric field, 248.

Helium in beryls of varied geological age (Rayleigh), 370.
Helium, intensity measurements of band spectrum (Johnson and Turner), 574
Hinshelwood (C. N.) *See* Bairstow and Hinshelwood.
Hoar (T. P) The mechanism of the oxygen electrode, 628.
Horn, transmission of infra-red radiation by a thin layer (Taylor), 598
Howarth (A.) *See* Jackson and Howarth.
Howell (O. R.) and Jackson (A.) The change in the absorption spectrum of cobalt chloride in aqueous solution, with increasing concentration of hydrochloric acid, 587.
Hurst (C.) Emission constants of metals in the near infra-red, 466.
Hydrocarbons, absorption spectra of burning (Egerton and Pidgeon), 26.
Hydrogen, atomic, preparation and behaviour of metals in (Pearson and others), 275.
Hydrogen and nitrous oxide, kinetics of reaction (Melville), 524.

Ions, passage of positive, through gases (Massey and Smith), 142.

Jackson (A.) *See* Howell and Jackson.
Jackson (J. M.) and Howarth (A.) Exchange of energy between inert gas atoms and a solid surface, 447.
Jackson (W.) Power loss phenomena in liquid dielectrics, 606.

Jay (A. H.) The thermal expansion of quartz by X-ray measurements, 237
Johnson (R. C.) and Turner (R. C) Some intensity measurements on the band spectrum of helium (He_2), 574.

Kinetics of reaction between hydrogen and nitrous oxide (Melville), 524.

Langstroth (G. O.) Perturbations in barium I spectrum, 286.
Lead, behaviour in atomic hydrogen (Pearson and others), 275
Lewis (W. B.) *See* Rutherford, Lewis and Bowden

Marsden (J.) *See* Richardson and Davidson
Massey (H. S W) and Smith (R. A) The passage of positive ions through gases, 142.
Massey (H. S. W) *See also* Childs and Massey.
Megaw (H. D) The thermal expansion of certain crystals with layer lattices, 198
Melville (H. W.) The kinetics of the reaction between hydrogen and nitrous oxide—I, 524
Metals, behaviour in atomic hydrogen (Pearson and others), 275.
Metals, emission constants in the near infra-red (Hurst), 466.
Methanol, catalytic decomposition on zinc (Steacie and Elkin), 457.
Miller (J. G. F) *See* Adam and Miller.
Mohr (C. B. O) *See* Nicoll and Mohr
Moment, electric estimation in solution (Fairbrother), 173
Mott (N F) *See* Taylor and Mott

Naphthalene crystalline structure, X-ray investigation (Robertson), 674
Neutron, the (Chadwick), 1
Neutrons, collisions with light nuclei (Feather), 689
Nicoll (F H.) and Mohr (C B O) The inelastic scattering of slow electrons in gases—III, IV, 320, 647
Nitrous oxide and hydrogen, kinetics of reaction (Melville), 524

Oxygen electrode, mechanism (Hoar), 628.

Pearson (T. G), Robinson (P L.) and Stoddart (E. M.) The behaviour of metals, particularly lead and bismuth, in atomic hydrogen, and attempts to prepare atomic hydrogen and hydrides, 275.
Pickett (L. W.) An X-ray study of *p*-diphenylbenzene, 333.
Propionic aldehyde, decomposition by homogeneous catalysis (Bairstow and Hinshelwood), 77.
Proteins, cataphoretic mobility of adsorbed (Dummett and Bowden), 382.

Quantization of the Kramers and Pauli model (Davidson), 269.
Quartz, thermal expansion by X-ray measurements (Jay), 237.

Radium C′, α-particles from, analysis by magnetic focussing method (Rutherford and others), 347.
Rao (B. V. Raghavendra) The first spark spectrum of gold, Au II, 118.
Rayleigh (Lord) Beryllium and helium. I.—The helium contained in beryls of varied geological age, 370.
Richardson (O. W.) and Davidson (P. M.) The spectrum of H_2. The bands ending on $2p\ ^3\Pi$ levels—Part III. Appendix by Marsden (J.) and Evans (W. M.), 40.

Richardson (O. W.) and Davidson (P. M.) The spectrum of H_2. The $3d^3\Delta$ and $4d^3$ levels, 63.
Roberts (J. K.) The exchange of energy between gas atoms and solid surfaces, 518.
Robertson (J. M.) The crystalline structure of naphthalene. A quantitative X-ray investigation, 674.
Robertson (J. M.) Fourier analysis of the durene structure, 659.
Robinson (B. W.) The reflections of X-rays from anthracene crystals, 422.
Robinson (P L.) *See* Pearson, Robinson and Stoddart.
Rosenhead (L.) Interference due to walls of a wind tunnel, 308.
Rotor, motion of, carried by a flexible shaft in flexible bearings (Smith), 92.
Rutherford (Lord), Lewis (W. B.) and Bowden (B. V) Analysis of the long range α-particles from radium C′ by the magnetic focussing method, 347.

Smith (D. M.) The motion of a rotor carried by a flexible shaft in flexible bearings, 92.
Smith (R. A.) *See* Massey and Smith.
Spectra, absorption of burning hydrocarbons (Egerton and Pidgeon), 26
Spectrum, absorption of chlorine monoxide (Bailey and Cassie), 129.
Spectrum, absorption of cobalt chloride (Howell and Jackson), 587.
Spectrum, band of He_2, intensity measurements (Johnson and Turner), 574.
Spectrum of barium I, perturbation (Langstroth), 286.
Spectrum of H_2 (Richardson and Davidson), 40, 63.
Spectrum, investigations in infra-red regions (Bailey and Cassie), 129.
Spectrum of the afterglow of carbon dioxide (Fowler and Gaydon), 362
Spectrum, spark of gold (Raghavendra Rao), 118.
Squire (H. B.) On the stability for three-dimensional disturbances of viscous fluid flow between parallel walls, 621.
Steacie (E. W. R.) and Elkin (E. M.) A comparison of the catalytic activity of liquid and solid surfaces. The decomposition of methanol on solid and liquid zinc, 457.
Stoddart (E. M.) *See* Pearson, Robinson and Stoddart.
Surfaces, liquid and solid, catalytic activity (Steacie and Elkin), 457.
Surface, solid, and energy exchange between gas atoms (Jackson and Howarth), 447.
Surfaces, solid, and exchange of energy between gas atoms (Roberts), 519.

Taylor (H. J.) The transmission of infra-red radiation by a thin layer of horn, 598.
Taylor (H M.) and Mott (N. F.) The internal conversion of γ-rays, 215.
Turner (R. C.) *See* Johnson and Turner.

Wilson (C. T. R.) On a new type of expansion apparatus, 88.
Wind tunnel, interference due to walls (Rosenhead), 308.

Zinc, scattering of electrons by vapour of (Childs and Massey), 509.

END OF THE ONE HUNDRED AND FORTY-SECOND VOLUME (SERIES A).

I. A. R. I. 75

PERIAL AGRICULTURAL RE[redacted]CH
INSTITUTE LIBRARY
NEW DELHI.

Date of issue.	Date of issue.	Date of issue.
26.11.64		